Physical Science Techniques for Non-Invasive, Quantitative Measurements within the Living Human Body

Professor Michael A Smith

BSc, MSc, PhD, CPhys, CSci, FIPSM, FInstP

Doctor of Science

The University of Edinburgh

2006

Contents

THE UNIVERSITY OF EDINBURGH

ABSTRACT OF THESIS

Name of Candidate: Professor Michael A Smith

Address :

Postal Code:

Degree: Doctor of Science

Title of Thesis: Physical Science Techniques for Non-Invasive, Quantitative Measurements within the Living Human Body

No. of words in the main text of Thesis:

5,500 words plus 129 scientific papers

The research in this thesis focuses on the use of a range of physical science techniques to perform quantitative measurements within the living human body in a non-invasive manner, for the purpose of understanding disease processes, diagnosing abnormality or monitoring therapeutic responses. The research publications cover work which has been undertaken over the last thirty years in the Universities of Edinburgh, London and Leeds. The research has not concentrated on one aspect of the physical sciences but has taken advantage of scientific and technological developments, encompassing neutron, X and γ ionising radiation, laser and THz non-ionising radiation, magnetism, radio-waves and a range of mathematical and computing techniques. Clinical applications have encompassed a wide range of diseases and conditions and include osteoporosis and other metabolic bone diseases, cardiac disease, vascular disease, rheumatoid arthritis and cancer.

Declaration and Acknowledgements

The nature of the research that I undertake often requires multidisciplinary collaboration between scientists and clinicians. The publications I have submitted are either purely my own work, the result of collaborative research where I have made a major contribution as joint researcher, or output from a research group. In the case of the latter I have either led or co-led the research group and have been responsible for both the strategic direction of the research and the day to day oversight of the research.

31st July 2006.

As a consequence, I have had the pleasure and privilege of working with many talented and inspirational colleagues whose support and contribution to my work I would like to acknowledge:

In Edinburgh:

Dr Peter Tothill, who started me on my research career, Prof Richard Eastell, Prof David Reid and Prof George Nuki in the area of Bone Measurement.

Dr John Ridgway, Prof Tony Bell, Dr Martin Been, Dr David Kean, Dr Lindsay Turnbull and Prof Jonathan Best in the area of Magnetic Resonance Imaging.

In London:

Dr Stephen Keevil, Dr Soundrie Padayachee, Dr Ted Baker, Prof Ray Gosling, Prof Michael Maisey and Prof Mike Richards in the area of Magnetic Resonance Imaging and Spectrocopy.

In Leeds:

Dr John Sutcliffe in the area of Body Composition Measurement

Dr John Truscott in the area of Bone Measurement

Dr Elizabeth Berry in the area of Image Analysis, Evidence Based Imaging and Terahertz Imaging and Sensing

Dr John Ridgway, Dr Steve Tanner and Dr Jim Meaney in the area of Magnetic Resonance Imaging

Prof Martyn Chamberlain (who also co-led the research group) in the area of Imaging and Sensing

I would also like to acknowledge my PhD students during this period: John Ridgway, Alison McKie, Maria Tarnowski, David Porter, Martin Graves, Stephen Keevil, Sylvester Yankuba, John Trustcott, Nasser Dennaoui, Sasha Radjenovic, Niall MacDougall, David Brettle, David Higgins and Gillian Walker. I would also like to acknowledge research fellows who have worked with me: Steve Kelly, Dr Tony Fitzgerald, Dr Graham Woodrow, Brian Oldroyd and Dr Chris Twelves.

Background

The publications which I have submitted for consideration for the award of DSc cover work which has been undertaken over the last thirty years during which I have worked in the Universities of Edinburgh, London and Leeds in association with NHS Teaching Hospitals. My research has focused on the use of physical sciences to perform quantitative measurements within the living human body in a non-invasive manner, for the purpose of understanding disease processes, diagnosing abnormality or monitoring therapeutic responses.

This underlying scientific theme has remained constant throughout my research career but it has been mediated by two other factors which I believe to be important in the area of applied medical science research. Both are associated with the transition of the development of an original idea to its eventual widespread availability in the health sector. I had always envisaged that any new medical technique should go through a natural, and logical, progression from basic scientific research to its eventual provision and availability in the health sector. Given that part of my personal motivation was to develop new techniques which would have an impact on healthcare, it was natural that I should take an increasing interest in the subsequent stages of this process after my initial contribution. The two factors to which I refer were therefore the clinical validation of new techniques and their commercial development.

At the start of my research career I had thought that my expertise and responsibility would, and indeed should, be concentrated in the early stages of this process, ie in the development of new techniques, and that appropriate processes and funding mechanisms were in place to investigate clinical effectiveness and efficacy. I subsequently recognised that this was naïve, a fact which I attribute to youthful inexperience, and I became aware that if I did not extend my research involvement further then appropriate validation would not take place. In addition this recognition of the importance of the need to evaluate new techniques stemmed from personal experience, as I recognized that the acceptance of new scientific techniques by health sectors was not necessarily evidence based. I became aware that the route from the assessment of the feasibility of the use of a new scientific technique in clinical practice, to finally a rigorous analysis of the efficacy and effectiveness of an investigative technique in routine clinical use, generally did not occur. This compromised the rapid implementation of new techniques into health provision.

In a number of cases the eventual outcome of my research has been associated with a medical device which has had commercial potential. From the start of my career I considered this to be part of the 'research pipeline', a concept which I have always had, long before 'knowledge transfer' became a significant part of University life. This was driven by the recognition that if any of the developments with which I was associated were to become widely available in the medical and health sector, they would need to be commercially produced and supported. This extension of my research into the commercial sphere exposed me to an additional critical environment which encompassed economic and financial issues as well as perceived user acceptance.

In my chosen field there has always been a close and synergistic link between the science and the technology. Often, particularly early in my career, there was a need to identify innovative scientific solutions to overcome problems which, we can now see with hindsight, could have been easily solved with later technology or as the technology matured. Obvious examples include computer power, firmware and software packages, non-magnetic materials, image storage devices, data communication protocols and micro-fabrication techniques. As I consider and review my early research I am conscious that I am doing so from the perspective of current technology and that initially I had a tendency to be somewhat dismissive of some of my early innovative work which had to overcome technological deficiencies. I have made every effort not to fall into this trap but include such work and the associated publications.

Because of the ongoing nature of developments in science and technology my research has not concentrated on one aspect of the physical sciences but has encompassed many, utilising neutron, X and γ ionising radiation, laser and THz non-ionising radiation, magnetism, radio-waves and a range of mathematical techniques. Likewise the clinical applications have also varied and include osteoporosis and other metabolic bone diseases, cardiac disease, vascular disease, rheumatoid arthritis and cancer. This variety is neither dilettantism nor simple opportunism on my part. Throughout my career I have recognised when it is time for a physical scientist such as myself to reduce my involvement in a subject area and pass the baton on to clinicians or the commercial sector. In such cases I have often retained a significant involvement but have transferred the main focus of my research attention to another area. Also my desire to pursue research at a high level has resulted in my willingness to transfer my attention to more promising scientific methods, when the opportunity arises, and to choose the clinical applications which are most important or which provide a challenging exemplar for the new techniques.

In addition to some of the scientific reasons for the evolution of my research, I would also like to highlight the two other factors which have had an impact. The first was the impact of career changes which have imposed both constraints and opportunities. These are generally associated with the equipment and facilities available and, probably more importantly, scientific and clinical colleagues with whom it is essential to undertake collaborative research. This collaborative approach to research is essential for high quality research into the non-invasive use of physical science in medicine. Throughout my career I have formed research teams and sometimes the presence or absence of a key team member has influenced the direction of the research. In my acknowledgements I highlight my key collaborators. The second factor was the external influence of funding priorities and opportunities. My research area requires significant equipment and recurrent expenditure on facilities and, as a consequence, is highly dependent on external funding. Generally the evolution of my research into a new area anticipated a change in funding priorities of which I was then able to take advantage (magnetic resonance imaging in the 1980s, evidence based medicine in the 1990s). Other research areas were affected by a relative lack of funding opportunities (neutron activation analysis after the 1970s, physical science aspects of bone measurement

in the 1980s, and magnetic resonance imaging in the 1990s). Far from criticising these changes in funding priorities, I would support the necessary change of emphasis into areas which offer, or potentially offer, better outcomes. In addition the funding priorities also reflect the correct emphasis away from 'near market' research.

In this review of my research it will be apparent that though the non-invasive use of physical science in medicine has remained constant, the primary focus of my research has changed with time. In addition, as with other things in life, though I became involved in new areas, association with pre-existing areas continued; as a consequence there is considerable overlap in time between different research areas. For ease of understanding I have tried to indicate the time-line of my research in the table below.

Number of papers in each research area during approximate five year periods

	79 - 84	85 - 89	90 - 94	95 - 99	00 - 05
Bone Measurement	27	10	10	4	
Magnetic Resonance	3	37	17	1	5
Body Composition Measurement		1	10	19	1
Image Analysis (generally MRI)				4	3
Evidence Based Imaging				5	6
Terahertz Imaging and Sensing					11

The table above includes the total number of my refereed publications in the different research areas. In my DSc submission I have not included all my research publications but have been selective and included those which contain the major research outputs. A small number of publications are referred to in the text in {these} brackets. These include patents, which relate to the research described but would not be appropriate as part of my DSc submission, and large systematic reviews, which are in the form of substantial monographs. For reasons of space hard copies have not been included, but electronic copies have been included on a accompanying CD.

The publications I am submitting for my DSc are listed chronologically under broad category headings, rather than in a continuous chronological list. I have only included a small number of published conference papers; these have all been refereed and the specific conferences are a recognised route for publication, often in a rapidly evolving field of research. A small number of publications arose following my PhD studies at the University of Edinburgh; these are indicated in the publication list with the symbol (*PhD) and I have included them for completeness.

Research Areas

Bone Measurement

At the start of my research career in Edinburgh in the early 1970s, one of the small number of physics techniques which had the potential to enable quantitative measurements to be made in-vivo was neutron activation analysis (NAA), and a number of research groups were investigating its development and application. My initial research focused on the development of techniques which could be used in practice on patients, in a clinical environment. Many other researchers were using neutron sources such as research reactors and cyclotrons, which may have been appropriate for the development of a research tool, but were clearly impractical for clinical use. I developed precise techniques for measuring bone calcium and other elements in the forearm and spine and applied them to the investigation of osteoporosis and bone disease associated with renal dialysis [1, 2, 3]. My scientific research had to overcome problems of relatively low neutron yield from the small Cf^{252} sources, minimise the effect of the variation in sensitivity with depth in tissue, design and construct detection systems for the relatively high γ radiation emitted and develop a computer technique for spectral analysis using matrix inversion. I also undertook the preliminary clinical evaluation, designing and managing the small trial in renal dialysis patients.

Whilst developing this technique I became aware of the limitations of studying a part of the body where there was insufficient accurate knowledge of the location of the area of measurement. Hitherto the research I had undertaken relied on accurate repositioning and sequential measurements or assumptions of internal localisation in the human body. Also the variation between people of different sizes was clearly a limitation in a fixed geometry and was particularly important in performing absolute measurements and determining the percentage difference from normal. This led me to become involved with two different approaches to resolve this underlying problem, both of which I pursued by attracting external funding to support additional research support staff.

The first was to extend NAA measurements to the whole human body [4, 11, 22] using a clinical cyclotron which had just been installed in the hospital. The spectral analysis programme I had developed was extended to measure a wider range of body elements including Ca, Na, Cl, P and N. Absolute measurements on patients were obtained by normalising the measurement using an equation based on the patient's stature; this enabled the results to be expressed as a percentage of normal. The seasonal variation in total body calcium was also measured [15]. The whole body technique was applied to a range of clinical conditions, particularly osteoporosis [12] and osteoarthritis [13, 20], rheumatoid arthritis [7, 17, 18], ankylosing spondylitis [16] and other osteopenic disorders [14, 19]

The second, and more far reaching, approach was to recognize the opportunities that medical imaging offered to localise accurately the site in the body where quantitative measurements were being performed. It was this which led me into the area of medical imaging. I was less interested in developing new imaging

techniques *per se* but rather I recognised the powerful combination of performing quantitative measurements and identifying where the information was coming from.

Whilst performing NAA measurements to measure bone calcium I had previously implemented a simple method to measure bone mineral of the wrist by measuring the absorption of γ radiation from a radionuclide source as it traversed the wrist. I had used it to measure demineralization in patients with Turner's syndrome [6] and had compared the changes measured using the two techniques [36]. It was natural to extend this work into two dimensions to obtain quantitative measurement of bone mineral in the spine. Two radionuclide energies were used, to correct for the body thickness; the technique was known as dual photon absorptiometry (DPA) and it was able to obtain both quantitative measurements and relatively low resolution images to obtain accurate and reproducible localization [8, 10]. This method was also developed further to measure bone mineral in the whole hand [21].

Whilst developing DPA I became aware of a potentially significant problem associated with the interference of one energy with the other which I termed the 'crossover correction' [5]. A consequence of an error in the crossover correction could, I hypothesised, be responsible for the variation in the decrease in bone mineral with age which was apparent at different international locations [9].

The focus of my research on bone and the increasing national interest on osteoporosis led me to consider methods of monitoring or measuring fracture healing using radionuclides. As a consequence I developed and evaluated a nuclear medicine technique to predict fracture healing in a relatively large clinical study [23].

After moving from Edinburgh I maintained my research interest in bone measurement, both in London where I offered some scientific advice and support to clinicians, but more so later in Leeds where I provided leadership to the Bone and Body Composition Research Group. The technology had advanced and commercially available dual energy X-ray based systems (DPX) were available to measure bone mineral. My research therefore followed the natural path of investigating the variation of bone mineral with age in large populations, measured using DPX [24, 28] and applying the technique to the study of a variety of bone diseases [27, 30, 32, 33].

In Leeds I also become interested in newer techniques to measure bone mineral. These included the use of ultrasound for measuring bone parameters and its relationship with measurements using photon absorptiometry [25]. To support this work it was necessary to resolve the difficult problem of simulating bone for ultrasound and so a phantom material for ultrasound was developed [29] and patented {34}. Availability of new technology enabled me to extend the technique of single photon absorptiometry, using a radiation sensitive CCD camera, to the challenging application of the measurement of neonatal bone mineral [26, 31].

Statistics

Whilst in the early phase of my research career my mathematical background and computing experience, coupled with my involvement in the clinical evaluation of the physical science techniques as well as their scientific development, caused me to become increasing involved in the statistical and data analysis aspect of research. Initially this led me to consider statistical issues associated with the comparison of techniques and the level of correlation which was possible due to inherent precision values [36].

Consideration of a possible clinical study of bone loss after surgery highlighted a potentially more important problem for research. This was the question of survival after surgery and whether there was a link to smoking status. An almost unique patient data set, recorded over several decades, had been maintained by a surgeon. This, coupled with the recently available computer power (even though the data were still entered on punch cards), enabled me to undertake a rigorous statistical analysis and demonstrate the relationship between survival after gastric surgery and smoking status [37, 38, 39].

Collaborative research with colleagues also led to a number of publications of a statistical nature [40, 41, 42] whilst I was in Edinburgh and London.

Magnetic Resonance

At the beginning of the 1980s, whilst still in Edinburgh, I recognized the limitations of neutron activation analysis in the clinical environment and also I felt that there was limited further physical science research to be done in the area of photon absorptiometry. I had become aware of exciting developments in in-vivo nuclear magnetic resonance and I therefore made a conscious decision to change the physical science techniques I would use for quantitative measurements in-vivo. Clearly a major difficulty was access to the very expensive equipment which was still in the early stages of development. I became involved with a proposal to seek funding to install the first pre-production prototype clinical MRI system in Scotland. As an MRC senior research fellow I was responsible for the scientific research of the programme. I therefore became actively involved in research to develop new techniques of magnetic resonance imaging (MRI) using the low field magnetic resonance system, and also to explore potential areas of clinical applications.

I published papers on some of the practical aspects of MRI [43, 46, 51, 59] and collaborated with radiologists on exploring its use for qualitative imaging of the brain, having extended the system to obtain sagittal images. However my main research interests were firstly the quantitative measurement of the magnetic resonance relaxation rate T_1, particularly in the brain and heart and secondly the quantitative measurement of velocity and flow.

In MRI the T_1 value is related to the ratio of free to bound water and, as a consequence, MRI offered a method to measure water content of tissue. With colleagues I studied changes in brain water in chronic alcoholic patients [44, 48,

62, 68] and, more importantly, related T_1 measurements to direct measurements of brain water content in patients with brain tumours [53, 56].

Though elsewhere the use of MRI was generally being investigated in the brain and CNS, we started investigating its use in the heart [45]. During this time my research group produced the first quantitative T_1 measurements in the human heart [49] which required the sychronisation of the MRI acquisition with the movement of the subject's heart. Qualitative cardiac images had recently been acquired elsewhere but there was much greater complexity involved in obtaining gated quantitative T_1. The technique was used to investigate acute myocardial infarction [47, 55, 60, 61] and monitor changes with time; there was a clear increase in T_1 in recent infarcts.

At the time there was some debate about the ability of T_1 and T_2 to be tissue specific and I contributed to this debate, based on our experience of quantitative measurements [50]. There was also a clinical interest in measuring the breast using MRI but the MRI system was insufficiently sensitive because of its vertical magnetic field and large body coil. Other MRI systems had horizontal magnetic fields which easily enabled specialist orthogonal vertical field surface coils to be developed. I developed an new surface coil for breast imaging for vertical field magnets [54] which was the subject of two patents {86, 87}.

The influence of movement on the phase of the NMR signal was known and, utilising this relationship, my research group was one of the first to develop a quantitative technique to measure fluid velocity in-vivo. We used two separate gradient pulse sequences which were subtracted to eliminate spatial phase variations and so produced an image which was directly related to velocity. We were already using gradient echoes for imaging so were able to develop MRI to produce velocity maps [52]. In addition to measuring blood velocity we explored its uses at low velocity levels, demonstrating the ability to measure the pulsatility of CSF [57] and its value for identifying communicating syringomyelia [58].

Having contributed significantly to the development of MRI science and technology at a low field strength I was approached to move to Guy's Hospital in London in 1986 to take on a senior academic position and continue research using one of the first high field MRI systems which had the field strength to offer the potential of in-vivo spectroscopic measurements.

Whilst in London I continued and developed my earlier interest in cardiac imaging and flow measurement, using the increased sensitivity and resolution of a much higher field strength magnet. I extended my cardiac research to the investigation of cardio-vascular abnormalities in infants [65, 66, 67] which concentrated on the accurate special localisation of the defect. I extended my research into MR flow measurements to the development of MR angiography [64, 70] and extending the quantification of it to the measurement of time-average flow [72, 73] and its evaluation against Doppler ultrasound.

The high field strength magnet offered the opportunity to measure, and potentially quantify, phosphorus metabolism. Previous research in the field had used surface coils to localise measurements, predominantly in muscle. My research, along with

a small number of other centres internationally, focused on image localised spectroscopic techniques [63] focusing on the effectiveness and characterisation of the localisation in-vivo [71, 75]. The technique was applied to breast tumours [69, 74, 77, 78] using customised breast coils.

Though this was the early days of MR spectroscopy, I made the decision not to continue in that area as I felt there were inherent scientific problems in utilising phosphorous MR spectroscopy for clinical usage. This also corresponded to a time, in the late 80s, where it was becoming increasingly difficult, if not impossible, for researchers in an academic environment to make the necessary scientific and technological changes to commercially produced MR systems to pursue research in certain areas. In addition this coincided with my view that image analysis would have an increasing role in the future and that a number of developments in imaging techniques, including MR, would require an image analysis approach

This awareness coincided with my decision to move to Leeds in 1989 to take up the chair in Medical Physics at the University of Leeds where, once I had raised funding to purchase MRI systems, I continued with applied MR research. I continued research in the area of angiography [76, 79] but also extended this to the development and implementation of perfusion measurements, particularly in infants, including neonates [80, 82]. The difficult task of attempting to measure perfusion in cardiac tissue was pursued by my research group, the first stage being the development of quantitative T_1 in different phases of the cardiac cycle in a single breath-hold [84]. Another potential method for estimating perfusion is the quantification of pharmacokinetic parameters and my research group developed a practical clinical technique [85] which is being used for cardiac and rheumatologic applications.

The use of MRI for quantitative radiation dose measurements had been around for many years. I felt that the technique could have practical use, with the increasing availability and usage of conformal radiotherapy, but I was concerned about the relatively poor quality of the evidence which I saw in published papers. On that basis my research group undertook to review the evidence and evaluate the performance of the latest generation of polymer gels used for dosimetry [81, 83].

During the period of my research in MRI, the technology had evolved from MRI systems in the laboratory which I could modify as required, through more restricted commercial systems which I could configure differently, to finally relatively closed commercial systems which could not be modified without extensive negotiation and delay. The opportunity for significant physics research in MRI was therefore severely restricted for someone like myself, working in the university and health sectors. I had recognised this growing restriction in the late 1980s at the same time as I recognised that many research problems may best be resolved by image analysis methods rather than by developments in MRI techniques. For this reason my research in image analysis, which only started to flourish in the early 1990s after my move to Leeds, has often focused on MRI; this work is described in the later section about image analysis.

Body Composition Measurement

In the 1980s there was interest in the measurement of body composition in vivo, particularly body fat and muscle mass, initially to monitor parentral nutrition and the after effects of surgery; of particular interest was the measurement of nitrogen as a better indicator of muscle mass. After moving from London to Leeds in 1989 I was able to utilise my experience in both neutron activation analysis and dual photon absorptiometry to provide leadership to a newly formed Bone and Body Composition Research Group.

I had previously been aware of the potential advantages of prompt neutron activation analysis to measure body nitrogen and initiated a research project whilst in Edinburgh [88] but recognised problems with that method associated with sensitivity. My move to Leeds in 1989 offered the unique opportunity to explore the use of the high and controllable output of neutron generators for body composition measurement. We developed a much improved pulsed neutron technique to measure body carbon, hydrogen and oxygen [89, 90] and considered whether it could be used to measure glycogen [91]. This work was extended to consider the measurement of total body water, fat and protein from the measurement of the ratio of the major elements [93].

We also undertook research into a recently published whole body electromagnetic method for body composition measurement which we thought may overcome some of the problems of bio-impedance methods [95]. However we found major scientific flaws in the technique [96], which to my knowledge is now no longer in use.

The commercially available techniques such as dual energy X-ray absorptiometry and bio-impedance analysis and laboratory techniques such as total body potassium offered an array of measurements of total body fat, fat-free mass, water, and lean-tissue mass. Research was undertaken to understand the relationship between the different methodologies [92, 94] with a particular focus on patients on renal dialysis [97, 98, 99, 100, 101, 102, 103, 105].

Image Analysis

My move to Leeds in 1989 coincided with my emerging view that the development of medical image analysis was of growing importance in the next stage in extracting quantitative information from MRI and other imaging techniques; indeed I had set up a medical image analysis group at Guy's Hospital just prior to my departure.

As outlined earlier I had become concerned that there should be a natural progression from basic scientific research, through applied research to a rigorous analysis of the efficacy and effectiveness of an investigative technique in routine clinical use. These three fundamental stages in research underpinned the creation of a multidisciplinary Centre of Medical Imaging Research (CoMIR), which I set up in Leeds in 1992 and of which I was Director until 1998, to undertake research in all these three areas. My own personal research which I pursued from the early 1990s in medical imaging was in magnetic resonance imaging (described above),

image analysis (described in this section) and evidence based imaging which developed beyond expectations and is described in the next section.

The possibility of using the spatial distribution of mineralisation in low resolution hip images obtained using DXA to improve the prediction of fracture risk was studied [106] and the image analysis methods developed demonstrated the benefit of such an approach. Unfortunately, however, it was beyond the scope of my research group to test the technique further by implementing it in a sufficiently large prospective clinical study.

New developments in MR offered the opportunity of superimposing darker grids onto tissue, so-called 'tagging'; these offered greater opportunity to quantify the movement of cardiac muscle during the cardiac cycle. Research was undertaken to perform the necessary simulation before the technique could be used for accurate quantification of heart movement [107, 109]. The increased usage of 3D data sets from MR and the need to combine them led to research to develop a mathematically robust method for 3D registration [110].

Familiarity with techniques for the extraction of quantitative information, such as texture from medical images, led to research into how, in effect, a reversal of the process could be used to create better psychophysical tests to access an individual's ability to view medical images [111]. The outcome of the evaluation of this method has just been accepted for publication.

Evidence Based Imaging

Over a decade before my first publication in evidence based imaging I had become concerned about issues associated with the assessment of health technologies [112], and I had become familiar with the debate around evidence based medicine. With the creation of CoMIR soon after my move to Leeds I ensured that there was a focus in the area of evidence based imaging, both in terms of primary research and also secondary research, ie the scientific evaluation of existing published material.

My emphasis on evidence based imaging was planned to coincide with changes in funding policy which offered the opportunity to focus staff and resources appropriately. Initial research highlighted, somewhat unexpectedly, the relatively poor quality of evidence in medical imaging research and the presence of bias in many studies [113]. It was clear that a simple focus on randomised controlled trials, as used in the Cochrane Collaboration, could not be applied to the evaluation of medical imaging research, and that we would need to undertake research into methodological issues.

For example it was necessary to develop a decision analytic model for the role of ultrasound in primary coronary stenting before a full review could be undertaken. In addition research had to be undertaken into the identification of studies for systematic reviews in medical imaging [114] and also how to undertake a review in a rapidly evolving field [116].

Extensive systematic reviews were undertaken in four areas of medical imaging: endoscopic ultrasound in gastro-oesophageal cancer [115] {118}; spiral and

electron beam computed tomography {119}; intravascular ultrasound-guided interventions in coronary artery disease {120}; and magnetic resonance angiography of carotid artery stenosis and peripheral vascular disease [117] {121}. These systematic reviews {118, 119, 120, 121} are large published monographs, each running to over 100 pages long, and their length precludes the inclusion of hard copies; instead copies have been included on a CD to be found on the back cover.

In 1998 I was President of the British Institute of Radiology and chose the subject of 'Evidence Based Imaging' for my Presidential Lecture giving me the opportunity to stimulate a wider debate in this area. However although I felt I had made significant progress in evidence based imaging I came to the conclusion that it was strategically appropriate to begin to withdraw from the field in the late 1990s for a number of reasons. Firstly it was difficult to continue our secondary research in medical imaging because the funding policy was to concentrate support in centres which specialised in systematic reviews, rather than specialist research centres such as CoMIR which also undertook systematic reviews; thus it was very difficult to recruit and retain the necessary expertise. Secondly we were unable to obtain and maintain the appropriate clinical support for good quality primary research.

Terahertz Imaging and Sensing

Throughout my career I had recognised the value of imaging for the localisation of quantitative measurements but I also recognised there were limitations about what could be measured utilising certain physical science techniques. In the late 1990s this led me to consider other parts of the electromagnetic spectrum where, perhaps, any signal variation could potentially be influenced more by cellular or molecular changes. As a consequence I developed an interest in the use of terahertz radiation [122] which could potentially act both as an imaging technique [123] and also a sensor in a localised region. I recognised that instead of using large volume images of a human subject to localise an abnormality and perform a relatively crude quantitative measurement, it may be possible to develop techniques that could be delivered using minimal invasive surgery techniques. Though these may only provide imaging information over a relatively small volume, they could produce much more valuable information about tissue at a highly localised point.

My research has been involved in understanding some of the science behind terahertz radiation and the subject is still in its early days of development. Research was undertaken to model the propagation of terahertz radiation through tissue [127, 129] and also catalogue the optical properties of tissue at terahertz frequencies [125, 132]. In developing an imaging technique we were surprised to identify gaps in data used to define safety criteria which could influence issues of safety in the terahertz region [126, 130]. As terahertz systems were developed to image tissue, we undertook research to determine how to evaluate image quality using test objects [124] and also the effect of frequency on image quality [131]. Multispectral clustering techniques were used for the extraction of quantitative information from the imaging data to classify histopathology [128].

Summary

The value and importance of the physical sciences for measurement of health and disease in-vivo has been demonstrated by my research. I recognise that I have been fortunate that my research has coincided with significant technological developments, opening up avenues of research that would have been unimaginable to my predecessors.

Working over a span of three decades I have contributed to fundamental and applied knowledge, changing my approach and methodology as opportunities present themselves, whilst retaining my focus on quantitative, non-invasive measurements in the human body.

Publications

Bone Measurement

1. Development of apparatus to measure calcium changes in the forearm and spine by neutron activation analysis using Cf-252 (*PhD)
    MA Smith and P Tothill
    Physics in Medicine and Biology 24, 319-329, 1979

2. Measurement of spinal calcium by in vivo neutron activation analysis in osteoporosis (*PhD)
    MA Smith, R Eastell, NSJ Kennedy, LG McIntosh, JD Simpson, JA Strong and P Tothill
    Clinical Physics and Physiological Measurement 2, 45-48, 1981

3. Long term effect of dialysate calcuim and 1α -OHD3 on bone calcium in haemodialysis patients as measured by neutron activation analysis of the forearm (*PhD)
    MA Smith, RJ Winney, JA Strong and P Tothill
    Nephron 28, 213-217, 1981

4. Total body neutron activation analysis of calcium: calibration and normalisation
    NSJ Kennedy, R Eastell, CM Ferrington, JD Simpson, MA Smith, JA Strong and P Tothill
    Physics in Medicine and Biology 27, 697-708, 1982

5. The crossover correction in dual photon absorptiometry with Gd-153
    MA Smith and P Tothill
    Physics in Medicine and Biology 27, 1515-1521, 1982

6. Bone demineralisation in patients with Turner's syndrome
    MA Smith, J Wilson and WH Price
    Journal of Medical Genetics 19, 100-103, 1982

7. Total body calcium in rheumatoid arthritis: effects of disease activity and corticosteroid treatment
    DM Reid, NSJ Kennedy, MA Smith, P Tothill and G Nuki
    British Medical Journal 285, 330-332 1982

8. Comparison between Gd-153 and Am-241, Cs-137 for dual photon absorptiometry of the spine
    MA Smith, D Sutton and P Tothill
    Physics in Medicine and Biology 28, 709-721, 1983

9. Intra-laboratory variations using dual photon absorptiometry
    MA Smith and P Tothill
    Physics in Medicine and Biology 28, 748-751, 1983

10. Dual photon absorptiometry of the spine with a low activity source of gadolinium 153
P Tothill, MA Smith and D Sutton
British Journal of Radiology 56, 829-835, 1983

11. Normal levels of total body sodium and chlorine by neutron activation analysis
NSJ Kennedy, R Eastell, P Tothill and MA Smith
Physics in Medicine and Biology 28, 215-222, 1983

12. The assessment of postmenopausal osteoporosis by total body neutron activation analysis
R Eastell, NSJ Kennedy, MA Smith, JD Simpson, JA Strong and P Tothill
Metabolic Bone Disease and Related Research 5, 65-67, 1983

13. Bone mass in nodal primary generalised osteoarthritis
DM Reid, NSJ Kennedy, MA Smith, P Tothill and G Nuki
Annals of the Rheumatic Diseases 43, 240-242, 1984

14. Changes in total body calcium after renal transplantation effect of low-dose steroid regime
R Eastell, NSJ Kennedy, MA Smith, P Tothill and JL Anderton
Nephron 40, 139-142, 1985

15. The seasonal variation of total body calcium
P Tothill, NSJ Kennedy, JJ Nicoll, MA Smith, DM Reid and G Nuki
Clinical Physics and Physiological Measurement 7, 361-367, 1986

16. Bone mass in ankylosing spondylitis
DM Reid, JJ Nicoll, NSJ Kennedy, MA Smith, P Tothill and G Nuki
Journal of Rheumatology 13, 932-935, 1986

17. Corticosteroids and bone mass in asthma: comparisons with rheumatoid arthritis and polymyalgia rheumatica
DM Reid, JJ Nicoll, MA Smith, B Higgins, P Tothill and G Nuki
British Medical Journal 293, 1463-1466, 1986

18. Total and peripheral bone mass in patients with psoriatic arthritis and rheumatoid arthritis
DM Reid, NSJ Kennedy, JJ Nicoll, MA Smith, P Tothill and G Nuki
Clinical Rheumatology 5, No 3, 372-278, 1986

19. Changes in total body calcium following surgery for primary hyperparathyroidism
R Eastell, NSJ Kennedy, MA Smith, P Tothill and CRW Edwards
Bone 7, 269-272 1986

20. Bone loss in rheumatoid arthritis and primary generalized osteoarthrosis: effects of corticosteroids, suppressive antirheumatic drugs drugs and calcium supplements
DM Reid, NSJ Kennedy, MA Smith, JJ Nicoll, N Brown, P Tothill and G Nuki
British Journal of Rheumatology 25, 253-259, 1986

21. Measurement of hand bone mineral content using single-photon absorptiometry
JJ Nicoll, MA Smith, DM Reid, E Law, N Brown, P Tothill and G Nuki
Physics in Medicine and Biology 32, 697-706, 1987

22. In-vivo precision of total body calcium and sodium measurements by neutron activation analysis
JJ Nicoll, P Tothill, MA Smith, DM Reid, NSJ Kennedy and G Nuki
Physics in Medicine and Biology 32, 243-246, 1987

23. Prediction of fracture healing in the tibia by quantitative radionuclide imaging
MA Smith, E Jones, R Strachan, P Tothill, JJK Best and SPF Hughes
Journal of Bone and Joint Surgery 69-B, 441-448, 1987

24. Premenopausal bone loss in the lumbar spine and neck of femur: a study of 225 Caucasian women
A Rodin, B Murby, MA Smith, M Caleffi, I Fentiman, MG Chapman and I Fogelman
Bone 11, 1-5, 1990

25. Bone ultrasound attenuation in women: reproducibility, normal variation and comparison woth photon absorptiometry
JG Truscott, M Simpson, SP Stewart, R Milner, CF Westmacott, B Oldroyd, JA Evans, A Horsman, CM Langton and MA Smith
Clinical Physics and Physiological Measurement 13, 29-36, 1992

26. The use of a radiation sensitive CCD camera system to measure bone mineral content in the neonatal forearm: a feasibility study
JG Truscott, R Milner, S Metcalfe and MA Smith
Physics in Medicine and Biology 37, 1391-1397, 1992

27. Primary Generalised Osteoarthritis and Bone Mass
LD Hordon, SP Stewart, PR Troughton, V Wright, A Horsman and MA Smith
British Journal of Rheumatology 32, 1059-1061, 1993

28. Variation in lumbar spine and femoral neck bone mineral measured by dual energy X-ray absorption: a study of 329 normal women
JG Truscott, B Oldroyd, M Simpson, SP Stewart, CF Westmacott, R Milner, A Horsman and MA Smith
British Journal of Radiology 66, 514-521, 1993

29. A phantom for quantitative ultrasound of trabecular bone
    AJ Clarke, JA Evans, JG Truscott, R Milner and MA Smith
    Physics in Medicine and Biology 39, 1677-1687, 1994

30. Comparison of changes in bone mineral in idiopathic and secondary
    osteoporosis following therapy with cyclical disodium etidronate and high
    dose calcium supplementation
    SM Orme, M Simpson, SP Stewart, B Oldroyd, CF Westmacott, MA Smith
    and PE Belchetz
    Clinical Endocrinology 41(2), 245-50, 1994

31. A portable system for measuring bone mineral density in the pre-term
    neonatal forearm
    JG Truscott, R Milner, PC Holland, C Wood and MA Smith
    British Journal of Radiology 69, 532-8, 1996

32. Assessment of renal osteodystrophy in dialysis patients: use of bone alkaline
    phosphatase, bone mineral density and parathyroid ultrasound in comparison
    with bone histology
    S Fletcher, RG Jones, HC Rayner, P Harnden, LD Hordon, JE Aaron, B
    Oldroyd, AM Brownjohn, JH Turney and MA Smith
    Nephron 75(4), 412-9, 1997

33. Regional bone mineral density after orthotopic liver transplantation
    SH Hussaini, B Oldroyd, SP Stewart, F Roman, MA Smith, S Pollard, P
    Lodge, JG O'Grady and MS Losowsky
    European Journal of Gastroenterology Hepatology 11(2), 157-63, 1999

Patents (copies not included)

34. Material to mimic bone and its interaction with ultrasound
    J Clarke, JA Evans, R Milner and MA Smith
    1994

35. Anthropomorphic spinal phantom
    R Milner, E Berry and MA Smith
    1999

Statistics

36. The comparison of neutron activation analysis and photon absorptiometry at the same part body site
MA Smith, RA Elton and P Tothill
Clinical Physics and Physiological Measurement 2, 1-7, 1981

37. Survival after peptic ulcer surgery
AH McLean Ross, J Anderson, WP Small and MA Smith
British Medical Journal 282, 1472, 1981

38. Late mortality after surgery for peptic ulcer
AH McLean Ross, MA Smith, JR Anderson and WP Small
New England Journal of Medicine 307, 519-522, 1982

39. Survival after surgery
WP Small, MA Smith and AH MacLean-Ross
British Medical Journal 289, 108-109, 1984

40. Metabolism of sodium pentosan polysulphate in man-catabolism of iodinated derivatives
IR MacGregor, J Davies, L Paton, DS Pepper, CV Prowse and MA Smith
Thrombosis and Haemostasis 51, 321-325, 1984

41. Correction factors for gravimetric measurement of peritumoural oedema in man
BA Bell, MA Smith, JL Tocher and JD Miller
British Journal of Neurosurgery 1, 435-440, 1987

42. Inter-individual differences in the pituitary-thyroid axis influence the interpretation of thyroid function tests
CA Meier, MN Maisey, A Lowry, J Muller and MA Smith
Clinical Endocrinology 39, 101-107, 1993

Magnetic Resonance Imaging

43. The installation of a commercial resistive NMR imager
MA Smith, JJK Best, RHB Douglas and DM Kean
British Journal of Radiology 57, 1145-1158, 1984

44. Brain water in chronic alcoholic patients measured by magnetic resonance imaging
MA Smith, J Chick, DM Kean, RHB Douglas, A Singer, RE Kendell and JJK Best
Lancet i, 1273-1274, 1985

45. Nuclear magnetic resonance imaging in hypertrophic cardiomyopathy
M Been, DM Kean, MA Smith, RHB Douglas, JJK Best, and AL Muir
British Heart Journal 54, 48-52, 1985

46. Two examples of CNS lipomas demonstrated by CT and low field MRI
DM Kean, MA Smith, RHB Douglas, CN Martyn and JJK Best
Journal of Computer Assisted Tomography 9(3), 494-496, 1985

47. Characterisation of acute myocardial infarction by gated magnetic resonance imaging
M Been, MA Smith, JP Ridgway, JWE Brydon, RHB Douglas, DM Kean, JJK Best and AL Muir
Lancet ii, 348-350, 1985

48. Brain water measured in volunteers after alcohol and vasopressin
AJ Mander, MA Smith, DM Kean, J Chick, RHB Douglas, AU Rehman, GJ Weppner and JJK Best
Lancet, ii, 1075, 1985

49. ECG gated T1 images of the heart
MA Smith, JP Ridgway, JWE Brydon, M Been, RHB Douglas, DM Kean, JJK Best and AL Muir
Physics in Medicine and Biology 31, 771-778, 1986

50. The absence of tissue specificity in MRI using in-vivo T1 or T2 determination - true biological variation or technical artefact?
MA Smith and DG Taylor
British Journal of Radiology 59, 82-83, 1986

51. A description of a low field resistive magnetic resonance imaging system and its application in imaging midline central nervous system pathology
DM Kean, MA Smith, RHB Douglas and JJK Best
Clinical Radiology, 37, 211-217, 1986

52. A technique for velocity imaging using magnetic resonance imaging
JP Ridgway and MA Smith
British Journal of Radiology 59, 603-607, 1986

53. Correlation of human NMR T1 values measured in vivo and brain water content
HL MacDonald, BA Bell, MA Smith, DM Kean, JL Tocher, RHB Douglas, JD Miller and JJK Best
British Journal of Radiology 59, 355-357, 1986

54. A surface coil design for a vertical field MRI system and its application in imaging the breast
MA Smith and DW Pye
Magnetic Resonance Imaging 4, 455-560 1986

55. Cardiac gating in nuclear magnetic resonance imaging
MA Smith
Journal of Medical Engineering and Technology 10(6), 325-328, 1986

56. Brain water measured by magnetic resonance imaging: correlation with direct estimation and changes after mannitol and dexamethasone
BA Bell, MA Smith, DM Kean, CNJ McGhee, HL MacDonald, JD Miller, GH Barnett, JL Tocher, RHB Douglas, JJK Best
The Lancet (i), 66-69, 1987

57. Demonstration of pulsatile cerebrospinal-fluid using magnetic resonance phase imaging
JP Ridgway, LW Turnbull and MA Smith
British Journal of Radiology 60, 423-427, 1987

58. Magnetic resonance flow imaging: a possible method for distinguishing communicating syringomyelia from cystic intraspinal lesions
LW Turnbull, JP Ridgway, MA Smith and JJK Best
British Journal of Radiology 60, 517-518, 1987

59. Cerebral and brain stem changes after ECT revealed by nuclear magnetic resonance imaging
AJ Mander, A Whitfield, DM Kean, MA Smith, RHB Douglas and RE Kendell
British Journal of Psychiatry 151, 69-71, 1987

60. Serial changes in the T1 magnetic relaxation parameter after myocardial infarction in man
M Been, MA Smith, JP Ridgway, RHB Douglas, DP De Bono, JJK Best and AL Muir
British Heart Journal 59, 1-8, 1988

61. Myocardial involvement in systemic lupus erythematosus detected by magnetic resonance imaging
M Been, BJ Thompson, MA Smith, JP Ridgway, RHB Douglas, JJK Best and AL Muir
European Heart Journal 9 1250-1256, 1988

62. Brain hydration during alcohol withdrawal in alcoholics measured by magnetic resonance imaging
MA Smith, JD Chick, HM Engelman, DM Kean, AJ Mander, RHB Douglas and JJK Best
Drug and Alcohol Dependence 21, 25, 1988

63. Magnetic resonance spectroscopy in-vivo
DA Porter, MA Smith
Journal of Biomedical Engineering 10, 562-567, 1988

64. Blood flow imaging by magnetic resonance
DJ West, M Tarnawski, MJ Graves, MG Taylor, S Padayachee, VT Ayton and MA Smith
Medicamundi 33, 101-111, 1988

65. Magnetic resonance imaging of the infant heart at 15T
MA Smith, EJ Baker, VT Ayton, JM Parsons, EJ Ladusans and MN Maisey
British Journal of Radiology 62, 367-370, 1989

66. High field strength magnetic resonance imaging of ventricular septal defects in infants
EJ Baker, VT Ayton, MA Smith, JM Parsons, EJ Ladusans, RH Anderson, M Tynan and NLK Fagg
British Heart Journal 62, 305-310, 1989

67. Magnetic resonance imaging of coarctation of the aorta in infants: use of high field strength
EJ Baker, VT Ayton, MA Smith, JM Parsons, EJ Ladusans, RH Anderson, M Tynan, AK Yates and PB Deverall
British Heart Journal 62, 97-101, 1989

68. Magnetic resonance imaging of the brain in alcoholics: cerebral atrophy, lifetime alcohol consumption and cognitive defects
JD Chick, MA Smith, HM Engleman, DM Kean, AJ Mander, RHB Douglas and JJK Best
Alcoholism: Clinical and Experimental Research 13, 512-517, 1989

69. Phospholipids are visible in P-31 NMR spectra of human breast tumours
M Lowry, DA Porter, CJJ Twelves, PE Heasley, PB Garlick, MA Smith, RD Rubens, MN Maisey and MA Richards
Biochemical Society Transactions 17, 1053-1054, 1989

70. The measurement and visualisation of vessel blood flow by magnetic resonance imaging
MA Smith
Clinical Physics and Physiological Measurement 11, 2, 101-123, 1990

71. A method for characterising localisation techniques in volume selected nuclear magnetic resonance spectroscopy
SF Keevil, DA Porter and MA Smith
Physics in Medicine and Biology 35(7), 821-834, 1990

72. The measurement of time-averaged flow by magnetic resonance imaging using continuous acquisition in the carotid arteries and its comparison with Doppler ultrasound
M Tarnawski, S Padayachee, DJ West, MJ Graves, V Ayton, MG Taylor and MA Smith
Clinical Physics and Physiological Measurement 11(1), 27-36, 1990

73. Measurement of time-averaged flow in the middle cerebral artery by magnetic resonance imaging
M Tarnawski, S Padayachee, MJ Graves, V Ayton, MG Taylor and MA Smith
British Journal of Radiology 64, 178-181, 1991

74. Visibility of phosholopids in ^{31}P NMR spectra of human breast tumours in-vivo
M Lowry, DA Porter, CJ Twelves, PE Heasley, MA Smith and MA Richards
NMR in Biomedicine 5, 37-42, 1992

75. Experimental characterisation of the ISIS Technique for volume selected NMR spectroscopy
SF Keevil, DA Porter and MA Smith
NMR in Biomedicine 5, 200-208, 1992

76. Rapid dynamic contrast-enhanced magnetic resonance imaging of the liver and portal vein
J Ward, D Martinez, AG Chalmers, J Ridgway, P Robinson and MA Smith
British Journal of Radiology 66, 214-222, 1993

77. Phosphorus-31 metabolism of human breast - an in-vivo magnetic resonance spectroscopy study at 1.5T
CJ Twelves, M Lowry, DA Porter, NA Dobbs, PE Graves, MA Smith and MA Richards
British Journal of Radiology 67, 36-45, 1994

78. Phosphorus-31 metabolism of post-menopausal breast cancer studied in vivo by magnetic resonance
CJ Twelves, DA Porter, M Lowry, NA Dobbs, PE Graves, MA Smith, Rubens RD and MA Richards
British Journal of Cancer 69(6), 1151-6, 1994

79. Stepping-table gadolinium-enhanced digital subtraction MR angiography of the aorta and lower extremity arteries: preliminary experience
JF Meaney, JP Ridgway, S Chakraverty, I Robertson, D Kessel, A Radjenovic, M Kouwenhoven, A Kassner and MA Smith
Radiology 211(1), 59-67, 1999

80. Quantitative comparison of intrabrain diffusion in adults and preterm and term neonates and infants
SF Tanner, LA Ramenghi, JP Ridgway, E Berry, MA Saysell, D Martinez, RJ Arthur, MA Smith and MI Levene
American Journal of Roentgenology 174(6), 1643-9, 2000

81. A systematic review of the precision and accuracy of dose measurements in photon radiotherapy using polymer and Fricke MRI gel dosimetry
ND MacDougall, WG Pitchford and MA Smith
Physics in Medicine and Biology 47, 107-121, 2002
Response to comments:
Physics in Medicine and Biology 48, L19 - 22, 2003

82. Cerebral perfusion in infants and neonates: preliminary results obtained using dynamic susceptibility contrast enhanced MRI
SF Tanner, LG Cornette, LA Ramenghi, LS Miall, JP Ridgway, MA Smith and MI Levene
Archives for Disease in Childhood 88(6), F525-530, 2003

83. Evaluation of the dosimetric performance of BANG3 polymer gels
ND MacDougall, ME Miquel, DJ Wilson, SF Keevil and MA Smith
Physics in Medicine and Biology 50, 1717 – 1726, 2005

84. T1 measurement using a short acquisition period for quantitative cardiac applications
DM Higgins, JP Ridgway, A Radjenovic, UM Sivananthan, and MA Smith
Medical Physics 32, 1738-1746, 2005

85. A method for pharmacokinetic modeling of dynamic contrast enhanced MRI studies of rapidly enhancing lesions acquired in a clinical setting
A Radjenovic, JP Ridgway and MA Smith
Physics in Medicine and Biology 51, N187-N197, 2006

Patents (copies not included)

86. Surface coils for magnetic resonance imaging
MA Smith 1986

87. Sympathetic resonance in magnetic resonance imaging
MA Smith 1986

Body Composition Measurement

88. Apparatus for the measurement of total body nitrogen using prompt neutron activation analysis with Californium-252
A Mackie, WJ Hannan, MA Smith and P Tothill
Journal of Medical Engineering and Technology 12, 152-159, 1988

89. A feasibility study for the simultaneous measurement of carbon, hydrogen and oxygen using pulsed 14.4MeV neutrons
JF Sutcliffe, AJ Waker, AH Smith, MCJ Barker and MA Smith
Physics in Medicine and Biology 36, 87-98, 1991

90. Inelastic scattering of pulsed 14.4 MeV neutrons as a function of depth in tissue and the half-life for radiative capture
JF Sutcliffe, AH Smith, AJ Waker, MCJ Barker and MA Smith
Physics in Medicine and Biology 36, 643-648, 1991

91. Can glycogen be measured by in-vivo neutron activation analysis?
JF Sutcliffe, AH Smith, RFGJ King and MA Smith
Physics in Medicine and Biology 37, 475-479, 1992

92. Comparison of measure of body composition in a trial of low dose growth hormone replacement therapy
SM Orme, JP Sebastian, B Oldroyd, SP Stewart, PJ Grant, MH Strickland, MA Smith and PE Belchetz
Clinical Endocrinology 37, 453-459, 1992

93. A theoretical analysis using ratios of the major elements measured by neutron activation analysis to derive total body water, protein and fat
JF Sutcliffe, AH Smith, MJC Barker and MA Smith
Medical Physics 20(4), 1129-34, 1993

94. Estimation of body composition from bioelectrical impedance of body segments: comparison with dual-energy X-ray absorptiometry
S Stewart, PN Bramley, R Heighton, JH Green, A Horsman, MS Losowsky and MA Smith
British Journal of Nutrition 69(3), 645-55, 1993

95. An investigation of an electromagnetic method for the measurement of body composition
JF Sutcliffe, SW Smye and MA Smith
Physics in Medicine and Biology 39, 1501-1507, 1994

96. A further assessment of an electromagnetic method to measure body composition
JF Sutcliffe, SW Smye and MA Smith
Physics in Medicine and Biology 40(4),659-70, 1995

97. Measurement of total body water and urea kinetic modelling in peritoneal dialysis
G Woodrow, B Oldroyd, JH Turney, PS Davies, JM Day and MA Smith
Clinical Nephrology 47(1), 52-57, 1997

98. Measurement of total body water by bioelectrical impedance in chronic renal failure
G Woodrow, B Oldroyd, JH Turney, PS Davies, JM Day and MA Smith
European Journal of Clinical Nutrition 50(10), 676-81, 1996

99. Four-component model of body composition in chronic renal failure comprising dual-energy X-ray absorptiometry and measurement of total body water by deuterium oxide dilution
G Woodrow, B Oldroyd, JH Turney, PS Davies, JM Day and MA Smith
Clinical Science 91(6), 763-9, 1996

100. Whole body and regional body composition in patients with chronic renal failure
G Woodrow, B Oldroyd, JH Turney, L Tompkins, AM Brownjohn and MA Smith
Nephrology Dialysis and Transplantation 11(8), 1613-8, 1996

101. Measurement of body composition in chronic renal failure: comparison of skinfold anthropometry and bioelectrical impedance with dual energy X-ray absorptiometry
G Woodrow, B Oldroyd, MA Smith and JH Turney,
European Journal of Clinical Nutrition 50(5), 295-301, 1996

102. Influence of changes in peritoneal fluid on body-composition measurements by dual-energy X-ray absorptiometry in patients receiving continuous ambulatory peritoneal dialysis
G Woodrow, B Oldroyd, JH Turney and MA Smith
American Journal of Clinical Nutrition 64(2), 237-41, 1996

103. Measurement of total body water and urea kinetic modelling in peritoneal dialysis
G Woodrow, B Oldroyd, JH Turney, PS Davies, JM Day and MA Smith
Clinical Nephrology 47(1), 52-7, 1997

104. Effects of orthotopic liver transplantation on body composition
SH Hussaini, B Oldroyd, SP Stewart, S Soo, F Roman, MA Smith, S Pollard, P Lodge, JG O'Grady and MS Losowsky
Liver 18(3), 173-9, 1998

105. Comparison of anthropometric equations for estimation of total body water in peritoneal dialysis patients
G Woodrow, B Oldroyd, A Wright, WA Coward, JG Truscott, JH Turney, AM Brownjohn and MA Smith
Nephrology Dialysis and Transplantation 18, 384-389, 2003

Image Analysis

106. Spatial distribution of femoral bone mineral in dual energy X-ray absorptiometry images: a possible technique to improve discrimination between normal and osteoporotic patients
E Berry, JG Truscott, SP Stewart and MA Smith
British Journal of Radiology 69(824), 743-50, 1996

107. Simulation of two-dimensional tagged MRI
WR Crum, E Berry, JP Ridgway, UM Sivananthan, LB Tan and MA Smith
Journal of Magnetic Resonance Imaging 7(2), 416-24, 1997

108. Preliminary experience with medical applications of rapid prototyping by selective laser sintering
E Berry, JM Brown, M Connell, CM Craven, ND Efford, A Radjenovic and MA Smith
Medical Engineering and Physics 19(1), 90-6, 1997

109. Frequency-domain simulation of MR tagging
WR Crum, E Berry, JP Ridgway, UM Sivananthan, LB Tan and MA Smith
Journal of Magnetic Resonance Imaging 8(5), 1040-50, 1998

110. Robust point correspondence applied to two and three dimensional image registration
E Guest, E Berry, RA Baldock, M Fidrich and MA Smith
IEEE Transactions on Pattern Analysis and Machine Intelligence 23, 165-79, 2001

111. Synthesis of texture from clinical images
DS Brettle, E Berry and MA Smith
Image and Vision Computing 21, 433-445, 2003

Evidence Based Medicine

112. Health technology assessment and the NHS R&D initiative
     MA Smith
     Journal of Medical Engineering and Technology 20(6), 192-5, 1996

113. The identification of bias in studies of the diagnostic performance of imaging modalities
     S Kelly, E Berry, P Roderick, KM Harris, J Cullingworth, L Gathercole, J Hutton and MA Smith
     British Journal of Radiology 70(838):1028-35, 1997

114. Identifying studies for systematic reviews: an example from medical imaging
     E Berry, S Kelly, J Hutton, KM Harris and MA Smith
     International Journal of Technology Assessment in Health Care 16(2), 668-72, 2000

115. A systematic review of the staging performance of endoscopic ultrasound in gastro-oesophageal carcinoma
     S Kelly, KM Harris, E Berry, J Hutton, P Roderick, J Cullingworth, L Gathercole, and MA Smith
     Gut 49 (4), 534 -530, 2001

116. How to undertake a clinically relevant systematic review in a rapidly evolving field
     ME Westwood, S Kelly, E Berry, JM Bamford, MJ Gough, CM Airey, LM Davies, JFM Meaney, J Cullingworth and MA Smith
     International Journal of Technology Assessment in Health Care 18(1), 24-32, 2002

117. Use of magnetic resonance angiography to select candidates with recently symptomatic carotid stenosis for surgery: systematic review
     ME Westwood, S Kelly, E Berry, JM Bamford, MJ Gough, CM Airey, , JFM Meaney, LM Davies J Cullingworth and MA Smith
     British Medical Journal 324(7331), 198-201, 2002

Substantial monographs (copies included on CD at the back of the thesis)

118. Systematic Review of endoscopic ultrasound in gastro-oesophageal cancer
     KM Harris, S Kelly, E Berry, J Hutton, J Cullingworth, L Gathercole, PJ O'Connor, JC Boyce and MA Smith
     Health Technology Assessment 2 (18), 1-134, 1998

119. A systematic literature review of spiral and electron beam computed tomography: with particular reference to clinical applications in hepatic lesions, pulmonary embolus and coronary artery disease
E Berry, S Kelly, J Hutton, KM Harris, P Roderick, JC Boyce, J Cullingworth, L Gathercole, PJ O'Connor, and MA Smith
Health Technology Assessment 3(18), 1-118, 1999

120. Intravascular ultrasound-guided interventions in coronary artery disease: a systematic literature review, with decision analytic modelling, of outcomes and cost-effectiveness
E Berry, S Kelly, J Hutton, HSJ Lindsay, JM Blaxill, JA Evans, J Connelly, J Tisch, GC Walker, UM Sivananthan and MA Smith
Health Technology Assessment 4(35), 1-108, 2000

121. The cost effectiveness of magnetic resonance angiography: carotid artery stenosis and peripheral vascular disease
E Berry, S Kelly, ME Westwood, LM Davies, MJ Gough, JM Bamford, JFM Meaney, CM Airey, J Cullingworth, M Barbieri, A Jackson and MA Smith
Health Technology Assessment 6(7), 1-155, 2002

Terahertz Imaging and Sensing

122. Terahertz Imaging
JM Chamberlain and MA Smith
Physics in Medicine and Biology 47, 2002

123. An introduction to medical imaging with coherent terahertz frequency radiation
AJ Fitzgerald, E Berry, NN Zinovev, GC Walker, MA Smith and JM Chamberlain
Physics in Medicine and Biology 47, 67-84, 2002

124. Evaluation of image quality in terahertz pulsed imaging using test objects
AJ Fitzgerald, E Berry, RE Miles, NN Zinovev, MA Smith and JM Chamberlain
Physics in Medicine and Biology 47, 3865-3873, 2002

125. Catalogue of human tissue optical properties at terahertz frequencies
AJ Fitzgerald, E Berry, NN Zinov'ev, S Homer-Vanniasinkam, RE Miles, JM Chamberlain and MA Smith
Journal of Biological Physics 129, 123-128, 2003

126. Do in vivo terahertz imaging systems comply with safety guidelines?
E Berry, GC Walker, AJ Fitzgerald, NN Zinov'ev, JM Chamberlain, SW Smye, RE Miles and MA Smith
Journal of Laser Applications 15(3), 192-198, 2003

127. Two methods for modelling the propagation of terahertz radiation in a layered structure
GC Walker, E Berry, SW Smye, NN Zinov'ev, AJ Fitzgerald, RE Miles, JM Chamberlain and MA Smith
Journal of Biological Physics 129, 141-148, 2003

128. Multispectral classification techniques for terahertz pulsed imaging: an example in histopathology
E Berry, JW Handley, AJ Fitzgerald, WJ Merchant, RD Boyle, NN Zinov'ev, RE Miles, JM Chamberlain and MA Smith
Medical Engineering and Physics 26, 423 - 430, 2004

129. Modelling the propagation of terahertz radiation through a tissue simulating phantom
GC Walker, E Berry, SW Smye, NN Zinov'ev, AJ Fitzgerald, RE Miles, JM Chamberlain and MA Smith
Physics in Medicine and Biology 49, 1853-1864, 2004

130. Terahertz Imaging and International Safety Guidelines
GC Walker, E Berry, NN Zinov'ev, AJ Fitzgerald, RE Miles, JM Chamberlain
and MA Smith
Medical Imaging 2002: Physics of Medical Imaging. Proceedings of SPIE
4682, 683-690, 2002

131. Effects of frequency on image quality in terahertz pulsed images
AJ Fitzgerald, E Dzontoh, T Loeffler, K Siebert, E Berry, NN Zinovev, RE
Miles, MA Smith and JM Chamberlain
Medical Imaging 2002: Physics of Medical Imaging. Proceedings of SPIE
4682, 107-116, 2002

132. Optical properties of tissue measured using terahertz pulsed imaging
E Berry, AJ Fitzgerald, NN Zinov'ev, GC Walker, S Homer-Vanniasinkam, CD
Sudworth, RE Miles, JM Chamberlain and MA Smith
Medical Imaging 2003: Physics of Medical Imaging. Proceedings of SPIE
5030, 459-470, 2003

133. Two methods for modeling the propagation of terahertz radiation in a layered
structure
GC Walker, E Berry, SW Smye, NN Zinov'ev, AJ Fitzgerald, RE Miles, JM
Chamberlain and MA Smith
Medical Imaging 2003: Physics of Medical Imaging. Proceedings of SPIE
5030: 647-655, 2003

Development of Apparatus to Measure Calcium Changes in the Forearm and Spine by Neutron Activation Analysis using Californium-252

M. A. SMITH, PH.D., and P. TOTHILL, PH.D., F.INST.P.

Department of Medical Physics and Medical Engineering,
Western General Hospital, Crewe Road, Edinburgh, EH4 2XU, U.K.

ABSTRACT. Techniques were developed to measure small changes of calcium in the forearm and spine *in vivo* by neutron activation analysis using two sources of ^{252}Cf in a hospital environment. Using purpose-built part-body counters and bilateral irradiation with 7·5 cm premoderation between the sources and the bone, peripheral bone was measured with a total source strength eventually as low as 50 mCi. Two methods of spectral analysis were used and compared. Patient studies of the forearm were successfully undertaken, with a precision of 2·6% which included patient movement, and an annual bone dose of less than 10 rem and skin dose of 35 rem from six measurements.

Two 100 mCi sources were used for measurements of the lumbar spine. Care was taken to minimise the problems of non-uniformity of activation which are present using unilateral irradiation. Emphasis was placed on measuring the bodies of the vertebrae with adequate sensitivity and uniformity, and the spinous processes and arches with low sensitivity. A whole body counter was used for the bilateral detection of the induced activity. The precision of the method was 3·0% with an annual peak bone dose of 2·1 rem and skin dose of 18 rem from three measurements.

I. Introduction

Since the first measurements *in vivo* on human volunteers by neutron activation analysis (Anderson, Osborn, Tomlinson, Newton, Rundo, Salmon and Smith 1964) the field has expanded to include both whole-body and part-body measurements of a range of body elements. The element that is of most clinical interest is calcium, and apparatus for measuring part-body calcium changes can be constructed relatively cheaply for use in a hospital environment.

Most part-body calcium measurements on patients have been performed on peripheral bone, and although large neutron sources have been used (Comar, Riviere, Raynaud and Kellershohn 1968), most studies have been performed with compact radionuclide neutron sources using the ^{48}Ca (n, γ) ^{49}Ca reaction. Measurements of the hand have been carried out using a single 25 Ci Am–Be source (Catto, McIntosh and MacLeod 1973), a single 75 mCi ^{252}Cf source (Guey, Leitienne, Zech and Traegar 1978) and a combination of two 100 mCi ^{252}Cf and four 10 Ci Pu–Be sources (Maziere and Comar 1976). No activation measurements have been performed on the forearm, the site which is used for bone mineral determination by photon absorptiometry (Cameron and Sorenson 1967). In order to make a direct comparison with absorptiometry and because

the long bones of the forearm could be easily immobilised during any measurements, the forearm was chosen as the site for our investigations of peripheral bone loss.

Although a method of utilising twelve 5 Ci Pu–Be sources has been used for calcium measurements of the trunk (McNeill, Thomas, Sturtridge and Harrison 1973), part-body measurements of the spine alone have only been performed using a cyclotron (Al-Hiti, Thomas, Al-Tikrity, Ettinger, Fremlin and Dabek 1976). We have developed apparatus which could be used in a hospital to measure the calcium changes in the lumbar spine using ^{252}Cf sources.

2. Neutron sources

Two ^{252}Cf sources were obtained for activation analysis. They had previously been housed for three years at the Scottish Universities Research and Reactor Centre where some physical evaluation had taken place (Boddy, Robertson and Glaros 1974) and a pneumatic delivery system developed (Glaros 1975), before being moved to Edinburgh. Although the ideal source strength for patient measurements has been stated as 200 mCi (Boddy *et al.* 1974) or between 500 mCi and 1500 mCi (Evans, Le Blanc and Johnson 1976), the total combined source strength that was available for patient measurements over a $2\frac{1}{2}$ year period was eventually as low as 50 mCi. At this point the sources were replaced by two 104 mCi sources, mainly for the purpose of spine measurements.

An activation chamber was constructed inside a room by building an L-shaped baffle of concrete blocks and wax. An access 0·75 m wide allowed entry into the 2·5 m × 1·4 m irradiation chamber where the sources were stored 3 m below ground.

3. Forearm measurements

3.1. *Activation*

Two designs of apparatus were used for activation measurements of the forearm, both using a bilateral irradiation geometry. The sources and limb were surrounded by a hydrogenous material, which acted as a neutron 'reflector', to increase the thermal flux through the bone.

The premoderator thickness was chosen not to give the maximum thermal flux, which occurs at a depth of approximately 1·5 cm, but to give the minimum absorbed radiation dose for a given induced activity. Combining data from the variations in dose and thermal flux with thickness of premoderator and activation measurements of a cadaver limb, it was possible to calculate the dose per fixed count for a range of premoderator thicknesses (fig. 1). The shape of the curve is a function of the activity of the source when patient measurements are made of radionuclides with short half-lives.

The first forearm irradiation geometry (A), 19·75 cm source separation, 6 cm Perspex premoderator and wax blocks above and below the limb has been previously described (Smith and MacPherson 1977, Smith, Tothill, Simpson, MacPherson, Merrick, Strong and Boddy 1978). This was improved upon and

the second irradiation geometry (B) consisted of the two sources inside cylindrical wax reflectors each side of a water bath into which the patient's arm was fixed at an angle of 45° (fig. 2). The dimensions of the tank were
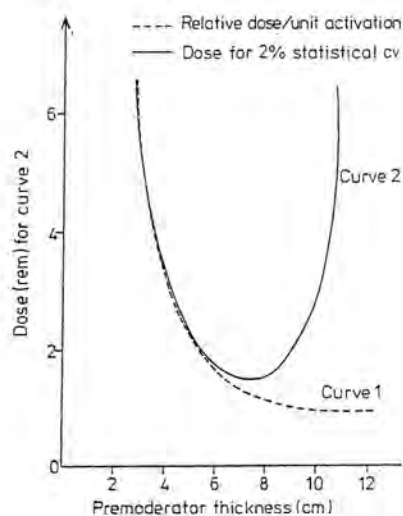

Fig. 1. Curve 1 shows the relative dose per unit activation for radionuclides with a long half-life. For induced radionuclides with a half-life comparable with the irradiation time, long irradiation times are not rewarding. Curve 2 shows the dose in rem required to obtain a statistical coefficient of variation of 2% when activating ^{48}Ca with a total ^{252}Cf activity of about 55 mCi.
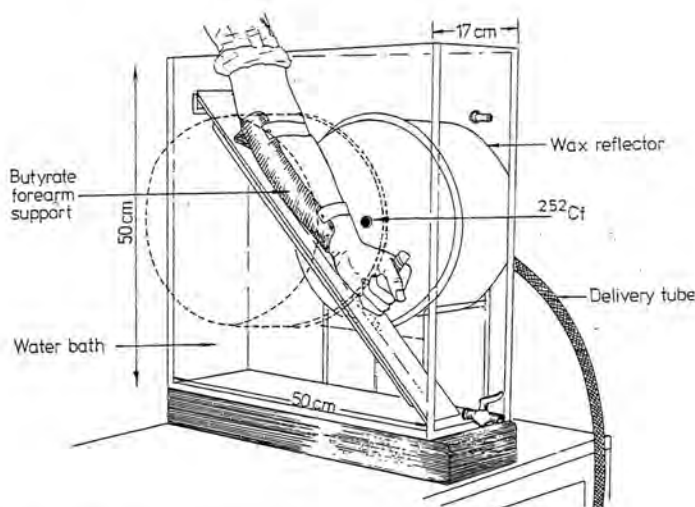
Fig. 2. Forearm irradiation geometry (B) incorporating a water bath to act as combined premoderator and reflector. The dotted lines indicate the position of the second wax reflector.

50 cm × 45 cm × 17 cm so that the water acted as a premoderator, giving a total of about 7·5 cm premoderation between source and bone, as well as a reflector. With the water bath the sensitivity of activation over a 25 cm length was found to be improved by a factor of 1·8 compared with the first irradiation geometry. Part of this improvement, about 30%, was due to the smaller source separation, but the major increase in sensitivity was due to the elimination of air gaps around the forearm. The latter also reduced the variation in calcium counts from patient to patient due to overlying soft tissue, increasing the possibility of absolute measurements.

During the 10 min activation period the patient gripped a Perspex rod and the forearm was restrained in a mould constructed from butyrate sheet. The variation in thermal fluence across the central 5 cm was ±4·2% and the full width at half maximum (FWHM) of the variation along the arm was 16·2 cm, measured using 1 cm diameter 0·0025 cm thick gold foils.

Dose measurements were performed in a phantom using gas flow ionisation chambers and a GM counter (Law, Lawson and Porter 1974). During a 10 min irradiation with a total source strength of 65 mCi the subject received a neutron dose of 0·68 rad and a gamma ray dose of 0·59 rad to the skin surface and a neutron dose of 0·20 rad and a gamma ray dose of 0·26 rad to the bone. Combining the variation of RBE with energy and the calculated neutron spectrum, a mean quality factor (QF) of 7·8 was obtained for the neutrons after 6 cm premoderation. The dose equivalent to the skin surface was therefore 5·8 rem and 1·8 rem to the bone. The gonad dose was less than 14 mrem taking the value QF = 10. For patient studies the irradiation time was kept constant so the maximum annual dose to the patient from six measurements was less than 10 rem to the bone or 4·5 rem averaged over the forearm.

3.2. *Detection*

A part-body counter (fig. 3) was built for the detection of induced activity in peripheral bones and the thyroid. Two 15 cm × 10 cm NaI detectors were encased in 5·0 cm thick lead and could be used in a bilateral geometry with or without a large central shield which could surround a limb such as the forearm. When used with the central shield there was a thickness of at least 7·5 cm of lead in all directions around the crystal except in the direction of the limb entrances of the central shield. All three sections could be moved around a large steel table 0·84 m above the floor. The background in the calcium region, 2·9 MeV to 3·3 MeV, with a 9 cm separation between the detectors in the central shield was 0·09 CPS and with a 12 cm separation without the central shield was 0·13 CPS. The variation in sensitivity at 2·75 MeV in the central 5 cm between the detectors for these separations was ±6% and ±5·8% respectively. The FWHM for the variation in detection sensitivity along the arm was 21·8 cm.

At the end of the irradiation period the patient was transferred to the part-body counter with a delay of 1 min. The forearm was counted for 1000 s

in the central shield of the counter with a detector separation of 9 cm, the forearm being constrained in the same way as for activation. The combination of activation and detection had a FWHM of 12·7 cm centred 13·5 cm from the centre of the fist (fig. 4).
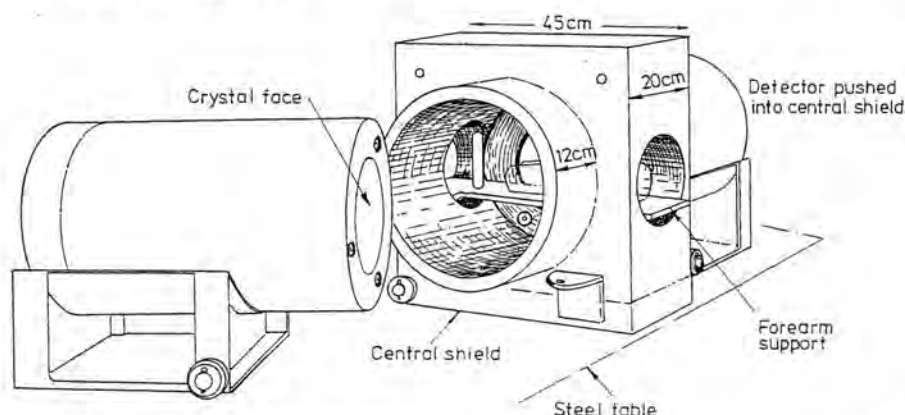

Fig. 3. Part-body counter. One detector had been removed from the central shield to show the position of the forearm support.
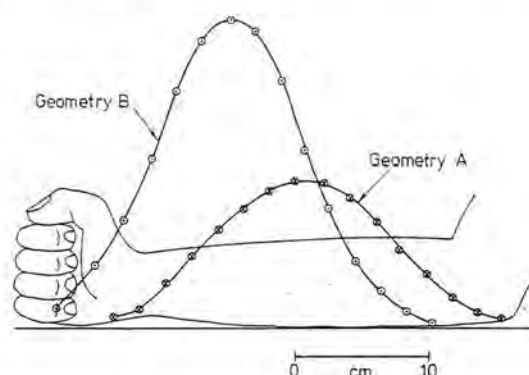

Fig. 4. Combined activation and detection profiles to show region of measurement of the forearm. The curves illustrate the improved sensitivity of calcium measurement using the water bath.

4. Data analysis and precision

The spectrum obtained from a forearm after a 10 min irradiation, 1 min delay and 1000 s count is shown in fig. 5. It was not possible to wait for the calcium to decay in order to calculate the contributions from ^{38}Cl and ^{24}Na to the calcium peak, because during this time there would be a significant decrease in the ^{24}Na peak due to redistribution in blood and soft tissue.

Two methods were used to calculate the ^{49}Ca contributions to the spectrum. In the first the patient spectrum and standard spectra of ^{24}Na and ^{49}Ca were integrated over the regions of the two photopeaks. Solutions of the two

simultaneous equations gave the sodium and calcium contributions in the two regions.

The second method used a computer to fit the standard spectra of [38]Cl, [24]Na and [49]Ca to the patient spectrum. Matrix algebra was used to fit simultaneously the three standard spectra using a least-squares technique. The intrinsic
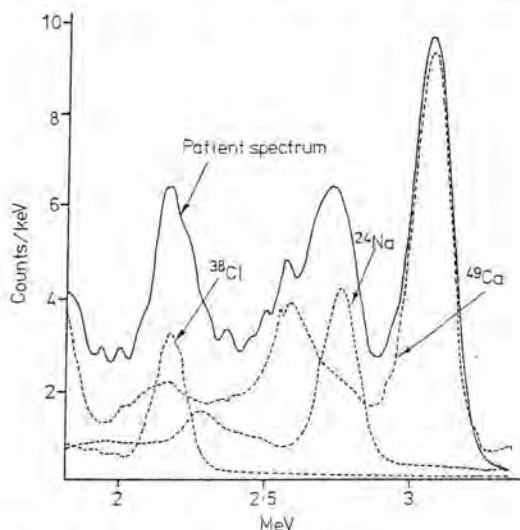
Fig. 5. Standard spectra fitted to a smoothed patient spectrum over the relevant 200 channels of the total spectrum.

precision of the two methods was compared by taking a single patient spectrum and randomly shifting each point in a Gaussian distribution within the limits of counting statistics. The coefficient of variation (cv) of the two methods based on manipulated spectra from a single patient spectrum was 2·4% and 2·1% respectively.

Precision measurements on a cadaver limb showed that with the low source activity, small changes in a patient could best be detected by performing sets of three repeated measurements at the beginning and end of a time period (e.g. six months) rather than six individual measurements performed throughout that time period. In addition, this irradiation programme enabled accurate repeatability figures to be obtained, which could include the effect of patient movement. From the many sets of repeated patient measurements the error due to movement (cv_m), which was independent of the number of counts measured, was calculated. This could then be combined with the statistical cv to give the overall precision (total cv) for each patient. Table 1 shows values for both irradiation geometries and both data processing techniques. The precision figures quoted were based on the mean calcium counts for both methods and the least significant change was calculated from the standard error of the mean of the sets of measurements, taking the level of significance at $P < 0.05$.

Table 1. Reproducibility of the two forearm irradiation apparatuses and methods of spectral analysis based on sets of repeated patient measurements

		cv_m (%)	Precision (%)	Least significant change (%)	No. of sets of patient measurements
Perspex pre-moderators and wax reflectors	Simultaneous equations	2·66	3·45	5·63	75
	Spectral stripping	2·20	3·14	5·13	
Water bath	Simultaneous equations	2·04	2·65	4·33	68
	Spectral stripping	1·93	2·57	4·20	

5. Spine measurement

It is recognised that ^{252}Cf is not the ideal source for measurements of the spine because of its relatively low mean neutron energy. However, extensive experiments were performed to determine the optimum irradiation geometry to measure changes in calcium in the lumbar spine using ^{252}Cf.

Changes in the bodies of the vertebrae are of most clinical interest, so good uniformity of activation and detection was sought in the region 5 cm to 9 cm below the skin surface, which is the approximate position of the region of interest (Brinkley and Masters 1967). In addition, effort was made to measure the region 0 cm to 5 cm deep with as low a sensitivity as possible so that calcium counts from the spinous processes and arches of the vertebrae contributed as little as possible to the total calcium counts detected. Thus changes in the bodies of the vertebrae, where the calcium losses are most important, would be most likely to be detected.

5.1. *Activation*

The variation in thermal neutron flux with depth was investigated in fourteen different irradiation geometries. Reflector position, thickness of premoderator and source to skin distance were varied and the effect of a thermal neutron absorber was investigated. The efficiency of activation, using both phantoms and a cadaver, and the dose were then measured in the geometries with reasonable thermal neutron flux profiles.

The flux profiles of the two irradiation geometries chosen as most suitable are shown in fig. 6. Geometry 1, to be used for the majority of patients, gave the best thermal fluence uniformity. The sources were situated 6 cm from the skin surface and no premoderator or reflector was used. Geometry 2 would only be used for patients of very small stature, where the bodies of the vertebrae were likely to be in the region 3 cm to 6 cm below the skin surface, and so would be measured fairly uniformly and with higher sensitivity. For this geometry the sources were situated 6 cm from the skin surface and surrounded

5.2. *Detection*

Counting was performed bilaterally with the patient supine in a shadow shield whole body counter incorporating four 15 cm × 10 cm NaI detectors, two above and two below, separated by 41 cm. In this position, a background of 0·25 CPS was obtained in the ^{49}Ca region. The variation in sensitivity in the approximate region of the vertebrae, 5 cm to 9 cm above the bed, was ± 8·0%. The variation along the spine 7 cm above the bed was 43·2 cm (FWHM) which was compatible with the activation profile 7 cm below the skin surface of 36·0 cm (FWHM).

A pilot study was carried out using the spine irradiation apparatus (geometry 1), sets of three measurements being performed on ten volunteers. The results showed that using two 100 mCi sources, the lumbar spine could be measured with a precision of around 3·0%. The dose, measured using nuclear emulsion films from a 200 s irradiation, would be 6 rem to the skin, 0·7 rem to the bone (0·4 rem averaged over the whole spine) and 0·2 rem to the female gonads. The mean calcium count from this dose would be approximately 2000 counts.

The 1000 s counting time was split into three periods of 200 s, 200 s and 600 s, the first two of these being used to determine the feasibility of phosphorus measurements, via the ^{31}P (n, α) ^{28}Al reaction (threshold 2·0 MeV, $T_{\frac{1}{2}} = 2·3$ min). The number of counts from ^{28}Al varied enormously, the statistical error being greater than 10% in five out of nine volunteers. Thus, as would be expected, the neutron energy of ^{252}Cf is too low for phosphorus activation.

6. Discussion

Apparatus has been developed to use the technique of neutron activation analysis to monitor calcium changes for use in a hospital. Sequential measurements of the forearm have been performed now for two years on over 90 patients and the technique has been proved to be a useful research tool. Significant changes both in individual patients and in groups of patients with respect to treatment have been detected and new forms of treatment evaluated (Winney, Tothill, Robson, Abbot, Lidgard, Cameron, Smith, MacPherson and Strong 1977).

The use of a water bath acting as premoderator and reflector, and the matrix method of spectral analysis have been shown to give the best precision. The advantage of this latter technique is, however, marginal when used with the water bath, and so the simultaneous equations method could be used with almost equal success for clinical measurements.

The characteristics of the forearm irradiation and detection apparatus compare favourably with other methods of monitoring sequential changes of calcium at peripheral sites. The precision value of 2·6% for a single measurement is better than those achieved by Catto *et al.* (1973) and Maziere and Comar (1976) who quote values of 5% and 3% respectively. The bone dose is also less, due both to the lower mean neutron energy and the relatively large amount of premoderator used. The precision of activation analysis of the forearm also

compares well with that achieved by bone mineral absorptiometry (Cameron and Sorenson 1967).

Tests performed on the spine apparatus suggested that, despite the low neutron energy, ^{252}Cf is suitable for measurements of the lumbar spine. The characteristics of the method compare well with the technique using more suitable higher energy neutrons from a cyclotron (Al-Hiti *et al.* 1976). This could be due to the reduction of lordosis in the patient obtained using a tilting chair and also better uniformity of detection obtained by the use of bilateral geometry.

Californium-252 is a particularly suitable source for neutron activation analysis in a clinical environment. It is the cheapest of all the radionuclide sources, although its relatively short half-life must be taken into account when planning long term clinical studies. The minimum initial total source activity required for a three-year study would be 100 mCi for the forearm and 200 mCi for the spine.

Résumé

Mise au point des appareillages destinés à mesurer les modifications du calcium dans l'avant-bras et dans la colonne vertébrale par une analyse par activation neutronique, en employant le californium 252

On a mis au point des techniques pour mesurer *in vivo* les petites modifications du calcium dans l'avant-bras et la colonne vertébrale, ce par une analyse par activation neutronique en utilisant deux sources de ^{252}Cf ambiance hospitalière. En employant des compteurs spécifiquement destinés au prélèvement de mesures sur certaines parties du corps, ainsi qu'une irradiation bilatérale avec une prémodération de 7,5 cm entre les sources et l'os, on a mesuré l'os périphérique avec une puissance globale de source dont la valeur a pu baisser jusqu'à 50 mCi. Deux méthodes d'analyse spectrale ont été employées et comparées. Sur six mesures, on a réussi à faire des études de l'avant-bras de patients, avec une précision de 2,6% compte tenu du mouvement du patient, et une dose annuelle de 10 rem à l'os, la dose au niveau de la peau étant de 35 rem.

Deux sources de 100 mCi ont été employées pour les mesure de la colonne lombaire. On a pris soin de minimiser les problèmes d'absence d'uniformité de l'activation auxquels on se heurte lorsque l'on utilise l'irradiation unilatérale. L'accent a été mis sur la mesure des corps de vertèbres, avec une sensibilité et une uniformité adéquates, ainsi que les arches et procès épineux avec basse sensibilité. Un compteur du corps entier a été employé pour la détection bilatérale de l'activité induite. La précision de la méthode s'est avérée être de 3% avec une dose osseuse annuelle de pointe de 2,1 rem et une dose de 18 rem au niveau de la peau, ce sur trois mesures prélevées.

Zusammenfassung

Entwicklung einer Apparatur zur Messung der Änderungen der Kalziumwerte im Vorderarm und im Rückgart mit Hilfe von analytischen Methoden auf der Basis von Neutronenaktivation unter Einsatz von Californium-252

Es wurden Methoden zur Messung geringfügiger Änderungen der Kalziummengen im Vorderarm und im Rückgrat entwickelt. Sie wurden am labenden Organismus, d.h. *in vivo*, durchgeführt und beruhen auf Neutronenaktivierung als analytische Methodik, bei der zwei ^{252}Cf-Quellen im Krankenhaus verwendet wurden. Unter Einsatz speziell gebauter Zähler zur Messung der Radioaktivität

in bestimmten Körperzonen und einer zweiseitigen Strahleneinwirkung bei einem, 7,5 cm langen Strahlenbremsvorsatz zwischen den Quellen und dem zu messenden Knochen wurden die Peripheriezonen von Knochen bei einer Gesamtstärke der Quelle, die zum Schluss nur noch 50 mCi betrug, gemessen. Angewandt wurden zwei verschiedene Methoden der Spektralanalyse und die so erhaltenen Werte wurden mit einander verglichen. Die Messung des Kalziummetabolismus im Vorderarm von Patienten wurde somit erfolgreich durchgeführt, indem eine Genauigkeit von 2,6% erreicht wurde, sofern man die Bewegung das Patienten noch mitberücksichtigt. Die jährliche Dosis für die Knochen lag unter 10 rem und diejenige für die Haut bei 35 rem. Diese Werte verstehen sich für sechs Messungen.

Zwei Strahlenquellen mit je 100 mCi wurden zur Messung des Kalziumwechsels im Rückgrat in der Lendengegend eingesetzt. Hierbei wurde vorsichtig arauf geachtet, diejenigen Schwierigkeiten so gering wie möglich au halten, welche sich aus der Ungleichförmigkeit der Aktivierung bei Verwendung einer einseitig wirkenden Bestrahlung ergeben. Das Schwergewicht wurde darauf gelegt, die Wirbelsäulenteile mit ausreichender Empfindlichkeit und Gleichförmigkeit sowie die Veränderungen der Wirbelsäule und der Wölbungen mit niedriger Empfindlichkeit zu messen. Zur Messung der induzierten Radioaktivität bei zweiseitiger Strahleneinwirkung wurde ein Zählinstrument gewählt, das den ganzen Körper erfasst. Die Genauigkeit der Methode betrug 3,0% bei einer jährlichen Spitzendosis für die Knochen von 2,1 rem und einer Dosis für die Haut von 18 rem. Diese Werte gelten für drei Messungen.

References

AL-HITI, K., THOMAS, B. J., AL-TIKRITY, S. A., ETTINGER, K. V., FREMLIN, J. H., and DABEK, J. T., 1976, *Int. J. Appl. Radiat. Isotopes*, **27**, 97.

ANDERSON, J., OSBORN, S. B., TOMLINSON, R. W. S., NEWTON, D., RUNDO, J., SALMON, L., and SMITH, J. W., 1964, *Lancet*, **ii**, 1201.

BODDY, K., ROBERTSON, I., and GLAROS, D., 1974, *Phys. Med. Biol.*, **19**, 853.

BRINKLEY, D., and MASTERS, H. E., 1967, *Br. J. Radiol.*, **40**, 66.

CAMERON, J. R., and SORENSON, J., 1967, *J. Bone Jt Surg.*, **49A**, 481.

CATTO, G. R. D., MCINTOSH, J. A. R., and MACLEOD, M., 1973, *Phys. Med. Biol.*, **18**, 508.

COMAR, D., RIVIERE, R., RAYNAUD, C., and KELLERSHOHN, C., 1968, *Radioactive Isotopes in Klinik und Forschung*, **8**, 186 (Munich: Urban and Schwarzenberg).

EVANS, H. J., LE BLANC, A. D., and JOHNSON, P. C., 1976, *Med. Phys.*, **3**, 148.

GLAROS, D., 1975, *Ph.D. Thesis*, University of Glasgow.

GUEY, A., LEITIENNE, P., ZECH, P. Y., and TRAEGER, J., 1978, in *Proc. Symp. Californium 252 Utilization, Brussels, 1976* (U.S.E.R.D.A.) in press.

LAW, J., LAWSON, R. C., and PORTER, D., 1974, *Phys. Med. Biol.*, **19**, 643.

MAZIERE, B., and COMAR, D., 1976, in *2nd East Kilbride Conf. on Progress and Problems of In-Vivo Activation Analysis*. Scottish Research and Reactor Centre Rep. No. 57/76.

MCNEIL, K. G., THOMAS, B. J., STURTRIDGE, W. C., and HARRISON, J. E., 1973, *J. Nucl. Med.*, **14**, 502.

SMITH, M. A., and MACPHERSON, J. N., 1977, *Calcif. Tissue Res.*, **22**, 568.

SMITH, M. A., TOTHILL, P., SIMPSON, J. D., MACPHERSON, J. N., MERRICK, M. V., STRONG, J. A., and BODDY, K., 1978, in *Proc. Symp. Californium 252 Utilization, Brussels, 1976* (U.S.E.R.D.A.) in press.

VARTSKY, D., and THOMAS, B. J., 1976, *Phys. Med. Biol.*, **21**, 139.

WINNEY, R. J., TOTHILL, P., ROBSON, J. S., ABBOT, S. R., LIDGARD, G. P., CAMERON, E. H. D., SMITH, M. A., MACPHERSON, J. N., and STRONG, J. A., 1977, *Clin. Endocr.*, **1**, 151s.

Short Communication

Measurement of spinal calcium by *in vivo* neutron activation analysis in osteoporosis

M A Smith†, R Eastell§, N S J Kennedy‡, L G McIntosh§, J D Simpson‡, J A Strong§ and P Tothill†

†Department of Medical Physics and Medical Engineering, Royal Infirmary and ‡Western General Hospital, Edinburgh, Scotland
§Department of Medicine, Western General Hospital, Edinburgh, Scotland

1. Introduction

Osteoporosis is the most common disease of bone, affecting in particular the elderly female population. The lumbar spine is of particular interest in the study of this disease for two reasons. Firstly, lumbar vertebral crush fracture is a common manifestation of osteoporosis, suggesting that the spine appears to be particularly vulnerable. Secondly, the normal turnover rate of bone at such trabecular sites is 8% per annum compared with 3% per annum in the cortical bone of the metacarpals or the radius (ICRP 23 1975). Any change or response to treatment may thus be made more apparent by measuring the lumbar spine than by using conventional techniques of metacarpal index or photon absorptiometry of the radius.

Methods for measuring changes in calcium content of the lumbar spine by *in vivo* neutron activation analysis have been described using ^{252}Cf (Smith and Tothill 1979), and elsewhere using a cyclotron (A1 Hiti *et al* 1976). No report of changes in spinal calcium content in response to treatment for osteoporosis has yet been published.

This study set out to evaluate the technique of part-body neutron activation analysis of the spine as a method for monitoring calcium changes in elderly osteoporosis patients.

2. Methods and patients

The apparatus used consisted of a modified dental chair that could tilt back to minimise patient movement. Two ^{252}Cf sources, each initially 2.96 GBq (80 mCi), were positioned behind the patient 6 cm from the skin surface and 20 cm apart, centred on the iliac crest. No premoderator or hydrogenous reflector was used. The patient was irradiated for 3.5 min. The induced activity was measured in a whole-body counter containing four 15 cm × 10 cm NaI detectors for 1000 s (Smith and Tothill 1979). As there was no collimation of the neutron flux, parts of the thoracic spine, sacrum and pelvis were also activated, in addition to the lumbar spine.

Twenty-three women presenting with fractured neck of femur were studied. Their mean age was 69.5 years (range 43–80 years) and all were post-menopausal. Twenty of these patients had normal blood biochemistry and were randomly allocated to one of four treatment groups: (a) placebo, (b) ethinyloestradiol (oestrogen) and calcium

supplement (Ca), (c) 1α-hydroxycholecalciferol (1αOHD$_3$) and Ca, (d) 1αOHD$_3$, oestrogen and Ca (Eastell *et al* 1980). Three patients with possible osteomalacia, as indicated by blood biochemistry, were given 1αOHD$_3$ and Ca.

The patients were measured at intervals of four months for one year. In addition to the measurement of spinal calcium, the mineral content of the non-dominant forearm was measured using photon absorptiometry at a site 5 cm proximal to the tip of the styloid process of the radius. Patients were assessed radiographically at their first and last visit to detect the occurrence of vertebral crush fractures during the period of the study. It was recognised that an increase in the thickness of soft tissue over the spine would decrease the efficiency of activation, so patients who showed a consistent weight increase of more than 5 kg during the year were omitted from the study.

3. Results

An average of 997 counts was measured in the [49]Ca photopeak in these patients. After correcting for decay of the [252]Cf, the annual rate of change in spinal calcium content was calculated by fitting a regression line to the four measurements. The combined residual sum of squares from the regression lines gave an overall estimate of reproducibility (coefficient of variation) of 5% for all the patient data.

Three patients showed a consistent weight increase (probably as a result of the oestrogen therapy), one suffered a crush fracture during the study and one was found to suffer from rheumatiod arthritis. The results of the remaining fifteen osteoporotic patients are shown in figure 1. A one-way analysis of variance (Kruskal and Wallis
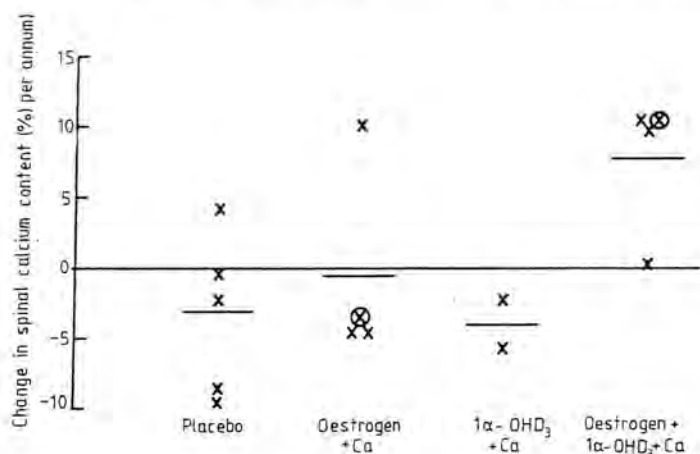

Figure 1. Annual changes in spinal calcium content in patients (♀) with fractured neck of femur. ⊗ represents changes over six months in patients who did not complete the study.

1952) suggested that the results were not of the same population ($p = 0.6$). The treatment that was expected to be of most benefit, 1αOHD$_3$, Ca and oestrogen (Marshall and Nordin 1977, Nordin *et al* 1980) was significantly better than placebo ($P < 0.05$). There were no other significant diffrerences between the groups. The predictable response to vitamin D therapy in the three osteomalacic patients was demonstrated by an increase in spinal calcium in all three patients, the increases being significant ($P < 0.05$) in two of the three.

Similar analysis of the photon absorptiometry measurements of the forearm gave a figure for the reproducibility of 4.4%. Analysis of the data suggested that all the results from the osteoporotic patients came from the same population ($p = 0.45$) and no significant differences were seen between groups. No significant correlation was found between changes in the forearm and spine ($r = 0.21$).

4. Discussion

The results of this study demonstrate that NAA of the spine using ^{252}Cf, perhaps the most convenient and inexpensive neutron source, can be sucessfully used to monitor calcium changes due to osteoporosis and its treatment in the elderly female population. The reproducibility figure of 5% is worse than the figure of 3% which had been achieved in a previous small pilot study (Smith and Tothill 1979) on a group of patients not suffering from osteoporosis. This can be accounted for by the lower calcium levels in the osteoporotic patients and hence a larger error due to counting statistics, plus their difficulty in sitting still during the activation period, due to pain in their recently fractured hip. The assesment of reproducibility in the osteoporotic group assumes a linear change with time; such an assumption may lead to an over-pessimistic figure for reproducibiltiy.

The expected 'best' treatment regime, Ca, 1αOHD$_3$ and oestrogen was shown to be significantly better ($P < 0.05$) than placebo by spine NAA. This result was not demonstrated by forearm absorptiometry, even though the latter had better reproducibility. The lack of correlation between changes in bone mineral in different parts of the skeleton confirms other findings (Aloia *et al* 1975, Cohn *et al* 1975, 1976, Dabek *et al* 1977, Harrison *et al* 1974).

The patients in the study were selected from a group of 180 patients presenting with fractured neck of femur over a seven month period. It had been hoped that about half of these would be suitable for the study, hence the four treatment groups, but the high morbidity and morality rates associated with this fracture reduced the available number considerably. The low admittance rate into the study was not due to difficulties associated with the NAA measurement technique.

Nonetheless there is one drawback of the technique. This is that an increase in body tissue in the region of the spine will affect the sensitivity of the activation. As some patients steadily increase their weight as a result of receiving oestrogen, these patients must be eliminated from any analysis of the results or, preferably, experiments must be performed to correct for variations in activation and detection efficiency.

Acknowledgments

References

Al-Hiti K, Thomas B J, Al-Tikrity S A, Ettinger K V, Fremlin J H and Dabek J T 1976 *Int. J. Appl. Radiat. Isot.* **27** 97–102
Aloia J F, Ellis K J, Zanzi I and Cohn S H 1975 *J. Nucl. Med.* **16** 196–9
Cohn S H, Ellis K J, Caselnova R C, Asad S N and Letteri J M 1975 *J. Lab. Clin. Med.* **86** 910–9

Cohn S H , Ellis K J, Martino A N, Asad S N and Letteri J M 1976 *Calcif. Tissue.* Res. **21** 216–20

Dabek J T, Robinson B H B, Naik R B and Al-Hiti K 1977 *Clin. Endocrinol.* **7** 147–50

Eastell R, Smith M A, Kennedy N S J, McIntosh L V, Simpson J D, Strong J A and Tothill P 1980 *Scott. Med. J.* **25** 174

Harrison J E, McNeill K G, Meema H E, Fenton S, Oeropoulos D G and Sturtridge W C 1974 *J. Nucl. Med.* **15** 929–34

I C R P 1975 *Reference Man; Anatomical, Physiological and Metabolic characteristics*, ICRP 23 (Oxford: Permagon) p 75

Kruskal W H and Wallis W A 1952 *J. Am. Stat. Assoc.* **47** 583–621

Marshall D H and Nordin B E C 1977 *Clin. Endocrinol.* **7** 159–68

Nordin B E C, Horsman A, Crilly R G, Marshall D H and Simpson M 1980 *Br. Med. J.* **280** 451–4

Smith M A and Tothill P 1979 *Phys. Med. Biol.* **24** 319–29

Long-Term Effect of Dialysate Calcium and 1α-Hydroxycholecalciferol on Bone Calcium Content in Haemodialysis Patients as Measured by Neutron Activation Analysis of the Forearm

M. A. Smith, R. J. Winney, J. A. Strong, P. Tothill

Department of Medical Physics and Medical Engineering and Department of Medicine, Western General Hospital and Medical Renal Unit, Department of Medicine, Royal Infirmary, Edinburgh, Scotland

Abstract. The effect of different concentrations of dialysate calcium and treatment with 1α-OHD₃ on bone calcium content in haemodialysis patients was investigated over a 2½-year period. Part-body neutron activation analysis of the forearm with ^{252}Cf was used to measure both an initial absolute calcium content and changes in the bone calcium. A highly significant inverse correlation ($r = -0.84$, $p < 0.001$) was found between the initial calcium content and the duration of previous dialysis utilising a dialysate calcium concentration of 1.75 mmol/l. No significant difference was found between the changes in bone calcium in patients who continued using a dialysate calcium of 1.75 mmol/l and those whose dialysate calcium was reduced to 1.375 mmol/l. There was a significant increase of 16.7% ($p < 0.01$) in bone calcium over the 2½-year period in the patients receiving 1α-OHD₃. The results of the study suggest that bone calcium loss is not necessarily influenced by dialysate calcium concentration but that 1α-OHD₃ has a beneficial long-term effect on bone calcium content.

Introduction

Renal osteodystrophy in haemodialysis patients is a complex mixture of osteomalacia, secondary hyperparathyroidism and osteoporosis. While it is now recognised that disturbance of vitamin D metabolism has a central role in the pathogenesis of renal osteodystrophy, the concentration of calcium in the dialysis fluid has also been thought to be of importance in haemodialysis patients [1]. However, while using a dialysate calcium concentration of 1.5 mmol/l or higher may prevent hypocalcaemia and improve calcium balance [2–5] there is still controversy regarding the effect of dialysate calcium concentrations on bone disease [6, 7]. By contrast, short-term treatment of renal osteodystrophy with synthetic active metabolites of vitamin D has produced promising improvement in renal bone disease [8] except when this is aluminium-induced [9].

The end result of all forms of renal osteodystrophy is loss of bone mineral and calcium which may result in bone pain and fractures. Since bone mineral content may change slowly as renal bone disease progresses, assessment of its response to treatment requires a means of detecting small changes in bone mineral or bone calcium content. Skeletal radiography is a qualitative technique which detects only severe changes while bone histology requires expertise for quantification of changes and since it is traumatic for the patient, is not ideal for frequent analyses. Neutron activation analysis (NAA) is a non-invasive and precise technique which measures calcium content and would be of value in quantitating small changes in the calcium content of bone. Its usefulness has been confirmed by a number of studies where use of this technique has detected changes in calcium content paralleling biochemical, radiological and histological changes [10].

This study assesses the effect of dialysate calcium and treatment with 1α-hydroxycholecalciferol (1α-OHD₃) on the calcium content of bone in haemodialysis patients over a 2½-year period using NAA to measure changes in calcium content of the forearm.

Patients and Methods

21 patients, aged 22–56 years (mean 40 years) had been established on haemodialysis from 2 to 11 years (mean 4.5 years). These were the

Table I. Initial sex distribution, mean age (range), duration of dialysis (range) and blood biochemistry (± 1 SD) prior to the start of the study

	Number in group		Age, years	Duration of dialysis months	Plasma calcium mmol/l	Plasma alkaline phosphatase U/l	Plasma parathyroid hormone μg/l
	♀	♂					
Group 1	1	4	42 (27–56)	45 (24–84)	2.65 ± 0.11	130 ± 60	1.03 ± 0.90
Group 2	2	5	42 (22–52)	65 (33–134)	2.49 ± 0.31	134 ± 64	1.29 ± 0.72
Group 3	3	4	36 (25–56)	53 (37–75)	2.53 ± 0.19	156 ± 113	1.19 ± 1.30

entire population of patients on home dialysis who had not been treated previously with vitamin D. Patients were dialysed for 5–8 h twice or thrice weekly using either Gambro 1M², 1M² coil or Cordis Dow 1.3M² hollow fibre. Prior to this study, dialysis on all patients was conducted with a dialysate calcium concentration of 1.75 mmol/l and magnesium concentration of 0.75 mmol/l; their diet contained 70 g of protein, 800 mg (20 mmol) of calcium and 1,100 mg (35.5 mmol) of phosphorus daily. In addition, patients received aluminium hydroxide if necessary to maintain the pre-dialysis plasma phosphate in the range 1.6–2.0 mmol/l.

The patients were randomly allocated into one of three treatment groups. Group 1 continued their treatment unchanged with a dialysate calcium concentration of 1.75 mmol/l. 2 patients failed to attend for the study leaving only 5 in the group. Group 2 contained 7 patients who were treated with a low dialysate calcium concentration of 1.375 mmol/l. Group 3 also contained 7 patients who were treated with a low dialysate calcium concentration of 1.375 mmol/l but in addition were given 1α-OHD₃ in an initial dose of 2 μg daily, adjusted later if necessary to avoid hypercalcaemia. The initial characteristics of each group are shown in table I. There were no significant differences between the groups at the start of the study.

The calcium content of the non-fistula forearm was measured by NAA at time zero before the treatment alteration, then at 8, 16 and 30 months after the start of the trial. 2 patients in Group 1 did not complete the study: 1 died of cardiac failure after 17 months and 1 had a fistula inserted in the arm being measured after 18 months. In Group 2, 2 patients also did not complete the study, 1 after 9 months due to hypocalcaemia and 1 after 17 months when 1α-OHD₃ treatment commenced. In Group 3, 1 patient died just before the final measurement whilst receiving treatment of oesophageal carcinoma. Throughout the period of this study, skeletal radiographs of the ankle, hand, pelvis, chest, lumbar spine and skull were taken to monitor extraosseous calcification.

The measurement of calcium content of bone using NAA involves irradiating the region of interest with neutrons which react with the isotope ^{48}Ca in bone to form unstable ^{49}Ca. This induced radioactivity, which has a half-life of 8.8 min, can then be measured with a gamma-ray detector to provide a relative estimate of the calcium content of the bone, expressed as measured ^{49}Ca counts. In our apparatus [11, 12] the forearm is irradiated with two neutron sources of ^{252}Cf and the activity measured with two 15×10 cm sodium iodide detectors placed one on either side of the forearm. A triple irradiation procedure was adopted at each visit giving a precision of 1.8%, the same apparatus and procedure being used on each occasion. The NAA results over the 2½ years of the study were expressed as a percentage of the initial value.

At the time of the last attendance at 30 months, irradiation apparatus using a water bath had been developed so an additional measurement was performed which enabled a more absolute calcium determination to be made using a normalisation procedure to correct for variations due to the patient's size [13]. This value, combined with the changes over the 2½-year period, enabled an initial absolute forearm calcium content to be established in the 14 patients who completed the study. A group of 18 patients awaiting treatment with lithium carbonate were used to define a normal range, so the initial forearm calcium in the renal patients could be expressed as a percentage of normal.

Analysis of data was made using non-parametric statistics unless otherwise stated and $p > 0.05$ was taken to be not significant.

Results

For the dialysis patients as a group the initial calcium content in the forearm prior to the start of the study was significantly lower than normal (mean 87%, $p < 0.05$, t test). A highly significant inverse correlation was found ($r = -0.84$, $p < 0.001$) between the initial bone calcium level and the duration of previous haemodialysis treatment (fig. 1).
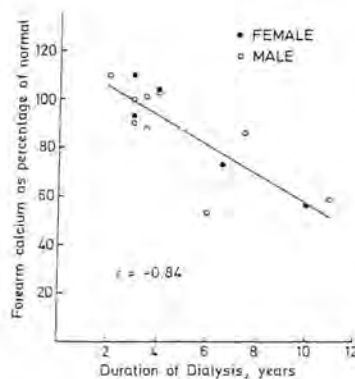

Fig. 1. Relationship between initial calcium content of the forearm, expressed as a percentage of normal, and duration of previous haemodialysis.
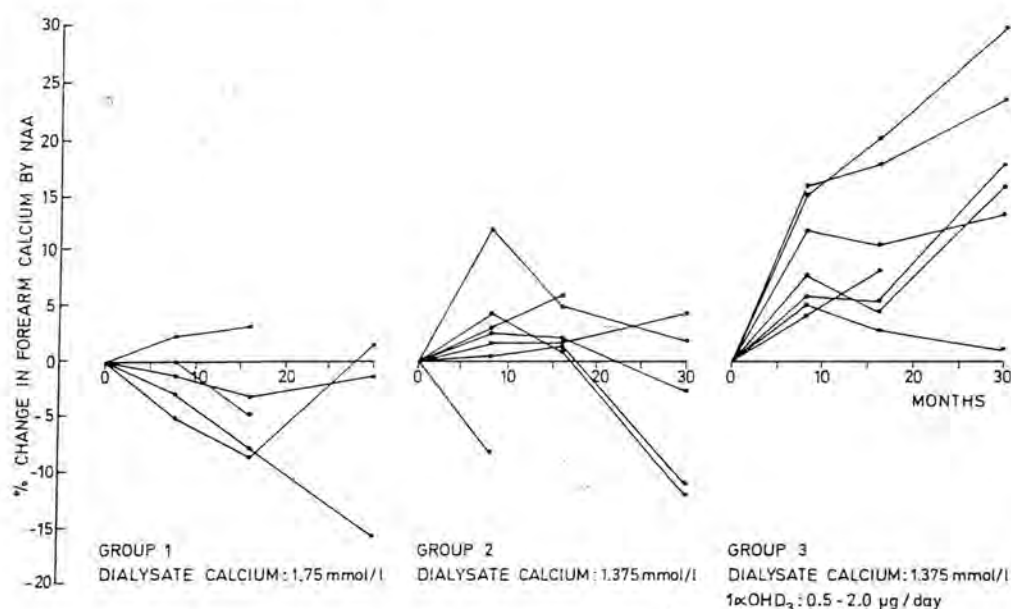
Fig. 2. Percentage changes in forearm calcium in individual patients in the three groups over a period of 2½ years expressed as a percentage of the initial value.

Table II. Mean percentage change (± 1 SD) in the non-fistula forearm calcium as measured by NAA in the three groups

	0–8 months	8–16 months	16–30 months	0–30 months
Group 1	−1.54 (± 2.80) (n = 5)	−2.84 (± 2.37) (n = 5)	+1.36 (± 8.75) (n = 3)	−5.29 (± 9.20) (n = 3)
Group 2	+2.10 (± 5.85) (n = 7)	−0.94 (± 3.48) (n = 6)	−6.22 (± 6.73) (n = 5)	−3.97 (± 7.42) (n = 5)
Group 3	+9.26 (± 4.82) (n = 7)	+0.63 (± 3.31) (n = 7)	+6.49 (± 5.37) (n = 6)	+16.65 (± 9.42) (n = 6)

n = Number of patients.

The percentage changes in calcium content of the non-fistula forearm in individual patients in the 3 groups over the period of study are shown in figure 2. The mean changes in NAA calcium in each group expressed as a percentage change over the different time periods are given in table II.

In the patients in Group 3 treated with 1α-OHD$_3$, there was a consistent increase in calcium content which was significantly greater than that in Group 1 (p < 0.01) and Group 2 (p < 0.02) over the initial period of 8 months [14], Group 2 (p < 0.01) over the 16- to 30-month period and in both groups (p < 0.01) over the complete time period of 2½ years. The change in calcium content in Groups 1 and 2 was variable but any differences between these two groups were not significant.

There was no increase in soft tissue or vascular calcification over the period of the study on skeletal radiographs.

Discussion

The reduced forearm calcium content in these patients at the onset of the study, as well as the clear relationship between the initial forearm calcium and the duration of haemodialysis treatment, indicates that prolonged use of a 'high' dialysate calcium concentration of 1.75 mmol/l did not prevent bone calcium loss in these patients. In addition we have also failed to detect any significant difference between changes in calcium content in patients treated with either a high or a low dialysate calcium concentration. These findings contrast with those in earlier studies which indicated that use of a dialysate calcium of 1.5 mmol/l or higher might prevent the loss of bone mineral [1, 3, 4], but confirm similar more recent observations [6, 7]. Thus, while the use of a dialysate calcium of 1.5 mmol/l or higher may

improve calcium balance and prevent hypocalcaemia [2, 5], the role of dialysate calcium in the pathogenesis of renal bone disease requires further study.

The significant increase in forearm calcium content in patients treated with 1α-OHD$_3$ compared to the untreated groups demonstrates the beneficial long-term effect of 1α-OHD$_3$ on bone calcium in haemodialysis patients. The rate of increase in bone calcium in patients treated with 1α-OHD$_3$ in this study was equivalent to 7.1% per annum over the whole period of observation. This compares with estimated increases of 3% per annum using whole body NAA over periods of 10–18 months [5] and 8.7% in 3 months using NAA measurements of the hand [15]. The increases in hand calcium by NAA in the short-term demonstrated by *Catto* et al. [15], however, did not continue in the long term [16; *Catto* pers. commun.]. While the reason for these differences in results of NAA using these two part-body sites is not clear, they may reflect regional differences in the skeletal response to 1α-OHD$_3$.

The increase in bone calcium in this study in response to 1α-OHD$_3$ occurred despite the use of a dialysate calcium concentration of 1.375 mmol/l at which calcium loss into the dialysate fluid might be expected. The 'low' dialysate calcium was chosen in this study in the light of previous experience when the use of a dialysate calcium of 1.75 mmol/l restricted the dosage of 1α-OHD$_3$ due to hypercalcaemia [17]. Since calcium absorption improves with 1α-OHD$_3$ it may be unnecessary, indeed undesirable, to use a 'high' dialysate calcium during treatment with 1α-OHD$_3$, particularly in view of the uncertainty about the influence of dialysate calcium on bone disease.

This study indicates that part-body in vivo NAA is a useful means of monitoring renal osteodystrophy. The hand is commonly chosen for NAA measurements on renal patients [18–20] but since NAA measurements of the hand have failed to demonstrate a long-term beneficial effect of 1α-OHD$_3$ on bone calcium, it is suggested that the forearm, which in any event contains more calcium, is more reliable and should be regarded as a more suitable site for monitoring renal bone disease using part body NAA.

References

1 Fournier, A.E.; Johnson, W.J.; Taves, D.R.; Beabout, J.W.; Arnaud, C.D.; Goldsmith, R.S.: Etiology of hyperparathyroidism and bone disease during chronic haemodialysis. J. clin. Invest. *50:* 592–598 (1971).

2 Wing, A.J.: Optimum calcium concentrations of dialysis fluid for maintenance haemodialysis. Br. med. J. *iv:* 145–149 (1968).

3 Bone, J.M.; Davison, A.M.; Robson, J.S.: Role of dialysate calcium concentration in osteoporosis in patients on haemodialysis. Lancet *i:* 1047–1049 (1972).

4 Goldsmith, R.S.; Johnson, W.J.: Role of phosphate depletion and high dialysate calcium on controlling dialytic renal osteodystrophy. Kidney int. *4:* 154 (1973).

5 Naik, R.B.; Dabek, J.T.; Heynen, G.; James, H.M.; Kanis, J.A.; Robertson, P.W.; Robinson, B.H.B.; Woods, C.G.: Measurement of whole body calcium in chronic renal failure: effects of 1α-hydroxyvitamin D$_3$ and parathyroidectomy. Clin. Endocrinol. *7:* 139–150 (1977).

6 Regan, R.J.; Peacock, M.; Rosen, S.M.; Robinson, P.J.; Horsman, A.: Effect of dialysate calcium concentration on bone disease in patients on haemodialysis. Kidney int. *10:* 246–255 (1976).

7 Junor, B.J.R.; Catto, G.R.D.: The effect of 1α-hydroxyvitamin D$_3$ on calcium and mineral content of bone in renal osteodystrophy. Clin. Endocrinol. *7:* 131–138 (1977).

8 Editorial: One-alpha. Lancet *i:* 973–974 (1978).

9 Pierides, A.M.; Simpson, W.; Ward, M.K.; Ellis, H.A.; Dewar, J.H.; Kerr, D.N.S.: Variable response to long term 1α-hydroxycholecalciferol in haemodialysis osteodystrophy. Lancet *i:* 1092–1095 (1976).

10 Cohn, S.H.; Ellis, K.J.; Vartsky, D.; Zanzi, I.; Aloia, J.F.: Medical application of in vivo neutron activation analysis. Int. Symp. Nuclear Activation Techniques in the Life Sciences, IAEA-SM-227/63, pp. 747–760 (1979).

11 Smith, M.A.; MacPherson, J.N.: Activation analysis by ^{252}californium for the estimation of the calcium content of bone. Calcif. Tissue Res. *22:* 568–571 (1977).

12 Smith, M.A.; Tothill, P.: Development of apparatus to measure calcium changes in the forearm and spine by neutron activation analysis using californium-252. Physics Med. Biol. *24:* 319–329 (1979).

13 Tothill, P.; Smith, M.A.; Simpson, J.D.; Chew, I.; MacPherson, J.N.; Winney, R.J.; Strong, J.A.: Clinical measurements of part-body calcium using neutron activation analysis. Int. Symp. Nuclear Activation Techniques in the Life Sciences. IAEA-SM-227/40, pp. 687–699 (1979).

14 Winney, R.J.; Tothill, P.; Robson, J.S.; Abbot, S.R.; Lidgard, G.P.; Cameron, E.H.D.; Smith, M.A.; MacPherson, J.N.; Strong, J.A.: The effect of dialysate calcium concentration and 1α-hydroxyvitamin D$_3$ on skeletal calcium loss and hyperparathyroidism in haemodialysis patients. Clin. Endocrinol. *7:* 151–158 (1977).

15 Catto, G.R.D.; MacLeod, M.; Pelc, B.; Kodicek, E.: 1α-hydroxycholecalciferol: a treatment for renal bone disease. Br. med. J. *i:* 12–14 (1975).

16 MacDonald, P.J.; Junor, B.J.R.; Fraser, R.A.; Smith, F.W.; Ettinger, K.V.; Catto, G.R.D.; Edward, N.; MacLeod, M.: Progressive renal bone disease – an assessment of long-term therapy with vitamin D analogues. Scott. med. J. *24:* 87–88 (1979).

17 Winney, R. J.; Bone, J. M.; Anderson, T. J.; Robson, J. S.: Treatment of renal osteodystrophy with 1α-hydroxycholecalciferol (1α-OH-D₃) in conjunction with a high dialysate calcium. Calcif. Tissue Res. 22: 94–100 (1977).

18 Catto, G. R. D.; McIntosh, J. A. R.; MacDonald, A. F.; MacLeod, M.: Haemodialysis therapy and changes in skeletal calcium. Lancet i: 1150–1152 (1973).

19 Maziere, B.; Kuntz, D.; Comar, D.; Ryckewaert, A.: In vivo analysis of bone calcium by local neutron activation of the hand: results in normal and osteoporotic subjects. J. nucl. Med. 20: 85–91 (1979).

20 Guey, A.; Leitienne, P.; Zech, P. Y.; Traeger, J.; Doyen, J. B.; Breton, J. P.: Utilisation d'un irradiateur neutronique chargé en californium-252 pour l'analyse in vivo du contenue calcique osseux de la main. Int. Symp. Nuclear Activation Techniques in the Life Sciences, IAEA-SM-227/94, pp. 701–717 (1979).

M. A. Smith, BSc, MSc, PhD, Department of Medical Physics and Medical Engineering, Western General Hospital (OPD), Crewe Road, Edinburgh EH4 2XU (Scotland)

Total body neutron activation analysis of calcium: calibration and normalisation

N S J Kennedy†, R Eastell‡, C M Ferrington†, J D Simpson†,
M A Smith§, J A Strong‡ and P Tothill§

† Department of Medical Physics and Medical Engineering,
‡ Department of Medicine, Western General Hospital, and
§ Department of Medical Physics and Medical Engineering, Royal Infirmary,
Edinburgh, Scotland

Abstract. An irradiation system has been designed, using a neutron beam from a cyclotron, which optimises the uniformity of activation of calcium. Induced activity is measured in a scanning, shadow-shield whole-body counter. Calibration has been effected and reproducibility assessed with three different types of phantom. Corrections were derived for variations in body height, depth and fat thickness. The coefficient of variation for repeated measurements of an anthropomorphic phantom was 1.8% for an absorbed dose equivalent of 13 mSv (1.3 rem). Measurements of total body calcium in 40 normal adults were used to derive normalisation factors which predict the normal calcium in a subject of given size and age. The coefficient of variation of normalised calcium was 6.2% in men and 6.6% in women, with the demonstration of an annual loss of 1.5% after the menopause. The narrow range should make single measurements useful for diagnostic purposes..

1. Introduction

Total body neutron activation analysis is now established as one of the most important methods of determining the elemental composition of the human body. It can be used to determine both the absolute amount and changes with time of certain body elements, in particular calcium, sodium, chlorine, phosphorus and nitrogen (Cohn 1981).

In the technique, the subjects are exposed to a beam of partially moderated fast neutrons which induces amongst others the reactions $^{48}Ca(n, \gamma)^{49}Ca$, $^{23}Na(n, \gamma)^{24}Na$, $^{37}Cl(n, \gamma)^{38}Cl$, $^{31}P(n, \alpha)^{28}Al$ and $^{14}N(n, 2n)^{13}N$. The radioactive isotopes produced then decay, emitting γ-rays which can be readily detected in a whole-body counter.

If the reproducibility of the method were good then small changes in the body elements with time might be detected relatively easily. Absolute quantification of the elements is more difficult, because of the natural variation in body dimensions and the difficulty of obtaining a suitable variable phantom of known composition for calibration. To overcome these problems several different approaches have been made. Nelp *et al* (1972) made repeated measurements on five cadavers of different sizes and then ashed the skeletons to determine the calcium content. Cohn and Dombrowski (1971) and Cohn *et al* (1972) used only one size of phantom for activation and depended on the invariant response of a 54-detector whole-body counter (Cohn *et al* 1969). Three sizes of phantom were used by Williams *et al* (1978); their patients

were then graded into three groups according to body habitus. Two different sizes of phantom were used by Spinks *et al* (1977) and the effects of varying thickness or adding wax around these phantoms were studied by Spinks (1979). The effect of varying the thickness of the trunk and thighs was also studied by McNeill *et al* (1974). Oxby and Brooks (1979) have tackled the problem of varying body dimensions by designing a complex phantom of variable shape and content.

This paper describes the technique used in Edinburgh to measure total body calcium (TBCa) with a high degree of precision and also our methods of overcoming the problems mentioned above. The technique of evaluating whether a subject contains a normal amount of calcium is in two parts. Firstly, corrections to eliminate the effects of variations in activation and detection efficiency due to varying body dimensions are made. This enables the absolute amount of calcium in the subject in grams to be evaluated and requires a variety of phantom measurements. Secondly, the normal predicted total body calcium is calculated using a formula derived from the results of a group of healthy normal volunteers aged 40–70 years. These results were used to obtain a range of normal values of the body elements of interest.

Total body calcium measurements of normal volunteers have also been made by Nelp *et al* (1972), Cohn *et al* (1976), Aloia *et al* (1978), and Chesnut *et al* (1981). Where appropriate, the results of these studies and the data presented in this paper will be compared and discussed.

2. Method

2.1. Neutron activation

The neutron source used for patient activation was a cyclotron producing neutrons of mean energy 6.5 MeV by the reaction of 15 MeV deuterons on a beryllium target (Williams *et al* 1979). During irradiation the subject was positioned in a moderator kiosk made from 3 cm thick polyethylene sheets mounted on a turntable. The thickness of the premoderator was chosen, after preliminary measurements, in order to minimise the variation in the thermal neutron flux through the patient. This was measured using a ^{235}U fission chamber with and without a cadmium shield; in a phantom 24 cm
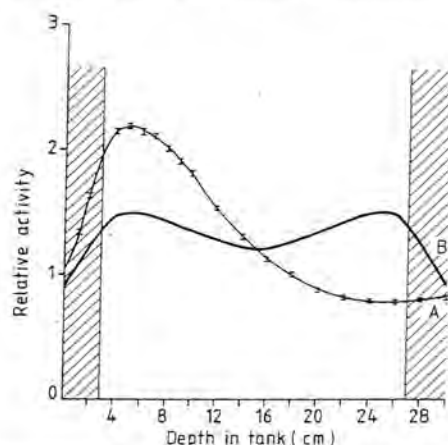

Figure 1. The thermal neutron flux profile through a water tank of depth 30 cm; A, with unilateral irradiation; B, with bilateral irradiation. Using the first and last 3 cm (shaded areas) as premoderator, the profile through a subject 24 cm deep may be observed.
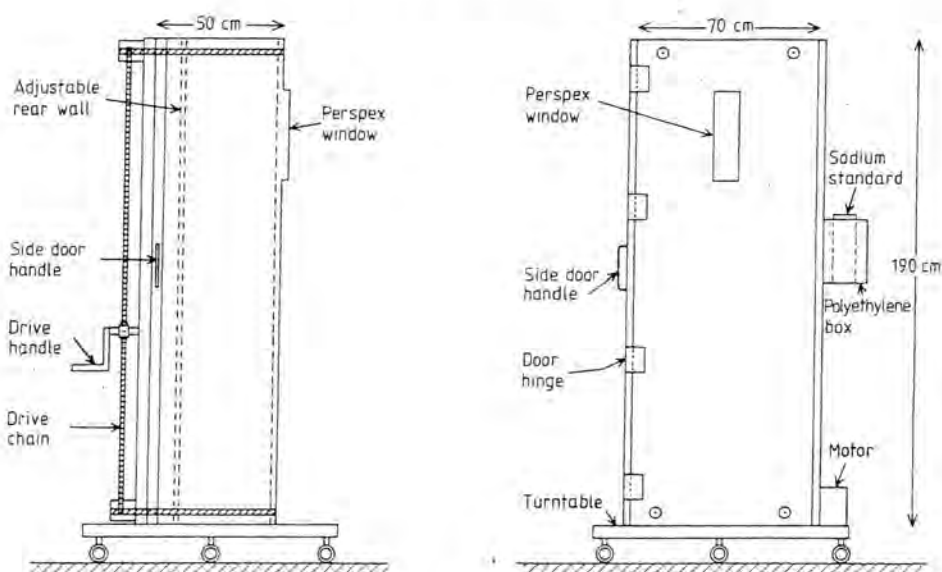
Figure 2. The irradiation enclosure. The rear wall is brought forward until the subject's trunk is in contact with both the front and rear walls. The depth of the perspex window was chosen so that the effect on the thermal neutron profile was equal to that of the 3 cm thick polyethylene walls.

deep this variation was ±7% (figure 1) and in a limb phantom 12.5 cm in diameter the variation was ±13%. The back wall of the kiosk was movable and was adjusted so that the subject's trunk was in contact with both the front and back walls (figure 2). This contact kept the subject in the correct position and gave extra support. The fixed neutron dose was given to the patient in two successive irradiations each lasting about 22 s, with the kiosk rotating through 180° in 18 s after the first irradiation and before the second. These times were checked with a stopwatch and a decay correction applied if necessary. The target to subject distance was 5.4 m.

Using a Geiger–Müller tube sheathed in 3 mm of ^{6}LiF, the photon absorbed dose was measured as 0.4 mGy. The total dose, measured at the position of the pelvis using a tissue-equivalent ionisation chamber, was 1.68 mGy, and was nearly constant with depth through the patient. Using a neutron quality factor of 10 therefore, the total dose equivalent received by the patient was 13.2 mSv. This dose was controlled by the neutron monitor chamber of the beam and the irradiation calibrated by activating simultaneously a container of Na_2CO_3 in a polyethylene jacket mounted on the side of the moderator kiosk. Possible long term variations in the neutron beam distribution were monitored by weekly measurements of the Bush phantom.

2.2. Measurement of induced activity

After irradiation, the patient was transferred to a shadow-shield whole-body counter containing four 15 cm diameter × 10 cm thick sodium iodide detectors, two above and two below the bed, arranged in line across the patient. The separation of the upper and lower counters was 40 cm. Four 200 cm scans at constant speed, each lasting five minutes, were then performed. The scan direction was simply reversed at the end of each scan. The time from the end of the irradiation to the start of the first scan was measured and was usually about 6 min.

The patient spectrum, covering the energy range 0–4 MeV, was recorded on a multichannel analyser. A twenty minute background count, measured using an inactive phantom, was then subtracted from the patient spectrum and the difference was punched out on paper tape for computer analysis.

2.3. Spectral analysis

The data were analysed by fitting five standard spectra, those of calcium, sodium, chlorine, phosphorus and potassium to the smoothed subject spectrum in the energy range 1.0–3.4 MeV, using a least squares technique (Smith *et al* 1976, Smith and Tothill 1979). The standard spectra were obtained by separately filling a phantom of human dimensions with appropriate solutions, activating the phantom and then recording the spectra on the whole-body counter. When the best possible fit to the subject's spectrum had been obtained, the amount of each standard required to make up the spectrum was listed. These amounts were then divided by the count from a twenty minute scan of the Na_2CO_3 standard. The values for each element were then corrected for radioactive decay.

In addition to the major elements of interest, some nuclides are activated which interfere with the measurement of the elements under analysis. The main interfering reaction in the measurement of calcium is the $^{37}Cl(n, p)^{37}S$ reaction, since the ^{37}S produced has a 5.06 min half-life and a gamma-ray energy of 3.1 MeV. The correction applied to the calcium content, obtained by activating chlorine in a water-filled phantom was 3.1% of the chlorine count corrected back to the reference time. By similar methods, the reaction $^{39}K(n, 2n)^{38}K^m$ was found to contribute 0.9% of the total counts in the chlorine region (2.00 to 2.32 MeV) and the $^{24}Mg(n, p)^{24}Na$ reaction contributed 0.8% of the total counts measured in the sodium region (2.57 to 2.92 MeV) when the composition of reference man (IRCP 1975), was assumed. The interferences from the last two reactions were regarded as negligible.

3. Results

3.1. Reproducibility

The reproducibilities of the measurements of calcium, sodium, chlorine and phosphorus were investigated by repeatedly measuring a phantom which consisted of hollow polyethylene sections containing known amounts of the elements of interest (Bush 1946). The water-filled weight of the phantom was 68.5 kg and its height 172 cm. Three separate filling mixtures were used (see table 1) and these mixtures were irradiated 3, 3 and 7 times respectively. In the final mixture, the total amounts

Table 1. Contents of phantoms (in g).

Element	Phantom composition			Reference man (IRCP 23)
	1	2	3	
Calcium	600	802	1009	1000
Sodium	60	70	84	100
Chlorine	50	61	70	95
Phosphorus	455	455	455	780
Potassium	120	120	130	140

of the various elements were similar to those in reference man (IRCP 1975) with the exception of phosphorus where more recent results imply that the quoted content is too high. There was no significant dependence of the counts obtained per gram of element on the ratio of the various elements in the phantom. The reproducibilities (coefficients of variation (CV)) of the measurements of the various elements, obtained from the 13 irradiations of the phantom, using the same dose as given to the patient, were ±1.7% for calcium, ±2.2% for sodium, ±4.3% for chlorine and ±4.3% for phosphorus. The values of the CV for calcium, sodium and chlorine reflect almost entirely the counting statistics for these elements. For a small female with only 500 g of calcium the CV for calcium would increase to about 3.0%. The reproducibility of the measurement of calcium was also investigated by repeatedly measuring a phantom consisting of a human skeleton with approximately 700 g calcium encapsulated in tissue-equivalent rubber. The reproducibility in this case, determined from 10 measurements, was 1.8% for calcium and 2.1% for sodium.

3.2. Measurement corrections

In this section the corrections required to allow for the influence of body habitus on the combined activation and counting efficiency are determined. These corrections are essential for accurately calculating the absolute amount of calcium in the subject.

3.2.1. Effect of height. The thermal neutron fluence at a depth of 5 cm, over an area 185 cm high and 60 cm wide at the subject irradiation position, was uniform to within ±8% with the maximum incident neutron flux around 85 cm above the chamber floor. The effect of varying height was tested by altering the height of the water filled phantom over the range 150 cm to 193 cm by inserting wax spacers between the various sections. The phantom was measured twice at each of five different positions. The range 150 cm to 172 cm was investigated by removing the pelvis section. The results obtained were fitted by the power law:

$$\% \text{ loss of counts} = 0.5 \text{ (subject height} - 1.5)^2 \times 100 \qquad \text{height} > 1.5 \text{ m.}$$

3.2.2. Effect of body build and body fat. The effect of variations in thickness of the subject, measured along the beam direction, was investigated using sections of the solution-filled phantoms of different sizes, but similar heights. Two repeated measurements were made at each of five different thicknesses i.e. 11, 14, 16, 18 and 24 cm. The decrease in measurement efficiency was 1.8% per cm increase in thickness of the chest section and 1.4% per cm increase in diameter of the limb section.

3.2.3. Effect of wall separation. Ideally the front and back premoderator sections of the activation chamber are positioned just to touch the subject's trunk at the front and back. The separation of the walls is dependent, therefore, on the subject's depth measured along the beam direction (figure 2). Due to patient apprehension in some cases this is not possible and the walls are positioned further back than normal. The effect of this extra separation was investigated by repeatedly measuring both the solution-filled and the skeletal phantoms, increasing the wall separation each time up to an air gap of 10 cm. Two repeated measurements were made at each of three different positions. The decrease in activation efficiency was 1.0% per cm increase in the air gap.

3.2.4. Absolute calibration of calcium. Using the results from sections 3.2.1 to 3.2.3, the mass of calcium in the subject in grams was calculated from the equation:

$$\text{TBCa} = \text{measured calcium} \times \text{height correction} \times \text{depth correction}$$
$$\times \text{fat correction} \times \text{wall correction}$$

where

$$\text{height correction} = 0.5 \,(\text{subject height} - 1.50)^2 + 1 \qquad \text{height} > 1.5 \text{ m}$$
$$= 1 \qquad\qquad\qquad\qquad\qquad\qquad \text{height} \leq 1.5 \text{ m}$$

$$\text{depth correction} = 1.6 \,(\text{Subject depth} - \text{TST} - 0.2) + 1$$

$$\text{fat correction} = 3.6 \left(\frac{\text{TST} + \text{LST}}{2} \right) + 1$$

$$\text{wall correction} = 1.0 \,(\text{wall separation} - \text{subject depth}) + 1.$$

All measurements are in metres and TST = mean torso skinfold thickness of subject, i.e. the mean of the subscapula and iliac crest measurements; LST = mean limb skinfold thickness of subject, i.e. the mean of the biceps and triceps measurement; 1.6 = mean fractional loss per m increase in depth; 3.6 = mean fractional loss per m increase in fat; 0.2 = reference depth, i.e. the depth of the trunk section of the solution filled phantom. The depth correction makes the assumption that the depths of the various limbs scale in proportion to the depth of the trunk.

The number of counts obtained per gram of element was checked by repeatedly activating three phantoms of different sizes similar to the Bush phantom but with the calcium and phosphorus contained in solid rods which simulated the human skeleton (Battye *et al* 1971). The results obtained for sodium and chlorine agreed within experimental error. However the calcium was on average 3.1% low and the phosphorus result 11.2% low compared with elements dispersed in solution. This effect might well be explained by the difference in the combined efficiency of activating and detecting the calcium and phosphorus when they are uniformly distributed in the phantom compared with when they are contained in a simulated skeleton. This effect has also been noted by Spinks *et al* (1977). The necessary change was therefore made to the conversion factor for calcium to give counts per gram of the element. The difference between the results of calcium and phosphorus was due to the fact that the latter undergoes a fast neutron reaction.

4. Normalisation procedures

To establish the range of normal values for total body calcium, 40 normal volunteers were measured: twenty males (six aged 40–49, eight aged 50–59 and six aged 60–69) and twenty females (two aged 40–49, ten aged 50–59 and eight aged 60–69). All the subjects were active and in good health. None had any history of disease that might be expected to influence calcium metabolism, and all had normal blood and urine biochemistry. There was a large variation in the total body calcium results for both groups (table 2). The females ranged from 596 to 1036 g with a mean of $821 \pm 15.2\%$ (cv), while the males ranged from 886 to 1428 g with a mean of $1143 \pm 11.7\%$. Since the total body composition of the various elements is clearly related to the subject's build, a mean value based on sex alone is inadequate. Therefore the dependence of the measured TBCa on height, span, weight, lean body mass (calculated from the

Table 2. Data for normal controls.

	Means and percent coefficients of variation	
	Male (CV)	Female (CV)
Number	20	20
Height (m)	1.770 (4.7)	1.622 (4.2)
Span (m)	1.843 (4.7)	1.655 (4.4)
Weight (kg)	81.8 (13.8)	63.7 (17.2)
Calcium (g)	1143 (11.7)	821 (15.1)

skinfold thickness measurement), age and number of years post-menopause was investigated by multiple linear regression analysis.

For males, this gave a formula for predicted total body calcium in grams (TBCa_p),

$$\text{TBCa}_p = 347 \, (\text{height})^{2.07} \qquad (r = 0.84, P < 0.001).$$

Total body calcium was also found to be strongly dependent on span

$$\text{TBCa}_p = 384 \, (\text{span})^{1.80} \qquad (r = 0.74, P < 0.001).$$

Height and span are measured in metres. Perhaps because the spread in age was small no significant dependence of total body calcium on age was observed. Weight and lean body mass also proved to be unimportant. The biological variation in normal TBCa due to size could be reduced by expressing the subjects result in terms of the ratio $\text{TBCa}/\text{TBCa}_p$. When height was used in the formula the CV in the male controls was reduced to 6.2%.

For the female controls, multiple regression gave

$$\text{TBCa}_p = 399 \, (\text{span})^{1.69} \exp(-0.015 \, Y) \qquad (r = 0.90, P < 0.001)$$

where span was measured in metres and Y is the subject's years post-menopause. This gave a highly significant correlation with an annual loss of calcium after the
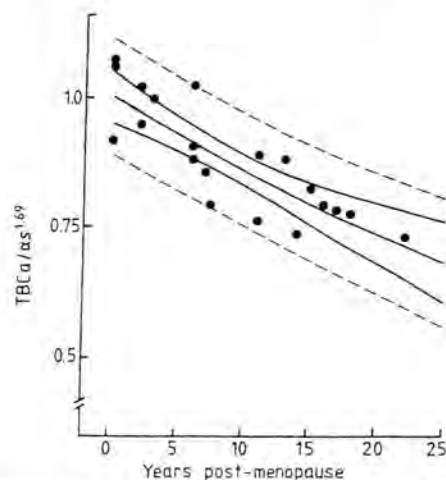
Figure 3. Total body calcium of normal women, normalised using the span (s), plotted against years post-menopause. The line representing a loss of 1.5% per annum is plotted with confidence and tolerance limits. α is a constant $= 399$; ●, normal women; ——, confidence limits, $P = 0.05$; – – –, tolerance limits, $P = 0.10$.

menopause of 1.5% (figure 3). An equally good correlation was obtained if a linear relationship between calcium and years post-menopause was assumed. Total body calcium, for the female controls, was also found to be strongly dependent on height

$$\text{TBCa}_p = 443 \, (\text{height})^{1.57} \exp(0.016 \, Y) \qquad (r = 0.87, P < 0.001).$$

Since total body calcium was more strongly correlated with span than with height and as height may be significantly reduced in patients with osteoporosis, it was decided to use span rather than height as a variable for normalisation for women. The coefficient of variation of total body calcium in normal women $\text{TBCa}/\text{TBCa}_p$, after normalisation improved to 6.6%.

The possibility was investigated that the correction factors, applied to the raw data, described in section 3.2.4 could be replaced with an extra normalisation factor, namely weight. Regression analysis performed on the uncorrected data for the male controls gave a low correlation with height, $r = 0.40$, compared to the corrected data, $r = 0.84$. The introduction of weight as a normalisation factor improved the correlation considerably

$$\text{TBCa}_p^1 = C_M \, (\text{height})^{2.15} \, (\text{weight})^{-0.34} \qquad (r = 0.80)$$

where the superscript indicates that this equation refers to the raw data, uncorrected for the height, build and body fat corrections derived in section 3.2.4.

A similar effect was obtained, using the uncorrected female data, after the introduction of a normalisation factor for weight

$$\text{TBCa}_p^1 = C_F \, (\text{span})^{1.66} \, (\text{weight})^{-0.18} \exp(-0.016 \, Y) \qquad (r = 0.89)$$

where C_M and C_F are constants.

This contrasts with the case of the corrected data, both male and female, where weight proved to be unimportant. Therefore to a large extent the correction factors described in section 3.2.4 and the introduction of weight as a normalisation factor fulfil a similar function. The CV of the $\text{TBCa}^1/\text{TBC}_p^1$ ratio was 7.0% for both men and women. When the ratio is used, the units of TBCa_p^1 can be left as ^{49}Ca counts. However, using the results from the calculations of TBCa_p, the values $C_M = 1447$ and $C_F = 870$ will give TBCa_p^1 in grams of calcium.

5. Discussion

The technique of total body neutron activation analysis presented in this paper with its precision of 1.8% on phantoms is suitable for detecting small changes in total body calcium. The process of correcting for varying body dimensions is most important for the accurate determination of the absolute amount of calcium in the body. When the corrections described in section 3.2.4 were applied to the raw data for our normal male volunteers they increased the estimated body calcium by 16% on average. The importance of such corrections has also been emphasised by Spinks (1979). Using a similar irradiation system, he found correction factors for total thickness and wax layer thickness which were close to ours. McNeill et al (1974) also studied the effect of body thickness on the efficiency of activation and measurements of calcium in the trunk. They found a reduction of calcium counts of 5% cm^{-1}. Their figure was somewhat higher than ours, probably because their Pu–Be sources were a fixed distance apart and fairly close to the subject's skin. Correction for body stature is important not only for absolute calcium determinations, but also for studying changes over a

period if the subject is likely to alter in weight. Some treatments which lead to osteodystrophy, or which are designed to avoid the condition, are liable in themselves to change the amount of fat in the body.

The establishment of a normal range of total body calcium for men and women is vital if full use is to be made of the absolute values. Total body calcium measurements of normal volunteers have been made by Nelp *et al* (1972), Cohn *et al* (1976), Aloia *et al* (1978) and Chesnut *et al* (1981). Partial body (trunk) measurements have been made by Harrison *et al* (1975) and by McNeill and Harrison (1977). The most comprehensive of these studies is that of Cohn *et al* (1976). They derived equations for predicting normal values based on measurements on 79 normal individuals, 48 in the age range covered by this study. Their whole body counter corrects for variations in response due to different body dimensions, but no attempt was made to separate variations in activation efficiency from the biological variations of actual calcium content in the normal population studied.

The equations developed by Cohn *et al* (1976), which incorporate height, age and total body potassium levels, therefore included a consideration of measurement errors, as well as statistical variations. The coefficient of variation of normalised total body calcium was 7.8% for men and 7.1% for women. As a result of the different approach to normalisation and because Cohn *et al* (1976) assumed a uniform age of menopause at 55, our values of total body calcium are not directly comparable with theirs. As in this study, Cohn *et al* (1976) found total body calcium in males to be dependent approximately on height squared. These results are in slight disagreement with the total body calcium study of Nelp *et al* (1972) and the partial body studies (trunk) of Harrison *et al* (1975) who found a near cubic relationship between calcium and height.

The percentage of calcium lost by normal women after the menopause of 1.5% per year from this study is slightly higher than that of 1.1% determined by Cohn *et al* (1976). They also calculated a rate of calcium loss of 0.4% per annum between the ages of 35 and 55. This is probably the combination of a lower (if existent) pre-menopausal bone loss and a higher post-menopausal loss from those normal women who were post-menopausal before the age of 55.

Although multiple regression analysis on our male data gave a mean loss of calcium with age of 0.1% per year, this result was not significantly non-zero. Cohn *et al* (1976) reported a mean annual loss of calcium for the average man of 0.70% after 50 years of age. However it is interesting to note that their result, whch was obtained by omitting their data for men over 80, leads to such a low predicted value of calcium for older men that the majority of their own male subjects aged 67 and over have $TBCa/TBCa_p$ values substantially greater than one.

In section 4 it was shown that the introduction of weight as a normalisation factor applied to the raw data, rather than using the correction factors described in section 3.2.4, implied that total body calcium was dependent partly on $(weight)^{-0.34}$ for males and $(weight)^{-0.18}$ for females. These values are in broad agreement with the exponent determined by Cohn *et al* (1976) of -0.25 (see appendix Cohn *et al* 1976, substituting K_p for K). We obtained no significant dependence on weight after multiple regression analysis was performed on the final data because of the correction factors used in section 3.2.4. For the determination of a narrow normal range of calcium values the use of weight as an extra normalisation factor would appear to be almost as good, and would be simpler than determining and applying the various correction factors for height, body fat and thickness. The success of weight as a normalisation factor presumably depends on its close correlation with body thickness. However the body

correction factors described in section 3.2.4 are important for the accurate determination of the absolute amount of calcium in grams in individuals whose size or shape differs, even by only a few centimetres, from the phantom used for calibration. The values of the correction factors are only applicable to the experimental arrangement used in this study. However if other research groups were able to calculate accurately the absolute amount of calcium in grams in their patients then the equations for $TBCa_p$ derived from our normal controls could be used to calculate the $TBCa/TBCa_p$ ratio.

We believe that the best approach is the one we have adopted, of first trying to establish an accurate measure of whole body calcium, making correction for all the variables likely to affect activation and detection efficiency, and then deriving normalisation factors which take into account variations of calcium with size, age and sex. The narrow ranges for normal subjects that we have observed, with coefficients of variation of 6.2% for men and 6.6% for women, may allow the technique of total body neutron activation analysis of calcium to be a useful diagnostic procedure.

Acknowledgments

Résumé

Analyse par activation neutronique du calcium de corps entier: calibration et normalisation.

Nous avons réalisé un système d'irradiation, utilisant un faisceau de neutrons émis par un cyclotron, qui optimise l'uniformité de l'activation du calcium. L'activité induite est mesurée par un compteur corps entier à balayage 'shadow shield'. Nous avons calibré les mesures et testé leur reproductibilité à partir de trois types différents de fantômes. Nous en avons déduit des corrections pour les variations de la taille du corps, de la profondeur et de l'épaisseur de la graisse. Le coefficient de variation pour les mesures repetées sur un fantôme anthropomorphe est de 1,8% pour une dose absorbée équivalente à 13 mSv (1,3 rem). Nous avons utilisé les mesures du calcium global du corps chez 40 adultes normaux pour déduire les facteurs de normalisation qui prédisent le taux normal du calcium chez un sujet d'âge et de taille donnés. Le coefficient de variation du calcium normalisé est de 6,2% chez l'homme et de 6,6% chez la femme avec une perte annuelle de 1,5% après la ménopause. Cette faible dispersion des valeurs rendrait utile une seule mesure à des fins diagnostiques.

Zusammenfassung

Ganzkörper-Neutronenaktivierungsanalyse von Kalzium: Kalibrierung und Normierung.

Mit Hilfe eines Neutronenstrahls aus einem Zyklotron wurde ein Bestrahlungssystem konstruiert zur Optimierung der Gleichförmigkeit der Kalziumaktivierung. Die induzierte Aktivität wurde in einem Ganzkörperzähler mit Schattenschutz gemessen. Eine Kalibrierung wurde durchgeführt. Die Reproduzierbarkeit wurde mit drei verschiedenen Phantomtypen bestimmt. Korrekturen für Änderungen der Körperhöhe, -tiefe und -dicke wurden abgeleitet. Der Variationskoeffizient für Wiederholungs-Messungen an einem anthropomorphen Phantom betrug 1.8% für eine Äquivalentdosis von 13 mSv (1.3 rem). Messungen des Ganzkörper-Kalziums bei 40 gesunden Erwachsenen wurden benutzt um Normierungsfaktoren

abzuleiten, die den normalen Kalziumgehalt eines Menschen bei vorgegebener Größe und Alter vorhersagen können. Der Variationskoeffizient von normiertem Kalzium var 6.2% bei Männern und 6.6% bei Frauen, mit einem jährlichen Verlust von 1.5% nach der Menopause. Der eingeschränkte Bereich könnte einzelne Messungen für diagnostische Zwecke brauchbar machen.

References

Aloia J F, Cohn S H, Ross P, Vaswani A, Abesamis C, Ellis K and Zanzi I 1978 *Am. J. Physiol.* **235** E82

Battye C K, Knight V, Marxhall T O, Knight A and Godfrey B E 1971 *Nucl. Instrum. Methods* **92** 601

Bush F 1946 *Br. J. Radiol.* **19** 14

Chesnut C H, Lewellen T K and Nelp W B 1981 in *Proc. Int. Symp. on Osteoporosis, Jerusalem, Israel*

Cohn S H 1981 *IAEA At. Energ. Rev.* **18** 599

Cohn S H and Dombrowski C S 1971 *J. Nucl. Med.* **12** 499

Cohn S H, Dombrowski C S, Pate H R and Robertson J S 1969 *Phys. Med. Biol.* **14** 645

Cohn S H, Shukla K K, Dombrowski C S and Fairchild R G 1972 *J. Nucl. Med.* **13** 481

Cohn S H, Vaswani A, Zanzi I, Aloia J F, Roginsky M S and Ellis K J 1976 *Metabolism* **25** 85

Harrison J E, Williams W C, Watts J and McNeill K G 1975 *J. Nucl. Med.* **16** 116

IRCP 23 1975 *Reference Man: Anatomical Physiological and Metabolic Characteristics* Publication No. 23 (Oxford: Pergamon)

McNeill K G and Harrison J E 1977 *J. Nucl. Med.* **18** 1136

McNeill K G, Kostalas H A and Harrison J E 1974 *Int. J. Appl. Radiat. Isot.* **25** 347

Nelp W B, Denny J D, Murano R, Hinn G M, Williams J L, Rudd T G and Palmer H E 1972 *J. Lab. Clin. Med.* **79** 430

Oxby C B and Brooks K 1979 *Phys. Med. Biol.* **24** 440

Smith M A and Tothill P 1979 *Phys. Med. Biol.* **24** 319

Smith M A, Tothill P, Simpson J D, MacPherson J N, Merrick M V, Strong J A and Boddy K 1976 *Californium-252 Radiobiology and Medical Applications*, U.S. Department of Energy Conference 760436 (Springfield, VA: NTIS) p 217

Spinks T J 1979 *Phys. Med. Biol.* **24** 976

Spinks T J, Bewlay D K, Ranicar A S O R and Joplin G F 1977 *J. Radioanal. Chem.* **37** 345

Williams E D, Boddy K, Harvey I and Haywood J K, 1978 *Phys. Med. Biol.* **23** 405

Williams J R, Bonnett D E and Parnell C J 1979 *Br. J. Radiol.* **52** 197

Scientific Note

The crossover correction in dual photon absorptiometry with ^{153}Gd

M A Smith and P Tothill

Department of Medical Physics and Medical Engineering, Royal Infirmary, Edinburgh, Scotland

1. Introduction

The measurement of the bone mineral content (BMC) by single photon absorptiometry has long been an established technique for the forearm. However, in the study of bone disease, the part-body site of most clinical interest is the lumbar spine. Recently, efforts have been made to measure the BMC using dual photon absorptiometry (DPA), the second photon energy being used essentially to correct for varying amounts of soft tissue within the trunk. The energy combinations that have been used are ^{241}Am and ^{137}Cs with energies at 60 keV and 660 keV and ^{153}Gd with energies at 44 keV and 100 keV, the latter being generally considered the most suitable energy combination for measurements of the spine.

Although reasonable figures of 2–3% for the precision (or reproducibility) have been obtained by the various methods, there is a degree of disagreement about the absolute measurements of BMC. This is particularly the case with cross-sectional data on normal volunteers, i.e. single BMC measurements on subjects of different ages. Two groups (Madsen 1977, Riggs *et al* 1981) have reported no increase in the rate of loss of BMC from the spine at the time of the menopause. The expected increase in the rate of loss after the menopause, as shown using total body neutron activation analysis (Cohn *et al* 1976, Smith *et al* 1980) and forearm absorptiometry (Mazess and Cameron 1974) has, however, been shown in the spine by two other groups (Krølner and Pors Nielsen 1980, Smith *et al* 1981) in cross-sectional studies and also in a longitudinal study (Krølner and Pors Nielsen 1981), where the bone loss was determined from repeated measurements on individual subjects over a period of time. It is not known whether this discrepancy between the various methods is due to differences in methodology or in the populations studied. Before accepting the latter the possibility of the former must be thoroughly investigated.

All but two of the methods of DPA (Roos 1974, Condon *et al* 1979) which have been used for patient or normal volunteer studies have used ^{153}Gd as the radionuclide source. Obviously there are several factors that influence the accuracy of the technique. This note considers one aspect of the methodology of DPA which is specifically important when using ^{153}Gd and which will affect the absolute determination of BMC. This is the contribution to the 44 keV energy window from the 100 keV energy caused by Compton events within the crystal and scatter within the patients. This will be referred to as the 'crossover correction' (XO) and is expressed as a percentage of the 100 keV photopeak.

2. Gadolinium-153

The radionuclide source [153]Gd has a half-life of 242 days with gamma-ray energies (plus approximate abundance) of 103 keV (23%), 97 keV (31%) and 70 keV (2.6%) and Eu K x-rays with energies 41 keV (86%) and 47 keV (23%). The peaks at 103 keV and 97 keV and at 41 keV and 47 keV cannot be resolved by NaI detectors and so are considered as 100 keV and 44 keV peaks respectively. The ratio of the 44 keV peak to the 100 keV peak is approximately 2:1 though this falls to about 1.4:1 from an encapsulated sealed source measured by a Ge(Li) detector, due mainly to the stainless steel window specified as 0.2–0.25 mm for our source, and to 1.1:1 from the same source measured by a 10 cm diameter, 5 cm thick NaI detector, additional attenuation arising in the crystal housing. The measurements described in this paper were performed using a 12 mm diameter sealed [153]Gd source (ref no X.92/1, Amersham 1978) of approximate activity 4 GBq, spectra of which are shown in figure 1.
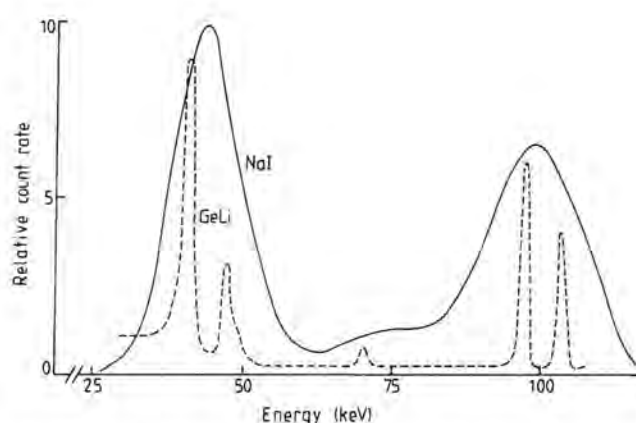
Figure 1. [153]Gd spectra measured by a NaI detector and by a GeLi detector.

3. Bone mineral calculation

The basic equations for calculating the BMC from two photon energies are quoted elsewhere (Roos and Sköldborn 1974) but can be simplified to

$$\text{BMC} \propto \ln(I_{100}) - \frac{\mu_{ST,\,100}}{\mu_{ST,\,44}} \ln(I_{44})$$

where I is the count rate of 100 keV or 44 keV radiation, μ_{ST} is the attenuation coefficients through soft tissue at 100 keV or 44 keV, and I_{44} is (measured count rate in 44 keV region) $-$ (XO/100) $\times I_{100}$ with XO the crossover correction (per cent).

The two criteria for accurate measurements of BMC by the technique of DPA using the above equation are that (i) the BMC must be independent of the thickness of soft tissue and (ii) the measured BMC must be proportional to the actual BMC. The XO will affect both the estimate of I_{44} and $\mu_{ST,\,44}$ in the above equation. The mean supine

anterior to posterior thickness (with range) at the lumbar region in 180 normal subjects and patients was found to be 22 cm (15–29 cm) in men and 19.8 cm (15–29 cm) in women. Criterion (i) must be verified over an appropriate range of soft tissue thicknesses. For criterion (ii) to be fulfilled the basic assumption that both 44 keV and 100 keV radiation have exponential attenuation in bone and soft tissue must be true. In particular the attenuation of the corrected 44 keV radiation through bone mineral or a similar material such as aluminium must be exponential.

4. Crossover correction

Experiments to investigate the xo were performed using a 13 mm diameter source collimator and a 20 mm square detector collimator with a separation between the two of 0.4 m. This collimation, which we have used for spine BMC measurements (Smith *et al* 1981), is slightly larger than that used by Wilson and Madsen (1977) and smaller than that used by Peppler and Mazess (1981). Some experiments were also performed using 6 mm diameter source and detector collimators, the size used by Riggs *et al* (1981) and smaller than that used by Krølner and Pors Nielsen (1980). The NaI detector used was 10 cm diameter, 5 cm thick, with an energy resolution of 20–25% over the energy range used.

The standard method adopted in the past to calculate the xo has been to use copper to filter out the 44 keV peak at the source collimator. This method was used with a 3.3 mm Cu filter and energy windows from 27–61 keV and 83–121 keV. Using the larger collimation the xo was found to vary with the thickness of soft tissue equivalent material (STEM) (figure 2) but the two criteria mentioned previously were
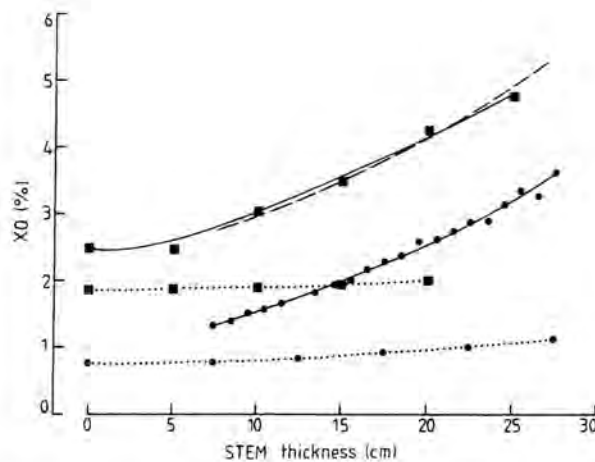

Figure 2. Variation in the xo with different thicknesses of STEM measured using: ●—● the standard Cu filter technique, 13 mm source and 20 mm detector collimators; ● · · · ● Cu filter, 6 mm source and detector collimators; ■—■ simulated spectrum with U and Hg, 13 mm and 20 mm collimators; ■ · · · ■ simulated spectrum, 6 mm collimators; —— using Cu filter multiplied by ratio of portions between the peaks, 13 mm and 20 mm collimators.

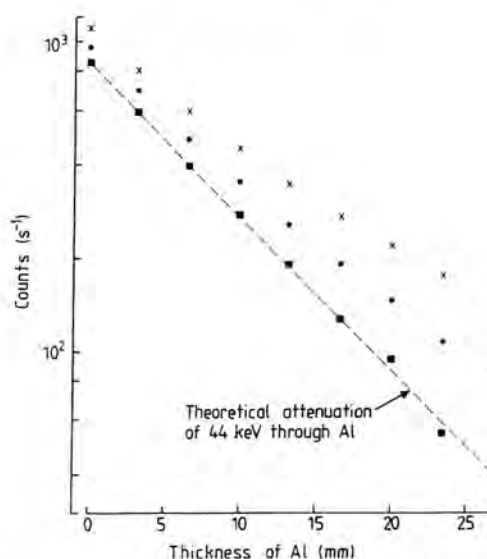not fulfilled (figure 3) due to an apparent underestimation of the xo. The possible reasons were investigated.

M A Smith and P Tothill

Figure 3. Attenuation of 44 keV radiation using 13 mm source and 20 mm detector collimators through Al within 20 cm STEM; ×, uncorrected; ●, corrected using XO from the standard Cu filter technique; ■, corrected using new XO values. The theoretical attenuation was calculated assuming narrow beam attenuation (McMaster *et al* 1969).

The error due to background may be negligible when measuring the BMC but becomes significant when calculating the XO values. More important than the room background were the Compton scatter contributions from [152]Eu contamination in the [153]Gd source. Lead 4 mm thick was used to filter out the [153]Gd to assess the contribution from the higher energy peaks of [152]Eu to the 44 keV and 100 keV channels. The variation in background, including [152]Eu, with thickness of STEM was
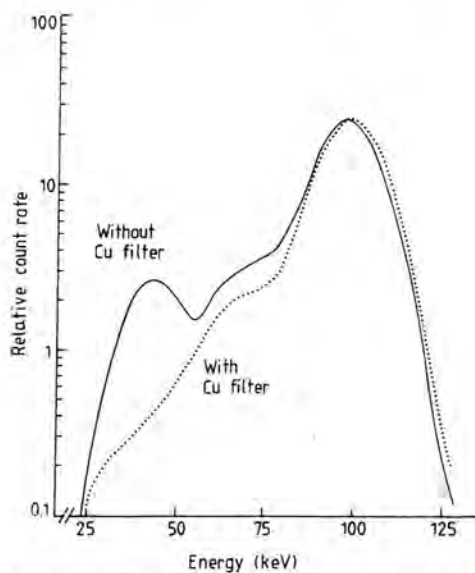
Figure 4. Spectra of [153]Gd through 10 mm Al and 20 cm STEM with and without 3.3 mm Cu filter.

measured and used to correct subsequent data. No corrections were ever required for counting losses.

The ^{153}Gd spectrum with STEM and aluminium in place to simulate the transmission through the lumbar spine was compared with the spectrum of the same arrangement with the Cu filter, both spectra having the same number of counts in the 100 keV channel (figure 4). It can be seen that the filtered ^{153}Gd spectrum appears to underestimate the contribution to the 44 keV channel. It seemed likely that the low abundance 70 keV peak in the ^{153}Gd spectrum contributes appreciably to the lower energy channel, but is severely attenuated by the copper used to eliminate the 44 keV radiation.

The possibility was investigated by using monoenergetic x-rays to simulate the upper portion of the ^{153}Gd spectrum. Between 4 and 70 GBq of ^{99}Tc^{m}, absorbed onto ion exchange resin, was used to produce the characteristic 70 keV and 100 keV x-rays from mercury and uranium respectively (figure 5). The Hg and U were placed
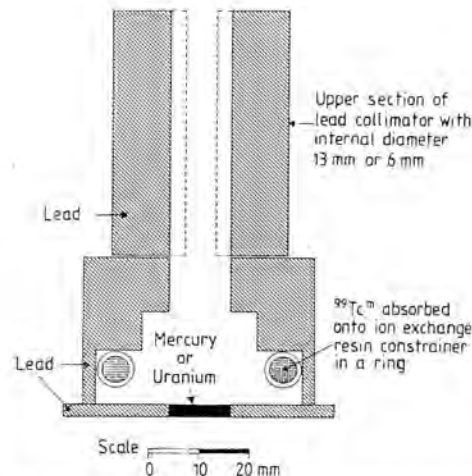
Figure 5. Vertical section through the circular source collimation used for measurements with the characteristic x-rays from mercury and uranium.

separately with the ^{99}Tc^{m} in the position of the ^{153}Gd source so that the geometry remained the same. The counts in the 44 keV region were expressed as a percentage of the counts in the respective photopeaks. The proportion of the 70 keV peak compared with the 100 keV peak from the ^{153}Gd source in air was 4.6% as measured by a Ge(Li) detector. This value combined with the relative attenuations of the 70 keV and 100 keV Hg and U peaks through STEM enabled the xo contribution from the 70 keV ^{153}Gd peak to be expressed as a percentage of the 100 keV peak. The results are shown in table 1 and the total xo value plotted in figure 2.

It was found empirically that if the xo derived from the use of the copper filter was multiplied by the ratio of the portions of the two spectra in figure 4 between the peaks (60–85 keV) the two criteria required in the calculation of bone mineral were fulfilled. The values of the xo calculated in this way for the 13 mm source and 20 mm detector collimation are shown in figure 2 for various thicknesses of STEM.

It can be seen that both the new methods of calculating the xo give the same result (figure 2). When these xo values were used for measurements on 10 mm Al in depths of water ranging from 8 cm to 27 cm no variation in the apparent mineral

Table 1. XO values for 44 keV region using Hg and U to simulate the upper part of the [153]Gd spectrum with 13 mm source and 20 mm detector collimators.

	Thickness of STEM (cm)					
	0	5	10	15	20	25
Using U. Percentage of 100 keV photopeak	2.0	1.9	2.3	2.5	3.1	3.4
Using Hg. Percentage of 70 keV photopeak	13.2	13.5	16.6	20.6	25.0	27.2
Combined U and Hg to simulate [153]Gd. Percentage of 100 keV photopeak	2.5	2.5	3.1	3.5	4.3	4.7

content was found. In addition the attenuation of the corrected counts in the 44 keV channel through Al in 20 cm scattering medium was exponential (figure 3).

5. Discussion

The importance of the correct calculation of the XO value for absolute measurements of spine BMC should not be underestimated. Although the actual percentage value may seem low, a XO value of only 3% would reduce the counts in the 44 keV region by 19% in a subject of average thickness (22 cm) and average bone density, and by 25% in a subject of thickness 27 cm (approximate normal mean + 2SD) and high bone density (approximate normal mean + 2SD). In a subject 22 cm thick the use of a XO value of 2.8%, obtained using the standard Cu filter technique, rather than the true value of 4.4%, will produce an error of 15% in the BMC measurement of a normal subject.

The XO values quoted vary considerably. Mazess *et al* (1974) quote 1.9%, Wilson and Madsen (1977) 3.0%, Wahner and Dunn (1980) 6.0% and Riggs *et al* (1981) 4-6% depending on the source. The commercial apparatus used by Krølner and Pors Nielsen (1980) has a XO of 'about 1%' (personal communication). Only Peppler and Mazess (1980) mention that XO varies with depth, 1.8% at 14 cm and 3.4% at 25 cm; Wilson and Madsen (1976) specifically state that it does not. Although, as we have shown, the XO will depend on the size of the beam, the variation in XO values quoted by different authors cannot be attributed to variations in collimator size and should not depend on the source. It has been suggested that 'beam hardening' could account for any deviation from an exponential by the 44 keV radiation (Krølner and Pors Nielsen 1980). We would suggest that an underestimation of the XO value could be the true cause. Similarly the non-linear relationship between measured BMC and actual BMC which sometimes has to be corrected for (Krølner and Pors Nielsen 1980) is due to the same effect.

The underestimation of the XO is due to the significant contribution from the small 70 keV [153]Gd peak which may be completely filtered out by Cu. This photopeak will produce an iodine escape peak at 40 keV. Thus, for example, in a 20 cm thick patient 70% of the total XO is due to the 100 keV peak and 30% due to the 70 keV peak.

The XO has been shown to vary with the thickness of the patient though when small collimation is used this variation is small. If, as is often the case, larger collimators need to be used to achieve acceptable count rates then a XO value appropriate for the patient's thickness must be used. The previous standard method of using Cu to filter the lower energy channel has been shown to be inadequate. It is suggested that

the true XO should be calculated by simulating the 100 keV and 70 keV peaks of the ^{153}Gd spectrum over a range of STEM from 12 cm to 28 cm.

Acknowledgments

References

Amersham Radiation Sources Catalogue 1978 p 441

Cohn S H, Vaswani A, Zanzi I and Ellis K J 1976 *Am. J. Physiol.* **230** 143

Condon B, Tothill P and Smith M A 1979 *Calcif. Tissue Int.* **27** s 29

Krølner B and Pors Nielsen S 1980 *Scand. J. Clin. Lab. Invest.* **40** 653

——1981 *Calcif. Tissue Int.* **33** s 171

Madsen M 1977 *Invest. Radiol.* **12** 185

Mazess R B and Cameron J R 1974 in *Proc. Int. Conf. Bone Mineral Meas.* NIH75-683228

Mazess R B, Wilson C R, Hanson J, Kan W, Madsen M, Pelc N and Witt R 1974 in *Proc. Symp. on Bone Mineral Determination, Aktiebolaget Atomenergi, Stockholm-Studsvik* **2** 40

McMaster W H, Kerr Del Grande N, Mallet J H and Hubbell J H 1969 *University of California Radiation Laboratory Report* UCRL-50174 SecII 53

Peppler W W and Mazess R B 1981 *Calcif. Tissue Int.* **33** 353

Riggs B L, Wahner H W, Dunn W L, Mazess R B, Offord K P and Melton L S 1981 *J. Clin. Invest.* **67** 328

Roos B 1974 *PhD Thesis* University of Gothenburg

Roos B O and Sköldborn H 1974 *Acta Radiol. Ther. Phys. Biol.* **13** 266

Smith M A, Kennedy N S J, Eastell R, Simpson J D, Strong J A and Tothill P 1980 *Nucl. Med. Commun.* **1** 166

Smith M A, Sutton D, Hannan J, Tothill P and Wilson J 1981 in *Proc. Symp. on Osteoporosis, Jerusalem* in press

Wahner H W and Dunn W L 1980 *Nucl. Med. Commun.* **1** 211

Wilson C R and Madsen M 1977 *Invest. Radiol.* **12** 180

Bone demineralisation in patients with Turner's syndrome

M A SMITH,* J WILSON,† AND W H PRICE†

*From *the Department of Medical Physics and Medical Engineering, The Royal Infirmary, Edinburgh, and
†MRC Clinical and Population Cytogenetics Unit and University Department of Medicine,
Western General Hospital, Edinburgh*

SUMMARY The hypothesis that the demineralisation associated with gonadal dysgenesis is analogous to post-menopausal osteoporosis was investigated. Bone mineral content of the distal forearm was measured in 11 adult patients with Turner's syndrome aged 18 to 57 years. As a group these patients were significantly demineralised ($p < 0.001$) when compared with normal subjects. A bimodal distribution of bone mineral was demonstrated, the eight patients below the normal range having a bone mineral content 73% of normal. This may be the usual bone mineral content for a large proportion of Turner's patients. No steady reduction in mineralisation with age was demonstrated. The number of osteoporotic type fractures was obtained from the records of 36 adult patients with Turner's syndrome. From the cumulative total years at risk (770 patient years) from the age of 15 years, it was found that the number of fractures of the distal radius corresponded to the normal premenopausal rather than post-menopausal fracture incidence. The absence of any reduction in bone mineral content with age and no clear evidence of an increase in frequency of fractures both suggest that the demineralisation associated with Turner's syndrome is not analogous to post-menopausal osteoporosis. The regular use of long term oestrogen therapy as a treatment for 'osteoporosis' in these patients is therefore not justified.

Qualitative assessment of skeletal radiographs from patients with Turner's syndrome has demonstrated that in this condition osteoporosis occurs with a frequency of between 60 and 80%.[1–4] In affected children bone histology has shown increased bone resorption with normal bone formation,[5] while radiographs of the second metacarpals show reduced total diameters and increased medullary diameters.[2 6]

The degree of demineralisation owing to osteoporosis can be assessed quantitatively using the technique of photon absorptiometry. The linear density of bone is obtained from the degree of attenuation of radiation from a monoenergetic radionuclide source.[7] This technique has been used to demonstrate demineralisation of the radius and os calcis in children and young adults.[5 8]

Oestrogen inhibits bone resorption in osteoporosis[9] and has been advocated for the treatment of post-menopausal osteoporosis.[10] The rationale behind this treatment is the prevention of the normal loss of bone mineral of about 1% per annum,[11] thus reducing the likelihood of debilitating fractures in later life. There are, however, disadvantages since

there is evidence that when it is terminated the mineral content falls to the level at which it would have been had no treatment been given.[12] Thus, to achieve a long term benefit, oestrogen therapy may have to be continuous. Other disadvantages include associated side effects such as increased incidences of abnormal uterine bleeding and endometrial carcinoma.[13–16]

The treatment of osteoporosis in patients with Turner's syndrome might depend on whether osteoporosis associated with gonadal dysgenesis is analogous to post-menopausal osteoporosis in normal women. If it is, there should be a steady decrease in bone mineral after the age of about 15 years combined with a raised incidence of fractures. In these circumstances long term oestrogen therapy would be indicated.

The present study was undertaken to investigate the bone mineral content (BMC) in adult patients with Turner's syndrome, and to assess the severity and age relationship of any deficit in bone mineralisation. The incidence of osteoporotic fractures has also been examined and compared with the incidence in the general population.

Patients and methods

The bone mineral content was studied in 11 adult patients with Turner's syndrome over a wide age range (18 to 57 years). These were available patients with Turner's syndrome in the south-east of Scotland who were over the age of 18 years and who had been registered with the MRC Cytogenetics Unit. They had all given informed consent to the investigation. Their mean height was 140·8 cm. Other details of the patients are given in table 1. For comparison we studied a group of 16 healthy premenopausal women of presumed normal karyotype aged 18 to 44 years. Within the group of 16 there was a subgroup of 11 short women with a mean height of 154·0 cm whose BMC measurements were used to establish the normal range. The remaining five were significantly taller with a mean height of 169·1 cm, and their BMC measurements were used to determine the effect of a height difference of 15 cm.

The BMC of the non-dominant forearm was measured by photon absorptiometry using a commercial 'Novo Osteodensitometer' which had a reproducibility of 1·4%.[17] The source and detector scan the forearm in a rectilinear motion from the distal end. The BMC is measured for each traverse, but is only stored once the gap between the radius and ulna exceeds 6 mm. A further five scans, 4 mm apart, are performed and the total BMC of the radius and ulna are recorded. The width of the radius and the ulna on the third and sixth traverse were measured from a chart recorder output and their sum total (W) used as a normalisation factor.

The medical records of the 11 patients with Turner's syndrome and of 25 others with the same diagnosis were examined. Their mean age was 36·4±8·4 years (±SD). The number of fractures since the age of 15 years of the type associated with osteoporosis, that is, of the distal radius and of the neck of the femur, was noted and compared with figures for a normal Scottish population.[18] The cumulative total years at risk in the group of 36 patients with Turner's syndrome was 770 patient years.

Results

The results of BMC measurements are displayed in fig 1. For three patients with Turner's syndrome they were within the normal range and for eight they were significantly low (five patients $p < 0.05$, three patients $p < 0.01$). The mean for the group of patients with Turner's syndrome was 2.31 ± 0.44 (arbitrary units ±SD) which is significantly lower ($p < 0.01$) than for the group of normal subjects, whose mean was 2.85 ± 0.27. The results of the group of taller normals (mean BMC = 2·94) demonstrated that a height difference of 15 cm did not significantly affect the normalised BMC values. It can be seen in fig 1 that the eight patients with values outside the normal range are perhaps a subgroup in themselves with a mean value of 2.07 ± 0.15 which is 73% of normal. Indeed, the three patients (CM, SG, MS) in the normal range were found to be biochemically hypothyroid, a condition which may be expected to increase bone mineral. One of these three patients (SG aged 36) was still menstruating spontaneously.
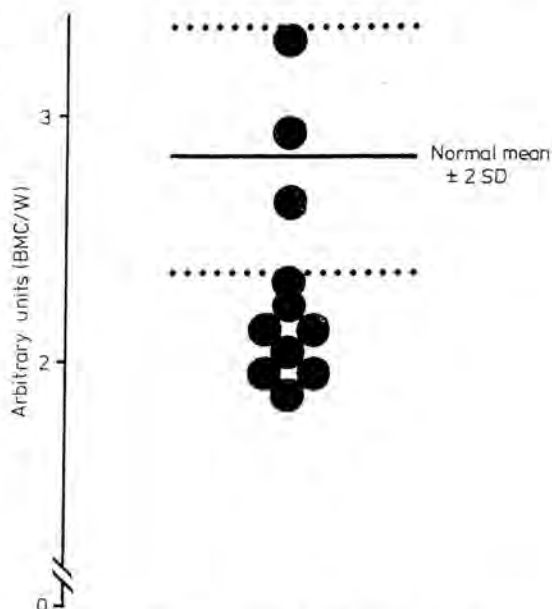
The values of BMC are plotted against age in

TABLE 1 *Details of patients with Turner's syndrome on whom the BMC of the distal forearm was measured*

Patient	Age	Karyotype	Oestrogen therapy
ES	18	45,X/46,Xi(Xq)	1978–
JC	26	45,X/46,XY	Never
CM	26	45,X	Never
MV	27	45,X	1972–1973
IC	35	45,X	1965–1977
SG	36	45,X/46,XY	1964–1965
HB	39	46,Xi(Xq)	1974–
MS	42	45,X	1956–1967
FS	47	45,X	1956–1961
ML	45	45,X	Irregularly until 1977
HS	57	45,X	Never

FIG 1 *BMC values in patients with Turner's syndrome compared with the normal range. Note the narrow spread in BMC values of patients below the normal range.*
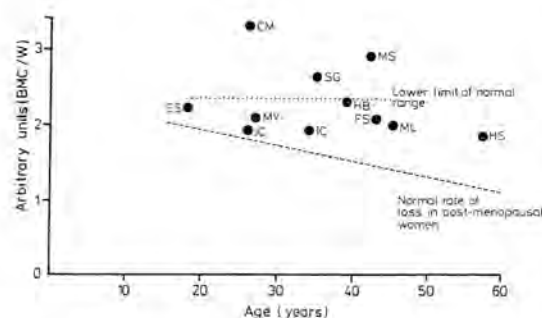
FIG 2 *BMC values in patients with Turner's syndrome plotted against age. The normal rate of loss in post-menopausal women is shown.*

TABLE 2 *Comparison of all quantitative studies of BMC in Turner's patients. Note the close agreement in the results of the three studies.*

BMC site	No of patients	Age range (yr)	No significantly demineralised	Mean BMC of demineralised patients (% of normal)	
Radius	8	9–19	6	71%	Brown et al[5]
Os calcis	6	17–28	3	72%	Risch et al[8]
Distal forearm	11	18–57	8	73%	Present study

fig 2. No significant correlation was found whether or not patients CM, SG, and MS were included in the analysis. It is apparent from fig 2 that there is no reduction in mineralisation with age as has been found in normal post-menopausal women. The dotted line in fig 2 corresponds to a loss of 1% per annum, the value obtained by BMC in post-menopausal women,[11] starting at the age of 15 years and with the BMC equal to the value for the sub-group of eight patients with reduced mineralisation.

There were only two osteoporotic type fractures in the group of 36 Turner patients. One patient had fractured the neck of the femur aged 32 years, and the other the distal radius aged 35 years. The incidence of fractures of the distal radius in the normal population is 0·55% per annum and 0·15% per annum for post-menopausal and premenopausal women, respectively.[18] Applying these values to the accumulated Turner patient years at risk, the expected number of fractures of the distal radius would be four at the post-menopausal fracture rate and one at the premenopausal rate. Similar analysis of neck of femur fractures could not be performed because the number of fractures based on the normal incidences was less than one for both pre- and post-menopausal periods. The patient with a fracture of the lower end of the radius (MS) had a normal BMC.

Discussion

The results are in good agreement with those obtained in another two studies of bone mineral content in Turner's syndrome.[5 8] In both these studies the mean BMC was significantly reduced and in both the values fell into two clear groups, those in the normal range and those which were distinctly low. All three studies therefore suggest a bimodal distribution with the mean for the lower

values being in close agreement in the three studies (table 2). This suggests that this may be the usual bone mineral content for the larger proportion of Turner patients. The proportion of patients with low values (73%) also agrees with the prevalence of 'osteoporosis' found radiologically.[1–4] The BMC values of the patients bore little or no relationship to whether oestrogen therapy had been administered previously (table 1). This was not surprising as it is known that any gain in bone mineral because of oestrogen therapy disappears once treatment is stopped,[12] and only two of the patients in this present study are currently receiving oestrogen (ES and HB). The values for both these patients are at the upper end of the range for the sub-group with low BMC values.

The failure to demonstrate a reduction in bone mineral content with age (fig 2) in this study is substantiated by measurements of metacarpal cortical thicknesses in 22 patients aged 18 to 56 years.[2] No reduction in cortical thickness in the older patients was observed although it was not commented on in the paper. This is contrary to the findings in post-menopausal women in whom there is a progressive reduction in BMC with age. If BMC had been reduced by 1% per annum in the patients with Turner's syndrome we would have expected to see it even with the relatively small numbers studied.

It had not been our clinical impression that the fracture rate in Turner patients was noticeably different from normal subjects of similar age. Unfortunately, it is not possible to draw firm conclusions from the analysis of fractures in this study because of the small numbers. However, the incidence of fractures of the distal radius does appear to be lower than the incidence in post-menopausal women and is comparable, in fact, to the incidence in women of similar age. A lower than expected fracture rate was also noted by Preger et al[2] in a group of over 50 Turner patients.

In conclusion, this study quantifies the bone mineral content in patients with Turner's syndrome. The absence of any reduction in BMC with age and no clear evidence of an increase in frequency of fractures both suggest that if osteoporosis is a

complication of Turner's syndrome it should not be
thought analogous to the osteoporosis that occurs in
post-menopausal women. It would not, therefore,
be possible to justify the regular use of long term
oestrogen therapy in patients with Turner's syndrome
on the grounds of 'osteoporosis'.

References

1 Finby N, Archibald RM. Skeletal abnormalities associated with gonadal dysgenesis. *AJR* 1963;**89**:1222–35.
2 Preger L, Steinbach HL, Moskowitz P, Scully AL, Goldberg MB. Roentgenographic abnormalities in phenotypic females with gonadal dysgenesis. *AJR* 1968;**104**:899–910.
3 Müller G, Gschwend N. Endokrine störungen und morbus Scheuermann. *Arch Orthop Unfallchir* 1969;**65**:357–62.
4 Beals RK. Orthopaedic aspects of the XO (Turner's syndrome). *Clin Orthop* 1973;**97**:19–30.
5 Brown DM, Jowsey J, Bradford DS. Osteoporosis in ovarian dysgenesis. *J Pediatr* 1974;**84**:816–20.
6 Garn SM, Poznanski AK, Nagy JM. Bone measurement in the differential diagnosis of osteoporosis and osteopenia. *Radiology* 1971;**100**:509–18.
7 Cameron JR, Sorenson J. Measurement of bone mineral in vivo: an improved method. *Science* 1963;**142**:230–2.
8 Risch WD, Banzer DH, Moltz L, Schneider U, Rudloff R. Bone mineral content in patients with gonadal dysfunction. *AJR* 1976;**126**:1302.
9 Riggs BL, Jowsey J, Kelly PJ, Jones JD, Maher FT. Effect of sex hormones on bone in primary osteoporosis. *J Clin Invest* 1969;**48**:1065–72.
10 Nordin BEC, Horsman A, Crilly RG, Marshall DH, Simpson M. Treatment of spinal osteoporosis in post-menopausal women. *Br Med J* 1980;**i**:451–4.
11 Mazess RB, Cameron JR. Bone mineral content in normal US whites. *International Conference on Bone Mineral Measurement* (NIH) 75-683, 1974:228–38.
12 Lindsay R, Hart DM, MacLean A, Clark AC, Kraszewski A, Garwood J. Bone response to termination of oestrogen treatment. *Lancet* 1978;**i**:1325–7.
13 Quint BC. Changing patterns in endometrial adenocarcinoma. *Am J Obstet Gynecol* 1975;**122**:498–501.
14 Smith DC, Prentice R, Thompson DJ, Herman WL. Association of exogenous estrogen and endometrial carcinoma. *N Engl J Med* 1975;**293**:1164.
15 Zeil HK, Finkle WD. Increased risk of endometrial carcinoma among users of conjugated estrogens. *N Engl J Med* 1975;**293**:1167.
16 Hammond CB, Jelovsek FR, Lee KL, Creasman WT, Parker RT. Effects of long-term estrogen replacement therapy. *Am J Obstet Gynecol* 1979;**133**:525–36.
17 Christiansen C, Rodbro P. Long-term reproducibility of bone mineral content measurements. *Scand J Clin Lab Invest* 1977;**37**:321–3.
18 Knowelden J, Buhr AJ, Dunbar O. Incidence of fractures in persons over 35 years of age. *Br J Prev Soc Med* 1964;**18**:130–41.

Total body calcium in rheumatoid arthritis: effects of disease activity and corticosteroid treatment

D M REID, N S J KENNEDY, M A SMITH,
P TOTHILL, G NUKI

Abstract

Rheumatoid arthritis may be associated with generalised as well as periarticular osteoporosis. To assess the extent of bone loss and the influence of corticosteroid treatment total body calcium was measured by in-vivo neutron activation analysis in 63 patients with rheumatoid arthritis treated with non-steroidal anti-inflammatory drugs alone and 31 treated with additional low-dose corticosteroids. The results were compared with those in 40 normal controls matched for age, sex, and menopausal state. There were significant reductions in mean total body calcium in the group treated with non-steroidal anti-inflammatory drugs (5·3% in men; 6·8% in women) and greater reductions in the corticosteroid-treated patients (11·5% in men, 15·5% in women). The reduction was correlated with disease duration and activity in the patients treated with non-steroidal anti-inflammatory drugs alone. Measured total body calcium was signifi-

Rheumatic Diseases Unit, Northern General Hospital, and Department of Medicine, Western General Hospital, University of Edinburgh

D M REID, MB, MRCP, lecturer
G NUKI, MB, FRCP, professor

Department of Medical Physics and Medical Engineering, Western General Hospital and Royal Infirmary of Edinburgh, University of Edinburgh

N S J KENNEDY, PHD, physicist
M A SMITH, MSC, PHD, senior physicist
P TOTHILL, PHD, FINSTPHYS, reader

cantly less than the values predicted when this relation was used in the corticosteroid-treated patients. The data suggest that increased bone loss in patients with rheumatoid arthritis treated with corticosteroids is attributable to drug treatment rather than disease activity.

Many patients with rheumatoid arthritis treated with low-dosage corticosteroids and some postmenopausal women with the disease are likely to be at risk from the complications of osteoporosis.

Introduction

Rheumatoid arthritis is thought to be associated with generalised[1][2] as well as periarticular osteoporosis, but considerable uncertainty exists regarding the extent of bone loss and its relation to the duration of disease, disease activity, and additional corticosteroid treatment. Most previous studies of osteoporosis in rheumatoid arthritis have used radiological or photon absorptiometric methods.[2] These techniques have the disadvantage of using single bone sites and may be particularly misleading in a disease associated with severe and variable localised periarticular osteoporosis. The only accurate method of measuring total bone mass in vivo is to measure total body calcium using neutron activation analysis.[3] To assess bone mass in rheumatoid arthritis and its relation to duration of disease, disease activity, and drug treatment we measured total body calcium in sizable groups of patients treated with non-steroidal anti-inflammatory drugs alone and with additional corticosteroids and compared the results with those obtained in controls matched for age, sex, and menopausal state.

Subjects and methods

We measured total body calcium in 63 patients (29 men, 34 women) with definite or classical rheumatoid arthritis[4] treated with non-steroidal anti-inflammatory agents alone and in 31 patients (nine men, 22 women) who were receiving in addition low-dosage corticosteroids (<10 mg prednisolone/day) (see table). The results were compared with those from 40 normal control subjects (20 men, 20 women).[5] Serum calcium, phosphate, and protein concentrations and alkaline phosphatase activity were measured in all subjects, and those with abnormalities of calcium metabolism or medical conditions associated with secondary osteoporosis were excluded.

Total body calcium was measured by in-vivo neutron activation analysis. Patients were irradiated for 20 seconds from front and back, while standing in a rigid polyethylene activation enclosure, using

neutrons from the Edinburgh MRC cyclotron. They were then transferred to a shadow shield whole-body counter, where the gamma radiation from calcium-49 induced from stable calcium-48 by neutron capture was measured for 20 minutes. The patient's total body calcium (in grams) was calculated by comparison with the energy spectrum from an activated anthropomorphic phantom containing a known quantity of calcium. Repeated measurements of the phantom gave a long-term precision of 1·8% for a radiation dose of 13 mSv (1·3 rem). Mean total body calcium (± 1 SD) in the control population was 1142·7 $\pm$ 133·8 g in men and 820·5 $\pm$ 124·5 g in women. Individual results were expressed as a percentage of the expected normal value for the patient's skeletal size (arm span) and menopausal state. The spread in the normal range was 7·8% in male controls and 6·5% in female controls.[5]

Clinical assessments undertaken at the time of measurement of total body calcium included measurements of articular index,[6] functional state,[7] Westergren erythrocyte sedimentation rate, duration of early morning stiffness, and rheumatoid factor titre.[8] Statistical analysis of results was performed using Student's t test for unpaired variables and by multiple linear regression analysis. The Mann-Whitney test was used for data not normally distributed and for small samples. All patients gave informed consent, and ethical approval was obtained from local and national committees.

Results

The table shows details of age, duration of disease, variables of disease activity, and corticosteroid dosage in the patients studied. Comparison of the results obtained in the control and patient groups (fig 1) showed a significant reduction in mean total body calcium in patients receiving non-steroidal anti-inflammatory drugs alone (men 5·3%, $p < 0.05$; women 6·8%, $p < 0.01$). Mean total body calcium was further reduced in patients receiving low-dosage corticosteroids compared with controls (men 11·5%, $p < 0.01$; women 15·5%, $p < 0.001$) and in women receiving low-dosage corticosteroids compared with those receiving only non-steroidal anti-inflammatory drugs (8·7%, $p < 0.02$).
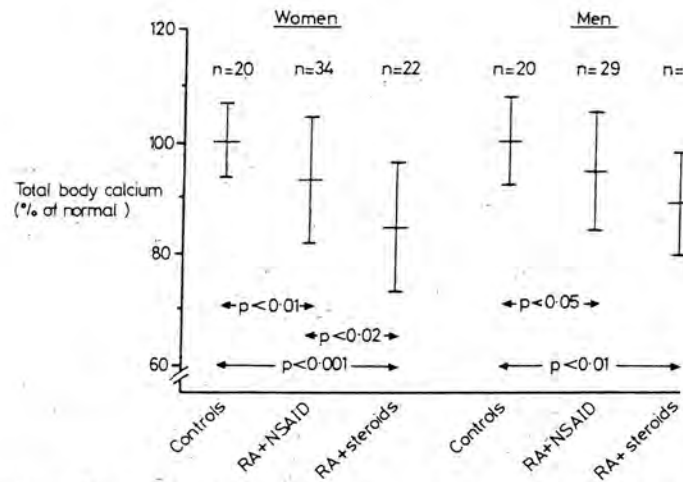
In patients receiving non-steroidal anti-inflammatory drugs total body calcium was not significantly correlated with any single index of disease activity or duration. Multiple linear regression analysis, however, showed a weak but significant correlation between total body calcium and a composite index of articular index, functional state, erythrocyte sedimentation rate, rheumatoid factor titre, and duration of disease ($r = 0.34$, $p < 0.01$) in 56 patients who had not received gold. A similar correlation was shown in 26 of the patients receiving corticosteroids ($r = 0.64$, $p < 0.01$), in whom there was also an inverse correlation between total body calcium and articular index ($r = -0.60$, $p < 0.01$).
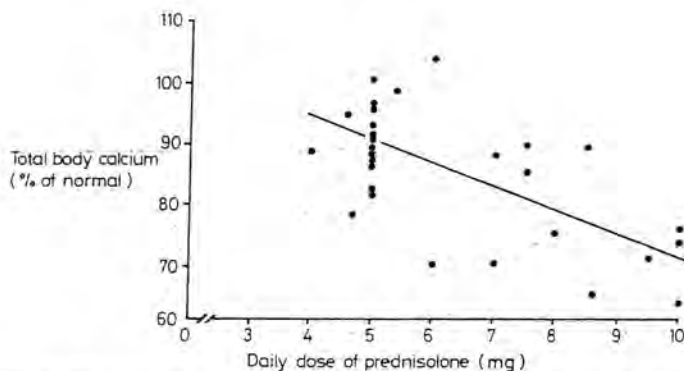
When the equation obtained by multiple linear regression analysis in patients receiving only non-steroidal anti-inflammatory drugs was used the mean total body calcium in patients receiving additional

Mean age and variables of disease in patients studied (ranges given in parentheses)

	Men		Women	
	NSAID* (n = 29)	Steroids (n = 9)	NSAID* (n = 34)	Steroids (n = 22)
Age (years)	51·7 (29–70)	53·6 (32–70)	52·4 (25–70)	56·1 (34–69)
Duration of disease (years)	8·5 (0·8–28)	5·7 (1·5–10)	8·2 (0·6–30)	12·3 (3–33)
Erythrocyte sedimentation rate (mm in first h)	35·9 (1–115)	31·9 (2–104)	39·5 (2–105)	35·0 (4–137)
Rheumatoid factor (1/titre)	392 (0–1280)	566 (0–1280)	345 (0–2480)	432 (0–1280)
Articular index	10·6 (0–21)	9 (0–18)	14·8 (4–31)	10·6 (1–23)
Functional state	2·14 (1–4)	1·89 (1–2)	1·99 (1–2·5)	2·00 (1–3)
Prednisolone (mg)		6·1 (4·6–9·5)		6·3 (4–10)
Duration of steroid treatment (years)		2·7 (1–6)		6·6 (2–22)

*NSAID = Non-steroidal anti-inflammatory drugs.

FIG 1—Total body calcium expressed as percentage of expected normal value (mean ± 1 SD) in male and female controls and patients with rheumatoid arthritis (RA) treated with non-steroidal anti-inflammatory drugs (NSAID) and corticosteroids.

FIG 2—Relation of total body calcium, expressed as percentage of mean normal value with daily dose of prednisolone (mg) in patients with rheumatoid arthritis treated with corticosteroids.

corticosteroids predicted from the duration of disease and variables of disease activity was found to be $93 \cdot 6 \pm 3 \cdot 7\%$ (range $87 \cdot 5 \text{-} 102 \cdot 3\%$). This was significantly higher ($p < 0 \cdot 005$) than the measured value in this group and similar to the measured value ($93 \cdot 2 \pm 10 \cdot 9\%$) for men and women in the group taking non-steroidal anti-inflammatory agents alone. No significant differences were found in erythrocyte sedimentation rate, functional state, and rheumatoid factor titre between the group receiving non-steroidal anti-inflammatory drugs alone and additional corticosteroids, although the duration of disease was 25% higher ($p < 0 \cdot 02$) and the articular index 20% lower ($p < 0 \cdot 05$ in the group receiving corticosteroids.

In patients receiving corticosteroids total body calcium was closely correlated with the mean daily dose of prednisolone ($r = -0 \cdot 66$, $p < 0 \cdot 001$) (fig 2) but not with duration of treatment or the total steroid dose (daily dose $\times$ duration of treatment).

Discussion

These studies show a significant reduction in mean total body calcium in patients with rheumatoid arthritis who had not received corticosteroid drugs and strongly suggest that the reduction in bone mass is an integral feature of the disease. The only previous studies of total body calcium in patients with rheumatoid arthritis showed conflicting results. In a small preliminary study Zanzi et al[9] found no reduction in seven women who had not received corticosteroids, while Kennedy et al[10] found an 18% reduction in 32 women compared with hypertensive controls. No details of drug treatment preceding the study were given in the latter paper.

By using localised methods of skeletal measurement several previous studies have suggested a relation between bone loss and duration of disease in rheumatoid arthritis,[11-13] while others have been unable to confirm this.[14-16] Most studies in which radiological or absorptiometric methods have been used, however, have suggested a relation between bone loss and variables of disease activity including erythrocyte sedimentation rate[13-15] and rheumatoid factor titre.[13]

Unfortunately, there is no good method by which overall disease activity over a period of time can be assessed. The composite index used in this study included the erythrocyte sedimentation rate and rheumatoid factor titres as indicators of disease activity at the time of measurement of total body calcium as well as functional state and duration of disease, which also reflect the clinical state over a prolonged period. Although the correlation between total body calcium and the composite index of disease duration and activity in patients who had not received corticosteroid treatment was relatively weak, it did permit total bone mass in the steroid-treated patients to be predicted. The striking discrepancy between measured and predicted total body calcium in the steroid-treated group suggests that loss of bone mass in these patients is directly attributable to the drug treatment and not a function of more prolonged or severe underlying disease. Some previous studies using less sophisticated methods have failed to show a relation between osteoporosis and corticosteroid treatment in patients with rheumatoid arthritis,[11 15 17] and it has been suggested that low-dosage treatment may be free from this risk and that improved mobility attributable to the use of corticosteroids may have the effect of reducing bone loss. Most studies, however, have shown evidence of increased bone loss in patients with rheumatoid arthritis treated with corticosteroids,[9 16 18] although this has not been correlated with steroid dosage. The finding that daily corticosteroid dosage is correlated with reduction in total body calcium while duration of corticosteroid treatment is not is consistent with the hypothesis that the histochemical changes and catabolic effects of corticosteroids on bone are most pronounced early in the course of treatment.[19 20]

Previous measurements of total body calcium in women with symptomatic postmenopausal osteoporosis have shown mean reductions of 16 and 18% greater than expected values.[3 21] This would seem to suggest that despite low mean daily doses of prednisolone (men 6·1 mg; women 6·3 mg) some male patients with rheumatoid arthritis treated with corticosteroids (mean reduction in total body calcium of 11·5%) and many female patients (mean reduction 15·5%) are at risk of osteoporotic complications. As a group patients treated with non-steroidal anti-inflammatory drugs alone, with a mean reduction in total

body calcium of only 5·3% in men and 6·8% in women, are probably not at high clinical risk of complications of osteoporosis. Since, however, the range of the reduction was wide (-20% to $+12\%$ in men; -33% to $+19\%$ in women) and many patients with rheumatoid arthritis are postmenopausal women, probably many individual patients who have not received corticosteroids will sustain clinically important reductions in skeletal mass. Although there has been an isolated report of spontaneous fractures in patients with rheumatoid arthritis who had not received corticosteroids,[22] there is clearly a need for epidemiological studies of the incidence of fracture in patients with this disease.

These studies also suggest that it will be important to try and establish the pathological basis of reduced bone mass in patients with rheumatoid arthritis as well as to determine to what extent this is the result of local and generalised osteoporosis.

References

[1] Duncan H, Frost HM, Villanueva AR, Sigler JW. The osteoporosis of rheumatoid arthritis. *Arthritis Rheum* 1965;8:943-54.

[2] Kennedy AC, Lindsay R. Bone involvement in rheumatoid arthritis. *Clin Rheum Dis* 1977;3:403-20.

[3] Cohn SH, Ellis KJ, Wallach S, Zanzi I, Atkins HL, Aloia JF. Absolute and relative deficit in total-skeletal calcium and radial bone mineral in osteoporosis. *J Nucl Med* 1974;15:428-35.

[4] Ropes MW, Bennett GA, Cobb S, Jacox R, Jessar AR. Proposed diagnostic criteria for rheumatoid arthritis. *Ann Rheum Dis* 1959;18:49.

[5] Kennedy NSJ, Eastell R, Ferrington CM, Simpson JD, Smith MA, Tothill P. Total body neutron activation analysis of calcium: calibration and normalisation. *Phys Med Biol* (in press).

[6] Ritchie DM, Boyle JA, McInnes JM, et al. Clinical studies with an articular index for the assessment of joint tenderness in patients with rheumatoid arthritis. *Q J Med* 1968;37:393-406.

[7] Steinbrocker O, Traeger CH, Batterman RC. Therapeutic criteria in rheumatoid arthritis. *JAMA* 1949;140:659-62.

[8] Podliachouk L, Eyquem A, Jacqueline F. Le diagnostic de la polyarthrite chronique évolutive par agglutination des globules rouges humains sensibilisés. *Annales de l'Institut Pasteur* 1958;94:659-62.

[9] Zanzi I, Roginsky MS, Ellis KJ, Blau S, Cohn SH. Skeletal mass in rheumatoid arthritis: a comparison with forearm bone mineral content. *American Journal of Roenterology, Radium Therapy, and Nuclear Medicine* 1976;126:1305-6.

[10] Kennedy AC, Boddy K, Williams ED, et al. Whole body elemental composition during drug treatment of rheumatoid arthritis: a preliminary study. *Ann Rheum Dis* 1979;38:137-40.

[11] McConkey B, Fraser GM, Bligh AS. Osteoporosis and purpura in rheumatoid disease: prevalence and relation to treatment with corticosteroids. *Q J Med* 1962;**55**:419-27.

[12] Kennedy AC, Smith DA, Buchanan WW, Anderson JD, Samuels BB, Jasani MK. Osteoporosis in rheumatoid arthritis. *Rheumatology* 1974; 4-25-35.

[13] Hancock DA, Asiedu-Offei S, Atkinson PJ, Reed GW, Wright V. Femoral bone mass in patients with rheumatoid arthritis and osteoarthritis. *Rheumatol Rehab* 1978;**17**:65-71.

[14] Oka M, Rekonen A, Kuikka J, Anttinen J. Bone mineral density in rheumatoid arthritis measured by the gamma transmission method. *Scand J Rheumatol* 1975;**4**:28-32.

[15] Virtama P, Helelä T, Kalliomäki JL. Osteoporosis in rheumatoid arthritis. *Acta Rheumatol Scand* 1968;**14**:276-84.

[16] Bjelle AO, Nilsson BE. Osteoporosis in rheumatoid arthritis. *Calcified Tissue Research* 1970;**5**:327-32.

[17] Kennedy AC, Smith DA, Anton HC, Buchanan WW. Generalised and localised bone loss in patients with rheumatoid arthritis. *Scand J Rheumatol* 1975;**4**:209-15.

[18] Hahn TJ, Boisseau VC, Avioli LV. Effect of chronic corticosteroid administration on diaphyseal and metaphyseal bone mass. *J Clin Endocrinol Metab* 1974;**39**:274-82.

[19] Duncan H. Osteoporosis in rheumatoid arthritis and corticosteroid induced osteoporosis. *Orthop Clin North Am* 1972;**3**:571-83.

[20] Jee WSS, Roberts WE, Park HZ, Julian G, Kramer M. Interrelated effects of glucocorticoid and parathyroid hormone on bone remodelling. In: Talmage RV, Munson PL, eds. *Calcium, parathyroid hormone and the calcitonins*. Amsterdam: Excerpta Medica, 1972:430-9. (ICS No 243.)

[21] Eastell R, Kennedy NSJ, Smith MA, *et al.* Total body calcium measurements in osteoporosis. *Calcif Tissue Int* 1981;**33**s:160.

[22] Haider R, Storey G. Spontaneous fractures in rheumatoid arthritis. *Br Med J* 1962;i:1514-6.

Comparison between ^{153}Gd and ^{241}Am, ^{137}Cs for dual-photon absorptiometry of the spine

M A Smith, D Sutton† and P Tothill

Department of Medical Physics and Medical Engineering, Royal Infirmary, Edinburgh, Scotland

Abstract. The bone mineral content (BMC) of the spine can be measured from the attenuation of two photon beams. An equation was derived for the theoretical precision of BMC measurement and validated experimentally. Though ^{153}Gd was found to possess the better energy combination, the precision due to the photon energy levels using ^{241}Am, ^{137}Cs was only 1.5 times the value obtained from ^{153}Gd. The available photon outputs from ^{241}Am and ^{153}Gd were investigated and with a 12 mm diameter disc source a theoretical precision of 1% could be obtained with source strengths 20 GBq ^{241}Am or 5 GBq ^{153}Gd in a 40 min and 20 min patient scan respectively. There was no great advantage in either energy combination when the problems of fat or patient dose were considered. Given the disadvantages of ^{153}Gd, its cost and availability, ^{241}Am, ^{137}Cs can be used as a practical alternative to measure spine BMC from a reconstructed bone mineral image.

1. Introduction

Dual-photon absorptiometry (DPA) to measure bone mineral content (BMC) was first proposed by Reed (1966). Subsequently interest concentrated on the forearm and single-photon absorptiometry became the method of choice (Cameron and Sorenson 1963, Christiansen and Rødbro 1977). More recently the technique of DPA has been used to measure the BMC of the spine, the site of most clinical interest, (Mazess *et al* 1974, Roos and Sköldborn 1974, Wilson and Madsen 1976, Price *et al* 1977, Condon *et al* 1979, Krølner and Pors Nielsen 1980, Wahner and Dunn 1980, Smith *et al* 1983) and whole body (Price *et al* 1977, Peppler and Mazess 1981), the second energy being used to compensate for variations in the thickness of overlying soft tissue.

The photon energies at 60 keV and 660 keV from ^{241}Am and ^{137}Cs respectively have been used by Roos and Sköldborn (1974) and Condon *et al* (1979). More commonly the radionuclide ^{153}Gd, with effective energies at 44 keV and 100 keV has been used (Mazess *et al* 1974, Wilson and Madsen 1976, Krølner and Pors Nielsen 1980, Wahner and Dunn 1980, Smith *et al* 1983). The reason for this is that it has become generally accepted that ^{153}Gd possesses the optimum energy combination for such work. Mazess *et al* (1974) state that ^{153}Gd is optimal for bones larger than the radius and ulna, citing the theoretical work of Judy (1971). However Judy (1971) concludes that the optimum lower energy for DPA is between 30 keV and 40 keV for a thickness of soft tissue of only 5 g cm^{-2}. Peppler and Mazess (1981) state that ^{153}Gd is optimal, citing the theoretical work of Hanson (1974) and Watt (1975). Hanson (1974), however, compared ^{153}Gd with ^{125}I, ^{241}Am for thicknesses of soft tissue ranging

---

† Present address: Department of Medical Physics, Essex County Hospital, Colchester, Essex, England.

up to $10 \, \text{g cm}^{-2}$. Watt (1975) does show the optimum lower energy to be 40 keV, but for a total sample thickness of only $15 \, \text{g cm}^{-2}$ and an upper energy of 400 keV. The suggestion that ^{153}Gd possesses the optimum lower energy is therefore interpreted from calculations using thicknesses that are of the order of half that found in human subjects in the region of the lumber spine. In addition, none of the theoretical analyses included all the variables associated with the bone mineral measurement.

Although ^{153}Gd may have nearly the optimum energy for BMC measurements of the spine, it has a relatively short half-life of 240 d compared with 458 yr for ^{241}Am. In addition, ^{153}Gd is more expensive and less readily available than ^{241}Am. The cost of ^{153}Gd, which has to be replaced annually, is therefore considerably greater than ^{241}Am.

Two factors, however, cause ^{241}Am to have a much lower photon output per unit volume than ^{153}Gd. The first is its much longer half-life. The second is the photons emitted per disintegration, 36% for ^{241}Am and 110% for the lower energy of ^{153}Gd. For a given output at the lower energy a much larger volume of ^{241}Am is therefore required and self absorption becomes significant. It is accepted that to reduce the error due to repositioning without excessively increasing the patient dose, the best method to measure spine BMC is to scan the patient and construct a bone mineral image which includes the region of the spine to be measured. The exact region of interest, for example the lumbar vertebrae L2, L3 and L4, can then be selected from the computer-processed bone mineral image. Such a technique requires sufficient resolution and sensitivity to produce an adequate bone mineral image. If narrow collimation of the source is used to produce the image then the maximum possible photon output from ^{241}Am is much lower than from a ^{153}Gd source, the activity of which is typically 37 GBq(1 Ci). However previous work using ^{153}Gd with lower activity of 7.4 GBq(200 mCi) (Smith *et al* 1983), showed that sufficient resolution to distinguish the separate lumbar vertebrae could be obtained with collimator sizes larger than had been used previously allowing the possibilities of higher activities of ^{241}Am to be considered.

This study was undertaken firstly to establish the optimum energy combination for DPA of the spine at realistic soft tissue and bone thicknesses, secondly to compare the relative merits of the energy combinations from ^{153}Gd and ^{241}Am,^{137}Cs and thirdly, given that adequate images can be produced with larger collimation than has been generally used, to determine whether ^{241}Am can produce a high enough photon output for DPA. The results would then determine whether ^{241}Am,^{137}Cs could be used in practice as an acceptable alternative to ^{153}Gd.

2. Methods

The content of either component of a two-phase system (e.g., bone and soft tissue) can be obtained from the attenuation of two suitable monoenergetic photon beams through the system, combined with the unattenuated count rates. For *in vivo* measurements of the spine a third phase, fat, is present. The assumption is made that the fat content is evenly distributed across the body. The BMC of the spine is therefore calculated using a region adjacent to the spine as the 'background' region, rather than the unattenuated through-air count rate (Roos *et al* 1980).

The relative merits of different energy combinations, irrespective of the actual count rate, were obtained using the following equations for the theoretical variance of the BMC measurement:

The measurement of BMC is obtained from four values

I_1 = total counts from energy 1 (lower) over the spine

I_2 = total counts from energy 2 (upper) over the spine

I_1^{bgd} = total counts from energy 1 over the soft tissue background

I_2^{bgd} = total counts from energy 2 over the soft tissue background

using the equation

$$M_b = K_\alpha[\ln(I_1^{bgd}/I_1) - K_\beta \ln(I_2^{bgd}/I_2)] \tag{1}$$

where

M_b is the BMC in g cm^{-2}

$K_\alpha = \mu_{s2}/(\mu_{b1}\mu_{s2} - \mu_{b2}\mu_{s1})$

$K_\beta = \mu_{s1}/\mu_{s2}$

μ is the mass attenuation coefficient $(\text{cm}^2\,\text{g}^{-1})$.

Subscripts s, b, 1 and 2 refer to soft tissue, bone and the lower and upper energies respectively. Also

$$I_1 = {}^*I_1 - \text{xo}\,I_2 \quad \text{and} \quad I_1^{bgd} = {}^*I_1^{bgd} - \text{xo}\,I_2^{bgd}$$

where ${}^*I_1$ and ${}^*I_1^{bgd}$ are the actual measured counts and xo is the contribution from the upper energy in the region of the lower energy referred to as the crossover correction (Smith and Tothill 1982).

The variance of the BMC measurement is given by

$$\sigma^2(M_b) = \left(\frac{\partial M_b}{\partial {}^*I_1}\right)^2 \sigma^2({}^*I_1) + \left(\frac{\partial M_b}{\partial I_2}\right)^2 \sigma^2(I_2) + \left(\frac{\partial M_b}{\partial {}^*I_1^{bgd}}\right)^2 \sigma^2({}^*I_1^{bgd}) + \left(\frac{\partial M_b}{\partial I_2^{bgd}}\right)^2 \sigma^2(I_2^{bgd})$$

$$= \left(\frac{\partial M_b}{\partial {}^*I_1}\right)^2 {}^*I_1 + \left(\frac{\partial M_b}{\partial I_2}\right)^2 I_2 + \left(\frac{\partial M_b}{\partial {}^*I_1^{bgd}}\right)^2 {}^*I_1^{bgd} + \left(\frac{\partial M_b}{\partial I_2^{bgd}}\right)^2 I_2^{bgd}$$

$$= \frac{K_\alpha^2}{I_1^{air}}\left[(C+A)(1+2\text{xo}K_\beta) + \left(\frac{C^2}{D} + \frac{A^2}{B}\right)z(\text{xo}+\text{xo}^2) + \frac{(D+B)K_\beta^2}{z}\right] \tag{2}$$

where

I_1^{air} = total counts at energy 1 through air—similarly I_2^{air}

$A = \exp(\mu_{s1}t_s + \mu_{b1}t_b) = I_1^{air}/I_1$

$B = \exp(\mu_{s2}t_s + \mu_{b2}t_b) = I_2^{air}/I_2$

$C = \exp(\mu_{s1}T_s) = I_1^{air}/I_1^{bgd}$

$D = \exp(\mu_{s2}T_s) = I_2^{air}/I_2^{bgd}$

t_b = thickness of bone (g cm^{-2}); this is equivalent to M_b in equation (1)

t_s = thickness of soft tissue overlying bone

T_s = thickness of soft tissue adjacent to bone

$z = I_2^{air}/I_1^{air}$.

To obtain the optimum value of z

$$\frac{\partial(\sigma^2(M_b))}{\partial z} = 0$$

$$z = \left(\frac{K_\beta^2(D+B)}{(C^2/D + A^2/B)(xo + xo^2)}\right)^{1/2}. \tag{3}$$

As would be expected the variance of the BMC is a function of sensitivity; in the case of the equation above, of the unattenuated lower energy count rate. However the equation for the variance of the BMC (equation 2) can be written as

$$\sigma^2(M_b) = \frac{\phi^2}{I_1^{air}}$$

where ϕ will be referred to as the comparative error function (CEF) and which is independent of the count rate. The CEF will be proportional to the coefficient of variation (CV) of the BMC measurement, which is usually defined as the precision or reproducibility.

The theoretical error analysis of spine BMC measurement using the equations above was performed for a range of energies, bone mineral values and soft tissue thicknesses. The range of the lower energy was 30 keV to 80 keV, the range of the upper energy 100 keV to 800 keV. Soft tissue values ranged from 5 g cm^{-2} to 30 g cm^{-2} and the bone mineral from 0.6 g cm^{-2} to 1.4 g cm^{-2}. The values for the bone mineral covered the range detected in patients and normal volunteers (Hansson and Roos 1980, Riggs *et al* 1981). The mass attenuation coefficients, derived from the data of Sorenson and Cameron (1974), are listed in table 1, the soft-tissue values being 85% muscle and 15% fat. When simulating ^{153}Gd, energies of 44 keV and 100 keV were used with $z = 1$. The value of $z = 1$ is higher than from the theoretical emissions but is the approximate ratio that has been observed from encapsulated sources (Peppler and Mazess 1981, Smith and Tothill 1982).

Table 1. Mass attenuation coefficients (cm^2 g^{-1})

	^{153}Gd		^{241}Am, ^{137}Cs	
	44 keV	100 keV	60 keV	660 keV
μ_b	0.790	0.203	0.402	0.076
μ_s (15% fat)	0.241	0.170	0.204	0.086
μ_m	0.245	0.170	0.205	0.086
μ_f	0.216	0.170	0.195	0.086

To examine whether ^{153}Gd possesses the ideal energies for spine BMC measurement, the CEF was determined over the energy ranges mentioned previously. The bone mineral values and soft tissue thicknesses used were more realistic than those used in previous analyses. The relative advantage, if any, of ^{153}Gd over ^{241}Am, ^{137}Cs due to the photon energy levels was investigated by studying the ratio of the CEFs, $\phi_{Am,Cs}/\phi_{Gd}$. The effects of the bone mass, soft tissue mass, xo and method of background calculation on the CEF ratio and the optimum value of z for ^{241}Am, ^{137}Cs were investigated.

The theoretical precision of spine BMC measurement using the ^{153}Gd and ^{241}Am, ^{137}Cs was compared with experimental reproducibility measurements on phantoms and normal volunteers. A 12 mm diameter sealed ^{153}Gd disc source (ref. no X.92/1, Amersham 1981) of activity 2.5–5.5 GBq(68–150 mCi) was used. The stainless steel 'window' for the source was specified as 0.2–0.25 mm. The ^{241}Am,^{137}Cs combination used a 5 mm diameter spherical ^{241}Am source of activity 7.4 GBq(200 mCi) (ref. no X.108, Amersham 1981). Again, the window for the source was stainless steel, 0.2–0.3 mm thick. The ^{137}Cs was a 2 mm diameter, 0.93 GBq(25 mCi) spherical bead placed behind the ^{241}Am. Bone mineral content measurements of the spine were obtained using a dual headed rectilinear scanner, the J&P Multipoise II, with NaI crystals 10 cm diameter and 5 cm thick. The top crystal was retained in use whilst the source was placed in the position of the lower one. The minimum scan speed was 5 mm s^{-1} with a stepping distance of 4 mm, so an average spine scan of 12 cm by 20 cm took 20 min. Two matrices of the high and low-energy transmission scans were stored on computer. At the end of the scan these could be combined to produce a two-dimensional bone mineral image of the lumbar spine on a colour TV display. Regions of interest around the vertebrae and a suitable background region could then be chosen. A variety of collimator sizes were used to vary the count rate and resolution though the separation remained constant at 0.4 m. In all cases there was sufficient resolution to define a region of interest around L2, L3 and L4.

Two types of phantom were used for experimental reproducibility measurements. The first consisted of the bones of a spine and pelvis encased in paraffin wax 15 cm thick. The bones were obtained from a cadaver and had a normal BMC (1.0 g cm^{-2}). The second was an anthropomorphic phantom consisting of a human skeleton encapsulated in tissue-equivalent rubber with a front to back thickness in the lumbar spine region of 22.5 cm. The BMC was lower than normal (0.8 g cm^{-2}) as was also confirmed by total body neutron activation analysis (Kennedy *et al* 1982). The precision of BMC measurements on human subjects was obtained from sets of two repeated measurements, separated by at least a week, on a number of normal volunteers. A single experienced operator analysed the scans used for the precision estimation so that the results would not contain any inter-observer error. Using equation (2) and measured values of A, B, C and D, the theoretical precision was calculated in all cases for comparison.

When comparing the two energy combinations the error due to fat must be considered. In equation (1) the assumption is made that the percentage of fat in the soft tissue is the same in both the background region and over the spine. The value for μ_s used assumes 15% fat and 85% muscle. If, however, there is a varying proportion of fat in the two regions then an error is introduced into the BMC calculation. To estimate the error in the BMC due to fat, associated with the two different energy combinations, the following equations were used in which the components of soft tissue, fat and muscle were considered separately:

$$I_1 = I_1^{air} \exp(-\mu_{m1}t_m - \mu_{b1}t_b - \mu_{f1}t_f)$$
$$I_2 = I_2^{air} \exp(-\mu_{m2}t_m - \mu_{b2}t_b - \mu_{f2}t_f)$$
$$I_1^{bgd} = I_1^{air} \exp(-\mu_{m1}T_m - \mu_{f1}T_f)$$
$$I_2^{bgd} = I_2^{air} \exp(-\mu_{m2}T_m - \mu_{f2}T_f).$$

Substituting in equation (1)

$$M_b = K_\alpha[t_b(\mu_{b1} - K_\beta\mu_{b2}) + (t_m - T_m)(\mu_{m1} - K_\beta\mu_{m2}) + (t_f - T_f)(\mu_{f1} - K_\beta\mu_{f2})]$$

where

T_m, T_f = thickness of muscle and fat (g cm^{-2}) adjacent to the bone

t_m, t_f = thickness of muscle and fat overlying the bone

μ_m, μ_f = mass attenuation coefficients of muscle and fat at energies 1 and 2.

Other factors in the equation have been defined previously.

The mass attenuation coefficients listed in table 1 were used and the values T_m, T_f, t_m and t_f were varied. The calculated BMC was compared with the true value t_b for both energy combinations.

The two energies can also be used to estimate the percentage fat in the background region adjacent to the spine. The error in the fat estimation due to counting statistics was calculated using equation (2), substituting the appropriate bone mineral parameters with those for fat and the soft tissue parameters with those for muscle. This enabled the precision of the percentage fat estimation to be obtained. The major source of error in the accuracy of the fat estimation is due to inaccuracies in the mass attenuation coefficients which are known typically to three decimal places. The constant K_a, which in the estimation of fat content becomes $\mu_{m2}/(\mu_{f1}\mu_{m2} - \mu_{f2}\mu_{m1})$, is affected most by errors in μ. The maximum variation in the estimation of the fat content was therefore calculated using the values of μ in table 1 plus and minus 0.0005.

The patient skin dose from the sources described previously was measured. An ionisation chamber was placed on the bed and surrounded by tissue-equivalent material. The dose was measured whilst the scanner operated in the same mode as was used for spine measurements.

Having obtained a comparison between ^{153}Gd and ^{241}Am, ^{137}Cs intrinsic to the photon energy levels, experimentally validated the theoretical precision estimation and considered the effect of fat and dose, the question of available count rate was investigated. The error due to counting statistics in DPA is determined principally by the lower energy count rate. For spine BMC measurements the source would have a single circular hole collimator, so a disc shaped source would give the highest output per unit volume. The degree of self absorption is negligible in a ^{153}Gd source but significant in a ^{241}Am source. The photon output for various sizes of ^{241}Am and ^{153}Gd sources of different activities was investigated. The photon output was measured using the two sources and detector described previously plus in addition a 12 mm diameter 11.1 GBq(300 mCi) ^{241}Am source (ref. no X.92/0, Amersham 1981) with 0.2–0.25 mm stainless steel window.

Previous research into DPA of the spine had shown that adequate resolution, sufficient to define the space between the lumbar vertebrae on a bone mineral image, could be obtained using a 12 mm diameter source collimator, a 20 mm square detector collimator and a separation between the two of 0.4 m (Smith *et al* 1983). The theoretical precision of spine BMC measurement for different activities of ^{153}Gd and ^{241}Am was calculated using values of I_1^{air} that could be obtained from commercially available sealed sources. The variation of precision with source activity was calculated assuming a 12 mm diameter disc source and source collimator, 20 mm square detector collimator, 0.4 m separation and a scan area of 12 cm by 20 cm. The time taken to scan this area was assumed to be 20 min or 40 min. The average area over L2, L3 and L4 was calculated from six volunteer scans, and theoretical precision was calculated for both a subject with normal spine bone mineral and soft tissue thickness and the 'worst' type of patient, one with dimineralised bone and a large thickness of soft tissue.
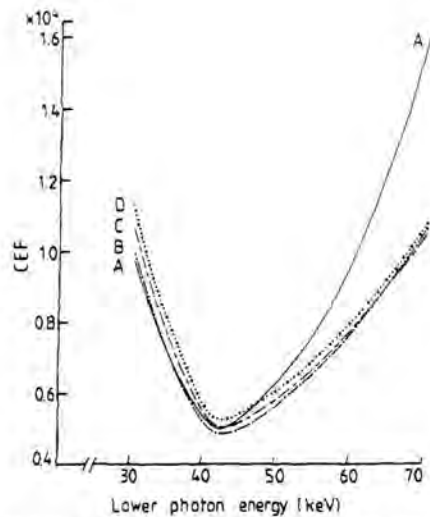
Figure 1. Variation in CEF for a range of lower and upper energy values. Curve A, 100 keV; B, 200 keV; C, 400 keV; D, 600 keV.

3. Results

The optimum energy combination to minimise the CEF for spine BMC measurements, assuming the optimum value of z, was found to be approximately 43 keV and 180 keV for a bone mineral of 1.0 g cm^{-2} and a soft tissue thickness of 20 g cm^{-2}. The variation in CEF is shown in figure 1 for a range of lower and upper photon energies. It can be seen that though there is a well defined minimum at approximately the same lower energy level, the upper energy level has little effect on the CEF.

The results of the CEF ratio for ^{241}Am,^{137}Cs and ^{153}Gd are shown in figure 2. A XO value of 4% was used and the assumption was made that the area to define the background level on the bone mineral image was the same as that used for the bone mineral region. Also shown in figure 2 is a histogram showing the distribution of
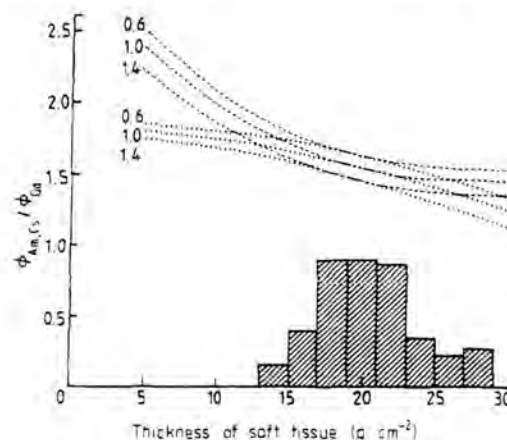
Figure 2. Ratio of CEF for a range of soft tissue thicknesses. BMC values of 0.6, 1.0 and 1.4 g cm^{-2} are used. Dashed line: $z = 1$ for ^{241}Am,^{137}Cs and ^{153}Gd. Dotted line: $z = 1$ for ^{153}Gd, optimum z for ^{241}Am,^{137}Cs. A histogram showing the variation in soft tissue thickness is also shown.

anterior to posterior thicknesses in the lumbar region of 180 patients and normal subjects. It can be seen that for measurements of the spine, though ^{153}Gd may possess nearly the optimum lower photon energy, the intrinsic error due to the photon energies using the energy combinations from ^{241}Am,^{137}Cs is only about 1.5 times greater than the error obtained using ^{153}Gd. The value of the xo was found to have little effect on the CEF ratio; for example if the bone mineral is 1.0 g cm^{-2} and the soft tissue thickness is 20 g cm^{-2} then a xo of 6% will increase the CEF ratio by 3.8% and a xo of 2% will reduce it by 6.4%.

Figure 3 shows the variation in z, the optimum ratio of the two values of z.
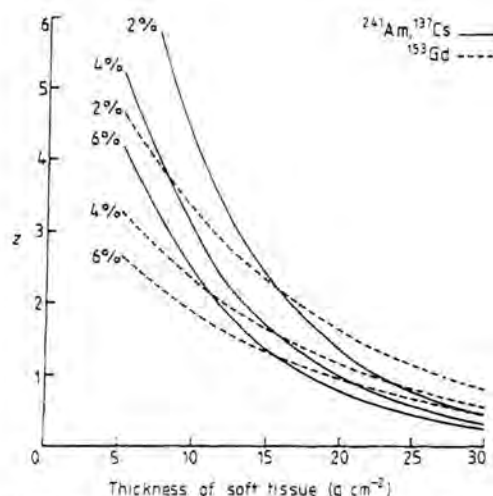
Figure 3. Variation in optimal value of z with soft tissue thickness. BMC value of 1.0 g cm^{-2} and xo values of 2%, 4% and 6% are used.

The results in table 2 show how well the theoretical error agrees with the experimental reproducibility. The large 4 cm diameter detector collimator used with ^{241}Am and the wax phantom showed the effect of increasing the ^{241}Am photon output. With this size collimator it was possible to distinguish the lumbar vertebrae on the bone mineral image of the phantom but not of the human subjects.

The error due to fat is shown in figures 4(a) and 4(b). It can be seen that with both a constant proportion of fat and different amounts of soft tissue and with different proportions of fat and the same amount of soft tissue the error in BMC is worse using ^{153}Gd by a factor of 1.3 compared with ^{241}Am,^{137}Cs. The precision of the fat estimation (CV) using the two energies in the region adjacent to the spine improves as the total soft tissue thickness decreases and the percentage fat increases. For a total soft tissue thickness of 20 g cm^{-2}, 15% fat and $I_1^{air} = 10^8$, the precision of the fat estimation using ^{153}Gd is 1.7% and using ^{241}Am,^{137}Cs is 3.8%. The maximum error in the fat estimation due to the assumed inaccuracies of the mass attenuation coefficients varies with the percentage fat content. With 15% fat the maximum error is 8% and 20% and with 30% fat the maximum error is 2.5% and 6.5% for ^{153}Gd and ^{241}Am,^{137}Cs respectively.

The skin dose was found to be 123 µSv when the ^{153}Gd activity was 10.6 GBq(286 mCi). The dose from the 7.4 GBq(200 mCi) ^{241}Am plus 0.93 GBq(25 mCi) ^{137}Cs combination was 14 µSv.

Table 2. Theoretical and experimental precision using phantoms and normal volunteers.

(i) Anthropomorphic phantom using ^{153}Gd.

Collimation		CV (%)		Number of measurements
Detector (cm × cm)	Source (mm)	Measured	Predicted	
2 × 2	13	1.1	1.2	10
2 × 2	10	2.0	1.5	10
2 × 2	8	2.1	1.8	10
2 × 2	6	2.5	2.4	10

(ii) Wax phantom using ^{153}Gd and $^{241}Am,^{137}Cs$.

Source	Detector collimation	CV (%)		Number of measurements
		Measured	Predicted	
$^{241}Am,^{137}Cs$	4 cm	0.6	0.90	10
^{153}Gd	2 cm × 2 cm	0.4	0.37	10

(iii) Normal subjects using ^{153}Gd and $^{241}Am,^{137}Cs$

Source	CV (%)		Number of measurements
	Measured	Predicted	
$^{241}Am, ^{137}Cs$ (Condon et al 1979)	2–3	2.64	12
^{153}Gd (Tothill et al 1981)	0.95	0.96	10
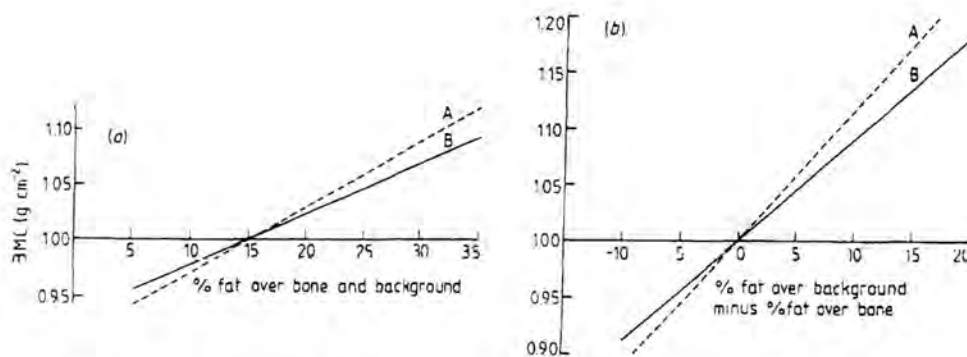
Figure 4. Variation in calculated BMC with non-uniform distribution of fat in background and over spine. (a) True BMC $1.0\,g\,cm^{-2}$, attenuation coefficients assume 15% fat. Percentage fat is constant over bone and in background but amount of soft tissue in background is $25\,g\,cm^{-2}$ and over bone is $15\,g\,cm^{-2}$. (b) Amount of soft tissue is constant, $20\,g\,cm^{-2}$, and true BMC $1.0\,g\,cm^{-2}$. Percentage fat over bone and in background is different. In each case, curve A, ^{153}Gd; curve B, $^{241}Am,^{137}Cs$.
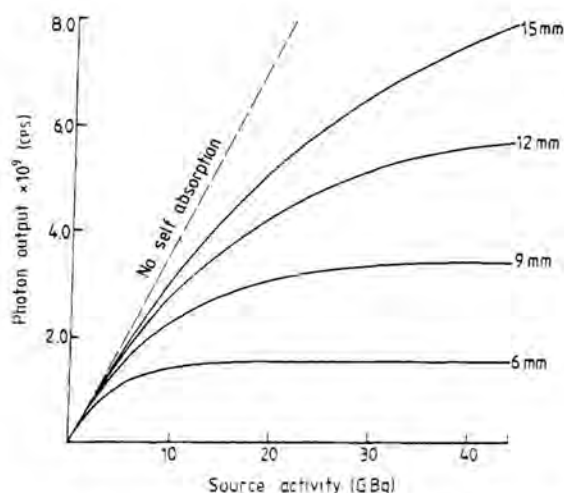
Figure 5. Variation in photon output with activity for disc sources of [241]Am with different diameters.

Various factors were found to affect the detected count rate from [241]Am and [153]Gd. It can be seen from figure 5 that the theoretical self absorption within a disc source is a major problem with [241]Am. The problem of self absorption is not significant however for [153]Gd, there being less than 1% with a source activity of 56 GBq(1.5 Ci). The stainless steel window of the source encapsulation was assumed to be 0.225 mm thick giving an attenuation of 19% and 39% at 60 keV and 44 keV respectively. An additional source of photon attenuation in the source is caused by the fact that [241]Am is mixed with a ceramic which does not form a perfect disc when set but has one concave face. This results in a reduction of approximately 15% in the photon output. An improvement in the output from a sealed source can be achieved if a 1 mm Be window is used. This will cause an attenuation of only 3% for both radionuclides. The photon output from the sealed source is also significantly attenuated in the housing around the NaI crystal, approximately 15% and 35% at 60 keV and 44 keV respectively.

The theoretical variation of precision with source activity is shown in figure 6. The value of I_1^{air} used is obtained from the theoretical output assuming attenuation by the factors described above and with a 1 mm Be window rather than stainless steel. The time spent over L2, L3 and L4 was taken as 357 s and 750 s for 20 min and 40 min patient scans respectively. It can be seen that with the collimation used, [153]Gd has an acceptable theoretical precision of less than 1.0% at activities down to 5 GBq(135 mCi). This is also the case when an activity of more than 20 GBq(540 mCi) of [241]Am is used with a 40 min scan time.

4. Discussion

The theoretical analysis of the variance of the bone mineral estimation is presented in a more comprehensive form than in previous studies. Wooten (1971) ignored the effect of xo and assumed four different optimum count times through bone and the adjacent background at the two energies, and also different optimum values of z. Hanson (1974) in his analysis ignored the xo, the error due to the background estimation and the ratio of the two energies. Roos (1974) dealt more thoroughly with
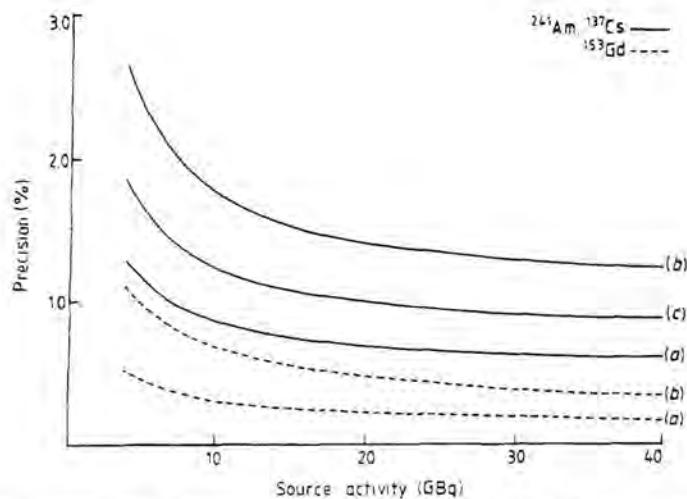
Figure 6. Variation in theoretical precision (CV) with activity of ^{153}Gd or ^{241}Am. (*a*) 20 g cm^{-2} soft tissue, 1.0 g cm^{-2} bone, 20 min scan. (*b*) 25 g cm^{-2} soft tissue, 0.8 g cm^{-2} bone, 20 min scan. (*c*) 25 g cm^{-2} soft tissue, 0.8 g cm^{-2} bone, 40 min scan.

the various factors but his analysis was very specific to his particular technique and he did not present a single equation of the total error that was generally applicable. The relative error function (REF) proposed by Judy (1971) and Watt (1975) also ignored the xo, assumed that the background is estimated from the unattenuated beams and that the ratio of the two energies was unity. In fact the REF is a special case of the CEF presented in this paper with xo = 0, $z = 1$ and $C = D = 1$. When these values were inserted into the equation for the CEF, identical results to those given in the paper by Watt (1975) were found.

The theoretical analysis confirms that ^{153}Gd possesses the ideal lower energy for spine BMC measurement, though the upper energy is rather lower than the optimum. Given that the upper energy is 100 keV, however, the actual ratio of the photon outputs is reasonably close to the optimum value. Though intrinsically the energy combination of ^{153}Gd is superior to $^{241}Am, ^{137}Cs$, the precision in BMC measurement is only increased by a factor of 1.5 if the latter is used. This suggests that $^{241}Am, ^{137}Cs$ is a practical proposition if a high enough output can be obtained.

Neither ^{153}Gd nor $^{241}Am, ^{137}Cs$ showed any clear advantage when the problem of fat was considered. Though ^{153}Gd estimates the fat content in the background region with greater precision and accuracy than $^{241}Am, ^{137}Cs$, a greater error is introduced in the BMC calculation using ^{153}Gd if the fat is not uniformly distributed over the spine.

There is also no particular advantage between the two energy combinations when the patient dose, which is very low in both cases, is considered. The skin dose to the patient from DPA of less than 150 μSv is far lower than other quantitative techniques, such as neutron activation analysis, where the dose can be of the order of 30–60 mSv (Al-Hiti *et al* 1976, Smith and Tothill 1979).

For clinical studies into metabolic disorders of the bone, such as osteoporosis, the precision of the technique needs to be around 2%, so the theoretical precision based on counting statistics should be ideally around 1%. Using the 2 cm square detector collimator and a 12 mm diameter disc source, which has been shown to give adequate resolution of the BMC image, theoretical and experimental results (figure 6 and

table 2) showed that this degree of precision could be obtained with a 20 min scan if at least 5 GBq(135 mCi) ^{153}Gd were used. Clearly the sensitivity of ^{241}Am could be increased by reducing the scan speed, but it is our experience that 40 min is about the maximum time that a patient will endure without becoming restless. Using the same collimation and a 40 min scan time, it is possible to achieve this precision if at least 20 GBq(540 mCi) ^{241}Am are used.

The cost of ^{241}Am is considerably less than ^{153}Gd, though the cost of the latter does vary in different countries. In Great Britain the cost of a 37 GBq(1 Ci) ^{241}Am 12 mm disc source with a Be window would be of the order of £2000 compared with £7000 for the same activity of ^{153}Gd. Given that ^{153}Gd needs to be replaced about every 12 months, there is a considerable financial advantage in developing apparatus which uses ^{241}Am. In addition the availability of ^{153}Gd is irregular.

The results in this paper show that activities down to 5 GBq(135 mCi) ^{153}Gd can be used suggesting that a 37 GBq(1 Ci) ^{153}Gd source could be used for about two years. To use activities over this range, the size of the collimation would have to be increased during the two year period to avoid dead-time errors at high activity and to give a high enough count rate at low activity. This would alter the geometry and also necessitate the use of different xo values (Smith and Tothill 1982) which could introduce errors into the BMC measurement. If longitudinal patient studies are to be undertaken, such as the study of osteoporosis covering a period of many years, then it would be desirable to use a technique whose parameters remain constant.

Acknowledgments

Résumé

Etude comparée du ^{153}Gd et du couple ^{241}Am,^{137}Cs pour les mesures d'absorption dans la colonne vertébrale en double énergie.

Le contenu minéral de l'os (BMC) peut être mesuré dans le rachis à partir de l'atténuation de deux faisceaux de photons. Une formule a été établie pour l'estimation théorique de l'incertitude qui affecte la mesure du BMC, et elle a été validée expérimentalement. Bien que le ^{153}Gd présente la meilleure combinaison d'énergies de photons, l'incertitude due aux niveaux d'énergies des photons du couple ^{241}Am,^{137}Cs est seulement 1,5 fois plus importante que celle correspondant au ^{153}Gd. Les flux de photons disponibles avec le ^{241}Am et le ^{153}Gd ont été mesurés et, pour une source ayant la forme d'un disque de 12 mm de diamètre, une incertitude théorique de 1% peut être obtenue lors de l'examen d'un patient avec 20 GBq de ^{241}Am (durée 40 min) et 5 GBq de ^{153}Gd (durée 20 min). Aucun avantage important n'apparaît avec l'une ou l'autre des combinaisons d'énergies pour la dose reçue par le patient ou les problèmes posés par la graisse. Aussi, compte-tenu des inconvénients du ^{153}Gd, en particulier son prix et sa disponibilité, il peut être remplacé en pratique par le couple ^{241}Am,^{137}Cs pour la mesure du BMC dans la colonne vertébrale à partir d'une image reconstruite du contenu minéral de l'os.

Zusammenfassung

Vergleich zwischen ^{153}Gd und ^{241}Am/^{137}Cs für 2-Photonenabsorptiometrie der Wirbelsäule.

Der Knochenmineralgehalt (KMG) der Wirbelsäule kann durch die Schwächung zweier Photonenstrahlen gemessen werden. Eine Gleichung für die theoretische Genauigkeit von KMG-Messungen wurde abgeleitet

^{153}Gd or $^{241}Am,$ ^{137}Cs for spine BMC   721

und experimentell bestätigt. Obwohl ^{153}Gd die günstigere Energiekombination besitzt, ist die Genauigkeit, die durch die Photonenergieniveaus bei Verwendung von ^{241}Am/^{137}Cs erreicht wird 1.5 mal größer als die für ^{153}Gd erhaltenen Werte. Die verfügbaren Photonenemissionen von ^{241}Am und ^{153}Gd wurden untersucht und mit einer Flächenquelle von 12 mm Durchmesser konnte eine theoretische Genauigkeit von 1% erreicht werden mit Quellstärken von 20 GBq ^{241}Am oder 5 GBq ^{153}Gd in einem 40- bzw. 20-minütigen Patienten-Scan. Es gab für beide Energiekombinationen keine großen Vorteile bei der Berücksichtigung der Fett- oder Patientendosis. Wegen der Nachteile von ^{153}Gd, Kosten und Verfügbarkeit, kann ^{241}Am/^{137}Cs als praktische Alternative zur Messung des KMB der Wirbelsäule aus einem rekonstruirten Bild des Knochen-minerals verwendet werden.

References

Al-Hiti K, Thomas B J, Al-Tikrity S A, Ettinger K V, Fremlin J H and Dabek J T 1976 *Int. J. Appl. Radiat. Isot.* **27** 97

Amersham 1981 *Radiation Sources Catalogue* (Amersham: The Radiochemical Centre)

Cameron J R and Sorenson J A 1963 *Science (New York)* **142** 230

Christiansen C and Rødbro P 1977 *Scand. J. Clin. Lab. Invest.* **37** 321

Condon B, Tothill P and Smith M A 1979 *Calcif. Tissue Int.* **27s** A8

Hanson J 1974 *Annual Progress Report* Bone Mineral Laboratory, University of Wisconsin p 73

Hansson T and Roos B 1980 *Spine* **5** 545

Judy P F 1971 *PhD Thesis* University of Wisconsin

Kennedy N S J, Eastell R, Ferrington C M, Simpson J D, Smith M A, Strong J A and Tothill P 1982 *Phys. Med. Biol.* **27** 697

Krølner B and Pors Nielsen S 1980 *Scand. J. Clin. Lab. Invest.* **40** 653

Madsen M 1976 *Invest. Radiol.* **12** 185

Mazess R B, Hanson J, Kan W, Madsen M, Pelc N, Wilson C R and Witt R 1974 in *Proc. Symp. Bone Mineral Determination, Stockholm-Studsvik* **2** 40

Peppler W W and Mazess R B 1981 *Calcif. Tissue Int.* **33** 353

Price R R, Wagner J, Larsen K H, Patton J A, Touya J J and Brill A B 1977 in *Medical. Radionuclide Imaging* STI/PUB/440 (Vienna: IAEA) vol. 2 p 145

Reed G W 1966 *Phys. Med. Biol.* **11** 174

Riggs B L, Wahner H W, Dunn W L, Mazess R B, Offord K P and Melton L J III 1981 *J. Clin. Invest.* **67** 328

Roos B 1974 *PhD Thesis* University of Gothenburg

Roos B O, Hansson T H and Sköldborn H 1980 *Acta Radiol. Oncol. Radiat. Phys. Biol.* **19** 111

Roos B and Sköldborn H 1974 *Acta Radiol. Ther. Phys. Biol.* **13** 266

Smith M A, Sutton D, Hannan W J, Tothill P and Wilson J 1983 *Osteoporosis* ed. J. Menczel (Chichester: Wiley) p 91

Smith M A and Tothill P 1979 *Phys. Med. Biol.* **24** 319

Smith M A and Tothill P 1982 *Phys. Med. Biol.* **27** 1515

Sorenson J A and Cameron J R 1974 *Instrumentation in Nuclear Medicine* ed. G J Hine and J A Sorenson (New York: Academic Press) p 353

Tothill P, Sutton D, Smith M A and Hannan W J 1981 *Calcif. Tissue Int.* **33s** 185

Wahner H W and Dunn W L 1980 *Nucl. Med. Commun.* **1** 211

Watt D E 1975 *Br. J. Radiol.* **48** 265

Wilson C R and Madsen M 1976 *Invest. Radiol.* **12** 180

Wooten W W 1971 *MS Thesis* University of California

but they have misrepresented the procedures of others and have alluded to intra-laboratory differences where none have been shown to exist.

Richard B Mazess†, Walter Peppler†,
Mark Madsen‡ and Charles Wilson§
† Medical Physics Division,
University of Wisconsin,
Madison, WI 53706, USA
‡ Dept of Medical Physics,
Jefferson Hospital,
Philadelphia, PA, USA
§ Medical Physics of Radiology,
Medical College of Wisconsin,
Milwaukee, WI 53226, USA

24 *February* 1983

Reference

Smith M A and Tothill P 1982 *Phys. Med. Biol.* **27** 1515–21

Intra-laboratory variations using dual-photon absorptiometry

The Editor,
Sir,

We welcome the letter by Mazess *et al* (previous letter), which provides further justification for our belief that technical problems in dual-photon absorptiometry (DPA) need to be explored. In our recent scientific note (Smith and Tothill 1982) we stated that there were intra-laboratory differences between cross-sectional studies of vertebral bone mineral content (BMC) in normal women as measured by DPA. Two groups have reported an increase in the rate of loss of BMC from the spine at the time of the menopause (Krølner and Pors Nielsen 1982, Smith *et al* 1983) whereas two other groups have not (Madsen 1977, Riggs *et al* 1981). Examples from two groups are shown in figure 1 illustrating this fairly fundamental disparity. Our own normal data (Tothill *et al* 1983) show that the units used to express the BMC, whether in grams (Krølner and Pors Nielsen 1980) or $g\,cm^{-2}$ (Riggs *et al* 1981), do not alter any age relationship. Nowhere in our scientific note did we state that the differences illustrated in figure 1 were due to the crossover corrections; we simply stated that 'It is not known whether this discrepancy between the various methods is due to differences in methodology or in the populations studied. Before accepting the latter the possibility of the former must be thoroughly investigated.'

We considered just one technical aspect of BMC measurement by DPA, the crossover correction, and though it was recognised that this would be influenced by both the NaI crystal and scatter within the patient it was considered unnecessary to separate the two components. There is a dearth of information in the literature about methods
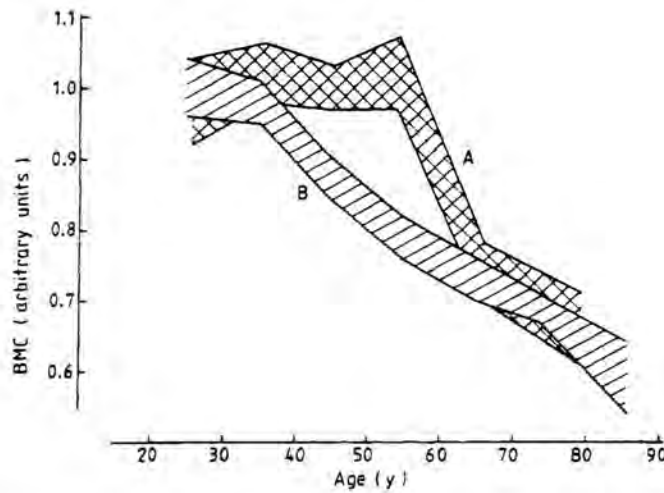
Figure 1. Variation in BMC of the lumbar vertebrae with age as measured by A, Krølner and Pors Nielsen (1982) in 70 normal women, and B, Riggs *et al* (1981) in 105 normal women. ±1 standard error about the mean for each decade is shown with the exception of the oldest women in A when the range 70–90 years is used.

used to determine the crossover correction. Mazess *et al* (1974) state that copper and aluminium were used to filter out the lower energy radiation. Other authors however (Wilson and Madsen 1977, Krølner and Pors Nielsen 1980, Wahner and Dunn 1980, Peppler and Mazess 1981, Riggs *et al* 1981) do not mention the absorber used to determine the crossover correction. It is not true that aluminium does not preferentially attenuate the 70 keV peak (Mazess *et al* 1983). Aluminium may be superior to copper but 5 cm of the former will attenuate the 70 keV peak 2.6 times more than the 100 keV peak, hence our rather complicated simulation of the upper end of the ^{153}Gd spectrum. Our empirical technique provided a satisfactory alternative, but would need to be validated for other apparatus.

Although previous literature of DPA techniques omitted many technical details, contradictions do appear to exist in the crossover correction values. Peppler and Mazess (1981) used a detector collimation of 8 mm × 25 mm and stated that the crossover correction varied with patient thickness from 1.8% to 3.4% whereas Wilson and Madsen (1977), using an even larger detector collimator of 12.5 mm × 37.5 mm, stated that the crossover correction was constant at 3%. Wahner and Dunn (1980) and Riggs *et al* (1981) used 6 mm detector collimation, the smallest used for DPA, but obtained crossover corrections of 6% and 4–6% respectively. The variation in crossover correction of 4–6% (Riggs *et al* 1981) was stated to be dependent on the source although no reason is apparent. The high value of 6% (Wahner and Dunn 1980) was due to the thin 1 mm NaI crystal used. If a thicker crystal were used which detected the 100 keV peak efficiently then this value would be reduced to about 2.5%. In the apparatus used by Krølner and Pors Nielsen (1980) however, which has a large detector collimator of 13 mm, a crossover correction of only 1% was used (personal communication).

In our original scientific note (Smith and Tothill 1982) and in this letter we do not intend criticism of any particular method of DPA for vertebral BMC measurements. Explanations may exist for many of the intra-laboratory differences but they need to be investigated with a degree of scientific thoroughness which hitherto has been absent.

Michael A Smith and Peter Tothill
Department of Medical Physics
  and Medical Engineering,
Royal Infirmary, Edinburgh EH3 9YW,
Scotland

17 *March* 1983

References

Krølner B and Pors Neilsen S 1980 *Scand. J. Lab. Invest.* **40** 653
Krølner B and Pors Nielsen S 1982 *Clin. Sci.* **62** 329
Madsen M 1977 *Invest. Radiol.* **12** 185
Mazess R B, Peppler W, Madsen M and Wilson C 1983 *Phys. Med. Biol.* **28** 747
Mazess R B, Wilson C R, Hanson J, Kan W, Madsen M, Pelc N and Witt R 1974 in *Proc. Symp. on Bone
    Mineral Determination, Aktiebolaget Atomenergi, Stockholm-Studsvik* **2** 40
Peppler W W and Mazess R B 1981 *Calcif. Tissue Int.* **33** 353
Riggs B L, Wahner H W, Dunn W L, Mazess R B, Offord K P and Melton L S 1981 *J. Clin. Invest.* **67** 328
Smith M A, Sutton D, Hannan J, Tothill P and Wilson J 1983 *Osteoporosis* ed J Menczel, G C Robin, M
    Makin and R Steinberg (Chichester: Wiley) p 91
Smith M A and Tothill P 1982 *Phys. Med. Biol.* **27** 1515
Tothill P, Smith M A and Sutton D 1983 *Br. J. Radiol.* to be published.
Wahner H W and Dunn W L 1980 *Nucl. Med. Commun.* **1** 211
Wilson C R and Madsen M 1977 *Invest. Radiol.* **12** 180

Dual photon absorptiometry of the spine with a low activity source of gadolinium 153

By P. Tothill, B.Sc., Ph.D., F.Inst.P., F.R.S.E., M. A. Smith, B.Sc., M.Sc., Ph.D. and *D. Sutton, B.Sc., M.Sc.

Department of Medical Physics and Medical Engineering, Royal Infirmary, Edinburgh EH3 9YW

ABSTRACT

Apparatus and data-processing techniques were developed to measure the bone mineral content (BMC) of the lumbar spine. ^{153}Gd was used as the dual photon source with an activity down to 7 GBq, lower than that adopted by other workers. The compromise between resolution and sensitivity was optimised. A reproducibility in normal subjects of 1.5% (coefficient of variation) was obtained. Normalisation procedures using parameters of the scan image and other indicators of body size such as span were developed, and reduced the coefficient of variation between normal subjects to 10% for men and 8% for pre-menopausal women. The absolute values of BMC are similar to those reported by others. Cross-sectional studies in women demonstrated an accelerated loss of BMC after the menopause.

Absorptiometry is well established as a method for measuring bone mineral. If a uniform overall thickness can be achieved, for example by using a water bath, and a two-phase system assumed, a single photon technique is adequate. Dual photon techniques have been used for some time to allow for varying thicknesses or an extra phase, and more recently have been applied to the study of the spine, the area of trabecular bone of most interest in diseases such as osteoporosis.

For the first measurements of bone mineral content (BMC) of the spine Roos and Sköldborn (1974) used the 60 keV radiation from ^{241}Am and 660 keV gamma rays from ^{137}Cs. They did not rely on retrospective choice of the site of analysis from a bone mineral image, but identified the scan position from a prior radiograph. Subsequent spine BMC measurements have generally used the radiations from ^{153}Gd, complex mixtures of X and γ rays effectively giving energies of 44 and 100 keV (Mazess et al, 1974; Wilson & Madsen, 1977; Price et al, 1977; Krølner & Pors Nielsen, 1980; Wahner & Dunn, 1980; Smith et al, 1983a). These authors have mostly selected the appropriate vertebrae from the processed image.

We set out to develop a scanning and data processing system for dual photon absorptiometry (DPA) of the spine. We were able to obtain only a lower-activity, larger-diameter ^{153}Gd source than had been used by previous workers and so had to investigate different

compromises between sensitivity and resolution. An appropriate collimation having been chosen, measurements were made of spinal BMC in a group of normal volunteers to establish the degree of variation and to provide a baseline against which to judge abnormality. Methods of normalisation of the data for body size were investigated. The results are presented here and compared with others from the literature.

METHODS

A standard dual-headed radionuclide scanner (J. & P. Engineering Ltd.) was adapted for transmission scanning. The ^{153}Gd source was mounted in the lower head and was initially of 18·5 GBq (500 mCi); its activity had decayed to about 7 GBq when the measurements on normal volunteers were made. The source was a disc, diameter 12 mm, in a stainless steel capsule (Amersham International X 92/1). The initial photon output was quoted by the supplier as 7×10^8 photons/s/steradian at 100 keV. The output at 44 keV was found to be about the same, there being appreciable attenuation in the 0.25 mm thick stainless steel exit face.

The detector was the standard 10×5 cm overhead NaI crystal of the scanner, which moved in synchronism with the source. The collimator face separation was 40 cm. The minimum reliable scanner speed of 5 mm s^{-1} was used, with a stepping distance between scans of 4 mm. A variety of single parallel-hole collimators, each of length 5 cm, was fitted to the source for measurements on a phantom, but once the optimum conditions had been determined a collimator of 13 mm diameter was used for all measurements on subjects. The detector collimator was 7.5 cm long and fixed at 20 mm square.

Two pulse-height analysers with window settings 32–56 keV and 75–125 keV were used to select the gamma-ray energies. Some of the results were obtained by recording data on a Digidek tape recorder for off-line transfer to a PDP 12 computer. Later a Cromemco microcomputer and TV monitor were interfaced to the scanner. Programs were written to correct for dead-time when necessary and the contribution from the higher energy radiation to the lower energy detection channel (the cross-over). The latter arises partly from scatter in the subject and partly from interactions in the detector

---

* Present address: Department of Medical Physics, Essex County Hospital, Colchester, Essex.

crystal; the correction was found to vary with patient thickness. To derive the cross-over with ^{153}Gd it is necessary to filter out the lower energy peak; the presence of a low abundance 70 keV peak creates complications (Smith & Tothill, 1982). The corrections were determined for each collimator combination used.

The bone mineral was calculated for each 4 mm cell using the equation derived by Roos and Sköldborn (1974)

$$M_b = \frac{\mu_{s2} \ln (I_{01}/I_1) - \mu_{s1} \ln (I_{02}/I_2)}{\mu_{s2}\mu_{b1} - \mu_{s1}\mu_{b2}} \quad (1)$$

where

M_b = bone mineral mass per unit area

μ = mass attenuation coefficient of soft tissue (s) and bone (b) at the lower energy (1) and higher energy (2)

I_0 = intensity of unattenuated beam

I = intensity of transmitted beam

Re-arranging equation (1),

$$M_b = \frac{(\mu_{s1} \ln I_2 - \mu_{s2} \ln I_1) - (\mu_{s1} \ln I_{02} - \mu_{s2} \ln I_{01})}{\mu_{s2}\mu_{b1} - \mu_{s1}\mu_{b2}} \quad (2)$$

In the soft-tissue area lateral to the spine, $M_b = 0$, and the second bracketed term containing the unattenuated beam intensities is equal to the first bracketed term. That area can be taken to constitute a background level above which the bone mineral values are calculated, and the expression then simplifies to

$$M_b = \frac{\mu_{s1} \ln I_2 - \mu_{s2} \ln I_1}{\mu_{s2}\mu_{b1} - \mu_{s1}\mu_{b2}} \quad (3)$$

The equations as presented here assume that soft tissue is homogeneous, whereas in practice it consists of mixtures of lean and adipose tissue which vary between patients. If the thickness of fat were uniform, the only error introduced would be in the values of μ_s chosen. Such uniformity is most unlikely, and non-uniformity leads to an incorrect choice of baseline (Roos et al, 1980). However, in common with other workers, we ignore the errors introduced by this factor.

The attenuation coefficients used in our calculations were derived from attenuation measurements through water and hydroxyapatite, and were as follows:

$$\mu_{s1} = 0.218, \ \mu_{s2} = 0.152, \ \mu_{b1} = 0.71, \ \mu_{b2} = 0.21$$
(all in cm^2 g^{-1}).

The ratio μ_{s2}/μ_{s1} is particularly important, as it was found from phantom measurements that the adoption of an incorrect ratio in the calculations led to an apparent change of bone mineral with water depth. Our ratio of 0.697 is close to the values used by other workers, even though individual values of attenuation coefficients may differ, perhaps due to different assumptions about the composition of soft tissue and bone mineral.

The bone mineral image is displayed on a colour

FIG. 1.

Monochrome display of bone mineral image.

monitor (Fig. 1). The original scan, over an area of about 12 cm wide and 20 cm long (taking about 20 min to perform), is positioned to include part of the pelvis, to facilitate identification of vertebrae on the image. Three lumbar vertebrae are included, cursors being positioned manually at the top of L2 and the bottom of L4. All cells in a vertical column between these limits are summed and a horizontal profile plotted (Fig. 2). Horizontal baselines are defined either side of the vertebrae, their selection adjacent to the bone edge being facilitated by vertical cursors. The bone mineral values are then integrated above the line joining the baselines. The results are expressed as a total in the three vertebrae, as bone mineral per unit length or unit area.

After reproducibility studies had been performed with anthropomorphic phantoms the optimum collimations were then used for repeated measurements on nine normal volunteers aged 21–58 years. Two measurements were made on separate days on each
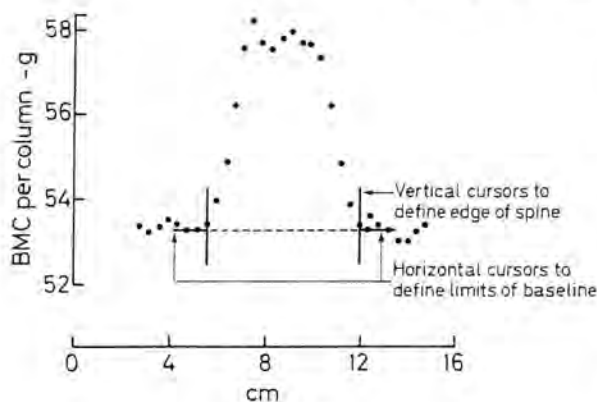
FIG. 2.

Profile of bone mineral content across vertebrae L2–4.

TABLE II

BONE MINERAL CONTENT EXPRESSED AS TOTAL IN L2–4(B), BMC PER UNIT LENGTH (B/L) AND PER UNIT AREA (B/A) AND NORMALISED FOR SPAN (BMI). MEAN VALUES WITH STANDARD DEVIATIONS OR COEFFICIENTS OF VARIATION IN BRACKETS

Sex	No.	Mean age	B g	B/L g cm^{-1}	B/A g cm^{-2}	BMI
M	18	33.9 (10.3)	62.1 (14.4%)	5.51 (11.2%)	0.98 (11.4%)	1.00 (9.8%)
F(all)	24	41.2 (12.8)	51.2 (20.1%)	4.95 (16.9%)	0.94 (16.7%)	
F($\leqslant$ 50y)	18	36.7 (11.4)	54.5 (15.8%)	5.23 (12.7%)	0.98 (12.3%)	1.00 (7.5%)

subject. Each bone mineral image was analysed by three operators.

The ^{153}Gd source with optimum collimation has been used to measure spine BMC in 24 normal women, aged 21–61 years, and 18 normal men aged 21–58 years. As there is a measure of subjectivity in the selection of the area of interest in the bone mineral image, all scans were analysed by the same operator.

The radiation dose to the skin was measured with a 1 litre ionisation chamber and found to be 140 μGy when the ^{153}Gd activity was 12 GBq.

RESULTS

From the experiments on models it was found that the precision improved as the sensitivity was increased by using larger diameter collimators, in spite of the worsening resolution (Table I). The experimental coefficients of variation were derived from 10 repeated measurements on an anthropomorphic phantom. The theoretical precision was based on counting statistics, taking into account the photon outputs at the two energies, the collimator geometries, the thickness of soft tissue, the bone mineral content, the detector efficiencies and the crossover correction. Details of the calculation are given elsewhere (Smith et al, 1983b).

TABLE I

EXPERIMENTAL AND THEORETICAL PRECISION USING AN ANTHROPOMORPHIC MODEL OF A HUMAN SKELETON IN TISSUE-EQUIVALENT RUBBER. 10 MEASUREMENTS. DETECTOR COLLIMATOR FIXED AT 20 × 20 mm

Source collimator diameter, mm	Coefficient of variation, % Measured	Predicted
6	2.5	2.4
8	2.1	1.8
10	2.0	1.5
13	1.1	1.2

The results of the repeated measurements on normal subjects, using the collimators that gave the highest precision in phantoms, were calculated as the average coefficients of variation (CV) obtained by dividing the differences between two measurements on each subject, expressed as a percentage of the mean, by 1.128 (Crow et al, 1960). The mean CV for operator 1, who had more experience than the others, was 1.0%, for operator 2, 1.5% and for operator 3, 3.3%.

The BMC values for the 42 normal subjects are summarised in Table II. In column 4 is the total mass of bone mineral in grams (B) in lumbar vertebrae 2, 3 and 4 as defined by the rectangle selected from the bone mineral image. For column 5 the total BMC values were divided by the length (L) of the rectangle in cm (along the spine) to give B/L. A further division by the width of the rectangle yielded the figures for BMC per unit area (B/A) in column 6. The best reproducibility was found by selecting the boundaries of the rectangle at the edge of the profile peak as illustrated in Fig. 2. The width of the rectangle was then such as to exclude the extremities of the transverse processes. A small amount of bone mineral was therefore included in the soft-tissue background. This leads to an inaccuracy analogous to that arising from non-uniform fat distribution.

The use of B/L or B/A gives a measure of normalisation for body size, but further relationships were sought, in the hope of minimising the variations in the values for the normal groups. The best correlation for the men and for the women aged 50 or less was between B/L and span. This linear relationship was used to derive formulae to give predicted BMC $(B/L)p$ for normal subjects.

For women $(B/L)p = 5.42 \times S - 3.50$,
$r = 0.81, p < 0.001$
For men $(B/L)p = 5.73 \times S - 4.61$,
$r = 0.48, p < 0.05$
where

S = span in metres.
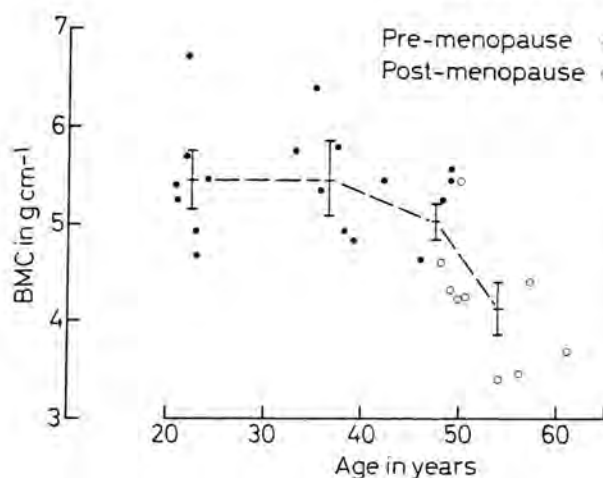
FIG. 3.

BMC per unit length (*B/L*) plotted against age for normal women. Error bars represent standard error of the mean for each decade.
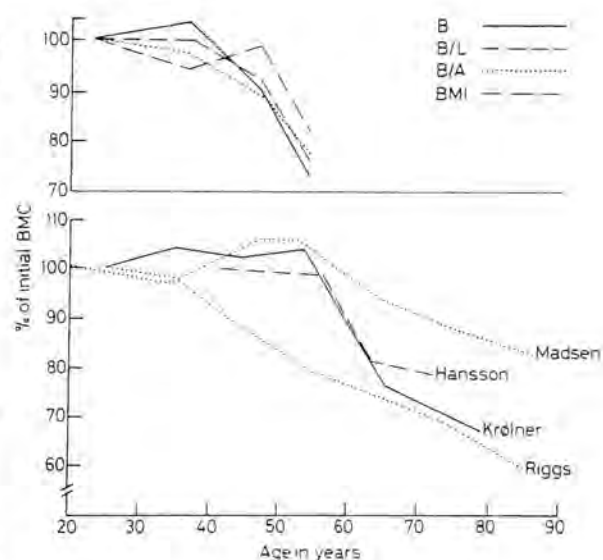

FIG. 4.

BMC plotted against age for normal women, mean results per decade. A (above) present authors' results expressed in different ways, B (below) results derived from other publications.

We can define a bone mineral index (BMI) as the ratio of *B/L* to (*B/L*)*p* for individual subjects. The mean values of the BMI are included in the last column of Table II. Normalisation using span was slightly better for *B/L* than for *B*.

When BMC was plotted against age for men, no correlation was found. For women there was a progressive loss of BMC with age above about 50 years. For example, *B/L* is plotted against age in Fig. 3, without normalisation for span. As there are relatively few points and a fair amount of scatter, a degree of smoothing has been obtained by calculating the mean BMC cm^{-1} for each decade. The same method of presentation, without data points or error bars, is used in Fig. 4A, to illustrate the different normalisation procedures and for comparison with other published results, the means for the first decade being set to 100%.

A further indication of age-related bone loss in women was obtained by correlating BMC with years post-menopause (*Y*). Only for the ratio BMI was the correlation significant ($r = -0.63$, $p < 0.05$, $n = 11$), the linear regression equation being $BMI = 0.995 - 0.017 \times Y$, corresponding to a rate of loss of 1.7% per annum soon after the menopause.

DISCUSSION

The main difference between our measurements of spine BMC and those of others using a similar technique was that the activity of our ^{153}Gd source was much lower, only about 7 MBq when most of the measurements on normal subjects were performed, compared with about 40 GBq in common use. Krølner and Pors Nielsen (1982b) quote the lowest activity employed, considering their source to be usable down to 15 GBq. We had already shown by theoretical analysis

and measurements on models that an acceptable precision (around 1%) could be obtained with this lower activity, using a coarser collimation to maintain sensitivity (Smith et al, 1983b). The results presented here confirm this finding in repeated measurements on normal subjects, the coefficients of variation of 1.0% and 1.5% for operators 1 and 2 being close to the theoretical CV based on counting statistics. The CV of 3.3% obtained by operator 3 is less acceptable, but he was inexperienced in the analysis, and we have found that practice brings a rapid improvement in the consistency of area selection.

The acceptable precision obtained with our activity means that a 20 GBq source could be used for about a year and 50 GBq for twice as long.

Another way in which our source differed was that it had an active diameter of 12 mm. The specific activity of ^{153}Gd is such that self-absorption of the X rays is not a limitation with smaller sources, and other workers have used lower diameters, giving a better resolution. Some have also improved resolution by using a smaller detector collimation. Our demonstration that satisfactory results can be obtained with a 12 mm source is not so important for ^{153}Gd, but is vital if ^{241}Am is considered for the lower energy photon beam. The long half-life of ^{241}Am, which makes it so attractive and economical a source, means that its specific activity is low. It is only possible to obtain sufficient photon output from ^{241}Am to give the required statistical precision if a diameter of at least 12 mm is used (Smith et al, 1983b).

Our measured radiation doses are similar to those

NOVEMBER 1983

Dual photon absorptiometry of the spine

published by others. For example, Krølner and Pors Nielsen (1980) quote a skin dose of 0.1 mGy and Wilson and Madsen (1977) approximately 0.02 mGy. In any case the doses are low enough to permit repeated observations in a wide category of subjects.

The BMC results for normal subjects are presented in Table II in different forms to allow comparison with other published results. Each form has its merits. As Krølner and Pors Nielsen (1980) have pointed out, the total BMC in a number of vertebrae (usually the second, third and fourth) is influenced least by vertebral crush fractures, which compress the vertebrae into a shorter length. On the other hand, no normalisation for body size is provided by this presentation and the consistency of the measurement is most critically dependent on the choice of boundaries between vertebrae. The total height of the three vertebrae is about 100 mm, corresponding to 25 scans at our 4 mm spacing. An inconsistency of boundary selection by one line, which is difficult to avoid, leads to an error of about 4%. This error can be much reduced, and some measure of normalisation for body size obtained, by expressing results as BMC per unit length. The penalty of this method is that crushed vertebrae may thereby appear to have a raised bone mineral content.

An advantage in expressing the result in terms of BMC per unit length is that the length is easily defined and so intercomparison of results using different techniques can be made. This may not be so if the result is expressed in terms of BMC per unit area, because the width of the vertebrae can be expressed in several ways. Our method was chosen to give the best reproducibility of selection of region of interest. Increasing the width of the chosen rectangle will not, beyond a certain level, affect the BMC value but will progressively decrease the BMC per unit area. Some centres do not use a rectangle but an irregular region of interest, calculated using an edge detection program. Thus though it may be possible for the different techniques to obtain comparable BMC or BMC per unit length values, there is likely to be considerable variation between values of BMC per unit area. This is illustrated in the results shown in Tables II and III.

Using our apparatus, the mean width, which was affected by the relatively coarse collimation, was about

5.5 cm; this is somewhat greater than the average width of the vertebral bodies, but less than the overall width of the transverse processes. By this exclusion we slightly underestimate the total bone mineral, but include all the trabecular bone of the bodies. The selection of a width large enough to encompass the whole bones would reduce the precision and the value of normalisation by width. The use of a finite beam width and scanning speed leads to an additional underestimate of BMC (West & Reed, 1970; Watt, 1973) but in common with others making measurements of the spine, we do not attempt to apply corrections.

Table II shows that the CV for the normal population studied was highest when total BMC was used (column 4). A reduction was obtained, as might be expected, when normalisation by length or area was applied (columns 5 and 6). The least variation was found when the additional factor of span was incorporated to give the predicted BMC per unit length, with which the measured value could be compared (column 7).

Our results can be compared with others from the literature. As all investigators have demonstrated a loss of BMC with age in women, it was thought best to present the mean values for the populations studied, together with the mean ages. These results are summarised in Table III, which can be compared with our Table II.

Roos et al (1980) relied on prior X-radiography to select a single vertebra and performed a single profile scan with a combined ^{241}Am/^{137}Cs beam.

The remaining authors used ^{153}Gd, but Madsen (1977) did not select the vertebrae from a bone mineral image, relying instead on a fixed scanning length of 10 cm starting at the level of the iliac crests. Riggs et al (1981) used lumbar vertebrae 1–4 and determined the area used for normalisation from an edge-detection program applied to the images. Krølner and Pors Nielsen (1982a) integrated profiles to obtain total BMC in vertebrae L2–4; although they express their results in arbitrary units with the dimensions of mass, it is clear from an earlier paper (Krølner & Pors Nielsen, 1980) that these units are equivalent to grams of hydroxyapatite.

It is seen from Tables I and II that our results are very similar to those already published.

TABLE III

MEAN VALUES OF LUMBAR BONE MINERAL CONTENT REPORTED BY VARIOUS AUTHORS

Authors	Sex	No.	Mean age	Vertebrae studied	B	B/L g cm^{-1}	B/A g cm^{-2}
Madsen (1977)	F	41	61	10 cm length		4.5	0.85
Roos et al (1980)	M	18	63.4	L 3		4.9	
Riggs et al (1981)	M	82	52	L1–4			1.22
	F	105	55	L1–4			1.08
Krølner & Pors Nielsen (1982a,b)	F	70	50.5	L2–4	44.5		

An examination of the loss of bone mineral from the spine with increasing age in women is important, as somewhat different patterns have been reported from the various cross-sectional studies considered here. Madsen (1977) fitted a linear regression to B/A over the whole age range, with a slope of 0.40% per annum at age 60. However, by re-analysing the data from his graph, it can be seen that there is no evidence of a loss below the age of about 50. For women over 50 a linear regression has a correlation coefficient of 0.565, $n = 31$, $p < 0.001$, with a slope of 0.75% per annum at age 60.

Hansson and Roos (1980) measured the bone mineral per unit length in single vertebrae removed at autopsy. They correlated B/L with age using a linear regression, showing a loss of 1.0% per annum at age 60. However, only 4 of the 18 women were below 50 years of age and the data do not permit deductions about possible changes of slope.

Riggs et al (1981) also used a single linear regression, this time of B/A against age, but justified it statistically, there being much larger numbers and no significant difference in the slope pre- and post-menopause. The rate of loss was 1.0% per annum at age 60.

Krølner and Pors Nielsen (1982a) considered that the distribution of lumbar BMC of normal pre-menopausal women showed skewness, as logarithmic transformation reduced the moment coefficient. However, analysis of their data shows that the skewness was not statistically significant. They found that BMC of pre-menopausal women was not related to age, whereas a significant reduction was found in the post-menopausal group, with an annual loss of 1.4%. They investigated several linear and polynomial regression equations, but chose to fit data to a gamma variate function, although a better fit was not obtained thereby. The function serves well enough at higher ages, but has the disadvantage that it introduces a maximum in the curve at about the age of 35. This is not in accord with the data and it seems a pity to distort the possible conclusions.

The data plotted in the four publications reviewed above have been analysed in the same way as our own data, mean values of BMC for each decade of age being plotted against the mean age in Fig. 4B.

Our own results, such as those presented in Figs. 3 and 4A, do not contain sufficient numbers or cover a wide enough age range for detailed analysis, but support the view that there is an increased loss of lumbar bone mineral after the menopause. Fig. 4A demonstrates that the normalisation procedure adopted does not affect the pattern of loss, suggesting that differences in Fig. 4B are due to some other cause.

When sufficient normal women have been measured, it should be possible to define the predicted normal lumbar BMC for a given age and size, as has been done for total body calcium (Cohn et al, 1976; Kennedy et al, 1982). The annual losses of lumbar bone mineral in post-menopausal women summarised here are not greatly different from those reported for total body

calcium, 1.1% (Cohn et al, 1976) and 1.5% (Kennedy et al, 1982).

The age-dependence of lumbar bone mineral in men has been reported by fewer authors. Hansson and Roos (1980), again using autopsy specimens from 15 subjects, found the slope of a linear regression of B/L against age to be the same as for women in terms of g cm^{-1}. Taking into account the higher mean BMC of the men, the proportional loss was lower, 0.76% per annum at age 60.

Riggs et al (1981) analysed the variation of lumbar BMC with age in 82 men. They found a small loss, of less than 0.2% per annum, with a significance of $p < 0.05$. With smaller numbers studied and a more restricted age range, it is not surprising that we demonstrated no change with age. Once again these results are similar to those from total body calcium determinations (Kennedy et al, 1982).

REFERENCES

COHN, S. H., VASWANI, A., ZANZI, I., ALOIA, J. F., ROGINSKY, M. S. & ELLIS, K. J., 1976. Changes in body chemical composition with age measured by total-body neutron activation. *Metabolism*, 25, 85–95.

CROW, E. L., DAVIS, F. A. & MAXFIELD, M. W., 1960. In *Statistics Manual* (Dover Publications, New York).

HANSSON, T. & ROOS, B. O., 1980. The influence of height and weight on the bone mineral content of lumbar vertebrae. *Spine*, 5, 545–551.

KENNEDY, N. S. J., EASTELL, R., FERRINGTON, C. M., SIMPSON, J. D., SMITH, M. A., STRONG, J. A. & TOTHILL, P., 1982. Total body activation analysis of calcium: calibration and normalisation. *Physics in Medicine & Biology*, 27, 697–707.

KRØLNER, B. & PORS NIELSEN, S., 1980. Measurement of bone mineral content of the lumbar spine, I. Theory and application of a new two-dimensional dual-photon attenuation method. *Scandinavian Journal of Clinical & Laboratory Investigation*, 40, 653–663.

——1982a. Bone mineral content of the lumbar spine in normal and osteoporotic women: cross-sectional and longitudinal studies. *Clinical Science*, 62, 329–336.

——1982b. Long-term reproducibility of dual-photon absorptiometry of lumbar vertebrae (lumbar BMC). In *Non-invasive Bone Measurements: Methodological Problems*, Ed. by J. Dequeker and C. C. Johnston, Jr. (IRL Press, Oxford/Washington) pp. 73–76.

MADSEN, M., 1977. Vertebral and peripheral bone mineral content by photon absorptiometry. *Investigative Radiology*, 12, 185–188.

MAZESS, R. B., HANSON, J., KAN, W., MADSEN, M., PELC, N., WILSON, C. R. & WITT, R. M., 1974. Progress in dual photon absorptiometry of bone. In *Proceedings, Symposium on Bone Mineral Determination*, Ed. by P. Schmeling (Aktiebolaget Atomenergi, Studsvik, Sweden), pp. 40–52.

PRICE, R. R., WAGNER, J., LARSEN, K. H., PATTON, J. A., TOUYA, J. J. & BRILL, A. B., 1977. Techniques for measuring

regional and total-body bone mineral mass to bone function ratios. In *Proceedings of Symposium on Medical Radionuclide Imaging*, Vol. II. (International Atomic Energy Agency, Vienna), pp. 145–158.

RIGGS, B. L., WAHNER, H. W., DUNN, W. L., MAZESS, R. B., OFFORD, K. P. & MELTON, L. J., III, 1981. Differential changes in bone mineral density of the appendicular and axial skeleton with aging. *Journal of Clinical Investigation, 67*, 328–335.

ROOS, B. O., HANSSON, T. H. & SKÖLDBORN, H., 1980. Dual photon absorptiometry in lumbar vertebrae: evaluation of the baseline error. *Acta Radiologica Oncology, 19*, 111–114.

ROOS, B. O. & SKÖLDBORN, H., 1974. Dual photon absorptiometry in lumbar vertebrae. I, Theory and method. *Acta Radiologica Therapy Physics Biology, 13*, 266–280.

SMITH, M. A., SUTTON, D., HANNAN, J., TOTHILL, P. & WILSON, J., 1983a. Dual photon absorptiometry for the determination of bone mineral content in the spine. In *Osteoporosis*, Ed. by J. Menczel, G. C. Robin, M. Makin & R. Steinberg (Wiley, London), pp. 91–97.

SMITH, M. A., SUTTON, D. & TOTHILL, P., 1983b. Comparison between [153]Gd and [241]Am, ^{137}Cs for dual photon absorptiometry of the spine. *Physics in Medicine & Biology, 28*, 709–721.

SMITH, M. A. & TOTHILL, P., 1982. The crossover correction in dual photon absorptiometry with [153]Gd. *Physics in Medicine & Biology, 27*, 1515–1521.

WAHNER, H. W. & DUNN, W. L., 1980. A new instrument for determination of bone mineral in the lumbar spine. *Nuclear Medicine Communications, 1*, 211–215.

WATT, D. E., 1973. Beam diameter and scan velocity effects on linear bone mass measurement by photon attenuation. *Physics in Medicine & Biology, 18*, 673–685.

WEST, R. R. & REED, G. W., 1970. The measurement of bone mineral *in vivo* by photon beam scanning. *British Journal of Radiology, 43*, 886–893.

WILSON, C. R. & MADSEN, M., 1977. Dichromatic absorptiometry of vertebral bone mineral content. *Investigative Radiology, 12*, 180–184.

Book review

Porphyrin Photosensitization (Advances in Experimental Medicine and Biology Vol. 160). Ed. by David Kessell and Thomas J. Dougherty, pp. ix + 294, 1983 (Plenum Press, New York/London), $42.50.
ISBN: 0–306–41193–8

For many years tumour tissues have been known to localise porphyrins, although the biochemical reasons for this are not understood. Nevertheless this finding is being exploited clinically both by using haematoporphyrins as photosensitisers as a means of eradication of tumours (PRT) and to aid tumour localisation. In 1981 a workshop was held in which workers involved in fundamental studies on porphyrin chemistry, physics and photobiology, along with those using porphyrins clinically, were brought together. This book contains the contributions of the participants and is an extremely useful source of information on the topic for all scientists and clinicians interested in this field of knowledge.

A series of articles on clinical aspects of haematoporphyrin photoradiation therapy is followed by a paper concerning the dosimetry of light in tissue by Doiron et al and a general review of photobiological considerations in photoradiation therapy by J. A. Parrish, both of which should be of widespread interest. The latter half of the book includes papers on the photochemical and photobiological mechanism of action of haematoporphyrin derivatives, including a report of a study by Michael Berns and co-workers using fluorescent analysis of cells with a laser light source. Each chapter ends with a useful list of references, so that people with no prior knowledge of the subject can use this as an original source of information.

D. J. G. DAVIES.

Normal levels of total body sodium and chlorine by neutron activation analysis

N S J Kennedy†‖, R Eastell‡, M A Smith§ and P Tothill§

† Department of Medical Physics and Medical Engineering, Western General Hospital, Edinburgh, Scotland
‡ Department of Medicine, Northwick Park Hospital, London, England
§ Department of Medical Physics and Medical Engineering, Royal Infirmary, Edinburgh, Scotland

Abstract. *In vivo* neutron activation analysis was used to measure total body sodium and chlorine in 18 male and 18 female normal adults. Corrections for body size were developed. Normalisation factors were derived which enable the prediction of the normal levels of sodium and chlorine in a subject. The coefficient of variation of normalised sodium was 5.9% in men and 6.9% in women, and of normalised chlorine 9.3% in men and 5.5% in women. In the range examined (40–70 years) no significant age dependence was observed for either element. Total body sodium was correlated with total body chlorine and total body calcium. Sodium excess, defined as the amount of body sodium in excess of that associated with chlorine, also correlated well with total body calcium. In females there was a mean annual loss of sodium excess of 1.2% after the menopause, similar to the loss of calcium.

1. Introduction

Total body neutron activation analysis can be used to determine the absolute amounts of certain body elements and also changes in these levels with time. At present, elements which may be measured by this technique include calcium, sodium, chlorine, phosphorus and nitrogen.

Absolute levels of total body sodium (TBNa) with or without total body chlorine (TBCl) in normal adults have been determined using neutron activation analysis by Chamberlain *et al* (1968), Rudd *et al* (1972), Ellis *et al* (1976) and Aloia *et al* (1980). Where appropriate the results of these studies and the data presented in this paper will be compared and discussed. TBNa has been shown to change in several disease states, e.g., renal failure (Cohn *et al* 1972), hypertension (Boddy *et al* 1978) and osteomalacia (Hosking *et al* 1972), and so techniques which allow the accurate evaluation of TBNa and TBCl are of considerable interest. For these to be of diagnostic significance it is necessary to establish normal ranges and develop normalisation procedures.

Most of the sodium in the body is extracellular, fairly rapidly exchangeable and associated with an equivalent amount of chlorine. The sodium in bone exchanges less rapidly and the chlorine concentration is much lower. The presence of a slowly-exchangeable pool of sodium has been demonstrated by the differences between the

---

‖ Present address: Department of Medical Physics, Ninewells Hospital, Dundee, Scotland.

values for exchangeable sodium as measured by isotope dilution techniques and total body sodium as measured by chemical analysis (Forbes and Lewis 1956) or by neutron activation analysis (Chamberlain *et al* 1968, Boddy *et al* 1978).

2. Methods

In the technique, the subjects are exposed to a beam of partially moderated fast neutrons which induces amongst others the reactions, $^{23}Na(n, \gamma)^{24}Na$, $^{37}Cl(n, \gamma)^{38}Cl$, $^{48}Ca(n, \gamma)^{49}Ca$, $^{31}P(n, \alpha)^{28}Al$ and $^{14}N(n, 2n)^{13}N$. The neutron source used for patient activation was a cyclotron producing neutrons of mean energy 6.5 MeV (Williams *et al* 1979). During irradiation the subject was positioned in a moderator kiosk which optimises the uniformity of activation of sodium and chlorine. The subject was then transferred to a shadow-shield whole-body counter where the γ-ray spectrum, covering the energy range 0 to 4 MeV, was recorded on a multichannel analyser. The data were analysed by fitting five standard spectra obtained from the activation of sodium, chlorine, calcium, phosphorus and potassium to the smoothed subject spectrum in the energy range 1.0 to 3.4 MeV, using a least squares technique (Smith and Tothill 1979). Corrections to eliminate the effects of variations in activation and detection efficiency with body size and position were then made, allowing the TBNa and TBCl content in grams to be determined accurately.

The technique of total body neutron activation analysis used in this study has been described in detail, with reference to measurements of calcium, by Kennedy *et al* (1982). The corrections were determined for each element using phantoms of several sizes, but there were no significant differences between those for calcium, sodium and chlorine. The coefficient of variation (CV) for repeated measurements of an anthropomorphic phantom was 2.1% for sodium and 4.3% for chlorine for an absorbed dose equivalent of 13 mSv. The phantom contained known amounts of sodium, chlorine, calcium, phosphorus, potassium and nitrogen, and there was no significant dependence of the counts obtained per gram of element on the ratio of the various elements in the phantom. Although no attempt was made in this study to determine total body nitrogen levels, a physiological amount of nitrogen (1960 g) was contained in the phantom. The importance of including nitrogen has recently been emphasised by Spinks and Bewley (1982).

Although this technique requires little patient preparation, it is important to check that the subject is not wearing thermal underwear which may contain significant levels of chlorine.

Since the chlorine space approximates extracellular fluid volume and the ratio of Na to Cl in the extracellular fluid has been estimated, the amount of sodium in excess of that associated with the chlorine space may be defined as the sodium excess value, Na_{ES}, (after Ellis *et al* 1976) and can be expressed in grams as

$$Na_{ES} = \text{TB}Na - 0.78 \text{ TB}Cl$$

where TBNa and TBCl are in grams. It is assumed that Na_{ES} represents most of the sodium resident in bone.

3. Results

3.1. Normal values

TBNa and TBCl measurements were made on a group of 36 normal volunteers, 18 male and 18 female, betweeen 40 and 70 years of age. All the subjects were active

and in good health. None had any history of disease that might be expected to influence their TBNa and TBCl levels, and all had normal blood and urine biochemistry. There was a considerable spread in the TBNa and TBCl results for both groups (see table 1). For the males the TBNa ranged from 74.8 g to 99.4 g with a mean of 83.7 g ± 8.2% (CV) while the TBCl ranged from 61.8 g to 93.4 g with a mean of 71.7 g ± 11.3%. The TBNa for the females ranged from 55.1 g to 75.9 g with a mean of 62.0 g ± 9.2% while the TBCl ranged from 46.5 g to 65.8 g with a mean of 53.4 g ± 10.2%.

Table 1. Data for normal controls.

	Mean (CV)	
	Male	Female
Number	18	18
Height (m)	178.3 (4.8)	160.9 (4.0)
Weight (kg)	81.3 (12.0)	62.5 (17.7)
Lean body mass (kg)	59.3 (11.7)	39.9 (12.6)
Age (y)	54.3 (16.5)	56.7 (10.9)
Sodium (g)	83.7 (8.2)	62.0 (9.2)
Chlorine (g)	71.7 (11.3)	53.4 (10.2)
Sodium excess Na_{ES}, (g)	27.7 (12.2)	20.5 (19.9)
Na_{ES}/kg calcium (g)	24.4 (9.1)	24.9 (17.5)

3.2. Normalisation procedures

As the total composition of the various elements in the body is related to the subject's build, the dependence of the measured TBNa and TBCl on height, weight, lean body mass (LBM) (calculated from the weight and skinfold thickness measurements), age and number of years post-menopause was investigated by multiple linear regression analysis.

For males, this gave a formula for predicted total body sodium ($TBNa_p$) in grams

$$TBNa_p = 19.2 \, (LBM)^{0.26}(height)^{0.71} \qquad (r = 0.72, \, P < 0.001)$$

and predicted total body chlorine ($TBCl_p$) in grams

$$TBCl_p = 11.3(LBM)^{0.37}(height)^{0.57} \qquad (r = 0.58, \, P < 0.05).$$

Height is measured in metres and LBM in kilograms. Similar equations were obtained when weight was used instead of LBM.

$$TBNa_p = 19.1(weight)^{0.23}(height)^{0.81} \qquad (r = 0.69, \, P < 0.001)$$

$$TBCl_p = 8.9(weight)^{0.40}(height)^{0.56} \qquad (r = 0.60, \, P < 0.05).$$

No significant dependence of TBNa and TBCl on age was observed. The biological variation in normal TBNa and TBCl due to body build could be reduced by expressing the results in terms of the ratios $TBNa/TBNa_p$ and $TBCl/TBCl_p$. This reduced the CV in the male controls to 5.8% for sodium and 9.2% for chlorine.

For the female controls, multiple regression analysis gave,

$$TBNa_p = 13.1(LBM)^{0.34}(height)^{0.63} \qquad (r = 0.72, \, P < 0.001)$$

$$TBCl_p = 5.2(LBM)^{0.59}(height)^{0.33} \qquad (r = 0.84, \, P < 0.001).$$

As with the male controls, similar equations were obtained when weight was substituted for LBM

$$\text{TBNa}_p = 19.1(\text{weight})^{0.16}(\text{height})^{1.09} \qquad (r = 0.72, P < 0.001)$$

$$\text{TBCl}_p = 9.8(\text{weight})^{0.31}(\text{height})^{0.88} \qquad (r = 0.81, P < 0.001).$$

No significant dependence on age was observed for either element. Using the ratios $\text{TBNa}/\text{TBNa}_p$ and $\text{TBCl}/\text{TBCl}_p$ the CV for sodium was 6.9% and for chlorine was 5.5%.

The TBNa and TBCl results for both male and female subjects are presented in figure 1. There was a good correlation between the TBNa and the TBCl results for males ($r = 0.89, P < 0.001$) and females ($r = 0.70, P < 0.005$) and when the sexes were combined ($r = 0.94, P < 0.001$).
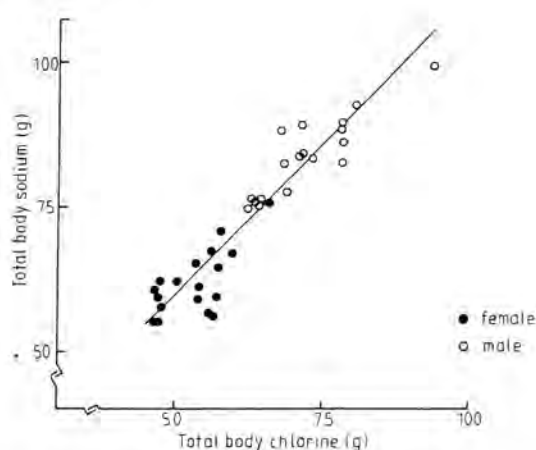
Figure 1. Relationship between total body sodium and total body chlorine. The regression line is calculated from male and female data combined.

Total body sodium was also found to be dependent on the subject's total body calcium (TBCa) ($r = 0.67, P < 0.01$). The TBCa results for these subjects were reported by Kennedy *et al* (1982). Significant dependence for TBCl on TBCa was found only for men ($r = 0.49, P < 0.05$).

There was a correlation between Na_{ES} and TBCa (figure 2). The relationship derived was

$$\text{Na}_{ES} = 19.9\,\text{TBCa} + 4.5 \qquad (r = 0.79, P < 0.001)$$

where Na_{ES} is measured in g and TBCa in kg, and the mean Na_{ES} per kg of TBCa was found to be 24.4 g for males and 24.9 g for females.

Although no correlation was found between TBNa and age, Na_{ES} was found to be correlated with years post-menopause in females ($r = 0.50, P < 0.05$) with an annual loss of Na_{ES} after the menopause of 1.2%. No significant dependence of Na_{ES} on age was observed for the male volunteers.

4. Discussion

The mean values of TBNa g/kg body weight for males, 1.03, and females, 0.99, are in good agreement with those values determined by Ellis *et al* (1976) of 1.08 for
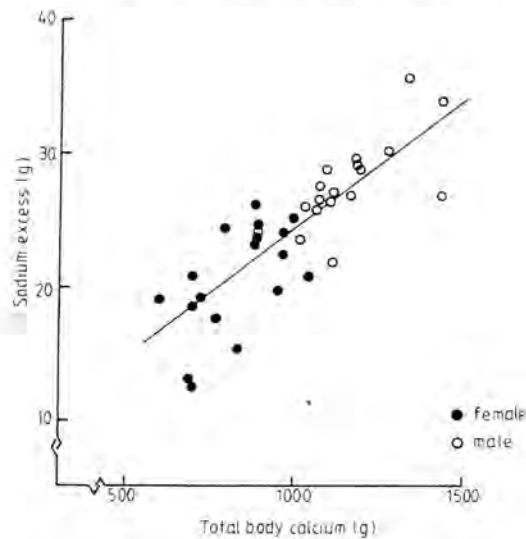
Figure 2. Relationship between sodium excess and total body calcium. The regression line is calculated from male and female data combined.

males and 0.98 for females. However the mean values of TBCl g/kg body weight for males, 0.88, and females, 0.85, are lower than those of Ellis *et al* (1976) of 0.99 for both sexes.

No dependence of either TBNa or TBCl on age was observed for either sex. Over the age range covered by this study, 40 to 70 years, this is largely in agreement with Ellis *et al* (1976), which is the most comprehensive of the other studies, although they did observe a slight decrease in TBNa in elderly females. Even when the varying body build of the subjects in this study was taken into account by plotting $TBNa/TBNa_p$ and $TBCl/TBCl_p$ against age, no significant correlation was obtained for either sex. The annual loss of Na_{ES} after the menopause of 1.2% is not significantly different from the loss of 1.5% per annum in TBCa in the same subjects (Kennedy *et al* 1982) and implies that an approximately equal percentage of calcium and sodium is lost from bone per year after the menopause. The lack of significant dependence of Na_{ES} on age for the male volunteers agrees with a similar result for TBCa.

The mean level of 24.3 g of Na_{ES} per kg of TBCa for males agrees well with that determined by Ellis *et al* (1976), for a similar age range, of 24.0 g/kg TBCa. However, their mean value of Na_{ES} for females, aged 40–70 y of 15.3 g/kg TBCa, and that of a later study by the same group, of 16.0 g/kg TBCa for females aged 50 to 59 y (Aloia *et al* 1980) are considerably lower than the 24.9 g/kg TBCa of our study. Ellis *et al* do not comment on the surprising difference they found between the sexes of the relationship of sodium excess to total body calcium.

The results from this study imply that the sodium excess represents around 33% of the TBNa for both male and female normal volunteers. This compares with values of 27% for males by Rudd *et al* (1972), 18% for males by Chamberlain *et al* (1972) and 27% for males and 23% for females by Ellis *et al* (1976).

The total body levels of sodium and chlorine determined in this study are in broad agreement with other studies, e.g., Anderson *et al* (1968), Rudd *et al* (1972) and Ellis *et al* (1976), and again suggest that the levels quoted by the International Commission

on Radiological Protection (ICRP 23) of 100 g for a 70 kg man for sodium and 95 g for chlorine are overestimates.

The narrow ranges for normal subjects that we have observed and the equations for predicting TBNa and TBCl should allow the technique of total body neutron activation analysis of sodium and chlorine to be a useful diagnostic procedure.

Acknowledgments

Résumé

Niveaux normaux du sodium et du chlore du corps entier par analyse par activation neutronique.

Nous avons utilisé l'analyse par activation neutronique *in vivo* pour mesurer le sodium et le chlore du corps entier chez des adultes normaux (18 hommes et 18 femmes). Nous avons introduit des corrections tenant compte des dimensions du corps. Nous en avons déduit des facteurs de normalisation permettant de prédire les niveaux normaux du sodium et du chlore chez un sujet. Le coefficient de variation du sodium normalisé est de 5,9% chez l'homme et 6,9% chez la femme, et celui du chlore normalisé est de 9,3% chez l'homme et de 5,5% chez la femme. Pour les deux éléments, nous n'avons observé aucune dépendance significative vis à vis de l'age dans la tranche d'age éxaminée (40–70 ans). Le sodium du corps entier est corrélé avec le chlore et le calcium du corps entier. L'excès de sodium, défini comme la quantité de sodium du corps en excédant par rapport à celui associé au chlore, est aussi bien corrélé avec le calcium du corps entier. Chez les femmes, on observe une perte moyenne annuelle du sodium en excès de 1,2% après la ménopause, similaire à la perte en sodium.

Zusammenfassung

Normaler Ganzkörper-Natrium- und -Chlorspiegel mit Hilfe der Neutronen-aktivierungsanalyse.

Der Ganzkörpergehalt an Natrium und Chlor wurde bei 18 männlichen und 18 weiblichen normalen erwachsenen Probanden mit Hilfe der *in vivo*-Neutronenaktivierungsanalyse gemessen. Korrektionen für die Körpergröße wurden entwickelt und Normierungsfaktoren wurden abgeleitet, die die Voraussage des normalen Natrium- und Chlorspiegels bei einem Menschen ermöglichen. Der Schwankungskoeffizient des normierten Natriums war 5.9% bei Männern und 6.9% bei Frauen. Der Schwankungskoeffizient des normierten Chlors betrug bei Männern 9.3% und bei Frauen 5.5%. Im untersuchten Bereich (40–70 Jahre) wurde für keines der beiden Elemente eine signifikante Altersabhängigkeit beobachtet. Das Ganzkörper-Natrium ist mit dem Ganzkörper-Chlor und dem Ganzkörper-Kalzium korreliert. Der Natrium-Überschuß, definiert als die Menge an Körper-Natrium, die über den mit dem Chlor verbundenen Anteil hinausgeht, ist ebenfalls eng mit dem Ganzkörper-Kalzium korreliert. Bei Frauen wurde ein mittlerer jährlicher Verlust des Natrium-Überschußes von 1.2% nach der Menopause festgestellt, ganz ähnlich wie der Verlust an Kalzium.

References

Aloia J F, Cohn S H, Abesamis C, Babu T, Zanzi I and Ellis K 1980 *J. Nucl. Med.* **21** 130
Anderson J, Osborn S B, Tomlinson R W S, Newton D, Rundo J, Salmon L and Smith J W 1964 *Lancet* **2** 1201
Boddy K, Brown J J, Davies D L, Elliott A, Harvey I, Haywood J K, Holloway I, Lever A F, Robertson J I S and Williams E D 1978 *Clin. Sci. Molec. Med.* **54** 187
Chamberlain M J, Fremlin J H, Peters D K and Philip H 1968 *Br. Med. J.* **2** 583
Cohn S H, Cinque T J, Dombrowski C S and Letteri J 1972 *J. Lab. Clin. Med.* **79** 978

Ellis K J, Vaswani A, Zanzi I and Cohn S H 1976 *Metabolism* **25** 645

Forbes G B and Lewis A M 1956 *J. Clin. Invest.* **35** 596

Hosking D J, Chamberlain M J, Fremlin J H and Jarves H 1972 *Br. Med. J.* **1** 19

ICRP 1975 *Reference Man: Anatomical, Physiological and Metabolic Characteristics* Report 23 (Oxford: Pergamon) pp 298, 314

Kennedy N S J, Eastell R, Ferrington C M, Simpson J D, Smith M A, Strong J A and Tothill P 1982 *Phys. Med. Biol.* **27** 697

Rudd T G, Pailthorp K G and Nelp W B 1972 *J. Lab. Clin. Med.* **80** 442

Smith M A and Tothill P 1979 *Phys. Med. Biol.* **24** 319

Spinks T J and Bewley D K 1982 *Phys. Med. Biol.* **27** 727

Williams J R, Bonnett D E and Parnell C J 1979 *Br. J. Radiol.* **52** 197

The Assessment of Postmenopausal Osteoporosis by Total Body Neutron Activation Analysis

R. EASTELL, N.S.J. KENNEDY, M.A. SMITH, J.D. SIMPSON, J.A. STRONG, and P. TOTHILL

Department of Medicine, Western General Hospital, Edinburgh, and Department of Medical Physics and Medical Engineering, Western General Hospital and Royal Infirmary, Edinburgh, UK.

Address for correspondence and reprints: Dr. R. Eastell, Northwick Park Hospital, Watford Road, Harrow, Middlesex HA1 3UJ, UK.

Abstract

Total body calcium (TBCa) was measured using a cyclotron for in vivo neutron activation analysis (IVNAA) in 20 healthy women, 15 women with vertebral compression fractures, and 8 women with wrist fractures. The precision of the technique, using phantoms, was 1.8% for a dose of 13 mSv. A formula for predicted TBCa (TBCa$_p$) was derived from the 20 normal women based on span and years postmenopause. The coefficient of variation of TBCa after normalization in the normal women was 6.6%. The mean TBCa values for the vertebral and wrist fracture groups were 69% and 84% of TBCa$_p$ for women at the time of the menopause. The low TBCa in the wrist fracture group was attributable to postmenopausal bone loss. Of the low TBCa in the vertebral fracture group, about half the loss could be attributed to postmenopausal age and half to other factors.

Key Words: Activation–Analysis–Osteoporosis.

Introduction

In vivo neutron activation analysis (IVNAA) is an established technique for measuring total body calcium (TBCa) and has been described by five other groups (Chamberlain et al., 1968; Cohn et al., 1976a; Palmer et al., 1968; Spinks et al., 1977; Kennedy et al., 1979) as well as by ourselves (Kennedy et al., 1982). Since 99% of TBCa is present in bone (Heany, 1963), IVNAA can be used to measure bone mass and in this way avoid the errors in sampling from different parts of the skeleton. Two other groups have reported TBCa in women with postmenopausal osteoporosis (Chesnut et al., 1977, Cohn et al., 1974).

In this report we describe a formula for predicting TBCa from the span and postmenopausal age based on a study of 20 normal women. This formula is then used to compare the bone mass of women with vertebral or wrist fractures with their expected bone mass. The degree of osteopenia associated with these two types of fracture is also calculated.

Patients and Methods

Twenty women aged 46–66 years were selected from volunteers who answered requests circulated in the hospital, in a factory, in the local press, and on BBC Radio Scotland. The criteria for selection were based on age (40–70 years) and the absence of a past history of back pain, fragility fractures, artificial menopause, rheumatic, hepatic, renal, or endocrine diseases, exposure to steroid or anticonvulsant therapy, or excessive alcohol intake. Screening tests to exclude occult malabsorption and disorders of calcium metabolism or of renal or hepatic function were undertaken as follows: serum or plasma calcium, phosphate, magnesium, alkaline phosphatase, albumin, parathyroid hormone, 25-hydroxycalciferol, iron, iron-binding capacity, ferritin, vitamin B$_{12}$ and folic acid, urinary calcium, phosphate, magnesium, hydroxyproline and creatinine clearance, and a full blood count.

Eight women with wrist fracture, aged 56–69 years, were selected from a consecutive series of patients attending the orthopedic clinic. Selection was made on the same basis as for the volunteers. Measurements of TBCa and of plasma and urine as for the normal women were made 1 year after the fracture.

Fifteen women aged 48–71 years were referred to the endocrine clinic for medical therapy of their vertebral osteoporosis. Back pain had been present for less than 2 years in 11 of the 15 women. At least two collapsed vertebrae were seen on a lateral radiograph of the thoracolumbar spine in all patients. No selection was made of these patients, and the same investigations as already described were performed together with isotope bone scans and bone biopsy when indicated.

TBCa was measured by IVNAA using the MRC cyclotron in Edinburgh (Williams et al., 1979) as the source of neutrons. The induced radiation was measured using four sodium iodine detectors mounted in a whole-body counter. Computer analysis of the spectrum and the value of a standard irradiated simultaneously with the subjects gave the TBCa in ^{49}Ca counts. The long-term precision, based on anthropomorphic phantom measurements, was 1.8% (coefficient of variation, CV) for a dose of 13 mSv (1.3 rem) (Kennedy et al., 1982). The effect on measurement efficiency due to variation in body size was determined experimentally. Calcium counts were converted to grams of calcium using a correction formula from phantom measurements. Biologic variation due to size and age was then reduced using multiple regression analysis of height, arm span, weight, age and years postmenopause, and lean body mass (% body fat was obtained using skin calipers) (Durnin and Womersley, 1974). The factors relating most closely to TBCa were found to be arm span and years postmenopause.

Informed consent was obtained from all patients. The study protocol was approved by the Hospital Ethics Committee and by ARSAC (Administration of Radioactive Substances Advisory Committee).

Results

The TBCa in normal women was 820 ± 124 g (mean ± standard deviation, SD). This gave a CV of 15.1% before any allowance was made for span or postmenopausal age. The greatest reduction in variance was achieved using the following formula to obtain the predicted TBCa (TBCa$_p$):

$$TBCa_p = \alpha s^{1.69} e^{-0.015y} \; (r = 0.90, P < 0.001)$$

where:

TBCa$_p$ is in grams
$\alpha = 399$
$s =$ arm span in meters
$y =$ years postmenopause

The arm span not only related more closely to TBCa than height but also eliminated the error due to loss of height associated with vertebral fractures. The formula applied to perimenopausal women and to women up to 22 years postmenopause. The regression is based on an exponential loss of bone mass starting at the time of the menopause. The estimated rate of bone loss was 1.5% per year. The ratio TBCa/TBCa$_p$ has been defined by Cohn et al. as the calcium ratio (Ca$_R$) (Cohn et al., 1974) and for our normal women was 1.00 with a CV of 6.6%.

The TBCa in women with vertebral and wrist fractures was 649 ± 87 g and 787 ± 72 g, respectively (mean ± SD). The values of span and postmenopausal age are shown in **Table I**. In the women with wrist fractures the Ca$_R$ was 1.00 ± 0.10, which was normal (**Fig. 1**). Six of the 15 women with vertebral fracture had postmenopausal ages greater than 22 years. This was the greatest postmenopausal age among the normal women; the formula for TBCa$_p$ cannot be extrapolated to cover the women in this group who were more than 22 years past the menopause. In the remaining 9 women the Ca$_R$ was 0.87 ± 0.06, significantly lower than in normal women (P < 0.01). Factors that may have contributed to this excessive bone loss were identified in 5 of the 9 patients, namely, prednisolone therapy for polymyalgia rheumatica, phenytoin therapy for epilepsy, previous history of thyrotoxicosis, atrophic gastritis, and moderate impairment of renal function (creatinine clearance 20 ml/min).

When TBCa was normalized for span alone (TBCa/$\alpha s^{1.69}$), i.e., $y = 0$ in the equation for TBCa$_p$, an estimate of osteopenia in the patients with fractures could be made by comparing the values with the Ca$_R$ of the normal women (**Fig. 2**). The TBCa/$\alpha s^{1.69}$ for women with vertebral and wrist fractures and for normal women were 0.69 ± 0.06, 0.84 ± 0.08, and 0.88 ± 0.11, respectively (mean ± SD). All the women with vertebral fractures had values less than 0.78, but 3 of the 8 women with wrist fractures and 5 of the 20 normal women also had values below 0.78.

Fig. 1. Calcium ratio (Ca$_R$) in normal women (○), women with wrist fracture (△), and women with vertebral fracture (□). Horizontal lines are mean Ca$_R$ ± 2 SD for normal women.
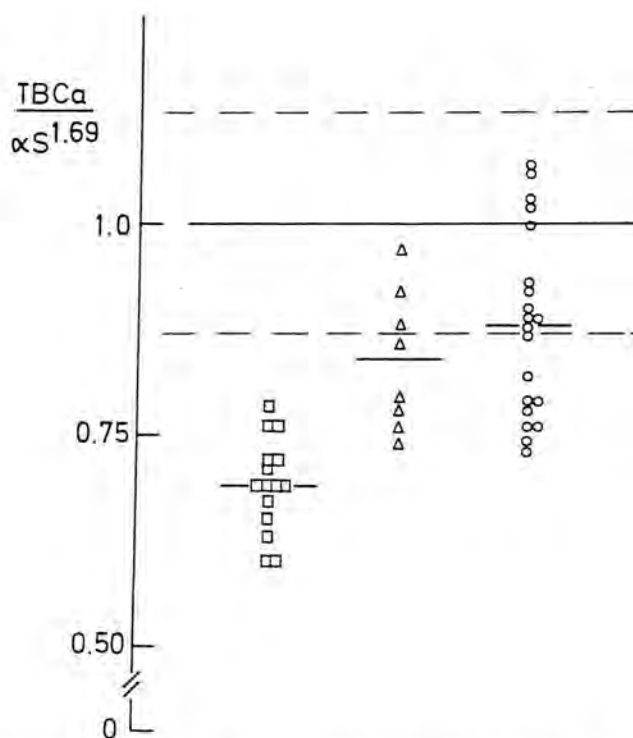
Fig. 2. Total body calcium normalized for span (TBCa/$\alpha s^{1.69}$) in normal women (○), women with wrist fracture (△), and women with vertebral fracture (□). Horizontal lines are mean Ca$_R$ ± 2 SD for normal women.

Table I. Span and postmenopausal age in normal women and women with vertebral and wrist fractures. The years postmenopause in the vertebral fracture group were significantly higher than in the normal women (P < 0.002).

Group	Number	Span (m) Mean ± SD	Postmenopausal age (yr) mean ± SD
Normal women	20	1.65 ± 0.07	8.9 ± 7.0
Vertebral fracture	15	1.66 ± 0.07	21.9 ± 8.4
Wrist fracture	8	1.66 ± 0.06	12.0 ± 5.9

Discussion

TBCa for the normal women (820 ± 124 g) was similar to that reported by Cohn et al. (1976b), namely, 804 ± 106 g for normal women aged 50–59 years. The TBCa for women with vertebral fractures (649 ± 87 g) resembled that described by Chesnut et al. (1977) (mean 688 g ± 94 g) and Cohn et al. (1974) (mean 590 g ± 108 g). However, some of the patients in the latter two groups did not have vertebral compression fractures but only demineralized vertebrae.

Different formulae for $TBCa_p$ have been reported. Cohn et al. (1976b) use age from birth, height, and total body potassium: the latter two also may be age dependent. Nelp et al. (1972) predict TBCa from the cube of the patient's height. In the present report it was noted that span was more effective than height in reducing variance, and we would prefer to use span, as it is unaffected by the height loss due to vertebral compression fractures.

The CV of $TBCa_p$ in normal women was 6.6% as compared with 7.1% reported by Cohn et al. (1976b). The latter group found that the rate of bone loss after the age of 55 years was 1.1% per year compared with the rate of 1.5% per year after the menopause in our group.

The Ca_R was 0.87 in the women with vertebral fractures, similar to the value of 0.82 found by Cohn et al. (1974). An early menopause in these two groups of women may explain in part their osteopenia. Additional factors, including a low TBCa at the time of the menopause or an accelerated loss of bone after the menopause, must also have been present. The normal Ca_R in the women with wrist fractures suggests that they were not specifically prone to fracture compared with other postmenopausal women.

Expressions such as $TBCa/\alpha s^{1.69}$ to describe the degree of osteopenia have not been reported previously. Although the sample size of 15 was small, in this group of women vertebral crush fractures occurred when total body calcium was below 80% of that predicted from span alone, i.e., $TBCa/\alpha s^{1.69}$ less than 0.78. However there was some overlap of these values with the other groups of women. It may be possible, therefore, to predict those women likely to sustain a vertebral fracture and to recommend treatment, estrogens, for example, aimed at preventing further loss of bone mass.

References

Chamberlain M.J., Fremlin J.H., Peters D.K. and Philip H.: Total body calcium by whole body neutron activation: new technique for study of bone disease. Br. J. Med. 2:581-583, 1968.

Chesnut C.H. III, Nelp W.B., Baylink D.J. and Denney J.D.: Effect of methandrostenolone on postmenopausal bone wasting as assessed by changes in total bone mineral mass. Metabolism 26:267-277, 1977.

Cohn S.H., Ellis K.J., Wallach S. et al.: Absolute and relative deficit in total-skeletal calcium and radial bone mineral in osteoporosis. J. Nucl. Med. 15:428-435, 1974.

Cohn S.H., Vaswani A., Zanzi I. and Ellis K.J.: Effect of aging on bone mass in adult women. Am. J. Physiol. 230:143-148, 1976a.

Cohn S.H., Vaswani A., Zanzi I. et al.: Changes in body chemical composition with age measured by total-body neutron activation. Metabolism 25:85-95, 1976b.

Durnin J.V.G. and Womersley J.: Body fat assessment from total body density and its estimation from skinfold thickness: measurements on 481 men and women aged 16 to 72 years. Br. J. Nutr. 32:77-97, 1974.

Heaney R.P.: Evaluation and interpretation of calcium-kinetic data in man. Clin. Orthop. 31:153-183, 1963.

Kennedy A.C., Boddy K., Williams E.D. et al.: Whole body elemental composition during drug treatment of rheumatoid arthritis: a preliminary study. Ann. Rheum. Dis. 38:137-140, 1979.

Kennedy N.S.J., Eastell R., Ferrington C. et al.: Total body neutron activation analysis of calcium: calibration and normalization. Phys. Med. Biol. 27:697-707, 1982.

Nelp W.B., Denney J.D., Murano R. et al.: Absolute measurements of total body calcium (bone mass) in vivo. J. Lab. Clin. Med. 79:430-438, 1972.

Palmer H.E., Nelp W.B., Murano R. and Rich C.: The feasibility of in vivo neutron activation analysis of total body calcium and other elements of body composition. Phys. Med. Biol. 13:269-279, 1968.

Spinks T.J., Bewley D.K., Ranicar A.S.O. and Joplin G.F.: Measurement of total body calcium in bone disease. J. Radioanal. Chem. 37:345-355, 1977.

Williams J.R., Bonnett D.E. and Parnell C.J.: The fixed horizontal neutron therapy beam at Edinburgh: dosimetry and radiation protection. Br. J. Radiol. 52:197-208, 1979.

RÉSUMÉ

Le calcium corporel total (Ca CT) a été mesuré par activation neutronique in vivo avec l'aide d'un cyclotron chez 20 femmes en bonne santé, 15 femmes ayant un tassement vertébral et 8 femmes atteintes de fracture de l'extrémité inférieure du radius. La précision de la technique, évaluée sur des fantômes, est de 1,8 pour cent pour une dose de 13 mSv. Une formule permettant de prédire le CaCT à partir du délai écoulé depuis la ménopause a été calculée pour les 20 femmes normales. Le coefficient de variation du CaCT après normalisation est de 6,6 pour cent dans la population témoin. Les valeurs moyennes du CaCT dans le groupe avec fracture vertébrale et dans celui avec fracture du radius étaient respectivement égales à 69 et 84 pour cent du CaCT des femmes au moment de leur ménopause. Le CaCT réduit dans le groupe avec fracture du radius peut être attribué à la perte osseuse post-ménopausique. La réduction du CaCT dans le groupe avec tassements vertébraux peut être imputée pour moitié environ à l'état post-ménopausique et pour moitié à d'autres facteurs.

Bone mass in nodal primary generalised osteoarthrosis

D. M. REID, N. S. J. KENNEDY, M. A. SMITH, P. TOTHILL, AND G. NUKI

From the Rheumatic Diseases Unit, Northern General Hospital, Department of Medicine, Western General Hospital and Departments of Medical Physics and Medical Engineering, Western General Hospital and Royal Infirmary of Edinburgh, University of Edinburgh

SUMMARY   Previous studies of patients with primary osteoarthrosis of the hip have suggested an increase in bone mass compared with control populations. Nodal primary generalised osteoarthrosis is known to have a strong familial tendency. To test the hypothesis that this tendency might also lead to increased bone mass, total body calcium has been measured by in-vivo neutron activation analysis and cortical area calculated from measurements of metacarpal indices in 15 female patients with primary generalised osteoarthrosis. The results have been compared with those from 12 healthy controls matched for age, menopausal status, and skeletal size. No significant differences were noted in the total body calcium or cortical area measurements between the 2 groups either before or after correction for skeletal size and menopausal status. No relationship was found between the grade of radiological osteoarthrosis in the hand and either bone mass parameter. Bone mass would not appear to be an important factor in the aetiopathogenesis of nodal primary generalised osteoarthrosis.

Osteoarthrosis (OA) is not a single disease but rather a pattern of biomechanical failure of joints[1] which may be secondary to a variety of disorders of bone or articular cartilage. Although most theories of the pathogenesis of OA are based on primary alterations in the articular cartilage,[2] Radin *et al.*[3][4] have suggested that the progressive wear of fibrillated articular cartilage seen in 'primary' OA results from stiffening of the subchondral bone. Clinical support for such a hypothesis comes from the observation that pathological changes of OA are unusual in femoral heads removed from patients with fractured necks of femur[5] and that bone mass appears to be increased in patients with primary OA of the hip when assessed by measurements of metacarpal indices[6] or photon absorptiometry.[7]

To examine this hypothesis further we have assessed bone mass in female patients with nodal primary generalised osteoarthrosis by measuring total body calcium and metacarpal indices and comparing the results with controls matched for age, skeletal size, and menopausal status.

Patients and methods

Fifteen female patients with nodal primary

generalised osteoarthrosis (PGOA) fulfilling the criteria defined by Kellgren and Moore[8] and 12 asymptomatic healthy women matched for age, skeletal size, and menopausal status have been studied. Serum calcium, phosphate, alkaline phosphatase, and albumin were measured in all subjects by standard methods, and persons with abnormalities of calcium metabolism or medical conditions known to be associated with secondary osteoporosis were excluded.

Total body calcium (TBCa) was measured by in-vivo neutron activation analysis. Patients were irradiated for 20 seconds from front and rear, while standing in a rigid polyethylene activation enclosure, by means of neutrons from the Edinburgh Medical Research Council Cyclotron. The patients were then transferred to a shadow-shield whole-body counter, where the gamma radiation from calcium ^{49}Ca induced from stable ^{48}Ca by neutron capture, was measured for 20 minutes. The patient's TBCa in grams was calculated by comparison with the energy spectrum from an activated anthropomorphic phantom of human dimensions containing a known quantity of calcium. Repeated measurements of the phantom gave a long term precision of 1·8% for a radiation dose of 13 mSv (1·3 rem).[9] The mean TBCa ± 1 SD in the control population was 842·0 ± 142·7 g. Individual results were expressed both in grams and

as a percentage of the expected normal value for the patient's skeletal size (arm span) and menopausal status. After correction for arm span and menopausal status the spread in the normal controls expressed as the coefficient of variation was reduced to 6·3%.

Metacarpal indices were measured by a variation of the technique described by Dequeker.[10] A single posteroanterior radiograph of the hands was taken at a uniform 1 metre tube-to-film distance using non-screen film. Morphometric measurements were performed at the right 2nd, 3rd, and 4th metacarpals. The length of each metacarpal was determined with a millimetre rule, and the external diameter (D) and the internal diameter (d) of the midshaft of the cortext were measured to the nearest 0·1 mm by means of a needle-tipped direct reading Vernier caliper. The cross-sectional cortical area was then calculated from the formula $\pi/4\ (D^2-d^2)$, but omitting $\pi/4$ by convention. The final figure was expressed as a mean of the 3 metacarpals. The precision of the technique, evaluated from 2 radiographs take at daily intervals in 10 young normal controls, was 2·0%. The mean cortical area in the control population was 46·3 mm², with a range from 37·5 to 52·9 mm².

The severity of radiographic osteoarthritic changes at the distal and proximal interphalangeal joints of each digit and at the carpometacarpal joint of the thumb was graded from 0 to 4 according to the criteria of the *Atlas of Standard Radiographs.*[11] A composite score was derived from the sum of the changes in each of the above joints giving a possible score of 0–80 considering both hands. All patients gave informed consent, and approval was obtained from local and national ethical committees.

Results

Details of age, menopausal status, span, height, and osteoarthrosis score for patients and controls are shown in Table 1. The results of TBCa and cortical

Table 1 *Mean age, menopausal status, span, height and osteoarthrosis score in patients with PGOA and controls; range given in parentheses*

	PGOA n = 15	Controls n = 12
Age (years)	58·5 (47–68)	55·5 (46–65)
Years after menopause	8·5 (0–20)	6·9 (0–22)
Arm span (cm)	166·2 (155–183)	163·1 (150–175)
Height (cm)	162·2 (156·5–170)	159·8 (151–173)
Osteoarthrosis score	36 (11–64)	3 (0–9)

Table 2 *TBCa expressed in grams and as a percentage of normal and cortical area in PGOA patients and controls. Mean values ± SD with the range given in parentheses*

	PGOA n = 15	Controls n = 12
TBCa in grams	830·6± 129·0 (590·2–1053·7)	842± 142·7 (596·0–1036·1)
TBCa–% or normal	99·5± 11·5 (83·0–120·1)	100± 6·31 (88·7–110·4)
Cortical area in mm²	47·0± 6·4 (36·1–56·0)	46·3± 5·2 (37·5–52·9)

area in the 2 groups are shown in Table 2. The mean TBCa in control and PGOA groups showed almost identical values, both when expressed in grams and when expressed as a percentage of the expected normal values for the patient's skeletal size and menopausal status. Mean cortical area measurements in the 2 groups again showed no significant difference.

Total body calcium was highly significantly correlated with cortical area (r = 0·722, p<0·001). TBCa and cortical area were not correlated with the osteoarthrosis score (TBCa: r = −0·289, cortical area: r = −0·173). There was no different in any of the indices of bone mass between patients who had or had not received nonsteroidal anti-inflammatory drugs.

Discussion

These studies suggest that there are no significant differences in total bone mass (measured by TBCa) or local bone mass (measured by cortical area) in patients with PGOA compared with matched controls. Statistical analysis of the data shows that mean differences in TBCa normalised for skeletal size and menopausal status ≥7·2% and cortical area ≥9·9% would have been significant at the 95% level in groups of this size.

Previous studies have only measured bone mass in patients with primary osteoarthrosis of the hip. Foss and Byers[6] first suggested that bone density measured by metacarpal indices was increased in patients with primary OA of the hip when compared with age matched normal subjects, but data on the skeletal size and extent of generalised osteoarthrosis in the patient group were not included. Roh et al.[12] found an increase in periosteal diameter (external cortical diameter) and cortical area in primary OA of the hip compared with an age matched normal range, but the differences in females may well have been attributable to increased skeletal size. More recent studies have failed to confirm such increases in bone density using measurements of cortical area and cortical thickness[13] or cortical area related to cross-sectional area.[14]

Photon absorptiometric methods have been used to estimate metacarpal[7] and radial bone mineral content[7 13 15] in patients with primary OA of the hip. The results have been conflicting: one study appeared to show an increase in bone mineral content of 13% at cortical and 23% at trabecular sites,[7] one showed an increase at a trabecular site alone,[15] and one showed no increase at either site.[13]

There are several possible explanations for the differences shown in these studies. The use of a stick as support might cause an increase in local bone mass, and this was eliminated in only 2 of the studies.[7 15] More important, patients and study groups have not been closely matched for skeletal size in any of the studies where increased bone mineral has been shown. In 2 of them the osteoarthrotic groups were indeed taller than the controls.[7 12]

No previous studies have corrected for menopausal status. As it is recognised that bone loss in females occurs at a rate of $1 \cdot 1\%$[16] to $1 \cdot 5\%$[9] per annum after the menopause and at a much slower rate before $(0 \cdot 37\%)$,[16] the small changes in the bone mineral content of the skeleton shown in some of the above studies may simply be related to different menopausal status.

Our failure to show increased total skeletal bone mass in patients with PGOA makes it very unlikely that bone mineral content is important in the aetiopathogenesis of this genetically determined condition. Nevertheless, these findings do not rule out the possibility of local increases in bone density in areas adjacent to affected joints, or very small increases in total bone mass.

References

1 Sokoloff L. The pathology of osteoarthrosis and the role of ageing. In: Nuki G, ed. *The aetiopathogenesis of osteoarthrosis.* Tunbridge Wells: Pitman Medical, 1980: 1–15.
2 Howell D S, Sapolsky A I, Pita J C, Woessner J F. The pathogenesis of osteoarthritis. *Semin Arthritis Rheum* 1976; **4:** 365–83.
3 Radin E L, Ehrlich M M, Weiss C A, Parker G H. Osteoarthrosis as a state of altered physiology. In: Buchanan W W, Carson Dick W, eds. *Recent advances in rheumatology.* London: Churchill-Livingston: 1976: 1–18.
4 Radin E L, Paul I L, Rose R M. Osteoarthrosis as a final common pathway. In: Nuki G, ed. *The aetiopathogenesis of osteoarthrosis.* Tunbridge Wells: Pitman Medical, 1980: 84–9.
5 Byers P D, Contepomi C A, Farkas T A. A post mortem study of the hip joint. *Ann Rheum Dis* 1970; **29:** 15–31.
6 Foss M V L, Byers P D. Bone density, osteoarthrosis of the hip, and fracture of the upper end of the femur. *Ann Rheum Dis* 1972; **31:** 259–64.
7 Roh Y S, Dequeker J, Mulier J C. Bone mass in osteoarthrosis measured in vivo by photon absorptiometry. *J Bone Joint Surg* 1974; **56A:** 587–91.
8 Kellgren J H, Moore R. Generalised osteoarthritis and Heberden's nodes. *Br Med J* 1952; i: 181–7.
9 Kennedy N S J, Eastell R, Ferrington C M, Simpson J D, Smith M A, Tothill P. Total body neutron activation analysis of calcium: calibration and normalisation. *Phys Med Biol* 1982; **27:** 697–707.
10 Dequeker J. Quantitative radiology: radiogrammetry of cortical bone. *Br J Radiol* 1976; **49:** 912–20.
11 Kellgren J H, Jeffrey M R, Ball J. The epidemiology of chronic rheumatism. *Atlas of standard radiographs of arthritis.* Oxford: Blackwell, 1963: 2.
12 Roh Y S, Dequeker J, Mulier J C. Cortical bone remodelling and bone mass in primary osteoarthrosis of the hip. *Invest Radiol* 1973; **8:** 251–4.
13 Alhava E M, Kettunen K, Karjalainen P. Bone mineral in patients with osteoarthrosis of the hip. *Acta Orthop Scand* 1975; **46:** 709–15.
14 Solomon L, Schnitzler C M, Browett J P. Osteoarthritis of the hip: the-patient behind the disease. *Ann Rheum Dis* 1982; **41:** 118–25.
15 Carlsson A, Nilsson B E, Westlin N E. Bone mass in primary coxarthrosis. *Acta Orthop Scand* 1979; **50:** 187–9.
16 Cohn S H, Vaswani A, Zanzi I, Aloia J F, Roginsky M S, Ellis K J. Changes in body chemical composition with age measured by total body neutron activation analysis. *Metabolism* 1976; **25:** 85–95.

Changes in Total Body Calcium after Renal Transplantation Effect of Low-Dose Steroid Regime

R. Eastell, N.S.J. Kennedy, M.A. Smith, P. Tothill, J.L. Anderton

Department of Medicine, Western General Hospital, Edinburgh, and Department of Medical Physics and Medical Engineering, Western General Hospital and Royal Infirmary, Edinburgh, UK

Key Words. Activation analysis · Homologous transplantation

Abstract. Total body calcium was measured in 8 men and 4 women, aged 20–51 years, undergoing kidney transplantation. The initial measurement was made within 8 weeks of operation and subsequent measurements up to 33 months postoperatively. Transplant rejection was prevented by low-dose prednisolone therapy (20 mg/day). 2 patients underwent parathyroidectomy for hypercalcaemia, and their total body calcium increased by 29 g (3%) and 66 g (8%). In the remainder the mean annual change was –0.9% (3.7, SD) over an average follow-up period of 17 months. This fall in total body calcium was statistically insignificant and was smaller than that previously described in patients treated with higher doses of steroids.

Introduction

Total body calcium (TBCa) can be used to measure long-term changes in calcium balance. We have applied this technique to 12 patients undergoing kidney transplantation. Previous prospective studies have shown that bone mass falls by between 5 and 7% in the 1st year after transplantation [*Lindsay* et al., 1976; *Aird and Pierides*, 1977]. However, these studies used higher doses of steroids than those used in the present study.

Patients and Methods

8 men and 4 women aged 20–51 years (mean 35.9) were studied. They had been on maintenance haemodialysis for 4–54 months (mean 23). The causes of renal failure were chronic glomerulonephritis (6), polycystic kidney disease (2), chronic pyelonephritis (1), obstructive nephropathy (1), malignant hypertension (1), and Goodpasture's syndrome (1). 2 patients had hypercalcaemia due to secondary hyperparathyroidism at the time of operation, 1 had aluminium-induced osteomalacia, and 1 had osteomalacia treated with alphacalcidol. 7 patients had arterial wall calcification.

9 patients received kidneys from cadavers and 3 from related donors. Antirejection treatment was given as described by *McGeown* et al [1977]. Azathioprine was given at a dose of 3 mg/kg/day and prednisolone at a dose of 20 mg/day. Subacute rejection episodes (average of 1 per patient, range 0–3) were treated with prednisolone

200 mg/day and reduced to 20 mg/day over 10 days. This dose was reduced to 10 mg/day over 10–33 months, unless chronic rejection developed (2 cases), and then the dose was increased to 20 mg/day.

TBCa was measured by in vivo neutron activation analysis using a cyclotron as the source of neutrons [*Kennedy* et al., 1982]. This method has a precision in anthropomorphic models of 1.8% for a dose of 13 mSv. Formulae have been described for predicting TBCa ($TBCa_p$) from height in men and from arm span and years postmenopause in women [*Kennedy* et al., 1982]. The ratio of TBCa to $TBCa_p$ is the calcium ration (Ca_R) and the mean value ± standard deviation (SD) for 20 healthy men was 1.000 ± 0.062 and for 20 women 1.000 ± 0.066. Initial measurements were made in the week prior to surgery in the 3 patients receiving kidneys from related donors and within 8 weeks of surgery in the remainder. Subsequent measurements were made at about 6-month intervals for up to 33 months (mean 17 months). Patients gave informed written consent, and the study was approved by the hospital ethics committee and the Administration of Radioactive Substances Advisory Committee.

Plasma calcium values were available immediately prior to operation and were subsequently measured monthly along with magnesium, protein, and creatinine. Plasma phosphate values were also available from before operation, and plasma parathyroid hormone (PTH), and plasma 25-hydroxyvitamin D were measured when the initial TBCa measurement was made; measurements were repeated at the end of the study. Radiographs were taken when considered appropriate by the physician in charge.

A paired t test was used to analyze the changes following kidney transplantation. Comparison with controls were made using the unpaired t test. Plasma alkaline phosphatase and 25-hydroxyvitamin measurements were $\log_e$-transformed prior to statistical analysis.

Table I. Initial TBCa results in patients undergoing renal transplantation

	Men	Women
TBCa, g		
Renal failure	1,006	685
Controls	1,143	821
Ca$_R$		
Renal failure	0.93*	0.82***
Controls	1.00	1.00

*p < 0.05; ***p < 0.001 (unpaired t test).

Table II. Initial plasma biochemistry and changes following renal allotransplantation in 10 patients

Variable	Initial value	Mean change, %	p
Alkaline phosphatase, U/l	72.2	−54	NS
Phosphate, mmol/l	1.69	−51	<0.02
Calcium, mmol/l	2.34	8	<0.05
Magnesium, mmol/l	1.26	−29	<0.002
Parathyroid hormone, g/l	0.82	−71	NS

NS = Not significant.
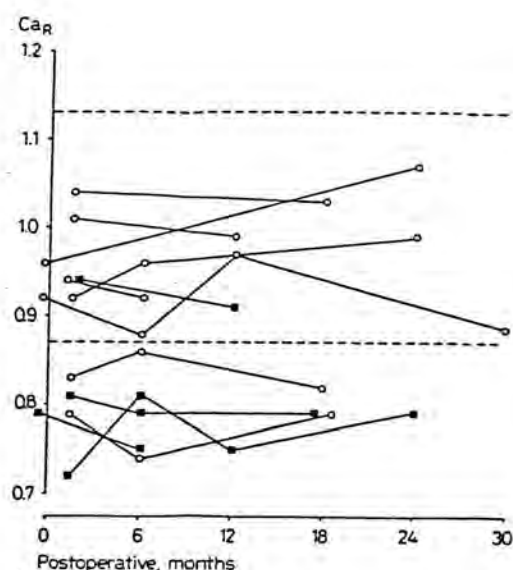
Fig. 1. Changes in Ca$_R$ in men (O) and women (■) following renal allotransplantation. Broken lines indicate 95% confidence limits for male and female controls.
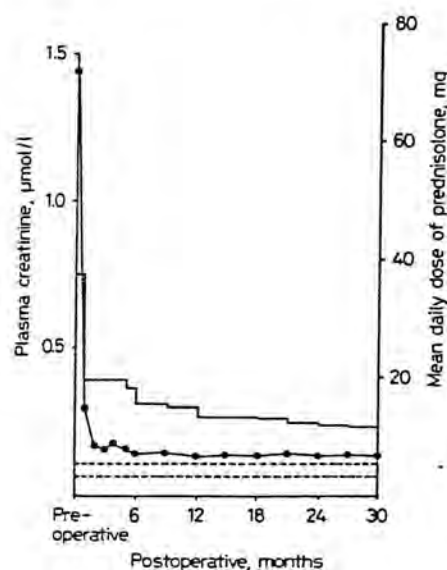
Fig. 2. Changes in plasma creatinine (.) and the mean daily dose of prednisolone (–) in 12 patients after renal allotransplantation. Broken lines indicate the laboratory reference range for plasma creatinine.

Results

Total Body Calcium

Initial values for TBCa and Ca$_R$ are shown in table I. The mean initial Ca$_R$ values in the 8 men showed a 7% reduction below the mean for male controls and in the 4 women an 18% reduction below the mean for female controls. 3 of the 4 women and 2 out of the 8 men had Ca$_R$ values less than 2 SD below the mean for the controls.

The 2 men who underwent parathyroidectomy 4 and 20 months after renal transplantation had increases in TBCa of 66 g (8%) over 10 months and 29 g (3%) over 18 months. In the remainder the mean change was calcu-lated from the initial and final measurements and was −0.9%/year, with 95% confidence intervals of −3.2–1.4%/year (fig. 1).

Biochemistry.

The initial biochemistry results are shown in table II. The elevated plasma creatinine fell gradually, but never into the normal range (fig. 2). 2 patients underwent parathyroidectomy, and so their data are excluded from the following results.

Plasma alkaline phosphatase and phosphate (table II) and plasma magnesium (fig. 3) all fell into the normal range. Plasma calcium gradually increased over the first 6
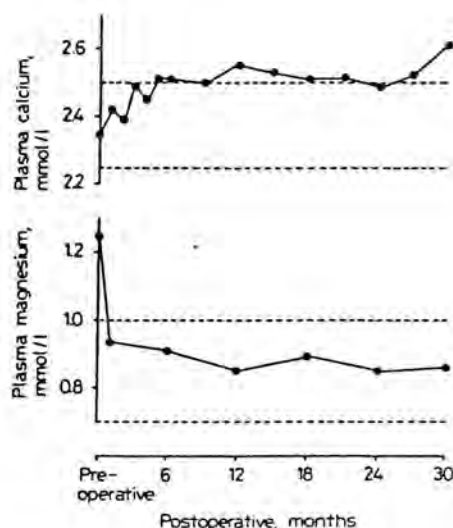
Fig. 3. Changes in plasma calcium and magnesium in 10 patients after renal allotransplantation. Broken lines indicate laboratory reference ranges.

months such that the mean value was at the upper limit of the reference range for the 30-month follow-up period (fig. 3). *1 z. einbf.*

Discussion

The annual reduction in TBCa of 0.9% was not statistically significant and was much smaller than the 7% fall in metacarpal bone density described by Lindsay et al. [1976] in the 1st year after renal transplantation. *Aird and Pierides* [1977] showed a fall of 5.1–5.4% in lower femur density over a similar period. Both groups used a higher dose of steroid, and this could account for the more rapid bone loss compared with the changes in the present study.

The insignificant change in TBCa contrasts with the dramatic biochemical changes. The time course of the return of plasma alkaline phosphatase, phosphate, and magnesium to normal, along with a reduction in plasma PTH almost to normal, corresponds with the bone biopsy findings of *Bortolotti* et al [1977]. They showed that the marrow fibrosis, excess osteoid, and increased bone resorption had resolved by 16–20 months after renal allotransplantation.

The persistent mild hypercalcaemia has been described in 21% of the 386 patients reported by *Chatterjee* et al. [1976], *David* et al. [1973], *Ibels* et al. [1978], and *Lee* et al. [1973]. It is associated with normal or raised plasma PTH levels [*Kleerekoper* et al., 1975]. This elevation may be due to the persistently impaired renal function. *Le-*

mann et al. [1979] have shown that plasma PTH rises when creatinine clearance falls below 50–80 ml/min (0.83–1.33 ml/s).

The initial low TBCa differs from the findings of others. *Cohn* et al. [1975] and *Denney* et al. [1973] reported normal mean TBCa values in patients on haemodialysis for chronic renal failure. The type of bone disease was reported to affect TBCa, the lowest values being found in those with osteomalacia and normal or high values in those with hyperparathyroidism. In the present series the low TBCa may be due to a higher frequency of osteomalacia, but unfortunately bone biopsies were not performed.

The healing of renal osteodystrophy after renal allotransplantation might be expected to be associated with an increase in TBCa, particularly in the patients with a predominantly osteomalacia type of bone disease. In the present series this effect was countered by the osteopaenic effect of the steroids. Ectopic calcification was present in more than half the subjects, but was always confined to blood vessel walls and was unlikely to have contributed much to TBCa [*Denney* et al., 1973]. Once the renal osteodystrophy has healed, the action of the steroids is unopposed and may be potentiated by the commonly associated mild hyperparathyroidism. This might account for the findings of *Andresen and Nielsen* [1982] of a low bone density in patients 67 months after renal transplantation; the mean value of bone mineral concentration of the radius and ulna was 25% below age- and sex-matched controls.

Acknowledgements

References

Aird, E.G.A.; Pierides, A.M.: Photon absorptiometry of bone after successful renal transplantation. Br. J. Radiol. *50:* 350–356 (1977).

Andresen, J.; Nielsen, H.E.: Interrelationship between metacarpal bone mass and bone mineral content in renal transplant recipients. Acta radiol. (Diag.) *23:* 513–516 (1982).

Bortolotti, G.C.; Feletti, C.; Scolari, M.P.; Bonomini, V.: Subclinical bone pathology after kidney transplantation in man. Calcif. Tissue Res. *22:* suppl. pp. 486–489 (1977).

Chatterjee, S.N.; Massry, S.G.; Friedler, R.M.; Singer, F.R.; Berne, T.V.: The incidence of persistent secondary hyperparathyroidism after renal transplantation. Surgery Gynec. Obstet. *143:*440–442 (1976).

Cohn, S.H.; Ellis, K.J.; Caselnova, R.C.; Asad, S.N.; Letteri, J.M.: Correlation of radial bone mineral content with total body calcium in chronic renal failure. J. Lab. clin. Med. *86:*910–919 (1975).

David, D.S.; Sakai, S.; Brennan, B.L.; Riggio, R.A.; Cheigh, J.; Stenzel, K.H.; Rubin, A.L.; Sherwood, L.M.: Hypercalcaemia after renal transplantation. Long-term follow-up data. New Engl. J. Med. *289:*398–401 (1973).

Denney, J.D.; Sherrard, D.J.; Nelp, W.B.; Chesnut, C.H, III; Baylink, D.J.: Total body calcium and long-term calcium balance in chronic renal disease. J. Lab. clin. Med. *82:*226–240 (1973).

Ibels, L.S.; Alfrey, A.C.; Huffer, W.E.; Weil, R., III: Aseptic necrosis of bone following renal transplantation. Experience in 194 renal transplant recipients and review of the literature. Medicine *57:*25–45 (1978).

Kennedy, N.S.J.; Eastell, R.; Ferrington, C.M.; Simpson, J.D.; Smith, M.A.; Strong, J.A.; Tothill, P.: Total body neutron activation analysis of calcium: calibration and normalization. Physics Med. Biol. *27:*697–707 (1982).

Kleerekoper, M.; Ibels, L.S.; Ingham, J.P.; McCarthy, S.W.; Mahony, J.F.; Stewart, J.H.; Posen, S.: Hyperparathyroidism after renal transplantation. Br. med. J. *ii:*680–682 (1975).

Lee, D.B.N.; Goldman, R.; Gonick, H.C.: Hypercalcaemia after kidney transplant. New Engl. J. Med. *289:*1256 (1973).

Lemann, XXXXX.

Lindsay, R.; McPherson, S.G.; Anderson, J.B.; Smith, D.A.: The value of bone density measurements in predicting the risk of developing avascular necrosis following renal transplantation. Calcif. Tissue Res. *21:*suppl., pp. 242–246 (1976).

McGeown, M.G.; Kennedy, J.A.; Loughridge, W.G.G.; Douglas, J.; Alexander, J.A.; Clarke, S.D.; McEvoy, J.; Hewitt, J.C.: One hundred kidney transplants in the Belfast City Hospital. Lancet *ii:*648–651 (1977).

Dr. R. Eastell,
Northwick Park Hospital,
Watford Road,
Harrow, Middx., HA1 3UJ (UK)

The seasonal variation of total body calcium

P Tothill†, N S J Kennedy†, J Nicoll†, M A Smith†, D M Reid‡ and G Nuki‡

† Department of Medical Physics and Medical Engineering, Royal Infirmary, Edinburgh EH3 9YW, Scotland
‡ Rheumatic Diseases Unit, University of Edinburgh, Edinburgh, Scotland

Abstract. Total body calcium was measured using *in vivo* neutron activation analysis in 156 patients with rheumatic diseases at six-month intervals. Evidence of seasonal variation was sought by relating deviation from a linear change to the month in which the measurement was made. A cyclic regression fitted to the data had an amplitude of 0.25% but a significance of only $P = 0.08$. The calcium balance studies of Malm were re-analysed to quantify the seasonal variation he had demonstrated in one group of men. The deduced variations of body calcium were highly significant, with a phase and amplitude very similar to the regression of our data. Both analyses differed from two previous reports of seasonal variations of part-body bone mineral of much greater amplitude and different phase.

1. Introduction

In 1958 Malm demonstrated a seasonal variation of calcium balance in a group of subjects maintained on a fixed intake over a long period (Malm 1958). This finding is compatible with subsequent studies of the seasonal variation of associated measurements of calcium biochemistry (Smith *et al* 1964, Stamp and Round 1974, Robertson *et al* 1974).

There have been two reports of direct measurements of bone mineral in limited parts of the skeleton which also showed seasonal variation (Aitken *et al* 1973, Krølner 1983). There do not appear to have been any studies of such an effect in the whole skeleton. As we have been carrying out longitudinal studies of total body calcium over an appropriate period it seemed worthwhile to examine the data for evidence of seasonal variation. Such a variation would be of direct physiological interest and also relevant to the interpretation of longitudinal studies of total body calcium.

2. Method

Total body calcium was measured by *in vivo* neutron activation analysis using a cyclotron source (Kennedy *et al* 1982). Corrections were applied for body size. The long term precision with anthropomorphic models was 1.8% and with patients 2.9% (Tothill *et al* 1984) for a dose-equivalent of 13 mSv. Three or four measurements of total body calcium were made at intervals of six months in 156 patients with various rheumatic diseases treated with a variety of agents (Reid *et al* 1984). 96 patients had rheumatoid arthritis, 9 psoriatic arthropathy, 19 primary generalised osteoarthrosis, 14 polymyalgia rheumatica and 18 ankylosing spondilitis. Permission was obtained from the local ethical committee and the Administration of Radioactive Substances Advisory Committee and the patients gave informed consent.

The rate of change of total body calcium was assessed by fitting a linear regression to the points for each patient. The possibility of a seasonal variation of total body calcium was investigated by relating the deviation of each point from the regression line to the month in which the measurement was made. Comparisons were made between mean deviations for monthly and three-monthly periods. In addition, a cyclic regression was fitted to the data.

Malm (1958) had demonstrated the existence of a seasonal variation of calcium balance by relating the proportion of 'better, poorer and intermediate' retentions to the month in which the observations were made. Such a method of analysis does not lend itself to the assessment of the significance or magnitude of the differences, so his data were subjected to re-analysis by the same techniques as were applied to our own.

3. Results

Our study commenced in mid 1980 and continued through 1983, although only 27 measurements were made in the last year. When mean deviations for each month of the study were plotted, no consistent pattern of variation was seen. As any seasonal changes were likely to be small compared with the spread of the data, results for each calendar month throughout the whole period were combined. The mean results for all subjects are shown in figure 1. Average deviations for each month are given, with standard errors. In addition, mean values are given for three-month periods. There is no significant difference between the mean values for any two months or quarters; the standard deviations and numbers of subjects were such that a difference of 0.7% in mean total body calcium between two three-month periods would have been significant at $P = 0.05$.
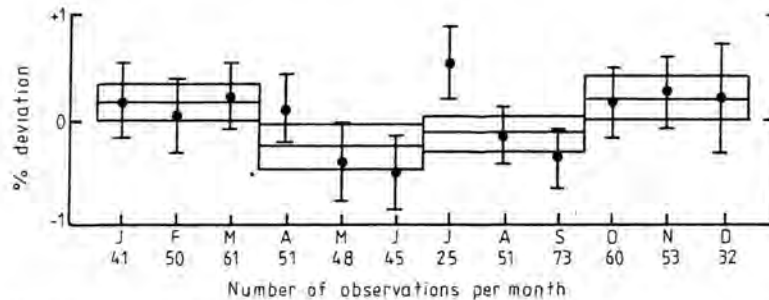
Figure 1. Variation of total body calcium with calendar month in which the measurement was made. Points are mean deviations from the regression line for each month, with standard errors. Blocks relate to means and standard errors for three-month periods. All subjects are included.

An expression of the form $x = a + b \cos(t + c)$ was fitted to all 590 observations using a least-squares method. x is the percentage deviation, t the month of the year and a, b and c are the parameters of the equation. a represents the mean value of x, b the amplitude of the oscillation and c the phase angle. The best-fit curve was

$$x = -0.002 + 0.253 \cos(30t - 19.37). \tag{1}$$

The correlation coefficient was $r = 0.070$, with a significance of $P = 0.08$.

The correlation coefficient provides a measure of the amount by which the residual variance of the data is reduced by the regression; in this case the reduction is barely significant.

A curve was also fitted to the mean monthly deviations

$$x = 0.032 + 0.187 \cos(30t - 8.93).$$ (2)

The regression ($r = 0.44$) had a significance of $P > 0.1$, reflecting the undue weight placed on the results from July, a month in which fewer than average measurements were made.

The data were also considered separately for women before and after the menopause and for men. No significant differences (at $P < 0.05$) between monthly or three-monthly mean values were seen and cyclic regressions were not significant. As mean rates of change were different in some of the disease and treatment groups (Reid *et al* 1984) the possiblity of seasonal variation was also examined in each of the groups separately. No evidence of such variation was found.

Malm (1958) considered seasonal variations of calcium balance in two groups of men studied for at least eight months. The first consisted of 16 men on a daily calcium intake of 950 mg. Over the whole period of study all but one of the subjects was in positive calcium balance. To quantify the variation, the mean of all 14-day calcium balances determined in a particular month was evaluated, together with its standard error. The results are plotted in figure 2(a). The three-month totals are also included. The numbers of observations varied slightly, averaging 31 per month. The difference between the highest positive balance in August and the lowest in April was significant ($P < 0.05$). When quarterly totals are considered the mean balances in the period July–September were greater than those in January–June, also with $P < 0.05$. The significance of the differences was calculated using tables of the Studentised range (Snedecor and Cochran 1980).

A cyclic regression was fitted to the data, the equation being

$$y = 73.9 + 45.0 \cos(30t + 86.6)$$ (3)

where the units of y are mg d^{-1} of calcium and t is in months. The correlation coefficient
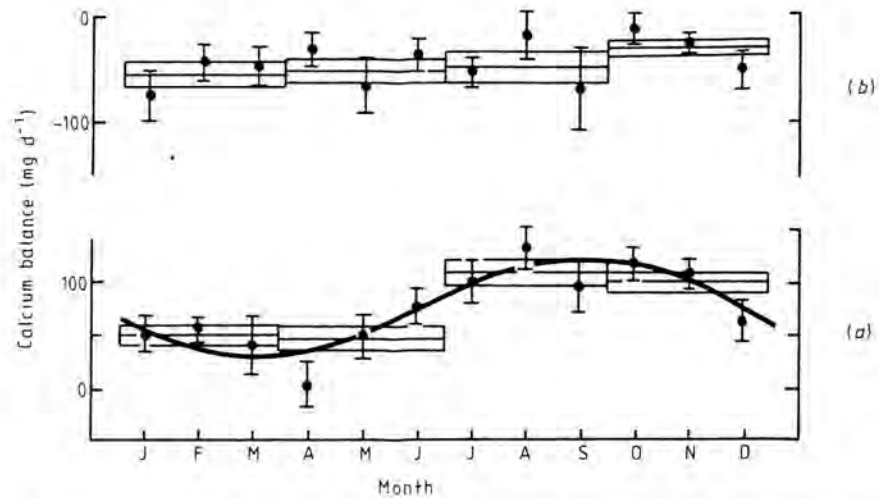
Figure 2. Malm's calcium balance data. Points are mean balances for each calendar month, with standard errors. Blocks relate to means and standard errors for three-month periods. (a) 16 men maintained for at least eight months with an intake of 950 mg d^{-1}; the full curve is the cyclic regression fitted to the data. (b) 10 men maintained for at least eight months with an intake of 450 mg d^{-1}.

is $r = 0.90$ and the regression is highly significant ($P < 0.001$); the amplitude is 45 mg d⁻¹. The curve is included in figure 2(a).

Variations in total body content of calcium can be obtained by integration of equation (3), giving

$$z = 2.25t + 2.58 \sin(30t + 86.6) \tag{4}$$

where z is the change in calcium content in g since the beginning of the year. The linear term reflects the overall positive balance of the subjects. The cyclic term has an amplitude of 2.6 g, with the phase shifted by three months compared with equation (3), so that the maximum positive deviation from a linear change occurs in December and the maximum negative deviation in June. The cyclic part of the regression is plotted in figure 3.
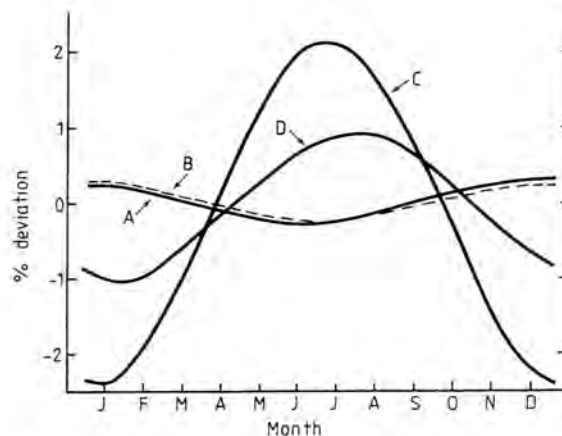
Figure 3. Cyclic regressions fitted to deviations from a linear change: A, total body calcium from Malm's balance data; B, total body calcium measured by us; C, metacarpal bone mineral reported by Aitken *et al*; D, spine bone mineral reported by Krølner.

The other group in which Malm claimed to have observed seasonal variation of calcium balance contained ten men maintained on a diet of only 450 mg d⁻¹. The mean monthly and three-monthly balances are plotted in figure 2(b). None of the differences between means was significant. The best-fit cyclic regression, $y = -44.5 + 7.73 \cos(30t + 91.7)$, was also not significant ($r = 0.29$, $P > 0.1$). Although this regression was not statistically significant, it may be noted that the phase was very similar to that observed for the high-level-intake regression.

4. Discussion

The first suggestion of possible seasonal variation of calcium balance came from McCance and Widdowson (1943). However, they made the finding in only three subjects. Malm (1958) demonstrated such an effect with more certainty by long-term balance studies on groups of subjects in a Norwegian state penitentiary, using closely controlled calcium intakes. Our study was the first to examine seasonal changes of total body calcium by direct measurement. The results suggest such a variation, but do not demonstrate it with a high degree of statistical significance.

Our re-analysis of Malm's data shows the magnitude and significance of seasonal variation based on long-term balance measurements. For the group of 16 men with a high calcium intake, the seasonal variation was highly significant. The maximum deviations of total body calcium from a linear change were 2.6 g. The calcium content of Reference Man is 1000 g (ICRP 1975) and our own measured mean value is 1143 g (Kennedy *et al* 1982) so that such an amplitude represents only about 0.25% of total body calcium. The dispersion of our results of TBCa measurements explains the difficulty that we have in detecting a change of this magnitude with any degree of significance. Nevertheless, although of marginal statistical significance, the curve fitted to our data is very similar in amplitude and phase to that derived from Malm's data. Both curves are included in figure 3.

Malm's observation of an apparent seasonal variation in the group of ten men with a low calcium intake was not, in fact, statistically significant.

The previous reports of the direct measurement of seasonal changes of bone mineral in humans have examined only a part of the skeleton. Aitken *et al* (1973) showed that the metacarpal mineral content of 48 post-menopausal women was 3.8% higher in the period May–August than in November–February. A cyclic regression fits very well to their data, with amplitude 2.3% and a maximum in July (figure 3).

Krølner (1983) similarly reported an increase of 1.7% in the lumbar spine bone mineral content of 26 normal women (nine of them post-menopausal) during July–September compared with January–March. There was a mean annual loss of 1% in this group and Krølner assessed the seasonal variation from deviations from a linear regression in the same way as we have. He fitted a cyclic regression equation, the amplitude of which corresponded to 1% of the spine bone mineral, with a maximum in August. This curve is also plotted in figure 3, which demonstrates that the two observations of bone mineral variation in parts of the body exhibit a greater amplitude than our deductions about total body calcium from Malm's balance data. They also show a different phase, with the maximum occurring about five months earlier.

Our results are not incompatible with Malm's observations. They are, however, at variance with the part-skeleton results; we could easily have detected changes of the magnitude reported by Aitken *et al* (1973) and Krølner (1983) if they had applied to the whole skeleton. It may be that seasonal variations are only apparent at certain bone sites. The greater variation in the spine than in the whole body might be thought to be due to the more rapid turnover of trabecular bone. However, the amplitude was even greater in the cortical bone of the metacarpals. It would perhaps be unwise to draw too many conclusions from different populations examined by different techniques.

We have to consider whether the likelihood of seasonal variation of TBCa in our patients might be different from that for normal subjects by virtue of their disease. Our population consisted of groups of patients, the majority of whom suffered from rheumatoid arthritis or primary generalised osteoarthrosis. Previous studies have shown that patients with these diseases do not have any disturbance of vitamin D metabolism (Bird *et al* 1980, 1982) and none of our patients had any abnormality of elementary calcium biochemistry. All were ambulant out-patients and it seems unlikely that the rheumatic diseases could affect any seasonal variation in calcium balance by either of the mechanisms that have been suggested, i.e. variable exposure to sunlight (Aitken *et al* 1973) or reduced exercise in winter (Krølner 1983).

One of our motives for undertaking this study was conern that seasonal variations might influence the interpretation of our longitudinal studies of TBCa. With the numbers

of our observations and their variance, the magnitude of any such seasonal variation is such that it does not complicate that interpretation.

Acknowledgments

Résumé

La variation saisonnière du contenu en calcium du corps entier.

Les auteurs ont mesuré, à six mois d'intervalle, le contenu en calcium du corps entier par analyse de l'activation neutronique *in vivo* sur 156 patients présentant des troubles rhumatismaux. Une variation saisonnière évidente a été recherchée en reliant l'écart à un changement linéaire au mois durant lequel la mesure était faite. Une régression cyclique ajustée aux données a présenté une amplitude de 0,25% mais une significativité de seulement $P = 0.08$. Les études par Malm de l'équilibre en calcium ont été analysées de nouveau pour quantifier la variation saisonnière qu'il avait démontré chez un groupe d'hommes. Les variations déduites du contenu en calcium du corps étaient hautement significatives, avec une phase et une amplitude tout à fait comparables à celles obtenues en ajustant la régression à nos données. Les deux analyses différaient de deux précédents rapports sur les variations saisonnières du contenu minéral osseux dans certaines parties du corps, présentant une amplitude beaucoup plus grande et une phase différente.

Zusammenfassung

Die jahreszeitliche Schwankung des Ganzkörperkalziums.

Mit Hilfe der *in vivo* Neutronenaktivierung wurde das Ganzkörperkalzium bei 156 Patienten mit rheumatischen Erkrankungen in 6-Monats-Intervallen gemessen. Es wurden Hinweise für jahreszeitliche Schwankungen gesucht, indem man die Abweichung von einer linearen Änderung in Beziehung setzte zu dem Monat, in dem die Messungen gemacht wurden. Eine zyklische Regression, mit der die Daten angepaßt wurden, hatte eine Amplitude bei 0.25%, aber eine Signifikanz von nur $P = 0.08$. Die Kalzium-Gleichgewichtsstudien von Malm wurden re-analysiert, um die jahreszeitlichen Schwankungen zu quantifizieren, die er in einer Gruppe von Männern gefunden hatte. Die abgeleiteten Schwankungen des Körperkalziums waren hochsignifikant mit einer Phase und Amplitude, die sehr ähnlich waren, wie die Regression der vorliegenden Daten. Beide Analysen unterscheiden sich von früheren Berichten jahreszeitlicher Schwankungen des Teilkörperknochenmineralgehaltes von viel größerer Amplitude und unterschiedlicher Phase.

References

Aitken J M, Anderson J B and Horton P W 1973 Seasonal variations in bone mineral content after the menopause *Nature* **241** 59–60

Bird H A, Peacock M, Storer J H and Wright V 1980 Comparison of serum 25-OH vitamin D concentrations in rheumatoid arthritis and osteoarthrosis *Br. Med. J.* i 1416

Bird H A, Wright V, Hennes U and Theiss E 1982 Comparison of serum 1,25-dihydroxycholecalciferol concentrations in rheumatoid arthritis and osteo-arthrosis *Ann. Rheum. Dis.* **41** 257–8

ICRP 1975 *Report of the Task Group on Reference Man No 23* (Oxford: Pergamon) p 296

Kennedy N S J, Eastell R, Ferrington C M, Simpson J D, Smith M A, Strong J A and Tothill P 1982 Total body neutron activation analysis of calcium: calibration and normalisation *Phys. Med. Biol.* **27** 697–707

Krølner B 1983 Seasonal variation of lumbar spine bone mineral content in normal women *Calcif. Tissue Int.* **35** 145–7

McCance R A and Widdowson E M 1943 Seasonal and annual changes in the calcium metabolism of man *J. Physiol.* **102** 42–9

Malm O J 1958 Calcium requirement and adaptation in adult men *Scand. J. Clin. Lab. Inv.* **10** (supplement 36) 1–290

Reid D M, Nicoll J, Brown N, Kennedy N S J , Tothill P, Smith M A and Nuki G 1984 Bone loss in rheumatoid arthritis and primary generalised osteo-arthrosis *Br. J. Rheumatol.* **23** 116–7

Robertson W G, Gallacher J C, Marshall D H, Peacock M and Nordin B E C 1974 Seasonal variations in the urinary excretion of calcium *Br. Med. J.* **iv** 436–7

Smith R W, Rizek J and Frame B 1964 Determinants of serum antirachitic activity: special reference to involutional osteoporosis *Am. J. Clin. Nutr.* **14** 98–108

Snedecor G W and Cochran W G 1980 *Statistical Methods* (Ames, IA: Iowa State University Press) p 234

Stamp T C B and Round J M 1974 Seasonal changes in human plasma levels of 25 hydroxyvitamin D *Nature* **247** 563–5

Tothill P, Nicoll J J, Kennedy N S J, Smith M A, Reid D M and Nuki G 1984 *Osteoporosis* ed C Christiansen, C D Arnaud, B E C Nordin, A M Parfitt, W A Peck and B L Riggs (Glostrup, Denmark: Department of Clinical Chemistry) pp 217–8

Bone Mass in Ankylosing Spondylitis

DAVID M. REID, JEREMY J. NICOLL, NORMAN S. J. KENNEDY, MICHAEL A. SMITH, PETER TOTHILL, and GEORGE NUKI

Abstract. To assess bone mass in ankylosing spondylitis (AS) we have measured total body calcium, bone mineral content of the lumbar spine and metacarpal indices in groups of patients with AS. Mean total body calcium was reduced by 5.3% ($p < 0.05$) in 20 patients compared with controls. The mean annual loss of bone, assessed over an 18 month period in 17 patients, was 2.9% ($p < 0.001$). Compared to controls, bone mineral content was increased by 28% ($p < 0.05$) in 8 male patients while metacarpal indices were normal in 18 male and female patients. The results of total body calcium measurements give support to the hypothesis of a minor increase in bone turnover in AS. The increased bone mineral content in the male patients may relate to syndesmophyte formation. (*J Rheumatol 1986;13:932-935*)

Key Indexing Terms:
ANKYLOSING SPONDYLITIS
TOTAL BODY CALCIUM

BONE MASS
SYNDESMOPHYTES

Although vertebral osteoporosis was originally considered to be an early radiological sign of ankylosing spondylitis (AS)[1,2], it is now recognized to occur as a late feature of the disease process[3,4]. Spontaneous fractures, a common consequence of vertebral osteoporosis, appear to be uncommon in AS, occurring only once in 212 patients in one report[5]. However, another group of investigators found 2 spontaneous fractures in a series of 50 patients, and the majority of subjects were said to have mild axial and appendicular osteoporosis[6].

To shed light on the presence and site of bone loss in AS we have measured total bone mass by total body calcium in patients with AS and related the results to those of vertebral bone mass measured by dual photon absorptiometry, peripheral bone mass measured by metacarpal indices and radiographic disease status measured by syndesmophyte count.

MATERIALS AND METHODS

Patients. We measured total body calcium in 20 randomly selected patients (14 men, 6 women) with AS as defined by the New York criteria[7] and compared the results with 52 age matched normal control subjects (27 men, 25 women). From within the total group 10 patients with AS (8 men, 2 women) had a single estimation of lumbar spine bone mineral content, 18 (13 men, 5 women) had a single measurement of metacarpal indices and

8 (7 men, 1 woman) had a syndesmophyte count. These patients were selected solely on willingness to attend for bone mass assessment. Bone mineral content results were compared with 36 normal control subjects (18 men, 18 women) and metacarpal indices with 45 normal controls consisting of 24 asymptomatic volunteers (12 men, 12 women) and 21 patients with primary generalized osteoarthritis (3 men, 18 women) who had been shown to have normal total bone mass[8].

Total body calcium measurement was repeated on 3 or 4 occasions over an 18 month period in 17 patients with AS (13 men, 4 women).

Serum calcium, phosphate, proteins and alkaline phospatase were measured in all subjects and those with abnormalities of calcium metabolism or medical conditions associated with secondary osteoporosis were excluded.

Methods. Total body calcium was measured by *in vivo* neutron activation analysis as described[9]. Neutrons produced from the Medical Research Cyclotron were directed at a patient standing in a rigid activation enclosure. The gamma rays produced by the reaction[48] $Ca(n, \gamma)$[49] Ca were measured in a whole body counter and compared with the results from a phantom to give a figure for total body calcium in grams. For longitudinal studies the measurement was repeated 3 or 4 times over an 18-month period and a regression line drawn through the values of total body calcium. From the slope of the regression line, the rate of change of total body calcium was calculated and expressed as a percentage of the initial value. In the initial studies the figure for total body calcium in grams was normalized for skeletal size (arm span) for both sexes and menopausal status in women using the regression formulae previously published[9]. The *in vivo* precision of the technique was 2.9%[10] for a radiation dose of 13 mSv.

Bone mineral content of the lumbar spine was measured by dual photon absorptiometry with an adapted dual headed rectilinear scanner using[153] Gd as a dual energy source[11]. The bone mineral image was displayed on a colour monitor and cursors placed at the top of lumbar vertebrae 2 (L2) and at the bottom of L4. The bone mineral content of the area within the cursors was calculated and divided by the vertical length to give bone mineral content in g/cm. The *in vivo* precision was reduced to 1.0% by an experienced operator. Predicted bone mineral content in patients with AS was calculated using the formula derived from the linear relationship found in normals between span and bone mineral content/unit length[11].

Metacarpal indices were measured by a variation of the technique described by Dequeker[12]. From nonscreen radiographs of the hands taken at a fixed 1 m source to film distance, the length (L) of the 2nd, 3rd and 4th metacarpals of the right hand were measured. At the mid-point of each metacarpal the external diameter (D) and the internal diameter (d) of the cortex were measured using a Vernier caliper. The mean cortical area as a percentage

of surface area [(D²-d²)/DL] was then calculated. The precision of the technique, evaluated from 2 radiographs taken at daily intervals in 10 young healthy controls was 2.0%.

The formation of bony bridging between the lateral and anterior borders of adjacent lumbar vertebrae from L1 to L5 was measured from posteroanterior and lateral films of the lumbar spine. Syndesmophytes were graded on a 0–3 scale with 3 equal to complete bony bridging. A final syndesmophyte count was recorded as a mean of the values at the 12 sites measured. Hence, no syndesmophytes would score 0 and a bamboo spine 3.

Statistical analysis was performed by Students's t test for unpaired variables. For small numbers and data not normally distributed, Wilcoxon's rank sum test and Kendall's rank correlation test were used.

RESULTS

Details of sex and age in controls and patients undergoing each assessment of bone mass are shown in Table 1. The results of normalized total body calcium, bone mineral content and metacarpal indices expressed as a percentage of normal are shown in Figure 1. Total bone mass was reduced by 5.3% (p<0.05) in AS compared with controls, when both sexes were considered together. The reduction was greater in the 6 female patients (9.7%, p<0.05) than in the males (2.4%), although the difference between the sexes did not reach statistical significance.

Bone mineral content of the lumbar spine was increased by 28% (p<0.05) in the 8 male patients measured but reduced in the 2 females. Metacarpal indices were normal in male and female patients with AS (Figure 1).

Details of disease duration and activity are shown in Table 2. None of the bone mass indices were related to disease duration or activity as measured by duration of early morning stiffness and erythrocyte sedimentation rate (ESR). The rate of change of total body calcium did not correlate with the change in the disease activity indices and was not related to the duration of disease. In addition, none of the bone mass indices was significantly related to the syndesmophyte count (mean ± 1SD=1.15 ± 0.85), when male and female

Table 2. *Results of disease activity indices expressed as the mean initial and mean change (± 1 SD) in male and female patients with AS undergoing measurements of total body calcium.*

	Male	Female
Duration of disease (years)	12.1 ± 6.8	14.3 ± 10.4
Initial EMS (min)	20.0 ± 25.9	114.2 ± 107.7
Change in EMS (min)	+3.5 ± 14.3	−46.2 ± 41.9
Initial ESR (mm/h)	24.8 ± 23.0	48.7 ± 40.4
Change in ESR (mm/h)	−5.5 ± 19.5	−31.7 ± 35.0

(EMS=duration of early morning stiffness; ESR=erythrocyte sedimentation rate)

patients were considered together. As syndesmophytes might be expected to increase spinal bone mineral, the difference in percentage of expected bone mass at lumbar and total bone sites (i.e., % bone mineral content – % total body calcium) was compared to the syndesmophyte count and a significant correlation was found (tau=0.571, p<0.01).

The annual rate of loss of total body calcium in the 17 patients with AS completing the longitudinal study (Table 3) was 2.9% (p<0.01), a figure not entirely explained by the large loss in the 4 female patients (5.2%), the male reduction also being significant.

Table 3. *The mean (± 1 SD) annual rate loss of total body calcium in male and female patients with AS*

Sex	No.	Annual Rate of Loss	Significance
Males	13	2.2 ± 2.6%	p<0.01
Females	4	5.2 ± 4.4%	–
Both	17	2.9 ± 3.2%	p<0.01

Table 1. *Sex, mean age and years post menopause (YPM) ± 1 SD in groups of patients with AS and controls undergoing total body calcium (TBCa), bone mineral content of the lumbar spine (BMC), metacarpal indices (MI) and syndesmophyte count (SC).*

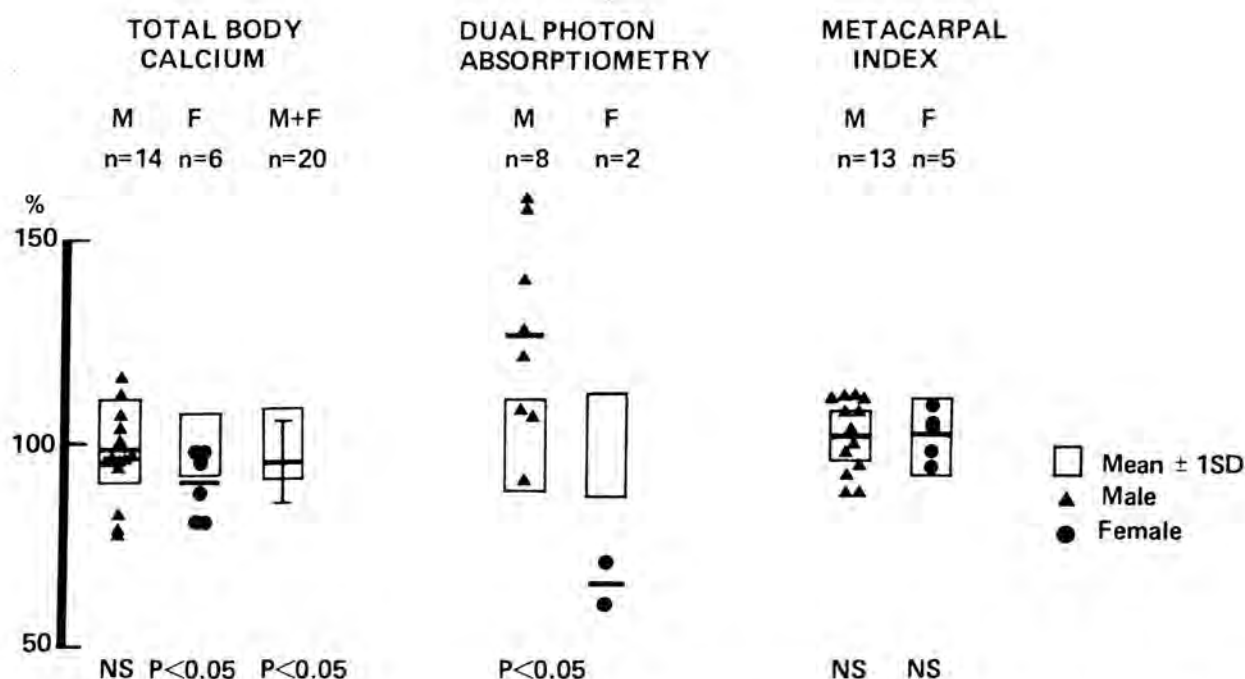|	Sex	AS Patients			Controls		
		No.	Mean Age	YPM	No.	Mean Age	YPM
TBCa	Males	14	41.7 ± 9.7	–	27	48.3 ± 13.1	–
	Females	6	39.7 ± 8.1	3.5 ± 5.9	25	52.6 ± 12.4	7.2 ± 6.9
BMC	Males	8	44.0 ± 10.4	–	18	33.9 ± 10.3	–
	Females	2	40.0 ± 11.3	7.0 ± 9.9	18	36.7 ± 11.4	3.2 ± 5.4
MI	Males	13	42.6 ± 9.5	–	15	46.6 ± 13.6	–
	Females	5	37.2 ± 7.5	4.2 ± 6.3	30	57.2 ± 6.1	8.6 ± 7.9
SC	Males	7	44.0 ± 10.4	–			
	Females	1	32	0			

Fig. 1. Results of normalized total body calcium expressed as a percentage of normal, bone mineral content of the lumbar spine expressed as a percentage of that predicted for each individual and metacarpal indices expressed as a percentage of the normal controls for male (▲) and female (●) patients with AS. The open blocks represent the mean ± 1 SD of the normal control subjects for each bone mass measurement. Significance values refer to the difference between patients and control values for each measurement.

DISCUSSION

In vivo methods of bone mass assessment have not previously been reported in patients with AS. However, radiographic studies have suggested that osteoporosis occurs both in the axial and appendicular skeletons[6], and using the technique of 24-h whole body retention of diphosphonate, bone turnover has been shown to be increased[13]. In our study total body calcium has been shown to be slightly, but significantly, reduced in patients with AS although much of the reduction occurred in the small group of female patients. In general the female patients had slightly more active disease than the males as measured by ESR and duration of early morning stiffness. However, as the differences did not reach statistical significance and the indices were not related to the results of total body calcium, it is not clear whether the slightly more active disease in females accounts for the lower bone mass. Although this small group of female patients was younger than controls, the age difference did not reach statistical significance using nonparametric tests. Total bone mass falls with age, but we have failed to show a relationship between age and total body calcium in normal premenopausal females either in this study or in previous work[9]. The lack of such a relationship has been suggested by other workers who only include an age correction factor for those women over the age of 55[14,15]. Accordingly it seems very unlikely that the difference in mean age between patients and controls accounts for the substantial differences in total body calcium.

Longitudinal total body calcium assessment gave support to the theory of a minor absolute reduction in bone mass as there was a significant annual loss of bone in males (2.2%) despite the young mean age of the group (42.6 years). Ethical considerations precluded the collection of control data for sequential measurements of bone mass, although previous work with the technique has shown an estimated annual reduction of total body calcium of only 0.7% in men over the age of 50 with no recorded loss before that age[16]. The rate of bone loss was not related to the activity of disease which tended to diminish during the study period.

If there is a reduction in total bone mass and an increased rate of bone loss, it is of interest to speculate where this might occur. Bone mineral content of the lumbar spine in 8 male patients was increased by 28% compared to controls but this increase is almost certainly explained by excess bone formation. The syndesmophyte count was correlated with the difference between the expected bone mass in the vertebrae and the total body while it was not related to lumbar spine bone mass alone. Hence, there is a strong suggestion that the increase in vertebral bone mineral content is caused by the presence of syndesmophytes. Using our current methods it is impossible to eliminate the effect on vertebral bone mass of syndesmophytes which become ossified when fully developed[17]. It remains possible that the vertebral bodies themselves are relatively osteopenic as suggested in pathological[18] and radiological studies[1,2,6]. The bone mineral content of the lumbar spine of the 2 female patients was markedly reduced and this is in keeping with the reduced total bone mass of the female patients.

The reduction in total body calcium in AS does not appear to be explained by reduced vertebral bone mass or by appendicular bone loss as metacarpal indices were normal in our patients. In order to be more certain of the site of bone loss it would be desirable to assess total, axial and appendicular bone mass simultaneously in the same groups of patients with AS and controls. This was not possible in our study.

The causes of increased bone loss in AS are unknown. Vertebral immobilization and changes in blood flow could be implicated, but the humoral factors responsible for increased turnover of vertebral bone have yet to be identified. Both immunoreactive parathyroid hormone (PTH)[19] and biologically active PTH[20] have been found to be elevated in some patients with AS but, in the absence of overt signs of hyperparathyroidism, both studies suggested that end organ failure might be responsible for the biochemical abnormality. We did not measure PTH values in our patients but we did not find any evidence of abnormal calcium biochemistry in our patients, and the only patient found to have a transient elevation in serum calcium was omitted from the analysis reported above. Many other biological mediators of bone resorption have recently been identified. From among these bone resorbing lympokines, interleukin 1, prostaglandins and vitamin D metabolites are all mediators that deserve further investigation in chronic inflammatory disorder such as AS.

ACKNOWLEDGMENT

REFERENCES

1. Buckley CW: Spondylitis deformans: Its differential diagnosis and treatment by physical methods. *Proc R Soc Med 1932;*26:105-110.
2. Steven GD: X-ray appearances in chronic rheumatism. *Ann Rheum Dis 1947;* 6:1-14.
3. Polley HF: The diagnosis and treatment of rheumatoid spondylitis. *Med Clin North Am 1955;* 39:509-528.
4. Wright V, Moll JMH: *Seronegative Polyarthritis.* Amsterdam: North Holland Publishing Company, 1976.
5. Wilkinson M, Bywaters EGL: Clinical features and course of ankylosing spondylitis. *Ann Rheum Dis 1958;*17:209-228.
6. Hanson CA, Shagrin JW, Duncan H: Vertebral osteoporosis in ankylosing spondylitis. *Clin Orthop Rel Res 1971;*74:59-64.
7. Bennett PH, Wood PHN: Population studies of the rheumatic diseases. In: *Proceedings of the Third International Symposium, New York, 1966.* Amsterdam: Exerpta Medica Foundation.
8. Reid DM, Kennedy NSJ, Smith MA, *et al:* Bone mass in primary generalized osteoarthrosis. *Ann Rheum Dis 1984;*43:240-242.
9. Kennedy NSJ, Eastell R, Ferrington CM, *et al:* Total body neutron activation analysis of calcium: calibration and normalisation. *Phys Med Biol 1982;*27:697-707.
10. Tothill P, Nicoll J, Kennedy NSJ, *et al:* The *in vivo* precision of total body calcium determinations by neutron activation analysis. In: Christiansen C, Arnaud CD, Nordin BEC, *et al,* eds. *Osteoporosis.* Denmark: Department of Clinical Chemistry, Glostrup Hospital, 1984;217-218.
11. Tothill P, Smith MA, Sutton D: Dual photon absorptiometry of the lumbar spine with a low activity source of ^{153}gadolinium. *Br J Radiol 1983;*56:829-835.
12. Dequeker J: Quantitative radiology: radiogrammetry of cortical bone. *Br J Radiol 1976;*49:912-920.
13. Steven MM, Sturrock RD, Fogelman I, *et al:* Whole body retention of diphosphonate in rheumatoid arthritis. *J Rheumatol 1982;*9:873-877.
14. Cohn SH, Vaswani A, Zanzi I, *et al:* Effect of aging on bone mass in adult women. *Am J Physiol 1976;*230:143-148.
15. Ott SM, Murano R, Lewellen TK, *et al:* Total body calcium by neutron activation analysis in normals and osteoporotic populations: a discriminator of significant bone mass loss. *J Lab Clin Med 1983;*102:637-645.
16. Cohn SH, Vaswani A, Zanzi I, *et al:* Changes in body chemical composition with age measured by total body neutron activation. *Metabolism 1976;*25:85-95.
17. Forestier J, Jacqueline F, Rotes-Querol J: *La Spondylarthrite Ankylosante.* Paris: Masson and Cie, 1951.
18. Fagge CH: Diseases etc. of the osseous system. 1. A case of simple stenosis of the ribs to the vertebrae and of the arches and articular processes of the vertebrae themselves. *Trans Pathol Soc London 1877;*28:201-206.
19. Fairney A, Wotjilewski H, Hart FD: Parathyroid hormone measurement in ankylosing spondylitis. In: Talmage RV, Owen M, Parsons JA. eds. *Calcium Regulating Hormones.* Amsterdam: Excerpta Medica 1975: 72-84.
20. Dunham J, Bourke BE, Bitensky L, *et al:* Circulating levels of biologically active parathyroid hormone in rheumatic diseases. *Ann Rheum Dis 1982;*41:569-573.

PAPERS AND SHORT REPORTS

Corticosteroids and bone mass in asthma: comparisons with rheumatoid arthritis and polymyalgia rheumatica

D M REID, J J NICOLL, M A SMITH, B HIGGINS, P TOTHILL, G NUKI

Abstract

Bone mass has previously been shown to be reduced at peripheral bone sites in patients with bronchial asthma receiving corticosteroids. To assess whether total bone mass is reduced in asthma total body calcium was measured by in vivo neutron activation analysis in patients receiving various treatments for asthma and compared with results from normal controls and patients with rheumatoid arthritis and polymyalgia rheumatica. Compared with controls total body calcium was reduced by 13·6% (p<0·001) in patients with asthma receiving daily oral corticosteroids but by only 9·0% (p<0·005) in a similar group of patients who had received oral calcium supplements at the start of their corticosteroid treatment. Total body calcium was also reduced in a group of patients receiving only inhaled corticosteroids (8·8%; p<0·001) but not significantly reduced in a small group of patients with asthma who had never received these drugs. When compared with controls a group of patients matched for age and for dose of corticosteroids given for rheumatoid arthritis had a similar reduction in total body calcium to the patients with asthma receiving daily oral treatment (17·7%; p<0·001), but no such reduction was shown in patients with polymyalgia rheumatica.

These findings suggest that the risk of bone loss with low dose oral corticosteroids is similar in asthma and rheumatoid arthritis. Further work is required to assess the clinical relevance of small losses of bone associated with the use of inhaled corticosteroids.

Introduction

Since Cushing's original description of the syndrome in 1932 it has been recognised that supraphysiological concentrations of endogenous corticosteroids are associated with excess bone loss.[1] The introduction of cortisone as a therapeutic agent was followed very shortly by case reports of spontaneous fractures during treatment,[2] and subsequently radiological osteoporosis was reported at various skeletal sites.[3 4] The cause of corticosteroid induced osteoporosis is now better understood[5] but there remains controversy about the dose and duration of treatment with synthetic corticosteroids necessary to induce osteoporosis.[6-8] Whether or not bone loss can be prevented by altering the route or timing of drug administration[8 9] remains uncertain. There is also continuing controversy whether patients with some diseases may be less susceptible.[10-13]

As there is a relative paucity of data on bone mass in asthmatics we have carried out measurements of total body calcium in groups of patients with bronchial asthma treated with oral and inhaled corticosteroids and compared the results with those in people who have not received steroids. The results were also compared from those from patients with rheumatoid arthritis and polymyalgia rheumatica receiving regular oral corticosteroid treatment and from controls matched for age and sex.

Patients and methods

We measured total body calcium in 70 patients with asthma (28 men, 42 women). The total group was subdivided according to current and previous treatment. Group 1 consisted of 23 patients (eight men, 15 women) who were receiving regular oral corticosteroids and had been doing so for at least two years. Group 2 consisted of a further 13 patients (two men) who were also receiving regular oral corticosteroids but who had received oral calcium supplements as calcium lactate gluconate three tablets a day (elemental calcium dose 1·2 g daily) at the start of their corticosteroid treatment and for two to 20 years thereafter. Group 3 consisted of 22 patients (11 men) whose only regular corticosteroid treatment was given by the inhaled route either as beclomethasone 100 µg four times daily or as betamethasone 200 µg four times daily. Sixteen patients (six men) in group 3 had also received a mean of 2·2 booster courses of oral corticosteroids, usually beginning with 40 mg prednisolone daily and reducing to nothing over seven to 10 days. Group 4

University Department of Medicine, Western General Hospital, Edinburgh

D M REID, MD, MRCP, lecturer, rheumatic disease unit
B HIGGINS, MRCP, registrar, respiratory disease unit
G NUKI, MB, FRCP, professor, rheumatic disease unit

University Department of Medical Physics and Medical Engineering, Edinburgh

J J NICOLL, PHD, senior physicist
M A SMITH, MSC, PHD, principal physicist
P TOTHILL, PHD, FINSTPHYS, reader

Correspondence to: Dr D M Reid, Rheumatology Department, City Hospital, Aberdeen AB2 1NJ.

consisted of 12 patients (seven men) who had never received corticosteroids either by inhalation or by the oral route.

The results from the four groups of patients with asthma were compared with those from 40 controls (20 men).[14 15] The results from patients in group 1 were further compared with those from 27 patients (eight men) with definite or classical rheumatoid arthritis,[16] matched for daily dose of prednisolone, and 12 patients (3 men) with polymyalgia rheumatica[17] who were receiving similar daily doses of oral corticosteroids.

All patients and controls who had abnormalities of calcium biochemistry or medical conditions known to be associated with secondary osteoporosis were excluded.

The corticosteroid dose for each patient was calculated retrospectively from the case records, supplemented when necessary by information from the patient. The total dose prescribed was expressed as the daily dose of prednisolone or equivalent averaged over the duration of treatment. Data on booster courses of the drugs were taken both from the case records and by direct questioning of the patient.

Total body calcium was measured by in vivo neutron activation analysis using the Edinburgh Medical Research Council cyclotron. Patients were irradiated with neutrons for 40 seconds while standing in a rigid polyethylene activation enclosure. Patients were then transferred to a shadow shield whole body counter, where γ radiation induced by the reaction calcium-48 (n, γ) calcium-49 was measured for 20 minutes. The patient's total body calcium was calculated in grams by comparison with the energy spectrum from an activated anthropomorphic phantom of human dimensions containing a known quantity of calcium. Repeated measurements of the phantom gave a long term precision of 1·8% for a radiation dose of 13 mSv (1·3 rem).[14] Normalisation was carried out by expressing individual results as a percentage of the expected normal value for the patient's skeletal size (arm span) in both sexes and menopausal state in women.[14] The in vivo precision of the technique was 2·9%.[18]

Statistical methods—Results were analysed by Student's *t* test for unpaired variables. The Mann-Whitney test was used for data not normally distributed and for small samples. By using Chauvenet's criterion[19]—a statistical technique designed to eliminate extreme values considered to occur by chance—two grossly aberrant total body calcium values from a woman in each of groups 1 and 2 were removed, leaving a total of 68 patients with asthma, whose results are reported.

Results

Table I gives details of age, duration of disease, corticosteroid and oral calcium treatment, and total body calcium values in grams in the four groups of patients with asthma. Patients in group 4 were significantly younger

TABLE I—*Sex ratio, mean age, years postmenopausal, duration of disease, and treatment in patients with asthma. (Mean values expressed with 1 SD in parentheses)*

	Group 1 (steroids alone; n=22)	Group 2 (steroids + calcium; n=12)	Group 3 (inhaled steroids; n=22)	Group 4 (no steroids; n=12)
Sex ratio (M:F)	8:14	2:10	11:11	7:5
Age (years)	54·1 (11·7)	60·8 (8·2)	55·6 (12·5)	37·9 (10·4)
No of women pre-/ postmenopausal	6/8	1/9	3/8	4/1
Years postmenopausal	5·0 (7·3)	11·4 (9·7)	10·0 (8·2)	0·5 (1·1)
Duration of disease (years)	23·3 (18·1)	30·6 (13·3)	15·8 (16·3)	12·0 (15·2)
Steroid dose (mg/day)	6·8 (1·9)	8·9 (1·4)	—	—
Duration of steroid treatment (years)	12·5 (6·4)	18·0 (3·8)	—	—
No of boosters [range]	—	—	2·2 [0-18]*	—
Duration of calcium treatment (years)	—	10·6 (6·8)	—	—
Total body calcium (g)	863 (173)	787 (151)	894 (160)	1029 (116)

Only 16 patients in group 3 given booster courses.

<0·001) than those in the three other groups. Duration of disease was greater in group 2 than in group 3 (by 14·8 years; p<0·05) and group 4 (by ·6 years; p<0·01). Patients in group 1 had received a lower dose of prednisolone (by 2·1 mg/day; p<0·01) and for a shorter period (by 5·5 years; <0·05) than those in group 2. Prenormalisation values for total body calcium in controls were 1142·7 (1SD 133·8) g for men and 820·5 (124·7) g for women, as previously reported.[14]

Comparison of normalised results obtained in the control and asthma groups (fig 1) showed a reduction in mean total body calcium in group 1

(13·6%; p<0·001), group 2 (9·0%; p<0·005), and group 3 (8·8%; p<0·001). There was also a significant difference in mean total body calcium between groups 1 and 4 (8·1%; p<0·05). No significant differences were found between men and women.

No correlations were shown between the duration of disease and total body calcium in any of the four groups with asthma nor between the duration of calcium treatment and total body calcium in patients in group 2.
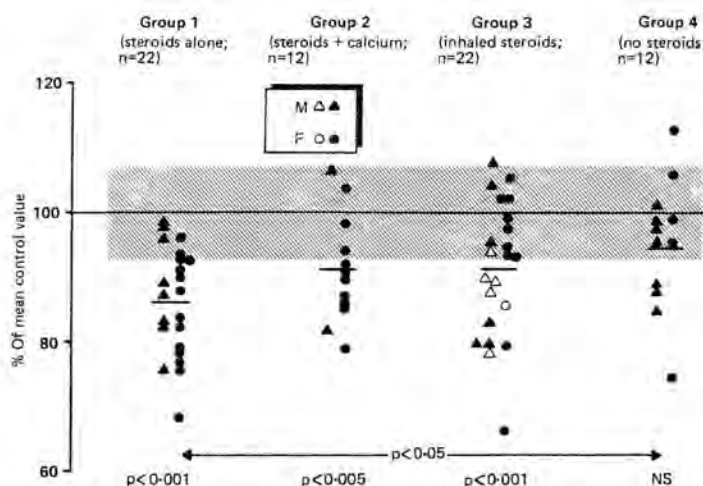
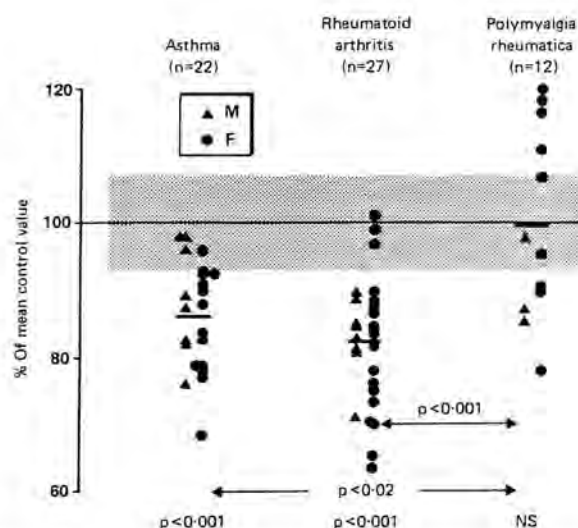

FIG 1—Total body calcium of patients with asthma expressed as percentage of mean of control population. Shaded area represents normal values (mean and 1 SD). In group 3 open symbols represent patients never given oral corticosteroids. Bars are means.

TABLE II—*Sex ratio, mean age, years postmenopausal, and details of corticosteroid treatment in controls and patients with asthma, rheumatoid arthritis, and polymyalgia rheumatica. (Mean values expressed with 1 SD in parentheses)*

	Controls (n=40)	Asthma (n=22)	Rheumatoid arthritis (n=27)	Polymyalgia rheumatica (n=12)
Sex ratio (M:F)	20:20	8:14	8:19	3:9
Age (years)	56·0 (7·5)	54·1 (11·7)	52·0 (11·8)	58·7 (10·2)
No of women pre-/postmenopausal	2/18	6/8	7/12	1/8
Years postmenopausal	8·8 (6·7)	5·0 (7·3)	6·8 (7·3)	11·8 (7·1)
Steroid dose (mg/day)	—	6·8 (1·9)	6·6 (1·9)	7·7 (1·5)
Duration of steroid treatment (years)	—	12·5 (6·4)	5·1 (4·4)	3·7 (3·3)
Total body calcium (g)	982 (206)	863 (173)	761 (155)	822 (173)

Table II gives details of sex ratio, age, corticosteroid treatment, and total body calcium values in group 1 patients with asthma and patients with rheumatoid arthritis and polymyalgia rheumatica. No significant differences were found between the patient groups with regard to age or corticosteroid treatment except that the patients with asthma had received oral steroids for longer than the patients with rheumatoid arthritis (7·4 years; p<0·001) and polymyalgia rheumatica (8·8 years; p<0·001).

Comparison of normalised results in these three groups with controls showed a reduction in mean total body calcium in patients with rheumatoid arthritis (17·7%; p<0·001) but none in those with polymyalgia rheumatica (fig 2). Compared with the group with polymyalgia bone mass was reduced in the patients with asthma (13·2%; p<0·02) and rheumatoid arthritis (17·3%; p<0·001). The apparent difference in mean total body calcium between the patients with asthma and those with rheumatoid arthritis did not reach statistical significance (0·1 >p>0·05).

The reduction in total body calcium was not related to the duration of treatment or the total steroid dose (daily dose × duration) in any of the groups but was correlated with the mean daily dose of prednisolone in those patients with rheumatoid arthritis (r=−0·605; p<0·001).

Discussion

Oral corticosteroid treatment has previously been associated with reduced bone mass in patients with bronchial asthma.[8 10] These

studies compared treated patients with normal controls using different measurements of forearm bone mass. Though unlikely, the possibility that bone mass might be reduced in asthma as a consequence of the disease itself was not considered. As bones contain 99% of the body's calcium content[20] it is a reasonable assumption that total body calcium is a measurement of total bone mass, particularly as it is extremely well correlated with the total bone mineral content of the skeleton measured by dual photon absorptiometry.[21] Hence this study confirms that reduced total bone mass does occur in patients with bronchial asthma treated with daily oral corticosteroids (group 1) when compared both with age matched normal controls and with young asthmatics who had never received steroids (group 4). Though this latter group was significantly younger than the controls, other studies have failed to show a relation between total body calcium and age in men or premenopausal women,[14] suggesting that the loss of bone in group 1 was attributable to steroid treatment rather than to age or disease.

FIG 2—Total body calcium of patients receiving corticosteroid treatment expressed as percentage of mean of control population. Shaded area represents normal values (mean and 1 SD). Bars are means.

The reduction in mean total body calcium of 13·6% in group 1 was substantial. Postmenopausal patients with crush fractures have a mean reduction in total body calcium of 16-20%,[22-24] suggesting that many patients with asthma treated with steroids are at risk of osteoporotic fractures. Indeed two patients in group 1 had sustained at least one atraumatic crush fracture before the measurement of total body calcium and a further patient had recurrent problems with multiple rib fractures.

Prevention of corticosteroid induced osteoporosis in patients with asthma, rheumatoid arthritis, and other diseases remains a severe therapeutic problem.[5] The use of alternate day corticosteroid regimens has not been shown to be advantageous.[9 10] In this study five patients in groups 1 and 2 who had received an alternate day regimen of corticosteroids for the first two to five years of treatment had a total bone mass which did not differ from that of patients who had received continuous daily treatment.

Despite higher daily doses and a longer duration of corticosteroid treatment a small group of patients (group 2) who had received oral calcium supplements at the start of treatment had a slightly greater mean total body calcium than those in group 1 (4·6%; 0·1>p>0·05). This suggests that the use of oral calcium supplements alone given at the start of corticosteroid treatment should be further investigated as a possible means of preventing osteoporosis. Other studies aimed at overcoming the calcium malabsorption known to be associated with corticosteroid treatment[25] have shown some benefit with 25-hydroxy vitamin D[26] but not with 1,25-dihydroxy vitamin D.[27]

The use of inhaled corticosteroids in asthma is almost certainly associated with a reduction in systemic side effects compared with oral treatment[28 29] but suppression of the hypothalamic-adrenal axis may occur with large doses.[30-32] There is little doubt that the main portion of the aerosol dose is deposited in the mouth and swallowed,[33] allowing gastrointestinal as well as pulmonary absorption. The finding that total body calcium was reduced in patients in group 3 by a mean of 8·8% compared with controls is therefore of concern. Sixteen of the 22 patients had received booster courses of oral corticosteroids, and such intermittent treatment has been associated with minor reductions of bone mass in patients with asthma.[8] The six patients who had never received oral treatment, however, had some of the lowest individual values of total body calcium (fig 1). This suggests that inhaled corticosteroids might be at least in part responsible for the reduction in group 3. The widespread and increasing use of high dose corticosteroid inhalers[34] suggests that further studies of bone mass in patients so treated should be undertaken. The pending development of inhaled corticosteroids which have an improved topical to systemic ratio[33 35] should be encouraged.

The effects of corticosteroids on bone mass in patients with asthma, rheumatoid arthritis, and polymyalgia rheumatica were compared (fig 2). Both patients with asthma and those with rheumatoid arthritis had reduced bone mass compared with patients treated for polymyalgia rheumatica but we were unable to confirm previous studies,[11 12] including our own preliminary data,[13] which suggested that corticosteroid treated patients with rheumatoid arthritis were more susceptible to bone loss than patients with asthma treated with similar daily doses. This study shows a small reduction in mean total body calcium (4·3%) in steroid treated patients with rheumatoid arthritis compared with asthmatics. As we have previously shown that total body calcium is reduced by 5·0-6·8% in patients with rheumatoid arthritis who have never received corticosteroids,[15] this reduction in bone mass may be attributable to the effects of the disease process, which causes appreciable bone loss at peripheral sites.[36]

Total body calcium is inversely related to the daily dose of prednisolone in patients with rheumatoid arthritis (r=-0·605; p<0·001). This finding raised the hypothesis that corticosteroid induced bone loss might occur early in the course of treatment,[15] and a recent longitudinal study has lent support to this theory.[37] Lack of a similar relation between total body calcium and daily steroid dose in asthma may reflect the wider fluctuations in individual steroid doses in these patients.

The explanation for the normal bone mass in patients with polymyalgia rheumatica is not clear. Women with polymyalgia rheumatica were older than those in the two other groups and the magnitude of the corticosteroid induced bone loss may not be apparent because of the substantial yearly 1·5% correction after the menopause.[14]

At present there is little convincing evidence for increased or decreased susceptibility to corticosteroid induced bone loss in patients with asthma or rheumatoid arthritis, though the position in patients with polymyalgia rheumatica may require further studies including larger numbers of subjects.

References

1 Cushing H. The basophil adenomas of the pituitary and their clinical manifestations. *Bulletin of the Johns Hopkins Hospital* 1932;50:137-95.
2 Boland EW, Headley NE. Management of rheumatoid arthritis with smaller (maintenance) doses of cortisone acetate. *JAMA* 1950;144:365-72.
3 Curtess PH, Clark WS, Herndon CH. Vertebral fractures resulting from prolonged cortisone and corticotropin therapy. *JAMA* 1954;156:467-9.

4 Murray RO. Radiological bone changes in Cushing's syndrome and steroid therapy. *Br J Radiol* 1960;33:1-19.
5 Baylink DJ. Glucocorticoid-induced osteoporosis. *N Engl J Med* 1983;309:306-8.
6 Hahn TJ, Boisseau VC, Avioli LV. Effect of chronic corticosteroid administration on diaphyseal and metaphyseal bone mass. *J Clin Endocrinol Metab* 1974;39:274-82.
7 Deding A, Taigaard S, Jensen MK, Rodbro P. Bone changes during prednisone treatment. *Acta Med Scand* 1977;202:253-5.
8 Adinoff AD, Hollister JR. Steroid induced fractures and bone loss in patients with asthma. *N Engl J Med* 1983;309:265-8.
9 Gluck OS, Murphy WA, Hahn TJ, Hahn B. Bone loss in adults receiving alternate day glucocorticoid therapy. *Arthritis Rheum* 1981;24:892-8.
10 Ruegsegger P, Medici TC, Anliker M. Corticosteroid induced bone loss. A longitudinal study of alternate day therapy in patients with bronchial asthma using computed tomography. *Eur J Clin Pharmacol* 1983;25:615-20.
11 Mueller MN. Effects of corticosteroids on bone mineral in rheumatoid arthritis and asthma. *American Journal of Roentgenology* 1976;12:1300.
12 Mueller MN, Mazess RB, Cameron JR. Corticosteroid therapy accelerated osteoporosis in rheumatoid arthritis. In: Mazess RB, ed. *International conference on bone mineral measurement*. Washington, DC: US Department of Health, Education, and Welfare, 1974:195-6. (DHEW publication 75/683.)
13 Reid DM, Nicoll JJ, Brown N, Smith MA, Tothill P, Nuki G. Bone mass in corticosteroid treated patients with rheumatoid arthritis, asthma and polymyalgia rheumatica. *Scott Med J* 1985;30:54-5.
14 Kennedy NSJ, Eastell R, Ferrington CM, *et al*. Total body neutron activation analysis of calcium: calibration and normalisation. *Phys Med Biol* 1982;27:697-707.
15 Reid DM, Kennedy NSJ, Smith MA, Tothill P, Nuki G. Total body calcium in rheumatoid arthritis: effects of disease activity and corticosteroid treatment. *Br Med J* 1982;285:330-2.
16 Ropes MW, Bennett GA, Cobb S, Jacox R, Jessar AR. Proposed diagnostic criteria for rheumatoid arthritis. *Ann Rheum Dis* 1959;18:49.
17 Hunder G, Hazelman BL. Giant cell arteritis and polymyalgia rheumatica. In: Kelley WN, Harris ED, Ruddy S, Sledge CB, eds. *Textbook of rheumatology*. Philadelphia: W B Saunders Co, 1985:1166-73.
18 Tothill P, Nicoll J, Kennedy NSJ, Smith MA, Reid DM, Nuki G. The in-vivo precision of total body calcium determinations by neutron activation analysis. In: Christiansen C, Arnaud CD, Nordin BEC, Parfitt AM, Peck WA, Riggs BL, eds. *Osteoporosis*. Denmark: Department of Clinical Chemistry, Glostrup Hospital, 1984:217-8.
19 Documenta Geigy. Chauvenet's criterion. In: *Scientific tables*. 5th ed. Basle: J R Geigy, 1956:47.
20 Fourman P, Royer P. *Calcium metabolism and the bone*. Oxford: Blackwell, 1968:20.
21 Mazess RB, Peppler WW, Chestnut CH, Nelp WB, Cohn SH, Zanzi I. Total body bone mineral by dual photon absorptiometry: II. Comparison with total body calcium by neutron activation analysis. *Calcif Tissue Int* 1981;33:361-3.
22 Cohn SH, Ellis KJ, Wallach S, Zanzi I, Atkins HL, Aloia JF. Absolute and relative deficit in total skeletal calcium and radial bone mineral in osteoporosis. *J Nucl Med* 1974;15:428-35.
23 Eastell R, Kennedy NSJ, Smith MA, Simpson JD, Strong JA, Tothill P. The assessment of postmenopausal osteoporosis by total body neutron activation analysis. *Metab Bone Dis Relat Res* 1983;5:65-7.
24 Ott SM, Murano R, Lewellen TK, Nelp WB, Chestnut CH. Total body calcium by neutron activation analysis in normals and osteoporotic populations: a discriminator of significant bone mass loss. *J Lab Clin Med* 1983;102:637-45.
25 Hahn TJ, Halstead LR, Baron DT. Effects of short term glucocorticoid administration on intestinal calcium absorption and circulating vitamin D metabolite concentrations in man. *J Clin Endocrinol Metab* 1981;52:111-5.
26 Hahn TJ, Halstead LR, Tietelbaum SL, Hahn BH. Altered mineral metabolism in glucocorticoid induced osteopenia: effect of 25-hydroxyvitamin D administration. *J Clin Invest* 1979;64:655-65.
27 Dykman TR, Haralson KM, Gluck OS, *et al*. Effect of oral 1,25-dihydroxyvitamin D and calcium on gluco-corticoid induced osteopenia in patients with rheumatic diseases. *Arthritis Rheum* 1984;27:1336-43.
28 Tse CST, Bernstein IL. Corticosteroid aerosols in the treatment of asthma. *Pharmacotherapy* 1984;4:334-42.
29 Spector SL. The use of corticosteroids in the treatment of asthma. *Chest* 1985;87(suppl):73-9.
30 Wyatt R, Waschek J, Weinberger M, Sherman B. Effects of inhaled beclomethasone dipropionate and alternate-day prednisone on pituitary-adrenal function in children with chronic asthma. *N Engl J Med* 1978;299:1387-92.
31 Toogood JH, Lefcoe NM, Haines DSM, *et al*. Minimum dose requirement of steroid-dependent asthmatic patients for aerosol beclomethasone and oral prednisone. *J Allergy Clin Immunol* 1978;61:355-64.
32 Gaddie J, Petrie GR, Reid IW, *et al*. Aerosol beclomethasone dipropionate; a dose response study in chronic bronchial asthma. *Lancet* 1973;ii:280-1.
33 Johansson SA, Anderson KE, Brattsand R, Gruvstad E, Hedner P. Topical and systemic glucocorticoid potencies of budesonide, beclomethasone dipropionate and prednisolone in man. *Eur J Respir Dis* 1982;122(suppl):74-82.
34 Anonymous. High-dose corticosteroid inhalers for asthma. [Editorial.] *Lancet* 1984;ii:23.
35 Lofdahl CG, Mellstrand T, Svedmyr N. Glucocorticoids and asthma. Studies of resistance and systemic effects of glucocorticoids. *Eur J Respir Dis* 1984;136(suppl):69-79.
36 Reid DM, Kennedy NSJ, Nicoll J, Smith MA, Tothill P, Nuki G. Total and peripheral bone mass in patients with psoriatic arthritis and rheumatoid arthritis. *Clinical Rheumatology* (in press).
37 Reid DM, Kennedy NSJ, Smith MA, *et al*. Bone loss in rheumatoid arthritis and primary generalised osteoarthrosis: effects of corticosteroids, suppressive anti-rheumatic drugs and calcium supplements. *British Journal of Rheumatology* 1986;25:253-9.

Total and peripheral bone mass in patients with psoriatic arthritis and rheumatoid arthritis

D.M. REID*, N.S.J. KENNEDY**, J. NICOLL**,
M.A. SMITH**, P. TOTHILL**, G. NUKI*

Rheumatic Diseases Unit, Northern General Hospital*, Department of Medicine, Western General Hospital* and Department of Medical Physics and Medical Engineering**, University of Edinburgh, Edinburgh, UK.

SUMMARY   *Psoriatic arthritis is thought to be associated with periarticular osteoporosis while rheumatoid arthritis may be associated with generalised as well as periarticular bone loss. To assess the extent of total and peripheral bone loss in these two diseases, total body calcium was measured by in vivo neutron activation analysis and peripheral bone mass was assessed by metacarpal indices in age-matched patients with psoriatic arthritis and rheumatoid arthritis treated with nonsteroidal anti-inflammatory drugs alone. In comparison with age and sex-matched normal controls, total and peripheral bone mass was normal in psoriatic arthritis. There were significant reductions in total (6.2% in men; 7.9% in women) and peripheral (10.9% in men; 12.8% in women) bone mass in patients with rheumatoid arthritis compared with controls. Peripheral bone mass was significantly correlated with the degree of radiographic damage in male and female patients with rheumatoid arthritis. The mean annual loss of total body calcium was insignificant in psoriatic arthritis (0.6% in men; 1.9% in women) but markedly greater in rheumatoid arthritis (4.4% in men; 2.7% in women). The data suggested that total and peripheral bone loss is greater in rheumatoid arthritis than psoriatic arthritis. Substantial reductions in peripheral bone mass in patients with rheumatoid arthritis not receiving corticosteroids may account in part for the small reductions in total bone mass.*

INTRODUCTION

There is little published information on the bone mass of patients with psoriatic arthritis (PA), although local osteoporosis is a

recognised radiological feature (1). This is not the experience of all investigators (2) and it is certainly limited in extent compared to that occurring in rheumatoid arthritis (RA) (3), where periarticular osteoporosis is an early radiological sign (4). Generalised osteoporosis is not thought to be a feature of PA (5) although it may occur in RA even in the absence of corticosteroids (6,7). To our knowledge no investigators have applied the in vivo methods of bone mass assessment to

patients with PA. As part of a large survey of bone mass in rheumatic diseases, we have have measured total bone mass, by total body calcium, and peripheral bone mass, by metacarpal indices, in a small group of patients with psoriatic arthritis and compared their results with those from a group of age and sex-matched patients with rheumatoid arthritis treated with nonsteroidal anti-inflammatory drugs alone.

PATIENTS AND METHODS

Twelve patients (6 males, 6 females) with PA, meeting the suggested diagnostic criteria of Wright and Moll (3), were enrolled in the study. All patients had a peripheral arthritis conforming to the PA$_1$ PA$_3$ and PA$_4$ sub-groups recognised by Moll and Wright (8). No patient had clinical evidence of spondylitis or sacro-iliitis (sub-group PA$_5$) nor were there any patients with arthritis mutilans (sub-group PA$_2$). All patients were sero-negative for rheumatoid factor and were receiving therapy with nonsteroidal anti-inflammatory drugs (NSAID) alone. No patient had received oral corticosteroids, suppressive anti-rheumatic drugs or immunosuppressive therapy.

Initial total body calcium (TBCa) has been assessed in the 12 patients with PA and compared with that of 45 patients (23 males, 22 females) with RA who were receiving NSAID alone and 36 controls (19 males, 17 females) (Table I).

The annual rate of change of TBCa has been assessed in 9 of the PA patients (5 males, 4 females) and compared with that of 13 age-matched patients (6 males, 7 females), with RA receiving NSAID alone (Table II).

Metacarpal indices have been measured in 11 of the PA patients and have been compared with results from 37 age and sex-matched patients (17 males, 20 females) with RA receiving NSAID alone and 27 controls (13 males, 14 females) (Table II).

TBCa was measured by in vivo neutron

Table I   *Male/Female ratio, mean ($\pm$ 1 standard deviation) age, yearsR post menopause and indices of disease activity in controlsa and patients with psoriatic arthritis (PA) and rheumatoidn arthritis (RA) included in initial total body calciumg measurement. Ranges given in parentheses. Statistical differences between PA and RA patients shown when signficant*

	Controls (n = 36)	Psoriatic Arthritis (n = 12)	Rheumatoid Arthritis (n = 45)
Male/female ratio	19/17	6/6	23/22
Age	45.2 ± 11.4	41 .5 ± 12.2	47.0 ± 9.2
(years)	(24-59)	(26-69)	(25-59)
Pre/post-menopause	8/9	5/1	13/9
Years post menopause	5.6 ± 2.9	19	5.4 ± 4.0
	(2-11)		(2-11)
Disease duration	—	7.1 ± 6.8	7.0 ± 7.1
(years)		(1-24)	(1-30)
Functional status	—	1.6 ± 0.5*	2.1 ± 0.6*
		(1-3)	(1-4)
ESR	—	18.8 ± 12.1*	35.4 ± 30.1*
(mm in 1st hour)		(2-40)	(1-115)
EMS	—	56.0 ± 72.5	79 .8 ± 89.7
(minutes)		(0-240)	(0-300)
Articular Index	—	5.4 ± 6.9*	12.4 ± 5.7*
		(0-22)	(0-21)

[ESR = erythrocyte sedimentation rate: EMS = duration of early morning stiffness: * = P < 0.01].

Table II *Mean age and years post menopause in controls and patientsR with psoriatic arthritis (PA) and rheumatoid arthritis (RA)a undergoing measurements of metacarpal indices (MI) and then rate of change in total body calcium (cTBCa).*

	Controls		Psoriatic Arthritis		Rheumatoid Arthritis	
	Men	Women	Men	Women	Men	Women
MI	(n = 13)	(n = 14)	(n = 6)	(n = 5)	(n = 17)	(n = 20)
Age	44.1	45.4	42.7	41.6	48.0	45 .9
(years)	(26-60)	(22-59)	(32-57)	(26-69)	(29-59)	(25 -58)
Pre/post-menopause	—	8/6	—	5/1	—	12/8
Years post menopause	—	5.8 (1-11)	—	19	—	1.8 (2-11)

	Controls		Psoriatic Arthritis		Rheumatoid Arthritis	
	Men	Women	Men	Women	Men	Women
cTBCa	—	—	(n = 5)	(n = 4)	(n = 6)	(n = 7)
Age	—	—	44.8	36.7	46.8	48.4
(years)	—	—	(37-57)	(31-45)	(32-59)	(34-57)
Pre/post-menopause	—	—	—	4/0	—	3/4
Years post menopause	—	—	—	0	—	7.2 (2-16)

Range shown in parentheses

activation analysis. Patients were irradiated for 40 seconds while standing in a rigid polyethylene activation enclosure, with neutrons from the Edinburgh Medical Research Council Cyclotron. The patients were then transferred to a shadow-shield wholebody counter, where gamma radiation induced by the reaction $^{48}Ca(n, 8)^{49}Ca$ was measured for 20 minutes. The patients' TBCa in grams was calculated by comparison with the energy spectrum from an activated anthropomorphic phantom of human dimensions containing a known quantity of calcium. Repeated measurements of the phantom gave a long term precision of 1.8% for a radiation dose of 13mSv (1.3 rem) (9). Individual results were expressed as a percentage of the expected normal value for the patient's skeletal size (arm span) in both sexes and menopausal status in women (9).

The rate of change of TBCa was calculated from 3 or 4 measurements of TBCa undertaken at 6-monthly intervals over an 18-month period. The TBCa in grams was plotted against time and from the slope of the regression line, the rate of change of TBCa was calculated and expressed as a percentage of the initial value. The in vivo precision of the technique, calculated from the deviation of individual points from the lines of regression representing the change in TBCa with time, was 2.9% in a large group of patients with rheumatic diseases (10).

Metacarpal indices were measured by a variation of the technique described by Dequeker (11). A single postero-anterior radiograph of the hands was taken at a constant 1 metre tube-to-film distance using nonscreen film. Morphometric measurements were performed at the right 2nd, 3rd, and 4th metacarpals. The length of each metacarpal was determined with a millimetre rule and the

external diameter (D) and the internal diameter (d) of the midshaft of the cortex were measured to the nearest 0.1mm by means of a needle-tipped direct reading Vernier caliper. To correct partially for the variation in skeletal size in the patient population, cortical area as a percentage of surface area $[(D^2-d^2)/DL]$ was calculated and the final figure expressed as a mean of the 3 metacarpals. Patient data were expressed as a percentage of the mean value of the control population. The precision of the technique, evaluated from 2 radiographs taken 24 hours apart in 10 young controls, was 2.0%(12).

Statistical analysis of results was performed using Student's t-test for unpaired variables. The Wilcoxon rank sum test was used for data not normally distributed and for small samples.

RESULTS

Details of male/female ratio, age, menopausal status and disease activity for the patients and controls undergoing initial total body calcium (TBCa) are shown in Table I. The patients with RA had more active disease in respect of their mean erythrocyte sedimentation rate, their functional status and their articular index. The age of the patients going on to complete 3 or 4 measurements of TBCa and those patients and controls who had metacarpal indices measured are included in Table II.

The results of initial TBCa measurement in males, females and both sexes together are shown in Table III. Patients with PA had a mean TBCa value which did not differ significantly from controls. Although the RA patients had reduced TBCa compared with PA patients, the results did not reach statistical significance. The RA patients did have reduced TBCa compared with controls and this reached signficance in females and both sexes when considered together. No relationship was found between age and TBCa in controls, patients with PA or patients with RA after the effect of the menopause was excluded.

The annual rate of change of TBCa in PA and RA patients is shown in Table IV. There was a significant mean annual loss of TBCa in the RA patients (-3.7%, p<0.005). The numbers in the PA group were small but the mean rate of change of TBCa was not significant in the male (-0.6%), the female (-1.9%) or the total group (-1.1%). The apparent difference between the rate of change of TBCa in RA and PA patients just failed to reach statistical significance (0.1>_ p>0.05). Annual change in TBCa was not related to disease duration or any one index of disease activity in the PA or RA groups.

The mean metacarpal indices for controls, PA and RA patients are shown in the figure. Cortical area as a percentage of surface area (D^2-d^2/DL) was normal in the small groups of male and female PA patients but significantly reduced in the groups of male and

Table III *Mean (= 1 standard deviation) initial total body calcium (TBCa), expressed as a percentage of the expected normal value, in male and female controls and patients with psoriatic arthritis and rheumatoid arthritis.*

	Controls	Psoriatic Arthritis	Rheumatoid Arthritis
Males	100.4 ± 11.4	98.5 ± 7.9	94.2 ± 10.2
Females	99.0 ± 8.0*	99.8 ± 11.1	91.1 ± 10.8*
Total	99.7 ± 9.9**	99.1 ± 9.7	93.3 ± 10.5**

[* = P<0.02 : ** = P<0.005]

Statistical difference between controls and patients with rheumatoid arthritis shown were significant.

Table IV   *Mean initial total body calcium (TBCa) expressed in grams and as a percentage of the expected normal value in patients with psoriatic arthritis and rheumatoid arthritis. Mean annual change in TBCa expressed as a percentage of the initial value in male, pre-menopausal and post-menopausal female patients. Range for each measurement shown in parentheses.*

	Psoriatic arthritis (n = 9)	Rheumatoid arthritis (n = 13)
Initial TBCa (grams)	1022.4 (821-1275)	913.5 (638-1196)
Initial % TBCa	100.4 (90.1 - 121.4)	92.7 (74.3 - 106.2)

	Psoriatic arthritis (n = 9)	Rheumatoid arthritis (n = 13)
Annual change in TBCa		
Males	-0.6% (+3.6 to -4.1)	-2.2% (+0.9 to -6.0)
Pre-menopausal females	-1.9% (+0.5 to -4.3)	-2.4% (-0.1 to -4.4)
M-Post-menopausal females	—	-4.8% (-2.6 to -7.1)
Males + females	-1.1%	-3.7%

female RA patients both in comparison with controls (males: 10.9%, $p < 0.01$; females: 12.8%, $p < 0.01$) and patients with PA (males: 10.6%, $p < 0.02$; females: 14%, $p < 0.02$). D^2-d^2/DL was not related to disease duration or any one index of disease activity in PA or RA with the exception of the Steinbrocker X-ray status (13) which was inversely related to the index in RA patients ($r = -0.35$, $p < 0.05$). Metacarpal indices were not related to age or years post-menopause in controls or patients with the exception of the female RA patients where there were significant relationships with age ($r = -0.50$, $p < 0.05$) and years post-menopause ($r = -0.65$, $p < 0.01$).

DISCUSSION

The results of initial total body calcium measurements strongly suggest that total bone mass is normal in patients with psoriatic arthritis. Such a suggestion is in keeping with a previously published view (5) and is given further support by the longitudinal study where the mean change in TBCa in the 9 patients with PA was only 1.1%. This was not statistically significant and as the figure also includes any loss of bone with age, the lack of significant change gives support to the hypothesis that psoriatic arthritis is not usually associated with generalised osteoporosis.

Local osteoporosis is a radiological feature of psoriatic arthritis (1) but we were unable to detect any local bone as measured by metacarpal indices (Fig. 1). However, in the patients with rheumatoid arthritis local bone mass was markedly reduced and was statistically less than that in psoriatic arthri-
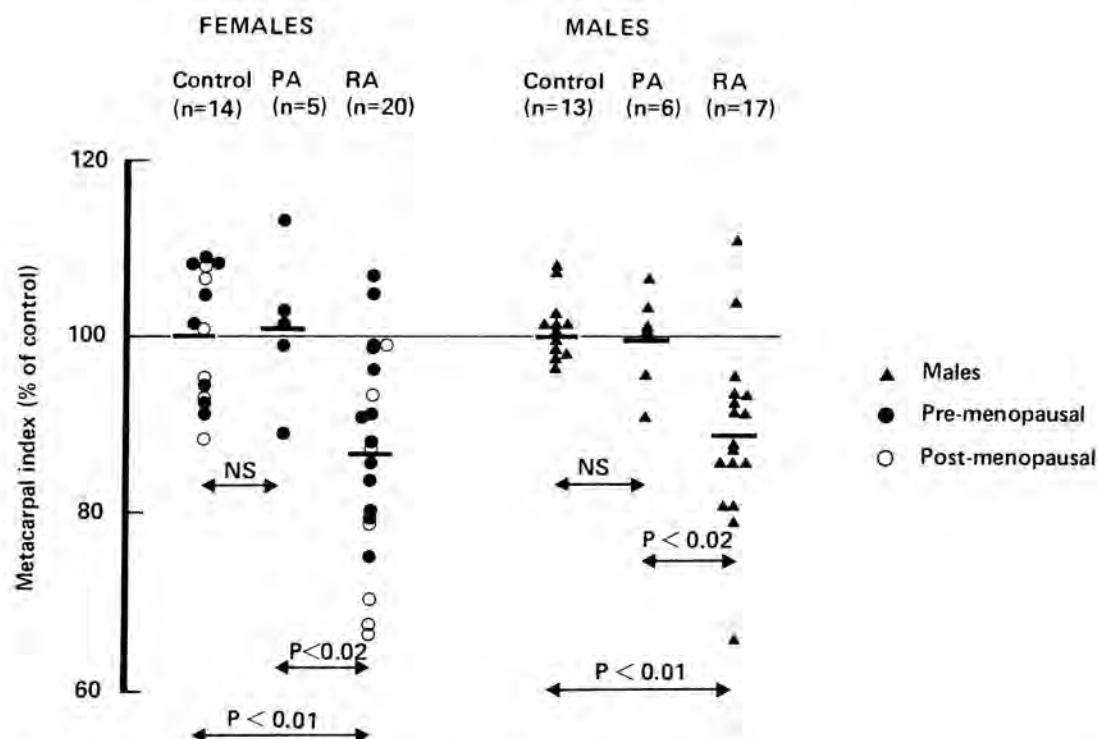
Fig. 1: Cortical area as a percentage of surface area [(D²-d²)/DL] of the 2nd, 3rd and 4th metacarpal bones in male (▲), pre-menopausal (●) and post-menopausal (o) female controls and patients with psoriatic and rheumatoid arthritis. Results expressed as a percentage of the mean of the controls.

tis. Similar trends were seen in the cross-sectional measurement of TBCa and also in the rate of change of TBCa, with RA patients showing reduced bone mass and a greater rate of bone loss than patients with PA. These results give support to the hypothesis that PA is a more benign condition as far as bone is concerned (3). Our PA patients had significantly less active disease than the RA patients and this may account for the differences in bone mass measurements, raising the possibility that biological mediators of bone resorption may be present in greater concentration in RA than in PA.

The reduction in local bone mass in RA is greater, in percentage terms, than the reduction in TBCa. Although the patients and controls having both bone mass measurements carried out were substantially the

same, there were some who did not undergo both measurements especially amongst the controls. Nevertheless, the substantial reduction in metacarpal indices (males: 10.9%, females: 12.8%) suggests a marked degree of local bone loss in RA which, if present in all peripheral bones, might account in part for the reduction in total bone mass shown in this study (males: 6.2%; females: 7.9%). A previous study where peripheral and total bone mass has been measured in the same group of patients showed an 8% reduction in total body bone mineral but a 19% reduction in the bone mineral content of the forearm (14).

We have previously reported the lack of relationships between TBCa and any one index of disease duration and activity in patients with RA (15). In addition no

relationship was found in this study between TBCa and Steinbrocker X-ray status. However, metacarpal indices have been shown to relate to X-ray status in RA (16) and this has been confirmed in our present study.

Peripheral bone loss in RA does seem to be related to the long-term disease activity and may account for some, if not all, of the reduction of TBCa. However, further work using improved methods of local bone mass assessment and relating any changes noted to total bone mass in the same groups of patients and controls will be required before this suggestion can be substantiated.

REFERENCES

1. Wright, V. Psoriatic arthritis. A comparative radiographic study of rheumatoid arthritis and arthritis associated with psoriasis. Ann Rheum Dis 1961, 20, 123-132.
2. Sherman, M.S. Psoriatic arthritis. - Observations on the clinical, roentgenographic and pathological changes. J Bone Jt Surg 1952, 34A, 831-852.
3. Wright, V., Moll, J.M.H. Seronegative polyarthritis. Amsterdam; Elsevier North Holland Publishing Company, 1976.
4. Bywaters, E. The early radiological signs of rheumatoid arthritis. Bull Rheum Dis 1960, 11, 231-4.
5. Genant, H.K. Radiology of rheumatic diseases. In: McCarty D.J., ed. Arthritis and Allied Conditions. New York: Lea Feabiger, 1979, 70-130.
6. Duncan, H., Frost, H.M., Villaneuva, A.R., Sigler, J.W. The osteoporosis of rheumatoid arthritis. Arthritis Rheum 1965, 8, 943-54.
7. Kennedy, A.C., Lindsay, R. Bone involvement in rheumatoid arthritis. Clin Rheum Dis 1977, 3, 403-20.
8. Moll, J.M.H., Wright, V. Psoriatric arthritis. Semin Arthritis Rheum 1973, 3, 55-78.
9. Kennedy, N.S.J., Eastell, R., Ferrington, C.M. et al. Total body neutron activation analysis of calcium: calibration and normalisation. Phys Med Biol 1982, 27, 697-707.
10. Tothill, P., Nicoll, J., Kennedy, N.S.J., Smith, M.A., Reid, D.M., Nuki, G. The in-vivo precision of total body calcium determinations by neutron activation analysis. In: Osteoporosis. Christiansen, C, Arnaud CD, Nordin BEC, Parfitt AM, Peck WA, Riggs BL. Eds. Denmark: Department of Clinical Chemistry, Glostrup Hospital, 1984, 217-8.
11. Dequeker, J. Quantitative radiology: Radiogrammetry of cortical bone. Br J Radiol 1976, 49, 912-20.
12. Reid, D.M., Smith, M.A., Kennedy, N.S.J., Tothill, P., Nuki, G. Comparison of metacarpal indices with total body calcium. Calcif Tiss Int 1983, 35s, A4, 16.
13. Steinbrocker, O., Traeger, C.H., Batterman, R.C. Therapeutic criteria in rheumatoid arthritis. J A M A 1948, 140, 659-62.
14. Skibsted Als, O., Gotfredsen, A., Christiansen, C. Relationship between local and total bone mineral in patients with rheumatoid arthritis and normal subjects. Clin Rheumatol 1983, 2, 265-71.
15. Reid, D.M., Kennedy, N.S.J., Smith, M.A., Tothill, P., Nuki, G. Total body calcium in rheumatoid arthritis: effects of disease activity and corticosteroid treatment. Br Med J 1982, 285, 330-2.
16. Bjelle, A.O., Nilsson, B.E. The relationship between radiological changes and osteoporosis of the hand in rheumatoid arthritis. Arthritis Rheum 1974, 44, 646-9.

Changes in Total Body Calcium Following Surgery for Primary Hyperparathyroidism

R. EASTELL, N.S.J. KENNEDY, M.A. SMITH, P. TOTHILL, and C.R.W. EDWARDS

Department of Medicine, Western General Hospital, Edinburgh, and Department of Medical Physics and Medical Engineering, Western General Hospital and Royal Infirmary, Edinburgh, UK.

Address for correspondence and reprints: Dr. R. Eastell, Mayo Graduate School of Medicine, 200 First Street S.W., Rochester, MN 55905, USA

Abstract

The aims of this study were to measure the deficit in total body calcium in patients with primary hyperparathyroidism and to observe whether this deficit was reversed by parathyroidectomy. Total body calcium was measured in five women and three men preoperatively, and the mean was found to be 11% below that of age- and sex-matched controls after normalization for postmenopausal age and body size ($P < 0.01$). Following parathyroidectomy, repeat total body calcium measurements showed an increase of 7.1% over an average period of 14 months ($P < 0.03$). In patients with primary hyperparathyroidism, total body calcium returns toward normal following surgical removal of the adenoma.

Key Words: Primary Hyperparathyroidism—Parathyroidectomy—Total Body Calcium—In Vivo Neutron Activation Analysis.

Introduction

Bone mass may be reduced in primary hyperparathyroidism. This has been found using techniques, such as in vivo total body neutron activation analysis (Cohn et al., 1973), photon absorptiometry of the radius (Pak et al., 1975, Pozzi-Mucelli et al., 1983; Posen et al., 1985), the lumbar spine (Seeman et al., 1982), and the third metacarpal (Genant et al., 1973), x-ray spectrophotometry of the radius and ulna (Dalen and Hjern, 1974), and quantitative computed tomography of the first and second lumbar vertebrae (Pozzi-Mucelli et al., 1983). These noninvasive techniques have shown mean reductions in bone of about 10% compared with age-matched controls. Low mean bone mass has been described in bones that are predominantly trabecular (Seeman et al., 1982; Pozzi-Mucelli et al., 1983) as well as in bones that are predominantly cortical in type. However, two studies have shown normal trabecular bone volume in bone biopsy specimens taken from postmenopausal women with primary hyperparathyroidism (Marcus et al., 1984; Charhon et al., 1982).

The skeleton is made up of approximately 80% cortical bone and 20% trabecular bone (Johnson, 1964). Therefore, total body calcium measurements are affected by changes in both trabecular and cortical bone, and the application of this measurement (=total body calcium) to patients with primary hyperparathyroidism should be appropriate. However, two studies of the effect of surgery for primary hyperparathyroidism on total body calcium have shown no overall beneficial effect (Cohn et al., 1973; Hosking et al., 1972). This is in contrast to prospective studies of regional bone mass, which have shown a beneficial effect of parathyroidectomy on bone density (Dalen and Hjern, 1974; Genant et al., 1973; Leppla et al., 1982). We report here the effect of parathyroidectomy on total body calcium of patients with primary hyperparathyroidism.

Patients and Methods

Patients

Eight patients with surgically proven primary hyperparathyroidism were studied. Age, sex, and clinical information are shown in **Table I.** Four of the five women were postmenopausal (1–11 years). The weight of the adenomata ranged from 0.17 to 1.59 g. Subperiosteal erosions were present on the hand radiograph of only one patient.

Twenty healthy women (aged 57.5 ± 6.5, SD) and 20 healthy men (aged 54.4 ± 8.8, SD) acted as controls.

Methods

Height was measured by wall-mounted ruler, arm span by wall-mounted graph paper, weight by Avery beam balance, and skinfold thickness by Harpenden calipers. These measurements were used in the normalization of total body calcium (Kennedy et al., 1982).

Biochemistry. Plasma and urinary calcium were measured by atomic absorption spectrophotometry and plasma alkaline phosphatase by the aminoantipyrene method. Immunoreactive parathyroid hormone (iPTH) was measured by a modification of the method of Woo and Singer (1974) (hormone antiserum complex precipitated by donkey antiguinea pig antiserum), which used polyvalent antibovine PTH antibody directed mainly against N-terminal PTH.

Total body calcium (TBCa). TBCa was measured by in vivo neutron activation as previously described (Kennedy et al., 1982). The method has a reproducibility of 1.8% (coefficient of variation of repeated measurements on phantoms) and a radiation dose equivalent of 1.3 rem (13 mSv). The reproducibility in vivo is 2.9% (coefficient of variation of repeated measurements on humans,

Table I. Laboratory results in eight patients with primary hyperparathyroidism

Patient No.	Age	Sex	Clinical Features	Plasma Ca (mg/dl)	Plasma iPTH (μg/l)	Plasma ALP (IU/l)	Urine Ca (mg/24 h)	TBCa (g)	Ca_R	Change in TBCa (g)
1	55	F	Hypertension Wrist fracture	11.1	2.20	141	492	672	0.720	80
2	61	F	Renal calculi Maturity-onset diabetes mellitus	10.3	0.53	88	460	697	0.911	142
3	46	F	Peptic ulcer	10.2	0.19	54	188	691	0.920	50
4	49	F	Peptic ulcer Polyuria, fatigue	10.2	0.41	64	480	663	0.716	106
5	50	F	Duodenitis	10.8	0.39	53	224	720	0.908	−26
6	64	M	Renal calculi Peptic ulcer	10.4	0.32	54	384	971	0.922	29
7	42	M	Renal calculi	10.6	0.31	65	516	1209	1.038	−9
8	37	M	Renal calculi Gout	11.4	0.38	71	412	1004	0.983	101
			Patients (n = 8)							
			Mean	10.6	0.44	70	395	820	0.890	59
			SD	0.4			124	206	0.115	59
			Controls (n = 40)							
			Mean	9.5	0.16	51	208		1.000	
			Mean ± 2SD	9.0–10.1	<0.33	30–80	8–408		0.870–1.130	
			P	<0.001	<0.001	<0.01	<0.01		<0.01	<0.03

Tothill et al., 1984). TBCa can be predicted from height in men and arm span and years postmenopause in women (Kennedy et al., 1982). The TBCa is expressed as a ratio of the observed to the predicted value (calcium ratio, Ca_R). The reference range of Ca_R was calculated from the 40 control subjects (mean ± 2 SD) and was 1.00 ± 0.13.

Statistical methods. The patient and control groups were compared by the Wilcoxon Rank Sum test. Changes following parathyroidectomy were compared using the paired t-test. The relationships between TBCa and biochemical measurements were assessed by linear correlation. Data for alkaline phosphatase and iPTH were analyzed after ln-transformation.

Results

Biochemistry. The results are shown in Table I, in which patients are compared with age-matched controls. In addition to the expected elevation in plasma calcium and iPTH, there were also increases in plasma alkaline phosphatase activity and urinary calcium excretion. Following parathyroidectomy plasma calcium fell into the normal range or below (1 patient), and plasma alkaline phosphatase activity fell by a mean of 22 IU/l ($P < 0.05$).

Total body calcium. The mean TBCa was 828 g (±206 g, SD). The mean Ca_R was 0.890 (±0.115, SD), that is, after normalization for body size and postmenopausal age there was an 11% reduction in bone mass ($P < 0.01$). Two of the eight patients had results below the 95% confidence intervals of Ca_R in controls **(Fig. 1).**

TBCa was remeasured 6–24 months (mean 14 months) after parathyroidectomy (Fig. 1). The mean increase was 59 g (range −29–142 g), equivalent to a mean rise of 7.1% in TBCa ($P < 0.03$). Only two of these eight patients had elevated plasma alkaline phosphatase activity preoperatively.

The weak relationships between the change in TBCa and initial urinary calcium excretion ($r = 0.40$), plasma alkaline phosphatase activity ($r = 0.50$), plasma iPTH ($r =$

0.22), and Ca_R ($r = -0.41$) did not reach statistical significance ($P > 0.05$).

Discussion

Cohn et al. (1973) found a mean Ca_R of 0.89 in nine patients with primary hyperparathyroidism, a result identical to that reported here. However, in the five patients they remeasured following parathyroidectomy there was no overall rise in TBCa. Similarly, Hosking et al. (1972) measured TBCa in 10 patients with primary hyperparathyroidism, and following parathyroidectomy half the patients showed a fall in TBCa, and in one this reduction was 30%. The patients studied by these groups had more severe hypercalcemia [mean plasma calcium 11.9 (Cohn et al., 1973) and 12.3 (Hosking et al., 1972), compared with 10.6 mg/dl in the present study] and higher plasma alkaline phosphatase activity. In patients with more severe hypercalcemia the osteopenia may not be reversible.

Three groups have reported increases in regional bone density following parathyroidectomy. In each study the size of the increase was similar to that reported in the present study. Pak et al. (1975) measured bone density of the distal radius by single photon absorptiometry and found normal values in men and premenopausal women and a 22% reduction in the bone density of postmenopausal women. The same group (Leppla et al., 1982) reported that after parathyroidectomy in postmenopausal women, as in the group of patients with primary hyperparathyroidism as a whole, there was a rise in bone density of 6.4% at 1 year. Over the following 2 years there was no further rise.

Genant et al. (1973) measured bone density of the third digit by photon absorptiometry and found a mean reduction of 13%. One to three years following parathyroidectomy there was a 7% rise in bone density. Dalen and Hjern (1974) measured bone density of the distal radius and ulna by x-ray spectrophotometry and found a mean reduc-
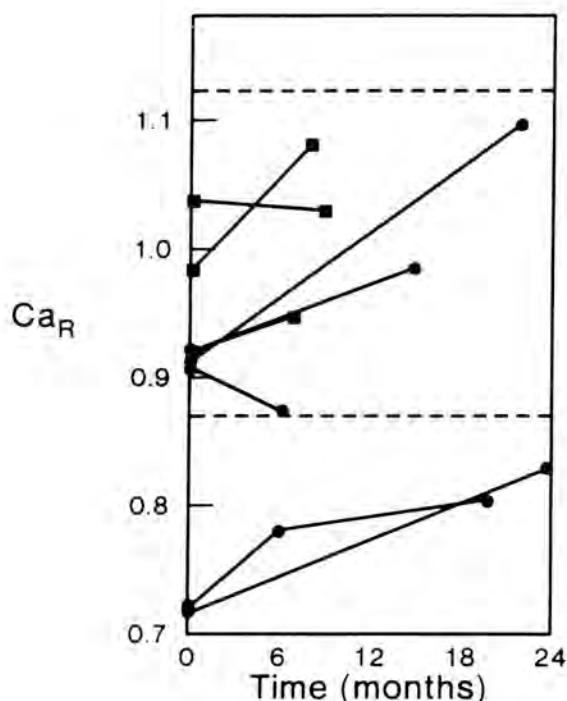
Fig. 1. Change in calcium ratio (Ca_R) following surgery for primary hyperparathyroidism in men (■) and women (●).

tion of 9%. One year after parathyroidectomy bone mass at this site had increased by 11.7%.

In a recently reported retrospective study Posen et al. (1985) found a 16% reduction in the density of the nondominant forearm measured by photon absorptiometry compared with age- and sex-matched patients who had undergone successful surgery for primary hyperparathyroidism.

What is the mechanism of increased bone mass following parathyroidectomy? Bone biopsy specimens taken from patients with primary hyperparathyroidism show an increase in the proportion of bone surfaces that are engaged in resorption. According to Parfitt (1980) the resorption phase leads to a transient deficit in bone mass, which is restored almost completely after the osteoblastic formation phase has finished. This ordinarily occurs in 2–3 months. In states of increased resorption there is a predictable increase in this transient pool of missing bone. Parathyroidectomy would cause an abrupt decrease in recruitment of resorption units, but those units already engaged in resorption would complete their remodeling cycles. This would explain why Leppla et al. (1982) found that the rise in bone density was almost complete at 6 months after parathyroidectomy. We were not able to delineate the time course of the change in total body calcium, since the dose of radiation used precludes multiple measurements.

Can the change in bone mass following surgery be predicted? No attempt was made by the three groups who have shown changes in regional bone mass to relate the changes to biochemical variables or initial bone mass. We were unable to predict changes in TBCa from baseline biochemical measurements or Ca_R.

The reduction in bone mass in patients with primary hy-

perparathyroidism may be associated with fragility fractures, such as vertebral crush fractures. For example, we found that the mean Ca_R in 14 women with postmenopausal osteoporosis and vertebral crush fractures was 0.87 (Eastell et al., 1983), a value similar to that found in the present study. Dauphine et al. (1975) found an increased prevalence of vertebral crush fractures in a case-control study of patients with primary hyperparathyroidism. Most of the patients with vertebral crush fractures in the latter study were postmenopausal women. The increase in total body calcium following parathyroidectomy may lower the risk of fracture.

Although all the patients in the present study had plasma calcium values of less than 12 mg/dl, most of them had complications of primary hyperparathyroidism. The results of this study may not apply to patients with mild, asymptomatic primary hyperparathyroidism. However, they do emphasize the need for a randomized, controlled trial of the effect of parathyroidectomy on bone mass in such patients.

References

Charhon S.A., Edouard C.M., Arlot M.E. and Meunier P.J.: Effects of parathyroid hormone on remodelling of iliac trabecular bone packets in patients with primary hyperparathyroidism. *Clin. Orthop.* **182**:255–263, 1982.

Cohn S.H., Roginsky M.S., Aloia J.F., Ellis K.J. and Shukla K.K.: Alterations in skeletal calcium and phosphorus in dysfunction of the parathyroids. *J. Clin. Endocrinol. Metab.* **36**:750–755, 1973.

Dalen N. and Hjern B.: Bone mineral content in patients with primary hyperparathyroidism without radiological evidence of skeletal changes. *Acta Endocrinol.* **75**:297–304, 1974.

Dauphine R.T., Riggs B.L., and Sholz D.A.: Back pain and vertebral crush fractures: An unemphasized mode of presentation for primary hyperparathyroidism. *Ann. Intern. Med.* **83**:365–367, 1975.

Eastell R., Kennedy N.S.J., Smith M.A., Simpson J.D., Strong J.A. and Tothill P.: The assessment of postmenopausal osteoporosis by total body neutron activation analysis. *Metab. Bone Dis. Rel. Res.* **5**:65–67, 1983.

Genant H.K., Heck L.L., Lanzl L.H., Rossman K., Horst J.V., and Paloyan E.: Primary hyperparathyroidism. A comparative study of clinical, biochemical, and radiological manifestations. *Radiology* **109**:513–524, 1973.

Hosking D.J., Chamberlain M.J. and Fremlin J.H.: Changes in total body calcium content in primary hyperparathyroidism. *Clin. Sci.* **43**:627–637, 1972.

Johnson L.C.: Morphologic analysis in pathology. In: Frost H.M. (ed) *Bone Biomechanics*, H.M. Frost, ed. Little, Brown and Co., Boston, 1964, p. 550.

Kennedy N.S.J., Eastell R., Ferrington C.M., Simpson J.D., Smith M.A., Strong J.A. and Tothill P.: Total body neutron activation analysis of calcium: Calibration and normalization. *Phys. Med. Biol.* **27**:316–334, 1982.

Leppla D.C., Synder W., and Pak C.Y.C.: Sequential changes in bone density before and after parathyroidectomy in primary hyperparathyroidism. *Invest. Radiol.* **17**:604–606, 1982.

Marcus R., Madig P., Crim M., Pont A. and Kosek J.: Conjugated es-

trogens in the treatment of postmenopausal women with hyperparathy- roidism. *Ann. Intern. Med.* **100**:633–640, 1984.

Pak C.Y.C., Stewart A., Kaplan R., Bone H., Notz C. and Browne R.: Photon absorptiometric analysis of bone density in primary hyperparathyroid- ism. *Lancet* **2**:7–8, 1975.

Parfitt A.M.: Morphologic basis of bone mineral measurements: Transient and steady state effects of treatment in osteoporosis. *Min. Elect. Metab.* **4**:273–287, 1980.

Posen S., Clifton-Bligh P., Reeve T.S., Wagstaffe C. and Wilkinson M.: Is parathyroidectomy of benefit in primary hyperparathyroidism? *Q. J. Med.* **54**:241–251, 1985.

Pozzi-Mucelli R.S., Kanton A.S., Genant H.K., Cann C.E., Ettinger B. and Kolb F.O.: Quantitative bone mineral analysis in primary hyperparathy- roidism. *J. Comput. Assist. Tomogr.* **7**:555, 1983.

Seeman E., Wahner H.W., Offord K.P., Kumat R., Johnson W.J., Riggs B.L.: Differential effects of endocrine dysfunction on the axial and appendic- ular skeleton. *J. Clin. Invest.* **69**:1302–09, 1982.

Tothill P., Nicoll J., Kennedy N.S.J., Smith M.A., Reid D.M. and Nuki G.: The in vivo precision of total body calcium determinations using neutron ac- tivation analysis. In: *Osteoporosis, Proceedings of the Copenhagen In- ternational Symposium on Osteoporosis.* C. Christiansen, C.D. Arnaud, B.E.C. Nordin, A.M. Parfitt, W.A. Peck and B.L. Riggs, eds. Glostrup, 1984, p. 217 (Abstr.).

Woo J. and Singer F.R.: Radioimmunoassay for parathyroid hormone. *Clin. Chim. Acta* **54**:161–168, 1974.

BONE LOSS IN RHEUMATOID ARTHRITIS AND PRIMARY GENERALIZED OSTEOARTHROSIS: EFFECTS OF CORTICOSTEROIDS, SUPPRESSIVE ANTIRHEUMATIC DRUGS AND CALCIUM SUPPLEMENTS

By D. M. REID[1], N. S. J. KENNEDY[2], M. A. SMITH[2], J. NICOLL[2], N. BROWN[1], P. TOTHILL[2] AND G. NUKI[1]

[1]*Rheumatic Diseases Unit, Northern General Hospital, Department of Medicine, Western General Hospital, and* [2]*Department of Medical Physics and Medical Engineering, University of Edinburgh, UK*

SUMMARY

The annual rate of bone loss in rheumatoid arthritis (RA) and primary generalized osteoarthrosis (PGOA) was determined by measurement of total body calcium (TBCa). The mean annual rate of bone loss in 24 patients with RA treated with nonsteroidal anti-inflammatory drugs (NSAIDs) alone was 3.4%. This rate of bone loss was not reduced in ten RA patients responding to suppressive antirheumatic drugs (4.3%) or seven patients receiving oral calcium supplements (4.5%). The mean annual rate of loss of TBCa in 19 patients with PGOA was 1.6%, a figure which probably represents age-associated bone loss. The rate of bone loss in PGOA was significantly less than that in RA patients not receiving corticosteroids. The mean annual rate of change of TBCa in 30 RA patients receiving corticosteroids (+0.7%) was significantly less than that in any of the other RA groups despite an initial normalized bone mass which was significantly less than in those RA patients receiving NSAIDs alone. The data supported the hypothesis that bone loss occurred early in the course of corticosteroid therapy and thereafter the drugs might have a protective effect on the loss of bone in RA.

KEY WORDS: Bone loss, Total body calcium, Rheumatoid arthritis, Osteoarthrosis, Corticosteroids, Suppressive antirheumatic drugs.

TOTAL bone mass has been shown to be reduced in rheumatoid arthritis (RA) [1–3] and further reduced by low-dose corticosteroid therapy [2, 3]. However, there is no literature on the rate of total bone loss in this disease although loss of bone from metacarpal sites has been shown to occur at rates of 2–4% per annum in patients receiving nonsteroidal anti-inflammatory drugs (NSAIDs), corticosteroids or penicillamine [4, 5].

Initial cross-sectional studies reported by us gave some support to the hypothesis that excess bone loss induced by corticosteroids occurred early in the course of therapy [2]. To test this hypothesis and to examine the effects on the rate of bone loss of oral calcium supplements and suppression of the disease process with antirheumatic drugs, we now report the results of an 18-month longitudinal study of total body calcium in RA. The results have been compared with those from patients with primary

generalized osteoarthrosis (PGOA) in whom total bone mass has been found to be normal [6].

METHODS

Patients

Seventy-one patients (30 males, 41 females) with definite or classical RA [7] underwent three or four measurements of total body calcium (TBCa) at 6-monthly intervals over 18 months. Twenty-four patients continued NSAIDs alone, 30 patients continued treatment with low-dose corticosteroids, ten patients commenced therapy with suppressive antirheumatic drugs (SARDs) in the form of gold or penicillamine and seven patients commenced oral calcium supplements (OCS) in the form of calcium lactate gluconate (Sandocal) one tablet t.d.s., giving an elemental calcium dose of 1.2 g/day. Those treated with SARDs responded clinically to the medication. All patients in the RA groups were receiving NSAIDs. A group of 19 patients (2 males, 17 females) with PGOA also had three or four measurements of TBCa and have been included as a 'disease control group'. Eight of these were receiving NSAIDs during the study

TABLE I
CLINICAL AND THERAPEUTIC DETAILS

	RA+NSAIDs	RA+SARDs	RA+steroids	RA+OCS	PGOA
Number	24	10	30	7	19
Male/female	10/14	5/5	10/20	5/2	2/17
Pre/postmenopausal	3/11	4/1	5/15	1/1	2/15
Age (range) years	55.9	42.5	52.3	53.7	58.4
	(32–70)	(25–62)	(25–69)	(48–55)	(47–68)
Years postmenopause (range)	10.4	0.2	8.8	6	9.8
	(0–21)	(0–1)	(0–22)	(0–12)	(0–30)

Male/female ratio, mean age and menopausal status of patients with primary generalized osteoarthrosis (PGOA) and rheumatoid arthritis (RA) treated with nonsteroidal anti-inflammatory drugs (NSAIDs) alone, additional suppressive antirheumatic drugs (SARDs), additional corticosteroids or additional oral calcium supplements (OCS) completing the 18-month study period (range shown in parentheses).

while the other 11 were treated with simple analgesics. All patients gave informed consent, and ethical approval was obtained from local and national committees.

Clinical and serological measurements

These were undertaken at each 6-monthly visit for TBCa estimation and included measurements of duration of early-morning stiffness, functional status [8], articular index [9], ESR and rheumatoid-factor titre [10]. A Steinbrocker radiographic grading [8] was determined from a hand radiograph at the beginning of the study. All patients had renal and liver function tests and calcium and phosphate biochemistry at the beginning of the study.

Total body calcium measurements

Our method for a single measurement of total body calcium (TBCa) has been fully reported [2, 11]. TBCa was carried out by *in-vivo* neutron activation analysis and calibration obtained by comparison with an anthropomorphic phantom. A figure for TBCa in grams was produced with an *in-vitro* precision of 1.8% [11] and an *in-vivo* precision over a period of 18 months of 2.9% [12]. Individual results in the cross-sectional studies were reported as a percentage of the expected normal value for the patient's skeletal size (arm span) and menopausal state derived from measurements in 40 normal subjects [11]. Longitudinal analysis was undertaken by calculating a best-fit linear regression for the three or four measurements of TBCa in grams. After deviant points were omitted using Chauvenet's criterion [13], the rate of change of TBCa was calculated from the slope of the regression line and expressed as a percentage of the initial value. Analysis demonstrated that the assumption of a linear fit was reasonable. In the long-

itudinal analysis no correction was made for the patient's skeletal size or menopausal status as the subjects acted as their own controls.

Statistical analysis

This was performed using Student's *t* test for paired and unpaired variables. The Mann–Whitney test was used for small samples.

RESULTS

The male/female ratio, age and menopausal status of the 71 RA and 19 PGOA patients who completed the longitudinal study are shown in Table I. There was a preponderance of females in all groups with the exception of the RA + OCS group. Patients in the RA + SARDs group were significantly younger than the NSAIDs (13.4 years, p < 0.02), the steroid (9.8 years, p < 0.05) and the PGOA (15.9 years, p < 0.005) groups.

Indices of disease duration and activity as well as details of corticosteroid therapy are displayed in Table II. The mean disease duration in the SARDs group was shorter than the other treatment groups but not significantly. However, the initial mean ESR in the SARDs group was significantly higher than that in the NSAIDs (34 mm/h, p < 0.025), steroid (32.7 mm/h, p < 0.05) and OCS (41.4 mm/h, p < 0.01) groups. The ESR fell significantly in the SARDs group during the study period (−32.8 mm/h, p < 0.001) but none of the indices changed significantly in the other groups.

The results of initial TBCa, expressed as a percentage of the expected normal values, are shown in Fig. 1. All the patients who continued with NSAIDs and who were to commence SARDs or OCS are contained in the RA plus no steroid group. The steroid-treated group had a significantly lower initial TBCa than the group

TABLE II
CHANGES OF DISEASE ACTIVITY

	RA+ NSAIDs	RA+ SARDs	RA+ steroids	RA+ OCS
Number	24	10	30	7
Duration of	10	6.2	10.3	10.2
disease (range)	(1–35)	(1.5–15)	(1–38)	(2–27)
Initial ESR	27.7	61.7	29	20.3
	±20.8	±38.0	±27.1	±13.1
Change in ESR	+5.7	−32.8	+0.7	−3.9
	±22.1	±19.4	±20.6	±12.4
Initial A.I.	12.7	14	8.7	8.9
	±6.2	±7.9	±6.4	±2.7
Change in A.I.	−1.9	−6	−1.9	−1.4
	±6.2	±8.5	±4.6	±5.3
Initial E.M.S.	45.4	113	45.3	91.7
	±52.1	±107	±76.6	±124
Change in E.M.S.	+1	−36	−3.6	−57
	±96.8	±85.9	±51.4	±111
Initial F.S.	2.0	2.3	1.8	1.6
	±0.3	±0.5	±0.5	±0.5
Radiographic	2.6	2.4	2.6	2.4
grade	±1.0	±0.8	±1.1	±0.8
Prednisolone dose (mg/day)			5.7 ±1.4	
Duration of therapy (years)			4.7 ±4.6	

Results of disease activity indices expressed as the mean initial and mean change in the index with the standard deviation. No change in functional status or radiographic grade occurred during the study.

NSAIDs = nonsteroidal anti-inflammatory drugs; SARDs = suppressive antirheumatic drugs; OCS = oral calcium supplements; ESR = erythrocyte sedimentation rate (mm/h); A.I. = articular index; E.M.S. = duration of early morning stiffness in minutes; F.S. = functional status.

who had not received corticosteroids (4.6%, p < 0.05) and the patients with PGOA (12.5%, p < 0.01). Both RA groups had a significantly reduced mean TBCa compared with the 40 normal controls previously reported [2, 11].

Comparison of the rate of change of TBCa in the four RA groups (Fig. 2) showed that they all had significant mean annual losses of TBCa (NSAIDs: 3.4%, p < 0.001; SARDs: 4.3%, p < 0.01; OCS: 4.5%, p < 0.01) with the exception of the steroid group. There were no significant differences between the annual rates of change of the NSAIDs, SARDs and OCS groups but all of these lost more calcium than the steroid group (NSAIDs: 4.1%, p < 0.05; SARDs: 5.0%, p < 0.01; OCS: 5.2%, p < 0.02). There was no tendency for the rate of bone loss to diminish in the

SARDs or OCS groups. In the steroid group there was no significant relationship between the rate of change of TBCa and the daily dose or duration of steroid therapy. The mean rate of change of TBCa was similar in males and females in all of the RA groups.

The 41 RA patients not treated with corticosteroids (i.e. the NSAIDs, SARDs and OCS groups combined) had a significantly increased rate of bone loss compared to the steroid group (−4.3%, p < 0.001) and the PGOA group (−2.0%, p < 0.025) although the latter group did show a significant annual loss of TBCa (−1.6%, p < 0.01).

The corticosteroid-treated patients have been sub-divided into those taking a low dose of prednisolone (≤5 mg/day) and a moderate dose of the drug (5.1–10 mg/day). Details of disease activity indices and corticosteroid therapy for the two subgroups are shown in Table III. All disease activity indices were greater in the moderate-dose group. The initial bone mass of the two groups was not significantly different but there was a significant difference between the rates of change of TBCa (Fig. 3). The mean rate
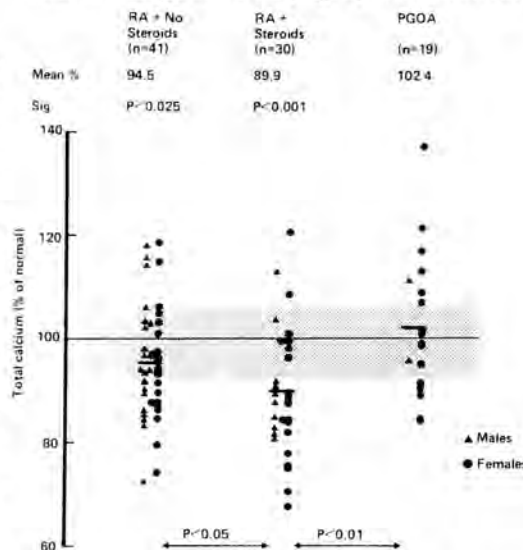

FIG. 1.—Initial normalized total body calcium (TBCa) expressed as a percentage of normal in male (▲) and female (●) patients with rheumatoid arthritis (RA) who were receiving nonsteroidal anti-inflammatory drugs (NSAIDs) alone or additional oral corticosteroids at the onset of the study. TBCa of patients with primary generalized osteoarthrosis (PGOA) are shown for comparison. Normal range displayed in the hatched area as the mean ±1 standard deviation.
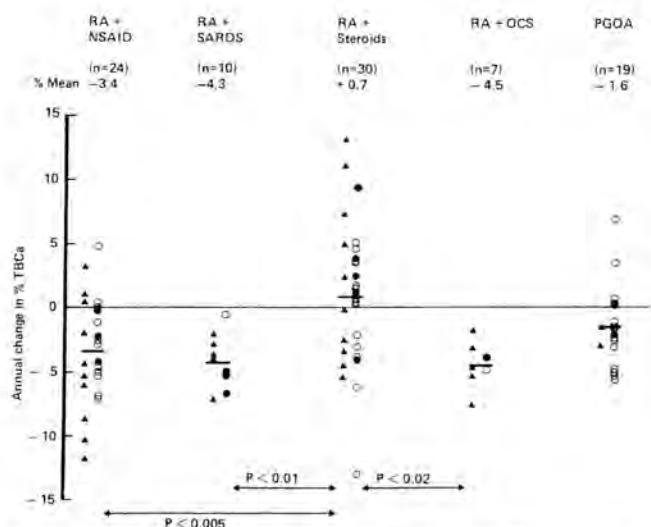
FIG. 2.—Annual rate of change of total body calcium (TBCa) expressed as a percentage of the initial value in male (▲), and premenopausal (●) and postmenopausal (○) female patients with rheumatoid arthritis (RA) treated with nonsteroidal anti-inflammatory drugs (NSAIDs) alone, suppressive antirheumatic drugs (SARDs), oral corticosteroids or oral calcium supplements (OCS) as well as in patients with primary generalized osteoarthrosis(PGOA).

of change in the moderate-dose group (−2.3% per annum) did not differ significantly from that in the NSAIDs, SARDs or OCS groups.

The annual rate of change was not related to disease duration or any one index of disease activity in any of the four groups. There was no difference between the rate of change of TBCa in those patients with seropositive or seronegative disease.

Annual change in TBCa was not significantly correlated with age or years postmenopause in females or age in males. However in the females, when considering 5-year postmenopause cohorts, the highest mean annual loss of TBCa was in the 5 years immediately after the menopause (0.1–5 years) both in the RA patients who did not receive corticosteroids (n = 6: 4.0%) and in the PGOA patients (n = 5: 3.2%).

DISCUSSION

Total bone mass has been shown to be reduced (by 5–8%) in patients with RA treated with NSAIDs alone and further reduced (by 11–15%) with low-dose corticosteroid therapy [2, 3]. Both these studies were cross-sectional and the rate of bone loss was difficult to estimate, particularly as there was no relationship between duration of

disease and total bone mass. Our longitudinal study reported here is the first account of the rate of loss of total bone mass in RA. The mean annual rate of loss of calcium in patients treated with NSAIDs alone was a substantial 3.4% per annum. Although the rate is similar to the 2–4% previously shown in longitudinal studies of photon absorptiometry of the forearm [4] and metacarpal indices [4, 5], these bone sites are close to areas of potentially inflamed synovium and therefore might lose bone at a faster rate than the total skeleton.

The annual rate of loss of TBCa in the RA patients receiving NSAIDs alone was greater than one would have expected from our cross-sectional study where TBCa was reduced by 5.3% in males and 6.8% in females [2]. However, in this study, the annual rate of loss of TBCa was relatively increased by expressing it as a percentage of the individual's initial value and also by omitting the age and menopausal corrections of our original studies [2, 6]. Furthermore, RA patients with more advanced, destructive disease may have an increased rate of bone loss [4] and hence loss of TBCa would tend to accelerate with time.

Loss of bone with age is greater in women than

TABLE III

AGE, YEARS POSTMENOPAUSE AND MEAN INDICES OF
DISEASE ACTIVITY AND CORTICOSTEROID THERAPY (± 1
STANDARD DEVIATION) IN THOSE TAKING LOW ($\leqslant 5$ mg
PREDNISOLONE/DAY) AND MODERATE (5.1–10 mg
PREDNISOLONE/DAY) DOSES OF CORTICOSTEROIDS

	Low	Moderate	Significance
Number	20	10	
Male/female ratio	8/12	2/8	
Age	48.8	59.1	p<0.02
	±13.9	±8.4	
Years postmenopause	7.1	11.2	NS
	±8.5	±6.4	
Duration of disease	6.9	15.1	NS
	±4.6	±12.6	
Initial ESR (mm/h)	20.6	45.7	NS
	±15.2	±37.6	
Initial A.I.	6.4	13	p<0.01
	±5.1	±6.6	
Initial E.M.S. (min)	17.7	100.5	p<0.01
	±35.4	±105.8	
Functional status	1.5	2.2	p<0.001
	±0.5	±0.7	
Radiographic grade	1.8	3.3	p<0.001
	±1.1	±0.7	
Prednisolone dose	4.9	7.4	p<0.001
(mg/day)	±0.2	±1.4	
Duration of therapy	3.2	7.3	NS
(years)	±2.2	±6.9	

ESR = erythrocyte sedimentation rate; A.I. = articular index; E.M.S. = duration of early morning stiffness; NS = not significant.

men [14], particularly immediately after the menopause [11, 15]. Rather surprisingly the mean rate of loss in our study was similar in males and females in all groups (Fig. 2). There was a tendency for those nearest to the menopause to have the greatest rate of loss of TBCa. In the light of these observations and because the groups were reasonably matched for years postmenopause, normalization for postmenopause time was not justified. The explanation for the substantial loss of bone in male RA patients is not clear. While there is a slow fall in bone mass with age in men it has been estimated at only 0.7% per annum after the age of 50 [16]. As the rate of bone loss is likely to be linear in males [17] and therefore we were not surprised to find no relationship between bone loss rates and age in men. Nevertheless, the rate of bone loss in males with RA must include an effect of ageing. We have shown total bone mass to be normal in PGOA [6], therefore the rate of bone loss in this condition was attributed to ageing.

The number of men measured was too small to comment on the rate of bone loss. It is reassuring to note that the mean loss of 1.5% per annum in women was very similar to the annual reduction in total bone mass in women found in cross-sectional studies of TBCa [11, 16].

The rate of bone loss in RA patients not treated with corticosteroids was significantly greater than in patients with PGOA, suggesting that bone loss, in excess of that due to ageing, is a feature of the former disease.

There were no significant differences between the annual loss of TBCa in the three nonsteroid-treated RA groups. The failure to demonstrate a reduction in the rate of bone loss in those responding to gold or penicillamine, or those taking calcium supplements was supported by finding no diminution in the rate of bone loss. The failure to prevent bone loss with SARDs is disappointing. Preliminary data had suggested that both gold [18–20] and penicillamine [21] might limit the degree of radiological destruction after a year of treatment. Indeed penicillamine may reverse the local bone loss associated with RA as measured by metacarpal indices [5, 22]. Penicillamine is a lathyritic agent which inhibits collagen cross-linking and synthesis, and theoretically could hasten the osteoporotic process by inhibiting collagen maturation in bone [23]. However, there was no significant difference in our study between the
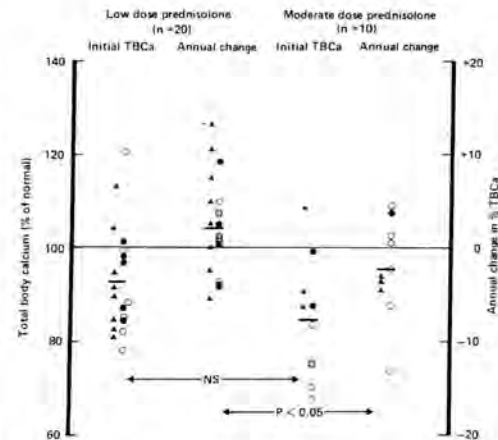

FIG. 3.—Initial normalized total body calcium (TBCa) expressed as a percentage of normal and annual rate of change of total body calcium (TBCa) expressed as a percentage of the inital value in male (▲), premenopausal (●) and postmenopausal female (○) patients with rheumatoid arthritis (RA) who were receiving low (≤5 mg/day) and moderate (5.1–10 mg/day) doses of prednisolone.

rate of loss of TBCa in those treated with penicillamine and gold.

The failure to prevent bone loss with oral calcium supplements is less surprising although oral calcium is thought to reduce the rate of bone loss in postmenopausal osteoporosis [24] and in corticosteroid-treated patients with rheumatoid arthritis [25]. The difference may be due to calcium malabsorption in postmenopausal osteoporosis [26] and in corticosteroid-induced bone loss [27] but not in RA [28]. However, a recent study has shown a mild degree of calcium malabsorption in early disease [29]. All our patients had RA for at least one year. Alternatively, most of the bone loss in RA patients treated with NSAIDs alone may take place at peripheral skeletal sites which may not be amenable to reversal by oral calcium supplements.

The data from the corticosteroid-treated patients give strong support to our hypothesis that bone loss due to prednisolone or its derivatives occurs early in the course of therapy [2]. This hypothesis is consistent with studies of the catabolic and histochemical effects of corticosteroids on bone in both animals [30] and humans [31, 32] and also with longitudinal studies of metacarpal indices [4] and bone histomorphometry [33] in RA and other diseases.

The failure of the steroid-treated patients to lose bone (Fig. 2) despite their initial reduced bone mass (Fig. 1) is perhaps surprising. It might reflect a tendency for those individuals with the lowest initial TBCa to lose the least bone [4]. However, we were unable to detect a relationship between the initial bone mass and the rate of loss in the steroid- or nonsteroid-treated patients. A more exciting possibility is that corticosteroid therapy might limit the degree of local bone damage at periarticular sites by reducing disease activity. Such a suggestion was made initially in the Medical Research Council trials of corticosteroids [34, 35] and has been given support in more recent studies [36, 37]. The subgroup of steroid patients who had received moderate doses of prednisolone (5.1–10 mg/day) had significantly greater mean loss of bone than the low-dose treated group (Fig. 3). The moderate-dose group was significantly older, had more severe disease and were significantly less mobile than the low-dose subgroup. These facts may explain the greater mean loss of TBCa in the former group of patients rather than their steroid therapy. Despite long-standing severe disease, the small group of patients receiving more than 5 mg of prednisolone daily

still had a lower rate of bone loss than the other RA patients. It is conceivable that corticosteroids, used in the treatment of RA, could induce bone loss early in the course of therapy, perhaps at an axial site, and thereafter prevent destructive bone loss at appendicular bone sites. Longitudinal studies assessing bone mass at both these bone sites and relating any loss to alteration of erosion formation will be necessary to explore such a hypothesis.

REFERENCES

1. Kennedy AC, Boddy K, Williams ED, et al. Whole body elemental composition during drug treatment of rheumatoid arthritis: a preliminary study. Ann Rheum Dis 1979;38: 137–40.
2. Reid DM, Kennedy NSJ, Smith MA, Tothill P, Nuki G. Total body calcium in rheumatoid arthritis: effects of disease activity and corticosteroid treatment. Br Med J 1982; 285:330–2.
3. Skibsted Als O, Gotfredsen A, Christiansen C. Relationship between local and total bone mineral in patients with rheumatoid arthritis and normal subjects. Clin Rheumatol 1983; 2:265–71.
4. Dequeker J, Wielandts L, Koentges D, Nijs J. The assessment of bone loss in rheumatoid arthritis. In: Feltkamp A, Van der Korst D, eds. Disease evaluation and patient assessment in rheumatoid arthritis. Alpen a/d Rijn: Stafleu's Scientific Publishing Company, 1982;54–63.
5. Schorn D, Mowat AG. Penicillamine in rheumatoid arthritis: wound healing, skin thickness and osteoporosis. Rheumatol Rehabil 1977;16:223–30.
6. Reid DM, Kennedy NSJ, Smith MA, Tothill P, Nuki G. Bone mass in primary generalised osteoarthrosis. Ann Rheum Dis 1984;43: 240–2.
7. Ropes MW, Bennett GA, Cobb S, Jacox R, Jessar AR. Proposed diagnostic criteria for rheumatoid arthritis. Ann Rheum Dis 1959; 18:49.
8. Steinbrocker O, Traeger CH, Batterman RC. Therapeutic criteria in rheumatoid arthritis. JAMA 1949;140:659–62.

9. Ritchie DM, Boyle JA, McInnes JM, *et al.* Clinical studies with an articular index for the assessment of joint tenderness in patients with rheumatoid arthritis. *Quart J Med* 1968; **37**:393–406.

10. Podliachouk L, Eyquem A, Jacqueline F. Le diagnostic de la polyarthrite chronique évolutive par agglutination des globules rouges humains sensibilisés. *Ann Inst Pasteur* 1958;**94**:659–62.

11. Kennedy NSJ, Eastell R, Ferrington CM, *et al.* Total body neutron activation analysis of calcium: calibration and normalisation. *Phys Med Biol* 1982;**27**:697–707.

12. Tothill P, Nicoll J, Kennedy NSJ, Smith MA, Reid DM, Nuki G. The *in-vivo* precision of total body calcium determinations by neutron activation analysis. In: Christiansen C, Arnaud CD, Nordin BEC, Parfitt AM, Peck WA, Riggs BL eds. *Osteoporosis*. Denmark: Department of Clinical Chemistry, Glostrup Hospital, 1984;217–8.

13. Documenta Geigy. Chauvenet's criterion. In: Geigy JR. *Scientific tables*. 5th ed. Basle, 1956;47.

14. Riggs BL, Wahner HW, Dunn WL, Mazess RB, Offord KP, Melton LJ. Differential changes in the bone mineral density of the appendicular and axial skeleton with ageing. *J Clin Invest* 1981;**67**:328–35.

15. Krolner B, Pors Nielsen S. Bone mineral content of the lumbar spine in normal and osteoporotic women: cross-sectional and longitudinal studies. *Clin Sci* 1982;**62**:329–36.

16. Cohn SH, Vaswani A, Zanzi I, Ellis KJ. Effect of aging on bone mass in adult women. *Am J Physiol* 1976;**230**:143–8.

17. Mazess RB. On aging bone loss. *Clin Orthop Rel Res* 1982;**165**:239–52.

18. Sigler JW, Vluhm GB, Duncan H, Sharp JT, Ensign DC, McCrum WR. Gold salts in the treatment of rheumatoid arthritis. *Ann Intern Med* 1974;**80**:21–6.

19. Luukainen R, Isomakii H, Kajander A. Effect of gold on the progression of erosions in RA patients. *Scand J Rheumatol* 1977;**6**:123–7.

20. Sharp JT, Lidsky MD, Duffy J. Clinical responses during gold therapy for rheumatoid arthritis. *Arthritis Rheum* 1982;**25**:540–9.

21. Gibson T, Huskison EC, Wojtulewski JA, *et al.* Evidence that D-penicillamine alters the course of rheumatoid arthritis. *Rheumatol Rehabil* 1976;**15**:211–5.

22. Schorn D. Osteoporosis in the rheumatoid hand—the effects of treatment with D-penicillamine and oral gold salts. *S Afr Med J* 1983;**63**:121–3.

23. Schorn D, Francis MJO, Loudon M, Mowat AG. Skin collagen biosynthesis in patients with rheumatoid arthritis. *Scand J Rheumatol* 1979;**8**:124–8.

24. Nordin BEC, Horsman A, Crilly RG, Marshall DH, Simpson M. Treatment of spinal osteoporosis in postmenopausal women. *Br Med J* 1980;**280**:451–2.

25. Nilsen KH, Jayson MIV, Dixon AStJ. Microcrystalline calcium hydroxyapatite compound in corticosteroid treated rheumatoid patients: a controlled study. *Br Med J* 1978; **2**:1124.

26. Gallagher JC, Riggs BL, Eisman J, Hamstra A, Arnaud SB, DeLuca HF. Intestinal calcium absorption and serum vitamin D metabolites in normal subjects and osteoporotic patients. *J Clin Invest* 1979;**64**:729–36.

27. Hahn TJ, Halstead LR, Baron DT. Effects of short term glucocorticoid administration on intestinal calcium absorption and circulating vitamin D metabolite concentrations in man. *J Clin Endocrinol Metab* 1981;**52**:111–5.

28. Kennedy AC, Lindsay R. Bone involvement in rheumatoid arthritis. *Clinics in the rheumatic diseases*, Eastbourne, E. Sussex: W B Saunders, 1977;403–20.

29. Sambrook PN, Abeyasekera G, Ansell BM, *et al.* Calcium absorption in rheumatoid arthritis. *Ann Rheum Dis* 1985;**44**:585–8.

30. Jee WSS, Park HZ, Roberts WE, Kenner GH. Corticosteroid and bone. *Am J Anat* 1970; **129**:477–81.

31. Duncan H. Osteoporosis in rheumatoid arthritis and corticosteroid induced osteoporosis. *Arthritis Rheum* 1967;**10**:216–27.

32. Rickers H, Deding A, Christiansen C, Rodbro P, Naestoft J. Corticosteroid-induced osteopenia and vitamin D metabolism: effect of vitamin D_2, calcium, phosphate and sodium fluoride administration. *Clin Endocrinol* 1982;**16**:409–15.

33. Lo Cascio V, Bonucci E, Imbimbo B, *et al.* Bone loss after glucocorticoid therapy. *Calcif Tissue Int* 1984;**36**:435–8.

34. Joint Committee of the Medical Research Council and Nuffield Foundation. A comparison of prednisolone with aspirin or other analgesics in the treatment of rheumatoid arthritis. *Ann Rheum Dis* 1959;**18**:173–8.

35. Joint Committee of the Medical Research Council and Nuffield Foundation. A comparison of prednisolone with aspirin or other analgesics in the treatment of rheumatoid arthritis. *Ann Rheum Dis* 1960;**19**:331–7.

36. Harris ED, Emkey RD, Nichols JE, Newberry A. Low dose prednisolone therapy in rheumatoid arthritis: a double blind study. *J. Rheumatol* 1983;**10**:713–21.

37. Million R, Poole P, Kellgren JH, Jayson MIV. Long-term study of management of rheumatoid arthritis. *Lancet* 1984:i:812–6.

Measurement of hand bone mineral content using single-photon absorptiometry

J J Nicoll†, M A Smith†, D Reid‡§, E Law†, N Brown‡, P Tothill† and G Nuki‡

† Department of Medical Physics and Medical Engineering, Royal Infirmary, Edinburgh EH3 9YW, UK
‡ Rheumatic Diseases Unit, Northern General Hospital, Ferry Road, Edinburgh, UK

Abstract. A single photon absorption imaging technique has been developed to assess the bone mass of the hand, especially in patients with rheumatoid arthritis or bronchial asthma. A modified rectilinear scanner images the hand by transmission scanning in a water bath with a 7.4 GBq ^{125}I source. A microcomputer is used to calculate the bone mineral distribution, and the total bone mineral content (BMC) of the hand is determined from that distribution. The precision (coefficient of variation) of the measurement is 1.9%. A control population of 20 men and 58 women has been studied to determine normal variations in hand bone mineral content with age, sex, body size, hand volume and years since menopause. The normal men are found to have an average hand BMC of 25.1 g with a coefficient of variation (CV) of 22%, which is reduced to 12% by normalising for body size using span. The normal women had an average hand BMC of 18.0 g ± 15%. The CV is reduced to 13% by normalising for span and years post-menopause.

1. Introduction

Single-photon absorptiometry (SPA) is an established technique for the measurement of forearm bone mineral content (BMC) using ^{125}I as the isotope source (Cameron *et al* 1968), but until now it had not been applied to the measurement of hand bone mineral. Neutron activation analysis is also used to measure bone *in vivo* and has been applied to the hand (Catto *et al* 1973, Maziere *et al* 1979). Maziere *et al* (1979) compared activation analysis of hand calcium using ^{252}Cf (132 controls, 45 osteoporotics) with SPA measurements of BMC in the radial epiphyses (37 controls, 13 osteoporotics) and found a strong correlation between the two. They preferred the NAA technique, which gave a coefficient of variation of 2.4% for repeated measurements on ten controls compared with 3.6% for the SPA. Some SPA measurements on patients were abandoned because results could not be reproduced. Maziere's preference for NAA of the hand was based upon the site of measurement rather than upon the technique. The radiation absorbed dose equivalent to the hand was 7.5 mSv. Smith *et al* (1981) compared part-body neutron activation analysis of the forearm with SPA of the radius 5 cm proximal to the styloid process, and found the two techniques to be equally sensitive *in vivo* methods for monitoring changes in calcified bone.

Total bone mass has been shown to be reduced by 5-8% in patients with rheumatoid arthritis who have been treated with non-steroidal anti-inflammatory drugs alone and further reduced in those patients receiving additional corticosteroid therapy

§ Current address: Rheumatology Department, City Hospital, Urquhart Road, Aberdeen, UK.

(Reid *et al* 1982, Als *et al* 1983). The site of bone loss in rheumatoid arthritis remains in doubt, although substantial reductions in peripheral bone mass may in part account for small reductions in the total bone mass in patients who have not received corticosteroids (Reid *et al* 1986). Substantial reductions in peripheral bone mass may relate both to periarticular osteoporosis and marginal bone erosion, which are radiological signs of rheumatoid arthritis (Bywaters 1960), especially in regions of the skeleton where small joints are involved, such as the hand. A method of evaluating hand bone mass could be useful not only to clarify the site of bone loss in RA but also as a potential measurement of long-term disease activity and to monitor treatment.

Apparatus was therefore designed to apply the technique of SPA with its established potential for precision and low radiation doses and its simple nucleonic requirements to the measurement of hand bone mineral.

2. Method

A J & P Multipoise dual-headed rectilinear scanner (J & P Engineering Ltd) is rotated until the scanning frames are vertical and modified by the addition of a rigid frame attached to one NaI detector (10 cm diameter, 5 cm thick) carrying a collimated ^{125}I source. The 1 mm diameter sealed source has an activity of 7.4 GBq on delivery and is used until it has decayed to about 1.5 GBq. The positions and orientation of the collimated source are adjusted to maximise the detected count rate. The detector collimator is circular with a diameter of 4 or 5 mm; the larger diameter being used to maintain the count rate as the source decays. The change of collimator does not degrade the image. No dead time correction is necessary. The hand is placed in a water bath at 35 °C between the source and detector (figure 1). Various widths of rigid air-filled perspex boxes are placed in the tank alongside the hand to reduce the water thickness as much as possible for an individual. Consideration was given to problems associated with rheumatoid arthritis when designing the apparatus, the most important feature being that some patients would be unable to straighten their fingers. For this reason the (flexed) hand is held immobile in the tank by water-filled balloons, rather than a rigid frame, for the duration of the scan. The apparatus is designed to scan the left hand at a speed of approximately 0.5 cm s^{-1} and a cell size of 4 mm, giving a total scan time of around 15 min.

The detected transmitted counts are collected into a 64×64 matrix by a Cromemco microcomputer. This transmission image (shown in figure 2(*a*)) is used to calculate a bone mineral image (figure 2(*b*)) by applying the following equation pixel by pixel:

$$M_B = [\rho_B/(\mu_B\rho_B - \mu_S\rho_S)] \ln I_0/I$$

where M_B is the bone mass per unit area, ρ_B and ρ_S are densities (g cm^{-3}) (the subscript 'B' indicating bone mineral and 'S' soft tissue or water) and μ_B and μ_S are mass absorption coefficients (cm^2 g^{-1}) of the bone mineral and soft tissue or water, respectively. The values used are those given by Cameron *et al* (1968). I_0 is the background intensity; this is determined from three regions of interest as shown in figure 2(*a*), and I is the transmitted intensity.

A rubber tourniquet is loosely applied around the wrist, 3 cm proximal to the radial styloid. The position is found using a specially made set of dividers. This band is clearly seen in the images (figure 2) and is used to define the limit of the hand. Total hand BMC is the sum of all pixels inside a region of interest, as shown in figure 2(*b*).

Hand volume, distal to the marker band, is measured by the displacement of water.
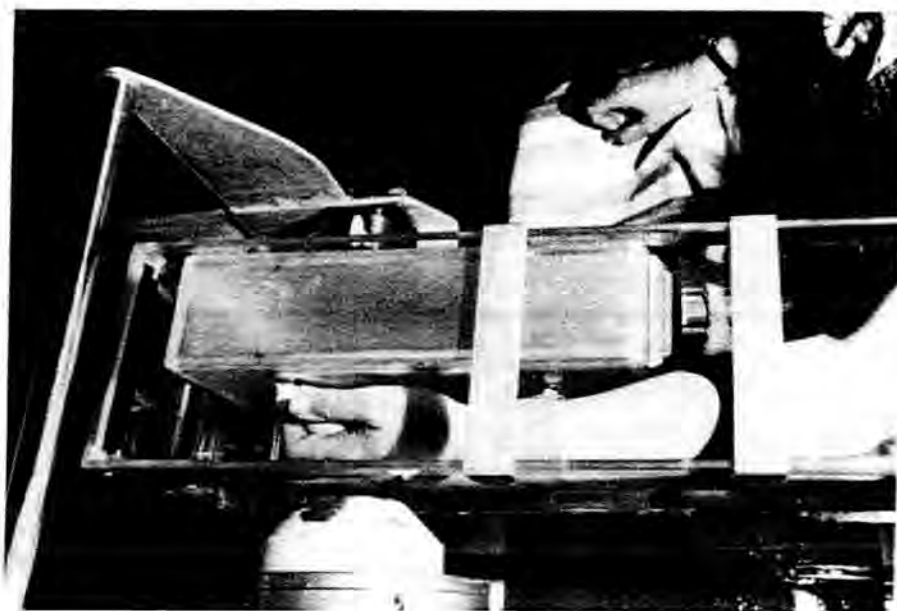
Figure 1. J & P rectilinear scanner modified for hand scanning. A ^{125}I source is mounted on a bracket facing the detector. The hand is placed in a water bath (35 °C) and held still by two water-filled balloons. A marker band is placed around the wrist, 3 cm proximal to the radial styloid.

3. Experimental results

Two to six repeat measurements were performed on ten volunteers on separate occasions over the life of a source (approximately five months), giving a precision (coefficient of variation) of 1.9%. The absorbed dose, measured using thermoluminescent dosimetry, was 6 μGy per scan.

The limit of measurement, 3 cm proximal to the radial styloid, was chosen arbitrarily. Figure 3 shows the variation in total BMC by movement of the upper limit for a typical male hand. Hand bone mineral is not unduly influenced by the position of the limit, and the relationship is linear. Errors introduced in the result by repositioning the marker band are incorporated in the precision measurement.

The measurement of hand BMC is quite a sensitive function of the measured background level; a 1% change in background giving a 2% change in hand BMC for an average female hand with a BMC of 19 g. The background count rate is well estimated; the counts in the three background regions give a coefficient of variation of 0.1% and the integral non-uniformity is less than 0.5%. This slight non-uniformity results from bowing of the tank walls when it is filled with water. More importantly, fat attenuates less than water or soft tissue and fat around the hand will give a locally raised background level. Increased transmission around the wrist may be clearly seen on some transmission images. The worst case seen, in a 109 kg female patient, shown in figure 4, gave an increased transmission of 15% at the side of the wrist. Using a simple cylindrical anatomy this gives a maximum localised error over the bone of 1.5% in transmitted counts or 3% in the BMC. However, this underestimate of the BMC is non-uniform, being directly dependent on an individual's fat distribution, and cannot be accurately measured. The effect is not included in the precision measurement as it predominantly affects the accuracy rather than the reproducibility.

J J Nicoll et al
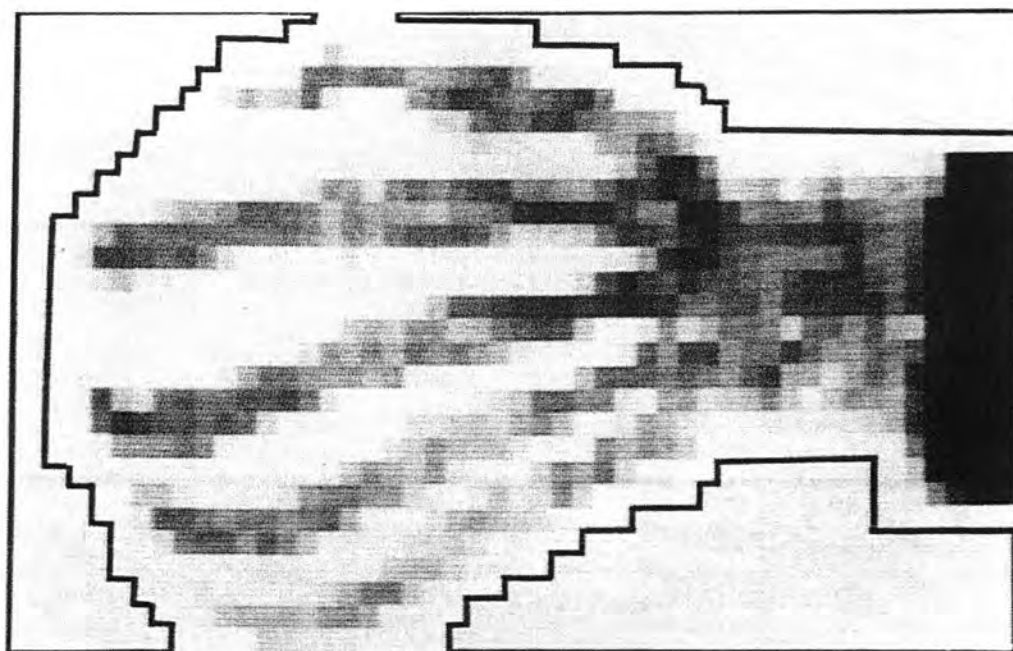
(a)
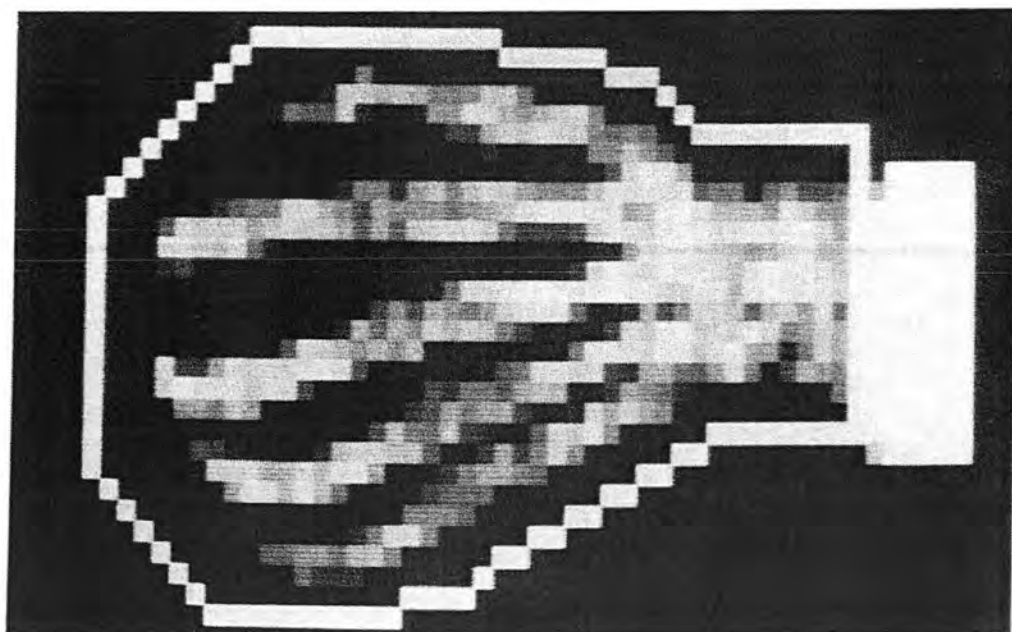
(b)

Figure 2. (a) Regions used to determine the background level on the transmission image. (b) Region used to determine hand BMC using the bone mineral image. The apparently very dense band around the wrist is the marker.
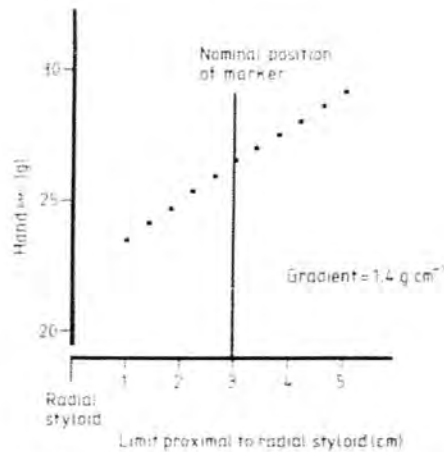
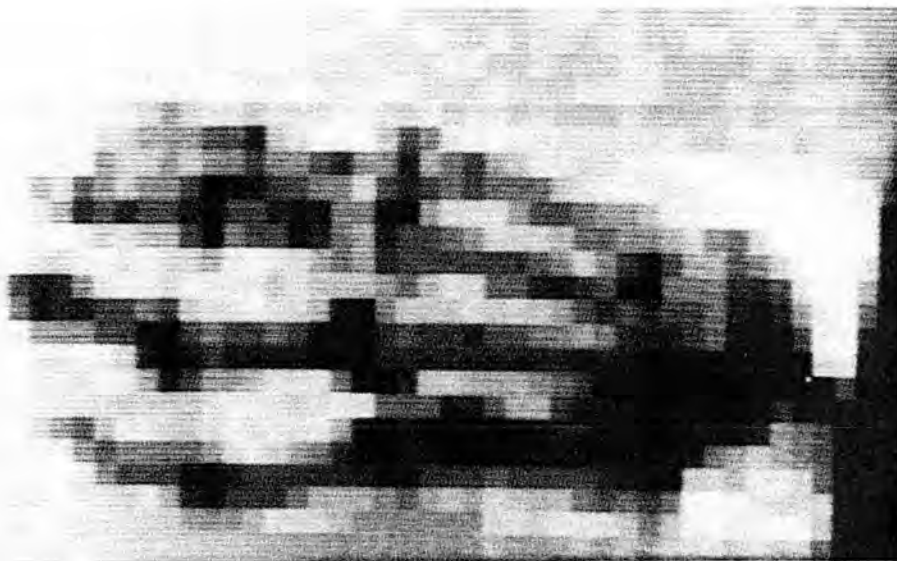**Figure 3.** Variation of hand BMC with position of wrist limit marker.

Figure 4. Transmission image of the hand of a 109 kg female showing increased transmission due to fat around the wrist.

4. Normalisation procedures

To establish a range of normal values for hand BMC, 78 normal volunteers were measured: 20 males (four aged 20–29, seven aged 30–39, two aged 40–49, four aged 50–59 and three aged 60–69) and 58 females (thirteen aged 20–29, seven aged 30–39, fourteen aged 40–49, twelve aged 50–59, eight aged 60–69 and four over 70). All the subjects were active, in good health and without any history of disease that might be expected to influence bone metabolism. The variation in hand BMC and in size is shown in table 1. The females ranged from 12.9 to 25.6 g with a mean of 18.0 g ± 15% (CV), while the males ranged from 14.6 to 34.9 g with a mean of 25.1 g ± 22% (CV).

Table 1. Data for normal controls. Means and standard deviation.

	Male (SD)	All female (SD)	Post-menopausal women (SD)
Number	20	58	23
Age (years)	43 (±14)	46 (±16)	62 (±8)
Years post-menopause	—	—	12.5 (±9.6)
Span (m)	1.85 (±0.09)	1.69 (±0.06)	1.66 (±0.06)
Hand volume (ml)	430 (±63)	327 (±39)	336 (±37)
Hand BMC (g)	25.1 (±5.5)	18.0 (±2.7)	16.7 (±1.9)

The dependence of measured hand BMC upon size parameters (hand volume, arm span, height and weight) and age was investigated using multiple regression analysis. The more significant results for men are shown in table 2(a) and for women in table 2(b). For women, years post-menopause is considered as an alternative age parameter. The biological variation in BMC due to size and age could be reduced by expressing the subjects' results as a ratio BMC/BMC_p. BMC_p is a predicted value obtained by using equations derived from the multiple regression analyses and is given in tables 2(a) and (b). These tables also contain the coefficients of variation (CV) of BMC/BMC_p for the control population when these predictive expressions are applied.

For men (table 2(a)), hand BMC is found to correlate equally well with hand volume and arm span. However, the correlation with age alone is poor ($r = 0.25$, $P > 0.3$), and the addition of age does not improve the correlation with either span or volume.

Amongst the female controls the biological variation was initially smaller (CV = 15%) (table 1), but correlations with size and age parameters were much weaker and hence a much smaller reduction in the CV was achieved by normalisation. Hand BMC correlates with span ($r = 0.36$, $P < 0.01$) or height ($r = 0.32$, $P < 0.02$) alone but not with volume alone. For women, both age ($r = 0.33$, $P < 0.02$) and years post-menopause ($r = 0.31$, $P < 0.02$) correlate with hand BMC and may be combined with a size parameter to improve the result. When this is done, age results in the lowest CV, giving 12.5% with volume and 12.2% with arm span. However, the most significant correlation ($r = 0.48$, $P = 0.001$) is for span and years post-menopause, a combination which gives a CV of 12.8%.

Figure 5 is the result of plotting hand BMC normalised using the expression given for span in table 2(b) ($BMC_p = 9.12S^{1.29}$) against age. By chance, all women over 50 are post-menopausal. The linear regressions are shown for the whole population, the pre-menopausal women and the post-menopausal women. The population as a whole shows a loss of 0.25% hand BMC per year with a significance $P < 0.05$. The pre-menopausal group show an increase which is not significant and the post-menopausal group show a loss of 0.4% hand BMC per year which is also insignificant.

5. Discussion

Single-photon absorptiometry can be usefully employed to make precise measurements of hand BMC and hence to study local bone loss. It is relatively insensitive to variations in placing and replacing the marker band, the effect of which is incorporated in the precision estimate. Fat deposits around the hand or wrist will result in a small inaccuracy in some patients.

Table 2. (*a*) Normalisation of male hand BMC for age and size parameters, showing the equations for the predicted hand BMC (BMC$_p$) with coefficient of variation (CV) of the normalised controls, correlation coefficients (*r*) and significances (*P*). Correlation with age alone was poor (*P* > 0.3) and has been omitted. (*b*) Normalisation of female hand BMC for age and size parameters, showing the equations for the predicted hand BMC (BMC$_p$) with coefficients of variation (CV), correlation coefficients (*r*) and significance (*P*).

(*a*)

Body size parameters	Age parameters	
	None	Age (*A*) in years
Hand Volume (*V*) in millilitres	BMC$_p$ = 2.12 × 10^{-2} $V^{1.7}$ CV = 11.8% r = 0.81 P < 0.0001	BMC$_p$ = 1.63 × 10^{-2} $V^{1.23}e^{0.0017A}$ CV = 11.7% r = 0.82 P < 0.0001
Span (*S*) in metres	BMC$_p$ = 3.07$S^{3.42}$ CV = 11.9% r = 0.80 P < 0.0001	BMC$_p$ = 3.07$S^{3.41}e^{0.0021A}$ CV = 11.9% r = 0.80 P < 0.0002
Height (*H*) in metres	BMC$_p$ = 3.28 $H^{3.6}$ CV = 15.0% r = 0.67 P < 0.001	BMC$_p$ = 2.49 $H^{3.81}e^{0.0038A}$ CV = 14.3% r = 0.72 P < 0.002

(*b*)

Body size parameters	Age parameters		
	None	Age (*A*) in years	Years post-menopause (*Y*) in years
None		BMC$_p$ = 20.02 $e^{-0.0027A}$ CV = 12.6% r = 0.33 P < 0.02	BMC$_p$ = 18.32 $e^{-0.0051Y}$ CV = 13.9% r = 0.31 P < 0.02
Hand volume (*V*) in millilitres	BMC$_p$ = 11.03 $V^{1.12}$ CV = 28.4% r = 0.07 P > 0.2	BMC$_p$ = 4.47 $V^{0.265}e^{0.0034A}$ CV = 12.5% r = 0.40 P < 0.02	BMC$_p$ = 5.37 $V^{0.21}e^{-0.006Y}$ CV = 13.9% r = 0.36 0 < 0.03
Span (*S*) in metres	BMC$_p$ = 9.12 $S^{1.29}$ CV = 13.8% r = 0.36 P < 0.01	BMC$_p$ = 12.45 $S^{0.91}e^{-0.0026A}$ CV = 12.2% r = 0.43 P < 0.01	BMC$_p$ = 9.40 $S^{1.29}e^{-0.0052Y}$ CV = 12.8% r = 0.48 P = 0.001
Height (*H*) in metres	BMC$_p$ = 10.0 $H^{1.20}$ CV = 14.2% r = 0.32 P < 0.02	BMC$_p$ = 12.8 $H^{0.90}e^{-0.0023A}$ CV = 18.0% r = 0.44 P < 0.01	BMC$_p$ = 11.3 $H^{1.00}e^{-0.0045Y}$ CV = 13.6% r = 0.42 P < 0.01

The variation in the control populations may be reduced by normalising for size and age. In the male controls there is no significant loss of hand BMC with age, and normalising for either span or hand volume gives an appreciable reduction in the coefficient of variation. We had thought that, since any variation due to mispositioning
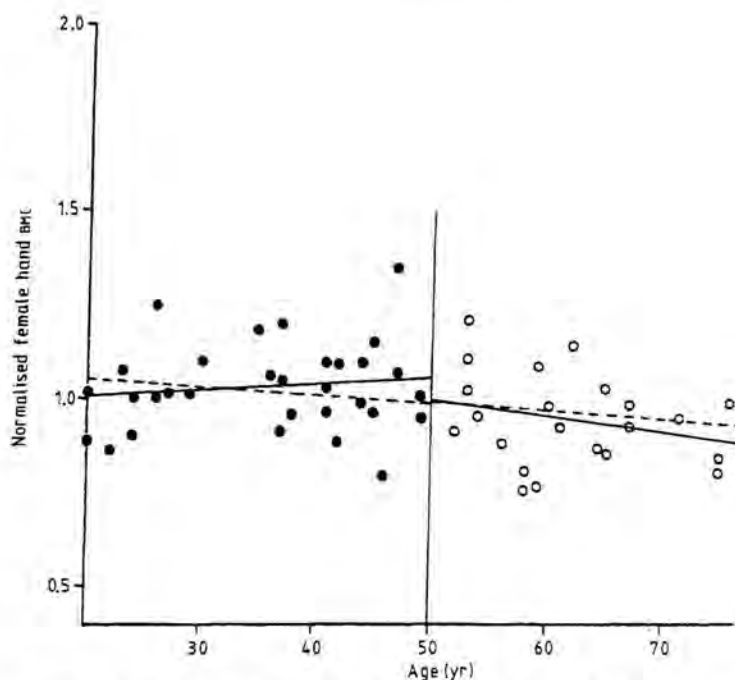
Figure 5. Variation of hand BMC normalised using span alone with age in female controls. ●, pre-menopausal—the full line represents the best fit to the data and has a gradient = 0.16% yr⁻¹, significance $P > 0.2$; ○, post-menopausal—the full line representing the best fit with a gradient = −0.41% yr⁻¹, significance $P > 0.2$. The broken line, representing the best fit to all the data, has a gradient = −0.24% yr⁻¹, significance $P < 0.05$.

of the marker band would be present in both the hand BMC and volume measurements, normalising for volume would help eliminate this source of error. However, if such an effect is present it is masked by the greater biological variation (15%) in this parameter, probably due to differences in soft tissue. The benefits of normalising the female control results are much less, with only a 2-3% reduction in CV although, since there is less biological variation initially, the normalised male and female controls have very similar CV.

The range of hand BMC obtained agrees well with the results found by Maziere *et al* (1979) who found 4.5-16 g of calcium distal to the radial and ulna styloid. Catto *et al* (1973) gave results for four patients in the range 5.9-13.6 g.

The normalisation procedures used by Maziere and co-workers are more direct, being based on an estimate of hand bone volume from a plane radiograph, and in the 20-60 age range they find a CV of 9% in men and 11% in women. However, this normalisation procedure is not open to us since we cannot expect to be able to flatten our patients' hands to obtain a suitable radiograph.

Age related loss of hand BMC is more apparent amongst the females although, as shown in figure 5, the rate of loss is small and the statistical significance is poor. These loss rates are much less than those reported previously for total body calcium where a post-menopausal loss of 1.5% per year was observed (Kennedy *et al* 1982). The age decade data given by Maziere *et al* (1979) for hand calcium suggest a loss rate of 1.3% per year amongst post-menopausal women if the menopause is assumed to occur at an age of 50. Dequeker (1976) used various hand bone indices from radiogrammetry

which suggest a loss rate of just under 1% per year following the menopause. However, none of these measurements are directly comparable, nor is it possible to calculate the significances from the published data.

The apparent change in the hand BMC loss rate at menopause, together with the improved correlation, leads us to use span and years post-menopause for normalising our female hand BMC. Span alone will be used for the male data.

Acknowledgments

Résumé

Mesure du contenu minéral des os de la main par absorptiométrie à photon unique.

Les auteurs ont développé une technique d'imagerie d'absorption à photon unique pour évaluer la masse osseuse de la main, en particulier pour des patients atteints de polyarthrite rhumatoïde ou d'asthme brochique. Les images de la main ont été obtenues sur un scintigraphe à balayage modifié, par des mesures de transmission dans un bac d'eau utilisant une source de ^{125}I de 7,4 GBq. Un micro-ordinateur permet de calculer la distribution minérale dans l'os, et le contenu minéral total des os (BMC) de la main est déterminé à partir de cette distribution. La dispersion des mesures est de 1,9% (coefficient de variation). Une population de contrôle de 20 hommes et de 58 femmes a été étudiée afin de déterminer les variations normales du contenu minéral osseux de la main en fonction de l'âge, du sexe, de la taille du corps, du volume de la main, et du temps écoulé après la ménopause. Les hommes normaux (témoins) ont un BMC moyen de la main de 25,1 g avec un coefficient de variation (CV) de 22% qui peut être amené à 12% en normalisant par rapport à la taille du corps, estimée avec l'empan. Les femmes normales (témoins) ont un BMC moyen de la main de 18,0 g ± 15%. Le CV est réduit à 13% en normalisant par rapport à l'empan et le temps écoulé après la ménopause.

Zusammenfassung

Messung des Knochenmineralgehaltes der Hand mit Hilfe der Einzel-Photon-Absorptiometrie.

Ein Einzel-Photon-Absorptions-Abbildungsverfahren wurde entwickelt, um die Knochenmasse der Hand zu bestimmen, insbesondere bei Patienten mit rheumatischer Arthritis oder Bronchialasthma. Ein modifizierter Scanner bildet die Hand ab durch Transmissionsabtastung in einem Wasserbad mit einer 7.4 GBq ^{125}I-Quelle. Ein Mikrocomputer wird verwendet zur Berechnung der Verteilung des Knochenminerals und der Gesamtknochenmineralgehalt (KMG) der Hand wird aus dieser Verteilung bestimmt. Die Genauigkeit (Variationskoeffizient) der Messung beträgt 1.9%. Eine Kontrollpopulation aus 20 Männern und 58 Frauen wurde untersucht, um die normalen Schwankungen im Knochenmineralgehalt der Hand in Abhängigkeit von Alter, Geschlecht, Körpergröße, Handvolumen und ggf. Jahre nach der Menopause zu bestimmen. Bei normalen Männern wurde ein KMG der Hand von 25.1 g festgestellt, mit einem Variationskoeffizienten (VK) von 22%, der auf 12% reduziert wird durch Normierung von Körpergröße und Handspanne. Bei normalen Frauen wird ein KMG von 18.0 g ±15% gefunden. Der VK wird auf 13% reduziert durch Normierung der Handspanne und der Jahre nach der Menopause.

References

Als O S, Gotfredsen A and Christiansen C 1983 *Clin. Rheumatol.* 2 265–71
Bywaters E 1960 *Bull. Rheum. Dis.* 11 231–4
Cameron J R, Mazess R B and Sorenson J A 1968 *Invest. Radiol.* 3 141–50
Catto G R D, McIntosh J A R and MacLeod M 1973 *Phys. Med. Biol.* 18 508–17

Dequeker J 1976 *Br. J. Radiol.* **49** 912-20
Kennedy N S J, Eastell R, Ferrington C M, Simpson J D, Smith M A, Strong J A and Tothill P 1982 *Phys. Med. Biol.* **27** 697-707
Maziere B, Kuntz D, Comar D and Ryckewaert A 1979 *J. Nucl. Med.* **20** 85-91
Reid D M, Kennedy N S J, Nicoll J J, Smith M A, Tothill P and Nuki G 1986 *Clin. Rheumatol.* **5** 372-8
Reid D M, Kennedy N S J, Smith M A, Tothill P and Nuki G 1982 *Br. Med. J.* **285** 330-2
Reid D M, Nicoll J J, Brown N, Kennedy N S J, Smith M A, Tothill P, Thompson A and Nuki G 1984 *Osteoporosis* ed C Christiansen *et al* pp 811-3
Smith M A, Elton R A and Tothill P 1981 *Clin. Phys. Physiol. Meas.* **2** 1-7

Scientific note

In vivo precision of total body calcium and sodium measurements by neutron activation analysis

J J Nicoll†, P Tothill†, M A Smith†, D Reid‡§, N S J Kennedy†‖ and G Nuki‡

† Department of Medical Physics and Medical Engineering, Western General Hospital, Edinburgh EH4 2XU and The Royal Infirmary, Edinburgh EH3 9YW, UK
‡ Rheumatic Diseases Unit, Northern General Hospital, Edinburgh, UK

1. Introduction

In vivo neutron activation analysis is an important established technique for determining body elemental composition. It may be used to determine both the absolute amount of some body elements or changes with time (Cohn 1981).

The MRC cyclotron in Edinburgh has been used as a neutron source for total body neutron activation analysis (TBNAA) of calcium (Kennedy *et al* 1982), sodium and chlorine (Kennedy *et al* 1983) using the reactions $^{48}Ca(n, \gamma)^{49}Ca$, $^{23}Na(n, \gamma)^{24}Na$ and $^{37}Cl(n, \gamma)^{38}Cl$ respectively.

We have derived absolute quantities of calcium and sodium by identifying and correcting for the body dimensions that affect the efficiency of activation and gamma-ray measurement (Kennedy *et al* 1982). However, it is often of more importance, particularly when measuring calcium, to determine changes within a patient over a long period of time.

The ability to detect such changes in body elements depends upon the reproducibility or precision of the method. This is defined as the coefficient of variation of repeated measurements over varying periods of time. The precision quoted by various centres making TBNAA estimations of total body calcium (TBCa), based on measurements of phantoms or cadavers, is shown in table 1. No measurements have yet been published of the long term *in vivo* precision of TBNAA based on repeated patient measurements. Since the typical dose is about 10 mSv it would not be ethical to activate human subjects repeatedly solely to obtain this information. However if patients are being measured over a long period of time to monitor either their bone loss as a result of disease or a change in bone calcium as a result of treatment, it is possible to use these results to obtain a measurement of the long term precision of TBNAA *in vivo*.

2. Method

One hundred and fifty nine male and female subjects participated in a clinical study to investigate bone loss in various rheumatic diseases. These patients attended for TBNAA on three or four visits, six months apart, over a period of up to 18 months. On

§ Present address: Rheumatology Department, City Hospital, Urquhart Road, Aberdeen, UK.
‖ Present address: Department of Medical Physics, Ninewells Hospital, Dundee, UK.

Table 1. Precision and dose for TBCa and TBNa measurements.

Neutron source	TBCa precision (%)	Method	TBNa precision (%)	Dose equivalent (mSv)	Authors
Cyclotron	2-3	8 measurements of 1 cadaver	—	15†	Chamberlain *et al* (1968)
Neutron generator	1.7	5 measurements of 1 phantom	—	6.4†	Cohn *et al* (1970)
Cyclotron	2	11 measurements of 3 cadavers	—	20†	Nelp *et al* (1970)
14 Pu–Be	1.1	Phantom	—	2.8†	Cohn *et al* (1972, 1976)
Two neutron generators	2.9	35+ measurements of various phantoms	—	10	Boddy *et al* (1973)
Cyclotron	2	Cadaver	—	10	Spinks *et al* (1977)
Cyclotron	1.8	13 measurements of 1 phantom	2.1	13†	Kennedy *et al* (1982, 1983)
Neutron generator	3.6	43 measurements of 1 phantom over 14 months	—	5	Burkinshaw (1985)
Neutron generator	3.0	5 measurements of 1 phantom	1.9	10	Sharafi *et al* (1983)

† A quality factor or relative biological effectiveness of 10 is given in the references cited.

each occasion they attended, simultaneous measurement was made of TBCa, total body sodium (TBNa) and total body chlorine (TBCl). The patients were activated in their normal clothing. This means that no reliable interpretation can be placed on the TBCl estimates as these are influenced by the chlorine content of their clothes, especially due to the use of thermal underwear in winter.

Corrections were applied for patient height, body thickness and fat layer and for air gap in the irradiation chamber (Kennedy *et al* 1982, 1983). Observed counts were related to those from a sodium standard irradiated at the same time and overall reproducibility was monitored by periodic activation of an an anthropomorphic model.

As a consequence of their disease or treatment, the patients' TBCa and TBNa might be expected to change with time and this was observed in most patient groups (Reid *et al* 1984). In calculating the *in vivo* precision, it was assumed that the changes would be linear over the period concerned. The results of patients who attended three or four times were analysed by fitting a linear regression to the TBCa and TBNa results plotted against time. The coefficient of variation of the deviation of the points from the regression line was calculated assuming a normal distribution and $(n-2)$ degrees of freedom, where n is the number of visits for that patient. Individual points which deviated by more than 3.4 standard deviations from the regression line were eliminated by applying Chauvenet's criterion (*Documenta Geigy* 1956). The mean of these coefficients of variation is taken to be the *in vivo* precision.

3. Results

After elimination for non-attendance and the application of Chauvenet's criterion, which removed 15 points, 590 points remained representing 156 patients with three or four TBCa results. The distribution of coefficients of variation is shown in figure 1.
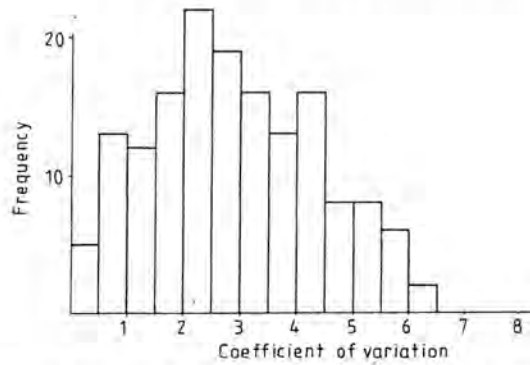
Figure 1. Deviation of TBCa results from regression (mean = 2.91, median = 2.76, mode = 2.25).
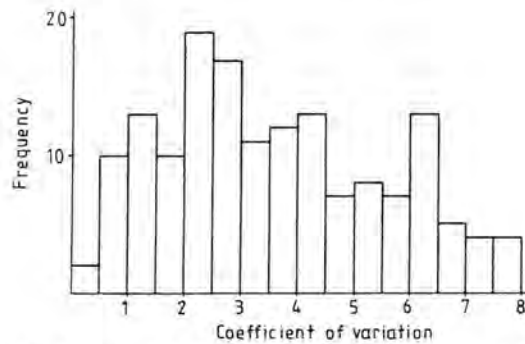

Figure 2. Deviation of TBNa results from regression (mean = 3.63, median = 3.30, mode = 2.25).

The *in vivo* precision is 2.9% compared with a precision of 1.8% obtained by repeated activation of an anthropomorphic model over a period of three months.

158 subjects with three or four TBNa results remained. The distribution of coefficients of variation is shown in figure 2. This gives an *in vivo* precision of 3.6% compared with a precision of 2.1% obtained from measurements of an anthropomorphic model.

4. Discussion

TBNAA is in regular use for determining body composition. In longitudinal studies it has successfully demonstrated changes in total body minerals as a result of disease or its treatment (Eastell *et al* 1985, Gruber *et al* 1984). Longitudinal studies have been over a variety of periods mainly in the range of six months to two years.

The application of TBNAA, however, requires a knowledge of the precision of the estimate. In the past this has been obtained from phantoms activated within a relatively short period of time. These models must represent the patient both in chemical composition and in the distribution of the elements. This has led to the development of complicated models, such as those of Oxby and Brooks (1979). Our technique of estimating the precision overcomes the limitations of anthropomorphic models. All the uncertainties in a single estimate are incorporated together with any long term variations in patient parameters (e.g. weight) and in the equipment. The assumption of linear changes in calcium and sodium seems to be reasonable (Tothill *et al* 1984) but if the changes are non-linear then the method is likely to overestimate the coefficient of variation. The true precision would then be better than that estimated by this

method. The distribution of the deviations from the regression lines are shown in figures 1 and 2. The use of the mean to describe the coefficient of variation is a conservative choice.

Inspection of table 1 shows that our *in vitro* precision compares favourably with that obtained by other authors. The difference observed between long term measurements *in vivo* and measurements based on the phantom (2.9 and 1.8% respectively for TBCa, and 3.6 and 2.1% for TBNa) is not surprising. Corrections for patient size and movement, neutron beam shape, and irradiation and measurement timing may not be completely adequate. The precision is still very satisfactory and allows the study of the effects of disease or treatment to be made with relatively small groups of subjects. We cannot tell how much deterioration of precision is to be expected with other systems as no previous estimates have been made *in vivo*. Cohn (1982) has reported a precision of 2.6% over a 4–5 year patient study compared with a phantom precision of 1% but without details of how this was measured. Some centres are able to use anthropomorphic models to monitor precision over long periods (Burkinshaw 1985) but this may not fully allow for effects due to changes in the patients' weight or body build between activations.

Acknowledgments

References

Boddy K, Holloway I and Elliott A 1973 *Int. J. Appl. Radiat. Isot.* **24** 428–30
Burkinshaw L 1985 Private communication
Chamberlain M J, Fremlin J M, Peters D K and Philip H 1968 *Br. Med. J.* **2** 581–3
Cohn S H 1981 *Med. Phys.* **8** 145–54
—— 1982 *Calcif. Tissue Int.* **34** 433–8
Cohn S H, Dombrowski C S and Fairchild R G 1970 *Int. J. Appl. Radiat. Isot.* **21** 127–37
Cohn S H, Shukla K K, Dombrowski C S and Fairchild R G 1972 *J. Nucl. Med.* **13** 487–92
Cohn S H, Vaswani A, Zanzi I and Ellis K J 1976 *Am. J. Physiol.* **230** 143–8
Documenta Geigy 1956 *Scientific Tables* (Basle: Geigy) 5th edn p 47
Eastell R, Kennedy N S J, Smith M A, Tothill P and Anderton J L 1985 *Nephron* **40** 139–42
Gruber H E, Ivey J L, Baylink D J, Matthews M, Nelp W B, Sisom K and Chesnut C H 1984 *Metabolism* **33** 295
Kennedy N S J, Eastell R, Ferrington C M, Simpson J D, Smith M A, Strong J A and Tothill P 1982 *Phys. Med. Biol.* **27** 697–707
Kennedy N S J, Eastell R, Smith M A and Tothill P 1983 *Phys. Med. Biol.* **28** 215–21
Nelp W B, Palmer H E, Murano R, Pailthorp K, Hinn G M, Rich C, Williams J L, Rudd T G and Denny J D 1970 *J. Lab. Clin. Med.* **76** 151–62
Oxby C B and Brooks K 1979 *Phys. Med. Biol.* **24** 440–2
Reid D M, Nicoll J, Brown N, Kennedy N S J, Smith M A, Tothill P and Nuki G 1984 *Br. J. Rheumatol.* **23** 116–7
Sharifi A, Pearson D, Oxby C B, Oldroyd B, Krupowicz D W, Brooks K and Ellis R E 1983 *Phys. Med. Biol.* **28** 203–14
Spinks T J, Bewley D K, Ranicar A S O and Joplin G F 1977 *J. Radioanal. Chem.* **37** 345–55
Tothill P, Nicoll J J, Kennedy N S J, Smith M A, Reid D M and Nuki G 1984 *Osteoporosis* ed C Christiansen, C D Arnaud, B E C Nordin, A M Parfitt, W A Peck and B L Riggs (Copenhagen: Glostrup Hospital Press) pp 217–8

PREDICTION OF FRACTURE HEALING IN THE TIBIA
BY QUANTITATIVE RADIONUCLIDE IMAGING

M. A. SMITH, E. A. JONES, R. K. STRACHAN, J. J. NICOLL, J. J. K. BEST, P. TOTHILL, S. P. F. HUGHES

From the Royal Infirmary, Edinburgh

The uptake of ^{99m}Tc-MDP was studied in 73 patients after a tibial fracture. The image obtained five minutes after injection during a period between one and four weeks after fracture was found to be related to the incidence of non-union after six months. A ratio of 1.3 between the uptake at the fracture site and at normal bone adjacent to it predicted non-union in an individual patient with a sensitivity of about 70% and a specificity of 90%.

It has been recognised for many years that there is an increased uptake of bone scanning agents at the site of a fracture and there have been several reports on bone scans as indicators of fracture healing. Various radionuclides such as ^{32}P (Tucker 1950), ^{85}Sr (Bauer and Wendeberg 1959; Muheim 1973), ^{87m}Sr (Illingworth and Schiess 1971; Johanssen 1973) and ^{18}F (Riggens et al. 1974) have been used to investigate fracture healing without a great deal of success. Technetium 99m-phosphate compounds such as ^{99m}Tc-Sn-pyrophosphate (Lund et al. 1978) have also been investigated but it is the compound ^{99m}Tc-methylene diphosphonate (MDP) which seems the most promising in the investigation of fracture healing (Hughes 1980).

Most of the research using MDP has concentrated on the qualitative assessment of scans recorded at two to four hours after injection. Matin (1979) and Desai et al. (1980), however, showed that there was increased uptake at fractures sites. Auchincloss and Watt (1982), in a study of fractures of the lower leg, demonstrated a significant relationship between uptake at the fracture site and time to union; they suggested that the two-hour scan may be of value in the prediction of delayed healing, though there was a considerable degree of overlap between the groups

in their study. However, Jacobs et al. (1981) and Gregg, Barsoum and Clayton (1983) came to the opposite conclusion. The only previous report on MDP uptake very soon after injection was a small study (Jacobs et al. 1981) which demonstrated a relationship between the rate of uptake and time to union.

It has been shown that the MDP uptake at two to four hours after injection is a function of both regional blood flow and bone formation (Lavender et al. 1979). Given the relatively slow transfer of MDP from blood through the bone fluids to bone itself with a peak at about one hour (Hughes et al. 1978; Makler and Charkes 1980), the uptake of MDP soon after injection should be largely dependent on blood flow alone. If the interruption of blood flow in the bone is the reason for the number of tibial fractures which fail to unite, then MDP uptake, particularly soon after injection, could be a valuable predictor of non-union. If bone blood flow is the predominant factor, then it is important that studies be made when the reactive increase in blood flow is maximal.

Previous studies using MDP to investigate fracture healing (Jacobs et al. 1981; Auchincloss and Watt 1982) have demonstrated that various indices are related to the time to union. Our aim was to conduct a prospective study to investigate the differences in early uptake of MDP between patients obtaining union in normal time and those developing non-union. We hoped to develop a technique which could predict non-union soon after fracture in order to allow consideration of an early prophylactic operation.

M. A. Smith, MSc, PhD, Senior Lecturer
Department of Radiological Sciences, United Medical and Dental School, Guy's Hospital, St Thomas Street, London SE1 9RT, England.

E. A. Jones, MSc, Senior Physicist
R. K. Strachan, FRCS, Lecturer
J. J. Nicoll, PhD, Senior Physicist
J. J. K. Best, FRCP, FRCR, Professor of Medical Radiology
P. Tothill, PhD, FInstP, FRSE, Reader in Medical Physics
S. P. F. Hughes, MS, FRCS Ed, FRCS, FRCSI, Professor of Orthopaedic Surgery
Departments of Medical Physics and Medical Engineering, Orthopaedic Surgery and Medical Radiology, The Royal Infirmary, Edinburgh EH3 9YW, Scotland.

Requests for reprints should be sent to Mr M. A. Smith.

PATIENTS AND METHODS

All patients aged from 16 to 55 years with a fractured tibia and a normal contralateral limb admitted to the Royal Infirmary, Edinburgh from January 1982 to July

Table I. Details of the 73 tibial fractures included in the study

	Number
Fracture of tibia and fibula	62
Fracture of tibia only	11
Type of fracture	
Transverse	24
Oblique	35
Spiral	14
Fixation	
Internal	4
External	13
Plaster	56
Compound injury (Gustilo and Anderson 1976)	
Grade 0	40
Grade 1	15
Grade 2	10
Grade 3	8
Comminution (Johner and Wruhs 1983)	
Type A	23
Type B	32
Type C	18
Clinical grading (Ellis 1958)	
Group I	13
Group II	48
Group III	12

1984 were considered for this study. Exclusions were those with severe multiple injuries and those who declined to take part. In all, 86 patients were accepted into the series, but 13 were subsequently withdrawn because of clinical problems or failure to attend. We accepted all types of tibial fracture (Table I) and all methods of management. There were 27 patients aged 15 to 19 years, 36 aged 20 to 29 years, 12 aged 30 to 39 years and 11 aged from 40 to 55 years.

In addition to the routine of management, each patient was examined by the same orthopaedic surgeon at monthly intervals in order to assess the state of healing of the fracture. He had no access to the results of the bone scan but, using a combination of radiographic and clinical criteria, recorded each patient as showing union, delayed union or non-union. Normal union was recorded for the fractures which had united within four months, and delayed union where fractures had united between four and six months. Non-union was recorded for those fractures which had not united by six months.

Our aim was to perform quantitative bone scans at two, six and 12 weeks after the injury. These times were chosen for a number of reasons. After a fracture there is an immediate decrease in blood supply to that bone; this is followed by an increase which reaches a maximum after 10 to 14 days in the canine tibia (Paradis and Kelly 1975; McCarthy and Hughes 1984). This increased blood flow is associated with new bone formation as the fracture heals. Two weeks after injury is a suitable time with respect to the mobility of the patient, and is also the time when the increased blood flow should reach a plateau. Operation for failure to unite is commonly considered after about 12 weeks; Jacobs et al. (1981) were able to show a difference in uptake between cases of

delayed and of non-union at this time. We therefore performed a scan at 12 weeks and also at an intermediate time to assess the healing process. The work of Lund et al. (1978) suggested that six weeks was an appropriate time.

At each visit, each patient was given an intravenous dose of 200 MBq of ^{99m}Tc-MDP; this is one-third of the dose normally given for a routine bone scan. Before the injection the radioactivity of the syringe was measured by scintillation counter against a ^{99m}Tc-MDP standard which was approximately 1% of the injected activity. The patient was positioned supine on a scanning bed below which a gamma camera had both lower legs in its field of view. A Technicare 110 gamma camera with a high sensitivity collimator and an MCS-560 computer processor were used. The ^{99m}Tc-MDP was administered as a bolus injection in the right antecubital fossa and was flushed through with 20 ml of saline. A dynamic series of 30×10 second images were obtained from the time of injection for 300 seconds. After this a static image was collected from 300 to 800 seconds post-injection. This static image was termed the "early uptake". After about two hours the patient returned to the scanning room and was positioned as before. A 300 second static scan was then collected which was termed the "late uptake". This late uptake scan was obtained with the same gamma camera but with a medium resolution, lower sensitivity collimator. After each early and late uptake scan the ^{99m}Tc-MDP standard was placed in the centre of the collimator field and measured for 100 seconds so that the absolute uptake at the fracture site could be determined.

The results from the bone scans were analysed using the computer to measure the radioactivity within regions of interest (Fig. 1). These were defined as: A, round the
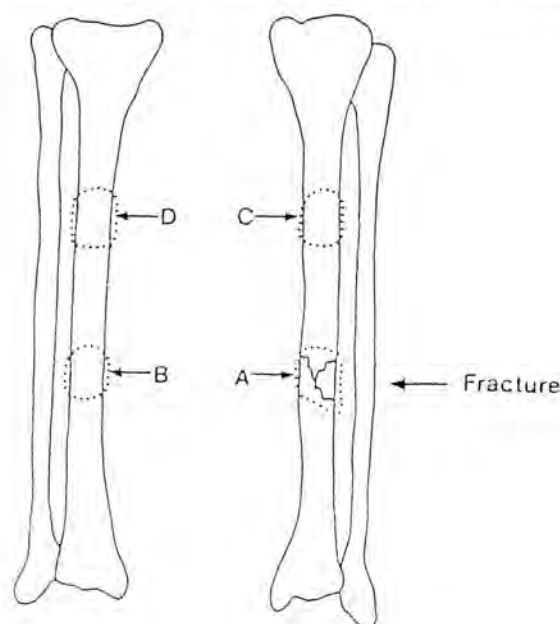

Fig. 1

Diagram to show the regions of interest A, B, C and D in relation to the site of the fracture.

Table II. The ratios between activity levels on "early uptake" and "late uptake" scans at the three visits for each of the groups (mean ± s.d.)

	Ratios												Number of patients		
	A/B			A/C			C/D			A/B ÷ C/D					
	U	D	NU	U	D	NU	U	D	NU	U	D	NU	U	D	NU
First visit															
Early	2.78	1.95	2.38	1.69	1.22	1.26	1.36	1.27	1.53	2.16	1.55	1.70			
	±1.18	±0.67	±0.74	±0.39	±0.12	±0.36	±0.44	±0.37	±0.48	±0.96	±0.38	±0.77			
Late	4.97	4.31	4.56	2.51	1.86	1.62	2.30	2.35	2.88	2.47	1.91	1.72	32	9	10
	±1.76	±1.60	±1.33	±0.99	±0.61	±0.57	±0.71	±0.98	±0.94	±1.49	±0.66	±0.75			
Second visit															
Early	2.38	2.16	2.03	1.84	1.65	1.79	1.12	1.14	1.05	2.20	1.99	2.06			
	±0.73	±0.61	±0.57	±0.55	±0.39	±0.69	±0.38	±0.30	±0.32	±0.60	±0.66	±0.80			
Late	6.78	6.34	5.45	3.23	2.82	2.41	2.09	2.40	2.35	3.29	2.69	2.49	34	8	12
	±2.52	±2.55	±1.51	±1.25	±0.80	±0.80	±0.56	±0.64	±0.74	±1.17	±0.96	±0.95			
Third visit															
Early	2.62	2.79	2.10	2.04	2.04	1.71	1.09	1.10	1.00	2.49	2.67	2.14			
	±1.29	±0.99	±0.63	±0.57	±0.56	±0.36	±0.37	±0.28	±0.23	±0.92	±0.97	±0.59			
Late	7.54	9.13	6.63	4.24	3.87	3.13	2.02	2.50	2.18	4.02	3.84	3.39	27	7	10
	±2.61	±2.89	±2.67	±1.79	±1.68	±1.09	±0.62	±1.25	±0.97	±1.76	±1.47	±1.43			

U, union
D, delayed union
NU, non-union

fracture site; *B*, over normal bone on the contralateral limb at the corresponding level; *C*, over normal bone above the fracture site; and *D*, over a corresponding region on the contralateral limb. When the fracture was too high in the tibia for enough normal bone to be available above it, region C, and therefore region D also, were chosen in normal bone below the fracture site. The selection of these regions of interest was made by the same author (EAJ) on each occasion after study of a radiograph of the fractured bone. The late uptake scan was often used to assist in the retrospective choice of the regions for the early scan. The measurement of MDP uptake from the images and the assessment of fracture healing were both performed double-blind. The ratios of A/B, A/C, C/D and (A/B) ÷ (C/D) were noted, after each result had been normalised for area. The latter two ratios were measured for comparison with the results of Auchincloss and Watt (1982). The attenuation of 141 keV gamma photons through the plaster on a fractured leg was between 3% and 5%, which is too small to distort the ratios significantly.

Since our results depended on the choice of the regions of interest, both intra-operator and inter-operator variations were investigated. The scans of 20 patients were re-analysed six months after the initial analysis by the original observer (EAJ) and the variation between measured uptakes at the fracture site were noted. Inter-observer variation was assessed by an independent re-analysis of the most appropriate ratio by a second observer using all the scans (JJN). Differences in the sensitivity and specificity of the technique between the two observers were noted. The sensitivity of the prediction of non-union was defined as the proportion of patients developing non-union who could have

been correctly identified. The specificity was defined as the proportion of patients obtaining normal union who could have been correctly predicted.

In addition, activity profiles along the length of the bone in the fractured leg were investigated. We also studied the automatic determination of the region of interest by the computer, and a range of computer programs was developed to define this region. After the operator had identified the approximate position of the region of high uptake at the fracture site, the program then included all pixels which showed more than a given percentage of the maximum uptake; cut-off levels of 70%, 80% and 90% were investigated.

RESULTS

Of the 73 patients admitted into the study, not all attended on all three occasions. Although it had been intended to obtain scans at two weeks, precise timing was not possible, so we analysed scans taken at the "first visit" from between one and four weeks after fracture. Two patients had evidence of infection at the time of scan and these results were excluded since infection is known to increase MDP uptake (Hughes et al. 1986). There were fewer exclusions from the results of scans taken between five and eight weeks after fracture, referred to as the "second visit", or between 10 and 15 weeks after injury, the "third visit".

The mean ratios obtained at each visit for the three groups of patients are listed in Table II. As would be expected, the ratios of most interest (A/B and A/C) tend to decrease in the patients who eventually showed non-union. For these ratios, the "non-union" group has a lower mean than the "union" group for both the early

Table III. The t value and significance of the difference between the groups with union and with non-union (Table II) for the ratios A/C and A/B on early and late uptake

	Ratio	t value of difference	Significance
First visit			
Early uptake	A/C	3.2	$p < 0.005$
	A/B	1.3	NS
Late uptake	A/C	3.5	$p < 0.005$
	A/B	0.8	NS
Second visit			
Early uptake	A/C	0.2	NS
	A/B	1.7	NS
Late uptake	A/C	2.6	$p < 0.05$
	A/B	2.2	$p < 0.05$
Third visit			
Early uptake	A/C	2.1	$p < 0.05$
	A/B	1.6	NS
Late uptake	A/C	2.3	$p < 0.05$
	A/B	0.9	NS

NS, not significant

and late uptake at each visit. Table III records the significance of the difference between the union and the non-union groups for each of the three visits and for the different ratios. As expected from other reports, there is frequently a significant difference between the groups designated union and non-union.

However, the degree of overlap between the results from these groups is more important; an indication of this overlap can be obtained from comparison of the t statistic for each group. The t values indicate that the best separation between the union and non-union groups can be obtained from the A/C ratio at the first visit. The only other significant differences between groups ($p < 0.05$) were obtained from the A/B $\div$ C/D ratio of the late uptake, recorded at the first visit and the second visit. Moreover, at the first visit the best separation of all was that obtained by using the A/C ratio of the "early uptake" (Fig. 2). Although at the first visit the t value for

Fig. 2 ▶

The results of the early uptake A/C ratio at the first visit related to the time to union. The dashed line represents the ratio 1.3.
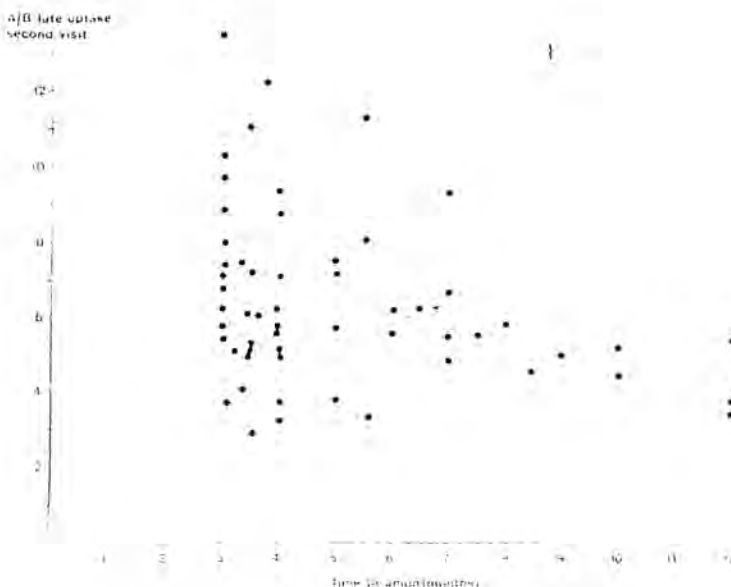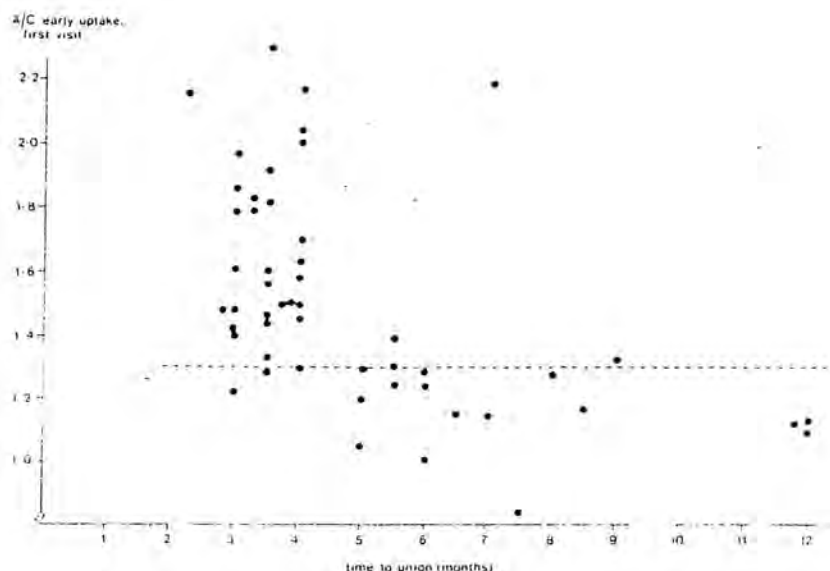
◀ Fig. 3

Results for the late uptake A/B ratio at the second visit related to the time to union.

Operator	Cut-off value of A/C ratio	Number of patients predicted to unite within 4 months (true total 19)	Sensitivity (per cent)	Number of patients with predicted delay or failure of union (true total 32)	Specificity (per cent)
EAJ	1.2	10	53	32	100
JJN		6	32	31	97
EAJ	1.3	16	84	29	91
JJN		12	63	28	88
EAJ	1.4	18	95	28	88
JJN		15	79	22	69

the late uptake A/C ratio was higher than the corresponding early uptake ratio, this was due to very high A/C values in the union group at late uptake even though separation was not as good. The possibility of improving the separation by using both early and late A/C ratios at the first visit was investigated. The product of these ratios gave no better separation between the groups than the early uptake A/C ratio at the first visit on its own. The late uptake A/B ratio at the second visit is shown in Figure 3.

The absolute uptake in region A, as a percentage of the injected activity, was calculated but no significant differences were found between the union and non-union groups at either the early or late uptakes at any of the three visits. No significant differences between the groups were found when the rate of uptake immediately after injection was calculated from the initial series of dynamic images.

The predictive value of the two-week, early uptake A/C ratio was investigated. The intra-observer variation in the analysis of these results was found to be a mean of 6% between the measured uptake at the fracture site on two occasions six months apart. More important, however, is the inter-observer variation, as the investigator's choice of the region C will have important implications. The sensitivity and specificity of the early uptake A/C ratio at two weeks was calculated independently by two of the authors using different A/C cut-off values and the results are given in Table IV. As expected, there are differences in the ratios and these are reflected in the variation in the sensitivity and specificity. It appears that a cut-off value of 1.3 for the ratios provides an acceptable compromise between sensitivity and specificity. Sensitivity varied from 63% to 84% and the specificity was from 91% to 88% for the two operators. Neither the use of longitudinal profiles or of computer programs to define the region of interest provided any improvement over a skilled operator, and, in fact, the results were significantly worse.

The timing of the early scan at the first visit is important in relation to the time of injection but less so with regard to the time since fracture. In eight patients, uptake was measured from a 15-minute dynamic series of images; this showed a steady increase in the activity at

the fracture site, and there was little variation from patient to patient (Fig. 4). This finding suggests that the A/C ratios illustrated in Figure 2 are likely to differ significantly if the measurements are performed at a different time after injection of the isotope.

The variation of early uptake A/C ratio with time since fracture in patients having normal union is illustrated in Figure 5. During the period from one week to four weeks after fracture there was no correlation between the A/C ratio and the time since fracture. Four patients had scans even earlier, between one and seven days after fracture, though these results were not included in the main analysis. Two of these patients had
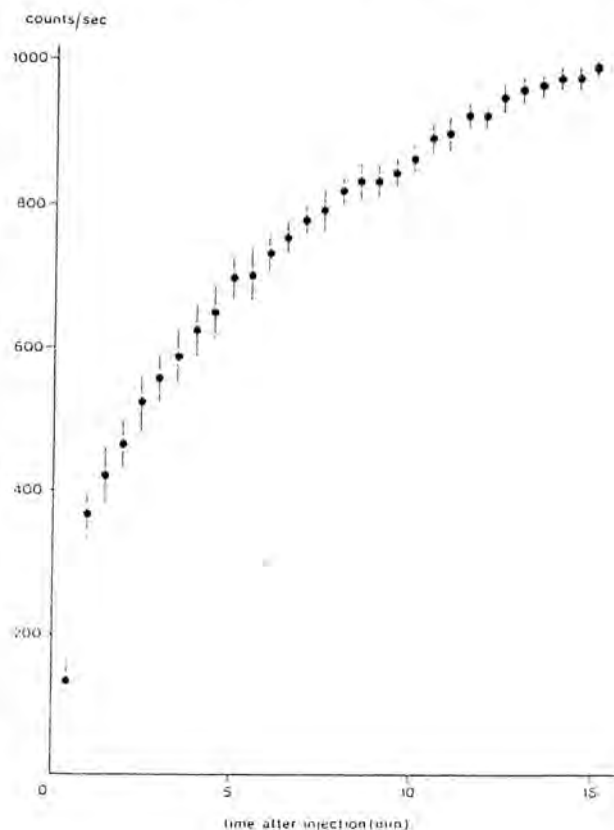

Fig. 4

Uptake at the fracture site during the first 15 minutes after injection, plotted as the mean ±2 standard errors from a series of eight patients.
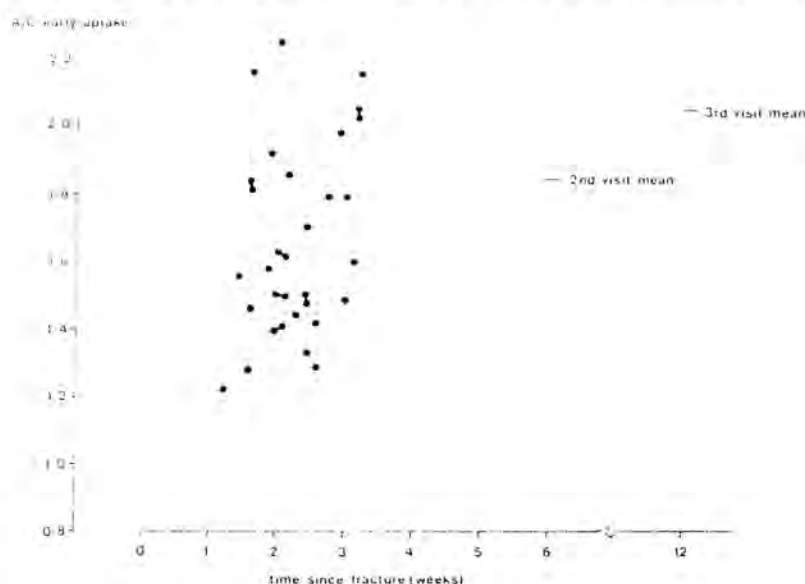
Fig. 5

Results for the early uptake A/C ratio at the first visit related to time since fracture. The open circles represent patients who were imaged less than one week after injury and were not included in the detailed analysis.

a very low ratio whereas those scanned after six days had results similar to those of the other patients. We concluded that the timing of the first scan after fracture is not particularly crucial to the ratio. Inspection of the bone scan images showed no appearance which was indicative of union or non-union, and in particular, no evident cold spots were seen in the scans of patients who proceeded to non-union.

DISCUSSION

Our results suggest that a quantitative MDP bone scan can help to predict non-union, but that the contralateral normal bone, as used by previous workers, does not provide a useful control site. Enough separation between the groups to enable a prediction to be made in an individual patient can only be achieved by using a normal region in the same limb as control.

One hypothesis is that, since disruption of the bone blood flow may be related to non-union, the early uptake result, which is predominantly related to blood flow, will be a better predictor than the late uptake, which is related to both blood flow and bone formation. This hypothesis can be extended, since it also explains why the greatest separation between the increased bone blood flow in bones which will unite, and its reduction in bones which will fail to unite, will be obtained at around the time of the maximum increase of blood flow. This period is likely to be nearer two weeks after injury than six or 12 weeks, and this explains our findings.

After a fracture blood flow increases to the whole of the bone, not just to the fracture site. This is why the use of a control region in the fractured limb rather than, as commonly chosen, a region in the contralateral normal leg, can compensate for variations between patients of the overall increase in blood flow. Thus the A/C ratio will

reflect variations in uptake at the fracture site alone. This may explain the smaller spread of the A/C ratios in the group obtaining union (coefficient of variation 23%) as compared with the A/B ratios of 42%.

Our results are in broad agreement with those of other workers. The mean values of the $A/B \div C/D$ and C/D ratios agree well with those reported by Auchincloss and Watt (1982), and the inverse relationship they found between the late uptake C/D ratio at six weeks and the time to union is also confirmed. Auchincloss and Watt (1982) state that this finding is "difficult to rationalise and no data are available to explain this observation". A possible explanation is that the fracture produces a general increase in blood flow and activity at C is increased relative to D. As the fracture heals, blood flow decreases and uptake at C decreases; failure to unite may result in the continued higher activity at C, resulting in the increased C/D ratio for those with non-union. This theory is substantiated by our results; the C/D ratio is similar in the union group at two weeks to that in the non-union group at six weeks.

Jacobs et al. (1981) also used a control region in the fractured limb and investigated early uptake, but our uptake curves over the first 15 minutes (Fig. 4) are significantly different from the example given in their paper. We do not agree that the uptake between 7 min and 15 min is a "linear phase" which is "more an index of the affinity of the bone for phosphate and thus correlated with bone formation". Our images of the late uptake from one day to three weeks after fracture confirm the findings of Gregg et al. (1983) that "neither the presence of a cold spot nor any other scintigraphic feature could be correlated with the progress or time to fracture union". It must be noted, however, that we were using a high sensitivity collimator with consequent low resolution.

The early uptake A/C ratio at the first visit demonstrates a separation between patients proceeding to union and those who develop non-union, and there are acceptable levels of sensitivity and specificity at a cut-off level of 1.3, even when different operators are analysing the results. However, the same data has been used both to develop and to assess the accuracy of the various cut-off values, so the values for sensitivity and specificity may be over-optimistic. There is therefore a need to test the technique in a further prospective study.

There are important practical implications for the timing of measurements. The fact that the best results were achieved as early as two weeks after fracture would allow changes to be made in the management of the patient far earlier than by other methods and these changes could reduce the mean time to union. The routine application of the technique is relatively easy because the "early uptake" can be investigated in only 10 minutes of the patient's time. The proportion of our patients recorded as suffering non-union was higher, at 20%, than the 13.5% quoted in a larger study by Ramadier et al. (1981). The reason is probably that we defined non-union as failure at six months; this is an important interval for clinical decision on further management. Auchincloss and Watt (1982) used the terms delayed union or unsatisfactory union for these patients and also had a lower incidence (11.5%) than in our study. This difference may be due to the higher proportion of severely injured limbs in our study: we had 16% and 66% respectively in Groups III and II (Ellis 1958) compared with 9% and 33% in Auchincloss and Watts' series.

REFERENCES

Auchincloss JM, Watt I. Scintigraphy in the evaluation of potential fracture healing: a clinical study of tibial fractures. *Br J Radiol* 1982;55:707-13.

Bauer GCH, Wendeberg B. External counting of Ca⁴⁷ and Sr⁸⁵ in studies of localised skeletal lesions in man. *J Bone Joint Surg [Br]* 1959; 41-B:558-80.

Desai A, Alavi A, Dalinka M, Brighton C, Esterhai J. Role of bo scintigraphy in the evaluation and treatment of nonunit fractures: concise communication. *J Nucl Med* 1980;2(10):913-

Ellis H. The speed of healing after fracture of the tibial shaft. *J Bo Joint Surg [Br]* 1958; 40-B:42-6.

Gregg PJ, Barsoum MK, Clayton CB. Scintigraphic appearance of tl tibia in the early stages following fracture. *Clin Orth* 1983;175:139-46.

Gustilo RB, Anderson JT. Prevention of infection in the treatment one thousand and twenty-five open fractures of long bone retrospective and prospective analysis. *J Bone Joint Surg [Ar* 1976;58-A:453-8.

Hughes S. Radionuclides in orthopaedic surgery. *J Bone Joint Surg [B* 1980;62-B:141-50.

Hughes S, Khan R, Davies R, Lavender P. The uptake by the canin tibia of the bone scanning agent ⁹⁹ᵐTc-MDP before and after a osteotomy. *J Bone Joint Surg [Br]* 1978;60-B:579-82.

Hughes SPF, Pinto MR, Fleming RH, McCarthy ID. The volume o distribution of albumin and methylene diphosphonate in norma and infected bone. *J Bone Joint Surg [Br]* 1986;68-B:841.

Illingworth GI, Schiess FA. Strontium 87m in the prognosis of fracture of the tibia. *Proc R Soc Med* 1971;64:633-4.

Jacobs RR, Jackson RP, Preston DF, Williamson JA, Gallagher J Dynamic bone scanning in fractures. *Injury* 1981;12:455-9.

Johanssen A. Fracture healing controlled by ⁸⁷Sr uptake. *Acta Orthop Scand* 1973;44:628-39.

Johner R, Wruhs O. Classification of tibial shaft fractures and correlation with results after rigid internal fixation. *Clin Orthop* 1983;178:7-25.

Lavender JP, Khan RAA, Hughes SPF. Blood flow and tracer uptake in normal and abnormal canine bone. *J Nucl Med* 1979;20:413-8.

Lund B, Lund JO, Sørensen OH, Lund B. Evaluation of fracture healing in man by serial ⁹⁹ᵐTc-Sn-pyrophosphate scintimetry. *Acta Orthop Scand* 1978;49:435-9.

McCarthy ID, Hughes SPF. Extraction of ⁹⁹ᵐTc-methylene diphos-phonate as a function of bone blood flow. In: Arlet J, Ficat RP, Hungerford DS, eds. *Bone circulation*. Baltimore, etc: Williams & Williams. 1984:167-70.

Makler PT Jr, Charkes ND. Studies of skeletal tracer kinetics. IV. Optimum delay time for Tc-99m (Sn) methylene diphosphonate bone imaging. *J Nucl Med* 1980;21:641-5.

Matin P. The appearance of bone scans following fractures, including immediate and long term studies. *J Nucl Med* 1979;20:1227-31.

Muheim G. Assessment of fracture healing in man by serial ⁸⁷ᵐStrontium-scintimetry. *Acta Orthop Scand* 1973;44:621-7.

Paradis GR, Kelly PJ. Blood flow and mineral deposition in canine tibial fractures. *J Bone Joint Surg [Am]* 1975;57-A:220-6.

Ramadier JO, Lecestre P, Camilleri A, Bomhart M, Mazas F, Witvoet J, Zueman P. Fractures ouvertes de jambe: étude de 818 cas. *Int Orthop* 1981;5:169-82.

Riggens RS, DeNardo GL, D'Ambrosia R, Goldman M. Assessment of circulation in the femoral head by 18F scintigraphy. *J Nucl Med* 1974;15:183-6.

Tucker FR. The use of radioactive phosphorus in the diagnosis of avascular necrosis of the femoral head. *J Bone Joint Surg [Br]* 1950;32-B:100-7.

Premenopausal Bone Loss in the Lumbar Spine and Neck of Femur: A Study of 225 Caucasian Women

A. RODIN,[1] B. MURBY,[2] M. A. SMITH,[3] M. CALEFFI,[4] I. FENTIMAN,[4] M. G. CHAPMAN[1] and I. FOGELMAN[2]

[1] *Departments of Gynaecology,*
[2] *Nuclear Medicine,*
[3] *Radiological Sciences and*
[4] *Oncology, Guy's Hospital, London, England*

Address for correspondence and reprints: Dr. Adam Rodin, Department of Gynaecology, Guy's Hospital, London, SE1, England.

Abstract

Two hundred and twenty-five premenopausal women were studied to evaluate age-related changes in trabecular bone mass. Measurements were made at the lumbar spine and femoral neck by dual photon absorptiometry. It was found that spinal bone density increased significantly from the 20s to reach a peak in the mid-30s. Identical trends were observed in total bone mass and bone mass normalized by length. Bone loss then proceeded at a rate of 1% per year, and by the early 50s, 10% of peak spinal density was lost. There was no peak in femoral neck density; loss commenced in the late 20s and continued at a rate of 0.4% per year. The cumulative premenopausal loss from the femur at 9% was comparable to that in the spine. It is concluded that significant amounts of trabecular bone are lost from both the spine and femoral neck before the menopause. The implications of these findings for the prevention of osteoporosis are discussed.

Key Words: Bone density–Dual photon absorptiometry–Menopause.

Introduction

Age is well recognized as an important determinant of bone density, but the natural history of age-related bone loss remains controversial. In women, cortical bone density shows little or no diminution until the menopause which is followed by a period of rapid bone loss (Riggs et al. 1981). Advances in technology have led to the introduction of dual photon absorptiometry and quantitative CT scanning and these techniques make it possible to measure bone density at the spine and femur, the clinically important sites where osteoporotic fractures tend to occur. These areas have a significant trabecular bone component and evidence is accumulating that cortical and trabecular bone exhibit different patterns of loss.

Three patterns of age-related changes in trabecular bone have been described. Riggs et al. (1981) demonstrated loss commencing in "young adulthood" and continuing in a linear manner throughout life. A second model suggests that trabecular bone behaves in a similar way to cortical bone; it is maintained until the menopause when loss commences (Aloia et al. 1985; Sambrook et al. 1987). Other groups have shown that trabecular bone mineral reaches a peak in the mid-30s, and this is followed by a progressive

Table I. Characteristics of the study population.

Age group (years)	n	Height (m) mean ± SD	Weight (kg) mean ± SD	Pill use (year) mean
18–22	55	1.65 ± 0.06	59.30 ± 8.07	1.5
21–25	69	1.63 ± 0.14	58.90 ± 7.11	2.4
24–28	41	1.65 ± 0.06	57.58 ± 12.0	2.9
27–31	33	1.63 ± 0.21	61.79 ± 10.0	2.9
30–34	27	1.66 ± 0.06	63.44 ± 9.59	3.1
33–37	19	1.62 ± 0.08	62.17 ± 11.5	2.3
36–40	28	1.62 ± 0.05	57.00 ± 17.0	2.0
39–43	30	1.62 ± 0.05	62.20 ± 9.99	1.8
42–46	23	1.63 ± 0.05	64.83 ± 8.36	2.0
45–49	17	1.60 ± 0.04	65.90 ± 11.2	2.5
48–52	15	1.56 ± 0.02	75.00 ± 14.3	1.9

loss (Krolner and Pors-Nielsen 1982; Cann et al. 1985). The aim of the present study is to establish the pattern of age-related alterations in trabecular bone in normal Caucasian women. An understanding of these changes may suggest alternative approaches to the prevention of osteoporosis.

Patients and Methods

Patients

The study population consisted of 225 Caucasian women whose ages ranged from 18 to 52 years. Women were recruited from the hospital staff and from outpatient clinics; approximately 50% of volunteers in each age group were staff members. They were all premenopausal with regular menstrual cycles. Subjects had no relevant medical history, and in particular, there was no history of bone or joint disease. None of the women were taking medication known to influence bone density. Women with a daily calcium intake of less than 500 mg, as assessed by questionnaire, were excluded as were those with a history of anorexia nervosa. In all cases, body mass index was <25 (weight in kilograms/(height in meters)^2). The characteristics of the study population are shown in Table I. Height and weight were similar in all age groups with the exception of the oldest group which was significantly shorter and heavier than other age groups. Current and past pill users were included in this study; we have previously shown that combined oral contraception does not influence bone density (Rodin et al. 1987).

All subjects gave informed consent for the study and approval was granted by the Ethical Committee, Guy's Hospital, London.

Methods

Individuals attended for densitometry on entry to the study and there was no grouping of measurements with time according to age. All scans were performed and analyzed by the same technician. Bone mineral was measured at the lumbar spine (L2–L4) and at the neck of femur by dual photon absorptiometry using a Novo 22a dual photon absorptiometer. Total bone mineral (BM), bone mineral per unit length (BM/L) and bone mineral per unit area or bone mineral density (BMD) were measured at both sites. The units used were respectively, grams hydroxyapatite (gHA), grams hydroxyapatite per unit distance between the top of L2 and the bottom of L4 (gHA/cm) and grams hydroxyapatite per unit area of L2 to L4 (gHA/cm^2) as measured by the edge detection algorithm. Reproducibility data was obtained by repeated measurements in 10 subjects at both sites at 12-week intervals, giving a precision of 2.2% for BM, 2.6% for BM/L and 2.0% for BMD in the lumbar spine, and 2.2% for BMD in the femoral neck.

In the analysis of the data subjects were grouped according to age. Overlapping 5 year groups were formed (18–22 years; 21–25 years; 24–28; 27–31; 30–34; 33–37; 36–40; 39–43; 42–46; 45–49 and 48–52). The mean BMD and standard error of mean were calculated for each group and plotted against the mean age for that group. Non-linear regression analysis was also performed on the whole data set. In order to confirm that the observed trends were independent of normalization, non-linear regression analysis was also performed on the BM and BM/L data in the spine. The significance of the difference between BMD at different ages was assessed using Students t test for unpaired data. To further analyze the significance of any visually identifiable peak linear regression, analysis was performed and rate of change in bone density was calculated.

Results

Second and higher order polynomial fits confirmed the existence and position of a peak in spinal BMD. Further confirmation was provided by the data on BM and BM/L (Fig. 1). The data were significantly correlated with a curve with a peak in the mid-30s ($r = 0.24$; $p < 0.001$). There was no
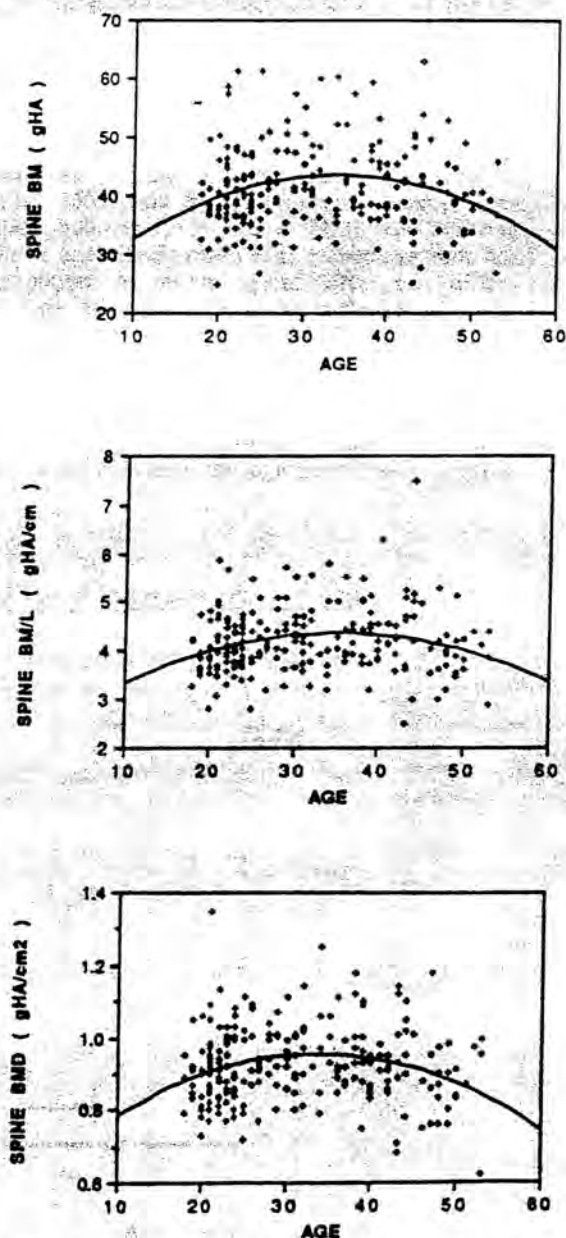

Fig. 1. Spinal BM, BM/L and BMD plotted against age for 225 premenopausal women. Second order polynomial fit shown.

correlation with a linear fit. There was a 5% increase in spinal bone density between the age groups 18–22 and 33–37 which was significant ($p = 0.03$). This was followed by a progressive decline at a rate of 1.0% per year. By the early 50s, 10% of peak spinal bone mass was lost and this represented a significant fall ($p = 0.016$) (Fig. 2).

A different pattern was exhibited by the femoral neck, the raw data of which showed a linear correlation with age ($r = 0.31$, $p < 0.001$). No improvement in fit was obtained using a second or higher order polynomial. Our study did not demonstrate a peak in femoral bone mass and loss of mineral commenced in the late 20s. The rate of loss was slower than that seen in the lumbar spine at 0.4% per year, however, by the early 50s, 9% of femoral bone mass was lost which represented a significant premenopausal fall ($p = 0.012$) (Fig. 3).

Discussion

In this study, we have demonstrated that significant premenopausal bone loss occurs from both the lumbar spine and neck of femur. Spinal bone density increases in the 20s to reach a peak in the mid-30s and then falls in an almost linear fashion. The femoral neck shows a different pattern of bone loss: peak density is presumably attained at an earlier age which cannot be defined from the present data. The rate of loss is slower than that seen in the spine, but as bone loss commences at an earlier age, by the late 40s the cumulative loss from peak density at both sites is comparable.

Previous studies offer conflicting evidence about the occurrence of premenopausal bone loss and the patterns of age-related changes in bone mineral. In a cross-sectional study of 105 normal women, Riggs et al. (1981), found that bone loss from the vertebrae begins in young adulthood

and is linear. However, the bulk of evidence now conflicts with this early model. Krolner and Pors-Nielsen (1982) examined lumbar spine bone mineral content in 70 women in relation to age. By fitting the data to a gamma variate function they showed a maximum spinal density at 34 years, but this method of statistical handling has been criticized (Tothill et al. 1983). Their own results support the view that there is increased loss of spinal bone mineral after the menopause, but insufficient numbers prevent detailed analysis in premenopausal women. This limitation also applies to other studies. Nilas and Christiansen (1987) carried out a cross-sectional study of 178 healthy women and found no evidence that substantial premenopausal bone loss occurs from any site. Hansson and Roos (1986) in agreement with our findings, noted a continuous age-related decrease of spinal bone density after the age of 35. Mazess et al. (1987) with a heterogeneous study population of 892 women derived from seven centers found a 10% decrease in spinal density in the decade preceding the menopause. A similar pattern was shown for femoral bone density. Schaadt and Bohr (1988), in a recent study, found that the bone mineral content of the femoral neck decreased linearly from the 30s. Premenopausal bone loss is also suggested by histomorphometric studies (Meunier et al. 1973; Marcus et al. 1983) and by postmortem investigations (Weaver and Chalmers 1966; Arnold 1973). The differing descriptions of age-related changes in trabecular bone are probably explained by technological differences, differences in data handling and differences in the sample sizes between the groups. Sambrook et al. (1987) pointed out the pitfalls of using cross-sectional data to draw conclusions about longitudinal changes in a population, and they emphasized the importance of adequate sample size.

Our data and results from previous studies provide a compelling body of evidence that significant loss of trabec-
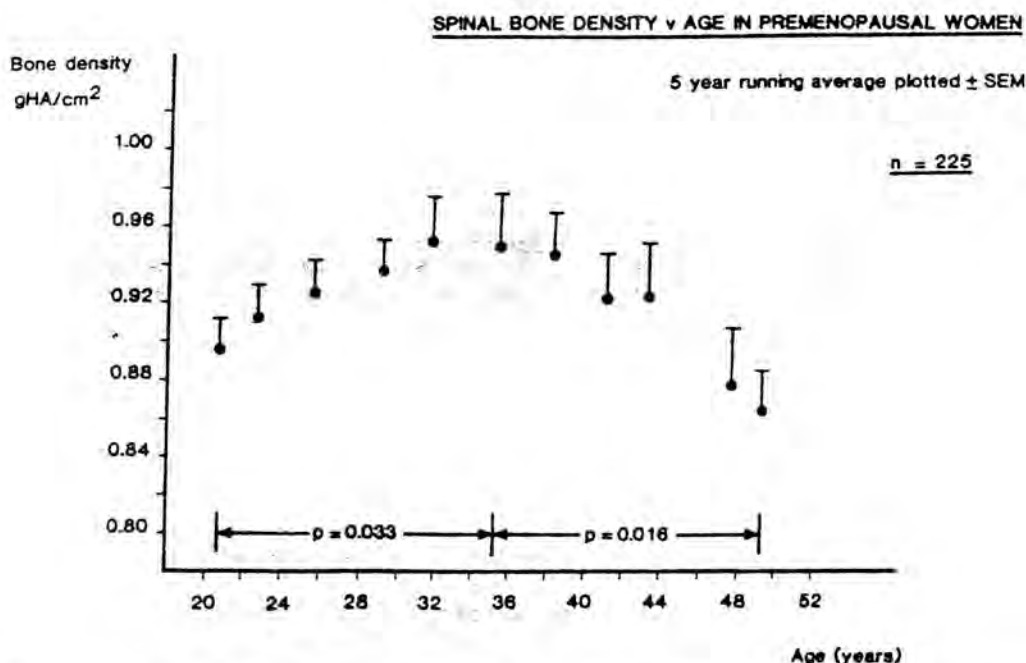

Fig. 2. Spinal BMD plotted against age in 225 premenopausal women. Mean BMD was calculated for 5 year overlapping groups and plotted against the mean age for that group.
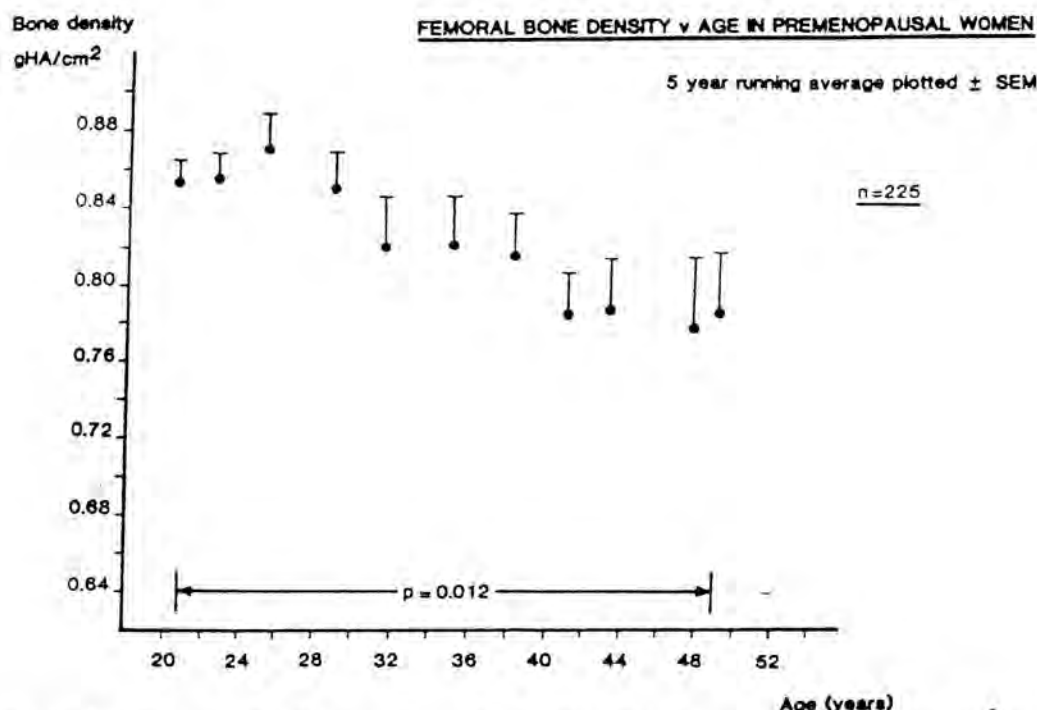
Fig. 3. Femoral BMD plotted against age for 225 premenopausal women. Mean BMD was calculated for 5 year overlapping groups and plotted against the mean age for that group.

ular bone occurs before the menopause. The finding of a peak in spinal bone density is supported by similar trends in BM and BM/L suggesting that this phenomenon is independent of area normalization. The significant increase in spinal bone density between the 20s and mid-30s may have important implications for the prevention of osteoporosis in later life. In addition, our study provides further evidence that trabecular bone at different anatomical sites exhibits different patterns of age-related density changes, but the reason for this variation is not fully understood.

The possibility that these patterns of changes in trabecular bone are biased by secular trends needs consideration. It seems unlikely, however, that the rise in spinal density seen between 18 years to the mid-30s could be due to such influences. The relatively short time scale argues against a secular effect. However, we cannot rule out the possibility that the differences between those at the age extremes of the study population are influenced by secular effects.

The mechanism of early bone loss remains unclear. The importance of oestrogen in maintaining skeletal bone mass is well established and there is evidence for accelerated bone loss after oophorectomy (Cann et al. 1980) or following a natural menopause (Gennant et al. 1984). Oestrogen replacement therapy is effective in preventing postmenopausal bone loss (Lindsay et al. 1976). However, the menopause is preceded by a transition phase which is characterized by rising gonadotrophin levels and falling total oestrogen output from the ovaries (Sherman et al. 1976). It therefore seems likely that the patterns of endocrine changes will vary between individuals, and we suggest that genetic and environmental factors interact to influence the timing and profile of the hormonal fluxes associated with the menopause. A proportion of women will therefore becomge relatively oestrogen deficient before the cessation of their menses, and it is well known that some develop

vasomotor instability and genital atrophy during the climacteric. It has been suggested that this relative deficiency of oestrogen may contribute to the loss of trabecular bone in premenopausal women (Johnston et al. 1985). It is possible that this effect contributes to spinal bone loss which commences in the mid-30s, but it does not adequately explain the pattern of loss seen in the femoral neck.

Prevention of osteoporosis is an important goal, and while hormone replacement therapy in the early premenopausal years is of proven efficacy (Lindsay et al. 1976), our findings raise the possibility that prophylaxis in premenopausal women should be considered. Two potential approaches are suggested: (a) spinal bone density increases in the young woman until the mid-30s, and if this can be enhanced the peak spinal bone density can be maximized; (b) if bone loss in the climacteric can be prevented or reduced, women would again reach the menopause with a better reserve. Exercise and calcium supplementation may be suitable strategies, but before any measures can be recommended they must be fully evaluated and ultimately they must be shown to reduce fracture risk.

References

Aloia, J. E.; Vaswani, A.; Ellis, K., et al. A model for involutional bone loss. *J. Lab. Clin. Med.* 106:630–637; 1985.

Arnold, J. S. Amount and quality of trabecular bone in osteoporotic and vertebral fractures. *Clin. Endocrinol. Metab.* 2:221–238; 1973.

Cann, C. E.; Gennant, H. K.; Ettinger, B.; Gordon, G. S. Spinal mineral

loss in oophorectomized women. *JAMA* 244:2056–2059; 1980.

Cann, C. E.; Genant, H. K.; Kolb, F. O.; Ettinger, B. Quantitative computed tomography for prediction of vertebral fracture risk. *Bone* 6:1–7; 1985.

Gennant, H. K.; Cann, C. E.; Ettinger, B., et al. Quantitative computed tomography for spinal mineral assessment. Christiansen, C.; Arnaud, C. D.; Nordin, B. E. C., et al., eds. *Osteoporosis I.* Aalborg Stiftsbogtrykkeri; 1984:65–71.

Hansson, T.; Roos, B. Age changes in the bone mineral of the lumbar spine in normal women. *Calcif. Tissue Int.* 38:249–251; 1986.

Johnston, C. C.; Hui, S. L.; Witt, R. M., et al. Early menopausal changes in bone mass and sex steroids. *J. Clin. Endocrinol. Metab.* 61:905–911; 1985.

Krolner, B.; Pors-Nielsen, S. Bone mineral content of the lumbar spine in normal and osteoporotic women. *Clin. Science* 62:329–336; 1982.

Lindsay, R.; Hart, D. M.; Aitken, J. M., et al. Long-term prevention of postmenopausal osteoporosis by oestrogen. *Lancet* 1:1038–1041; 1976.

Marcus, R.; Kosek, R. J.; Pfefferbaum, A.; Horning, A. Age-related loss of trabecular bone in premenopausal women: a biopsy study. *Calcif. Tissue Int.* 35:406–409. 1983.

Mazess, R. B.; Barden, H. S.; Ettinger, M., et al. Spine and femur density using dual-photon absorptiometry in US white women. *Bone and Mineral* 2:211–219; 1987.

Meunier, P.; Courpron, P.; Edouard, C., et al. Physiological senile involution and pathological rarefaction of bone. *Clin. Endocrinol. Metab.* 2:239; 1973.

Nilas, L.; Christiansen, C. Bone mass and its relationship to age and the menopause. *J. Clin. Endocrinol. Metab.* 65:697–702; 1987.

Riggs, B. L.; Wahner, H. W.; Dunn, W. L., et al. Differential changes in bone mineral density of the appendicular and axial skeleton with aging. *J. Clin. Invest.* 67:328–335; 1981.

Rodin, A.; Fogelman, I.; Chapman, M. G. Combined oral contraception as a determinant of bone mass. *Abstracts from the International Symposium on Osteoporosis, Denmark.* Osteopress; 1987:54

Sambrook, P. N.; Eisman, J. A.; Furler, S. M.; Pocock, N. A. Computer modeling and analysis of cross-sectional bone density studies with respect to age and the menopause. *J. Bone Min. Res.* 2:109–114; 1987.

Schaadt, O.; Bohr, H. Different trends of age-related diminution of bone mineral content in the lumbar spine, femoral neck and femoral shaft in women. *Calcif. Tissue Int.* 42:71–76; 1988.

Sherman, B. M.; West, J. H.; Korenman, S. G. The menopausal transition; analysis of LH, FSH, Estradiol and progesterone concentrations during menstrual cycles of older women. *J. Clin. Endocrinol. Metab.* 42:629–636; 1976.

Tothill, P.; Smith, M. A.; Sutton, D. Dual photon absorptiometry of the spine with a low activity source of gadolinium 153. *Br. J. Radiology* 56:829–835; 1983.

Weaver, J. K.; Chalmers, J. Cancellous bone; its strength and changes with aging and an evaluation of some methods for measuring its mineral content. I. Age changes in cancellous bone. *J. Bone Joint Surg.* 48A:289; 1966.

Bone ultrasonic attenuation in women: reproducibility, normal variation and comparison with photon absorptiometry

J G Truscott†, M Simpson†, S P Stewart†, R Milner†, C F Westmacott†, B Oldroyd†, J A Evans†, A Horsman‡, C M Langton§ and M A Smith†

† MRC Bone Mineralisation Group, Department of Medical Physics, University of Leeds, The General Infirmary, Leeds LS1 3EX, UK
‡ Department of Applied Biology, University of Hull, Hull HU6 7RX, UK
§ Department of Applied Physics, Sheffield City Polytechnic, Sheffield S1 1WB, UK

Abstract. The reproducibility of two methods of measuring broadband ultrasonic attenuation (BUA) in the calcaneus have been studied. An improvement in reproducibility *in vivo* from 9.6% to 2.8% between old and new techniques has been observed. Measurements of the calcaneus using BUA were correlated with measurements of bone mineral density measured by dual energy x-ray absorptiometry in the lumbar spine, femur and total body and bone mineral content in the distal and proximal forearm measured by single photon absorptiometry. For the older BUA technique the correlation coefficients ranged between $r = 0.27$ and $r = 0.34$. For the newer BUA technique the correlation coefficients ranged between $r = 0.49$ and $r = 0.62$ and were all significant ($P < 0.001$).

1. Introduction

Osteoporosis affects an increasing fraction of the elderly population and can result in fractures of the wrist, spine and hip. Bone loss is more rapid from these sites of high trabecular content (Genant and Cann 1981). Non-invasive bone measurement for the management and diagnosis of osteoporosis is currently carried out using single photon absorptiometry (SPA) of the forearm (Cameron and Sorenson 1963), dual photon absorptiometry (DPA) of the spine (Roos and Skoldborn 1974) and more recently by dual energy x-ray absorptiometry (DEXA) of the proximal femur, lumbar spine and total body (Mazess *et al* 1989). Whilst all these methods are reasonably precise and accurate they do expose the subject to ionising radiation and they only measure the area density (g cm^{-2}) of the bone.

Langton *et al* (1984) suggested that measurement of broadband ultrasonic attenuation (BUA, dB MHz^{-1}) of the calcaneus can give a direct interpretation of the structure of the bone as well as bone density. The calcaneum is chosen as it is a site containing a high percentage of trabecular bone and may have a composition similar to other bones, such as the vertebrae and femur, which are more commonly measured for BMD. Poll *et al* (1986) later suggested that a reproducibility figure for this method of 3.9% could be obtained by measuring both heels and taking the average BUA value. Since then, other workers have obtained improved reproducibility values *in vitro* for the method of 2.2% (McKelvie *et al* 1989) and 2.4% (McCloskey *et al* 1990a). The majority of the BUA measurements reported by other workers were made using the original commercial machine which measured BUA, the Walker Sonix UBA 1001, which has since been superseded by the Walker Sonix UBA 575.

In this study we examine the reproducibility of both the old and new techniques for measuring BUA in the calcaneus and correlate them with SPA of the forearm and DEXA of the lumbar spine, femur and total body. The normal variation of the newer BUA technique and comparison with DEXA of the spine and femur is also assessed in a group of women in whom we measured BUA of the calcaneus and BMD of the femur and spine on the same day.

2. Methods

2.1. Ultrasound equipment

We measured BUA in the right heel using two machines, the Walker Sonix UBA 1001 and the Walker Sonix UBA 575. With the UBA 1001, the patient sits with his/her foot in a room temperature water bath between two fixed 25 mm diameter transducers, both resonant at 1 MHz, one acting as a transmitter, the other as a receiver. The aim was to position the foot accurately so that the calcaneus lay between the two transducers. A series of short bursts of varying ultrasound frequency from 200 - 600 kHz in 16 kHz steps is transmitted through the water without the foot in the bath and the transmitted amplitude at each frequency recorded. A similar series of measurements is made through the water with the heel inserted in the bath. As the difference between the ultrasound signal amplitude for water and for water plus heel at each frequency sample point is due to the attenuation caused by the heel, an attenuation spectrum can be constructed. The slope of the best straight line fitted to this spectrum (dB MHz^{-1}) is the reported measurement of BUA. The measurement is repeated until three consecutive values are obtained that are within 0.5 dB MHz^{-1} of each other. This usually takes about 3 min, the delay probably being caused by air trapped in the pores which is released in this period.

The fundamental basis of the UBA 575 is the same as the UBA 1001 but several changes in technique have been made. The transducers have been changed to 19 mm diameter with 500 kHz resonant frequency and signal amplitudes are recorded at 12 equally spaced intervals between 200 and 600 kHz. The heel is still placed in a water bath but now the transducers are made to carry out a rectilinear scan of nine sample points on a 3 × 3 grid in a region of 22 mm × 22 mm located around the region of minimum density in the calcaneus. This region was located by the manufacturers from a study of x-ray films of the calcaneus. The calculation of BUA at each of these sample points is done as previously but the nine values obtained are subjected to a weighted averaging algorithm to produce a single value for BUA. The total measurement time is about 5 min.

2.2. Wetting agents

One problem with BUA measurement in water is that air nucleates on the skin and surface hair forming bubbles at the interface between skin and water. These bubbles cause anomalous attenuation and can be a source of unreliability in the results. To overcome this a wetting agent is added to the water and this releases the absorbed air within the water and on the skin. The detergent recommended by the manufacturer is not widely available and we had to select another capable of giving reliable results. The detergents (and concentrations) that we tested were Ark (4%), Ecover (2%,4%), Quadralene (6%,8%), Stardrops (1%,2%) and Triton X100 (2%). The last of these is a commercial wetting agent and the remainder household detergents. Ark and Ecover were abandoned as they produced a precipitate in the water bath which was opaque to ultrasound. Triton X100 was not used after an initial trial as it tended to gel at room temperature. Using each of the other solutions we made five measurements of BUA using the UBA 575 on each of three phantoms of

different BUA (described in section 2.3). In each case a pooled coefficient of variation (CV) was calculated and used as an indicator of reproducibility.

Prior to the reproducibility studies we found two other sources of variability in BUA measurement which could be easily removed. The first of these was due to talcum powder on the feet of patients. This causes a precipitate in the water bath and can be removed by prebathing the foot before immersion in the scanner. The second source of variability was due to body oils or creams applied to the heel which can be removed with an alcohol swab prior to scanning.

2.3. Reproducibility

The *in vitro* reproducibility studies were performed using phantoms, representing high, medium and low values of BUA which are made by Walker Sonix and are constructed from room temperature vulcanised silicone in which glass beads are suspended. The phantoms were stabilised in the scanner so that there was a minimal change in position and orientation between scans. On the UBA 1001 37 measurements were made on two phantoms (high and medium BUA) over 13 months. On the UBA 575 64 scans were made on all three phantoms over a period of three months.

The *in vivo* reproducibility studies were performed using cooperative volunteers who were measured repeatedly with a reasonable time interval between measurements. On the UBA 1001 three volunteers were studied on 13 occasions with an interval of about a month between measurements. On the UBA 575, five volunteers were studied on five occasions with an interval of one day between measurements. In addition, the short term reproducibility *in vivo* was measured from two scans made within five minutes of each other on 30 female volunteers, the foot being removed from the bath and dried between scans. The effects of the various detergent solutions as described in section 2.2. was determined prior to the evaluation of reproducibility of the UBA 575.

2.4. Bone mineral measurement using absorptiometry

We measured BMC in the forearm at two sites using a Nuclear Data 1100A scanner. This SPA technique uses an ^{125}I source of 5.5 - 7.4 GBq activity. The patients' arm is held in a water bath and the scanner finds the site at which the radius and ulna are separated by an 8 mm gap. From this point five scans are carried out at 4 mm intervals proximally and four scans at 2 mm intervals distally. The proximal and distal groups of scans are each averaged and the measurement at each of these two sites is given as bone mineral content normalised for both fat cover and bone width and expressed in arbitrary units which can be converted to g cm^{-2}. Nilas *et al* (1985) report a reproducibility of 1 - 1.5% (coefficient of variation) for the two forearm scan sites. The skin entrance dose associated with this technique is between 30 and 50 μSv.

To measure BMD in the spine, femur and total body we used a Lunar Radiation DPX scanner. The DEXA technique uses a filtered x-ray tube to obtain the dual energy beam required. The scanning and analysis procedures on this scanner are controlled by the manufacturers software version 3.2. The measurements we use are the bone mineral densities (BMD g cm^{-2}) of the lumbar spine (L2-L4), femoral neck, trochanter, Ward's triangle, and total body. The reproducibility obtained by us for the spine, femur and total body *in vivo* are 1.2%, 1.7% and 0.7% respectively. The skin entrance dose per scan associated with these techniques is 14 μSv each for spine and femur and 1 μSv for a total body scan.

2.5. Statistical methods

For reproducibility measurements the coefficient of variation has been calculated. With sets of paired data this is obtained from an analysis of the squares of the differences. For multiple measurements on subjects the overall CV is obtained from a pooled variance. This analysis and the calculation of the correlation coefficients was obtained using Statgraphics v3.0 as were the tests for normality and the pooled Students t-test.

3. Subjects

On the UBA 1001 we made BUA measurements on 264 women aged 19 to 81 years (group 1), comprising 131 asymptomatic normals, 83 patients with endocrine disorders, 12 with asthma and 38 volunteers who were unclassified. Of these women, 261 had spine and femur BMD and 60 had total body BMD measurements. SPA of forearm was also carried out on 249 of these women.

We made BUA measurements using the UBA 575 on 191 women aged 22 to 79 years (group 2), comprising 112 asymptomatic normals, 60 patients with endocrine disorders, 6 with osteoarthritis and 13 volunteers who were unclassified. Of these 190 had spine and femur BMD and 114 had total body BMD measurements. Forearm BMC measurements were made on 103 of these women. On the occasions when measurements were made on the same patient using different techniques they were carried out at the same visit.

The above measurements were made for use in a study of the correlation between the different techniques of bone measurement and so no exclusions were considered merited. To study the normal variation of each of the methodologies when applied to the same group, a subset of 70 women aged 50 to 59 years (group 3) was selected from group 2. These women were taking part in an hormone replacement therapy study and had presented for prophylactic screening with no symptoms of bone disease and comprise the whole of this age group. On groups 1 (UBA 1001) and 2 (UBA 575) we performed correlation analysis between BUA and each of the BMD and BMC measurement techniques described above. For group 3 we calculated mean and standard deviation (SD) for the measurements obtained using each technique and for each technique we also calculated the coefficient of variation within the group.

4. Results

In the assessment of the wetting agents the pooled values of CV over the three phantoms measured on the UBA 575 for Quadralene (6%,8%) were 0.52% and 1.99% respectively and for Stardrops (1%,2%) were 2.00% and 0.39% respectively. On the basis of these results we determined to use Stardrops (2%) in our future patient work.

The *in vitro* reproducibility measured in phantoms over a period of 13 months on the UBA 1001 was 3.1%, on the UBA 575 the equivalent reproducibility value measured over a period of 3 months was 2.2%. We measured reproducibility *in vivo* over a 13 month period on the UBA 1001 to be 9.6%. On the UBA 575 the reproducibility measured over a 5 day period was 2.8%. In addition to the above reproducibility measurements we measured the reproducibility *in vivo* on the UBA 575 in the short term to be 3.5%.

Summary statistics for subject groups 1 and 2 for each of the measurement techniques used are given in table 1. The smaller samples used for total body BMD in groups 1 and 2 and the forearm SPA samples drawn from group 2 were checked to ensure that the mean value of BUA in these samples was representative of the BUA of the group from which they

Table 1. Summary statistics for group 1 (UBA 1001) and group 2 (UBA 575) for heel BUA (dB MHz^{-1}), BMD (g cm^{-2}) at various sites, BMC (g cm^{-1}) in the forearm, height (cm) and weight (kg) comprising sample size (*n*), mean, standard deviation (SD), minimum and maximum values.

	Group 1					Group 2			
	n	Mean	SD	Min	Max	n	Mean	SD	Min	Max
Heel BUA	264	96.7	20.9	28.2	157.2	191	62.5	14.2	26	99
Spine BMD	261	1.054	0.200	0.503	1.543	190	1.057	0.204	0.520	1.579
Femoral neck BMD	261	0.879	0.148	0.520	1.333	190	0.868	0.152	0.518	1.343
Trochanter BMD	261	0.719	0.122	0.366	1.052	189	0.711	0.131	0.421	1.051
Ward's BMD	261	0.743	0.191	0.318	1.290	190	0.752	0.194	0.292	1.213
Total body BMD	60	1.088	0.100	0.887	1.276	114	1.095	0.110	0.786	1.463
Proximal forearm BMD	249	1.315	0.246	0.750	1.840	103	1.358	0.227	0.800	1.840
Distal forearm BMC	249	0.969	0.199	0.540	1.510	103	0.977	0.194	0.540	1.450
Height	264	160.5	6.5	144	176	191	160.5	7.5	135	177
Weight	264	63.5	11.4	43	107	191	62.6	10.4	35	93

were drawn. Pooled *t*-tests revealed no significant differences in BUA values between any of these samples and the group mean values. The correlation coefficients of the different techniques for groups 1 and 2 and their significances are given in table 2. None of the variates used in the correlation analysis departed significantly from being normally distributed. Scatter plots of the correlated variates did not depart from linearity confirming the validity of the use of correlation analysis. It can be seen from table 2 that although the correlations between BUA and other measurements in group 1 are significant, they are all relatively weak. Group 2 shows an improvement in the correlation coefficients all of which are highly significant.

The spread of the normal data in group 3 using the different techniques is given in table 3. Examination of the CVs of the various measurements reveals little difference between the spread of the normal range using the different techniques. The CV of heel BUA is, however, the largest.

Table 2. Correlation coefficients (*r*), for group 1 (UBA 1001) and group 2 (UBA 575), for various bone mineral measurement techniques compared to BUA in the right calcaneus, with significance values (*P*) and sample sizes (*n*). BMD is measured in g cm^{-2}.

Measurement technique	Group 1			Group 2		
	r	P	n	r	P	n
Spine BMD	0.34	<0.001	261	0.61	<0.001	190
Femoral neck BMD	0.27	<0.001	261	0.60	<0.001	190
Trochanter BMD	0.33	<0.001	261	0.58	<0.001	189
Ward's triangle BMD	0.29	<0.001	261	0.62	<0.001	190
Total body BMD	0.31	<0.02	60	0.54	<0.001	114
Proximal forearm BMC	0.30	<0.001	249	0.49	<0.001	103
Distal forearm BMC	0.29	<0.001	249	0.55	<0.001	103

Table 3. Summary statistics for heel BUA (dB Mhz^{-1}) and BMD (g cm^{-2}) comprising mean, standard deviation (SD) and percentage coefficient of variation (CV) for group 3.

Measurement technique	Mean	SD	CV
Heel BUA	65.61	12.45	18.98
Lumbar spine BMD	1.06	0.15	14.58
Femoral neck BMD	0.87	0.12	13.96
Trochanter BMD	0.72	0.11	15.53
Ward's triangle BMD	0.75	0.13	17.39

5. Discussion

The reproducibility figures obtained suggested an improvement with the UBA 575 over the earlier UBA 1001. This was particularly demonstrated by the *in vivo* data. However, the *in vivo* reproducibility data from the two machines are not entirely comparable due to the differences in time intervals used. The possible presence of a gradual variation in BUA using the UBA 1001 over the 13 month period was investigated by a further analysis of the data. The reproducibility was assessed from the differences between successive measurements; this gave a value of 9.4% suggesting that the relatively poor reproducibility was not due to a gradual long term variation. The improvement in precision in the UBA 575 equipment is probably due to several factors including a change in resonant frequency of the transducers, a change to rectilinear scanning, the addition of a foot restraint, the selection of wetting agent and the thorough cleaning of the foot before placement in the water bath.

Many groups have tried to correlate BUA of the calcaneus with different bone measurement techniques at other sites. With SPA of the distal forearm correlation coefficients of $r = 0.8$ (Poll *et al* 1986), $r = 0.77$ (McCloskey *et al* 1990b) and $r = 0.64$ (Rossman *et al* 1989) have been demonstrated. A study has also been reported which showed no correlation between BUA of the calcaneus and SPA of the forearm (Resch *et al* 1990). For DPA of the femoral neck Rossman *et al* (1989) report a correlation coefficient of 0.41 whilst for the lumbar spine they give $r = 0.66$. For the spine McCloskey *et al* (1990b) give $r = 0.72$. For all these previously reported studies reasonable numbers (*n* between 44 and 72) were used for the correlations.

Quantitative computed tomography (QCT), a technique developed in different forms by Cann and Genant (1980) and Ruegsegger *et al* (1976) has revealed a quite strong correlation ($r = 0.85$) between BUA of the calcaneus and forearm cortical bone mineral content, but a far weaker relationship ($r = 0.66$) with trabecular bone mineral in the same limb (Hosie *et al* 1987). However when BUA and QCT are carried out at the same site correlations of $r = 0.92$ in excised os calces (McKelvie *et al* 1989) and $r = 0.80$ in calcaneal core samples (McCloskey *et al* 1990a) have been observed. Both of these groups report correlations of BUA with physical density of approximately 0.8. However McKelvie *et al* (1989) rejected a large proportion of their calcaneal core samples (15%) before correlating physical density with BUA. In the studies using QCT the group sizes for correlation analysis ranged between 24 and 28.

The 25 mm core samples measured by McCloskey *et al* (1990a) were the same diameter as the ultrasound transducers which may result in significant diffraction artefacts. The core samples used above were all taken from similar sites where the structure and orientation of trabeculae could be expected to be similar. Evans and Tavakoli (1990) used samples taken from different regions of bovine femora excised at random angles, thus a difference in

structure and orientation between samples could be expected. This is probably why they observed such a weak correlation ($r = 0.33$, $n = 27$) between BUA and physical density. Unless substantial scattering of the ultrasound beam is occurring the trabecular orientation should make little difference to the measurement of attenuation. Evans and Tavakoli (1990) also considered samples with a range of density ($1.15 - 1.4$ g cm^{-3}) which had a higher upper limit than other workers. At higher densities errors in the measurement increase, which would diminish the correlation further.

Comparison of our correlation coefficients, of BUA with other techniques, for group 1 (UBA 1001) and group 2 (UBA 575) shows a significant improvement in correlation with the newer of the two methods of measuring BUA. This improvement is probably attributable to the improvement in reproducibility leading to less variability in BUA measurement with the newer method. When we compare the correlations of group 2 BUA with other techniques to those correlations reported by other workers, with the exception of the femoral neck (Rossman *et al* 1989), all our correlations are weaker, although we have substantially larger groups.

The weak correlations that have been obtained in our study could be due to either or both of the following factors: (i) BUA values may reflect, in some way, both density and structure. We may, therefore, not expect the correlation with only bone density to be particularly good. (ii) The correlation between bone density in the calcaneus and other sites in the body may not be particularly strong.

Other methods of assessing the utility of BUA measurements have been suggested in terms of diagnostic predictive power. Several workers observe that those patients at high risk of fracture can be sorted from the normal population (Langton *et al* 1984, Miller and Porter 1987, Johnson and Porter 1987). Murray *et al* (1987) showed that patients with osteoporosis could be identified, Fordham *et al* (1987) that patients with rheumatoid arthritis differed from controls and Jones *et al* (1987) that active and sedentary groups could, be separated. The problem still remains that, although groups can be separated, given a single measurement of BUA it is often difficult to assign an individual to a group with any degree of confidence.

Acknowledgements

References

Cameron J R and Sorenson J A 1963 Measurement of bone mineral in vivo: An improved method *Science* **142** 230-2

Cann C E and Genant H K 1980 Precise measurement of vertebral mineral content using computed tomography *J. Comput. Assist. Tomogr.* **4** 493-500

Evans J A and Tavakoli M B 1990 Ultrasonic attenuation and velocity in bone *Phys. Med. Biol.* **35** 1387-96

Fordham J N, Langton C and Tulsidas H 1987 Ultrasonic measurements of bone density in rheumatoid arthritis and osteoarthritis *Ultrasonic Studies of Bone* eds S B Palmer and C M Langton (Bristol: IOP Publications) pp 47-53

Genant H K and Cann C E 1981 Vertebral mineral determination using quantitative computed tomography *Osteoporosis: Recent Advances in Pathogenesis and Treatment* eds H F Deluca *et al* (Baltimore: University Park Press) pp 37-47

Hosie C J, Smith D A, Deacon A D and Langton C M 1987 Comparison of broadband ultrasonic attenuation of the os calcis and quantitative computed tomography of the distal radius *Clin. Phys. Physiol. Meas.* **8** 303-8

Johnson K and Porter R W 1987 Broadband ultrasonic attenuation in patients with fracture of the distal radius *Ultrasonic Studies of Bone* eds S B Palmer and C M Langton (Bristol: IOP Publications) pp 65-6

Jones P R M, Langton C M and Carr H 1987 Broadband ultrasonic attenuation studies in sedentary and active young male adults and in bovine cancellous and cortical bone *Ultrasonic Studies of Bone* eds S B Palmer and C M Langton (Bristol: IOP Publications) pp 37-45

Langton C M, Palmer S B and Porter S W 1984 The measurement of broadband ultrasonic attenuation in cancellous bone *Eng. Med.* **13** 89-91

McCloskey E V, Murray S A, Charlesworth D, Miller C, Fordham J, Clifford K, Atkins R and Kanis J A 1990a Assessment of broadband ultrasound attenuation in the os calcis *in vitro Clin. Sci.* **78** 221-5

McCloskey E V, Murray S A, Miller C, Charlesworth D, Tindale W, O'Doherty D P, Bickerstaff D R, Hamdy N A T and Kanis J A 1990b Broadband ultrasound attenuation in the os calcis: relationship to bone mineral at other skeletal sites *Clin. Sci.* **78** 227-33

McKelvie M L, Fordham J, Clifford C and Palmer S B 1989 *In vitro* comparison of quantitative computed tomography and broadband ultrasonic attenuation of trabecular bone *Bone* **10** 101-4

Mazess R B, Sorenson J A, Hanson J A, Collick B D and Smith S W 1989 Dual energy X-ray absorptiometry (DEXA) *Osteoporosis and Bone Mineral Measurement* eds E F J Ring, W D Evans and A S Dixon (York: IPSM Publications) pp 62-71

Miller C G and Porter R W 1987 Broadband ultrasonic attenuation as a predictive index for hip fracture in the elderly *Ultrasonic Studies of Bone* eds S B Palmer and C M Langton (Bristol: IOP Publications) pp 55-63

Murray S A, Miller C and Kanis J A 1987 Specificity and sensitivity of ultrasound attenuation in bone *Ultrasonic Studies of Bone* eds S B Palmer and C M Langton (Bristol: IOP Publications) pp 67-72

Poll V, Cooper C and Cawley M I D 1986 Broadband ultrasonic attenuation in the os calcis and single photon absorptiometry in the distal forearm: a comparative study *Clin. Phys. Physiol. Meas.* **7** 375-9

Resch H, Pietschmann P, Bernecker P, Krexner E and Willvonsender R 1990 Broadband ultrasound attenuation: a new diagnostic method in osteoporosis *Am. J. Roentgenol.* **155** 825-8

Roos B O and Skoldborn H 1974 Dual photon absorptiometry in lumbar vertebrae. 1. Theory and method *Acta. Radiol. Ther. Phys. Biol.* **13** 266-80

Rossman P, Zagzebski J, Mesina C, Sorenson J and Mazess R 1989 Comparison of speed of sound and ultrasound attenuation in the os calcis to bone density of the radius, femur and lumbar spine *Clin. Phys. Physiol. Meas.* **10** 353-60

Ruegsegger P, Elsasser U, Anliker M, Gnehm H, Kind H and Prader A 1976 Quantification of bone mineralisation using computed tomography *Radiology* **121** 93-7

NOTE

The use of a radiation sensitive CCD camera system to measure bone mineral content in the neonatal forearm: a feasibility study

J G Truscott, R Milner, S Metcalfe and M A Smith

The Centre for Bone and Body Composition Research, Institute of Physical Sciences, Department of Clinical Medicine, University of Leeds, Wellcome Wing, The General Infirmary, Leeds LS1 3EX, UK

1. Introduction

Single photon absorptiometry (SPA) was first suggested by Cameron and Sorenson (1963) for the measurement of bone mineral content (BMC) in the distal forearm *in vivo* and quickly gained currency as a quantitative method of bone mineral measurement giving a precision of approximately 2% with a radiation dose of approximately 0.15 mGy similar to the dose for a forearm x-ray film exposure. Adaptations of the method to measure the neonatal forearm met with some success (Steichen *et al* 1980, Greer *et al* 1982) but until 1986 (James *et al* 1986b) an instrument designed specifically to measure the forearm bones of premature neonates had not been constructed. With a dose to the subject of only 0.03 mGy and accuracy of 5% this machine enabled growth and mineralization data to be obtained for fetal mineralization (Ryan *et al* 1988), osteopenia of prematurity (James *et al* 1986a) and the repletion of mineral in osteopenia of prematurity (Congdon *et al* 1990).

Unfortunately a subset of preterm babies were too sick to be amenable to this measurement technique as they could not be moved from incubator to measuring instrument. In many situations it is important to measure BMC in these babies at this very early stage and to continue to monitor it in order to evaluate the efficacy of both treatment and feeding regimes. To study such babies in the incubator it would be necessary to construct a hand-held instrument which was portable, compact, light and accurate. Such a device should only expose the baby to a low radiation dose. It was felt that an isotope transmission device with a radiation sensitive charge coupled device (CCD) camera offered the likeliest solution to the problem.

2. Methods

The development of CCD video cameras which are sensitive to a range of x and γ ray energies (Arndt and In'T Veld 1988) suggested a method of measurement of BMC in the forearm using video techniques. The schematic diagram of an idealized version of

such a system is shown in figure 1. The ideal system would consist of an isotope source of monochromatic γ-ray photons of sufficient intensity located close to the arm to make the system as compact as possible. Correction for geometric distortion could be carried out relatively easily. The forearm would be enclosed in a parallel-sided soft tissue equivalent bolus material to provide a fixed thickness path in which the only changes in transmitted intensity would be due to changes in equivalent bone thickness. The radiation sensitive CCD video camera would convert each γ-ray photon arriving at the detector into a visible light photon which is converted to a specific charge on the CCD. The video circuitry produces a TV frame every 40 ms in which the grey level of each pixel is representative of the charge per element on the CCD. This information is digitized using a frame grabber under computer control. With the frame grabber operating in real time, the area to be measured could be viewed on the monitor before the data was captured. Each captured frame would then be added into a frame store until there were sufficient counts per pixel to reduce the measurement variance to an acceptable level.

The feasibility of using a CCD camera was investigated using a model of the neonatal forearm and the following apparatus. The CCD video camera was a Phototonic Science X-ray Imager on loan for a day from the manufacturers. This camera has a detector quantum efficiency (DQE) of 10–12% for energies of 5 to 200 keV covering the photopeak of ^{125}I at 27.5 keV. The effective detector pixels are 80 μm square working into the CCD by light pipe coupling to give 753×581 pixels. Digitization and sequential frame addition was carried out using a PC Vision Plus 8 bit frame grabber having two 512×512 pixel frame stores, controlled by an IBM PC using ITEX PC plus software. The limit of an 8 bit frame store meant that in practice in order to avoid overflow we could only collect 32 frames which is equivalent to an integration period of 1.28 s. The source used was an ^{125}I 1 mm point emitter of activity 1.13 GBq.

The forearm was modelled by a water-filled syringe of 21.7 mm diameter located 74.3 mm from the source and 14.0 mm from the detector surface with two aluminium tubes of diameters 3 mm and 2 mm having a wall thickness of 0.15 mm suspended centrally in the water. These sizes were typical of neonatal forearm bone sizes measured on x-rays. The forearm model was measured in air without a soft tissue equivalent bolus to provide a flat-sided soft tissue path. At this stage we make no attempt to
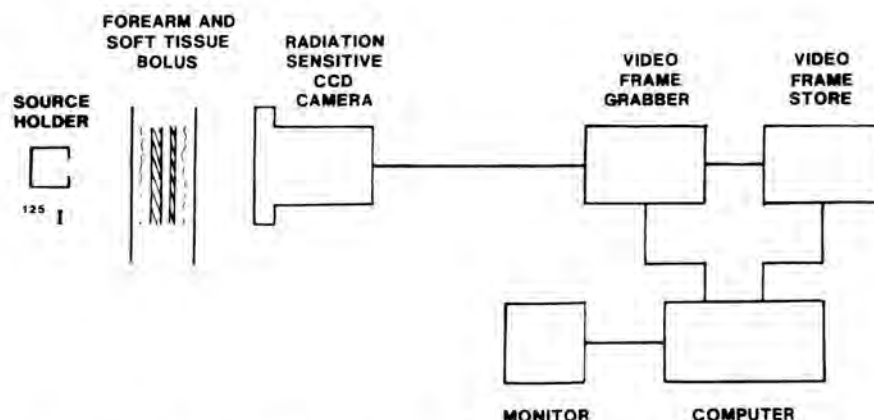
Figure 1. Schematic diagram of an idealized system for measuring BMC in the neonatal forearm.

correct for geometric distortion and differences in intensity caused by the cone beam geometry in the system.

3. Theory

With reference to the transmission image, the bone mass per unit area (M_B) can be calculated pixel by pixel by the application of the following equation:

$$M_B = [\rho_B/(\mu_B\rho_B - \mu_S\rho_S)] \ln(I_0/I) \qquad M_B = k_B \ln(I_0/I) \qquad (1)$$

where $k_B = \rho_B/(\mu_B\rho_B - \mu_S\rho_S)$. μ_B and μ_S are the mass absorption coefficients for bone mineral ($2.40 \text{ cm}^2 \text{ g}^{-1}$) and water or soft tissue ($0.35 \text{ cm}^2 \text{ g}^{-1}$) respectively. ρ_B and ρ_S are the values of density for bone mineral (1.85 g cm^{-3}) and water or soft tissue (1.00 g cm^{-3}). I is the intensity through 'bone' and I_0 is the background intensity. In the neonatal forearm phantom, bone has been replaced by aluminium having a density of 2.6989 g cm^{-3} and a mass absorption coefficient of $4.00 \text{ cm}^2 \text{ g}^{-1}$, thus we can calculate M_A the mass of aluminium per unit area.

We wished to study the relationship between the precision of the technique and the exposure time so that the minimum investigation time is achieved. This is particularly important in the measurement of preterm neonates. The variance of the mass per unit area is given by

$$\sigma^2(M_B) = \left(\frac{\partial M_B}{\partial I}\right)^2 \sigma^2(I) + \left(\frac{\partial M_B}{\partial I_0}\right)^2 \sigma^2(I_0) = \left(\frac{\partial M_B}{\partial I}\right)^2 I + \left(\frac{\partial M_B}{\partial I_0}\right)^2 I_0$$

$$= \left(\frac{k_B}{I}\right)^2 I + \left(\frac{-k_B}{I_0}\right)^2 I_0 = k_B^2 \frac{(I+I_0)}{II_0}$$

and so

$$\sigma(M_B) = k_B \left(\frac{I+I_0}{II_0}\right)^{1/2}. \qquad (2)$$

4. Results

The transmission image in figure 2 results from the capture of 32 frames of the neonatal phantom with the experimental system described above. Cursor regions A and C are 60×200 pixels (4.8×16 mm), cursor B is 80×200 pixels (6.4×16 mm) just covering the width of the larger aluminium tube in the phantom. These represent reasonable useful sizes for cursors *in vivo*. The equivalent mass of aluminium was calculated taking the mean of regions A and C for the background intensity I_0. Substituting into equation (1) produces a value of 0.0909 g cm^{-2} for M_A. This compares well with the known value of M_A of $0.0864 \pm 0.0093 \text{ g cm}^{-2}$; a difference of 5.3%.

The variation of the intensity across the phantom bone was studied using a region 250 pixels long but only 2 pixels wide. The plot of intensity across the aluminium phantom is shown in figure 3. This may be a more appropriate method of analysis *in vivo* as interpolation using the through tissue counts may give a more accurate estimation of the background count intensity.
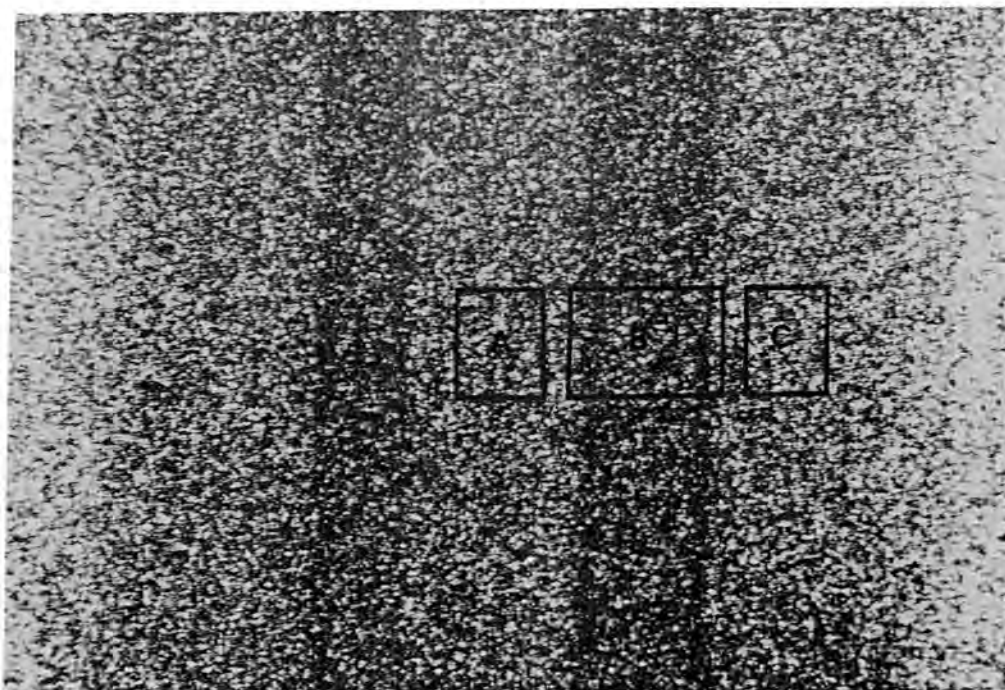
Figure 2. Image of the sum of 32 frames of raw data obtained from measurement of the neonatal forearm phantom.
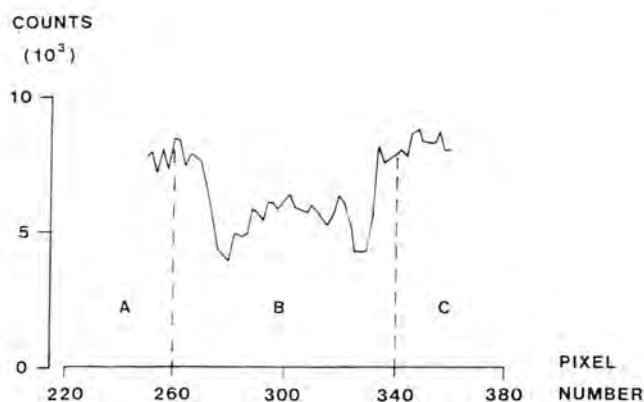
Figure 3. Linescan data for measurements of counts made across the neonatal forearm phantom plotted against distance expressed as pixel number between regions A and C.

Substitution into equation (2) gives a value for $\sigma(M_A)$ of 0.0009 g cm^{-2}. This is equivalent to a coefficient of variation (cv) of 0.99%. The computed skin entrance dose for the experimental system with a 1.13 GBq source and an integration period of 1 second is 0.046 μGy, computed from measurements made on a 3.5 GBq source in a similar configuration, several orders of magnitude less than the other techniques mentioned in the introduction. The variation of the theoretical precision versus time and dose for a 3.7 GBq activity source is shown in figure 4. This shows that at 3.7 GBq
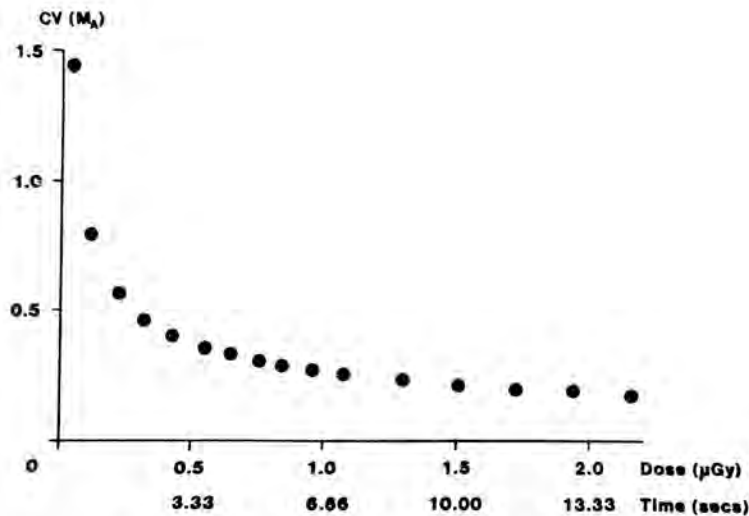
Figure 4. Graph of the percentage error in the measurement of M_A as a function of dose (μGy) and time (seconds).

it could be possible to reduce the integration period to as little as 3 seconds and still have a theoretical measurement error of less than 0.5%.

5. Discussion

While the physical size of the neonatal forearm means that an increase in cursor size is unlikely to be achieved, reduction in the measurement error could be brought about in a number of ways. The source we used in this evaluation was depleted and use of a fresh source of 7.4 GBq would increase the photon flux by at least a factor of 6. The position of the source in the experimental system is by no means optimal as the distance away from the object tends to make the system too cumbersome for use in an incubator. Moving the source closer to the object would also have the added advantage of increasing the flux and reducing the exposure time required. The use of a CCD camera working at video rate into an 8 bit frame grabber and frame store produces a grey level limit of 256 levels per pixel effectively limiting exposure time to 1.28 s with the photon flux available to us before overflow started to occur. The exposure time will be reduced with a higher flux source but will still only give a grey level resolution of 256 levels. An increase in grey level resolution could only be achieved by the use of a higher resolution frame grabber of 12 or 16 bits. Further, the system that we used in the feasibility experiment is by no means ideal as the addition of each captured frame into the frame store took about 30 seconds. This limit could be overcome in two ways. Firstly, by staying with the same technology and using higher resolution frame grabbers and stores with virtually instantaneous summation facility, which although increasing the cost considerably would allow the retention of real time viewing of the measurement site. The second possibility is to switch from real time video mode to still camera mode where the x-ray sensitive CCD is operated in integrating mode, exposed for a fixed period and then the charge is read off and converted to a digital signal directly representing photon events per pixel. This system loses the ability to view the measurement site at the time of measurement and suffers the further disadvan-
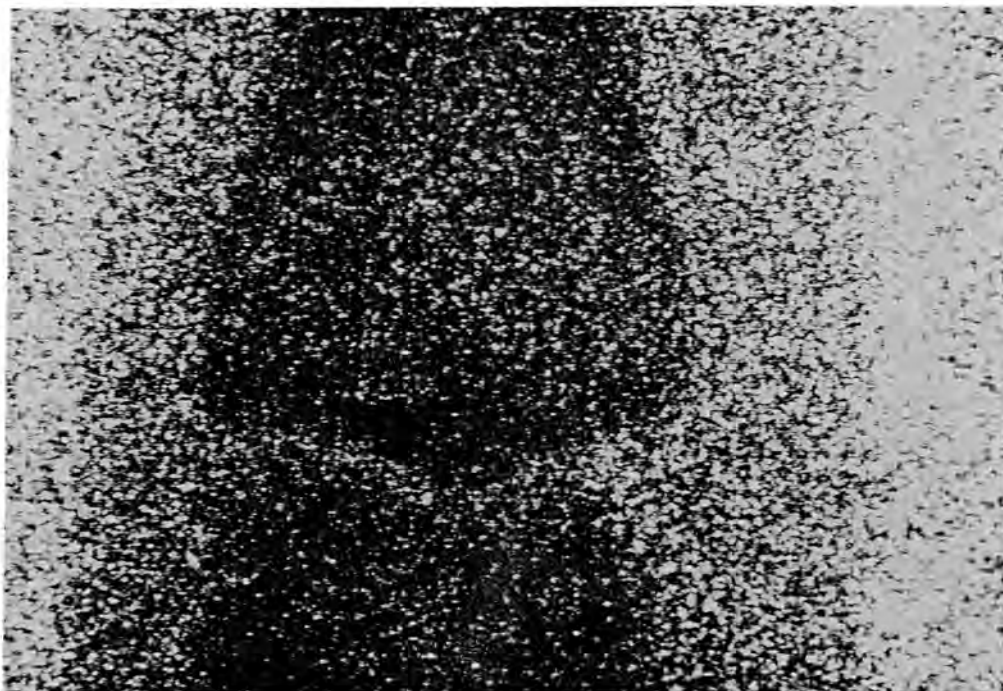
Figure 5. Image of the sum of 32 frames of raw data obtained from measurement of the distal and middle inter phalangeal joint of the middle finger in an adult.

tage of requiring to be cooled to liquid nitrogen temperatures to suppress electronic noise in the device. Both these techniques would allow us to increase exposure time to 10 s which we feel is the limit imposed by subject movement.

It may be possible to avoid using a bolus for the baby's arm altogether if we can adequately fit a line representing the background intensity. If this cannot be done satisfactorily then the tissue equivalent bolus need not be parallel sided. It may be possible to produce a short source to detector distance and a non-linear bolus geometry which could compensate for any variation in path length.

Although the technique was originally envisaged for the measurement of neonatal BMC there is no reason why it should not be extended to the adult appendicular skeleton. Figure 5 shows an image of the distal and middle inter-phalangeal joint of the middle finger of an adult captured using the evaluation system. The manufacturers have indicated that they could reduce the size of the video camera to 164 mm, with the drive electronics housed up to 1 metre away, making it feasible to place such a system in an incubator. In either neonates or adults this technique could provide a quick and accurate method of measuring BMC in the appendicular skeleton which may be adapted to suit many measurement environments and different measurement sites.

Acknowledgments

References

Arndt U W and In'T Veld G A 1988 Further developments of an X-ray television detector *Advances in Electronics and Electron Physics* ed B L Morgan (London: Academic)

Cameron J R and Sorenson J 1963 Measurement of bone mineral *in vivo*: An improved method *Science* **142** 230–2

Congdon P J, Horsman A, Ryan S W, Truscott J G and Durward H 1990 Bone mineral repletion in preterm infants after 40 weeks postconception *Archives of Diseases in Childhood* **65** 1038–42

Greer F, Lane J, Weiner S and Mazess R B 1982 An improved technique for accurate determination of bone mineral content (BMC) and identifying disorders of bone mineral metabolism in low birthweight infants *Pediatric Res.* **16** 163A (Abstract)

James J R, Congdon P J, Truscott J, Horsman A and Arthur R 1986a Osteopenia of prematurity *Archives of Diseases in Childhood* **61** 871–6

James J R, Truscott J, Congdon P J and Horsman A 1986b, Measurement of bone mineral content in the human fetus by photon absorptiometry *Early Human Development* **13** 169–81

Ryan S, Congdon P J, James J, Truscott J G and Horsman A 1988 Mineral accretion in the human fetus *Archives of Diseases in Childhood* **63** 799–808

Steichen J J, Edwards N and Tsang R C 1980 Adaptation of direct photon absorptiometry for measurement of bone mineral content in small infants *Proc. Fourth Int. Conf. on Bone Mineral Measurement (Toronto, 1978)* ed R B Mazess (Washington, DC: US Dept of Health and Human Services) (NIH No. 80-1938) pp 87–91

PRIMARY GENERALIZED OSTEOARTHRITIS AND BONE MASS

L. D. HORDON*, S. P. STEWART†, P. R. TROUGHTON*, V. WRIGHT*, A. HORSMAN‡
and M. A. SMITH†

*Rheumatology and Rehabilitation Research Unit and †Centre for Bone and Body Composition Research,
Department of Clinical Medicine, University of Leeds, ‡Department of Applied Biology, University of Hull*

SUMMARY

The association of OA with increased bone mass is controversial. This study measured BMD at the hip and spine and total body bone mineral (TBBM) by dual energy X-ray absorptiometry, and BMD at the distal forearm by single photon absorptiometry in 20 post-menopausal women with primary generalized OA. The data were compared with those from 89 normal controls. Osteoarthritic women had significantly increased BMD at the spine ($P<0.001$), distal forearm ($P<0.05$) and increased TBBM ($P<0.01$), but no difference was seen at the femoral neck. These differences were not explained by obesity. The influence of mobility is discussed.

KEY WORDS: Dual energy X-ray absorptiometry, Single photon absorptiometry, Spine, Distal forearm, Femoral neck.

ALTHOUGH the negative association between OA of the hip and femoral neck fracture is well recognized [1–4], it is not clear whether patients with OA have greater bone mass than normal people. A number of studies have been performed comparing bone mass in patients with OA of the hip with controls, but results are conflicting, perhaps due to the selection of subjects, the different techniques and sites used for bone measurement, and the heterogeneous nature of OA of the hip [3–6].

Fewer studies have been performed in patients with primary generalized osteoarthritis (PGOA) but results are also conflicting. Studies using metacarpal morphometry) and neutron activation analysis to measure total body calcium [7], quantitative computed tomography of the forearm [8] and single photon absorptiometry of the forearm [9] have shown no difference between osteoarthritic subjects and controls. However a relationship between trabecular bone volume in iliac crest biopsies and radiological grade of OA at the hand was found in one post-mortem study [10].

The aim of our study was to assess BMD at potential osteoporotic fracture sites (lumbar spine, distal forearm and hip) and total body bone mineral (TBBM) in women with PGOA and compare this with data from normal women.

PATIENTS AND METHODS

Twenty postmenopausal women aged 52–79 yr (median 68 yr), attending a rheumatology clinic for treatment of PGOA were recruited. All women had clinical and/or radiological OA affecting three or more groups of joints as described by Kellgren and Moore [11]. Details of joint involvement are given in Table I. Women with hysterectomy were excluded as age of menopause was unknown although one woman with simultaneous hysterectomy and bilateral oopho-

rectomy was included. Women with a history of disease or drug therapy potentially affecting bone mass were also excluded e.g. diabetes, thyroid disease, oral steroid therapy, anticonvulsant treatment. Although women with fractures were not specifically excluded, none were known to have vertebral or hip fractures and only one had a previous Colles' fracture. A second patient sustained a Colles' fracture after the study was completed. Six patients used one or more sticks for walking and two of these six also used wheelchairs for outings. Data from 89 normal postmenopausal women aged 50–79 yr (median 62 yr) recruited locally from hospital and university staff and randomly from a list of postmenopausal women attending an inner city general practice were used as controls [12]. Women with hysterectomy, thyroid disease and other endocrine disorders, liver, kidney or chronic gastrointestinal disease, known osteoporotic fracture, impaired mobility or who had received steroid, hormone replacement therapy or other treatment potentially affecting bone, were excluded from the control population. All study and control subjects were of caucasian origin.

BMD (bone mineral content/bone width, arbitrary units) was measured at the distal forearm by single photon absorptiometry. Bone mineral content (BMC, g) and BMD (g/cm^2) were measured at the lumbar spine ($L_2L_3L_4$) and femoral neck by dual energy X-ray absorptiometry using a Lunar DPX Bone Densitometer

TABLE I
JOINT INVOLVEMENT IN OSTEOARTHRITIC PATIENTS

Joints	No. of patients
Distal interphalangeal	20
Proximal interphalangeal	13
First carpo-metacarpal	12
First metatarso-phalangeal	15
Knee	18
Cervical spine	6
Lumbar spine	9
Hip	3
Shoulder	2
Ankle	1

TABLE IV
RELATIONSHIPS BETWEEN AGE, HAQ SCORE AND BONE MINERAL MEASUREMENTS IN OSTEOARTHRITIC WOMEN GIVEN AS THE
COEFFICIENT OF CORRELATION

	Age	Spine BMD	Femoral BMD	Forearm BMC/BW	TBBM
Spine BMD	−0.33 N.S.				
Femoral BMD	−0.5 *	0.71 **			
Forearm BMC/BW	−0.75 **	0.52 *	0.66 **		
TBBM	−0.68 **	0.60 **	0.72 **	0.61 **	
HAQ score	0.58 **	−0.40 *	−0.60 **	−0.70 ***	−0.58 **

BMC, Bone mineral content; BW, bonewidth; TBBM, total body bone mineral content; HAQ, Stanford Health Assessment Questionnaire.
* $P <0.05$; ** $P <0.01$; *** $P <0.001$.

showing this was not simply a local effect due to artefact. Mean lumbar BMD was 7.3 g higher in osteoarthritic patients than controls, whilst mean TBBM was 132 g higher in osteoarthritic patients than controls (Table III). The possible contribution of degenerative disease in the lumbar spine to the difference in TBBM is therefore small. In addition there was a strong correlation between lumbar BMD and distal forearm, femoral neck and TBBM measurements.

We conclude that women with PGOA have greater bone mass than controls at the distal forearm and spine and greater TBBM, although bone mass at the femoral neck is not increased. These differences are not due to obesity. It is possible that impaired mobility in the osteoarthritic women could explain the lack of difference in bone mass at the femoral neck. The cause of the increase in bone mass in women with PGOA is unknown, but the results of this study would support the hypothesis that oestrogen excess may be involved in the pathogenesis of OA [20].

REFERENCES
1. Byers PD, Contepomi CA, Farkas TA. Postmortem study of the hip joint. *Ann Rheum Dis* 1970;**29**:15–31.
2. Weintroub S, Papo J, Ashkenazi M, Tardiman R, Weissman SL, Salama R. Osteoarthritis of the hip and fractures of the proximal end of the femur. *Acta Orthop Scand* 1982;**53**:261–4.
3. Solomon L, Schnitzler CM, Browett JP. Osteoarthritis of the hip: the patient behind the disease. *Ann Rheum Dis* 1982;**41**:118–25.
4. Foss MVL, Byers PD. Bone density, osteoarthrosis of the hip and fracture of the upper end of the femur. *Ann Rheum Dis* 1972;**31**:259–64.
5. Roh YS, Dequeker J, Mulier JC. Cortical bone remodelling and bone mass in primary osteoarthritis of the hip. *Invest Radiol* 1973;**8**:251–4.
6. Alhava EM, Kettunen K, Karjalaimen P. Bone mineral in patients with osteoarthrosis of the hip. *Acta Orthop Scand* 1975;**46**:709–15.

7. Reid DM, Kennedy NSJ, Smith MA, Tothill P, Nuki G. Bone mass in nodal primary generalised osteoarthritis. *Ann Rheum Dis* 1984;**43**:240–2.
8. Price T, Hesp R, Mitchell R. Bone density in generalised osteoarthritis. *J Rheumatol* 1987;**14**:560–2.
9. Cooper C, Poll V, McLaren M, Daunt S O'N, Cawley MD. Alterations in appendicular skeletal mass in patients with rheumatoid, psoriatic and osteoarthropathy. *Ann Rheum Dis* 1988;**47**:481–4.
10. Gevers G, Dequeker J, Gensens P, Nyssen-Behets C, Dhem A. Physical and histomorphological characteristics of iliac crest bone differ according to the grade of osteoarthritis at the hand. *Bone* 1989;**10**:173–7.
11. Kellgren JH, Moore E. Generalised osteoarthritis and Heberden's nodes. *BMJ* 1952;**ii**:181–7.
12. Truscott JG, Oldroyd B, Simpson M *et al*. Variation in lumbar spine and femoral neck bone mineral measured by dual energy X-ray absorptiometry: a study of 329 normal women. *Br J Radiol* in press.
13. Fries JF, Spitz P, Kraines RG, Holman HR. Measurement of patient outcome in arthritis. *Arthritis Rheum* 1980;**23**:137–45.
14. Pocock N, Eisman J, Guinn T, Sambrook P, Kelly P, Freund J, Yeates M. Muscle strength, physical fitness and weight but not age predict femoral neck bone mass. *J Bone Miner Res* 1989;**4**:441–8.
15. Knight SM, Ring EFJ, Bhalla AK. Bone mineral density and osteoarthritis. *Ann Rheum Dis* 1992;**51**:1025–6.
16. Wahner HW. Measurement of bone mass and bone density. *Endocrinol Metab Clin North Am* 1989;**18**:995–1012.
17. Reid IR, Evans MC, Ames R, Wattie DJ. The influence of osteophytes and aortic calcification on spinal mineral density in post-menopausal women. *J Clin Endocrinol Metab* 1991;**72**:1372–4.
18. Resnick D, Niwayama G. Degenerative disease of the spine. In: Resnick D, Niwayama G, eds. *Diagnosis of bone and joint disorders*, 2nd edn. Philadelphia: WB Saunders, 1988;1480–561.
19. Orwoll ES, Oviatt SK, Mann T. The impact of osteophytic and vascular calcifications on vertebral mineral density measurements in man. *J Clin Endocrinol Metab* 1990;**70**:1202–7.
20. Spector TD, Campion GD. Generalised osteoarthritis: a hormonally mediated disease. *Ann Rheum Dis* 1989;**48**:523–7.

TABLE II

AGE AT MENOPAUSE AND BMI IN OSTEOARTHRITIC WOMEN AND CONTROLS

	Osteoarthritic	Controls
Age at menopause (yr)	48.4 ± 6.1	49.2 ± 4.0
BMI (kg/m²)	26.8 ± 4.1	24.9 ± 3.9

Results are expressed as means ± S.D.

(Lunar Radiation Corporation, Madison, WI, USA). TBBM (g) was also measured by this technique. Osteoarthritic patients completed a Stanford Health Assessment Questionnaire (HAQ) [13] in order to assess their functional ability.

Statistical analysis

Within group data were correlated using Spearman rank correlation (rho). Data on age of menopause and BMI from osteoarthritic women and controls were compared by separate variance t-tests. Differences in spine, femoral neck, distal forearm and TBBM measurements between the two groups were compared using an unbalanced analysis of covariance with age as covariant and significant difference of the F statistic for the elevation was tested after the regression lines were shown to have similar slopes.

All data were analysed on Unistat IV statistical software.

RESULTS

There was no significant difference in age at menopause or BMI between osteoarthritic women and controls (Table II). Women with OA scored a mean of 0.81 ± 0.64 (S.D.) on the HAQ.

BMC and BMD were significantly higher at the spine ($P < 0.001$) and BMD at the distal forearm was also increased ($P < 0.05$) in osteoarthritic women compared with controls. TBBM was higher in the osteoarthritic group ($P < 0.01$). BMC and BMD at the femoral neck were not significantly increased in osteoarthritic women (Table III).

Relationships between bone mineral measurements, age and HAQ score are shown in Table IV. There was a significant negative correlation between HAQ score and spinal, femoral neck, forearm and TBBM measurements. There was a significant positive correlation of HAQ score with age.

DISCUSSION

Women with PGOA have more bone at the distal forearm and spine and greater TBBM than controls, although no significant increase in bone mass was seen at the femoral neck in osteoarthritic women. These differences were not due to obesity as BMI was similar in control and study groups.

Some of the osteoarthritic women had impaired mobility and it is possible this may have influenced bone mass at the femoral neck, reducing differences from controls. Certainly the HAQ score correlated negatively with bone mineral measurements, but as age was also related to HAQ score this should not be over interpreted. It is of interest that muscle strength has been shown to predict bone mass in the femur and forearm, but not the spine in healthy postmenopausal women [14]. A regional increase in BMD adjacent to an osteoarthritic joint has been proposed as a mechanism for increased bone mass in OA [15]. If this theory is correct, the low prevalence of OA of the hip in our study population (Table I) could provide an alternative explanation for the lack of difference at the femoral neck from controls. However, this theory would not explain the increased BMD at the distal forearm in osteoarthritic women.

Neither osteoarthritic women nor controls had a routine lateral lumbar spine X-ray. The presence of osteophytes and degenerative disease at the facet joints can produce artefacts affecting lumbar BMD measurements [16], although the extent to which these measurements are affected is controversial [15]. Spinal osteophytes are present in the majority of 'normal' postmenopausal women [17, 18], but account for only 4% of the variance in lumbar BMD [17]. However, only half this effect is artefactual and lumbar osteophyte score is related to femoral BMD [17]. Exclusion of subjects from a study population because of degenerative changes may thus potentially bias the study group. In men, osteophytes make a greater contribution to lumbar BMD [19], perhaps because of lower age-related bone loss, or sex differences in osteophyte formation [18].

Although we cannot exclude an influence of degenerative disease on lumbar BMD, not only was bone mass increased at the spine, but also at the distal forearm, and TBBM was also elevated in the osteoarthritic group

TABLE III

COMPARISON BETWEEN BONE MINERAL MEASUREMENTS AT THE SPINE, FEMORAL NECK, DISTAL FOREARM AND TOTAL BODY BONE MINERAL IN OSTEOARTHRITIC PATIENTS AND CONTROLS

		OA, $n = 20$	Control, $n = 89$	F-statistic
Spine	BMC (g)	48.8 ± 9.8	41.5 ± 9.3	12.24***
	BMD (g/cm²)	1.12 ± 0.18	1.00 ± 0.17	11.39***
Femoral neck	BMC (g)	4.34 ± 0.68	4.13 ± 0.78	2.79 N.S.
	BMD (g/cm²)	0.87 ± 0.12	0.85 ± 0.13	2.80 N.S.
Distal forearm	BMC/BW (arbitrary units)	0.94 ± 0.18 ($n = 18$)	0.90 ± 0.16 ($n = 89$)	5.52*
Total body bone mineral	(g)	2377 ± 350 ($n = 20$)	2245 ± 305 ($n = 39$)	7.11**

BMC, Bone mineral content; BW, bonewidth.
Results expressed as means ± S.D.
* $P < 0.05$; ** $P < 0.01$; *** $P < 0.001$.

Variation in lumbar spine and femoral neck bone mineral measured by dual energy X-ray absorption: a study of 329 normal women

[1]J G TRUSCOTT, [1]B OLDROYD, [1]M SIMPSON, [1]S P STEWART, [1]C F WESTMACOTT, [1]R MILNER, [2]A HORSMAN and [1]M A SMITH

[1]Centre for Bone and Body Composition Research, Insititute of Physical Sciences, Department of Clinical Medicine, University of Leeds, Wellcome Wing, The General Infirmary, Leeds LS1 3EX and [2]Department of Applied Biology, University of Hull, Hull, UK

Abstract

Reference ranges used in dual energy X-ray absorptiometry (DXA) have previously used piecewise linear fits to the whole data set for spine or femur bone mineral density (BMD) as a function of age. In a study of 329 Caucasian normal women we present a refinement to the normal range by fitting straight lines between quinquennial mean values of BMD for each site measured (lumbar spine, femoral neck and Ward's triangle). From the age of 40 years onwards the premenopausal women demonstrated minimal loss of BMD whereas postmenopausal women showed a rapid loss amounting to 27% in the lumbar spine, 27% in the femoral neck and 38% in the Ward's triangle region in the age range under examination. Comparison of quinquennial means for pre and postmenopausal women in age bands 45–49 years and 50–54 years shows that at these ages postmenopausal BMD is significantly lower than premenopausal BMD ($P < 0.05$). This finding suggests that separate normal ranges should be used for pre and postmenopausal women. As reduction in the production of oestrogen is a major factor in postmenopausal bone loss and oestrogen function is related to years since menopause (YSM), a more logical way of displaying postmenopausal normal BMD ranges would be in terms of YSM rather than chronological age. Such data are given in this paper.

The measurement of bone mineral has long been recognized as important for the study of osteoporosis. Originally instruments were developed to measure bone mineral in the forearm (Cameron & Sorenson, 1963) but in the early 1980s techniques were developed to measure the sites of most clinical interest directly, *i.e.* the spine and femoral neck. The techniques for measuring the spine and femoral neck use the same basic principle; the differential attenuation that occurs between bone and soft tissue when gamma or X-ray photons of two different energies pass through the body. A measurement of the relative attenuation, coupled with the mass attenuation coefficient gives a measurement of the bone mineral. The region is studied by moving the source and detector in a rectilinear motion across the patient and producing an image in which each pixel is representative of the mineral content. The integration of the data over the appropriate region of interest (ROI) gives the bone mineral content (BMC) in grams.

Though the BMC for a given anatomical ROI may be an important parameter in its own right it is clear that its value will be dependent upon the size of the individual; large subjects will tend to have a higher BMC than small subjects. To compensate for this the BMC is divided by the area of the bone obtained from the image to produce bone mineral density (BMD) in units of g cm^{-2}. It should be noted that the BMD is not the measurement of volume density but is the area normalized BMC. BMD appears to have become the measurement of choice but care must be taken with its use.

Early instruments used two gamma ray energies obtained from isotope sources, initially a combination of ^{241}Am and ^{137}Cs and subsequently ^{153}Gd which became the basis of a number of commercial systems. The isotope techniques for measuring BMD were referred to as dual photon absorptiometry (DPA) (Reed, 1966). This gave a reasonable precision at about 8% (Tothill et al, 1983) but often the quality of the images was poor and in many patients it was difficult to identify the areas to measure. A significant improvement in signal-to-noise ratio in the image was obtained with the use of X-ray tubes as the photon source (Sartoris et al, 1985). The more recent development is referred to as quantitative digital radiography (QDR) or DXA (Mazess et al, 1988). The two abbreviations refer to the same basic principle and we shall adopt the latter irrespective of the commercial system used. The improved photon output of DXA over DPA results in benefits in terms of improved resolution, improved precision or shorter scan times.

The initial spine BMD results showed a significant variation in age relationship with different systems (Smith et al, 1983). At the time it was thought that there could be some national differences in BMD although technical explanations were also felt to be a possibility. It must be remembered that the BMD is the ratio of the BMC to the area of the bone. It is quite conceivable that different techniques can calculate the BMC reliably but that different algorithms used for edge detection, to calculate the area of the bone, are likely to differ significantly from system to system. As a consequence it may be the denominator in the ratio, *i.e.* the area, that is the principal cause of variation between different systems.

The variation in BMD of the spine and femoral neck using either DPA or DXA in Caucasian females in several countries is illustrated in Figures 1a and 1b. The data was extracted from the references listed in Table I which also gives the age range of each of the studies and the number of subjects involved. There are discrepancies between the data from each country, which may reflect differences in either the control population or the technique used. However, much depends upon the size of the data set and consequently the statistical model that can justifiably be used. This study was initiated to enable us to obtain a comprehensive normal range of BMD values for Caucasian females in the United Kingdom (UK). It was also recognized that an individual may suffer a crush fracture which is caused by a vertebral body having a lower BMC and may result in a lower than normal vertebral area. In such a situation the BMD, which is the ratio of the two, can appear in the normal range. As a consequence the normal data were analysed to obtain the vertebral area in the normal population which could be used to give an indication as to whether BMD or BMC values should be used in the assessment of that individual.

Methods

Reference subjects

The reference sample for the spine BMD measurements consisted of 329 women aged between 20 and 81 years, of whom 174 were premenopausal and 155 were postmenopausal. The mean age at menopause was 49.1 (4.5) years, the figure in brackets is the standard deviation. For the femur measurements the sample consisted of 327 women from the above set aged between 21 and 81 years of whom 173 were premenopausal and 154 were postmenopausal with a mean age at menopause of 49.1 (4.4) years. The women were recruited mainly from hospital and university staff by advertising locally and from the list of a local general practitioner (GP). The GP contacted every third woman on his list of Caucasian females in the age range 55–80 years and invited those with no known disorders to participate in the study of whom approximately 30% attended. On the basis of responses to a questionnaire women with endocrine disorders, adrenal disorders, malignancy, chronic gastrointestinal or liver disease, Paget's disease, diabetes, rheumatoid arthritis or renal stones were excluded. Women on steroid therapy, hormone replacement therapy, anticonvulsant drugs, sodium fluoride, heparin, thyroxin or with a history of hip, spine or wrist fracture or extended immobilization were all excluded. The exclusion also extended to women who had undergone hysterectomy or oophorectomy and subjects with histories of drug or alcohol abuse. Spine X-rays were not taken in this study for ethical reasons so that some women who may possibly have asymptomatic vertebral wedge or crush fractures were not identified and thus not excluded. It is recognized that the reference data presented in this study is not a statistically representative sample of the local population. In particular there is no representation of non-Caucasian races and there will

Table I. Major studies using DPA or DXA listed chronologically including first author, number of subjects, measurement site and age range

| First author	Year	Number	Site	Age range (years)
Riggs	1981	105	Spine	20–89
Krolner	1982	70	Spine	19–88
Tothill	1983	24	Spine	21–61
Guesens	1986	156	Spine	20–85
Hansson	1986	214	Spine	35–80
Mazess	1987	892	Spine/Femur	20–79
Nilas	1987	178	Spine	29–78
Elders	1988	286	Spine	46–55
Pocock	1988	179	Spine/Femur	20–83
Ribot	1988	510	Spine	25–70
Schaadt	1988	113	Spine/Femur	20–89
Stevenson	1989	284	Spine/Femur	21–68
Aloia	1990	376/257	Spine/Femur	20–80
Elliott	1990	462	Spine/Femur	20–84
*Hall	1990	165	Spine	4–80
Rodin	1990	225	Spine/Femur	18–52

All DPA scans except *which is DEXA.
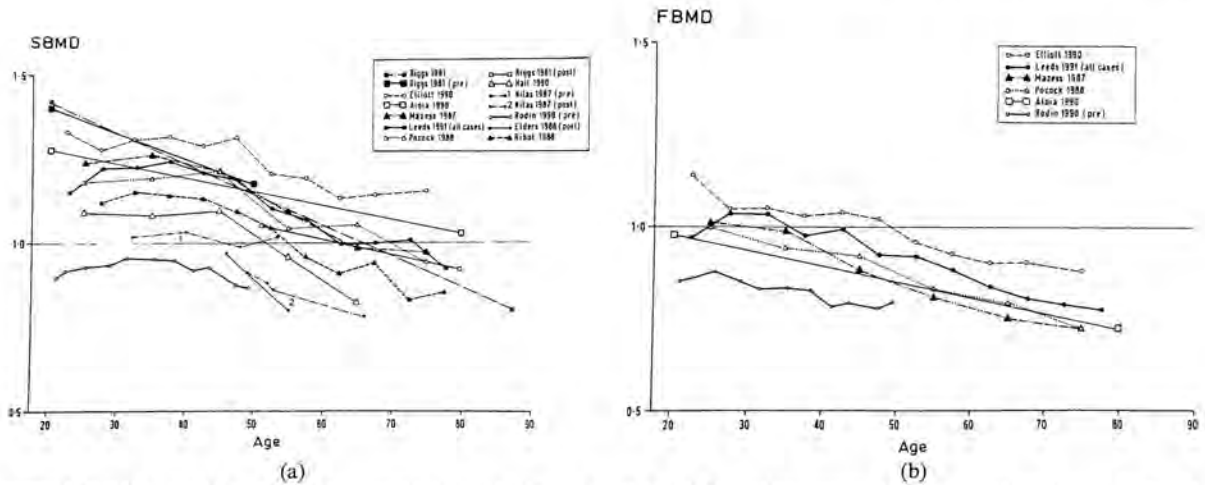
Figure 1. BMD (g cm⁻²) in the lumbar spine (a) and the femoral neck (b) of Caucasian women plotted against age (years) gathered by different measurement centres throughout the world. (●——● Leeds 1991 refers to this paper.)

be a higher proportion of social classes I, II and III than will be present in the local population.

Scanning techniques and scan analysis

Scanning was carried out using a Lunar DPX machine on sites in the femoral neck and lumbar spine (Mazess et al, 1989). Analysis of the scans was carried out using the manufacturer's software version 3.2. The effective dose equivalent for each examination is 1 μSv and was measured by the local radiation protection service.

Precision

Precision is defined as the ability of a method to obtain the same value with repeated measurements. *In vivo* precision represents variations in patient positioning and instrumentation errors, while *in vitro* precision is determined by instrumentation error alone. 15 subjects (seven male, eight female; mean age 43 years) had lumbar spine and femur scans on two occasions with an interval of 28–90 days (mean 55 days) between scans. The coefficient of variation (CV) for the lumbar spine, femoral neck and Ward's triangle was 1.18%, 1.69% and 3.13%, respectively. The manufacturer's aluminium spine and femur phantoms were scanned five times per day for 7 days in a low attenuation plastic tank filled with a nominal fat solution (25% isopropyl alcohol, 75% water) to a depth of 15 cm to measure the *in vitro* precision. The CV for spine, femoral neck and Ward's triangle regions of the phantoms was 0.45%, 1.00% and 0.84%, respectively.

Data analysis

A number of different analyses were undertaken to obtain normal data that could be used for comparison with patients who may have a degree of crushing of one or more of the vertebrae. If this is not known then the total BMD of L2–L4 may give an erroneous result. The total area of L2 + L3 + L4 was noted. In this paper we present the normal results as means and standard deviations. For comparison with the normal ranges of the commercial company (Lunar Corporation) straight lines were fitted to the normal data. The assumption has been made by the company that there is constant BMD early in life and then two different linear rates of loss later in life. Least squares techniques are used to identify the slopes of these losses and the break points, *i.e.* the age at which the rate of loss changes.

Results

The results for the normal vertebral BMD and associated areas are given in Table II, grouped into 5 year age bands for all women and separately for pre and postmenopausal women. The data for BMD of the femoral neck and Ward's triangle regions are given in Table III, grouped in the same way. The BMD data for spine, femoral neck and Ward's triangle are given, grouped into 5 year bands of years since menopause (YSM), in Table IV. The results of the variation of BMD with age are shown graphically in Figure 2a for the spine, Figure 3a for the femoral neck and Figure 4a for Ward's triangle. In each case the figure contains the raw data, the quinquennial mean values and straight lines joining those mean values. The results of the variation of BMD with YSM are shown in Figure 2b for the spine, Figure 3b for the femoral neck and Figure 4b for Ward's triangle. In each case the figure contains the raw data, the mean value of BMD for the 5 year band and straight lines joining the mean values.

Further investigation of the effect of the menopause was carried out by comparing the mean BMD values in the three quinquennia, 40–44.9 years, 45–49.9 years and 50–54.9 years, in the lumbar spine, femoral neck and Ward's triangle. Pooled Student's *t*-tests show that in the 40–44.9 year band there is no significant difference
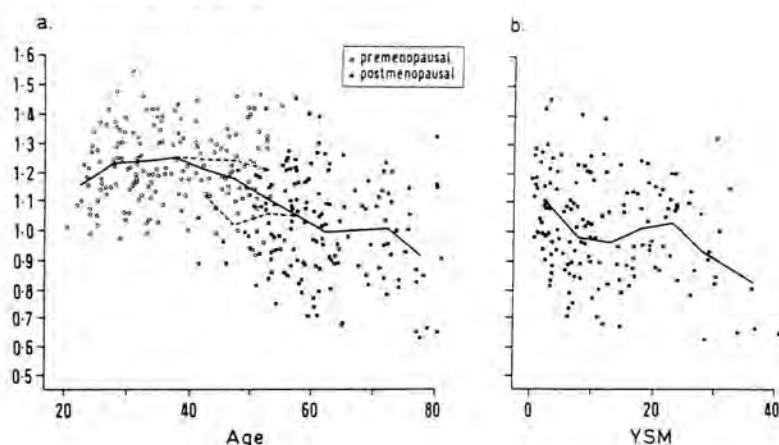
Lumbar Spine BMD

Figure 2. BMD (g cm^{-2}) in the lumbar spine plotted against (a) age (years), unbroken line joining means for all women, upper broken line joining means for premenopausal women, lower broken line joining means for postmenopausal women, and (b) years since menopause (YSM) for postmenopausal women.
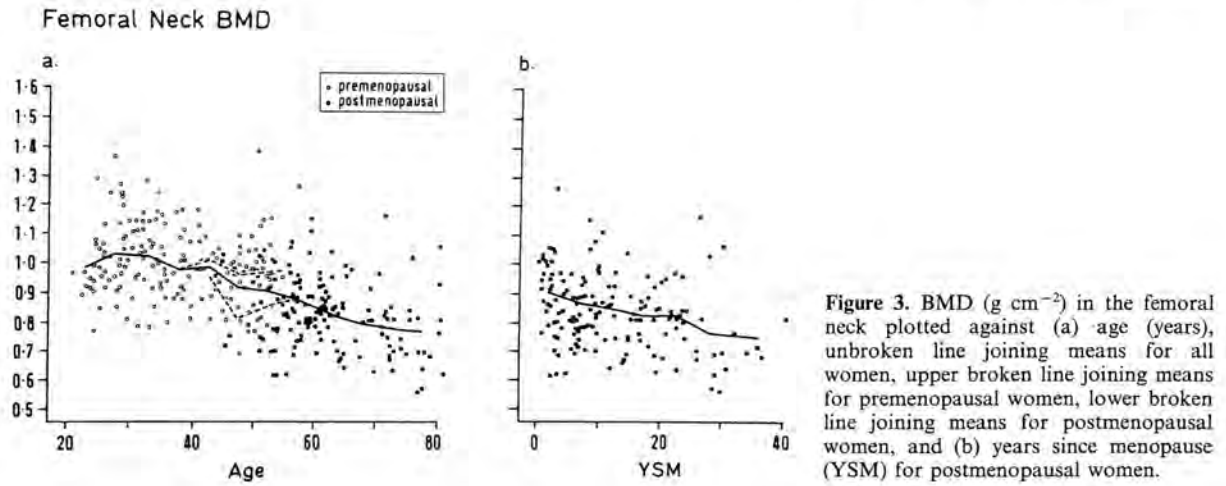
between the pre and postmenopausal groups, in the 45–49.9 year quinquennia the difference between the two groups at all three sites is highly significant ($P < 0.001$) and in the 50–54.9 year band is still significant ($P < 0.05$). The importance of separating reference data into premenopausal and postmenopausal groups is highlighted by this finding.

The results of comparing the linear fits to the data

Table II. Mean and standard deviation values for measurements made on lumbar vertebrae L2 to L4 of area, BMC and BMD listed for all women and for pre and postmenopausal women by age band including the number in each group

Ageband (years)	Number			Spine area (cm²)			Spine BMD (g cm^{-2})		
	All	Pre	Post	All	Pre	Post	All	Pre	Post
20–24	15	15		41.77 4.01	41.77 4.01		1.154 0.110	1.154 0.110	
25–29	32	32		42.41 4.50	42.41 4.50		1.231 0.123	1.231 0.123	
30–34	38	38		41.80 3.50	41.80 3.50		1.230 0.144	1.230 0.144	
35–39	24	24		41.41 2.64	41.41 2.64		1.245 0.118	1.245 0.118	
40–44	22	18	4	44.23 3.08	44.05 2.61	45.03 5.14	1.210 0.130	1.231 0.110	1.117 0.187
45–49	35	28	7	43.34 3.88	43.61 3.89	42.23 3.92	1.184 0.146	1.229 0.118	1.002 0.095
50–54	45	19	26	41.46 4.80	42.23 4.93	40.90 4.71	1.098 0.176	1.201 0.164	1.023 0.146
55–59	39		39	41.61 4.16		41.61 4.16	1.065 0.175		1.065 0.175
60–64	37		37	40.29 4.33		40.29 4.33	0.989 0.182		0.989 0.182
65–69	9		9	41.84 3.74		41.84 3.74	0.990 0.130		0.990 0.130
70–74	19		19	40.75 5.51		40.75 5.51	1.002 0.144		1.002 0.144
75–81	14		14	41.09 6.11		41.09 6.11	0.915 0.226		0.915 0.226

Femoral Neck BMD

Figure 3. BMD (g cm^{-2}) in the femoral neck plotted against (a) age (years), unbroken line joining means for all women, upper broken line joining means for premenopausal women, lower broken line joining means for postmenopausal women, and (b) years since menopause (YSM) for postmenopausal women.

with the commercial company's normal range showed negligible differences between the two data sets (Mean Z-score of differences 0.062). However, it should be noted that the results from Leeds were included in the data base of the commercial company and account for some 36% of the data used to construct their spine normal range and about 43% of the data used in the construction of their femur normal range.

Table III. Mean and standard deviation values for BMD measurements made in the femoral neck and Ward's triangle regions listed for all women and for pre and postmenopausal women by ageband including the number in each group

Ageband (years)	Number			Femoral neck BMD (g cm^2)			Ward's triangle BMD (g cm^{-2})		
	All	Pre	Post	All	Pre	Post	All	Pre	Post
20–24	15	15		0.975 0.114	0.975 0.114		0.944 0.171	0.944 0.171	
25–29	31	31		1.041 0.134	1.041 0.134		1.002 0.143	1.002 0.143	
30–34	38	38		1.037 0.119	1.037 0.119		0.978 0.150	0.978 0.150	
35–39	24	24		0.978 0.108	0.978 0.108		0.899 0.143	0.899 0.143	
40–44	22	18	4	0.988 0.091	0.995 0.094	0.956 0.073	0.895 0.099	0.896 0.104	0.892 0.083
45–49	35	28	7	0.921 0.107	0.949 0.095	0.809 0.075	0.830 0.137	0.867 0.119	0.683 0.100
50–54	45	19	26	0.914 0.152	0.981 0.151	0.864 0.134	0.800 0.164	0.873 0.158	0.747 0.150
55–59	38		38	0.880 0.134		0.880 0.134	0.741 0.154		0.741 0.154
60–64	37		37	0.833 0.097		0.833 0.097	0.693 0.122		0.693 0.122
65–69	9		9	0.799 0.110		0.799 0.110	0.608 0.123		0.608 0.123
70–74	18		18	0.784 0.124		0.784 0.124	0.642 0.140		0.642 0.140
75–81	15		15	0.768 0.153		0.768 0.153	0.621 0.183		0.621 0.183

Wards' Triangle BMD
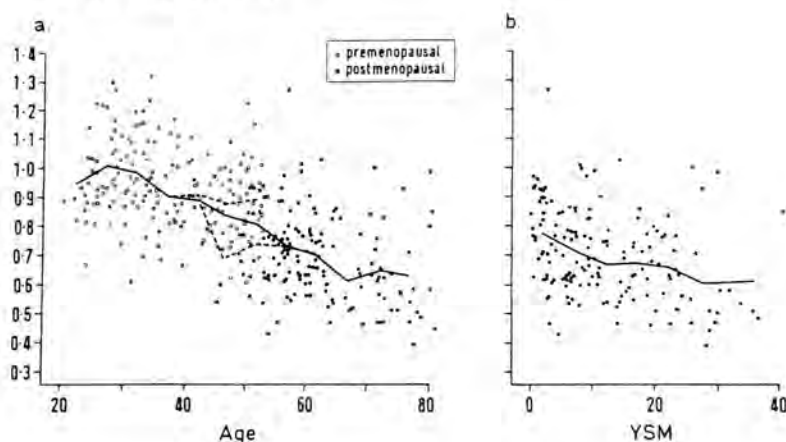
Figure 4. BMD (g cm^{-2}) in Ward's triangle plotted against (a) age (years), unbroken line joining means for all women, upper broken line joining means for premenopausal women, lower broken line joining means for postmenopausal women and (b) years since menopause (YSM) for postmenopausal women.

Discussion

Both the spine and femur data display an effect caused by the menopause with the end point BMD value of the premenopausal data being higher than the starting point data of the postmenopausal data in each case (Figures 2a, 3a, 4a). A small study by Tothill et al (1983) demonstrated an increased loss of bone from the spine after the menopause but this study was not supported by a larger study from Hansson & Roos (1986). By comparing the BMD values of premenopausal women who are over 45 years of age with the BMD values of postmenopausal women within 5 years

of menopause we can establish whether or not this difference is significant. The outcomes of these tests are given in Table V. It can be seen that in every site measured the difference between the two groups is highly significant, ranging from 7.9% to 11.3%.

In this set of data (Table II) peak BMD in the spine occurs in the 35–39.9 year band with very little loss taking place in the premenopausal women from the time at which peak BMD is attained onwards. In the UK this is earlier than the ages reported by Hall et al (1990) but consistent with the findings of Rodin et al (1990). In other countries we find agreement only with Elliott et al (1990). Krolner & Nielsen (1982), Schaadt & Bohr (1988), Guesens et al (1986) and Ribot et al (1988) all find that the peak occurs earlier. Postmenopausally the pattern is more confusing (Figure 2b) with a 10 year

Table IV. Mean and standard deviation values for BMD measurements of the lumbar vertebrae (L2–L4), femoral neck (FBMD) and Ward's triangle (WBMD) listed for postmenopausal women by YSM including the number (n) in each group

YSM (years)	n	SBMD (SD) (g cm^{-2})	n	FBMD (SD) (g cm^{-2})	WBMD (SD) (g cm^{-2})
0–4.9	42	1.091 0.155	41	0.886 0.137	0.771 0.158
5–9.9	41	0.987 0.157	40	0.845 0.110	0.716 0.125
10–14.9	18	0.965 0.218	20	0.827 0.127	0.673 0.153
15–19.9	20	1.019 0.128	19	0.815 0.081	0.665 0.099
20–24.9	17	1.042 0.117	17	0.823 0.092	0.658 0.112
25–29.9	11	0.941 0.193	9	0.759 0.208	0.602 0.220
> 30	6	0.816 0.212	8	0.756 0.134	0.623 0.184

Table V. Results of Student's *t*-tests comparing spine BMD (SBMD), femoral neck BMD (FBMD) and Ward's triangle BMD (WBMD) in two groups of women; premenopausal older than 45 years and postmenopausal within 5 years of menopause, for whom percentage differerence is given, including mean, standard deviation (SD) and number of subjects (n) for each group

		Premen Age > 45	Postmen YSM < 5	P	% Difference
SBMD (gm cm^{-2})	Mean	1.218	1.091	0.00009	10.4
	SD	0.138	0.155		
	n	47	42		
FBMD (gm cm^{-2})	Mean	0.962	0.886	0.007	7.9
	SD	0.121	0.137		
	n	47	41		
WBMD (gm cm^{-2})	Mean	0.869	0.771	0.002	11.3
	SD	0.135	0.158		
	n	47	41		

band of loss followed by a 10 year period of apparently little change, then loss taking place from this time onwards. When we look at this data set as a whole (Figure 2a) the pattern is simpler, showing a rise of BMD during the 20–40 year age range with peak density achieved in the 35–39.9 year band. This is followed by a steady loss amounting to about 27% in the following 42.5 years. This is consistent with the total bone loss of 25% reported by Hall et al (1990) in UK populations covering the same age range as our data. In other countries where Caucasian female populations covering the same age range have been studied, percentage bone losses have been closely comparable with ours with one striking exception. Riggs et al (1981) reported a loss of 47% in the BMD of lumbar vertebrae L1 to L4 but the age range in their study is from 20 to 90 years.

In the femoral neck (Table III) peak BMD is attained in the 25–29.9 year band with bone loss proceeding at a negligible rate before the menopause. Postmenopausally we observe a steady loss with years since menopause, the total loss in the period considered being some 27%. In the UK the total bone loss of 26% reported by Stevenson et al (1989) agrees with our data although they do report the loss phase starting at less than 30 years of age. Elsewhere in the world the data of Mazess et al (1987) (25%) compares closely with this data whereas Elliott et al (1990) report a lower age for both attainment of peak bone mass (20–25 years) and for onset of loss (25–30 years). Pocock et al (1987) also report loss starting earlier (mean age 25 years) than our estimate but proceeding at a comparable rate to achieve a slightly higher total loss (30%) by age 83 years.

In Ward's triangle, peak BMD is attained in the 25–29.9 year age band with loss commencing in the 30–34.9 year age band. Once again the premenopausal bone loss from this time is negligible. Postmenopausally, however, the bone loss is steady and rapid by comparison with the femoral neck, with total loss in the period amounting to some 38%. This very high rate of loss would make Ward's triangle an attractive site for measurement if the *in vivo* precision could be improved.

The data display two stages of bone loss consistent with the classification of Type I and Type II osteoporosis (Riggs & Melton, 1983). Type I is most active in the 15–20 years immediately after the menopause when the rate of loss can be as much as three times higher than normal. The loss is predominantly from trabecular bone and manifests itself in the form of vertebral and Colles' fractures. Type I osteoporosis is apparently linked to oestrogen deficiency in some, as yet unclear, way. Type II osteoporosis is apparent in women over 75 years of age and presents in the form of vertebral wedge fractures and hip fractures. The mechanism of loss is related to senescence with loss taking place in both cortical and trabecular bone.

The value of considering the vertebral geometry can only be assessed following a study of patients with a variety of established symptoms of osteoporosis; this analysis is currently being pursued. Our preliminary findings suggest that when a patient is referred for a bone mineral measurement the vertebral geometry should be considered in addition to the BMD.

Normal ranges should be developed which split data for pre and postmenopausal women. As reduced oestrogen levels are associated with postmenopausal bone loss and oestrogen levels decline with years since menopause it may be more logical to express postmenopausal normal ranges in terms of YSM rather than chronological age.

References

ALOIA, J F, VASWANI, A, ROSS, P & COHN, S H, 1990. Aging bone loss from the femur, spine, radius and total skeleton. *Metabolism, 39,* 1144–1150.

CAMERON, J R & SORENSON, J A, 1963. Measurement of bone mineral *in vivo*: an improved method. *Science, 142,* 230–232.

ELDERS, P J M, NETELENBOS, J C, LIPS, P ET AL, 1988. Accelerated vertebral bone loss in relation to the menopause: a cross-sectional study on lumbar bone density in 286 women of 46 to 55 years of age. *Bone Min., 5,* 11–19.

ELLIOT, J R, GILCHRIST, N L, WELLS, J E ET AL, 1990. Effects of age and sex on bone density at the hip and spine in a normal caucasian New Zealand population. *NZ Med. J., 103,* 33–36.

GEUSENS, P, DEQUEKER, J, VERSTRAETEN, A & NIJS, J, 1986. Age, sex and menopause related changes of vertebral and peripheral bone: population study using dual and single photon absorptiometry and radiogrammetry. *J. Nucl. Med., 27,* 1540–1549.

HALL, M L, HEAVENS, J, CULLUM, I D & ELL, P J, 1990. The range of bone density in normal British women. *Br. J. Radiol., 63,* 266–269.

HANSSON, T & ROOS, B, 1986. Age changes in the bone mineral of the lumbar spine in normal women. *Calcif. Tissue Int., 38,* 249–251.

KROLNER, B & NIELSEN, S P, 1982. Bone mineral content of the lumbar spine in normal and osteoporotic women: cross-sectional and longitudinal studies. *Clin. Sci., 62,* 329–336.

MAZESS, R B, BARDEN, H S, ETTINGER, M ET AL, 1987. Spine and femur density using dual-photon absorptiometry in US white women. *Bone Min., 2,* 211–219.

MAZESS, R B, SORENSON, J & HANSON, J, 1988. Performance of an X-ray dual-photon scanner. In *Bone Mineral Measurement by Photon Absorptiometry: Methodological Problems,* ed. by J Dequeker, P Geusens and H W Wahner (Leuven University Press, Leuven), pp. 157–164.

MAZESS, R B, SORENSON, J A, HANSON, J A ET AL, 1989. Dual energy X-ray absorptiometry (DEXA). In *Osteoporosis and Bone Mineral Measurement*, ed. by E F J Ring, W D Evans and A S Dixon (Institute of Physical Sciences in Medicine, York), pp. 62–71.

NILAS, L & CNRISTIANSEN, C, 1987. Bone mass and its relationship to age and the menopause. *J. Clin. Endocrinol. Metabol., 65,* 69–702.

POCOCK, N A, EBERL, S, EISMAN, J A ET AL, 1987. Dual-photon bone densitometry in normal Australian women: a cross-sectional study. *Med. J. Australia, 146,* 293–297.

REED, G W, 1966. The assessment of bone mineralisation from the relative transmission of ^{241}Am and ^{137}Cs radiation. *Phys. Med. Biol., 11,* 174.

RIBOT, C, TREMOLLIERES, F, POUILLES, J M ET AL, 1988. Influence of the menopause and aging on spinal density in French women. *Bone Min., 5,* 89–97.

RIGGS, B L, WAHNER, H W, DUNN, W L ET AL, 1981. Differential changes in bone mineral density of the appendicular and axial skeleton with aging. *J. Clin. Invest., 67,* 328–335.

RIGGS, B L & MELTON III, L J, 1983. Evidence for two distinct syndromes of involutional osteoporosis. *Am. J. Med., 75,* 899–901.

RODIN, A, MURBY, B, SMITH, M A ET AL, 1990. Premenopausal bone loss in the lumbar spine and neck of femur: A study of 226 Caucasian women. *Bone, 11,* 1–5.

SARTORIS, D, SOMMER, F G, MARCUS, R & MADWIG, P, 1985. Bone mineral density in the femoral neck. *AJR, 144,* 605–611.

SCHAADT, O & BOHR, H, 1988. Different trends of age-related diminution of bone mineral content in the lumbar spine, femoral neck and femoral shaft in women. *Calcif. Tissue Int., 42,* 71–76.

SMITH, M A, SUTTON, D & TOTHILL, P, 1983. Comparison between ^{153}Gd and ^{241}Am, ^{137}Cs for dual-photon absorptiometry of the spine. *Phys. Med. Biol., 28,* 709–721.

STEVENSON, J C, LEES, B, DEVENPORT, M ET AL, 1989. Determinants of bone density in normal women: risk factors for future osteoporosis? *Br. Med. J., 298,* 924–928.

TOTHILL, P, SMITH, M A & SUTTON, D, 1983. Dual photon absorptiometry of the spine with a low activity source of gadolinium 153. *Br. J. Radiol., 56,* 829–835.

Book reviews

Endosonography in Obstetrics and Gynecology. By G Bernaschek, J Deutinger and A Kratochwil, pp. xii + 187, 1990 (Springer Verlag), DM248.00.
ISBN 0-387-508285

Endosonography in Gastroenterology, Gynecology and Urology. By G Feifel, U Hildebrandt and N J Mortensen, pp. 217, 1990 (Springer Verlag), DM248.00.
ISBN 3-540-505032

Endosonography. Ed. by Bruno D Fornage, pp. iv + 186, 1990 (Kluwer Academic Publishers), £77.00.
ISBN-0-7923-00475

Endosonography—the use of specially designed ultrasound probes for insertion into various body orifices—is a significant advance in the practice of ultrasonography. High frequency transducers can be placed close to the organ of interest in order to generate high resolution images which can dramatically increase the yield of clinically useful information.

These probes are now offered by nearly all ultrasound equipment manufacturers and most ultrasound departments are being asked to provide an endosonographic service. There is clearly a need for books which can provide instruction on techniques and advice on image interpretation, and the appearance of these three volumes in the bookshops is timely.

The first book listed above has three authors—Bernaschek, Deutinger and Kratochwil—and is written as a conventional textbook providing a comprehensive coverage of all applications of endosonography in obstetrics and gynecology.

It is well written and is systematic in its approach. It is well illustrated and all the scans are presented in a uniform format using a standardized presentation of scan planes, and there is a good selection of references to the literature.

The same publishers, Springer Verlag, have produced the second volume, edited by Feifel, Hildebrandt and Mortensen. This is a collection of six entirely separate review articles, each with its own author or team of authors. As well as covering the history and physics/instrumentation of endosonography, there are chapters on the upper GI tract, rectum, prostate and gynecology. The coverage is selective and both the style and presentation of images are non-uniform.

The third book is edited by Bruno Fornage who has enlisted the help of 17 co-authors. It has a broad scope, covering upper and lower GI tract, urological, gynecological and obstetric applications, but is rather patchy and variable in the depth of its coverage, *e.g.* transvaginal Doppler techniques receive only cursory mention. The orientation of the scans varies both within and between chapters and the quality of some of the illustrations is disappointing.

In conclusion, most ultrasound departments will be looking for a teaching and reference text on endosonography in obstetrics and gynecology, and the book by Bernaschek, Deutinger and Kratochwil is to be highly recommended. For departments and libraries looking for a book giving an overview of all applications of endosonography, Fornage is recommended, while this reviewer has difficulty in identifying a prospective market for Feifel et al.

H C IRVING

A phantom for quantitative ultrasound of trabecular bone

A J Clarke, J A Evans, J G Truscott, R Milner and M A Smith

Centre for Bone and Body Composition Research, University of Leeds, Wellcome Wing, Leeds General Infirmary, Leeds LS1 3EX, UK

Abstract. The propagation mechanisms of ultrasound in trabecular bone are poorly understood and have been the subject of extended debate; also, the reproducibility of ultrasonic measurements on bone *in vivo* using commercial ultrasound heel-scanning devices is such that the interpretation of the obtained data is difficult. In this paper we describe recent developments in the production of a bone-mimicking material which is well suited to the task of routine monitoring of commercial ultrasound bone scanners. The material, based on a standard epoxy resin is fabricated to a pre-determined porosity value by the inclusion of a marrow-mimicking material thereby introducing a known and controlled mean pore size.

Measurements of the velocity and attenuation of the material have been performed over a range of porosity values from 10% to 80% in the frequency range 500–900 kHz; also, broadband ultrasonic attenuation (BUA) values have been obtained from commercial equipment. The material displays velocities in the range 1844–3118 m s^{-1} and attenuation ranging from 7.0 to 17.7 dB cm^{-1} at 500 kHz.

1. Introduction

The rapidly increasing use of ultrasound to detect and monitor bone pathology, in particular osteoporosis, has led to the development of several commercially available devices. Such devices typically measure the rate of change of attenuation of ultrasound with frequency (broadband ultrasound attenuation or BUA) between 0.2 and 0.6 MHz, and also the velocity of sound (Langton *et al* 1984, 1990).

Currently, at least two of the commercial manufacturers offer phantoms for use with their own scanners. However, at best these devices are suitable for monitoring temporal changes in scanner performance. There is no independently validated data on their acoustic parameters and in one case the machine is set in a different mode before the phantom can be used because the acoustic properties differ significantly from those of the os calcis. In neither case is there any attempt to simulate the architecture of the heel nor is it certain that the phantoms themselves have good long-term stability. There is a clear requirement for a phantom, constructed from a material which will mimic acoustically the properties of ultrasound in trabecular bone in this frequency range. Such a phantom would enable intercomparisons to be made between results from different commercial ultrasound bone systems and provide the necessary calibration for long term longitudinal patient studies. Furthermore, the propagation of ultrasound, particularly in trabecular bone, is still poorly understood and so there is a need for a material which could be used to simulate bone in a controlled, reproducible and realistic manner.

This paper describes a new material, made from a mixture of an epoxy resin and gelatine which mimics the speed and attenuation of sound through trabecular bone and which can be formed into a phantom of a specific size and shape.

2. Trabecular-bone-mimicking material

2.1. Requirements of the material

The bones of the human skeleton can be divided into two types: cortical bone and cancellous, or trabecular, bone. The latter has a porous structure made up of cortical trabecules, the pores being filled with bone marrow.

Cortical bone is relatively straightforward to mimic, as it has a homogenous, compact structure. Trabecular bone, having a composite structure is more problematic. The size, shape and concentration of pores varies between skeletal sites; the proportion by volume which is marrow is known as the porosity. Hence there is a requirement for the bone phantom material to be able to mimic porosity in a controllable way. We therefore aimed to have a two component material, one component being ultrasonically equivalent to cortical bone, and the other equivalent to bone marrow. The two components were to be geometrically arranged in a manner comparable to trabecular bone with variable, but controlled, porosity.

The specification for the two materials was that they should match the velocity and attenuation of cortical bone and marrow over as wide a range of conditions as possible. Unfortunately there is significant variation in the reported values for both parameters for cortical bone and almost no data for either quantity in bone marrow. Table 1 summarizes some of the published values, although in all but one case, these refer to animal samples.

Table 1. The ultrasonic characteristics of the constituents of trabecular bone. Note, all data are from bovine bone samples except the data marked with an asterisk (*) which are from human bone. ± values refer to 1 standard deviation.

Material	Velocity (m s^{-1})	Attenuation at 1 MHz (db cm^{-1})	Reference
Cortical bone	3461 ± 104	8.36 ± 1.37	Tavakoli (1991)
Cortical bone	$3250 \pm 196^*$	—	André *et al* (1980)
Cortical bone	—	6.9 ± 0.6	McKelvie and Palmer (1987)
Bone marrow	1435 ± 10	0.50 ± 0.05	Tavakoli (1991)

2.2. Materials to simulate cortical bone and marrow

An extensive search for synthetic materials possessing similar ultrasonic characteristics to those of cortical bone and marrow was made using the techniques described below. This concluded that the optimal values were not achievable. However, materials were found which gave a reasonable match.

The cortical bone mimic is a two-part epoxy compound normally used for the encapsulation of electrical components. It is available commercially as Araldite CW 1302 liquid epoxy resin and is used in conjunction with Araldite HY 1300 hardener in the proportions recommended by the manufacturer. Its ultrasonic velocity is within the published values for bone, although the attenuation coefficient is about 50% less (see table 2 below).

A number of materials were identified as potential marrow mimics but most were rejected since no practical means could be found of creating the required structure when dispersing in the epoxy compound. It was therefore decided to evaluate the use a gelatine/water mixture in the proportions of 11 g of dry gelatine to 150 ml of water. This

concentration was chosen as a compromise between the increased mechanical stiffness at higher concentrations and the lower sound velocities at lower concentrations. This concentration has useful mechanical properties as it can be formed into relatively stable pore-shaped granules, but has the disadvantage that its attenuation coefficient is an order of magnitude too low and its velocity some 6% too high. Nevertheless it was hoped that this would prove to be of little significance as the high acoustic losses in trabecular bone are more dependent on the scatter arising from the geometrical arrangement of its constituents than absorption by the constituents themselves; also, the discrepancy in velocity should be reduced in the composite material. The acoustic properties of the materials are displayed in table 2.

Table 2. The ultrasonic characteristics of the constituents of the bone phantom (Truscott *et al* 1993). The ranges quoted refer to standard deviation values.

Material	Velocity (m s^{-1})	Attenuation at 1 MHz (dB cm^{-1})
Bone mimic	3168 ± 8	3.7 ± 0.3
Marrow mimic	1519 ± 3	0.051 ± 0.004

2.3. Manufacture of the trabecular bone material

The two components were combined so as to resemble the structure of cancellous bone in the following manner. Firstly the gelatine was extruded twice through a 1.12 mm mesh to produce roughly cubic granules of side approximately 1 mm. This was then added to the liquid epoxy in volumes, calculated by means of weight and density, to give the required porosity and then mixed until a uniform distribution of gelatine particles had been achieved. The material was then de-gassed in a vacuum chamber at 3 Torr to remove any air pockets, then poured into moulds and left to harden.

This process, which is the subject of a patent application, produces a material consisting of gelatine pores enclosed in a matrix of epoxy. This differs from trabecular bone in as much as the gelatine cavities are essentially separated from each other (giving a so-called closed cell structure). In trabecular bone the cells are interconnected giving an open cell structure through which the marrow can flow. Figure 1 compares the cross sections of a sample of 60% porosity, the head of a femur and a lumbar vertebra.

Eight samples having porosities in the range 10% to 80% were made. The volumes of epoxy and gelatine required to give the various porosities were obtained by weighing, these weights being calculated after careful measurement of their densities. Values of the porosity of each sample were then obtained by relating their density to those of their constituents. All density measurements were made using Archimedes' principle.

3. Measurements on the trabecular phantom material

3.1. Instrumentation

Velocity and attenuation measurements at different frequencies were carried out using the experimental set-up shown in figure 2. This consists of a cubic ultrasonic water tank of side 15 cm with two identical 0.75 MHz broadband transducers centrally mounted in cut-outs on opposite faces so as to be in direct contact with the water. A 2% solution of a
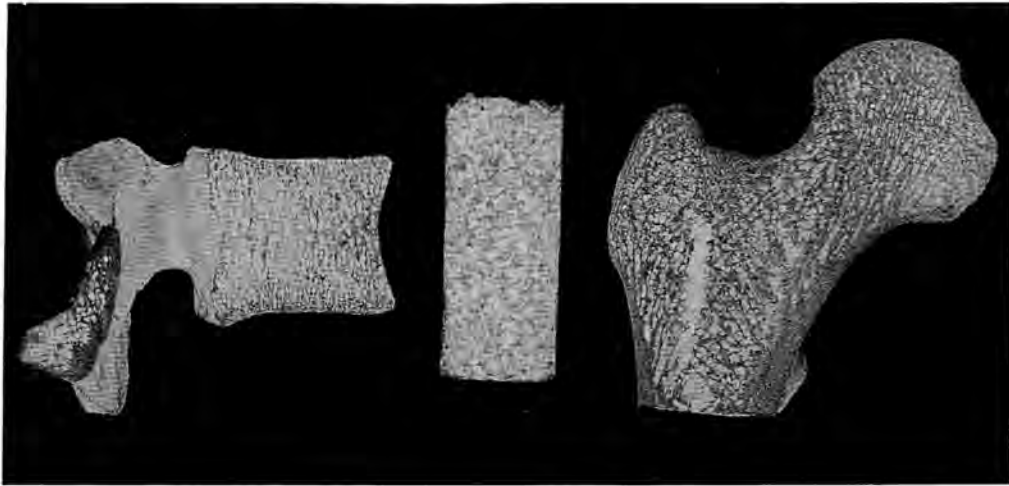
Figure 1. Cross sections of a lumbar vertebra, (left), the bone phantom (centre), and the head of a femur (right).
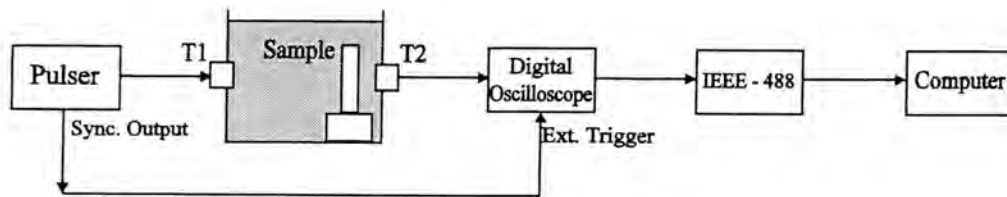
Figure 2. Block diagram of the experimental set-up.

proprietary detergent (Stardrops) was added to improve wetting. Transducer T1 is excited by a 1 kV pulse of duration 0.1 μs. This produces a broadband ultrasound pulse of length approximately 7 μs. The output from transducer T2 is captured by a digital oscilloscope and then transferred to floppy disc via an IEEE-488 interface and computer.

3.2. Velocity

The velocity of ultrasound in the phantoms was determined using the 'time of flight' method where the difference in the time taken for an ultrasound pulse to travel between the two transducers both with and without a sample of known thickness in place is noted. The velocity can then be calculated using the equation

$$V_s = \frac{d_s V_w}{d_s - V_w \Delta t} \tag{1}$$

where V_s is the velocity of sound in the sample, V_w is the velocity of sound in water, d_s is the sample thickness and Δt is the (time of flight in water only) − (time of flight with sample present). The measured ultrasonic velocities of the phantom material were compared with two theoretical velocities. The first uses the relationship described by Wyllie *et al* (1956)

who suggested that the ultrasonic velocity in a porous material could be predicted by the equation

$$\frac{1}{V_p} = \frac{\phi}{V_b} + \frac{1-\phi}{V_a}$$ (2)

where V_p is the predicted velocity in the material, V_a is the velocity in the matrix material, V_b is the velocity in the pore material and ϕ is the porosity of the material.

This equation was derived by analysing the times taken for a pulse to traverse a composite material made up of two slabs possessing different acoustic velocities. The porosity is defined in terms of the slab thicknesses and thus the equation is essentially one-dimensional.

The alternative hypothesis which we propose is that the velocity may change linearly with volume fraction and would therefore be more accurately predicted by the simpler expression

$$V_p = V_a(1 - \phi) + V_b\phi.$$ (3)

Here the predicted velocity is directly dependent on the porosity (i.e. the relative volumes of pore and matrix materials) and as such should correspond more closely to the structure of the phantom material. There are potentially a number of other formulations but, in this case, a reasonable agreement with experiment was found with this simple version.

3.3. Attenuation

When assessing the ultrasonic attenuation in a material, allowance has to be made for reflection losses at the water–sample interfaces. This was achieved by measuring the transmitted amplitude for a number of thicknesses of each sample. It was assumed that the reflection losses would be constant for each thickness and hence changes in received amplitude would be due solely to losses within the sample.

The reduction in sample thickness was achieved by milling. This ensured that the sample faces were parallel and hence kept the experimental errors to a minimum; also, care was taken not to reduce the sample thickness to a degree where reverberations of ultrasonic pulses inside the sample would affect the amplitude measurements. A thickness range of 8–20 mm was found to be acceptable.

The received pulses were digitized and subjected to a fast Fourier transform (FFT). This produced a spectrum from which amplitudes at different frequencies could be obtained.

The attenuation coefficient of the phantom was determined graphically. This involved plotting $20 \log_{10}$(amplitude) at a given frequency against sample thickness in cm. The slope of the resultant straight line should therefore be equal to the attenuation coefficient, α, given in dB cm^{-1}, thus;

$$\alpha = \frac{20}{ds_1 - ds_2} \log_{10}\left(\frac{A_1}{A_2}\right)$$ (4)

where ds_1 and ds_2 are sample thicknesses and A_1 and A_2 are the signal amplitudes at those thicknesses.

3.4. Broadband ultrasonic attenuation (BUA)

Commercial BUA devices generally measure the rate of change of attenuation with frequency between roughly 200 kHz and 600 kHz although the technique has only been applied to specific measurements on the os calcis (Langton *et al* 1984). However, although an attempt is made to correct for water and diffraction losses, the sample thickness is not taken into account. Furthermore, there is an implicit assumption that the attenuation is linear with frequency over that range. The equipment used for our attenuation measurements had a poor signal to noise ratio below 400 kHz and therefore results are given within the frequency range 500–900 kHz. Although this is not ideal, we were able to confirm the validity of the data by measuring BUA values in a commercial BUA scanner as described below.

In this study the BUA value was measured in a number of our samples using a commercial device (Walker Sonix UBA 575). These samples were all rectangular blocks of dimensions 50 mm × 50 mm × 20 mm and were positioned with the 20 mm axis parallel to the ultrasonic beam.
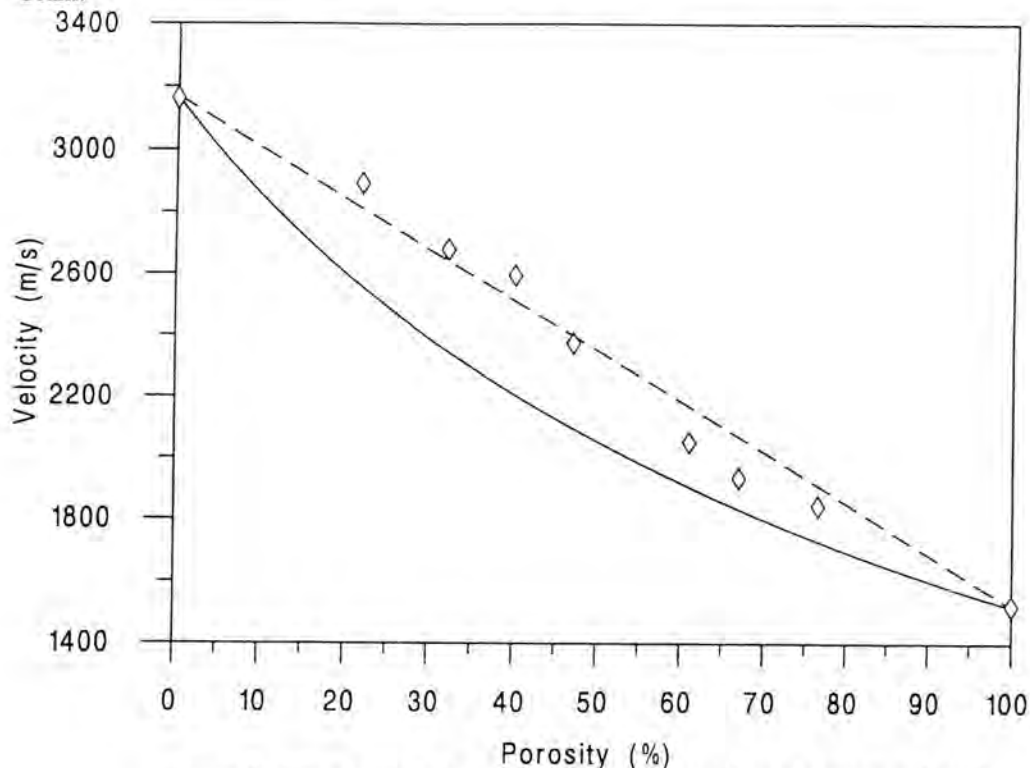
Figure 3. The relationship between porosity and velocity for the phantom, and predicted velocities (——) according to Wyllie *et al* (1956), and (– – –) proposed. Error bars (indicating ± one standard error of the mean) lie within data symbols.

4. Results and discussion

The variation of velocity in the trabecular phantom material for different values of porosity is shown in figure 3. It can be seen that the measured velocities seem to correspond better to the predicted velocity using equation (3) rather than equation (2). Ideally, the

lower limit of these values would be reduced further to provide a more comprehensive coverage of the range of velocity values quoted for trabecular bone (see table 3) although the range of reported values is large (McKelvie and Palmer 1987, Miller *et al* 1993). This could be achieved by replacing the gelatine with another material of lower velocity, and we are currently exploring a number of options. Since pulsed ultrasound was used for the measurement of velocities, the possibility of some dispersion cannot be entirely ruled out. Similarly, there was some initial concern about the possible errors due to non-linear propagation. This was investigated by sending pulses with amplitudes differing by 10 dB through the same material under the same conditions. The received signals were Fourier transformed and compared. Above 1 MHz, differences of up to 1 dB were found, the data points below 1 MHz had identical values within the limits of experimental precision and it was concluded that non-linear errors were negligible.
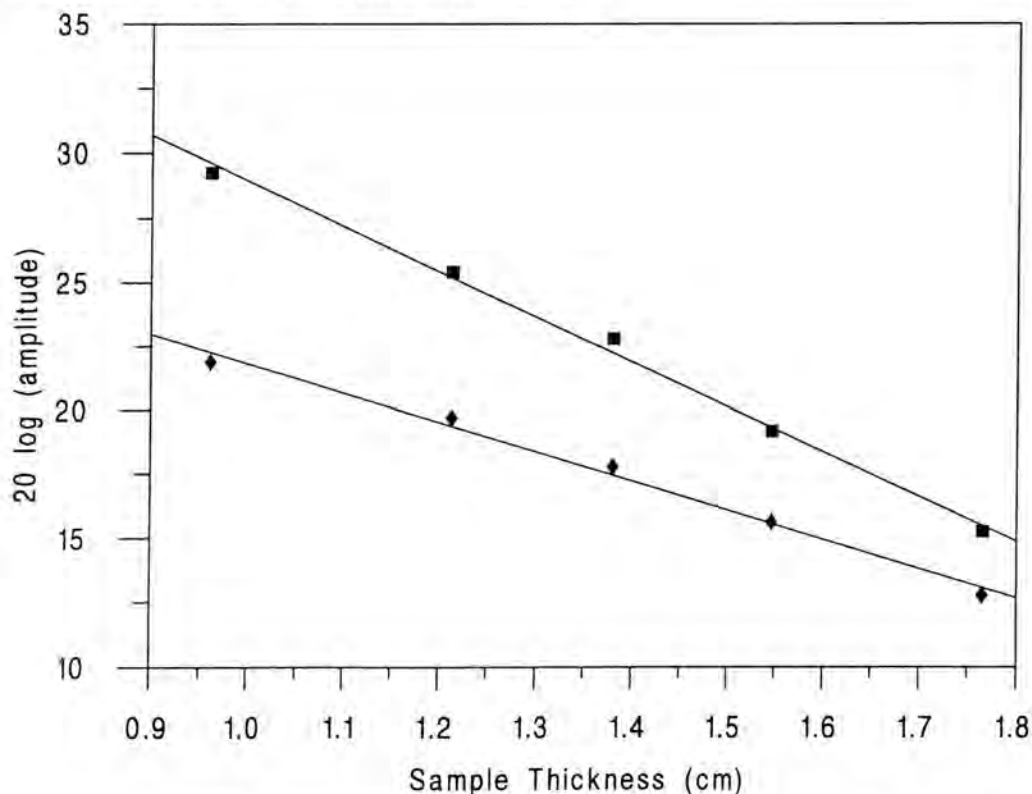
Figure 4. Example of the determination of attenuation coefficient of the 50% porous sample at (♦) 0.5 MHz and (■) 0.75 MHz. The respective gradients and r^2 values are (♦) 11.45, 0.99 and (■) 17.57, 0.99.

As stated above, the attenuation coefficient, α, at each frequency, was determined using a range of thicknesses as shown in figure 4. A linear least-squares regression was applied to the data points, the gradient of which gave the attenuation coefficient, α, in dB cm^{-1}. The correlation coefficient r^2 had values for all samples ranging from 0.83 to 0.99 with a mean value of 0.97. The attenuation coefficients obtained for the various samples over a range of porosities and frequencies, including those of 0% porosity (pure epoxy) and 100% porosity (pure gelatine), are displayed in figure 5. It can be seen that whilst the attenuation
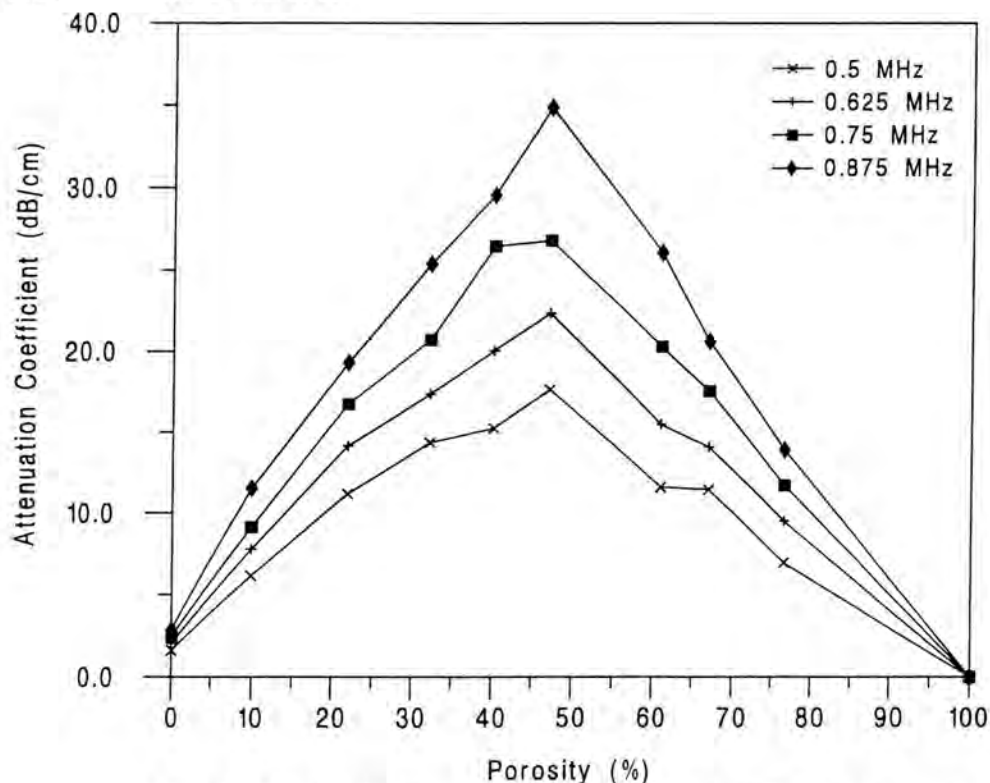
Figure 5. The relationship between the porosity and attenuation coefficient of the material.

in very low and very high porosity samples is relatively small it increases as the porosity is changed and passes through a peak at roughly 50%.

The results for BUA obtained from the Walker Sonix UBA 575 are displayed in figure 6. The general shape of the data points shows a similarity to those in figure 5, both peaking at around 50% porosity.

It is too early to report on the long-term stability of these phantoms, although we are in the process of carrying out the relevant measurements. However, it is clear that some form of encapsulation is needed to prevent the gelatine from drying out. Present signs indicate that if a thin shell of epoxy is added, it not only provides a suitable seal but it also mimics the outer cortical shell. The temperature dependence of the values is also relevant since some equipment operates at 37 °C while others use room temperature. We have performed tests on the temperature dependence of the 80% porosity phantom which indicate that it has a temperature coefficient of roughly -1.5 m s^{-1} per °C for velocity and -0.06 dB MHz^{-1} per °C for BUA.

As mentioned previously, much work has been done on the ultrasonic characteristics of bone taken from various sources, both human and animal. The most pertinent results, however, are those relating to large volumes of cancellous bone, as it has been suggested that these would be more sensitive to changes in bone metabolism (Langton 1984). A comparison of the results from previous work (McKelvie and Palmer 1987) and those from the present study is shown in table 3. The data were obtained from bone mimics with porosities in the range 47%–76% and cancellous bone with densities quoted as being between 940 kg m^{-3} and 1170 kg m^{-3}.

Table 3. A comparison of the ultrasonic characteristics of the bone mimic and real bone.

	Bone mimic	Trabecular bone
Attenuation at 0.5 MHz (dB cm^{-1})	7.0–17.7	6.0–16.0[a]
Velocity (m s^{-1})	1844–3118	1465[b]–2084[c]
BUA (dB MHz^{-1})	24–76	26–99[d]

[a] Tavakoli (1991).
[b] Miller *et al* (1993).
[c] McKelvie and Palmer (1987).
[d] Truscott *et al* (1992).
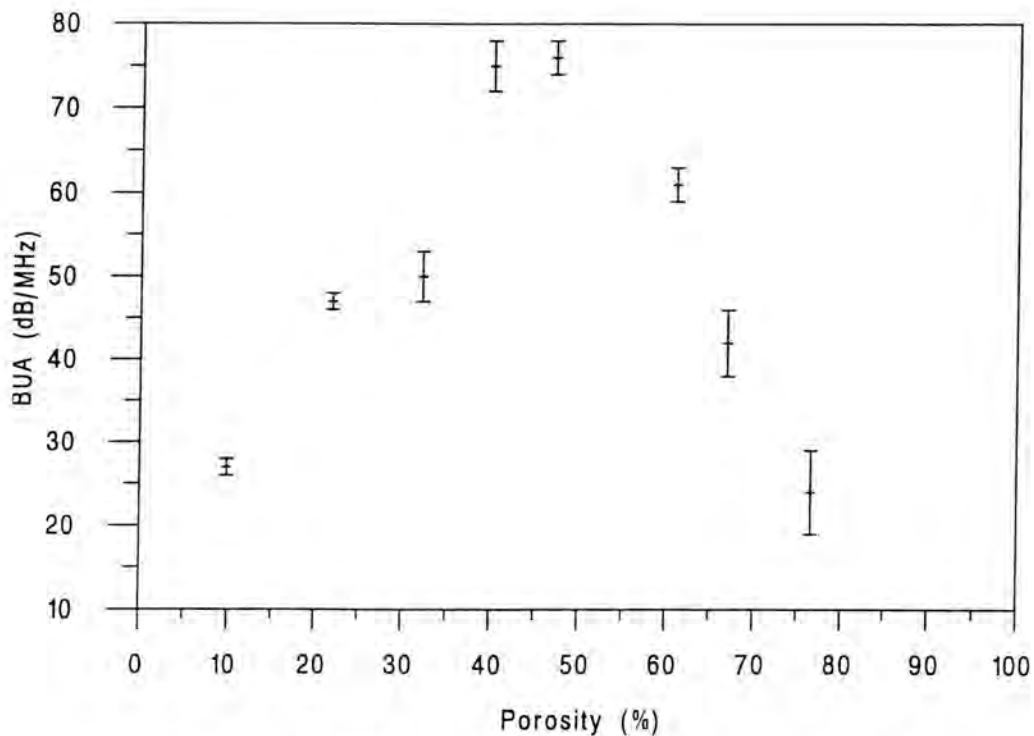
Figure 6. The relationship between the porosity and the BUA of the material. Error bars indicate one standard error of the mean.

The peak in the attenuation at 50% porosity implies that the highly attenuating nature of the material is predominantly due to the scatter arising from the geometrical arrangements of its constituents; this is often referred to as the 'architecture' of trabecular bone. This seems not to have been reported in ultrasonic studies of real bone, probably because the full range of porosities is not readily available in biological samples.

The location of the peak in attenuation at 50% porosity could be explained as follows. A standard pore size was used for all samples, the porosity being altered by changing the pore density. It seems likely, therefore, that at high densities there is a degree of connectivity between adjacent pores. Now if, as mentioned above, the attenuation is due to inhomogeneities in the material, we can consider these inhomogeneities to be gelatine pores in an epoxy matrix on one side of the peak (0%–50%) whereas on the other side

(50%–100%) it is the gelatine which forms the continuous phase with particles of epoxy forming the scatterers. It is then not unreasonable to assume that the attenuation in both cases should be a maximum when the number of scatterers per unit volume is a maximum. It is clear that this is not an entirely accurate model for cancellous bone, where changes in both pore size and density take place. This may mean that in trabecular bone the attenuation peak occurs at a porosity other than 50%.

As previous workers have shown, the attenuating properties of the os calcis diminish with decreasing density (McCloskey *et al* 1990, McKelvie and Palmer 1987). Now it can be assumed that in this case density and porosity are inversely proportional and hence the attenuation in the os calcis decreases with increasing porosity. If, therefore, the attenuation coefficients of various porosities of trabecular bone display a similar peak to that given by the phantom, then the porosity of the os calcis should be greater than 50%. Although several studies into the properties of the os calcis have been undertaken, no direct information on its porosity was found. Density values obtained by means of the Archimedes' principle are available. However, these measurements can be unreliable if great care is not taken to exclude all air from the sample or if there is a degree of uncertainty about the nature of the pore-filling material. For example, McKelvie and Palmer (1987) measured the density of samples of os calcis to lie in the range 940 to 1170 kg m^{-3}, despite the density of marrow being (970 ± 60) kg m^{-3} and that of cortical bone (1990 ± 27) kg m^{-3} (ICRP 1975). Nevertheless, in general the densities of the os calcis always give a porosity well in excess of 50%. This is also relevant when considering the BUA values obtained. Several reports (Evans and Tavakoli 1990, Tavakoli and Evans 1991) have concluded that there is a high correlation (0.8 to 0.9) between trabecular bone density and BUA *in vivo* and *in vitro* and therefore changes in porosity, and hence also density, over a wide range may not be particularly relevant in the os calcis where there appears to be a relatively small range of values.

The existence of a peak in attenuation as the porosity is changed means that a lower than normal attenuation measurement at a particular skeletal site cannot be interpreted as an indication of osteoporotic bone without knowledge of the porosity of that bone. In fact, if attenuation measurements of a particular bone either fall on the 'wrong' side of the peak or straddle the peak this would lead to false conclusions being drawn as to the condition of the bone.

The nature of the ultrasonic attenuating mechanism in porous materials is the subject of debate. Two models have been suggested, one based purely on multiple scatter and the other including losses due to viscoelastic mechanisms first described by Biot (1956, 1962). Biot theory treats attenuation as an effect of the viscous forces that are created as fluid is moved though the porous matrix. The theory therefore requires a fluid filled, permeable structure rather than the closed cell structure filled with semi-solid gelatine which comprises the phantom. Since our inclusions are of the order of 1 mm in diameter and the wavelength is similar, then it is inevitable that scatter will be significant. In fact, it seems probable that it is the dominant mechanism in this phantom material.

The trabecular phantom material displays ultrasonic characteristics which are similar to those of trabecular bone, both velocity and attenuation being highly dependent on porosity; also, the range of velocities, attenuation coefficients and BUA values achievable match those found in real bone.

It seems probable that the dominant attenuating mechanism is scatter due to the material's closed cell structure. Varying the porosity while using standard pore sizes changes the number of scatterers and hence changes the attenuating characteristics. The number of scatterers could also be altered by varying the pore size whilst keeping the

porosity constant. Hence it is possible that for this material the attenuation and velocity are independently variable, although further work is required in order to verify this. Another important potential development is the introduction of anisotropy into the phantom material. This would be readily achievable by using gelatine strands aligned in some way rather than the isotropic cubes described here. Such a material would have the advantage of being able to mimic the directionality of the structures in the os calcis, thereby making the phantom more realistic. However, in clinical practice, the os calcis is always examined in the same plane and therefore anisotropic influences should be minimal. Work to investigate this is now underway.

Acknowledgment

References

André M P, Craven J D and Greenfield M A 1980 Measurement of the velocity of ultrasound in the human femur *in vivo Med. Phys.* **7** 324–30
Biot M A 1956 Theory of propagation of elastic waves in fluid-saturated porous solid *J. Acoust. Soc. Am.* **28** 168–91
—— 1962 Generalised theory of acoustic propagation in porous dissipative media *J. Acoust. Soc. Am.* **34** 1254–64
Evans J A and Tavakoli M B 1990 Ultrasonic attenuation and velocity in bone *Phys. Med. Biol.* **35** 1387–96
ICRP 1975 Report of the task group on reference man *ICRP Report* 23 p 97
Langton C M 1984 The measurement of broadband ultrasonic attenuation in cancellous bone *PhD Thesis* University of Hull
Langton C M, Ali A V, Riggs C M, Evans G P and Bonfield W 1990 A contact method for the assessment of ultrasonic velocity and broadband attenuation in cortical and cancellous bone *Clin. Phys. Physiol. Meas.* **11** 243–9
Langton C M, Palmer S B and Porter R W 1984 The measurement of broadband ultrasonic attenuation in cancellous bone *Eng. Med.* **13** 89–91
McCloskey E V, Murray S A, Charlesworth D, Miller C, Fordham J, Clifford K, Atkins R and Kanis J A 1990 Assessment of ultrasound attenuation in the os calcis *in vitro Clin. Sci.* **78** 221–7
McKelvie M L and Palmer S B 1987 The interaction of ultrasound with cancellous bone *Ultrasonic Studies of Bone (Institute Of Physics, Short Meetings Reports 6)* ed S B Palmer and C M Langton (Bristol: Institute of Physics) ch 1, pp 1–13
Miller C G, Herd R J M, Ramalingan T, Fogelman I and Blake G M 1993 Ultrasonic velocity measurements through the calcaneus: which velocity should be measured? *Osteoporosis Int.* **3** 31–5
Tavakoli M B 1991 An investigation of ultrasonic attenuation and velocity in bone *PhD Thesis* University of Leeds
Tavakoli M B and Evans J A 1991 Dependence of the velocity and attenuation of ultrasound in bone on the mineral content *Phys. Med. Biol.* **36** 1529–37
Truscott J G, Simpson M, Stewart S P, Milner R, Westmacott C F, Olroyd B, Evans J A, Horsman A, Langton C M and Smith M A 1992 Bone ultrasonic attenuation in women: reproducibility, normal variation and comparison with photon absorptiomety *Clin. Phys. Physiol. Meas.* **13** 29–36
Truscott J G, Milner R, Clarke A J, Evans J A 1993 Towards an ultrasonic bone phantom *Abstracts of the IPSM Golden Jubilee Congr. (Bristol, 1993)* (York: IPSM) p 151
Wyllie M R J, Gregory A R and Gardner L W 1956 Elastic wave velocities in heterogeneous and porous media *Geophysics* **21** 41–70

Comparison of changes in bone mineral in idiopathic and secondary osteoporosis following therapy with cyclical disodium etidronate and high dose calcium supplementation

S. M. Orme, M. Simpson*, S. P. Stewart*, B. Oldroyd*, C. F. Westmacott*, M. A. Smith* and P. E. Belchetz
*Department of Endocrinology and *Centre for Bone and Body Composition Research, Institute of Physical Sciences, Department of Clinical Medicine, University of Leeds, The General Infirmary at Leeds, Leeds, UK*

Summary

OBJECTIVE Our clinical practice has been to offer treatment with cyclical disodium etidronate and high dose calcium supplements (1500–1600 mg/day) to all female patients with osteoporosis who are unable or unwilling to take hormone replacement therapy (HRT), and male osteoporotics. In a retrospective study we compared the effect of this treatment on measures of bone mineral over a 12-month period in women with post-menopausal and secondary osteoporosis. We also assessed its effects in 10 male osteoporotics.

DESIGN A retrospective analysis of 83 consecutive patients with osteoporosis who completed 12 months of treatment with disodium etidronate and calcium and who had a dual energy X-ray absorptiometry (DEXA) scan at baseline and following 12 months of therapy.

PATIENTS The study included 73 women (45 post-menopausal and 28 secondary osteoporotics) and 10 men with established osteoporosis as shown by spinal and femoral bone mineral densities (BMD) > 2 standard deviations (SD) below young normals, and radiological evidence of osteoporosis.

MEASUREMENTS Each patient had routine biochemistry at baseline, an X-ray of thoracic and lumbar spine and a DEXA scan of lumbar spine (L2–L4) and femoral neck. The DEXA scan was repeated following 12 months of therapy.

RESULTS There was no difference between increase in spinal BMD in the post-menopausal (5·7%) versus secondary osteoporotic group (6·7%). There was a significant increase in spinal BMD at 12 months in the 10 male osteoporotics (9·0%, $P < 0.01$). No overall change in femoral neck BMD was noted.

CONCLUSIONS Cyclical disodium etidronate given with high dose calcium supplements is equally effective in increasing spinal bone mineral density in post-menopausal and secondary osteoporosis. It also results in a significant rise in spinal bone mineral density in male osteoporotics. Whether this produces a reduction in fracture rates is unknown.

Correspondence: Dr S. M. Orme, Department of Diabetes, Royal Hallamshire Hospital, Glossop Road, Sheffield S10 2JF, UK.

Osteoporosis is characterized by an absolute decrease in the amount of bone, leading to an increased number of fragility fractures principally of the vertebrae, proximal femur and distal radius. Bone loss occurs because of an imbalance between bone resorption and formation, with the former exceeding the latter (Eastell *et al.*, 1988). Measures of bone mass correlate inversely with fracture rate (Jensen *et al.*, 1983). In post-menopausal women oestrogen deficiency, and consequently negative calcium balance, is a major cause of osteoporosis (Nordin & Morris, 1989; Nordin *et al.*, 1991). In patients with secondary osteoporosis due to thyrotoxicosis or steroid therapy, bone resorption is stimulated and intestinal calcium absorption is inhibited (Meunier *et al.*, 1984; Baran & Braverman, 1991). In steroid induced osteoporosis, bone formation is also inhibited by a direct effect on osteoblasts (Bressot *et al.*, 1979). Anti-resorptive therapy combined with adequate calcium supplementation would therefore be a rational therapy for these forms of osteoporosis.

Bisphosphonates have complex actions on bone. They act mainly as anti-resorptive agents, limiting the accession of osteoclast precursors to bone, the formation of osteoclasts (Boonekamp *et al.*, 1986) and direct bone resorption by mature osteoclasts (Carono *et al.*, 1990). They may also act through osteoblasts affecting their proliferation and inhibiting the secretion of osteoclast stimulating factors (Khoker & Dandona, 1989). They have been shown to provide protection against osteopaenia in a rat model (Wronski *et al.*, 1991). In a clinical study, the bisphosphonate (3-amino-1-hydroxypropylidene)-1,1-bisphosphonate (APD)

given continuously with 1 g of calcium supplements per day has been shown to increase vertebral bone mineral density in patients treated with corticosteroids (Reid *et al.*, 1988). Tiludronate has shown a more modest benefit when given continuously without calcium supplements in post-menopausal osteoporosis (Reginster *et al.*, 1989). More recently, well designed clinical trials have reported that 400 mg of disodium etidronate daily, given for 2 weeks, followed by 500 mg of calcium supplements for 11 weeks, in repeated cycles over 2 and 3 years, resulted in an increase in spinal bone mineral and reduced the rate of vertebral fractures in post-menopausal osteoporosis (Storm *et al.*, 1990; Watts *et al.*, 1990).

Our clinical practice has been to treat all patients with established osteoporosis, who are not suitable for, or who refuse, hormone replacement therapy (HRT) (including secondary osteoporosis and male patients) with repeated cycles of disodium etidronate, 400 mg per day for 2 weeks followed by at least 1500 mg of calcium supplements per day for 11 weeks (recommended daily requirement for post-menopausal women, Consensus Development Conference, 1987). In a retrospective study, we have compared the effect of this treatment on spinal and femoral bone mineral in a group of post-menopausal women with that in a group of women with secondary osteoporosis. We have also evaluated its effect on 10 male patients with osteoporosis.

Patients

The study contained 45 women with post-menopausal osteoporosis (mean age 64.4 ± 1.2 years) and 28 women with secondary osteoporosis (mean age 60.5 ± 1.9). Mean Z scores at baseline in these groups were comparable (see Table 1). The group with secondary osteoporosis included patients with previous thyrotoxicosis (8), on oral steroid therapy (7), and with early surgical menopause (13). All other causes of secondary osteoporosis (such as coeliac disease, anorexia nervosa and acromegaly) were excluded because they represented only single cases. We also included 10 males with osteoporosis (see Table 2); the causes were idiopathic osteoporosis (7), hypogonadism (2) and previous gastric surgery (1). Male patients with hypogonadism were on stable treatment with testosterone supplements for at least 1 year prior to treatment with etidronate; their treatment was not altered during the period under study. Osteoporosis was defined as a spinal or femoral Z score of > 2 SD below young normals or X-ray evidence of osteoporosis, such as vertebral body collapse. Vertebral collapse was defined as a reduction in the height of the whole or anterior vertebral body of $> 20\%$. In a number of cases

Table 1 Details of female patients

	Post-menopausal women ($n = 45$)	Secondary osteoporosis ($n = 28$)	Significance P
Age	64.4 ± 1.2	60.5 ± 1.9	NS
Age at menopause	46.2 ± 0.7	43.0 ± 1.1	$<; 0.001$
Years since menopause	16.7 ± 1.3	16.5 ± 2.0	NS
Height (cm)	155.8 ± 0.9	155.1 ± 1.5	NS
Weight (kg)	56.6 ± 1.5	57.3 ± 2.3	NS
Z-score*			
spine	-3.45 ± 0.20	-3.25 ± 0.28	NS
femur	-2.39 ± 0.18	-2.51 ± 0.19	NS

Paired *t*-test (mean $\pm$ SEM).
* Number of SD below young normals.

spinal Z scores were artefactually increased by vertebral collapse or abdominal aortic calcification, in which case patients were classified as osteoporotic by virtue of X-ray evidence of vertebral collapse.

Patients were excluded from the study for the following reasons: co-treatment with hormone replacement therapy (3), inability to take calcium supplements (2), and treatment with minocycline (which may bind calcium/etidronate in the gut) for acne (1). Treatment was generally well tolerated with only two patients who were unable to take calcium supplements withdrawing.

Methods

All patients had a clinical assessment, routine biochemical tests to exclude metabolic bone disease or other causes of osteopaenia, and standard spinal X-rays at baseline. They

Table 2 Details of male patients

	Male osteoporotic ($n = 10$)
Age	49.5 ± 5.4
Height (cm)	163.0 ± 10.2
Weight (kg)	68.3 ± 8.0
Z score*	
spine	-3.59 ± 0.28
femur	-1.19 ± 0.52

Mean $\pm$ SEM.
* Number of SD below young normals.

each underwent a DEXA scan (Lunar Corporation, Madison, Wisconsin, USA) of the lumbar vertebrae (L2–L4) and femoral neck (reproducibility in normal controls 1·18% in spine and 1·69% in femur) (Truscott *et al.*, 1993). Z score (number of SD below young normals) was derived from a study of 329 normal women (Truscott *et al.*, 1993) and 122 normal men (unpublished data) from the local population. Measurements were performed at baseline and after 12 months treatment in all cases.

Treatment consisted of disodium etidronate (400 mg to be taken in the middle of a 4-hour fast at night for 2 weeks), followed by 1500–1600 mg of calcium supplements per day for 11 weeks. The calcium supplements were given according to patient preference. Each patient started on Sandocal (calcium lactate gluconate/calcium carbonate, Sandoz) 400 mg twice during the day and 800 mg at night initially. Twelve were changed subsequently to Calcichew (calcium carbonate, Shire Pharmaceuticals) 500 mg thrice daily as they found the initial treatment unpalatable. Each cycle was repeated every 3 months.

Statistics

Statistical analyses were performed with paired Student's *t*-test or Wilcoxon signed rank test. Comparisons of more than two data sets were done by one-way ANOVA with the Bonferroni adjustment when comparing individual groups. All data were expressed as mean ± SEM. Level of significance was set at a P value of < 0.05.

Table 3 Measures of bone mineral in post-menopausal and secondary osteoporotic women at baseline and 12 months

	0	12 months	Significance P
Post-menopausal			
Spinal BMD	0.765 ± 0.025	0.808 ± 0.025	< 0.0001
Spinal BMC	28.65 ± 1.16	30.21 ± 1.13	< 0.0001
Secondary osteoporosis			
Spinal BMD	0.789 ± 0.0348	0.842 ± 0.03	< 0.0001
Spinal BMC	30.20 ± 1.72	33.20 ± 1.65	< 0.005
Post-menopausal			
Femoral BMD	0.695 ± 0.019	0.708 ± 0.017	NS
Femoral BMC	3.36 ± 0.09	3.43 ± 0.10	NS
Secondary osteoporosis			
Femoral BMD	0.699 ± 0.025	0.714 ± 0.027	NS
Femoral BMC	3.47 ± 0.164	3.47 ± 0.165	NS

Paired *t*-test (mean ± SEM.)
BMD, Bone mineral density (g/cm²); BMC, bone mineral content (g hydroxyapatite).

Table 4 Comparison of BMD in sub-groups of patients with secondary osteoporosis at baseline and 12 months

	0	12 months	Significance P
Post thyrotoxicosis ($n = 8$)			
Spinal BMD	0.858 ± 0.036	0.902 ± 0.028	< 0.05
Femoral BMD	0.679 ± 0.022	0.707 ± 0.025	< 0.05
Steroid therapy ($n = 7$)			
Spinal BMD	0.608 ± 0.08	0.684 ± 0.075	< 0.05
Femoral BMD	0.606 ± 0.08	0.583 ± 0.074	NS
Early surgical menopause ($n = 13$)			
Spinal BMD	0.844 ± 0.04	0.889 ± 0.033	< 0.01
Femoral BMD	0.756 ± 0.027	0.778 ± 0.034	0.052

Wilcoxon signed rank test (mean ± SEM).
BMD, Bone mineral density (g/cm²).

Results

There was no significant difference between the post-menopausal women ($n = 45$) and those with secondary osteoporosis ($n = 28$) in terms of age, years since menopause, height, weight or Z scores at baseline (see Table 1). The secondary osteoporosis group tended to have an earlier menopause, 43.0 ± 1.1 years versus 46.2 ± 0.7 years ($P < 0.01$). The spinal Z scores in all three groups were not significantly different (ANOVA $F = 0.3033$), but the femoral neck Z scores were significantly higher in the male group (Table 2) when compared with the post-menopausal and secondary osteoporotic groups ($P < 0.05$, $P < 0.01$ ANOVA; Bonferroni correction) (Table 1).

Spinal BMD and bone mineral content (BMC) rose in all groups (Tables 3 and 5). Percentage changes in BMD and BMC in the post-menopausal women and secondary osteoporotics were not significantly different (Fig. 1). There was no change in spinal area (L2–L4) between baseline and 12 months in either the post-menopausal or

Table 5 Measures of bone mineral in 10 male osteoporotic patients at baseline and 12 months

	0	12 months	Significance
Spinal BMD	0.795 ± 0.034	0.867 ± 0.033	$P < 0.005$
BMC	34.73 ± 2.29	38.35 ± 2.38	$P < 0.005$
Femoral BMD	0.800 ± 0.043	0.806 ± 0.041	NS
BMC	4.31 ± 0.245	4.32 ± 0.204	NS

Wilcoxon signed rank test (mean ± SEM).
BMD, Bone mineral density (g/cm²); BMC, bone mineral content (g hydroxyapatite).
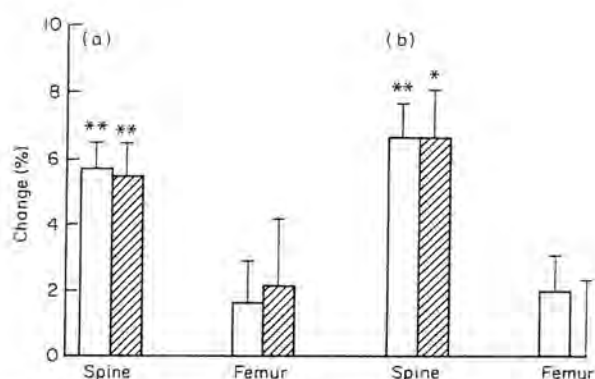
Fig. 1 Percentage changes in ▨, BMC and ☐, BMD in a, post-menopausal women and b, secondary osteoporotics following 12 months of therapy. *$P < 0.005$; **$P < 0.0001$.

secondary osteoporotic groups (37.25 ± 0.65 vs $37.20\,cm^2$ ± 0.61; 38.9 ± 1.04 vs $38.85\,cm^2 \pm 0.98$). There was no significant difference between percentage increase in spinal BMD (ANOVA $F = 0.906$) or spinal BMC (ANOVA $F = 1.557$) between groups (Figs 1 and 3). There was no significant change in femoral neck BMC or BMD in any of the groups studied (Tables 3 and 5). As femoral Z score in the male group was significantly higher than in the female groups they were not compared.

Baseline spinal BMD was significantly lower in the steroid group compared with the post-thyrotoxicosis and post-surgical menopause groups (ANOVA, Bonferroni correction
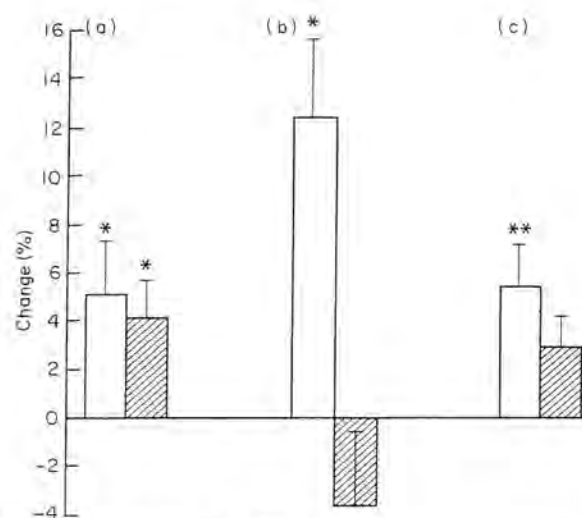
Fig. 2 Percentage changes in BMD in secondary osteoporotics. ☐, Spine; ▨, femur. a, Post thyrotoxicosis ($n = 8$); b, steroid therapy ($n = 7$); c, surgical menopause ($n = 13$). *$P < 0.05$; **$P < 0.01$.
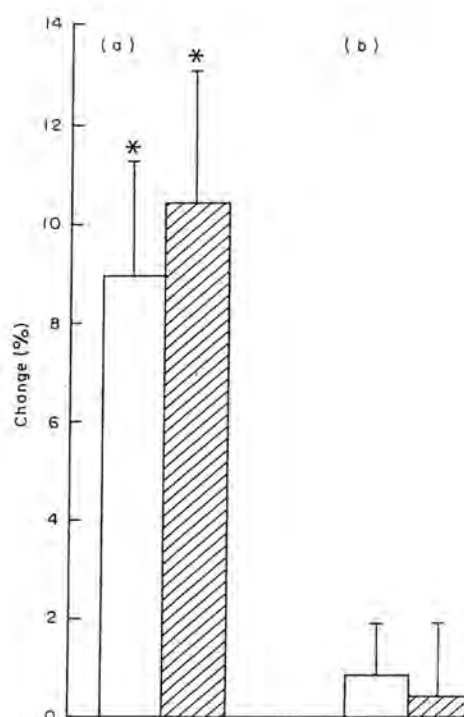
Fig. 3 Percentage changes in ▨, BMC and ☐, BMD in a, spine; b, femur in 10 male patients. *$P < 0.005$.

$P < 0.05$, $P < 0.01$) (Table 4). Femoral neck BMD at baseline was also significantly lower in the steroid group compared with the post-surgical menopause group, but not the post-thyrotoxicosis group (ANOVA, Bonferroni correction $P < 0.05$) (Table 4). Spinal BMD increased in all sub-groups of secondary osteoporosis (Table 4). Percentage changes in spinal BMD were not significantly different in the sub-groups of secondary osteoporosis (ANOVA $F = 2.786$) (Fig. 2). However, there was a significant difference between percentage changes in femoral neck BMD between groups (ANOVA $F = 4.18$, $P < 0.05$) (Fig. 2) with a significant increase in the post-thyrotoxicosis group ($P < 0.05$) and a 'borderline' increase in the early surgical menopause group ($P = 0.052$) (Fig. 2, Table 4). Both groups were significantly different from the steroid group ($P < 0.05$, $P < 0.05$ ANOVA, Bonferroni correction). No patient suffered an extra-axial fracture during the study period. We have no data on spinal fracture rate.

Discussion

The increase in spinal BMD and BMC in post-menopausal women and secondary osteoporotics were comparable and significantly different from baseline. The mean increases in

BMD and BMC in both groups were similar and the mean spinal areas (L2–L4) were unchanged. This indicates a real increase in bone mineral and not an artefactual increase in BMD produced by further vertebral collapse.

In the two major studies previously referred to (Storm *et al.*, 1990; Watts *et al.*, 1990) the former quoted a 5·3% increase in spinal BMC at 3 years and the latter a 5·2% increase in BMD at 2 years. A recent study (Miller *et al.*, 1991) has shown a 15·7% increase in spinal BMD over 2 years in 47 post-menopausal women treated with a similar regimen to that of Watts *et al.* (1990) except that they may have received a higher dose of calcium and vitamin D (total daily calcium intake 1500 mg/vitamin D 400–800 IU). A subsequent similar study (Silberstein *et al.*, 1992) has reported a mean increase of 6·6% in spinal BMD at 12 months, despite removing 15 of 42 patients from analysis due to technical difficulties in measuring BMD in spondylotic spines and 3 patients for not responding to treatment. All crushed vertebrae were excluded from analysis. They reported a mean increase in femoral neck BMD of 4·8% in 28 of 42 patients who 'responded' to treatment, with a fall in femoral neck BMD of 3·9% in the 14 'non-responders'. Watts *et al.* (1990) excluded from analysis any vertebra which suffered a crush fracture either at baseline or during the study. Their results show a greater than 1% increase in spinal BMD in the control group which is contrary to the well recognized decline in spinal BMD in post-menopausal osteoporotics shown in longitudinal studies. This increase in the control group was not found by Storm *et al.* (1990) who did not exclude any vertebra from analysis and quoted spinal BMC. Watts's regimen was similar to Storm's except for phosphate pretreatment (2 g per day for 3 days) to stimulate 'osteoblast activity' prior to the commencement of etidronate. Both studies showed evidence of a reduction in the incidence of spinal fractures compared with controls. No consistent increase in femoral BMD was found by Watts *et al.* (1990) and all three femoral neck fractures which occurred in the study period were in the two treatment groups. Storm *et al.* (1990) did not report any hip data.

We have found no overall changes in femoral neck BMD or BMC at one year. However, there appeared to be a small increase for patients with previous thyrotoxicosis, with a value of borderline significance for those with an early post-surgical menopause. The lack of any significant change in bone mass at the femoral neck could be interpreted as a beneficial effect in view of the expected bone loss at this site in most of the patients studied. The less marked benefit of anti-resorptive therapy on the femoral neck may result from the lower percentage of trabecular bone and higher percentage of cortical bone in the femoral neck, compared with the vertebrae. Evidence suggests that cortical osteo-

clasts are less sensitive to etidronate than trabecular osteoclasts (Chappard *et al.*, 1991).

In conclusion, cyclical disodium etidronate given with high dose calcium supplements results in a significant increase in spinal bone mineral density and content in post-menopausal osteoporotics, women with secondary osteoporosis and male osteoporotics. The increase may be greater than that produced by a lower daily dose of calcium, but direct comparisons between studies is not possible. The impact of this treatment regimen on fracture rate is not known.

References

Baran, D.T. & Braverman, L.E. (1991) Editorial: Thyroid hormones and bone mass. *Journal of Clinical Endocrinology and Metabolism*, **72**, 1182–1183.

Boonekamp, P.M., van der Wee-Pals, L.J.A., Van Wiik-vanLennep, M.M.L., Thesing, C.W. & Bijvoet, O.L.M. (1986) Two modes of action of bisphosphonates on osteoclastic resorption of mineral matrix. *Bone Mineral*, **1**, 27–39.

Bressot, C., Meunier, P.J., Chapuy, M.C., Lejeune, E., Edouard, C. & Darby, A.J. (1979) Histomorphometric profile, pathophysiology and reversibility of corticosteroid-induced osteoporosis. *Metabolic Bone Related Research*, **1**, 303–311.

Carano, A., Teitelbaum, S.L., Konsek, J.D., Schlesinger, P.H. & Blair, H.C. (1990) Bisphosophonates directly inhibit the bone resorption activity of isolated avian osteoclasts *in vitro*. *Journal of Clinical Investigation*, **85**, 456–461.

Chappard, D., Petitjean, M., Alexandre, C., Vico, L., Minaire, P. & Riffat, G. (1991) Cortical osteoclasts are less sensitive to etidronate than trabecular osteoclasts. *Journal of Bone and Mineral Research*, **6**, 673–679.

Consensus Development Conference (1987) Prophylaxis and treatment of osteoporosis. *British Medical Journal*, **295**, 914–915.

Eastell, R., Delmas, P.D., Hodgson, S.F., Eriksen, E.F., Mann, K.G. & Riggs, B.L. (1988) Bone formation in older normal women: concurrent assessment with bone histomorphometry, calcium kinetics and biochemical markers. *Journal of Clinical Endocrinology and Metabolism*, **67**, 741–748.

Jensen, G.F., Christiansen, C., Boesen, J., Hegedüs, V. & Transbol, I. (1983) Relationship between bone mineral content and frequency of postmenopausal fractures. *Acta Medica Scandinavica*, **213**, 61–63.

Khokher, M.A. & Dandona, P. (1989) Diphosphonates inhibit human osteoblast secretion and proliferation. *Metabolism*, **38**, 184–187.

Meunier, P.J., Dempster, D.W., Edouard, C., Chapuy, M.C., Arlot, M. & Charhon, S. (1984) Bone histomorphometry in corticosteroid-induced osteoporosis in Cushing's syndrome. *Advanced Experimental Medical Biology*, **171**, 191–200.

Miller, P.D., Neal, B.J., McIntyre, D.O., Yanouver, M.J., Anger, M.S. & Kowalski, L. (1991) Effect of cyclical therapy with phosphorus and etidronate on axial bone mineral density in postmenopausal osteoporotic women. *Osteoporosis International*, **1**, 171–176.

Nordin, B.E. & Morris, H.A. (1989) The calcium deficiency model for osteoporosis. *Nutrition Reviews*, **4**, 65–72.

Nordin, B.E., Need, A.G., Chatterton, B.E., Horowitz, M. & Morris, H.A. (1990) The relative contributions of age and years since menopause to postmenopausal bone loss. *Journal of Clinical Endocrinology and Metabolism*, **70**, 83–88.

Nordin, B.E., Need, A.G., Morris, H.A., Horowitz, M. & Robertson, W.G. (1991) Evidence for a renal calcium leak in postmenopausal women. *Journal of Clinical Endocrinology and Metabolism*, **72**, 401–407.

Reginster, J.Y., Deroisy, R., Denis, D., Collette, J., Lecart, M.P., Sarlet, N., Ethgen, D. & Franchimont, P. (1989) Prevention of postmenopausal bone loss by Tiludronate. *Lancet*, **ii**, 1469–1471.

Reid, I.R., Alexander, C.J., King, A.R. & Ibbertson, H.K. (1988) Prevention of steroid-induced osteoporosis with (3-amino-1-hydroxypropylidene)-1,1-bisphosphonate (APD). *Lancet*, **i**, 143–146.

Silberstein, E.B. & Schnur, W. (1992) Cyclic oral phosphate and etidronate increase femoral and lumbar bone mineral density and reduce lumbar spine fracture rate over three years. *Journal of Nuclear Medicine*, **33**, 1–5.

Storm, T., Thamsborg, G., Steiniche, T., Genant, H.K. & Sørensen, O.H. (1990) Effect of intermittent cyclical Etidronate therapy on bone mass and fracture rate in women with postmenopausal osteoporosis. *New England Journal of Medicine*, **322**, 1265–1271.

Truscott, J.G., Oldroyd, B., Simpson, M., Stewart, S.P., Westmacott, C.F., Milner, R., Horsman, A. & Smith, M.A. (1993) Variation in lumbar spine and femoral neck bone mineral measured by dual energy X-ray absorption: a study of 329 normal women. *British Journal of Radiology*, **66**, 514–521.

Watts, N.B., Harris, S.T., Genant, H.K., Wasnich, R.D., Miller, P.D., Jackson, R.D., Licata, A.A., Ross, P., Woodson, G.C., Janover, M.J., Mysiw, W.J., Kohse, L., Rao, M.B., Steiger, P., Richmond, B. & Chesnut, C.H. (1990) Intermittent cyclical etidronate treatment of postmenopausal osteoporosis. *New England Journal of Medicine*, **323**, 73–79.

Wronski, T.J., Yen, C-F. & Scott, K.S. (1991) Estrogen and Disphosphonate treatment provide long-term protection against osteopenia in ovariectomized rats. *Journal of Bone and Mineral Research*, **6**, 387–394.

A portable system for measuring bone mineral density in the pre-term neonatal forearm

[1]J G TRUSCOTT, MSc, CPhys, [1]R MILNER, [2]P C HOLLAND, MBBS, FRCP, [2]C WOOD, MBBS, MRCP and [1]M A SMITH, PhD, FInstP

[1]Centre for Bone and Body Composition Research, University of Leeds, Wellcome Wing, and [2]Department of Paediatrics, Clarendon Wing, The General Infirmary, Leeds LS1 3EX

Abstract

Current systems used to measure bone mineral content (BMC) in the neonate have the major drawback that the child must be well enough to be moved to the scanner. Consequently, low birth weight pre-term neonates, a group at particular risk of mineral compromise, cannot be measured. This paper describes a portable neonatal bone mineral device capable of measuring bone mineral in the incubator. It uses a radiation sensitive, charge coupled device (CCD) to acquire a bone mineral image enabling bone mineral to be measured at various sites. It measures bone mineral density (BMD) with a precision of 5.5 mg cm^{-2} *in vivo*, reduced to 7.5 mg cm^{-2} when repositioning between scans is taken into account. The procedure takes under 5 min with an image acquisition time of 30 s and an absorbed radiation dose to skin of 6 µSv. Calibration has been undertaken with aluminium foils of differing thickness to confirm the linearity of the system throughout the intended measurement range. A regression line fitted to the data demonstrated linearity and correlation between BMD and aluminium thickness with $r = 0.99$ ($p < 0.0001$). Preliminary measurements on pre-term neonates show values of BMD ranging from 43 to 115 mg cm^{-2} in babies aged 23–41 weeks post-conception. These figures are within the linear range of the system.

Improvements in neonatal intensive care have resulted in increased survival rate of very premature babies of less than 28 weeks gestation. The incidence of osteopenia of prematurity has been shown to be in excess of 50% in these particular infants [1]. This high incidence may be explained by the fact that the fetal skeleton is most intensively mineralized during the third trimester of pregnancy when about 70% (30 g) of calcium may be incorporated [2, 3]. This means that the very premature infant tends to have low bone mineral content (BMC). Conventional feeding regimes lead to far lower mineral accretion rates than those achieved *in utero* [4]. Because of the need to understand and overcome this problem both calcium metabolism and skeletal mineralization of the human fetus and neonate have been the subject of intensive study [5] but the lack of a simple, accurate and safe means of determining BMC has been a limiting factor in progress in the field.

For many years radiography was used but radiographs appear normal until a deficit in BMC of the order of 20% is present [6]. Lack of consistency in sequential radiographs due to variations in both exposure and development parameters mean that this technique is unsuitable for following infants undergoing different nutritional regimes. The application of photon absorptiometry to the determination of BMC in infants by Steichen et al [7] in 1978 was a major advance in the

field as it allowed the direct measurement of bone mineral content without the intermediate use of film with all its problems.

Neonatal bone, even at term, contains only relatively small amounts of mineral, typically 0.2 g cm^{-2} [8]. To measure these very small amounts of mineral, we built and validated the first machine designed specifically to measure the very small bones in the neonatal forearm [9]. Using this instrument we then went on to define osteopenia of prematurity [10], to describe the pace of mineral incorporation into bone *in utero* [11] and also after birth [12]. This system also allowed us to measure mineralization in a number of pathological conditions [13] and different nutritional regimes [14]. Prior to this we described the apparent resolution of osteopenia of prematurity in pre-term babies [15]. One major problem with this study was that the babies had to be well enough to be moved to the measuring instrument. The size of the samples and sensitivity of the instrument meant that a difference of less than or equal to 15% between normal term and premature babies at 71 weeks post-conception would not have been statistically significant. This latter problem could have been addressed by increasing the size of the study groups but the problem of moving the babies to the scanner proved more intractable. The sickest pre-term babies were not and could not be included in our studies using the, then, current technology. These babies, typically, fail to thrive and have mineralization patterns markedly different from those of premature babies who are well at birth and normal for dates.

Lyon et al [16] reported a system for the measurement of bone mineral in babies who were ill enough to warrant intensive care. This system required the observer to obtain two X-ray films of the forearm at 40 kV and 120 kV using a mobile X-ray unit. The films were subsequently digitized using a light box and video camera and a form of dual energy X-ray absorptiometry was carried out. More recently Williams et al [17] have been using this technique to measure premature babies in the incubator. Although offering a method which causes minimal disturbance to the baby, the problems associated with film radiography still affect this system and are reflected in the reproducibility in phantom measurements of between 6% and 9.2% noted by the authors. This technique underestimates the value of bone mineral in phantom sets by between 15.6% and 18.5%. They also give no suggestions as to why this inconsistency in the underestimate occurs, but it is obviously a major problem with this technique. All estimates of reproducibility and accuracy are based on phantom work and one would anticipate that these values would deteriorate *in vivo*.

This paper describes a new measurement instrument which is: (1) portable; (2) compact enough to be placed in the incubator; (3) fast enough in operation to cause minimal disturbance to the neonate; (4) capable of imaging a section of the forearm in a reproducible manner; (5) low dose enough to allow measurements to be made at frequent intervals. Apart from the obvious advantages in the solution of the problem which made the design desirable, several other advantages accrue. As we can measure a neonate almost immediately after birth we should be able to separate the maternal *in utero* effects on mineralization, such as placental insufficiency, from the environmental effects experienced *post-partum*. Such a system would also allow the effects of differing nutritional regimes to be assessed whilst the baby is in the incubator. Similarly the effects of various therapies, on bone, could be monitored at regular intervals.

Apparatus
Equipment design
It is usual for forearm bone mineral scanners to measure bone mineral across a region, often scanning a larger region to identify an appropriately reproducible site. In adults, the point of separation between the distal radius and ulna has often been used. In neonates, little is known about mineralization along the bones of the forearm and so we had no preconceived notion about the optimum site for measurement, both in terms of reproducibility or clinical value. For this reason it was felt that it would be ideal to obtain a map of bone mineral values of a relatively large proportion of the distal forearm.

The equipment was developed using a radiation sensitive charge coupled device (CCD) camera which offered the following advantages:

(1) A two-dimensional (2D) image of bone mineral content of the distal and mid-forearm could be obtained.

(2) No scanning mechanism and so no moving parts would be involved. Thus the technology could be robust enough to be portable within a neonatal intensive care unit.

(3) The device could be sufficiently compact to fit into an incubator.

(4) The sensitivity of radiation sensitive CCDs would allow sufficient data to be acquired in 1 or 2 s with a low radiation dose [18].

The block diagram for the system is shown in Figure 1. Photons are produced at 27.5 keV by the decay of an ^{125}I point source of half life 60 days. A cone beam of photons from the source is passed through the baby's forearm which is held in a water bolus between two parallel sheets of Perspex. Photons are differentially absorbed by bone of varying mineral content and hence the photon beam falling on the front part of the detector has different intensities per unit area. Each of these intensities will be inversely proportional to the bone mineral in the beam.

A bone mineral equivalent image can be calculated on a pixel by pixel basis by the application of the equation:

$$M_B = [\rho_B/(\mu_B\rho_B - \mu_S\rho_S)] \ln(I_O/I). \quad (1)$$

where μ_B and μ_S are the mass attenuation coefficients for bone mineral $(3.1704 \text{ cm}^2 \text{ g}^{-1})$ and water/soft tissue $(0.48016 \text{ cm}^2 \text{ g}^{-1})$ respectively. ρ_B and ρ_S are the density values for bone mineral $(3.225 \text{ g cm}^{-3})$ and water/soft tissue (1.0 g cm^{-3}) respectively. I is the photon intensity of an image pixel of the sample. I_O is the photon intensity in the same pixel through the water bolus alone. M_B represents bone mass per unit area and is in units of g cm^{-2} above the soft tissue/background level (which is an arbitrary baseline).

To calculate BMC (grams) the bone image must be integrated within a region of interest (ROI) and an equivalent area in the non-bone background subtracted. The area normalized BMC (BMD) can then be calculated by dividing the BMC by the area of the ROI. Because of the mass attenuation coefficient used these values are in grams of hydroxyapatite.

Most other single photon absorptiometry (SPA) adult forearm BMC techniques do not use two separate acquisitions. In this system the I_O data are acquired mainly to compensate for the different radiation path length which results from using a point source with a 2D detector array rather than a single collimated detector. Consequently, with a sample of uniform thickness in the beam, the acquired image of the signal intensity would be maximum at the centre and gradually decrease radially towards the edge of the image. This is due to the increase in radiation path length with distance from the centre (the inverse square law effect) coupled with an increase in sample thickness as the radiation beam passes through with increasing obliquity. The contribution of both these effects could be calculated mathematically from the precise geometry of the apparatus and correction could be made to the image. However, it was felt
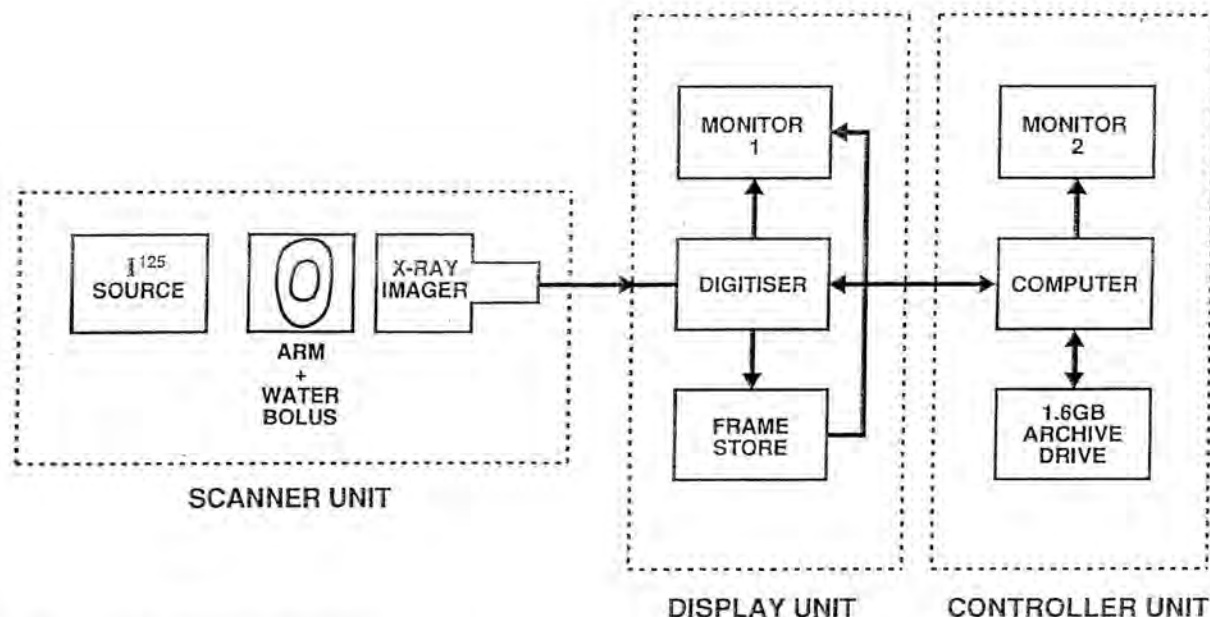
Figure 1. Block diagram of apparatus.

that the use of an I_0 image would be more reliable for longitudinal studies as the precise equipment geometry could change over a long time period.

Equipment construction

A Photonic Science X-ray Imager is used; this is a high performance X-ray sensitive video camera, consisting of a thin polycrystalline layer of gadolinium oxysulphide on a fibre optic substrate, optically coupled to a high resolution, low light level, intensified CCD imager. The active imaging area is a 50 mm diameter circle and the captured image region is a rectangular region 40 mm wide by 30 mm deep. A thin aluminium foil in front of the gadolinium oxysulphide scintillator makes the imager light-tight allowing operation under normal ambient lighting conditions. Using an image intensifier and coherent fibre optic components the image is transferred from the scintillator to a solid state (CCD) image sensor.

The camera electronics produce an output signal in the form of a monochrome composite video signal of 1 volt peak to peak into a 75 Ω load complying with Comité Consultatif Internationale de Radiodiffusion (CCIR) video standards. This video signal provides the input to a Data Translation DT2867 integrated image processor and precision frame grabber with a 16 bit full image buffer (Data Translation, Marlboro, MA, USA). This card, which is controlled by a 80486 personal computer running at 66 MHz, is capable of real time image capture. We use it to capture images of 768 pixels across a video scan line and 512 pixels (lines) in the frame with an effective pixel size of 52 μm square, from which we use a region of 32 mm by 24.5 mm. The digital image may be viewed in real time before data accumulation takes place. When positioning is satisfactory a simple

button press will start data collection by adding captured frames to the frame store until an image with sufficient detail is obtained. These data are then stored as a 16 bit image file and archived on a 1.6 GB hard disk drive for later analysis; an image of the water bolus on its own is also captured and stored for use as background in the calculation of a bone mineral image. The specification for this system was determined after a previously reported feasibility study [18].

The internal construction of the system is shown diagrammatically in Figure 2 and illustrated in Figure 3(a). The ^{125}I source, 2 mm diameter, of initial activity 200 mCi, is held in a shielded container. In front of the container is a simple shutter operated by a self contained subminiature time delay relay unit controlled by a timer dial and push button shutter release. The source, which has a half life of 60 days, is renewed at 120 day intervals. Constant path length is maintained by the Perspex sided forearm and bolus holder located between the source and the camera. Source-to-detector distance is 9 cm and the source-to-sample distance is approximately 6.2 cm with 3.5 cm between the faces of the forearm holder. The bolus is a water filled condom which is wrapped around the forearm. It fills the space between the Perspex sides of the positioning device. An air gap between the positioning device and the detector minimizes the effect of scatter in the image. The video output, camera power and control signals are coupled between computer and instrument via an insulated cable at the rear of the unit. Electrical construction and safety are consistent with IEC 601/1 and comply with all regulations for safety of the patient and operator. In use, the instrument is encased in a non-conducting Perspex casing giving electrical isolation to both user and subject. The size of the instrument is 52 cm by 20 cm. The controlling computer

534
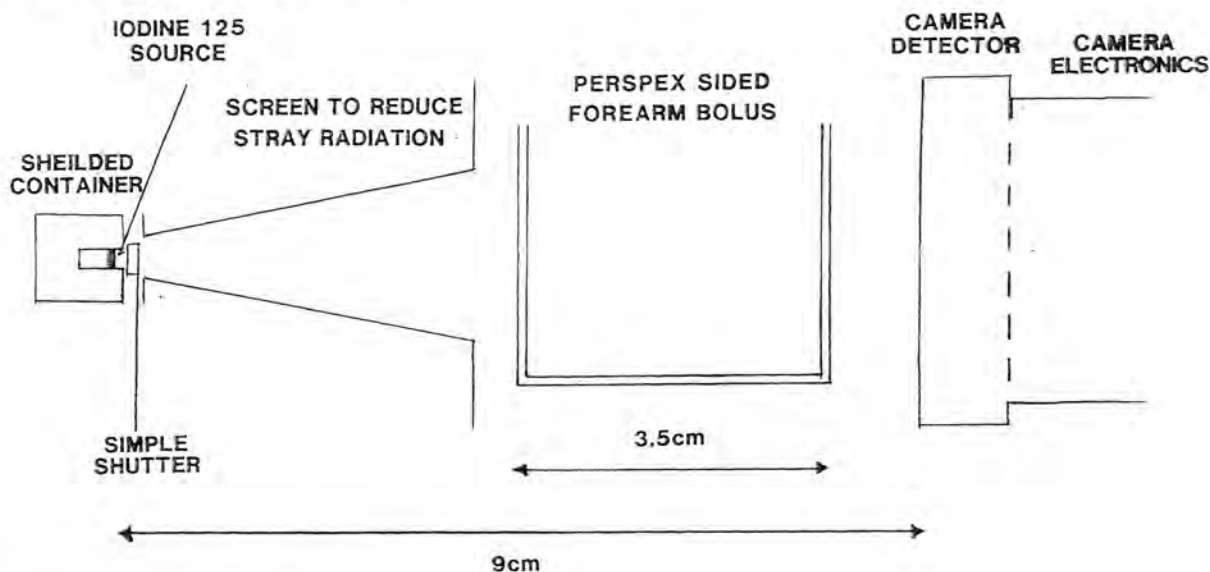
Figure 2. Diagram of apparatus design.
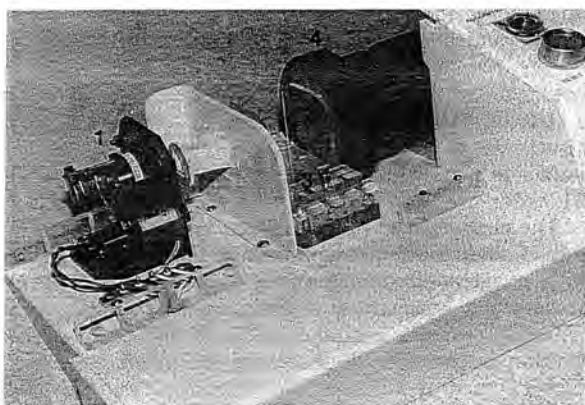
Figure 3. (a) Photograph of apparatus without protective cover. [125]I source container (1), shutter (2), bolus holder (3), camera (4). (b) Photograph of apparatus in incubator with baby.

is an IPC Porta PC P5-486 with docking station (IPC Corporation (UK), Lancashire, UK) having a footprint of 37 cm by 27 cm working into a Panasonic 5 inch monochrome monitor of size 15 cm by 25 cm (Matsushita Electric Industrial Co. Ltd, Osaka, Japan). This compact controlling system is mounted on a small trolley to improve mobility. The scanner is shown in use in an open incubator in Figure 3b, where it may be seen how compact the instrument is. This figure shows an open incubator in order not to obscure the view of the instrument in use. It is equally functional in a closed incubator.

Data acquisition software, which controls both the camera and the DT2867 frame grabber and frame store, was supplied by Photonic Science, the manufacturer of the X-ray imager. The software allows the user to specify

real time viewing of the video image on the monitor, thus permitting the positioning of the forearm before data collection is commenced. Data collected are specified as a number of consecutive "grabbed" video frames added into the frame store. Any number of frames between one and 9999 may be specified but the user should be careful that no pixels overflow (they have a 16 bit limit). Once a satisfactory image is obtained it may be named and saved to disk. Files are later transferred to an archive and analysis system based on a DAN 66 MHz 486 desk top PC system with 1.6 GByte hard drive.

Data analysis

A typical digital image is shown in Figure 4. Working on a pixel by pixel basis a bone mineral image is
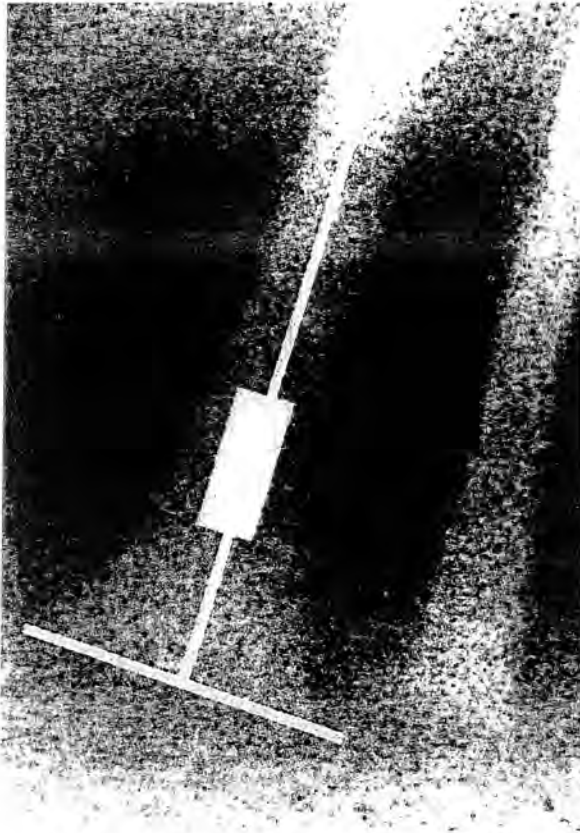
Figure 4. Bone mineral image with cursor positioned for data analysis.

calculated and, if required, displayed. Visible bone parts of the image are actually the mineralized section of the radius and ulna. Bone mineral values can be obtained by integrating through an ROI placed in this mineralized section. Currently we are investigating methods for placing the ROI and as a guide have developed a "T" shaped cursor which the operator can place with the bar of the "T" at the end of the mineralized portion of the radius and the tail of the "T" along the axis of the bone as shown in Figure 4. The operator can then opt to position the ROI either at a fixed distance from the end of the bone or at a percentage of the bone length from its end. The length of the radius can be calculated by measuring the palpated distance between the ulnar styloid process and the olecranon and applying the regression equation established by James et al [9]. Results in this paper have been obtained using an ROI 1.5 mm × 5 mm located 1 cm from the mineralized end of the radius axial to the shaft.

Calibration and preliminary validation

The system was checked for linearity in the biological range of interest by measuring aluminium foil. Differing numbers of pieces of 15 μm thick aluminium foil were placed in a water bath in the scanner, measures of its

thickness were obtained, and BMD equivalent values were calculated. These are shown plotted against the number of foils in Figure 5. Linear regression analysis applied to these points demonstrated a correlation coefficient of 0.999 ($p < 0.0001$) indicating a high degree of linearity in the mineral range of interest.

The reproducibility of the system was measured *in vivo* by two experiments. In the first of these two consecutive measurements were made on a set of 20 subjects without repositioning the forearm between scans. In the second, 16 subjects were scanned twice with the arm being removed from the system between scans. The precision was then calculated for each case using the method outlined by Bland [19]. This gave values of 5.5 mg cm^{-2} (8%) and 7.5 mg cm^{-2} (11%) respectively. The whole measurement procedure for a single scan took 5 min of which 30 s was patient acquisition time.

The absorbed radiation dose to skin associated with a single acquisition is approximately 6 μSv. This dose was calculated based on an air kerma rate of 30 μGy h^{-1} GBq^{-1} at 1 m [20] which allows for both γ and X-radiation. It should be remembered that this dose is given to a small portion of the forearm when comparing it with the typical dose for a paediatric chest X-ray of 40 μGy. As the forearm contains only skin, bone and muscle and the beam impinges on a very small region of the forearm the effective dose to the subject is negligible.

After establishing this linear relationship and the precision of the system we went on to measure pre-term babies at a range of gestational ages from 23 weeks to 41 weeks.

The measurement procedure was well tolerated by the babies studied. All measurements were made at less than 48 h of age and included babies of extreme prematurity undergoing mechanical ventilation. None of them showed any physiological evidence of distress or deterioration in their condition during the image collection. Despite their requirement for intensive care, the most immature babies were often easier to measure than their more mature counterparts as they tended to be less active. More active babies required more patience to
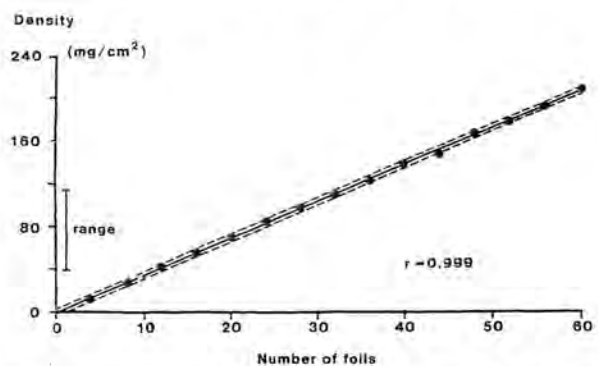
Figure 5. Theoretical bone mineral equivalent using aluminium foils *versus* calculated BMD. The horizontal dotted lines indicated the approximate range of BMD values for neonates.

10. JAMES, J R, CONGDON, P J, TRUSCOTT, J ET AL, Osteopenia of prematurity, *Arch. Dis. Child.*, *61*, 871–876 (1986).

11. RYAN, S, CONGDON, P J, JAMES, J ET AL, Mineral accretion in the human fetus, *Arch. Dis. Child.*, *63*, 799–808 (1988).

12. HORSMAN, A, RYAN, S W, CONGDON, P J ET AL, Bone mineral content and body size 65 to 100 weeks postconception in preterm and full term infants, *Arch. Dis. Child.*, *64*, 1579–1586 (1989).

13. RYAN, S W, VARIEND, S, JAMES, J ET AL, Mineral content of rib bone in infant deaths, *Arch. Dis. Child.*, *63*, 848–850 (1988).

14. HORSMAN, A, RYAN, S W, CONGDON, P J ET AL, Bone mineral accretion rate and calcium intake in preterm infants, *Arch. Dis. Child.*, *64*, 910–918 (1989).

15. CONGDON, P J, HORSMAN, A, RYAN, S W ET AL, Spontaneous resolution of bone mineral depletion in preterm infants, *Arch. Dis. Child.*, *65*, 1038–1042 (1990).

16. LYON, A S, HAWKES, D J, DORAN, M ET AL, Bone mineralisation in preterm infants measured by dual energy radiographic densitometry, *Arch. Dis. Child.*, *64*, 919–923 (1989).

17. WILLIAMS, J R, DAVIDSON, F, MENON, G and McINTOSH, N, A portable dual energy X-ray absorptiometry technique for the measurement of bone mineral in preterm infants, *Paediatr. Res.*, *36*, 351–357 (1994).

18. TRUSCOTT, J G, MILNER, R, METCALFE, S and SMITH, M A, The use of a radiation sensitive CCD camera system to measure bone mineral content in the neonatal forearm: a feasibility study, *Phys. Med. Biol.*, *37*, 1391–1397 (1992).

19. BLAND, M, *An Introduction to Medical Statistics* (Oxford University Press, Oxford), pp. 276–278 (1993).

20. INTERNATIONAL COMMISSION ON RADIOLOGICAL PROTECTION, *Protection Against Ionising Radiation From External Sources Used in Medicine, Publication No 35* (Pergamon Press, Oxford) (1981).

S. Fletcher[a]
R.G. Jones[b]
H.C. Rayner[a]
P. Harnden[b]
L.D. Hordon[c]
J.E. Aaron[d]
B. Oldroyd[c]
A.M. Brownjohn[a]
J.H. Turney[a]
M.A. Smith[c]

[a] Department of Renal Medicine,
[b] Institute of Pathology, General Infirmary at Leeds,
[c] Centre for Bone and Body Composition Research, and
[d] Department of Human Biology, University of Leeds, UK

Assessment of Renal Osteodystrophy in Dialysis Patients: Use of Bone Alkaline Phosphatase, Bone Mineral Density and Parathyroid Ultrasound in Comparison with Bone Histology

Abstract
Bone biopsies were studied in 73 patients to determine if a two-site radio-immunometric assay for serum bone alkaline phosphatase (BAP), total serum alkaline phosphatase (ALP), serum intact parathyroid hormone (iPTH), hand X-rays, regional bone mineral density (BMD) measurements and parathyroid enlargement detected by ultrasonography could accurately predict renal osteo-dystrophy. In the patients studied 57 had hyperparathyroid bone disease, 4 mixed renal osteodystrophy, 3 adynamic bone disease, 1 osteomalacia and 8 normal histology. Serum BAP, ALP and iPTH correlated positively with mineral apposition rate, osteoblastic, osteoid and eroded surface. In the diagnosis of hyperparathyroid bone disease serum iPTH was the most sensitive investigation, detecting 81% of patients at a level >100 pg/ml but with a specificity of only 66%. Serum BAP was more sensitive, 70% at a level of >10 ng/ml, than serum total ALP, 30% at a level of 300 IU/l, with similar specificities, 92 and 100%, respectively. Ultrasound detection of an enlarged parathyroid gland had a sensitivity of 64% and a specificity of 100% for the diagnosis of hyperparathyroid bone disease. Hand X-rays had a poor sensitivity, 47%, but a high specificity, 92%, for the detection of hyperparathyroid bone disease. The majority of patients had regional BMD values within the normal reference range and this test was of poor discriminatory value. The non-invasive markers were unable to distinguish between patients with low turnover, mild hyperparathyroidism and patients with normal histology. In conclusion the measurement of serum iPTH is a useful screening tool for the detection of hyperparathyroid bone disease which can be confirmed by the finding of a raised serum BAP or parathyroid enlargement. For definitive diagnosis, however, the gold standard remains bone biopsy and at present one cannot recommend any non-invasive method as an adequate substitute.

Introduction

Bone disorders resulting from abnormalities in mineral metabolism are common in patients with renal disease, and their diagnosis and treatment remains a considerable challenge to clinical nephrologists [1]. A reliable diagnosis of metabolic bone disease can be obtained from a transiliac bone biopsy, but this is an invasive procedure unsuited for repeated routine use. Biochemical and radiological investigations are used to try to identify high and low turnover renal osteodystrophy (ROD). Hand X-rays, despite their poor sensitivity, have traditionally been used to detect hyperparathyroid bone disease [2]. Serum intact parathyroid hormone (iPTH), even though not a direct product of bone metabolism, is currently accepted as the most clinically useful marker of high turnover ROD [3, 4]. Adynamic bone disease, which is being diagnosed with increasing frequency in chronic renal failure, is particularly difficult to establish with traditional markers of bone turnover [5, 6]. The inability to diagnose metabolic bone disease accurately in uraemic patients from serum biochemistry has led to continuing work to develop plasma markers of bone turnover. Serum osteocalcin and collagen breakdown products are renally excreted and although they accurately predict bone turnover in non-renal and pre-dialysis patients, due to the interference of breakdown products their use is limited in dialysis patients [7, 8].

Alkaline phosphatase (ALP), a product of osteoblasts, has a long history as a marker of bone turnover in metabolic bone disease [9]. Common routine measurement of serum total ALP lacks specificity for bone disease due to the inclusion of the activity of all isoenzymes, principally from liver, bone, gut and kidney in biochemical assays [10]. Serum bone-specific alkaline phosphatase (BAP) has shown a greater correlation with abnormal histology in renal failure than serum total ALP [11], but the accurate measurement of specific isoenzymes has required complicated separation techniques based upon electrophoresis, whereas more routine methods of isoenzyme separation, including thermal stability, have provided only a qualitative differentiation of limited clinical value [12–14]. The recent development of a direct radio-immunoassay, using two monoclonal antibodies to BAP, enables a more precise assessment of osteoblastic activity [15].

The aim of the present study is to determine the relative efficacy of certain non-invasive techniques to diagnose renal bone disease using histologically and histomorphometrically defined bone biopsies. In particular, the use of BAP as a plasma biochemical index of bone forma-

tion, regional bone mineral density (BMD) measurement, hand X-ray analysis, and ultrasound examination of the neck for parathyroid enlargement was evaluated.

Subjects and Methods

Patients

Seventy-three patients (39 male; 34 female) were recruited, in this cross-sectional study, from the dialysis units of Leeds General Infirmary and St. James's University Hospital (age range 23–78 years, median 48; time on dialysis 0–14 years, median 3). All patients were medically stable with no changes in therapy for at least 6 months prior to their biopsy. In the 3 months preceding their biopsy there was no change in the dosage or method of administration of vitamin D, although there were minor modifications of dietary phosphate and phosphate binders. Bone biopsies were performed on 39 patients with a known elevated serum iPTH, 32 prior to entering a trial of pulsed calcitriol, and 7 at the time of parathyroidectomy. Thirty-three patients were biopsied when an opportunity arose for a general anaesthetic, 19 at the time of transplantation, 9 when peritoneal dialysis catheters were inserted or repositioned, and 5 at the time of miscellaneous operations unrelated to dialysis. A single patient with clinical features of chronic aluminium overload and a positive desferrioxamine stimulation test was biopsied to assess the severity of aluminium deposition prior to treatment. Forty-six patients were on peritoneal dialysis and 28 were on haemodialysis. Table 1 lists the causes of end-stage renal failure in the subjects. All patients gave informed consent and the study was approved by the local Ethics Committees of both hospitals.

Bone Histology

Anterior iliac crest bone biopsies were taken from the 73 patients, 20 of whom had received tetracycline double labelling; 250 mg of oxytetracycline was taken twice daily for 4 days, followed 10 days later by 150 mg of demeclocycline twice daily for 4 days, and bone biopsy 4 days later. Biopsies were taken using a Sheffield trephine with a 7-mm diameter bore (Bolton Surgical Services Ltd., Sheffield, UK). All patients were under general anaesthesia with 2% Marcaine locally infiltrated and a 100 mg diclofenac suppository for analgesia. Patients tolerated the procedure well but there was one case of persistent haemorrhage (which settled when packed) and two wound infec-

Table 1. Distribution of renal disease in the study population

Disease	n
Glomerulonephritis	18
Chronic interstitial nephritis	18
Diabetes	11
Hypertension and renovascular	10
Polycystic	9
Hereditary (Fabry's, Alport's)	4
Vasculitis	3

tions requiringantibiotics. All biopsies underwent histological examination, 57 were examined histomorphometrically, fragmentation during the collection process making the rest unsuitable for the latter procedure.

The tetracycline-labelled specimens were fixed immediately in 70% alcohol, while the remainder were fixed in 10% phosphate-buffered formalin, pH 7.3. Undecalcified specimens were dehydrated in alcohol, cleared in xylene and embedded in methyl methacrylate. Sections, 10 μm thick, were cut on a Jung k heavy duty microtome (Reichert-Jung, Heidelberg) and stained for histomorphometry [16] with either 1% toluidine blue stain for 30 min or a modification of the Goldner stain [4]. In addition, sections 5–7 μm thick were stained with 1% solochrome azurine, pH 5, for approximately 18 h for the identification and localisation of aluminium impeding the bone surface [17]. The relative surface extent of aluminium staining was subjectively assigned as <10% (normal-low Al deposition), 10–33% (low-moderate Al deposition), 33–60% (moderate-high Al deposition) and >60% (extensive Al deposition) [17]. Other sections were stained with haemoxylin and eosin for routine histological examination. Histomorphometry was possible on 57 biopsies using a semiautomatic image analysing system OsteoMeasure (OsteoMetrics Inc., Atlanta, USA) and an epifluorescence microscope with ultraviolet light for the analysis of the tetracycline labels. In addition to the relative bone area within each specimen, a comprehensive range of formation and resorption variables was measured without prior knowledge of the corresponding biochemistry. On the basis of the histology the biopsies were classified according to the following criteria:

(1) normal bone biopsies: no evidence of increased or decreased bone turnover and normal osteoid distribution and thickness;

(2) adynamic bone disease: low bone formation rate with flat osteoblasts, few osteoid seams and rare osteoclasts and resorption cavities;

(3) osteomalacia: low and diffuse uptake of tetracycline, wide and extensive osteoid seams from which cuboidal-shaped osteoblasts are often absent and rare osteoclasts and resorption cavities;

(4) mixed renal osteodystrophy: combination of osteomalacia and hyperparathyroidism with poor mineralisation and wide and extensive osteoid seams in conjunction with increased numbers of cuboidal-shaped osteoblasts, osteoclasts and resorption cavities indicative of hyperparathyroidism;

(5) hyperparathyroid bone disease: (a) mild – localised areas of increased osteoblastic and osteoclastic activity, a slight increase in osteoid tissue and resorption cavities but no evidence of peritrabecular fibrosis; (b) moderate – more general increase in osteoblastic and osteoclastic activity, with increased osteoid tissue, resorption cavities with clearly defined but limited peritrabecular fibrosis; (c) severe – extensive osteoblastic and osteoclastic activity with increased osteoid tissue, usually of normal thickness, resorption cavities which are increased in both extent and depth, areas of woven bone and extensive peritrabecular fibrosis.

Biochemical Analysis

The following biochemical measurements were made on stable patients under standard conditions: serum calcium, phosphate, bicarbonate, and total ALP (range 100–300 IU/l; BM Hitachi Autoanalyser, Boehringer Mannheim, Poole, Dorset, UK), serum iPTH (Nichols Institute, normocalcaemic range 11–55 pg/ml) and serum BAP (Tandem OSTASE Hybritech, San Diego, Calif., USA, reference range <19 ng/ml), serum aluminium (atomic absorption, Perkin-Elmer, reference range 0.00–1.85 μmol/l). Standard calcium was cal-

culated by the equation of Payne et al. [18]: Std Ca = Ca + (40 – albumin) × 0.025.

The samples were drawn from peritoneal dialysis patients immediately prior to their biopsy and for haemodialysis patients these samples were taken prior to dialysis. There was no significant difference in their serum calcium, phosphate, bicarbonate, total ALP and iPTH between these study samples and the routine pre-dialysis samples taken to monitor the adequacy of dialysis. In the 15 patients who underwent fine needle aspiration of their parathyroid glands, there was no significant difference between the biochemical values drawn prior to their gland aspiration and those taken prior to bone biopsy which was performed after the glands were sampled.

BMD Measurement

BMD of the lumbar spine (L2–L4), right femoral neck and total body were determined in 65 patients prior to biopsy, by dual energy X-ray absorptiometry (DEXA) using a Lunar DPX-L bone densitometer (Lunar Radiation Co., Madison, Wisc., USA). Software version 1.3y was used for analysis of spine and femoral neck with extended research mode selected for total body analysis. Results were expressed as Z scores, the number of standard deviations of the measured value from age- and sex-predicted normal values obtained from a local population, reference range ± 2 SD [19]. Single photon absorptiometry of the dominant arm was performed using a Nuclear Data (ND1100A) bone densitometer. Bone mineral measurements were made at sites distal (approximately 25% trabecular bone) and proximal (approximately 7% trabecular bone) to an 8-mm gap between the radius and ulna [20]. Scan analysis was made using VO3 software. Z scores were derived by comparison with a local control group.

Radiographic Analysis

Hand X-rays were performed on all patients prior to biopsy. Images were obtained using a mammographic technique (Fuji MA Mammography cassette loaded with CEA MA Mammography film, processed through a Kodak X-OMAT Processor). All X-rays were examined by a single radiologist blinded to histology. The severity of acro-osteolysis of the terminal phalanx and subperiosteal erosions were graded in each case and radiological evidence of hyperparathyroidism was considered if grade 2 acro-osteolysis or grade 1 subperiosteal erosions were present [21, 22].

Ultrasonography

High resolution ultrasound of the neck was performed on 53 patients, prior to biopsy (Ultramark 9 with a L10–5 MHz linear array broadband transducer, Advanced Technology Laboratories, Bothwell, Wash., USA) by 2 radiologists blinded to histology. The detection limit was 0.016 cm³. Since normal parathyroid glands could not be detected, identification of parathyroid tissue was considered a positive scan. Each gland was measured in three dimensions (X, Y, Z) and the volume calculated, assuming it to be an ellipsoid [23]. In 15 patients cytological examination of ultrasound-guided fine needle aspirates confirmed the presence of parathyroid cells whilst elevated aspirate iPTH concentrations indicated a functioning adenoma.

All results are expressed as mean ± SD with Student's t test and Pearson product-moment correlation used as appropriate, using ASTUTE statistical calculator computer program.

Fletcher/Jones/Rayner/Harnden/Hordon/
Aaron/Oldroyd/Brownjohn/Turney/Smith

Table 2. Bone biopsy results with ancillary biological and biochemical data

Histology	n	Age years	Time on dialysis years	Standard calcium (2.2–2.4 mmol/l)	Phosphate (0.8–1.2 mmol/l)	Bicarbonate (22–26 mmol/l)	Total ALP (100–300 IU/l)	Bone ALP (0–19 ng/ml)	iPTH (11–55 pg/l)	Serum aluminium (0.0–1.85 μmol/l)
Normal	8	52.8±12.1	1.5±0.9	2.46±0.23	1.83±0.23	21.7±3.0	147±63	4.24±1.68	99±102	0.36±0.12
Adynamic	3	54.0±10.6	1.7±1.1	2.43±0.18	1.98±0.31	15.6±2.6	161±53	9.9±3.3	140±187	0.59±0.49
Osteomalacia	1	48	1	2.5	1.59	25.6	116	6.9	28	0.28
Mixed	4	51.5±3.5	1.3±0.5	2.56±0.28	2.3±0.2	20.0±2.4	161±43	7.02±1.6	68±70	0.38±0.12
Mild HPT	11	42.7±12.2	3.5±4.6	2.42±0.1	1.89±0.14	19.8±3.2	126±35	5.73±2.7	54±27	0.52±0.27
Moderate HPT	17	43.6±12.3	3.1±3.6	2.39±0.03	2.01±0.43	20.2±4.8	237±78**	15.8±10.4*	405±232**	0.75±0.35
Severe HPT	29	48.6±13.6**	4.1±3.7	2.5±0.25	2.06±0.55	20.7±4.4	361±190**	43.9±31.5**	780±455**	0.80±0.48

Results are shown as mean ± SD. Reference values and units for each parameter are indicated.
Statistically different values when compared with the patients with normal histology are shown as
* $p < 0.05$; ** $p < 0.01$; *** $p < 0.001$. HPT = Hyperparathyroidism.

Table 3. Histomorphometric and histodynamic data for the study population

Histology	n	Bone volume BV/TV (23.19±4.37%)	Osteoid volume OV/BV (1.48±0.93%)	Osteoid thickness O.Th (10.34±2.1 μm)	Total osteoid surface OS/BS (12.10±4.64%)	Osteoblast surface Ob.S.BS (3.9±1.94%)	Eroded surface ES/BS (4.09±2.33%)	Osteoclast surface Oc.S/BS (0.69±0.61%)	Mineral appositional rate MAR (0.63±0.2 μm/day)
Normal	6	22.38±7.64	1.63±2.51	8.82±2.09	7.37±10.97	0.51±0.21	3.14±3.47	1.14±1.13	–
Adynamic	2	20.91	0.45	7.68	3.41	–	5.79	1.62	–
		21.59	0.59	11.1	4.94	0.77	–	–	–
Osteomalacia	1	23.04	13.19**	19.17**	32.59**	0.56	1.36	0.159	
Mixed	3	31.39±15.12	8.57±3.71**	14.89±3.74*	43.12±11.31**	0.24	2.49±2.74	1.62	0.86
Mild HPT	9	22.24±4.94	1.91±2.00	10.98±2.34	8.1±6.96	0.68±0.25	2.12±2.63	0.43±0.28	0.58±0.14
Moderate HPT	12	21.77±4.56	6.49±4.34*	11.47±2.98	25.49±16.41	1.35±0.99	6.66±3.23	1.69±1.17	1.21±0.43
Severe HPT	24	23.37±7.02	12.05±8.69**	16.39±7.35**	37.96±16.66**	2.53±2.51**	9.73±4.64**	2.46±2.46	1.11±0.47

Values are shown as mean ± SD. Where the number of patients is <2 individual values are given.
Statistically different values when compared with the patients with normal histology are shown as
* $p < 0.05$; ** $p < 0.01$; *** $p < 0.001$. HPT = Hyperparathyroidism.

Results

Histology

The histological results classification of the 73 bone biopsies with ancillary biological and biochemical data are shown in table 2. There were 57 patients with predominant hyperparathyroid bone disease which included 1 patient with severe hyperparathyroid bone disease and severe aluminium deposition. There were 4 patients with mixed ROD and 4 patients with low turnover ROD, comprising 3 adynamic and 1 case of osteomalacia. There were 8 patients with normal bone histology. The high incidence of hyperparathyroidism in this study can be accounted for by patient selection. There was no statistical difference in age between histological subgroups. Hyper-parathyroid patients tended to be on dialysis longer than other histological subgroups, although this reached significance only between severe hyperparathyroid and normal histology.

The histomorphometry of the 57 undamaged bone biopsies is shown in table 3. The patients with normal and mild hyperparathyroidism on bone biopsy had histomorphometric parameters comparable with the range of the normal population included in the Osteo Measure software package and with our own previously published data. One of the adynamic biopsies had a raised osteoclast surface but the overall histomorphometric and histological picture was that of low bone formation. In the absence of aluminium staining a diagnosis of adynamic bone disease was reached by the 2 observers independently.

Table 4. The correlation between the biochemical markers of bone turnover and histomorphometric variables

	Total ALP	Bone ALP	PTH
Total osteoid surface	0.44**	0.58***	0.46**
Osteoid thickness	0.22	0.35*	0.31*
Osteoblast surface	0.51***	0.49**	0.37*
Eroded surface	0.40**	0.36*	0.51***
Osteoclast surface	0.16	0.16	0.20
Mineral appositional rate	0.42**	0.54***	0.49*

The data is presented as the r values obtained by Pearson product-moment correlation. Statistically significant values are shown as * p < 0.05; ** p < 0.01; *** p < 0.001.

The incidence of bone surface aluminium deposition was low; 7 patients (9.6% of the 73 biopsies) had mild deposition, 2 (2.7%) had moderate deposition and the patient with clinical aluminium toxicity had severe deposition. At the time of biopsy 11 (15%) were being prescribed aluminium phosphate binders, although 35 (48%) had been prescribed aluminium hydroxide at some time on dialysis. Mean serum aluminium levels were within the reference range for all histological groups. The patient with severe aluminium depositions had been prescribed aluminium hydroxide for 9 years as a phosphate binder with a serum aluminium within the normal range throughout this time. Persistent bone pain and myopathy raised the clinical suspicion of aluminium toxicity, which was confirmed by a desferrioxamine stimulation test and a bone biopsy. There was no correlation between the severity of bone aluminium deposition and serum aluminium.

Histopathological examination of the marrow revealed 2 unsuspected cases of non-Hodgkin's lymphoma.

Biochemistry
There was no statistically significant difference in plasma standard calcium, phosphate and bicarbonate concentrations between the subgroups studied, mean levels lying within the adult reference range. Mean serum iPTH levels were raised in all subgroups except the patient with osteomalacia. Mean serum total ALP and BAP levels were within the reference range for all subgroups except those with severe hyperparathyroidism. Moderate and severe hyperparathyroidism showed significant elevated serum iPTH, total ALP and BAP when compared with patients with normal histology (table 2).

Serum BAP, total ALP and iPTH all correlated significantly with mineral apposition rate, osteoid surface, osteoblast surface and eroded surface (table 4). There was a low degree of correlation between the osteoclast surface and the plasma markers of bone turnover. There was a wide variation in the values for osteoclast surface within the histological groups as exemplified by the adynamic patient described previously which the authors are unable to explain.

In the diagnosis of hyperparathyroid bone disease a serum iPTH >100 pg/ml had a specificity of 66% and a sensitivity of 81%. A serum BAP >10 ng/ml had a specificity of 92% and a sensitivity of 70%. A serum total ALP >300 IU/l had a specificity of 100% but a sensitivity of 30%. When the investigations were used in combination a serum iPTH >100 pg/ml and a serum BAP >10 ng/ml produced a specificity of 100% and a sensitivity of 66%. A serum iPTH >100 pg/ml and a serum total ALP >300 IU/l had a combined specificity of 100% but a sensitivity of 30%.

Bone Mineral Density
BMD for each histological group is shown in table 5. Mean Z scores for each histological subgroup, except for the spinal measurements for patients with mixed ROD, were within 2 SD of a matched control population. Patients with normal bone histology had a negative mean Z score in the axial skeleton reflecting a loss of mineralisation. There was a negative relation between severity of hyperparathyroid bone disease and BMD in all regions measured. Patients with mixed, mild and moderate hyperparathyroid bone disease had a higher mean axial BMD measurement than patients with normal histology or adynamic bone disease. In the forearm there was an increasing differential loss of BMD between the proximal and distal forearm with increasing severity of hyperparathyroid bone disease which reached significance in patients with severe hyperparathyroidism, p < 0.005.

Radiology
There was no radiological evidence of hyperparathyroid bone disease in the histologically defined mild subgroup. Four moderate patients and 23 severe patients had radiological evidence of hyperparathyroid bone disease on hand X-rays (table 6). There was no significant difference between the detection rate of subperiosteal erosions and acro-osteolysis in patients with hyperparathyroid bone disease. The specificity of a positive hand X-ray for the diagnosis of hyperparathyroid bone disease was 92% and the sensitivity 47%. When combined with a serum

Fletcher/Jones/Rayner/Harnden/Hordon/
Aaron/Oldroyd/Brownjohn/Turney/Smith

Table 5. Regional BMD expressed as a Z score ± SD

Histology	Number	Spine	Femur	Total body	Distal forearm	Proximal forearm
Normal	7	0.38±0.21	−0.87±1.1	−0.93±1.4	−0.87±1.2	−0.83±1.2
Adynamic	1	1	−0.86	−0.57	−0.23	−1.85
Mixed	4	2.85±1.98	−0.09±1.1	−0.10±0.78	0.01±1.58	−0.17±2.12
Mild HPT	9	0.49±1.1	−0.4±1.3	0.05±0.56	0.03±1.0	−0.16±0.9
Moderate HPT	15	−0.06±1.3	−0.24±0.87	−0.32±1.27	−0.5±1.4	−0.81±1.5
Severe HPT	25	−0.77±1.6	−0.95±0.9	−1.44±1.5	−1.23±1.5	−1.94±1.9

HPT = Hyperparathyroidism.

Table 6. Radiological evidence of hyparathyroidism in hand X-rays from the study population

Histology	Number	Acro-osteolysis		Subperiosteal erosion	
		grade I and II	grade III	grade I	grade II and III
Normal	8	8	0	8	0
Adynamic	3	2	1	2	1
Osteomalacia	1	1	0	1	0
Mixed	4	4	0	4	0
Mild HPT	10	10	0	10	0
Moderate HPT	17	14	3	13	4
Severe HPT	29	10	19	6	23

HPT = Hyperparathyroidism.

iPTH >100 pg/ml the specificity and sensitivity remained the same.

Parathyroid enlargement was only detected in patients with hyperparathyroid bone disease (Table 7). There was no correlation between parathyroid gland volume and serum iPTH levels. The specificity of the detection of an enlarged parathyroid gland in the diagnosis of hyperparathyroid bone disease was 100% with a sensitivity of 68%. When combined with a serum iPTH >100 pg/ml the specificity and sensitivity remained the same.

Discussion

The histological response of bone to the metabolic disorder of chronic renal failure is modified by age, sex, underlying renal pathology, duration of chronic renal failure, exposure to aluminium, medication and mode of dialysis, leading to considerable individual variation in

Table 7. Detection of parathyroid enlargement by ultrasound in the study population

Histology	Number	Parathyroid enlargement		Volume, cm³ (mean ± SEM)
		not detected	detected	
Normal	5	5	0	−
Adynamic	1	1	0	−
Osteomalacia	0	0	0	−
Mixed	3	2	1	0.02
Mild HPT	6	5	1	0.07
Moderate HPT	12	7	5	0.09±0.03
Severe HPT	26	2	24	0.30±0.48

HPT = Hyperparathyroidism.

type and severity of ROD [24]. An accurate histological diagnosis may be provided by a bone biopsy but, because bone is a dynamic organ, the nature and severity of any pathology may change with time. Regular, repeated bone biopsies are generally an unacceptable method of monitoring ROD due to the degree of discomfort suffered by the patients. The measurement of plasma biochemical markers of bone metabolism are used frequently to discriminate between high and low turnover metabolic bone disease in non-renal patients. However, ROD is more difficult to accurately diagnose using non-invasive methods, particularly in the early stages, because traditional biochemical markers lack specificity and their metabolism may be altered in the presence of uraemia [25].

In this study BAP, total ALP and serum iPTH correlated significantly with histomorphometric measurements of osteoblastic activity. In patients with normal histology, low turnover and mild hyperparathyroid bone disease there was no significant difference in serum BAP, total ALP and iPTH levels. Markers of bone turnover were unable to differentiate the bone pathologies in these patients. It was surprising that the histomorphometric parameters within these subgroups were all within the reference range, despite the clear diagnostic histological differences. A serum iPTH greater than 55 pg/l, the upper reference limit for normocalcaemic non-renal patients, was the most sensitive investigation for the detection of hyperparathyroid bone disease. A mean serum iPTH of 54 pg/l was observed in the mild subgroup, several patients with clear histological disease having 'normal' iPTH values, i.e. <55 pg/l. However, a mean serum calcium of 2.41 mmol/l for this group suggests that there is a failure of PTH suppression within this group and the selection of an isolated value for iPTH without regard to prevailing calcium levels is inappropriate. We do not have enough data in the present study to identify an appropriate index value which would combine calcium and iPTH values. In any event, lowering the limit below 55 pg/l to increase sensitivity of detection of the mild cases proves unacceptable due to the loss of specificity. An elevated mean serum iPTH was also found in several patients in the adynamic, normal and mixed ROD subgroups, reducing the specificity of a raised serum iPTH for the diagnosis of hyperparathyroid bone disease.

The normal reference range for serum BAP is quoted as less than 19 ng/ml, but in this study all but 1 of the patients with low turnover or normal histology had a serum BAP of less than 10 ng/ml. A serum BAP greater than 10 ng/ml gave a sensitivity similar to serum iPTH but with a greater specificity for the diagnosis of hyperparathyroid bone disease where all the subgroups were included.

BMD measurements were made in only 1 patient with adynamic bone disease and this study cannot comment on the diagnostic value of DEXA scanning to distinguish between high and low turnover ROD. Within the hyperparathyroid group there was a negative correlation between increasing severity of hyperparathyroid bone disease and BMD, although the mean values in all three subgroups were within 2 SD of a matched control population. DEXA scanning has little value in the diagnosis of hyperparathyroid bone disease, but it may have the potential to monitor its progress once it has been histologically diagnosed. Confirmation would require a longitudinal study. Increased bone turnover leads to cancellisation of cortical bone leading to a loss of bone volume principally in the appendicular skeleton [24]. The proximal forearm has a higher proportion of cortical bone than the distal forearm [26]. Increasing severity of hyperparathyroidism caused a greater differential loss of BMD in the proximal than the distal forearm, which was statistically significant in the patients with severe hyperparathyroid bone disease. The forearm, which reflects the changes in bone turnover occurring with hyperparathyroidism, can therefore be used for repeat measurements rather than subjecting the patients to total body scanning.

Using a higher cut-off of iPTH of 100 pg/l gave a specificity of 66% and sensitivity of 81%, the loss of sensitivity being attributable to the number of patients with mild bone disease who had normal or only marginally elevated iPTH values.

Parathyroid volume measured at the time of parathyroidectomy has been shown to correlate with the maximal iPTH secretion, the shift in calcium set point and with the duration and severity of renal failure [27]. Advances in ultrasound technology have improved the sensitivity and specificity of detection of the parathyroid glands. In this study the detection of an enlarged parathyroid gland was more sensitive and specific than for the diagnosis of hyperparathyroid bone disease than the radiological changes on a hand X-ray. Ultrasonography would be the appropriate radiological investigation to confirm the diagnosis of hyperparathyroid bone disease in patients with an elevated iPTH.

Fletcher/Jones/Rayner/Harnden/Hordon/
Aaron/Oldroyd/Brownjohn/Turney/Smith

Conclusions

At present there are no humeral markers or radiological markers capable of totally replacing a bone biopsy in the diagnosis of ROD. The measurement of serum iPTH was the most sensitive test in detecting hyperparathyroid bone disease but was not highly specific particularly when considering early and mild disease. When raised serum iPTH was combined with an elevated BAP or the detection of an enlarged parathyroid gland, the specificity of the diagnosis was increased. The use of a number of non-invasive investigations, combined with sound clinical judgement, may detect metabolic bone disease when present in the majority of patients, although a minority may still require a bone biopsy.

Acknowledgements

References

1 Malluche HH: Renal Bone Disease 1990. An unmet challenge for the nephrologist. Kidney Int 1990;38:193–211.
2 DeVita MV, Rasenas LL, Bansal M, Gleim GW, Zabetakis PM, Gardenswartz MH, Michelis MF: Assessment of renal osteodystrophy in hemodialysis patients. Medicine 1992;71: 284–290.
3 Andress DL, Endres DB, Maloney NA, Kopp JB, Coburn JW, Sherrard DJ: Comparison of parathyroid hormone assays with bone histomorphometry in renal osteodystrophy. J Clin Endocrinol Metab 1986;63;1163–1169.
4 Coen G, Mazzaferro S: Bone metabolism and its assessment in renal failure (editorial). Nephron 1994;67:383–401.
5 Sherrard DJ, Hercz G, Pei Y, Maloney NA, Greenwood C, Manuel A, Saiphoo C, Fenton SS, Segre GV: The spectrum of bone disease in end-stage renal failure – an evolving disorder. Kidney Int 1993;43:436–442.
6 Malluche HH, Monier Faugere MC: Risk of adynamic bone disease in dialyzed patients. Kidney Int Suppl 1992;38:S62–S67.
7 Delmas PD, Wilson DM, Mann KG, Riggs BL: Effect of renal function on plasma levels of bone Gla protein. J Clin Endocrinol Metab 1983;57:1028–1030.
8 Coen G, Mazzaferro S, Bonucci E, Taggi F, Ballanti P, Bianchi AR, Donato G, Massimetti C, Smacchi A, Cinotti GA: Bone GLA protein in predialysis chronic renal failure: Effects of 1, 25(OH)2D3 administration in a long-term follow-up. Kidney Int 1985;28:783–790.
9 Delmas PD: Biochemical markers of bone turnover for the clinical assessment of metabolic bone disease. Endocrinol Metab Clin North Am 1990;19:1–18.
10 Reck R, Jaster D: (Isoenzymes of alkaline phosphatase – their determination and clinical significance for orthopedics). Beitr Orthop Traumatol 1988;35:89–94.

11 Naik RB, Gosling P, Price CP: Comparative study of alkaline phosphatase isoenzymes, bone histology, and skeletal radiography in dialysis bone disease. BMJ 1977;i:1307–1310.
12 Onica D, Sundblad L, Waldenlind L: Affinity electrophoresis of human serum alkaline phosphatase isoenzymes in agarose gel containing lectin. Clin Chim Acta 1986;155:285–293.
13 Ewen CM: Separation of alkaline phosphatase isoenzymes and evaluation of the clinical usefulness of this determination. Am J Clin Pathol 1974;61:142–154.
14 Moss DW: Alkaline phosphatase isoenzymes. Clin Chem 1982;28:2007–2016.
15 Hill CS, Wolfert R: The preparation of antibodies which react preferentially with human bone alkaline phosphatase and not liver alkaline phosphatase. Clin Chim Acta 1990;186: 315–321.
16 Aaron JE, Makins NB, Sagreiya K: The microanatomy of trabecular bone loss in normal aging men and women. Clin Orthop 1987;215: 260–271.
17 Denton J, Freemont AJ, Ball J: Detection and distribution of aluminium in bone. J Clin Pathol 1984;37:136–142.
18 Payne RB, Carver ME, Morgan DB: Interpretation of serum total calcium: Effects of adjustment for albumin concentration on frequency of abnormal values and on detection of change in the individual. J Clin Pathol 1979;32:56–60.
19 Truscott JG, Oldroyd B, Simpson M, Stewart SP, Westmacott CF, Milner R, Horsman A, Smith MA: Variation in lumbar spine and femoral neck bone mineral measured by dual energy X-ray absorption: A study of 329 normal women. Br J Radiol 1993;66:514–521.

20 Nilas L, Borg J, Gotfredsen A, Christiansen C: Comparison of single- and dual-photon absorptiometry in postmenopausal bone mineral loss. J Nucl Med 1985;26:1257–1262.
21 Ritz E, Prager P, Krempien B, Bommer J, Malluche HH, Schmidt Gayk H: Skeletal X-ray findings and bone histology in patients on hemodialysis. Kidney Int 1978;13:316–323.
22 Sundaram M, Joyce PF, Shields JB, Riaz MA, Sagar S: Terminal phalangeal tufts: Earliest site of renal osteodystrophy findings in hemodialysis patients. AJR Am J Roentgenol 1979;133: 25–29.
23 Fukagawa M, Kitaoka M, Yi H, Fukuda N, Matsumoto T, Ogata E, Kurokawa K: Serial evaluation of parathyroid size by ultrasonography is another useful marker for the long-term prognosis of calcitriol pulse therapy in chronic dialysis patients. Nephron 1994;68:221–228.
24 Hamdy NA, Risteli J, Risteli L, Harris S, Beneton MN, Brown CB, Kanis JA: Serum type I procollagen peptide: A non-invasive index of bone formation in patients on haemodialysis? Nephrol Dial Transplant 1994;9:511–516.
25 Masters PM, Jones RG, Purves D, Cooper EH, Cooney JM: Commercial osteocalcin assays give clinically discordant results. Clin Chem 1994;40:358–363.
26 Hernandez D, Concepcion MT, Lorenzo V, Martinez ME, Rodriguez A, De Bonis E, Gonzalez Posada JM, Felsenfeld AJ, Rodriguez M, Torres A: Adynamic bone disease with negative aluminium staining in predialysis patients: Prevalence and evolution after maintenance dialysis. Nephrol Dial Transplant 1994;9:517–523.
27 Wallfelt CH, Larsson R, Gylfe E, Ljunghall S, Rastad J, Akerstrom G: Secretory disturbance in hyperplastic parathyroid nodules of uremic hyperparathyroidism: Implication for parathyroid autotransplantation. World J Surg 1988; 12:431–438.

Regional bone mineral density after orthotopic liver transplantation

S. Hyder Hussaini[a], Brian Oldroyd[b], Sheena P. Stewart[b], Fiona Roman[b],
Michael A. Smith[b], Stephen Pollard[a], Peter Lodge[a], John G. O'Grady[a] and
Monty S. Losowsky[a]

Objectives Although there is a fall in lumbar spine bone
mineral density (BMD) after liver transplantation, little is
known about femoral neck or total body BMD. Therefore
we determined: (a) the proportion of patients with pre-
existing hepatic osteopenia before transplantation and (b)
the effects of transplantation on global and regional BMD.

Design Retrospective analysis of BMD measurements of
patients before and up to 2 years after liver transplantation.

Methods BMD was assessed by dual energy X-ray
absorptiometry in 56 patients, before and at regular
intervals after liver transplantation, for up to 24 months, to
measure total body, lumbar spine (L2–L4) and femoral
neck BMDs.

Results Pre-transplant, 23% of patients had osteoporosis
(a negative Z score > 2). Paired data before and after
transplantation revealed no change in total body BMD.
However, there was a fall in lumbar spine BMD (1.04 ± 0.03
to 1.02 ± 0.03 g/cm^2; $P < 0.04$) at 1 month after
transplantation. The reduction in lumbar spine BMD was
seen up to 12 months, BMD at 18–24 months being similar
to pre-transplant values. Femoral neck BMD also fell

(0.96 ± 0.06 to 0.83 ± 0.04 g/cm^2; $P < 0.03$), but only after
6–9 months, thereafter remaining below pre-transplant
values until the end of the follow-up period.

Conclusions Although osteopenia is common in patients
with liver disease, total bone density does not fall after
transplantation. Nonetheless regional lumbar spine and
femoral neck bone density does fall after transplantation
with a risk period for femoral neck fracture which may
extend for up to 2 years. *Eur J Gastroenterol Hepatol*
11:157–163 © 1999 Lippincott Williams & Wilkins

Introduction

Patients with chronic liver disease suffer from bone
disease [1–3]. Osteomalacia occurs particularly in pa-
tients with cholestatic disease and is secondary to
vitamin D deficiency [4,5]. Reduced bone mineral
density (BMD), known as osteopenia, is present in up
to 40% of patients with chronic liver disease [6,7].
Osteopenia results in a two-fold increase in the rate of
axial spinal and appendicular peripheral spontaneous
bone fracture in patients with chronic liver disease
compared to healthy controls [6].

Orthotopic liver transplantation (OLT) is an estab-
lished treatment for patients with end-stage chronic
liver disease with 1 year survival rates for elective
patients of over 90% [8]. In some patients undergoing
liver transplantation, pre-existing bone disease may
deteriorate due to factors such as prolonged bed rest,
immobilization [9] and immunosuppressive therapy

[10–12]. Nonetheless, good graft function after liver
transplantation might be expected to overcome the
osteoporotic effects of the underlying liver disease. The
initial studies of bone disease following liver trans-
plantation have found a high rate of atraumatic bone
fracture [13–15] and a fall in BMD immediately after
transplantation [14,16,17]. However, long-term studies
suggest an overall improvement in BMD following
transplantation [14,17]. Immunosuppressive regimens
utilizing relatively high doses of steroids, especially in
the early post-operative period, may in part have been
responsible for these high fracture rates post-trans-
plantation [13,17]. Osteopenia in the non-transplant
population is a heterogeneous disorder with marked
anatomical regional variations in bone density [18–20].
The initial studies of BMD after transplantation
focused on the changes of lumbar spine BMD
[14,16,17], which consists of predominantly trabecular
bone. Only one small series has examined the effects of

OLT on regional bone density [21]. Therefore, in a cohort of patients undergoing OLT for end-stage chronic liver disease we determined the following: (a) the proportion of patients with pre-existing hepatic osteopenia before transplantation and (b) the effects of transplantation on global and regional BMD. Furthermore, we assessed whether duration of hospital stay, dose of steroids, number of rejection episodes, presence of cholestatic liver disease, age and sex were potential risk factors for post-transplant osteopenia.

Methods

Patients

We retrospectively identified all patients who underwent dual energy X-ray absorptiometry (DEXA) scanning before and after liver transplantation between September 1989 and December 1994. Fifty-six patients (33 female) with end-stage chronic liver disease were identified, with a mean age of $51 \pm SEM$ 1.5 y (range 24–69 y). Some of the patients studied have been reported in a separate, but related study concerning the changes in body composition after liver transplantation [22]. Thirty-three patients had cholestatic liver disease, 24 with primary biliary cirrhosis (18 female), seven with primary sclerosing cholangitis (three female), and two with secondary biliary cirrhosis (two female). A total of nine patients had alcohol-related cirrhosis (three female) and five had chronic autoimmune cirrhosis (four female). Of the remaining 10 patients, three had cryptogenic cirrhosis (two female), four had neoplastic disease (one female), one patient had hepatitis B cirrhosis and one suffered from alpha-1 antitrypsin deficiency.

All patients were diagnosed on the basis of biochemical, immunological or serological markers, together with liver histology when appropriate. The diagnosis of cryptogenic cirrhosis was made if a liver biopsy demonstrated cirrhosis with no diagnostic features, with the exclusion of excess alcohol intake and following laboratory findings of: (a) no autoantibodies and normal immunoglobulins (to exclude autoimmune liver disease), (b) negative viral serology for hepatitis B and C and, (c) normal studies for iron, copper and alpha-1 antitrypsin. All patients with primary biliary cirrhosis received 100 000 units intramuscular of vitamin D (calciferol) per month.

Transplantation details

Clinical data were available in 43 patients with regard to disease severity before transplantation. Six of the 43 patients were Child–Pugh [23] class A, 33 were class B and 4 were class C. All patients were given triple immunosuppressant therapy consisting of cyclosporin (or tacrolimus in seven patients), azathioprine and prednisolone. In 41 patients details of steroid dosage, duration of hospital stay and number of rejection episodes were available. Patients received a median

dose of prednisolone of 20, 12.5, 10, 7.5, and 7.5 mg at time intervals of 1, 2–5, 6–9, 12 and 18–24 months, respectively. The mean duration of hospital stay after transplantation was 32 ± 7 days (range 14–96 days; median 28 days). Ten (25%) patients had an episode of cholestasis after transplantation due to a bile duct stricture or cholestatic hepatitis. Only five (8%) patients experienced an episode of post-transplant hepatitis. One patient who was re-transplanted for recurrent hepatitis B did not receive any prednisolone postoperatively, to minimize the risk of hepatitis B recurrence.

Controls

A group of 329 women (age range 20–81 y) and 115 men (age range 20–78 y) were recruited locally as controls [24]. Subjects with a history of prolonged immobilization, fractures affecting the hip, spine or wrist, medical conditions or on medication known to affect BMD were excluded as control subjects.

Bone mineral density measurements

Total body, lumbar spine (L2–L4) and right femoral neck BMD were measured by dual energy X-ray absorptiometry using a Lunar DPX Bone Densitometer (Lunar Radiation Corporation, Wisconsin, USA). Analysis of the bone scans was made using the manufacturer's software (version 3.6) which calculated bone mineral content (g) and bone area scanned (cm^2). Hence BMD was calculated (g/cm^2) and Z scores derived subsequently, corrected for age and sex, were used in data analysis. The Z score for BMD is the number of standard deviations above or below the mean BMD for an age and sex-matched normal population. Patients were assessed before transplantation, at 1, 2–5, 6–9, 12 and 18–24 months after transplantation.

Statistical analysis

The number of patients studied at each of these time periods was variable. Thus, bone mineral content was analysed as paired data for each time period compared to pre-transplant values, and tested for statistical significance with the paired t-test. P values of < 0.05 were considered to be statistically significant.

To determine possible risk factors for osteopenia, patients were stratified into those with negative Z scores ≥ 1. The World Health Organization defines osteopenia as a BMD of > 1 SD below the mean for a healthy young population [25]. Since we wished to compare patients with liver disease with controls of the same sex and similar age, we defined osteopenia as BMD > 1 SD below that for an age and sex-matched control population, that is a negative Z score of > 1. Osteoporosis was defined as a negative Z score of > 2. Risk factors for osteopenia, i.e. severity of liver disease, age, gender and cholestatic chronic liver disease, were

compared before and after transplantation with the non-parametric heteroscedastic *t*-test. Further possible risk factors for osteopenia, namely duration of hospital stay, dose of steroids and numbers of rejection episodes were then compared in those with and without osteopenia after transplantation using the non-parametric analysis. Since multiple analyses, to determine risk factors for bone disease, were performed on the same dataset before and after transplantation, only *P* values of < 0.01 were taken as demonstrating a significant difference. The results were expressed as mean values ± standard error of the mean (SEM), unless otherwise stated. Excel software version 5.0 (Microsoft Corporation, 1 Microsoft Way, Redmond, WA 98052-6399) was used to analyse data.

Ethical considerations
The study was approved by the Ethics Committee of St James's University Hospital.

Results
Pre-transplant bone mineral density
The data for total body, lumbar spine and femoral neck BMD for controls and patients in all subjects and stratified for gender are shown in Fig. 1. The total body BMD of 1.15 ± 0.01 g/cm^2 in controls was significantly greater than the BMD of 0.62 ± 0.15 g/cm^2 in patients ($P < 0.001$). Similar differences were seen for lumbar spine (1.16 ± 0.02 vs 0.49 ± 0.15 g/cm^2; $P < 0.001$) and femoral neck (0.94 ± 0.02 vs 0.52 ± 0.13 g/cm^2; $P < 0.002$) BMD in controls and patients, respectively. As can be seen from Fig. 1, the pattern of osteopenia was unchanged when stratified for gender, although the difference in BMD was more marked between women and their controls.

The number of patients with osteoporosis defined as a negative Z score of > 2 or osteopenia defined as a negative Z score of > 1 is shown in Fig. 2. A total of 13 (23%) of 56 patients studied had osteoporosis, i.e. either total body, lumbar spine or femoral neck negative Z scores of > 2. However, the numbers of patients with total body, lumbar spine or femoral neck osteoporosis was variable, highlighting the fact that the osteoporosis was rather heterogeneous. Whole body DEXA results detected only an extra two patients to those with osteoporosis at either femoral or lumbar spine sites.

The prevalence of osteopenia was far greater than that of osteoporosis, with 32 (57%) of 56 patients with either total body, lumbar spine or femoral neck negative Z scores of > 1. No additional patients with osteopenia were detected with whole body DEXA scanning.

Pre-transplant determinants of osteopenia
Although total body BMD for patients with cholestatic liver disease was lower (1.04 ± 0.03 g/cm^2) than for

Fig. 1
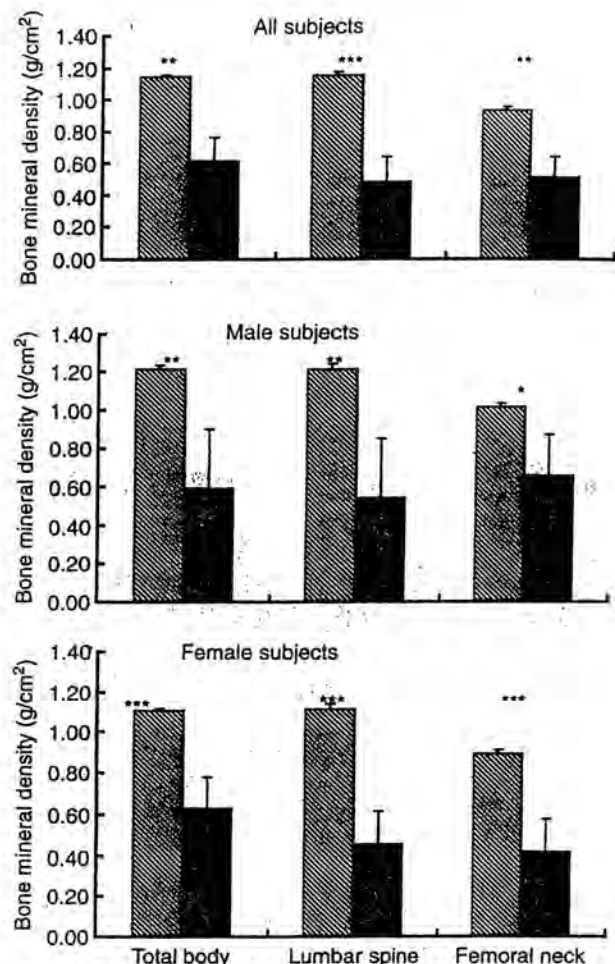
The data for total body, lumbar spine and femoral neck absolute bone mineral density (g/cm^2) of patients (■) and controls (▨) in all subjects and stratified for gender. The mean values are represented by the bars with the SEMs depicted as lines. Any statistical differences between controls and patients are shown as the following: * $P < 0.03$; ** $P < 0.007$; *** $P < 0.0001$.

patients with non-cholestatic liver disease (1.15 ± 0.02; $P < 0.002$), this difference was not statistically significant when corrected for age and sex as Z scores (-0.90 ± 0.26 vs -0.70 ± 0.96; $P = 0.07$). Similarly no significant difference was seen in lumbar spine (-0.96 ± 0.22 vs -0.63 ± 0.19) or femoral neck (-0.57 ± 0.30 vs -0.32 ± 0.23) Z scores from patients with cholestatic and non-cholestatic liver disease, respectively.

No significant differences in Z scores were observed between patients with a Child–Pugh (CP) score of < 7 (range 5–7; median 7) and those with a CP score > 7 (8–13; 9.5) for: (a) total body (-0.52 ± 0.25 vs -0.48 ± 0.34); (b) lumbar spine (-0.72 ± 0.20 vs -0.75 ± 0.29);

Fig. 2
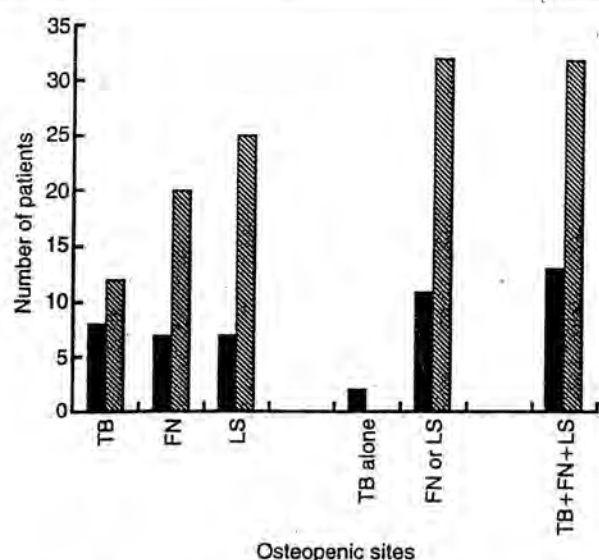
The regional variation in bone density is depicted as the number of patients with osteoporosis (negative Z score of > 2; ■) or osteopenia (negative Z score of > 1; ▧). The histogram shows the number of abnormal Z scores at: total body (TB), lumbar spine (LS) or femoral neck (FN) sites; total body alone or combined lumbar spine and femoral neck measurements and as combined total body, lumbar spine or femoral neck measurements.

or (c) femoral neck $(-0.63 \pm 0.25$ vs $-0.17 \pm 0.47)$ BMD.

Bone mineral density after liver transplantation
The paired data for BMD after transplantation are given in Fig. 3. The numbers of patients studied at 1, 2–5, 6–9, 12 and 18–24 months were 30, 23, 26, 17 and 11 patients, respectively. Total body BMD fell slightly at 2–5 months from 1.12 ± 0.03 to 1.11 ± 0.03 g/cm^2, although this just failed to reach statistical significance $(P = 0.053)$. Thereafter total BMD remained stable.

Immediately after transplantation, there was a fall in lumbar spine BMD, which persisted over the next 12 months. However in the 11 patients studied before and 18–24 months after transplantation no difference in BMD was observed. In contrast to lumbar spine BMD, there was no fall in femoral neck BMD immediately after transplantation. Nonetheless, significant reductions in femoral neck BMD were observed after 6–9 months which were sustained at 18–24 months after OLT.

Symptomatic non-traumatic fractures
The patients included in this study did not undergo systematic axial and spinal screening radiology to determine the rate of asymptomatic fractures. However, the rate of symptomatic bone fractures was 11% (six of

Fig. 3
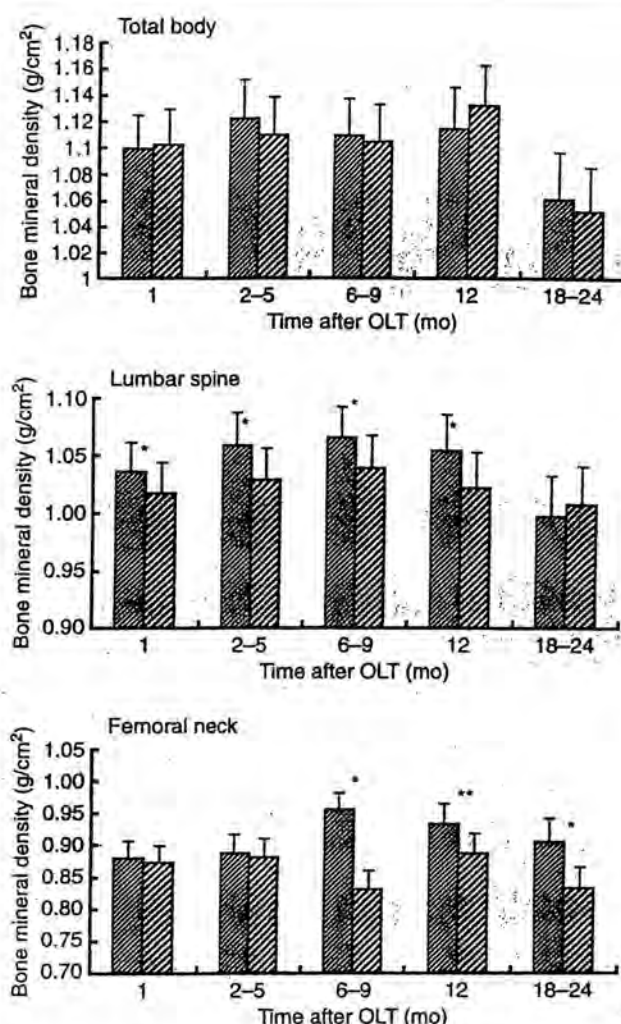
Paired data of bone mineral density (g/cm^2) expressed as mean ± SEM before and after orthotopic liver transplantation (OLT) for total body, lumbar spine and femoral neck measurements. Paired data that show a significant fall in bone mineral density are shown as follows: $*P < 0.05$; $**P < 0.004$. ▧, Pre-OLT; ▨, post-OLT.

56 patients) at 2 years. The details of the fractures with BMD before and at the time of fracture are given in Table 1. Only one patient with primary biliary cirrhosis (PBC) experienced a fracture of the lumbar spine, the remaining five patients sustaining femoral neck fractures. All the patients were female, four with PBC, five over the age of 50 years. Four patients had negative Z scores > 0.5 pre-transplantation and all had a negative Z score > 0.5 at the time of fracture.

Post-transplant determinants of osteopenia
No differences in BMD were found between patients stratified for age, gender, disease severity or disease type. Neither the dose of steroids administered at each

Patient	Age (y)	Disease	Site of fracture	Time post-transplantation (mo)	Z score at site of fracture	
					Pre-transplantation	At time of fracture
1	58	PBC	LS	4	−0.56	−0.56
2	44	CC	FN	12	0.40	−0.77
3	65	PBC	FN	24	−2.12	−1.98
4	52	PBC	FN	2	−0.88	−1.62
5	59	ALD	FN	8	−0.20	−0.86
6	59	PBC	FN	9	−2.86	−2.82

Demographic details of the six female patients who experienced symptomatic atraumatic bone fractures after liver transplantation at either femoral neck (FN) or lumbar spine (LS) sites with Z scores corresponding to the site of fracture before transplantation and at a time period nearest to the time that the bone fracture occurred. PBC, primary biliary cirrhosis; ALD, alcohol-related liver disease; CC, cryptogenic cirrhosis.

time interval nor the duration of hospital stay was significantly different in patients with or without osteopenia (i.e. negative Z scores of > 1) post-transplantation. Overall, 18 (44%) of the 41 patients had between one and three episodes of acute cellular rejection with no significant difference in the number of rejection episodes between those with or without osteopenia.

Discussion

Our results confirm that there is a loss of BMD after liver transplantation [14,16,17,26]. However, we have reported the effects of transplantation on both trabecular and cortical bone, rather than trabecular bone alone [14,16,17,26]. We consider this to be important since osteopenia is a heterogeneous disorder with variable bone density depending on the site examined [21].

The paired data did show a significant, though small, fall in lumbar spine bone density, confirming the findings of other groups [14,16,17,26]. Thereafter there was no improvement over pre-transplant values in lumbar spine BMD up to 24 months post-transplantation. In contrast to our data, Eastell *et al.* [17] found that lumbar spine BMD returned to the pre-operative values by about 12 months and was convincingly greater than pre-transplantation BMD by 2 years. The delay in recovery of lumbar bone density that we found confirms the observations of Arnold *et al.* [14], who documented an early fall in BMD within 3–6 months, which thereafter remained unchanged in the majority of patients up to 24 months after liver transplantation. However, long-term studies of bone density are required to determine the degree of reversibility of post-transplant osteopenia, especially in transplant programmes which use long-term corticosteroid therapy.

The timing of the changes of bone density in the femoral neck was different to that in the lumbar spine, with a fall in femoral BMD after transplantation, confirming regional differences in another, smaller, study which examined both femoral and lumbar BMD after transplantation [21]. A possible explanation for the discordance in the fall of femoral neck and lumbar spine BMD may have been the large time used in the early time periods. Thus a subtle femoral BMD in the 2–5 month period may have been missed. Nonetheless using this time scale we were able to demonstrate a significant fall in lumbar BMD in the early post-transplant period. Femoral bone density 2 years after OLT was still significantly lower than pre-transplant bone density. Thus the period for bone fracture may extend beyond the first year and perhaps still exists 2 years following transplantation.

The regional variation in osteopenia before and after transplantation, observed in the current study, has been documented previously in studies of bone loss in liver disease patients with osteoporosis [18–20]. Lumbar spine is predominantly made up of trabecular whilst proximal femur consists of mainly cortical bone. Trabecular bone has a higher turnover rate compared to cortical bone [27] which may account for the variation in bone loss.

The regional loss of bone density without any total BMD has been demonstrated previously in renal [28] transplantation, but has not been observed following liver transplantation. Following renal transplantation these changes have been attributed to differing regional skeletal responses to immunosuppression [29,30] or a redistribution of bone content from trabecular to cortical bone sites [30]. The findings of an initial fall of lumbar spine bone content and subsequent fall in femoral neck bone density little change in total body BMD support the theory with that there is a redistribution rather than absolute loss of bone following transplantation. However, in terms of practice, the measurement of total BMD, in addition to lumbar spine and femoral neck BMD, is of benefit, since only two further cases of 'osteoporosis'

were detected before transplantation and no overall changes in BMD were seen after transplantation.

The regional variations in bone density shown in the current study, together with the definitions used for osteopenia and osteoporosis, demonstrate the difficulty in defining the exact prevalence of bone disease patients with chronic liver disorders. In the current series, 23% of our patients had osteoporosis and 57% were osteopenic, although the exact figures would vary, depending on which region of the body was studied. Although these prevalence rates are comparable to earlier data [6,7], we would suggest that both lumbar spine and femoral neck BMD need to be assessed in order to accurately determine the prevalence of osteopenia in patients with chronic liver disease.

The small numbers of patients with cholestatic liver disease in our study, together with the fact that these patients received early transplantation and vitamin D supplementation prior to transplantation, may account for the absence of a relationship between cholestatic disease and bone density found by some [31], but not all, authors [17,32]. Furthermore, the short duration of hospital stay and relatively low dose of steroids administered were probably responsible for these factors not being implicated in the development of post-transplant bone disease. The median CP scores for the group of patients with mild (7) and those with moderate severity (9.5) liver disease were similar, with only four patients with class C disease. This skew in the distribution of disease severity towards milder disease may account for the similar BMD in patients with mild or moderate severity chronic liver disease before transplantation.

Since patients were not investigated systematically for evidence of asymptomatic fractures, we believe that the low fracture rate of 11% in the current series underestimates the true asymptomatic fracture rate. Others have reported a fracture rate of 20–65% in the first year of transplantation [13–15,17,33]. However, an alternative explanation for the low fracture rate is the relatively small magnitude of the reduction in BMD after transplantation. The quantitative fall in lumbar spine BMD was lower than some reports [13,15,17], although similar to others [14]. Moreover a recent study [34] reported no reduction in bone density in 82 patients undergoing transplantation. We speculate that the reason for the diminished reduction in BMD after transplantation, compared to a decade ago, is a consequence of earlier liver transplantation, shorter hospital stays and the use of steroids in lower dosages (with steroid withdrawal in some programmes).

In conclusion, although osteopenia is common in patients with chronic liver disease, total bone density does not fall after transplantation. Nonetheless regional

lumbar spine and femoral neck bone density does fall after transplantation with a risk period for femoral neck fracture which may extend for up to 2 years. However the magnitude of the fall in bone density after transplantation has declined over the last decade. This suggests that the prevalence rate of asymptomatic fracture should be reassessed with the use of modern transplantation techniques.

References

1   Atkinson M, Nordin BEC, Sherlock S. Malabsorption and bone disease in prolonged obstructive jaundice. Q J Med 1956; 25:299–312.
2   Summerskill WHJ, Kelly PJ. Osteoporosis with fractures in anicteric cirrhosis: observations supplemented by microradiographic evaluation of bone. Proc Mayo Clin 1963; 38:162–174.
3   Paterson CR, Losowsky MS. The bones in chronic liver disease. Scand J Gastroenterol 1967; 2:293–300.
4   Reed JS, Meredith SC, Nemchausky BA, et al. Bone disease in primary biliary cirrhosis: reversal of osteomalacia with oral 25-hydroxyvitamin D. Gastroenterology 1980; 78:512–517.
5   Dibble JB, Sheridan P, Hampshire R, et al. Osteomalacia, vitamin D deficiency and cholestasis in chronic liver disease. Q J Med 1982; 201:89–103.
6   Diamond T, Stiel D, Lunzer M, et al. Osteoporosis and skeletal fractures in chronic liver disease. Gut 1990; 31:82–87.
7   Bonkovsky HL, Hawkins M, Steinberg K, et al. Prevalence and prediction of osteopenia in chronic liver disease. Hepatology 1990; 12:273–280.
8   Bismuth H, Farges O, Castaing D, et al. Evaluation of results of liver transplantation: experience based on a series of 1052 transplantations. Presse Medicale 1995; 24:1106–1114.
9   Hulley SB, Vogel JM, Donaldson CL, et al. The effect of supplemental oral phosphate on bone mineral changes during prolonged bed rest. J Clin Invest 1971; 50:2506–2518.
10   Lukert BP, Raisz LG. Glucocorticoid induced osteoporosis: pathogenesis and management. Ann Intern Med 1990; 112:352–364.
11   Rich GM, Mudge GH, Laffel GI, et al. Cyclosporine A and prednisolone associated osteoporosis in heart transplant recipients. J Heart Lung Transplant 1992; 11:950–958.
12   Shane E, Rivas MC, Silverberg SJ, et al. Osteoporosis after cardiac transplantation. Am J Med 1993; 94:257–264.
13   Haagsma EB, Thijn CJ, Post JG, et al. Bone disease after orthotopic liver transplantation. J Hepatol 1988; 6:94–100.
14   Arnold JC, Hauser D, Ziegler R, et al. Bone disease after transplantation. Transplant Proc 1992; 24:2709–2710.
15   Meys E, Fontanges E, Fourcade N, et al. Bone loss after orthotopic liver transplantation. Am J Med 1994; 97:445–450.
16   Porayko MK, Wiesner RH, Hay JE, et al. Bone disease in liver transplant recipients: incidence, timing, and risk factors. Transplant Proc 1991; 23:1462–1465.
17   Eastell R, Dickson ER, Hodgson SF, et al. Rates of vertebral bone loss before and after liver transplantation in women with primary biliary cirrhosis. Hepatology 1991; 14:296–300.
18   Riggs BL, Wahner HW, Dunn WL, et al. Differential changes in bone mineral density of the appendicular and axial skeleton with aging: relationship to spinal osteoporosis. J Clin Invest 1981; 67:328–335.
19   Mazess RB, Peppler WW, Chesney RW, et al. Does bone measurement on the radius indicate skeletal status? J Nucl Med 1984; 25:281–288.
20   Eastell R, Wahner HW, O'Fallon WM, et al. Unequal decrease in bone density of lumbar spine and ultradistal radius in Colles' and vertebral fracture syndromes. J Clin Invest 1989; 83:168–174.
21   Abdelhadi M, Eriksson SAV, Ljusk Eriksson S, et al. Bone mineral status in end-stage liver disease and the effects of liver transplantation. Scand J Gastroenterol 1995; 30:1210–1215.
22   Hussaini SH, Oldroyd B, Stewart SP, Soo S, Roman F, Smith MA, et al. The effects of orthotopic liver transplantation on body composition. Liver 1998; 18:173–179.
23   Pugh RN, Murray-Lyon IM, Dawson JL, et al. Transection of the oesophagus for bleeding oesophageal varices. Br J Surg 1973; 60:646–649.
24   Truscott JG, Oldroyd B, Simpson M, et al. Variation in lumbar spine and femoral neck bone mineral measured by dual energy X-ray absorption: a study of 329 normal women. Br J Rad 1993; 66:514–521.
25   Kanis JA, Melton LJ III, Christiansen C, et al. The diagnosis of osteoporosis. J Bone Min Res 1994; 9:1137–1141.

26 McDonald JA, Dunstan CR, Dilworth P, *et al.* Bone loss after liver transplantation. *Hepatology* 1991; 14:613–619.

27 Parfitt AM. The physiological and clinical significance of bone histomorphometric data. In: *Bone Histomorphometry. Techniques and Interpretations*. Recker R. (editor). Boca Raton, Florida: CRC Press; 1983. pp. 143–223.

28 Almond MK, Kwan JTC, Evans K, *et al.* Loss in regional bone mineral density in the first 12 months following renal transplantation. *Nephron* 1994; 66:52–57.

29 Stewart AF, Adler M, Byers CM, *et al.* Calcium homeostasis in immobilisation: an example of resorptive hypercalciuria. *N Engl J Med* 1982; 306:1136–1140.

30 Horber FF, Casez JP, Steiger U, *et al.* Changes in bone mass early after kidney transplantation. *J Bone Min Res* 1994; 9:1–9.

31 Almdal T, Schaadt O, Vesterdal Jørgensen J, *et al.* Vitamin D, parathyroid hormone, and bone mineral content of lumbar spine and femur in primary biliary cirrhosis. *J Int Med* 1989; 225:207–213.

32 Guañabens N, Parés A, Mariñoso L, *et al.* Factors influencing the development of metabolic bone disease in primary biliary cirrhosis. *Am J Gastroenterol* 1990; 85:1356–1362.

33 Navasa M, Monegal A, Guanabens N, *et al.* Bone fractures in liver transplant patients. *Br J Rheumatol* 1994; 33:52–55.

34 Hawkins FG, Leon M, Lopez MB, *et al.* Bone loss and turnover in patients with liver transplantation. *Hepatol Gastroenterol* 1994; 41:158–161.

The comparison of neutron activation analysis and photon absorptiometry at the same part-body site

Michael A Smith†, Robert A Elton‡ and Peter Tothill†

Department of Medical Physics and Medical Engineering†, and Medical Computing and Statistics Unit‡, University of Edinburgh, Edinburgh, Scotland

Abstract. Two non-invasive methods of bone measurement were, for the first time, compared at the same part-body site. Bone calcium, using *in vivo* neutron activation analysis, and bone mineral, using photon absorptiometry, were measured in the forearm in a group of renal patients. A highly significant correlation was obtained from absolute values ($r = 0.91$) which was reduced after normalisation ($r = 0.75$). Percentage changes, over periods totalling 31.3 patient years, were also highly significantly correlated ($r = 0.61$, $P < 0.001$). The precision of the techniques accounts for the spread of the bivariate data and the estimated line of the true relationship was not significantly different from the line described if the percentage changes measured by the two techniques were equal. The two basic techniques were shown to be equally sensitive *in vivo* methods for monitoring calcified bone in patients suffering from metabolic bone disease.

1. Introduction

In metabolic bone disorders such as renal osteodystrophy, osteomalacia and osteoporosis, the loss of calcified bone will increase the tendency to fracture. It is therefore necessary to establish a means of quantifying any such bone loss, both for the routine management of patients and also to evaluate possible therapeutic regimes.

The two most precise non-invasive techniques of investigating the bone status are neutron activation analysis (NAA) and photon absorptiometry. NAA has been used clinically to measure both whole-body calcium and part-body calcium whilst photon absorptiometry has been used principally to measure the bone mineral content (BMC) of the forearm. The two techniques measure similar, though not identical, parameters. NAA measures purely calcium; photon absorptiometry, on the other hand, reflects total mineral content, usually in a small volume of bone.

Comparisons have been made in clinical studies between absolute values, normalised values (a correction being made to eliminate the variation in patient size) and fractional changes over a time period using the two techniques. Highly significant correlations have been found between absolute photon absorptiometry and both whole-body and part-body NAA (Chesnut *et al* 1973, Cohn *et al* 1974, 1975, 1976, Harrison *et al* 1974, Manzke *et al* 1975, Naik *et al* 1977, Zanzi *et al* 1978, Maziere *et al* 1979). As both techniques give values that are dependent on the size of the patient, these correlations are to be expected. The correlation coefficients were reduced when normalisation procedures were adopted in an attempt to correct for the size of the patient (Cohn *et al* 1974, 1975, Manzke *et al* 1975). The significant correlations that exist after normalisation may reflect the inadequacies of the normalisation procedures rather than demonstrating any relationship between the techniques themselves.

The most important comparison is therefore between changes measured over a period by the two methods. All such comparisons reported so far have failed to demonstrate any significant correlation (Harrison *et al* 1974, Aloia *et al* 1975, Cohn *et al* 1975, 1976, Dabek *et al* 1977) though 'reasonable agreement' was found in one study (Harrison *et al* 1974). It must be noted that different body sites were used for the two techniques so the lack of correlation could therefore reflect the different rates of change in bone at different sites in the body rather than differences between the two methods.

This study seeks to obtain a valid comparison of the two methods by comparing absolute, normalised and percentage changes measured by photon absorptiometry and NAA at the same part-body site, measurements of the forearm being correlated in a long-term clinical study.

2. Methods and patients

The main purpose of our research work has been the development and evaluation of NAA to measure forearm calcium. Care was taken in the design and construction of the apparatus to obtain a high level of precision. Photon absorptiometric measurements however were performed using available apparatus which had been constructed many years earlier in our workshop with the aim of monitoring bone mineral content in renal patients.

2.1. Part-body NAA

The calcium in the forearm was activated using two ^{252}Cf neutron sources positioned one either side of the forearm. The induced ^{49}Ca activity was then measured by two $15 \text{ cm} \times 10 \text{ cm}$ NaI detectors, also in a bilateral arrangement (Smith and MacPherson 1977, Smith and Tothill 1979). The irradiation apparatus had initially been designed to measure only changes in forearm calcium. Three repeated measurements were performed at each visit producing a precision of the calcium measurement of 1.8%. At the final visit an additional measurement was performed using the apparatus which was more suitable for absolute calcium measurements. Immersion of the forearm in a water bath (Smith and Tothill 1979) eliminated the variation in the sensitivity of activation due to soft tissue around the bone. The precision of a single measurement of absolute forearm calcium was 2.6%. To normalise for body stature the absolute calcium values were divided by the cube of the patient's height, this factor giving the smallest spread of the data from a series of normal forearm measurements (Tothill *et al* 1979).

The bilateral geometry effectively eliminated errors due to minor patient movement. The design of the apparatus, with the arm always held rigidly in the same arm rest, eliminated any subjective choice of the measurement site and hence inter-operator error. The efficiency of activation and detection are not uniform along the length of the forearm, the combination approximating to a normal distribution of full width at half maximum of 14 cm centred 19 cm from the centre of the fist. It is therefore not appropriate to express the results in grams of calcium. The measurements are 'absolute' in the sense that the ^{49}Ca counts recorded depend only on the mass of calcium and its distribution along the sensitive volume, and not on such factors as the thickness or composition of overlying tissue. The results are expressed as 'calcium counts', corrections being derived for such factors as source decay by measurements on a calcium standard.

2.2. Photon absorptiometry

The bone mineral content of the radius was measured using the techniques described by Cameron and Sorenson (1963). Calipers were used to define the measurement site 5 cm from the styloid process after which the forearm was positioned horizontally with the inside of the forearm uppermost in a water bath. A 1.665 GBq (45 mCi) ^{241}Am source and NaI detector with a collimation of 0.5 cm × 1.2 cm, scanned across the radius, counting for 5 s every millimetre (approximate count rate, 6×10^3 CPS). Three repeated scans across the radius were performed and the data were stored on punched tape for computer analysis. The precision of the BMC measurement on normal volunteers was approximately 3.5%. The width of the radius, obtained by plotting the BMC values across the forearm, was used as the normalisation factor.

It is recognised that neither the site nor the source were ideal for BMC measurements. The former was used to be consistent with previous studies whilst the latter was used for financial reasons. Our method of photon absorptiometry was more prone to patient movement and repositioning errors than NAA; in addition, varying amounts of overlying fat would affect the BMC measurements.

Only about 10% of the bone at the 5 cm site is trabecular (Melsen *et al* 1979) so both NAA and photon absorptiometry are measuring predominantly cortical bone.

2.3. Patient group

Nineteen renal patients undergoing chronic haemodialysis at home were followed for 22 months in a study to evaluate the effect of dialysate calcium levels and treatment with 1α-hydroxycholecalciferol. The same NAA apparatus was used to measure the forearm calcium at times 0, 8 and 22 months to determine the percentage changes over the first 8-month and then subsequent 14-month period. Changes in bone mineral content by photon absorptiometry were also measured over the same periods. Of the 19 patients at the start of the study, 18 were measured at eight months and the surviving 16 at 22 months. In addition absolute forearm calcium was measured at 22 months.

Absolute and normalised part body calcium and bone mineral content were correlated in 16 patients and percentage changes were correlated from 34 sets of data totalling 31.3 patient years. Regression analysis of the second kind (Documenta Geigy 1970) was performed on the data and $P > 0.05$ was taken to be non-significant. Having performed the regression analysis on the percentage changes measured by NAA and photon absorptiometry a χ^2 value was calculated which established whether the known errors of the two methods could account for any observed spread of the bivariate data about a straight line (see Appendix 1).

3. Results

The results of the absolute measurements are displayed in figure 1 and the results of the percentage changes in figure 2. As it is the percentage difference between the two sets of measurements which is plotted in figure 2, the error becomes the precision $\times \sqrt{2}$, i.e. 5.0% and 2.6% for BMC and NAA respectively. The estimated line of the true relationship (see Appendix 1) is displayed. This would only correspond to the major axis of the ellipse (figure 2) if the precisions of the two techniques were identical. Tolerance ellipses ($P = 0.05$) are displayed with the data and the results of the regression analysis are given in table 1. The result of the χ^2 analysis of the data in figure 2 was $\chi^2 = 36.2$ ($P = 0.30$).
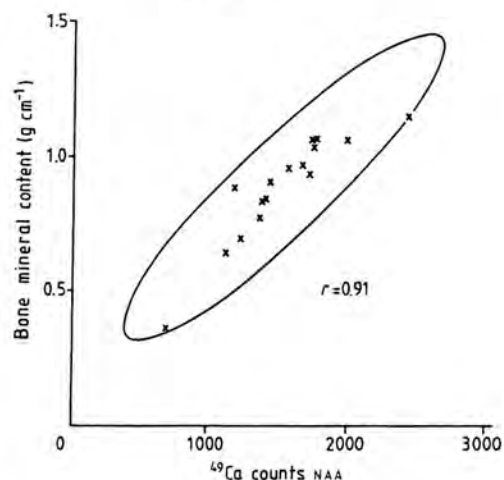
Figure 1. Correlation of absolute bone mineral content (BMC) measured by photon absorptiometry against forearm calcium measured by NAA.
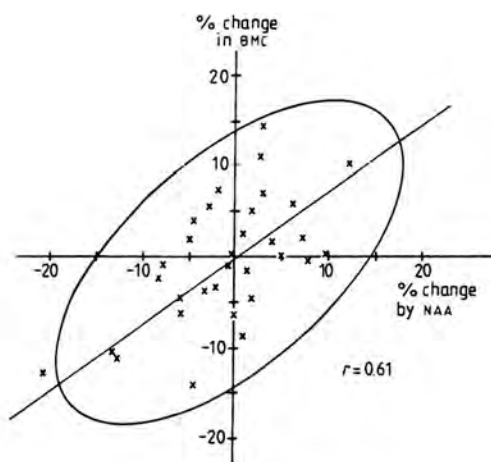
Figure 2. Correlation of percentage changes in bone mineral content (BMC) by photon absorptiometry against percentage changes in forearm calcium by NAA. Estimated line of true relationship is displayed.

Table 1. Correlation coefficients.

	n	r	P
Absolute values	16	0.91	<0.001
Normalised values	14	0.75	<0.01
Percent changes	34	0.61	<0.001

n = number of sets of patient measurements.

4. Discussion

This group of renal patients proved to be an ideal one to correlate NAA with photon absorptiometry because not only did they have a wide variation in absolute NAA values but also some large percentage changes over the period of the study. The NAA results are supported by clinical findings; a highly significant inverse correlation ($r = -0.84$, $P < 0.001$) was found between the normalised forearm calcium and the duration of dialysis and the patients receiving 1α-hydroxycholecalciferol were shown to increase significantly their forearm calcium during the study (Winney *et al* 1977, Smith *et al* 1979, 1981).

The correlation coefficient $r = 0.91$ for absolute values falling to $r = 0.75$ after normalisation agrees very well with the values found in comparisons between whole body NAA and forearm photon absorptiometry (Cohn *et al* 1975, Manzke *et al* 1975) and is better than values obtained by Maziere *et al* (1979) and Harrison *et al* (1974) who compared forearm photon absorptiometry with part-body NAA of the hand and trunk respectively. The decrease in the correlation coefficient from 0.91 to 0.75 after normalisation suggests that the high correlation between absolute values is due to a large extent to the size of the patient. As neither of the normalisation factors are perfect, the true correlation is probably lower still. This inability to eliminate completely the effect of stature means that the most important information can only be obtained by comparing the changes measured by the two techniques.

There are two important questions that need to be answered from the analysis of the percentage changes. Firstly, are changes in calcified bone measured by NAA and photon absorptiometry related and, secondly, if this is so, which is the more sensitive method.

This study is the first to show a highly significant correlation ($r = 0.61$, $P < 0.001$) between changes measured by NAA and photon absorptiometry. In addition the χ^2 value obtained showed that the errors of the techniques could account for the spread of the bivariate data. This is further demonstrated by the fact that 80% of the data points in figure 2 are within one standard deviation of the estimated line of the true relationship, suggesting that the scatter about the line is due to the known measurement errors. Consequently, if a perfect correlation between the methods did exist, the data would not be distributed along a straight line but in an ellipse of comparable width to the one obtained in this study.

Information about which of the two methods is the more sensitive is obtained from the estimated line of the true relationship of the data (figure 2). This line crosses the axes extremely close to the origin and the slope of the line appears to suggest that NAA is the more sensitive, as would be expected due to the better precision of the method. However, the 95% confidence interval of the line contains the line $Y = X$ so the line through the origin with slope unity is not significantly different from the estimated line of the true relationship of the data.

The discussion must now be extended to consider how the results from our specific methods of NAA and photon absorptiometry can be used to draw more general conclusions about the two techniques. In our hands NAA has a better precision, although figures of 1% have been quoted for some photon absorptiometry apparatus (Christiansen and Rodbro 1977). If, in figure 2, the BMC had the same precision as NAA then the line of relationship would be the major axis of the ellipse, which has a slope of 0.95. Thus NAA and photon absorptiometry, generally speaking, are equally sensitive *in vivo* techniques for monitoring bone status in the forearm in patients suffering from metabolic bone disease. An implication of the findings is that the lack of correlation of

changes found by others is due to real physiological differences between parts of the body and not to the use of alternative measurement techniques.

Appendix 1.

The equation to calculate χ^2 to test whether the specified error variances of the NAA and photon absorptiometry measurements are large enough to account for the observed spread of the bivariate data about a straight line (Sprent 1966) is as follows:
Let

$$(S_x)^2 = \text{error variance of } x\text{-axis}$$

where

$$S_x = \text{precision of NAA measurement} \times \sqrt{2}.$$

Similarly for the y-axis for photon absorptiometry.
Then

$$\chi^2 = \frac{S_{yy} - 2bS_{xy} + b^2 S_{xx}}{(S_y)^2 + b^2 (S_x)^2} \quad (n-1 \text{ degrees of freedom})$$

where

$$b = \frac{S_{yy} - \lambda S_{xx} + [(S_{yy} - \lambda S_{xx})^2 + 4\lambda S_{xy}^2]^{1/2}}{2S_{xy}}$$

and

$$\lambda = (S_y/S_x)^2$$
$$S_{xx} = \sum (x_i - \bar{x})^2, \qquad S_{yy} = \sum (y_i - \bar{y})^2$$
$$S_{xy} = \sum (x_i - \bar{x})(y_i - \bar{y}).$$

b is the slope of the estimated line of the true relationship between x and y.

Acknowledgments

Résumé

Comparaison en une même partie du corps de l'analyse par activation neutronique et de la mesure par absorption des photons.

Pour la premiere fois, une étude comparative de deux méthodes non-invasives de mesure de l'os ont été comparées, en une même partie du corps. Nous avons mesuré, au niveau de l'avant-bras, dans un groupe de patients ayant une atteinte rénale, le calcium osseux, en utilisant l'analyse par activation neutronique *in vivo* et l'os minéral, en utilisant la mesure par absorption des photons. Nous avons obtenu une correlation hautement significative pour les valeurs absolues ($r=0,91$), celle-ci diminue apres normalisation ($r=0,75$). Les changements en pourcentage, sur une periode totale de 31,3 années-malades, sont également corrélés de maniere hautement significative ($r=0,61$), $P<0,001$). La distribution de ces données bivariates est

expliquée par la précision des techniques. La ligne de régression estimée à partir des vraies valeurs ne diffère pas significativement de celle obtenue en supposant que les changements en pourcentage mesurés par les deux techniques sont égaux. Nous avons montré que ces deux techniques de base, de surveillance *in vivo* de l'os calcifié, chez des patients souffrant de maladies osseuses metaboliques, ont une sensibilite égale.

Zusammenfassung

Ein Vergleich zwischen Neutronenaktiviersungsanalyse und Photonenabsorptiometrie bei gleicher Teilkörperlage.

Zwei nicht-invasive Methoden zur Messung am Knochen werden bei gleicher Teilkörperlage verglichen. Mit der *in vivo* Neutronenaktivierungsanalyse wurde das Kalzium im Knochen, mit der Photonenabsorptiometrie der Mineralgehalt des Knochens im Vorderarm von Nierenpatienten gemessen. Aus den Absolutwerten ($r = 0.91$) erhielt man eine hochsignifikante Korrelation, die nach der Normalisierung ($r = 0.75$) reduziert wurde. Prozentuale Änderungen waren ebenfalls hochsignifikant korreliert ($r = 0.61$, $P = 0.001$). Die Genauigkeit, die man erhält durch das Spreizen der zweidimensionalen Werte und die geschätzte Linie der wahren Beziehung, war nicht sehr verschieden von der Linie, wenn die gemessenen prozentualen Änderungen bei beiden Techniken gleich waren. Es wird gezeigt, daß beide Techniken gleich empfindliche *in vivo* Methoden zur Darstellung verkalkter Knochen sind bei Patienten, die an einer Stoffwechselkrankheit leiden.

References

Aloia J F, Ellis K J, Zanzi I and Cohn S H 1975 *J. Nucl. Med.* **16** 196–9
Cameron J R and Sorenson J 1963 *Science, NY* **142** 230
Chesnut C H, Manzke E, Baylink D and Nelp W B 1973 *J. Nucl. Med.* **14** 386
Christiansen C and Rodbro P 1977 *Scand. J. Clin. Lab. Invest.* **37** 321–3
Cohn S H, Ellis K J, Caselnova R C, Asad S N and Letteri J M 1975 *J. Lab. Clin. Med.* **86** 910–9
Cohn S H, Ellis K J, Martino A N, Asad S N and Letteri J M 1976 *Calcif. Tissue Res.* **21s** 216–20
Cohn S H, Ellis K J, Wallach S, Zanzi I, Atkins H L and Aloia J F 1974 *J. Nucl. Med.* **15** 428–35
Dabek J T, Robinson B H B, Naik R B and Al-Hiti K 1977 *Clin. Endocrinol.* **7s** 147–50
Documenta Geigy Scientific Tables 1970 7th edn pp. 179–83
Harrison J E, McNeill K G, Meema H E, Fenton S, Oeropoulos D G and Sturtridge W C 1974 *J. Nucl. Med.* **15** 929–34
Manzke E, Chesnut C H, Wergedal J E, Baylink D J and Nelp W B 1975 *Metabolism* **24** 605–15
Maziere B, Kuntz D, Comar D and Ryckewaert A 1979 *J. Nucl. Med.* **20** 85–91
Melsen F, Mosekilde L, Nielsen H E and Christensen P 1979 *Calcif. Tissue Int.* **27s** 28
Naik R B, Dabek J T, Heynen G, James H M, Kanis J A, Robertson P W, Robinson B H B and Woods C G 1977 *Clin. Endocrinol.* **75** 139–45
Smith M A and MacPherson J N 1977 *Calcif. Tissue Res.* **22s** 568–71
Smith M A and Tothill P 1979 *Phys. Med. Biol.* **24** 319–29
Smith M A, Tothill P, Simpson J D, MacPherson J N, Winney R J and Strong J A 1979 *Calcif. Tissue Int.* **27s** 43
Smith M A, Winney R J, Strong J A and Tothill P 1981 *Nephron* in press
Sprent P 1966 *J. Royal Stat. Soc.* **28**B 278–84
Tothill P, Smith M A, Simpson J D, Chew I, MacPherson J N, Winney R J and Strong J A 1979 in *Nuclear Activation Techniques in the Life Sciences*, ST1/PUB/492 (Vienna: IAEA) pp 687–99
Winney R J, Tothill P, Robson J S, Abbot S R, Lidgard G P, Cameron E H D, Smith M A, MacPherson J N and Strong J A 1977 *Clin. Endocrinol.* **7s** 151–8
Zanzi I, Colbert C, Bachtell R, Thompson K, Aloia J and Cohn S 1978 *Am. J. Roentgenol.* **131** 551

SIR,—Your recent leading article (4 April, p 1096) draws conclusions with which we cannot entirely agree. Certainly patients who undergo surgery for peptic ulcer are at increased risk of dying prematurely. This was the conclusion in our article to which you refer,[1] and was re-emphasised in an extended study (on 779 males aged 30-59 years operated on from 1947 to 1965) recently presented to the British Society of Gastroenterology. Over a 15-32-year follow-up period highly significant increases in mortality occurred in all age groups. In both studies we found that the major contribution to this excess mortality was provided by diseases which have close associations with cigarette smoking (carcinoma of the lung and oesophagus, ischaemic heart disease, and chronic bronchitis and emphysema[2]). In our experience gastric carcinoma was no more common than predicted for an age-matched Scottish population. Eighty-four per cent of the patients studied were smokers prior to operation and this proportion of smokers remains unchanged among our patients now undergoing highly selective vagotomy.

Surgically treated ulcer patients as a group are heavy cigarette smokers. The crucial question therefore is not whether 5% or more of the survivors of the "gastrectomy bonanza" will subsequently develop carcinoma of the stomach but whether patients coming to surgery can be persuaded to cease smoking. Otherwise the trend towards premature death will not diminish with the abandonment of gastrectomy and patients undergoing highly selective vatogomy will die as prematurely as their gastrectomised predecessors.

A H McLean Ross
John Anderson
W P Small

Gastric Follow-up Clinic,
Department of Surgery,
Western General Hospital,
Edinburgh EH4 2XU

M A Smith

Department of Medical Physics,
Royal Infirmary,
Edinburgh EH3 9YW

[1] Din NA, Small WP. Gut 1974;15:335.
[2] Doll R, Peto R. Br Med J 1976;ii:1525-36.

LATE MORTALITY AFTER SURGERY FOR PEPTIC ULCER

A. Hugh McLean Ross, M.B., Ch.B., Michael A. Smith, Ph.D., John R. Anderson, M.B., Ch.B., and William P. Small, Ch.M.

Abstract To examine the claim that life expectancy is reduced after curative peptic-ulcer surgery, we studied mortality and its causes in 779 men with peptic ulcer treated surgically between 1947 and 1965. The minimum follow-up period of survivors was 15 years.

There was an excess mortality in the three major age groups (30 to 39, 40 to 49, and 50 to 59 years at operation), as compared with the general population (P<0.001), with a mean shift of 9.1 years in the survival curve. Surgery was not the direct cause of death. In particular, the eight deaths from carcinoma of the stomach were no more than expected. Excess mortality was due to smoking-associated disease, which accounted for 200 deaths. Eighty-three per cent of the patients were cigarette smokers.

We conclude that substituting highly selective vagotomy for gastrectomy will not lead to improved survival, because 80 per cent of patients now having operations for ulcer are heavy cigarette smokers. (N Engl J Med. 1982; 307:519-22.)

T HE long-term survival of patients who undergo curative surgery for peptic ulcer has attracted relatively little recent attention.[1] In 1958 Krause showed that patients tended to die prematurely in the years after Pólya gastrectomy[2]; the major contributors to this excess mortality were tuberculosis, carcinoma of the gastric remnant, suicide, and alcoholism. In the same year Balint confirmed that the number of deaths from pulmonary tuberculosis was significantly increased after gastric surgery; this report also added ischemic heart disease and carcinoma of the lung to the list.[3] Other diseases since linked with gastric surgery include carcinoma of the esophagus,[4] certain neurologic disorders,[5] and gallstones.[6]

The general increase in life expectancy since the reports of Krause and Balint, together with earlier claims that patients who had undergone surgery for ulcer were bad risks in life-insurance terms,[7] prompted us to review the mortality trends in men undergoing curative peptic-ulcer surgery.

The aims of our study were twofold: to determine whether there was still a tendency for patients to die prematurely after a successful peptic-ulcer operation, and if so, to determine which factors contributed to the excess mortality.

METHODS

The records of all men between 30 and 59 years old who underwent peptic-ulcer surgery in the Western General Hospital between 1947 and 1965 were reviewed. These records are completed at the time of surgery and updated at regular intervals thereafter by standardized questionnaires or personal interviews.

Three categories of patients were excluded from the analysis: those who died within one year of surgery, those who underwent simple closure of a perforated ulcer, and those in whom peptic ulcer subsequently recurred.

The patient's age at operation, the date of operation, the type of operation, the smoking status at operation, the age at death, and the cause of death were recorded. The cause of death in patients who died at home during the study period was taken as the underlying cause registered on the death certificate.

Of the 856 patients in the series, 77 (9 per cent) were excluded either because their records were incomplete or because they were lost to follow-up by the end of 1979. The study population therefore comprises 779 patients. By the end of 1979, 360 patients had died.

Six hundred seventy (86 per cent) of the 779 patients were treated by gastrectomy, and 101 (13 per cent) by drainage with or without vagotomy.

Method of Analysis

Actuarial survival curves were constructed to assess the mortality rate for each of three 10-year age groups: 30 to 39, 40 to 49, and 50 to 59 years at operation. These curves were compared with curves of expected survival calculated for the general population from life-table figures obtained from the Faculty of Actuaries of Edinburgh and appropriate to the period and the age groups under study. All patients were included in the calculation of the percentage surviving at 5, 10, and 15 years after surgery. In order to calculate the percentage surviving 20 and 25 years after surgery, subgroups of patients who underwent surgery before 1955 were used. The numbers of patients in the subgroups from 30 to 39, 40 to 49, and 50 to 59 years old were 85, 157, and 132, respectively.

The expected numbers of deaths from individual diseases were obtained from figures published by the Registrar General for Scotland (RGS).[8] For this purpose, the study group was not divided into the three groups used for the survival analysis. Two methods of calculating the expected number of deaths were used. When available from the RGS statistics, the death rate (expressed as the number of deaths per year per 100,000 population) was used. Data were analyzed in three five-year periods from 1965 (when input into the study group had ceased and the size of the group was 701 patients) until 1980. The age spectrum of the study group for each such period was calculated in 10-year intervals and combined with data from the RGS for the same age decades. The RGS data used were those for the middle year of each period (1967, 1972, and 1977). The three causes of death analyzed by this method were ischemic heart disease, chronic bronchitis and emphysema, and carcinoma of the lung.

For the causes of death for which the death rate per 100,000 population was not published, a second method was used. The study group was split into five periods from 1955 to 1980. As before, the RGS figures used were those for the middle year of each period, considered in 10-year age intervals. For each disease, the number of deaths per year recorded in the RGS figures was expressed as a percentage of the total number of deaths from all causes in the same age group. This was then combined with the total number of deaths in the corresponding age group of the study population for the particular five-year period, resulting in the expected number of deaths from a particular cause. This method of analysis alone was applied to six causes of death: carcinoma of the stomach, carcinoma of the pancreas, carcinoma of the esophagus, carcinoma of the colon and rectum, suicide, and cirrhosis of the liver. It was also employed for ischemic heart disease, chronic bronchitis, and carcinoma of the lung for the period from 1955 to 1965, when death rates expressed as deaths per year per 100,000 population were not published. Both methods of analysis took account of variations in causes of death with age and time.

When appropriate, the chi-square test was used to assess significance. When the expected number of deaths was less than five and the chi-square method was consequently invalid, the probability was calculated directly from the equation of the binomial distribution.[9]
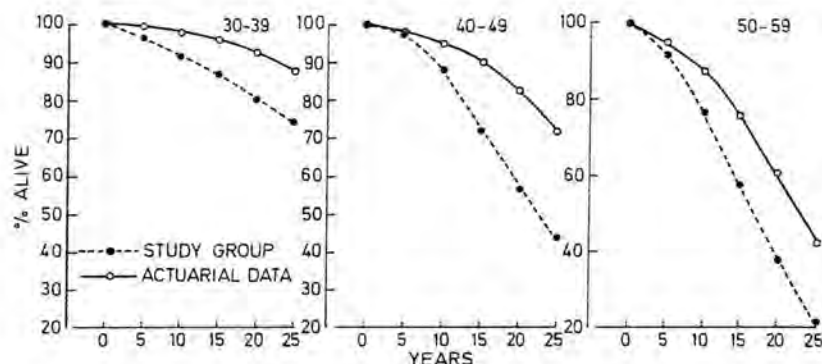
Figure 1. Survival Curves for the Three Age Groups (30 to 39, 40 to 49, and 50 to 59 Years at Operation).

Curves for expected survival were calculated from general-population data obtained from the Faculty of Actuaries of Edinburgh.

RESULTS

When the life-table survival curves for each of the three age groups studied are compared with the survival curves predicted for the general population, it is seen that the study population had a significant increase in mortality rate (Fig. 1) ($P<0.001$ in each age group). Figure 2 shows the death rate per year for each age group at operation over the first 15 years after the the operation. The curve for the study group (which includes a figure for 20 to 29-year-old patients who underwent surgery for peptic ulcer during the same period) is shifted to the left, indicating premature mortality; the mean shift of the curve is 9.1 ± 0.1 years.

Table 1 shows the number of deaths from individual diseases by age group during the study.

Deaths from diseases that have been identified as having close associations with smoking,[10] diseases that have been related to the sequelae of gastric surgery,[2] and other diseases with significant variations from the predicted values are detailed in Table 2.
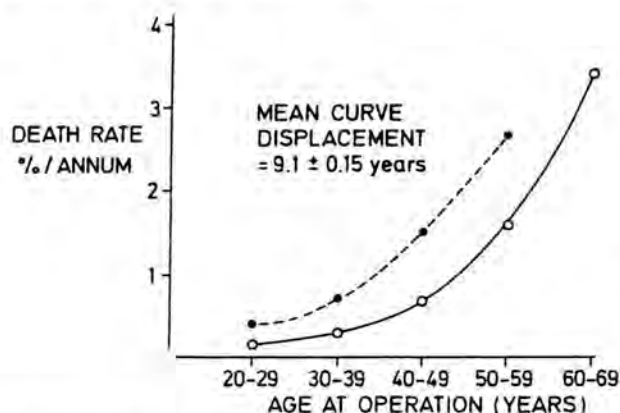
Figure 2. Death Rates for Each Age Group during the First 15 Years after Surgery.

The study group is represented by the dashed line, and actuarial data by the solid line. The figures include data for patients between 20 and 29 years old who underwent surgery in the same period.

Eighty-three per cent of the patients were cigarette smokers at the time of operation.

There were eight deaths from carcinoma of the stomach; the average time from gastrectomy to death from carcinoma was 18.9 years.

There were significant increases in the numbers of deaths from cirrhosis of the liver, suicide, carcinoma of the colon and rectum, and carcinoma of the pancreas.

DISCUSSION

Since Krause[2] first identified the increased risk of premature death in the years after peptic-ulcer surgery, this finding has been confirmed by others.[3,11,12]

Earlier, the nature of the link between the increased incidences of ischemic heart disease, of tuberculosis,[13] of carcinoma of the lung, esophagus, or stomach, of suicide, and of alcoholism after peptic-ulcer surgery was not always clear. However, the growing realization of the part played by smoking in the causation of a number of these diseases clarifies the relation of gastric surgery to shortening life expectancy.[10,14,15]

Our study confirms a tendency for patients who have undergone a curative ulcer operation to die prematurely in the years after the operation. The shortening of life expectancy was approximately nine years — a figure similar to that calculated several years ago with some of the population data presented here.[11] The trend toward premature death occurred in each age group at operation that we studied.

Thus, persons who have had surgery for ulcer are indeed bad risks in life-insurance terms. The question is why.

Of the four causes originally shown to be related to gastrectomy, pulmonary tuberculosis has now been virtually eliminated. We could attribute only two deaths to this disease.

An increased incidence of gastric carcinoma after gastrectomy has been reported,[16-18] but we found that it was no more common than predicted for an age-matched Scottish population. Stalsberg[19] suggested

that the increase in incidence occurs only 15 years or more after surgery; before then, the incidence may be decreased.[20] The average interval between gastrectomy and death from gastric carcinoma was 18.9 years in our study, so that insufficient time may have elapsed. If a subsequent increase does occur, its contribution to the overall excess mortality will be small.

Thus, of Krause's original four contributors, only alcoholism (as measured by liver cirrhosis) and suicide have in our experience contributed to the excess mortality. But numerically the excess was small. The major contribution was from the diseases that are closely associated with smoking. In men these diseases are identified as carcinoma of the lung and other respiratory sites, carcinoma of the esophagus, tuberculosis, chronic bronchitis and emphysema, pulmonary heart disease, aortic aneurysm, hernia, and ischemic heart disease.[10] In our study tuberculosis, hernia, and aortic aneurysm accounted for only three deaths. Overall, deaths due to the other five diseases were significantly more common than predicted for an age-matched Scottish population (P = 0.025), although individually these increases over the predicted values did not reach statistical significance. In particular, the number of deaths from ischemic heart disease, though increased, was not significantly different from the predicted value. Doll and Peto have shown that in men the link between ischemic heart disease and smoking is

Table 1. Causes of Death According to Age Group.*

CAUSE OF DEATH	AGE GROUP AT DEATH (YR)						
	TOTAL	30–39	40–49	50–59	60–69	70–79	≥80
	no. of deaths						
Ischemic heart disease	128	1	4	36	65	19	3
Carcinoma of the lung	47	—	1	8	28	10	—
Cerebrovascular accident	29	—	2	5	13	9	—
Chronic bronchitis and emphysema	22	—	—	4	14	4	—
Bronchopneumonia	21	—	—	5	7	6	3
Carcinoma of the colon and rectum	16	—	1	2	11	2	—
Carcinoma of the pancreas	11	—	3	2	5	1	—
Suicide	10	—	4	3	1	2	—
Carcinoma of the stomach	8	1	—	1	4	1	1
Accident	8	—	2	4	2	—	—
Hepatic cirrhosis	7	—	2	3	2	—	—
Peripheral vascular disease	6	—	—	2	2	2	—
Carcinoma of the prostate	5	—	—	—	3	2	—
Pulmonary embolism	5	—	—	2	3	—	—
Other malignant diseases	21	—	—	12	5	3	1
Other gastrointestinal diseases	4	—	—	1	2	1	—
Other respiratory diseases	3	—	—	2	—	1	—
Other vascular diseases	3	—	1	1	1	—	—
Miscellaneous	6	—	1	2	—	3	—

*Diseases that caused five or more deaths in the series are listed individually.

Table 2. Actual and Predicted Numbers of Deaths from Individual Diseases, 1955–1979.*

CAUSE OF DEATH	NO. OF DEATHS		P VALUE †
	ACTUAL	PREDICTED	
Ischemic heart disease and pulmonary heart disease ‡	128	112.5	NS
Chronic bronchitis and emphysema ‡	22	19.9	NS
Carcinoma of the lung and other respiratory sites ‡	47	35.7	0.05
Carcinoma of the esophagus ‡	3	2.7	NS
All smoking-associated diseases	200	170.8	<0.025
Carcinoma of the stomach	8	10.4	NS
Suicide	10	3.0	<0.05
Cirrhosis	7	2.2	<0.05
Carcinoma of the colon and rectum	16	8.9	<0.01
Carcinoma of the pancreas	11	3.9	<0.01

*Diseases with established links with smoking, diseases traditionally linked with gastric surgery, and other diseases with significant differences from the predicted number of deaths are listed.

†NS denotes not significant.

‡Smoking-associated disease.

strongest under the age of 45.[10] In patients over this age, the connection with smoking becomes weaker. Since the majority of our patients had the operation in their 40s, this may explain the insignificance of the rise over the predicted values.

Confirming the findings of others,[19,21] we found no significant increase in carcinoma of the esophagus. Although suicide and alcoholism are both traditionally regarded as potential sequelae of gastric surgery, both have established connections with smoking status. Possibly, they are related to the patient's psychological background as well as the need for peptic-ulcer surgery.

Carcinomas of the colorectum and of the pancreas were significantly increased in our study population, and these are also related to smoking status, although in the case of colorectal carcinoma the association is limited to carcinoma of the rectum.[10] No connection between these diseases and gastric surgery has been described, to our knowledge.

Thus, we found that diseases known to be related to smoking contributed more toward mortality than diseases traditionally linked with the sequelae or gastric surgery.

Eighty-three per cent of our patients were habitual cigarette smokers at the time of operation, and few ceased to smoke after surgery. The trend continues into the 1980s. Eighty per cent of our male patients presently undergoing highly selective vagotomy for chronic peptic ulceration are cigarette smokers, and this is occurring in a population in which the proportion of male smokers is diminishing. Clearly, the men who come to surgery for duodenal ulcer represent a select group.

Recently it has been suggested that the crucial question determining the fate of patients undergoing surgery for peptic ulcer is whether 5 per cent or more will subsequently have gastric-remnant carcinoma.[22] Should this occur, it will have relatively little impact on the problem of premature death after peptic-ulcer surgery.[23] Of much greater numerical importance is the problem of premature death caused by diseases associated with cigarette smoking. Despite reductions in the number of men in the general population who smoke, no such reduction is apparent in the group of patients with chronic peptic ulceration who require surgical treatment. The increase in premature death after surgery that cures ulcer will therefore continue, and since this increase is unrelated to the operation, the move from gastrectomy toward more conservative physiologic operations will not be followed by a significant improvement in life expectancy.

We are indebted to the staff of the Gastric Follow-Up Clinic and the Department of Medical Physics and Engineering for their invaluable assistance during this study, and to Prof. Sir Richard Doll for his helpful comments.

REFERENCES

1. Small WP. The long term results of peptic ulcer surgery. Clin Gastroenterol. 1973; 2:427-45.
2. Krause U. Late prognosis after partial gastrectomy for ulcer. Acta Chir Scand. 1958; 114:341-54.
3. Balint JA. Pulmonary tuberculosis and partial gastrectomy. Gastroenterologia. 1958; 90:65-84.
4. Shearman DJC, Finlayson NDC, Arnott SJ, Pearson JG. Carcinoma of the oesophagus after gastric surgery. Lancet. 1970; 1:581-4.
5. Williams JA, Hall GS, Thompson AG, Cooke WT. Neurological disease after partial gastrectomy. Br Med J. 1969; 3:210-2.
6. Horwitz A, Kirson SM. Cholecystitis and cholelithiasis as a sequel to gastric surgery: a clinical impression. Am J Surg. 1965; 109:760-2.
7. Sircus W, Small WP. The problem of peptic ulcer. Scott Med J. 1964; 9:453-68.
8. Registrar General for Scotland. Annual reports: Mortality statistics 1957, 1962, 1967, 1972, 1977.
9. Siegel S. Nonparametric statistics: for the behavioural sciences. New York: McGraw-Hill, 1956.
10. Doll R, Peto R. Mortality in relation to smoking: 20 years' observations on male British doctors. Br Med J. 1976; 2:1525-36.
11. Din NA, Small WP. Death after partial gastrectomy — a long term study. Gut. 1974; 15:335.
12. Skarstein A. Partial gastrectomy for peptic ulcer by the Krønlein method: long term results 12 years later with particular reference to general health condition and working capacity. Scand J Gastroenterol. 1980; 15: Suppl 64:1-7.
13. Wheldon EJ, Venables CW, Johnston IDA. Late metabolic sequelae of vagotomy and gastroenterostomy. Lancet. 1970; 1:437-40.
14. Doll R, Hill AB. Lung cancer and other causes of death in relation to smoking. Br Med J. 1956; 2:1071-81.
15. Crofton E, Crofton J. Influence of smoking on mortality from various diseases in Scotland and in England and Wales: an analysis by cohorts. Br Med J. 1963; 2:1161-4.
16. Stalsberg H, Taksdal S. Stomach cancer following gastric surgery for benign conditions. Lancet. 1971; 2:1175-7.
17. Helsingen N, Hillestad L. Cancer development in the gastric stump after partial gastrectomy for ulcer. Ann Surg. 1956; 143:173-9.
18. Domellöf L, Eriksson S, Janunger K-G. Late precancerous changes and carcinoma of the gastric stump after Billroth I resection. Am J Surg. 1976; 132:26-31.
19. Stalsberg H. Carcinoma of the oesophagus after gastric surgery. Lancet. 1972; 1:381.
20. De Jode LR. Gastric carcinoma following gastro-enterostomy and partial gastrectomy. Br J Surg. 1961; 48:512-4.
21. MacDonald JB, Waissbluth JG, Langman MJS. Carcinoma of the oesophagus and gastric surgery. Lancet. 1971; 1:19-20.
22. After gastrectomy. Br Med J. 1981; 282:1096-7.
23. McLean Ross AH, Anderson J, Small WP, Smith MA. After gastrectomy. Br Med J. 1981; 282:1472.

Late mortality after vagotomy and drainage for duodenal ulcer

SIR,—In their report (5 May, p 1335) on the survival of 711 patients who underwent truncal vagotomy and drainage for peptic ulcer Mr P C H Watt and others refer to our previously published study of 779 men undergoing surgery for peptic ulcer mainly by gastrectomy.[1] Direct comparison is not possible. The Belfast series included men and women patients, our series was restricted to men. The inclusion of women may explain the discrepancy between actual/predicted ratios (APR) for lung cancer (Belfast 3·35, Edinburgh 1·32). The actuarial curves show a greater reduction in survival for women than men. To compare the two studies it would be interesting to know the significance levels for survival and for individual disease incidence for the group of men only.

Whatever the reason for any discrepancies between the calculated APRs in Edinburgh and Belfast, there is clearly a real difference in the number of deaths due to gastric carcinoma, which accounts for 7·1% of all deaths in the Belfast study, compared with only 2·2% in the Edinburgh study. As all patients had vagotomy and drainage in the Belfast study compared with less than 13% in the Edinburgh study, the type of operation may explain the difference, though longer follow up may be required before increases are seen after gastrectomy.

None the less, of greater importance is the confirmation by Watt et al of the much larger contribution to excess mortality from disease having close associations with smoking (ischaemic heart disease, lung and oesophageal carcinoma, and chronic bronchitis).[2] One hundred and forty one of their patients died of these conditions while only 16 died of gastric carcinoma, emphasising the need to influence smoking habits if late mortality is to fall appreciably.

Finally, they confirm our finding of a statistically significant excess mortality from colorectal carcinoma following gastric surgery (APR 1·8, p = 0·01). Although not a major contributor to excess mortality, the increased incidence of colorectal carcinoma is academically stimulating in the search for factors of aetiological importance in the development of such tumours.

A H McLEAN ROSS
J R ANDERSON
M A SMITH
W P SMALL

Gastric Follow-Up Clinic,
Western General Hospital,
Edinburgh EH4 2XU

1 McLean Ross AH, Smith MA, Anderson JR, Small WP. Late mortality after surgery for peptic ulcer. N Engl J Med 1982;307:519-22.
2 Doll R, Peto R. Mortality in relation to smoking: 20 years observations on male British doctors. Br Med J 1976;ii:1525-36.

Metabolism of Sodium Pentosan Polysulphate in Man – Catabolism of Iodinated Derivatives

I. R. MacGregor[1], J. Dawes[2], L. Paton[3], D. S. Pepper[1], C. V. Prowse[3] and M. Smith[4]

From the Scottish National Blood Transfusion Service Headquarters Unit Laboratory[1], the MRC/SNBTS Blood Components Assay Group[2], Edinburgh, the S-E Scotland Blood Transfusion Service[3] and the Department of Medical Physics and Medical Engineering[4], Royal Infirmary, Edinburgh, Scotland, U.K.

Key words

Heparin analogue – SP54 – Metabolism – Iodinated derivatives – Organ distribution

Summary

An iodinated derivative of the heparin analogue SP54 has been prepared and used in conjunction with unlabelled SP54 to study the catabolism and organ distribution of this potential antithrombotic agent in healthy human volunteers. As observed previously with ^{125}I-heparin, we found that the ^{125}I-SP54 was rapidly cleared from the circulation, returning later in a desulphated form. Organ distribution studies with ^{123}I-SP54 suggested that the liver and spleen were major sites of desulphation. Gel filtration and Polybrene binding showed the presence of sulphated macromolecular SP54 and desulphated macromolecular and depolymerised SP54 in post-injection urines. No depolymerised material was present in plasma suggesting depolymerisation occurs in the kidney.

Introduction

Studies have demonstrated that heparin analogues which are relatively inactive in vitro may be potent anticoagulants in vivo and have led to a reappraisal of such properties (1, 2, 3). Pentosan polysulphate (SP54) is a semisynthetic linear polymer of $(1\rightarrow4)$ linked β-D-xylopyranose residues which contains $\cong$ 1.8 sulphate groups per monosaccharide unit and has a mean molecular weight of 6,000 daltons. It is less active than heparin in vitro but exhibits marked anticoagulant activity after injection in man. Several workers have shown that the inhibition of factor Xa activity in vivo is greater than obtained with a similar weight of injected heparin while thrombin inhibition is less (4, 5, 6, 7). Fischer et al. have also demonstrated that inhibition of factor Xa generation may be an important mechanism of SP54's activity (8). Such results have prompted clinical trials of the antithrombotic efficacy of SP54 which suggest that it can prevent postoperative thromboembolic complications (9, 10).

We have, therefore, investigated the catabolism of SP54 in man in view of its potential clinical use as an antithrombotic drug. Studies on the catabolism of heparin and its analogues have been previously hampered by the lack of a labelled molecule combining high specific activity with retention of biological activity but we have described the preparation and use of an iodinated derivatised heparin which possessed both properties (11). We have used a similar approach with SP54 by preparing a derivative containing tyrosyl residues via which the molecule can be iodinated using the conventional chloramine T method.

Correspondence to: Dr. I. R. MacGregor, Scottish National Blood Transfusion Service, Headquarters Unit Laboratory, 2 Forrest Road, Edinburgh EH1 2QN, Scotland, U.K.

The labelled SP54 has been used to study the catabolism of SP54 after intravenous and subcutaneous injection in human volunteers and to determine its organ distribution. The results indicate that the catabolism of SP54 follows similar general pathways to those previously described for heparin (11).

Materials and Methods

Derivatisation and Iodination of SP54

Gel filtered fractions of SP54 (Bene-Chemie, W. Germany) were provided by Drs. Tangen and Granath, Pharmacia. Their mean molecular weights were 3,000, 6,000 and 10,000 daltons as determined by low angle light scattering.

Fractionated SP54 was converted from the sodium salt to the tetrabutylammonium salt, freeze dried and dissolved in 0.5 ml dimethylsulphoxide to a concentration of 40 mg/ml. It was then reacted with 14 mg of carbonyldiimidazole at 56° C for 45 min following which 36 mg tyrosyl hydrazide was added and allowed to react overnight at 20° C. The tyrosyl-SP54 derivative was then converted to the Na^+ salt by adding excess sodium chloride, gel filtered on Sephadex LH-20 (Pharmacia, U. K.) in distilled water, and finally freeze dried. Tyrosyl incorporation was determined from the dry weight and absorption using a molar extinction coefficient E_{1cm}^{280} of 4.55×10^3.

10μg aliquots of derivatised SP54 were iodinated with ^{125}I or ^{123}I ($Na^{125}I$ and $Na^{123}I$, carrier free, Amersham, U. K.) using the chloramine T method of Greenwood et al. (12). The fraction of mean molecular weight 6,000 was used in all metabolism experiments.

Characterisation of ^{125}I-SP54

The molecular size distribution of ^{125}I-SP54 was compared with that of underivatised SP54 by gel filtration on a 95 × 3.6 cm column of Sephadex G-50 (Pharmacia, U. K.). The column was developed with 13 mM trisodium citrate, 150 mM NaCl, pH 6.7 and 8.3 ml fractions were collected. The elution position of underivatised SP54 was determined by measuring metachromasia with azure A (13), while that of the ^{125}I-SP54 was measured by gamma counting (NE-1600 γ counter, Nuclear Enterprises, U. K.).

The labelled and underivatised SP54 preparations were chromatographed on a 7 × 5.6 cm column of protamine agarose using an exponential gradient of 13 mM trisodium citrate, pH 6.7 containing from 0 to 3 M NaCl and were detected as described above. Salt concentration was measured conductimetrically.

Biological activity of derivatised SP54 was measured in an activated partial thromboplastin time assay (APTT) in vitro by adding known concentrations to a normal human citrated plasma pool (14). The APTT calibration curve was compared with that obtained using underivatised SP54.

Injection of ^{125}I-SP54 in Human Volunteers

Five healthy volunteers were fully informed of the procedures and aims of the study. Their weights ranged from 52–77 kg (mean 68) and their ages from 28–44 years (mean 34). Four subjects were injected intravenously with either 0, 0.1, 1, 7 or 50 mg SP54 containing 370 kBq ^{125}I-SP54, one subject receiving tracer alone and tracer plus 50 mg SP54 at an interval of 3 weeks. The fifth volunteer was injected subcutaneously with 50 mg SP54

containing 370 kBq ^{125}I-SP54. The actual amount of injected radioactivity was measured by counting a known fraction of the total volume of injection. 30 mg potassiumiodide was given orally each day to the subjects up to one week after injection. The unlabelled SP54 was an unfractionated sample used clinically.

Blood samples were taken at various times after injection by clean venepuncture from the antecubital veins and processed as described later. Urine samples of measured volume were collected at known times after injection.

Clearance of ^{125}I-SP54

Whole blood, platelet poor plasma (PPP), packed blood cells and urine obtained at various times after injection were counted for radioactivity in a gamma counter with the counts being corrected for background counts. The binding capacity of ^{125}I-SP54 for the polybasic chemical Polybrene (Aldrich, U. K.) was determined by end over end mixing of 5 ml plasma or urine with 0.2 ml of a slurry of Polybrene immobilised by linkage to epoxy agarose 6B (Pharmacia, U. K.). The molecular size distribution of ^{125}I-SP54 in plasma or urine was estimated by gel filtration on Sephadex G-50 as described above.

Organ Distribution of ^{123}I-SP54

Prior to injection, the syringe containing 10.0 MBq ^{123}I-labelled SP54 and 1 mg unlabelled SP54 was measured against an ^{123}I standard of approximate activity 30 MBq. The subject was then injected in front of a Scintag-Berthold gamma camera and a series of nine anterior views at 5 min intervals starting 7.5 min after injection, were stored on a Technicare MCS 560 computer processor. Immediately following this a single 5 min posterior view was recorded. The net detected ^{123}I counts in the liver and spleen were obtained for each image using variable regions of interest on the computer. The absolute uptake, as a percent of the administered activity, was obtained by relating the geometric mean of the 45 min and 50 min anterior and posterior image to the ^{123}I standard which was also counted using the gamma camera. The uptake in the liver plus spleen was also measured at 3 hr and 43 hr after injection using a profile scan on the whole body counter. The separate retention in the liver and spleen at 3 hr and 43 hr could not be obtained because of the absence of lateral resolution in the whole body counter profile. In all calculations of the ^{123}I retention, allowances were made for radioactive decay.

Results

Characterisation of Iodinated SP54

In initial labelling experiments with molecular weight fractions of SP54, ^{125}I was preferentially incorporated, on a weight basis, into the lowest molecular weight fraction of 3,000 daltons. This was thought to be due to derivatisation proceeding via the
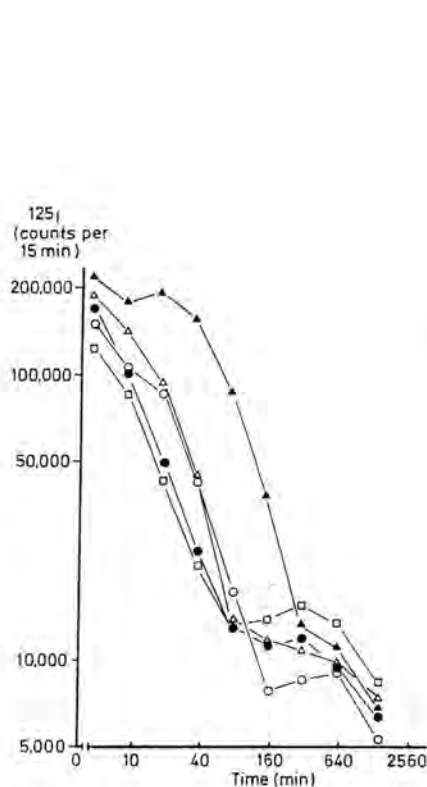
Fig. 1
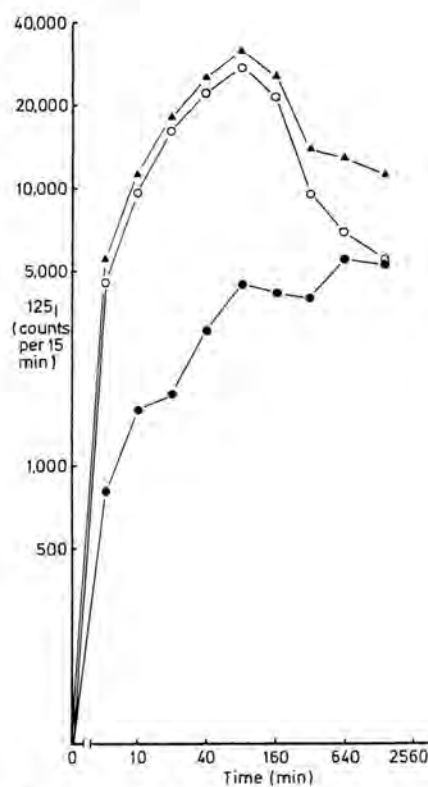
Fig. 2
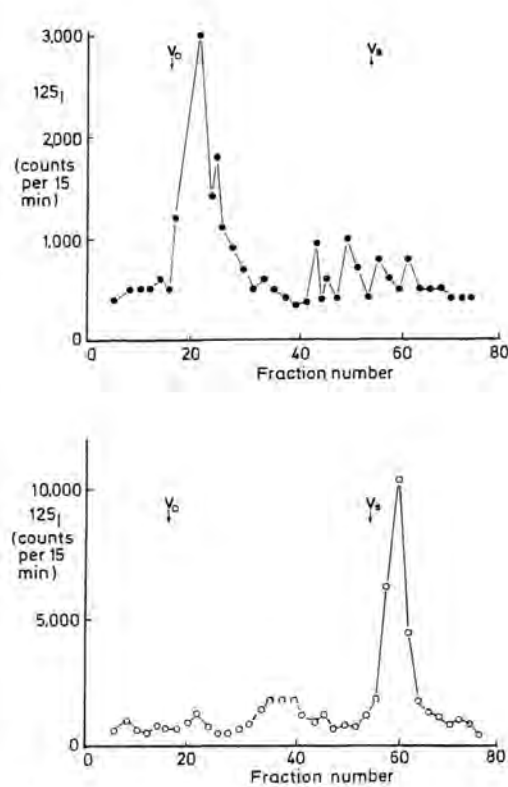
Fig. 3

Fig. 1 Clearance of ^{125}I-SP54 from the circulation. Radioactivity was monitored in blood samples taken at various times after intravenous injection of (nominal) 370 kBq ^{125}I-SP54, with 50 mg SP54, ▲–▲; with 7 mg SP54, ○–○; with 1 mg SP54, △–△; with 0.1 mg SP54, ●–●; and without unlabelled SP54 □–□. 5 ml sample volumes were counted throughout.

Fig. 2 Absorption and clearance of ^{125}I-SP54 in the circulation after subcutaneous injection. Radioactivity was monitored in samples taken at various times after subcutaneous injection of (nominal) 370 kBq ^{125}I-SP54 with 50 mg unlabelled SP54. Radioactivity in whole blood, ▲–▲; in plasma, ○–○; and in packed cells, ●–●. 5 ml sample volumes were counted throughout.

Fig. 3 Elution profile of gel-filtered radioactivity in plasma and urine obtained after i. v. injection of ^{125}I-SP54. Radioactivity was measured in fractions obtained after gel filtration of 5 ml plasma obtained at 320 min after injection of 370 kBq ^{125}I-SP54, ●–●; or 5 ml urine at 90 min after injection, ○–○; on a 95 × 3.6 cm column of Sephadex G-50 equilibrated with 13 mM citrate, 150 mM NaCl, pH 6.7. V_0 = void volume and V_s = solvent volume of the column.

reducing end of the molecule, rather than at free hydroxyl groups throughout the molecule, since the charge density of each labelled fraction was similar. Accordingly, a fraction of SP54 whose mean molecular weight was 6,000 was used for derivatisation and iodination and this exhibited a major elution peak coincident with that of unlabelled SP54 upon gel filtration. A second peak of radioactivity, which averaged 10% of the applied load, eluted in the solvent volume of the Sephadex G-50 column. Tyrosine was typically incorporated at 0.5 mole per mole of SP54.

Labelled and native SP54 eluted from protamine agarose at a similar salt concentration of 1.7 M NaCl. Up to 14% of the labelled material did not bind to the solid phase in 13 mM citrate.

Biological activity of the derivatised SP54 preparation of mean molecular weight 6,000 daltons was assessed by prolongation of the APTT of normal human plasma containing from 0–10 µg/ml derivatised SP54 or unmodified SP54. The activity of the derivatised SP54 averaged 69% of the activity of unmodified SP54, tested at three different concentrations.

Clearance of Injected ^{125}I-SP54

Radioactivity was initially cleared from the blood with a half-life of between 13–18 min at all i.v. doses except 50 mg where the half-life was 45 min, assuming zero order kinetics (Fig. 1). 90% of the radioactivity had been removed within 80 min of injection for the lower doses and within 240 min for the highest dose. Most remaining radioactivity was cleared in a second phase over the next 24–96 hr. The clearance of ^{125}I-SP54 from plasma and blood was initially similar, but the radioactivity in plasma decreased more rapidly than in whole blood, due to the progressive association of ^{125}I-SP54 with the packed cell fraction as shown in Table 1.

After s.c. injection of 50 mg SP54 with 370 kBq ^{125}I-SP54 radioactivity became detectable at 5 min post-injection and the peak radioactivity in the blood occurred at 80 min as shown in Fig. 2.

Appearance of ^{125}I-SP54 in Urine

Radioactivity was detectable in urine within an hour of i.v. injection. The recovery of radioactivity in the urine within 24 hr following both i.v. and s.c. injection averaged 31% of the

Table 1 ^{125}I-SP54 associated with plasma or packed cells

Time after injection of 7 mg SP54 plus 370 kBq ^{125}I-SP54 (min)	Radioactivity expressed as % of counts in whole blood	
	Plasma	Packed cells
5	100	0
10	98	2
20	101	0
40	97	3
80	93	6
160	70	32
320	67	34
640	67	35
1440	61	38

Radioactivity due to plasma trapped in the packed cell fraction was estimated and subtracted to allow the calculation of cell associated ^{125}I-SP54

injected dose (range 22–43%) and was not related to the dose of unlabelled SP54.

Characterisation of ^{125}I-SP54 in Plasma and Urine

a) *Affinity for immobilised Polybrene.* The percentage of radioactivity in plasma which bound to immobilised Polybrene decreased with time after injection and the rate of decrease in binding was less after 50 mg unlabelled SP54 than after the lower doses (Table 2). ^{125}I-SP54 with affinity for immobilised Polybrene was present in urine samples obtained soon after injection but not in later samples. Early urine samples contained more Polybrene-binding material after injection of ^{125}I-SP54 with 50 mg unlabelled SP54 than for the lower doses of cold SP54. Thus in the initial urine sampled 95 min after injection of 50 mg SP54, 78% of the radioactivity bound to Polybrene agarose while in the urines at 48 and 90 min after injection of 0.1 mg SP54 the binding was 43 and 9% respectively. With all doses the binding in urine was less than 10% by 6 hr after injection.

Fig. 4

Fig. 5

Fig. 4 Elution profile of gel-filtered radioactivity in urines obtained after i.v. injection of ^{125}I-SP54 with 7 mg SP54. Radioactivity was measured in fractions obtained after gel filtration of 5 ml urine obtained at 125 min, ●–●; and 425 min, ○–○ after injection of 370 kBq ^{125}I-SP54 with 7 mg SP54. 50% of the former and 3% of the latter sample bound to solid phase Polybrene. Other details are as described in the legend to Fig. 3 except that the eluting buffer contained 3 M NaCl.

Fig. 5 Distribution of ^{123}I-SP54 in the liver and spleen after intravenous injection. The retention of ^{123}I by the liver, ●–●; and the spleen, ○–○; was assessed as described in the text after i.v. injection of 10.0 MBq ^{123}I-SP54 with 1 mg SP54.

323

Table 2 Relationship between binding of ^{125}I-SP54 in plasma to immobilised Polybrene and time after injection showing the influence of accompanying dose of unlabelled SP54

Dosage of unlabelled SP54 (mg) injected together with 370 kBq ^{125}I-SP54	Time after injection (min)					
	5	10	20	40	80	160
–	93	93	82	84	57	29
0.1	81	77	87	58	33	18
1	91	91	90	84	45	19
7	89	84	89	80	42	28
50	75	79	87	88	84	70

Binding shown as % of total counts added to binding system

b) *Molecular size of ^{125}I-SP54 in plasma and urine assessed by gel filtration.* Figure 3 shows the elution profiles of gel filtered plasma and urine obtained after injection of 370 kBq ^{125}I-SP54 in the absence of any unlabelled SP54. Radioactivity in the plasma sample obtained at 320 min after injection, eluted in a major peak prior to the solvent volume demonstrating its macromolecular nature. In contrast, radioactivity in a urine sample obtained 90 min after injection eluted almost entirely in the solvent volume of the column, indicating that it was associated with low molecular weight material (<1,000 daltons). Samples of urine obtained at various times after injection of ^{125}I-SP54 plus 7 mg unlabelled SP54 were also gel filtered. Figure 4 shows the elution profile of urines sampled at 125 and 425 min after injection. Radioactivity in the first sample was associated both with macromolecular and degraded material while that in the later sample was entirely associated with low molecular weight material in the solvent volume of the column.

Radioactivity bound to Polybrene-agarose after adsorption of post-SP54 plasma (as described in section [a]) was eluted with 5 M NaCl and gel filtered on Sephadex G-50 using 13 mM citrate containing 3 M NaCl. The radioactivity eluted entirely before the solvent volume indicating the absence of any low molecular weight degraded material (results not shown).

Organ Distribution of ^{123}I-SP54

^{123}I-SP54 was prepared immediately before injection and coeluted with unlabelled SP54 when filtered on Sephadex G-50. 88% of the labelled SP54 had high affinity for immobilised Polybrene. After i.v. administration of 10.0 MBq ^{123}I-SP54 with 1 mg unlabelled SP54 images taken at 5 min intervals from 7.5 to 47.5 min showed progressive uptake of ^{123}I by the liver and spleen (Fig. 5), such that at 50 min 60% and 7.5% of the dose respectively was associated with these organs. A profile scan at 3 hr post-injection showed 60% of the activity in the liver plus spleen and 13% in the bladder. By 43 hr post-injection the liver plus spleen retention was 37%. Urine collected over 18 hr post-injection contained 35% of the administered activity while stools passed at 18 and 42 hr post-injection contained 0.13% and 0.07% respectively.

Discussion

Radioactively labelled heparin has been used by several groups to study the metabolism of heparin in a number of species (15–18). The most commonly used labels have been ^{35}S and ^{3}H both of which are rather unsuitable for use in man. The former label is quickly detached from the polysaccharide chain during the desulphation reactions and cannot be used to follow the subsequent metabolism of desulphated material. The latter label is

hazardous and it is consequently difficult to administer sufficient labelled material for accurate counting. We have previously shown that iodination of a derivatised heparin resulted in a labelled material of high specific activity which retained several of the biological activities characteristic of heparin (11) and which was suitable for injection in man.

A similar approach was chosen with SP54 and the following criteria led us to conclude that the labelled molecule can be successfully used as a tracer of SP54 metabolism in human volunteers. Firstly, the derivatisation of SP54 involves activation of ring hydroxyls or reducing end groups with carbonyldiimidazole to give an imidazolyl carbamate derivative which reacts with tyrosyl hydrazide to yield tyrosine coupled to SP54 via a urethane linkage (19). This linkage is very stable under the conditions used in the chromatographic experiments and those existing in plasma. Secondly, the labelled SP54 exhibited similar affinities for protamine and Polybrene to native SP54 and the molecular size distribution taking into account the effect of substitution of the derivatising groups was also similar. Thirdly, the labelled SP54 retained biological activity as assessed by the APTT assay.

The kinetics of clearance of ^{125}I-SP54 could not be accurately determined due to probable redistribution following the bolus injection. Even so it was clear that ^{125}I-SP54 was removed from the circulation more slowly when injected together with 50 mg of unlabelled SP54. These results again point to the similar properties of ^{125}I-SP54 and native SP54, in this case competing for the same mechanism of uptake from the blood-stream. A point of inflection in the plasma clearance curves which was also previously observed after injection of ^{125}I-heparin (11) represents the reappearance of ^{125}I-SP54 or its degradation products from extravascular sites.

Peak absorption of ^{125}I-SP54 occurred after subcutaneous injection at 80 min post-injection, and followed a similar time course to that observed for biological activity in other studies (5, 6, 7, 8). These results demonstrate the suitability of the tracer for following uptake and clearance of SP54 by the subcutaneous route.

The redistribution of ^{35}S-labelled SP54 from the plasma to the packed red cells has been noted in the rat. In the present experiments 30–40% of labelled material in later samples was associated with cells (shown to be leukocytes by cell fractionation), but this total radioactivity only represented about 2% of the injected dose. Binding to cellular elements of the blood is therefore not a major metabolic pathway for SP54 clearance which, like heparin, is probably mainly removed by the reticuloendothelial system (20).

Gel filtration and Polybrene-binding experiments showed that only macromolecular ^{125}I-SP54 was present in plasma and that the proportion with affinity for Polybrene decreased with time after injection. We conclude that the material without affinity is macromolecular desulphated SP54 and that the probable sites of desulphation are the liver and spleen which are rich sources of sulphatases (21). The ^{123}I-SP54 imaging data supports this conclusion since a major portion of the label became localised in these organs.

From the absence of depolymerised ^{125}I-SP54 in plasma it appears that the kidney is the site of depolymerisation. Only depolymerised label was found in the urine after injection of ^{125}I-SP54 alone while after injection of ^{125}I-SP54 with high doses of unlabelled SP54 both macromolecular label (some with affinity for Polybrene) and depolymerised label was detected. These results demonstrate the saturation of the desulphation and depolymerisation mechanisms at pharmacologically relevant doses of SP54. Such saturation has also been observed with clinical doses of heparin (22), although the enzymic pathways for

SP54 catabolism must differ from that of heparin due to structural differences and remain to be defined.

References

1 Thomas D P, Lane D A, Michalski R, Johnson E A, Kakkar V V. A heparin analogue with specific action on antithrombin III. Lancet 1977; 1: 120–2.

2 Lane D A, Michalski R, Van Ross M E, Kakkar V V. Comparison of heparin and a semisynthetic heparin analogue, A 73025. Br J Haematol 1977; 37: 239–45.

3 Thomas D P, Barrowcliffe T W, Johnson E A, Stocks J, Dawes J, Pepper D S. A heparin analogue that releases endogenous heparan sulphate. Thromb Haemostas 1979; 42: 418 (Abstr.).

4 Soria C, Soria J, Rychewaert J J, Holmer E, Caen J P. Anticoagulant activities of a pentosane polysulphate: comparison with standard heparin and a fraction of low molecular weight heparin. Thromb Res 1980; 19: 455–63.

5 Ryde M, Eriksson H, Tangen O. Studies on the different mechanisms by which heparin and polysulphated xylans (PZ 68) inhibit blood coagulation in man. Thromb Res 1981; 23: 435–45.

6 Vinazzer H, Haas S, Stemberger A. Influence on the clotting mechanism of sodium pentosan polysulphate (SP54) in comparison to commercial beef lung sodium heparin. Thromb Res 1980; 20: 57–68.

7 Bergqvist D, Nilsson I M. A sulphated polysaccharide – the effects in vivo and in vitro on the haemostatic system in healthy volunteers. Thromb Res 1981; 23: 309–15.

8 Fischer A M, Merton R E, Marsh N A, Williams S, Gaffney P J, Barrowcliffe T W, Thomas D P. A comparison of pentosan polysulphate and heparin. II: Effects of subcutaneous injection. Thromb Haemostas 1982; 47: 109–13.

9 Bergqvist D, Efsing H O, Hallböök T, Lindblad B. Prevention of postoperative thromboembolic complications: a prospective comparison between Dextran 70, Dihydroergotamin heparin and a sulphated polysaccharide. Acta Chir Scand 1980; 146: 559–68.

10 Bergqvist D, Ljunger H. A comparative study of Dextran 70 and a sulphated polysaccharide in the prevention of postoperative thromboembolic complications. Br J Surg 1981; 68: 449–51.

11 Dawes J, Pepper D S. Catabolism of low-dose heparin in man. Thromb Res 1979; 14: 845–60.

12 Greenwood F C, Hunter W M, Glover J S. The preparation of ^{131}I-labelled human growth hormone of high specific radioactivity. Biochem J 1963; 89: 114–23.

13 Lam L H, Silbert J E, Rosenberg R D. The separation of active and inactive forms of heparin. Biochem Biophys Res Comm 1976; 69: 570–7.

14 Cash J D, Gader A M A, Mulder J L, Cort J H. Structure activity relations in the fibrinolytic response to vasopressin in man. Clin Sci Molec Med 1978; 54: 403–9.

15 Losito R, Barlow G, Lemieux E. ^{3}H-heparin and antithrombin III in the isolated liver perfusion. Thromb Res 1977; 10: 83–9.

16 de Swaart C A M, Sixma J J, Andersson L-O, Holmer E, Verschoor L, Nijmeyer A. Kinetics in normal humans of anticoagulant activity, radioactivity and lipolytic activity after intravenous administration of (^{35}S) heparin and (^{35}S) heparin fractions. Scand J Haematol 1980; 25: (Suppl 36) 50–63.

17 Kitani T, Nagarajan S C, Shanberge J N. Effect of protamine on heparin-antithrombin III complexes – in vivo studies. Thromb Res 1980; 17: 375–82.

18 Effeney J D, Case S A, Graziano C, Blaisdel F W. Distribution and clearance of radioactive heparin. Surg Forum 1979; 30: 198–9.

19 Bethell G S, Ayers J S, Hancock W S, Hearn M T W. A novel method of activation of cross-linked agarose with 1,1-carbonyldiimidazole which gives a matrix for affinity chromatography devoid of additional charged groups. J Biol Chem 1979; 254: 2572–4.

20 Mahadoo J, Hiebert L, Jaques L B. Vascular sequestration of heparin Thromb Res 1977; 12: 79–90.

21 Farooqui A A. Sulfatases, sulfate esters and their metabolic disorders. Clin Chim Acta 1980; 100: 285–99.

22 McAllister B M, Demis D J. Heparin metabolism: isolation and characterisation of uroheparin. Nature 1966; 212: 293–4.

ORIGINAL ARTICLE

Correction Factors for Gravimetric Measurement of Peritumoural Oedema in Man

B. A. BELL, M. A. SMITH, J. L. TOCHER & J. D. MILLER

University Department of Clinical Neurosciences, Western General Hospital, Crewe Road, Edinburgh EH4 2XU, Scotland

Abstract

The water content of samples of normal and oedematous brain in lobectomy specimens from 16 patients with cerebral tumours has been measured by gravimetry and by wet and dry weighing. Uncorrected gravimetry underestimated the water content of oedematous peritumoural cortex by a mean of 1.17%, and of oedematous peritumoural white matter by a mean of 2.52%. Gravimetric correction equations calculated theoretically and from an animal model of serum infusion white matter oedema overestimate peritumoural white matter oedema in man, and empirical gravimetric error correction factors for oedematous peritumoural human white matter and cortex have therefore been derived. These enable gravimetry to be used to accurately determine peritumoural oedema in man.

Key words: *Brain oedema, specific gravity, gravimetry.*

Introduction

Interest in gravimetry of the brain began 135 years ago in Devon, with Sir Charles Bucknill's measurements on the brains of deceased lunatics[1]. A century after Bucknill's studies, Lowry used gravimetry to study changes in brain volume produced by freezing[2], and in 1971 Nelson and his colleagues introduced microgravimetry for the measurement of cerebral oedema induced by water intoxication in mice[3]. Nelson's technique was subsequently refined in the cat[4], and has been widely applied to other animals and to man.

The estimation of tissue water content, and hence oedema, from gravimetric measurements requires the specific gravity of the tissue solids to be known. This is a constant in oedema produced by water intoxication[3], but varies when the oedema fluid contains protein, and

when the blood volume in the tissue changes[5]. Marmarou and his colleagues derived a correction for the white matter of the cat brain made oedematous by the direct infusion of serum, which introduced an error in uncorrected gravimetric water content measurements that approached 4.5%[5]. This serum infusion oedema model is designed to simulate vasogenic oedema in which vascular permeability to plasma proteins is abnormal. Whilst it is suggested that the correction factors derived from these experiments might allow gravimetry to accurately measure water content in cryogenically induced oedema, the possibility that a different experimental model and different species may introduce new errors is discussed, and no correction to account for blood volume changes is made[5].

An assessment of the accuracy of gravimetry

to measure clinical brain oedema in man has not been made, and this is what has been done in the study reported here.

Patients and Methods

Neurosurgical operative treatment offered the opportunity to measure brain water in 16 patients with intrinsic supratentorial tumours of glial or metastatic origin. There were 14 men and two women, with an age range of 39–73 years (mean 58 years), and all were investigated with preoperative CT (computed X-ray transmission tomography) and NMR (nuclear magnetic resonance) imaging of their tumour. Surgery followed MRI (magnetic resonance imaging) within 24 h, and 7 patients had a frontal lobectomy, 4 a temporal lobectomy, and 5 an occipital lobectomy. The lobectomy specimens were sealed in copolymer film (Ethicon Ltd, Edinburgh, Scotland) to prevent evaporative water loss, and taken from the operating theatre to an adjacent laboratory.

Eleven samples of oedematous peritumoural cortex were obtained from the specimens, and 13 samples of oedematous peritumoural white matter. Thirteen samples of normal cortex and 8 of normal white matter were obtained from the poles of the lobectomy specimens in those patients whose MRI showed a normal longitudinal relaxation time (T_1) at the poles of the lobe to be resected.

Each tissue sample was divided, and part of it was weighed in its fresh state on a small piece of dry aluminium foil that had an accurately predetermined weight. The sample was then dried in an oven at 80°C, and re-weighed at 24 h intervals until it reached a constant weight, which was then recorded. The wet tissue weight (W) was obtained by subtraction of the foil weight from the fresh weight, and the dry tissue weight (D) by subtraction of the foil weight from the dried weight. The wet tissue weights ranged from 8.9 to 484.1 mg, with a mean of 102.8 mg. Water content was expressed as a percentage by weight of the fresh tissue using the formula:

$$\% \text{ water} = \frac{W-D}{W} \times 100$$

The remainder of each fresh tissue sample was then divided into three portions weighing approximately 5 mg each, and they were placed in a calibrated layered oil density column for specific gravity measurements[3,4,5]. Tissue water content was calculated from the specific gravity of fresh tissue (SG) using the equation:

$$\frac{\text{weight of water}}{\text{weight of brain}} = \frac{m}{SG} - b$$

where

$$m = \frac{SG\text{solids}}{SG\text{solids} - 1}$$

and

$$b = \frac{1}{SG\text{solids} - 1} \quad \text{(Marmarou[4])}$$

and

$$SG\text{solids} = \frac{1}{1 - \dfrac{(SG-1) \times W}{D \times SG}} \quad \text{(Nelson[3])}$$

(SGsolids = derived specific gravity of the solid component of normal brain tissue)

For our samples of normal brain, $m = 4.688$ and $b = 3.688$ for cortex, and $m = 7.430$ and $b = 6.430$ for white matter. These values are similar to those derived for man by Takagi and his associates[6]. Modified formulae were also derived for man using Marmarou's theoretical equations[5] for both oedmatous cortex, where $m = 8.145$ and $b = 7.005$, and for oedematous white matter, where $m = 15.905$ and $b = 14.566$. (For the derivation of these values of m and b please refer to the appendix).

Results

For the 13 samples of normal cortex, the mean ($\pm$ standard deviation) water content measured by wet and dry weighing was 80.96% ($\pm 0.86\%$), and derived from specific gravity measurements was 81.01% ($\pm 0.92\%$). The specific gravity of the solid component of normal human cortex was 1.2711 (± 0.0230).

For the 8 samples of normal white matter, the mean water content measured by wet and dry weighing was 70.23% (±0.88%), and derived from specific gravity measurements was 70.25% (±1.18%). The specific gravity of the solid component of normal human white matter was 1.1555 (±0.0086).

The specific gravity of the solid component of the brain increased as peritumoural oedema increased, for both cortex and white matter. The rise in specific gravity of the tissue solids was greater in cortex, where it averaged 0.0181 per 1% oedematous water increase (Fig. 1), compared to an average rise of 0.0044 per 1% oedematous water increase for white matter (Fig. 2).

For the 11 samples of oedematous peritumoural cortex, the mean water content measured by wet and dry weighing was 83.54%, and derived from uncorrected specific gravity measurements using Nelson's formula[3] was 82.37%. The cortex results are presented graphically in Fig. 3, and the progressive underestimate of water content with increasing oedema is apparent from the slope of the regression line of the data (0.3841) compared with the line of identity for the two different measuring techniques which has a slope of unity. For the 13 samples of oedematous peritumoural white matter, the mean water content measured by wet and dry weighing was 77.74%, and derived from uncorrected specific gravity measurements using Nelson's formula[3] was 75.22%. The white matter results are presented graphically in Fig. 4, and also show a

FIG. 1. Change in specific gravity of cortex solids with increasing oedema.
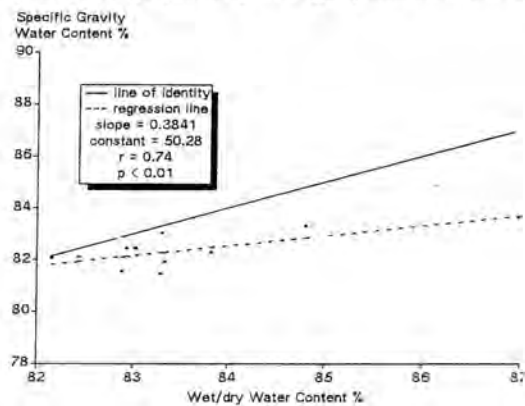
FIG. 3. Oedematous cortex water content derived by Nelson's equation.

FIG. 2. Change in specific gravity of white matter solids with increasing oedema.
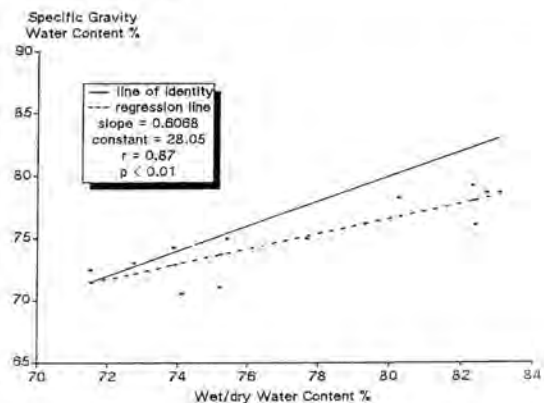
FIG. 4. Oedematous white matter water content derived by Nelson's equation.

progressive underestimate of water content with increasing oedema, although with less error than in cortex, as the slope of the regression line for the data (0.6068) is closer to unity.

Discussion

Many workers who quantify cerebral oedema with gravimetry have recognised the potential for the errors highlighted by Marmarou and his colleagues and have avoided calculating water content from specific gravity measurements[5]. They express their results directly as specific gravity figures, and take a fall in specific gravity to indicate cerebral oedema. This may not always be a valid interpretation. Taking as an example a 1 ml sample of normal human white matter:

Example 1
Fresh weight $= 1.0417\,g$
Specific gravity $= 1.0417\,g/1ml = 1.0417$
Dry weight $= 0.3104\,g$
Water content from wet
  and dry weights $= 70.21\%$
Water content from
  SG (Nelson[3]) $= 70.21\%$

For the same 1ml sample made oedematous by adding 0.5ml of pure water to it:

Example 2
Fresh weight $= 1.0417 + 0.5000\,g = 1.5417\,g$
Specific gravity $= 1.5417g/1.5\,ml = 1.0278$
Dry weight $= 0.3104\,g$
Water content from wet
  and dry weights $= 79.87\%$
Water content from
  SG (Nelson[3]) $= 79.87\%$

If 0.5 ml of normal human plasma containing 0.036 g of plasma protein is substituted for water as the oedema fluid:

Example 3
Fresh weight $= 1.5417\,g + 0.0360\,g = 1.5777\,g$
Specific gravity $= 1.5777\,g/1.5ml = 1.0518$
Dry weight $= 0.3104\,g + 0.0360\,g = 0.3464\,g$
Water content from wet
  and dry weights $= 78.04\%$
Water content from
  SG (Nelson[3]) $= 63.41\%$

In these examples it has been assumed that none of the protein from the plasma oedema has been cleared from the oedematous tissue, and the approximation that 1 ml water weighs 1 g at the temperature at which weighing was performed has been accepted. With these limitations, the extent of the error introduced by plasma protein in oedema fluid is apparent in Example 3, with an erroneous fall in water content calculated using the uncorrected equation[3]. This erroneous fall in water content would also be construed from the measured rise in specific gravity to 1.0518. Specific gravity and water content derived by Nelson's formula[3] are directly mathematically related, and the acceptance that calculated water content figures are inaccurate means that the underlying specific gravity figures are an equally inaccurate indicator of oedema.

Specific gravity figures alone cannot therefore be quoted when quantifying oedema, and the derivation of a correction factor to allow water content to be calculated from specific gravity, as advocated by Marmarou and his colleagues[5], is essential for each particular experimental protocol, or clinical aetiology. To test whether Marmarou's corrections derived from the serum infusion white matter oedema model in the cat are applicable to clinical peritumoural oedema in man, we have compared white matter water content measured by wet and dry weighing, with water content calculated from the specific gravity of the same samples by Marmarou's derived equation corrected for man (Fig. 5). Marmarou's equation progressively overestimates water content for this type of oedema in man, as the slope of the regression line for the data (1.3044) exceeds unity. Deriving a corrected equation for human cortex in accordance with Marmarou, a closer

estimate of water content is obtained from specific gravity measurements of oedematous peritumoural cortex (Fig. 6).
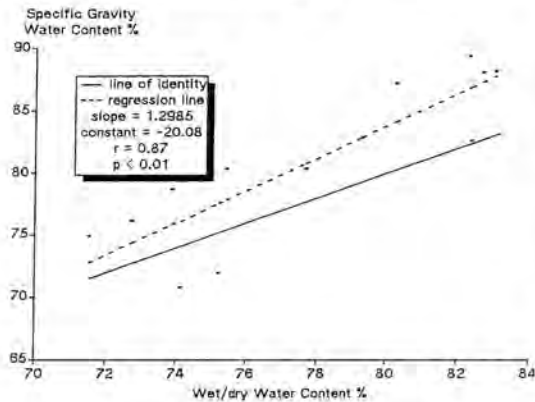
Specific Gravity
Water Content %

FIG. 5. Oedematous white matter water content derived by Marmarou's equation.

Specific Gravity
Water Content %
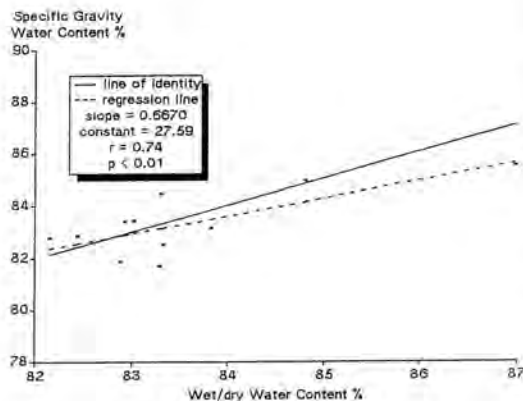
FIG. 6. Oedematous cortex water content derived by Marmarou's equation.

The reason why Marmarou's corrected equation overestimates oedema in peritumoural white matter relates to the degree of the increase in the specific gravity of tissue solids that occurs with increasing white matter oedema. Marmarou assumes in his equations that the protein content of vasogenic oedema fluid equals that of serum. This latter assumption will lead to an overcorrection if in fact the oedema fluid contains less protein than plasma. This is highly likely in the case of peritumoural

white matter oedema in man, where the leak in the blood brain barrier may be partially selective and exclude some plasma proteins from the oedema fluid. Some of the proteins that are extravasated into the oedema fluid may also be cleared from the tissue by reabsorption into the vascular compartment, further reducing the equilibrium protein content of the fluid. The measured rise in the specific gravity of tissue solids for a 1% increase in oedematous water content is less for human peritumoural white matter (0.0044 from Fig. 2) than for peritumoural cortex (0.0181 from Fig. 1), and this disparity between the two tissues is likely to be accounted for by a lower protein content of white matter oedema fluid compared to cortex oedema fluid.

Empirical correction factors can be derived from the regression line equations of our data in Figs. 3 and 4. The error for oedematous cortex shown in Fig. 3, can be corrected by subtracting the constant (50.28) from the uncorrected specific gravity derived water content and multiplying the result by 2.603 (the reciprocal of the slope of the regression line). The error for oedematous white matter shown in Fig. 4, can be corrected by subtracting the constant (28.05) from the uncorrected specific gravity derived water content and multiplying the result by 1.648 (the reciprocal of the slope of the regression line).

It must be stressed that these correction factors are for uncorrected water content derived from specific gravity measurements by Nelson's formula[3], and apply only to peritumoural oedema in man. They cannot be applied to animals, or where oedema in man has been produced by pathological processes other than a tumour. All measurements of brain oedema, where the oedema fluid is not pure water, must initially use wet and dry weighing as a reference standard to allow the derivation of correction factors for subsequent gravimetric estimations. Gravimetry alone in these circumstances cannot measure brain oedema accurately, and the error is in the specific gravity values themselves (Example 3) as well as in the water content figures derived from them by uncorrected equations.

Address for correspondence: B. A. Bell, Atkinson Morley's Hospital, Copse Hill, Wimbledon, London SW20 0NE.

References

1 Bucknill JC. On the specific gravity of cerebral substance, and on atrophy of the brain. Lancet 1852; 2:588–90.

2 Lowry OH. The quantitative histochemistry of the brain. J Histochem Cytochem 1953; 1:420–7.

3 Nelson SR, Mantz M-L, Maxwell JA. Use of specific gravity in the measurement of cerebral edema. J Appl Physiol 1971; 30:268–71.

4 Marmarou A, Poll W, Shulman K, Bhagavan H. A simple gravimetric technique for measurement of cerebral edema. J Neurosurg 1978; 49:530–7.

5 Marmarou A, Tanaka K, Shulman K. An improved gravimetric measure of cerebral edema. J Neurosurg 1982; 56:246–53.

6 Takagi H, Shapiro K, Marmarou A, Wisoff H. Microgravimetric analysis of human brain tissue. Correlation with computerized tomography scanning. J Neurosurg 1981; 54:797–801.

7 Diem K, ed. Documenta Geigy Scientific Tables. 6th edn. Manchester: Geigy Pharmaceutical Co, 1962; 546–53.

Appendix

Derivation of m and b for human brain, where the oedema fluid is pure water, from Marmarou[4]:

$$m = \frac{SG\text{solids}}{SG\text{solids} - 1} \quad \text{and } b = \frac{1}{SG\text{solids} - 1}$$

For our samples of normal human cortex, mean SGsolids $= 1.2711$, therefore:

$$m = \frac{1.2711}{0.2711} = 4.688 \quad \text{and } b = \frac{1}{0.2711} = 3.688$$

For our samples of normal human white matter, mean SGsolids $= 1.1555$, therefore:

$$m = \frac{1.1555}{0.1555} = 7.430 \quad \text{and } b = \frac{1}{0.1555} = 6.430$$

Derivation of m and b for human brain, assuming the oedema fluid contains the same amount of protein as plasma, from Marmarou[5]:

Equation A10[5] $m =$
$$\frac{(\text{Brain Water} - \text{Plasma Water}) \times (SG\text{brain} \times SG\text{plasma})}{(SG\text{plasma} - SG\text{brain})}$$

Equation A11[5] $b =$
$$\frac{(\text{Plasma Water} \times SG\text{plasma}) - (\text{Brain Water} \times SG\text{brain})}{(SG\text{plasma} - SG\text{brain})}$$

For normal man, SGplasma $= 1.0264$ and Plasma Protein $= 0.0720$ g protein/ml plasma[7].

$$\text{Plasma Water} = 1 - \frac{\text{Plasma Protein}}{SG\text{plasma}} = 1 - \frac{0.0720}{1.0264} = 0.9299$$

For our samples of normal human cortex, mean Brain Water $= 0.8096$ g water/g brain (by wet/dry weighing), and mean $SG = 1.0422$.

Therefore:
$$m = \frac{(0.8096 - 0.9299) \times (1.0422 \times 1.0264)}{(1.0264 - 1.0422)}$$
$$= 8.145$$

and
$$b = \frac{(0.9299 \times 1.0264) - (0.8096 \times 1.0422)}{(1.0264 - 1.0422)}$$
$$= 7.005$$

For our samples of normal human white matter, mean Brain Water $= 0.7023$ g water/g brain (by wet/dry weighing), and mean $SG = 1.0417$.

Therefore:
$$m = \frac{(0.7023 - 0.9299) \times (1.0417 \times 1.0264)}{(1.0264 - 1.0417)}$$
$$= 15.905$$

and
$$b = \frac{(0.9299 \times 1.0264) - (0.7023 \times 1.0417)}{(1.0264 - 1.0417)}$$
$$= 14.566$$

Editorial comment

The gravimetric method has been shown by many authors to be a useful technique for measurement of brain tissue water. It allows us to measure water content of small samples rapidly and accurately and has considerable advantages over conventional oven drying methods. This article by Dr Bell and his colleagues, emphasises an important point which is crucial to the correct application of the gravimetric methodology. Specifically, one must determine the nature of the edema fluid before using the appropriate equations, which convert the gravimetric measures directly to water content. In this study, it has been shown that the fluid, which exudes from the tumorous site in man, differs from that of serum. Thus, new conversion factors are necessary in order to accurately measure water content in adjacent tissue. Accordingly, it would seem proper that studies of tumorous edema in man utilise the equations described in this report. Complexities arise when compressive effects of the tumor volume result in barrier compromise or ischemia, in which case the nature of the extracellular fluid is difficult, if not impossible, to define. Under these circumstances, conventional wet/dry techniques share the same errors as gravimetry and given a choice, the features of small sampling and rapid determination offered by gravimetry remain attractive.

ANTHONY MARMAROU

Interindividual differences in the pituitary–thyroid axis influence the interpretation of thyroid function tests

C. A. Meier*, M. N. Maisey*, A. Lowry*, J. Müller† and M. A. Smith*‡

*Department of Radiological Sciences, UMDS, Thyroid Clinic, Guy's Hospital, London SE1 9RT, UK and †Department of Nuclear Medicine, University Hospital, CH-4051 Basel, Switzerland

Summary

OBJECTIVE We investigated interindividual differences in the shape, slope and setpoint of the pituitary–thyroid axis (PTA) in normal persons. Based on these physiological data we propose a novel bivariate concept for the interpretation of thyroid function tests which is less biased by interindividual differences in the PTA than the currently used univariate approach.

DESIGN In two separate trials (A and B), healthy volunteers were given small, increasing doses of T3 (7.5–45 μg/day orally) over 5 days. The regulation characteristics of the individual PTAs and the effects of age and gender were assessed by general linear regression models. In addition, serum samples were collected from normal persons to establish the proposed bivariate approach for the interpretation of thyroid function tests.

SUBJECTS The regulatory characteristics of the PTA were determined in a total of 21 normal volunteers (eight females, 13 males; age 24–49 years). Single blood samples were collected from 257 normal volunteers. The participants had no history of pituitary or thyroid disease.

MEASUREMENTS Free and total thyroid hormone and TSH concentrations were determined in the serum. All samples from one person were analysed in the same assay in duplicate.

RESULTS A log-linear relationship between T3 and TSH was found to describe best the individual PTA (multiple $r = 0.96$). However, significant differences in the setpoint ($P < 0.001$) and to a lesser degree in the slope ($P \leqslant 0.05$) of the PTA were detected; this variability was not dependent on age or gender. Since these findings invalidate the assumptions on which the current univariate interpretation of thyroid function tests is based, we propose a novel model for the evaluation of thyroid function tests derived from the experimentally determined shape and average slope of the PTA.

CONCLUSIONS The presence of significant age and gender-independent interindividual variations in the setpoint of the pituitary–thyroid axis raises conceptual problems with the current approach for interpreting thyroid function tests. An easy to use graphical bivariate representation of the normal ranges for thyroid function tests is presented and exemplified by the thyroid hormone and TSH measurements in a large reference population. This concept should improve the diagnostic accuracy in the borderline-normal, and particularly subclinical hypothyroid region of these hormone measurements.

‡ Present address: Department of Medical Physics, University of Leeds, Leeds General Infirmary, Great George Street, Leeds LS1 3EX, UK.

Correspondence and present address: Dr Christoph A. Meier, Thyroid Unit, Room 4-767, University Hospital, CH-1211 Geneva 14, Switzerland.

To assess the thyroid function of a patient, the thyroid hormone and TSH concentrations are measured in the serum. The results are formally interpreted independently of each other, i.e. by applying separate normal ranges for T3, T4 and TSH levels (Caldwell et al., 1985; Klee & Hay, 1987; Helfand & Crapo, 1990; Liewendahl, 1990; Surks et al., 1990). Nevertheless, many clinicians intuitively reason that, for example, a low-normal T4 level is more likely to be indicative of early hypothyroidism when accompanied by a high-normal rather than a low-normal TSH level. Presently, however, no method exists which permits this knowledge to be exploited quantitatively. The categorization of primary thyroid disorders into subclinical and overt hypo and hyperthyroidism is a direct consequence of this univariate approach as shown in Fig. 1. Two fundamental problems are raised by such a classification.

(1) When interpreting the thyroid function tests in a patient, the thyroid hormone and TSH levels are implicitly assumed to be uncorrelated in an individual normal person within the normal range of the hormone concentrations. If a correlation between these parameters exists, the individual shape, slope and setpoint of this relationship influence the extension of the individual normal range as represented by the maximally allowed variations of thyroid hormone and TSH levels within the normal range derived from a population (Fig. 1, see legend) thus introducing an unpredictable bias.

101
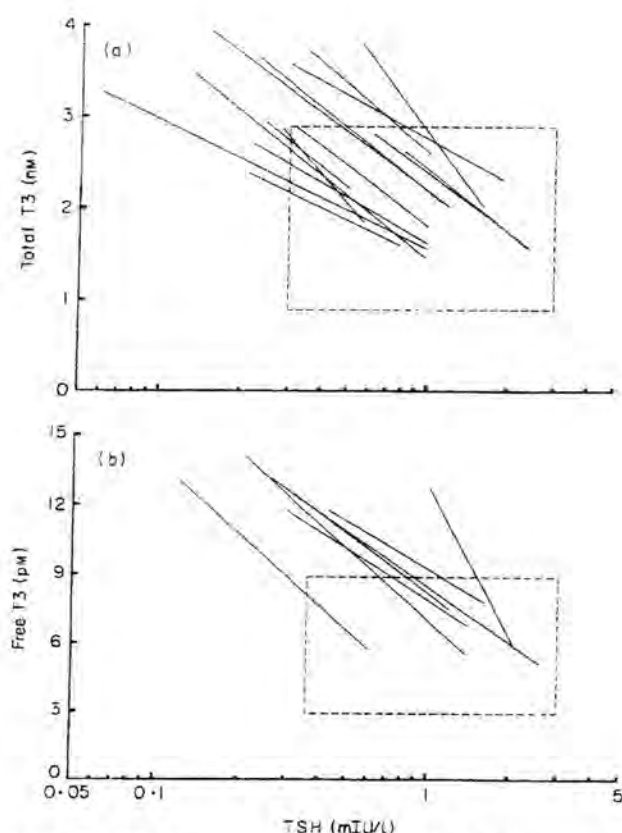
Fig. 2 Graphical representation of the individual pituitary thyroid axes. A curve of the shape $T3 = M \log(TSH) + N$ has been fitted to the hormone levels of each individual person (mean $r = 0.96$). Note the interindividual differences in the regulation characteristics and its influence on the individual normal range (dashed lines represent the univariate normal range for the hormone assays; see Subjects and methods). a, Individual axes from study A ($n = 14$). b, Individual axes from study B ($n = 7$).

measure the FT4 serum levels within a range of 0–93 pmol/l, the normal range being 9–24.5 pmol/l (intra-assay CVs 9 and 4%, respectively). The concentration of TSH was determined with the ultrasensitive RIA-gnost hTSH assay using a normal range of 0.3–3.0 mIU/l. The intra-assay CVs for 0.13 mIU/l were 20 and 3% for 5 mIU/l.

Study B. The FT3 serum concentrations were measured using the Amerlex-M RIA kit (Amersham Inc., UK) covering a range of 0–40 pmol/l with a normal range of 2.9–8.9 pmol/l. The intra-assay CV was 3% at 5.0 pmol/l. The Amerlex-M Free T4 RIA was utilized to measure the FT4 serum levels within a range of 0–130 pmol/l, the normal range being 9.4–25 pmol/l. The intra-assay CV was 4% at 14.8 pmol/l. The concentrations of TSH in the sera were determined with the ultrasensitive Amerwell TSH immunoradiometric assay (monoclonal) using a normal range of

0.36–3.25 mIU/l. The sensitivity was better than 0.06 mIU/l and the intra-assay CV for 0.8 mIU/l was 4.4%.

All samples from one person were analysed in the same assay in duplicate. The normal ranges given above are those currently in use by the respective laboratories and were utilized in Fig. 2.

Statistical methods

The data transformations, summary statistics, generalized linear regression modelling, Wilcoxon signed rank test, Kolmogorov–Smirnov and chi-squared goodness-of-fit tests were carried out on an IBM-PC with SYSTAT 5.03 (Systat Inc., Evanston IL, USA). Analysis of covariance with a repeated measures design was used to compare the slope and intercept of multiple regression lines (Neter *et al.*, 1990). Similar multiple regression models were specified to test the influence of sex and age on the interindividual differences in the pituitary–thyroid axis. Unless stated otherwise the results were expressed as mean ± one standard deviation ($\bar{x} \pm$ SD).

Results

Table 1 summarizes the hormone levels of the 21 persons from studies A and B after the administration of the T3 doses indicated. In study A, the TSH and FT4 concentrations had already declined significantly on day 2. Until and including day 4 the TT3 levels remained within the normal range accompanied by steadily declining TSH concentrations, demonstrating the continuous regulation of TSH by T3 within the normal range of the hormone concentrations. Because a small threshold in the pituitary–thyroid regulation could not be excluded from these data, this possibility has been investigated by the measurement of the TSH levels every 20 minutes after a single oral dose of 6 µg T3 was given to a healthy person. This resulted in a decline of TSH levels by 0.6 mIU/l within 4 hours (duplicate experiment in one person, controlled for circadian rhythmicity; data not shown). Taking into account the slightly different dosage regimen, study B showed a similar time course of the relative hormone level changes.

The regulation characteristics of the individual feedback axes were investigated by fitting a separate line through the T3 *vs* TSH data points of each person using multiple regression with a repeated measures factor. The residual mean squares were significantly lower when a regression line was fitted through the log-transformed rather than the linear TSH levels ($P < 0.0005$ in studies A and B); hence a logarithmic curve described the individual relationship between TT3/TSH in study A (multiple $r = 0.97$) and FT3/TSH in study B (multiple $r = 0.95$) well. However, a signifi-

Fig. 3 Representation of the proposed modified bivariate concept for the interpretation of thyroid function tests. The FT3 and TSH levels of 257 normal individuals were plotted and a univariate normal range box (dashed lines) based on the 2·5th and 97·5th percentiles was calculated. Three classic bivariate confidence ellipses (for 95·45, 99·73 and 99·99% corresponding to the probabilities of ± 2 SD, ± 3 SD and ± 4 SD, respectively) are shown in solid lines. The zones (stippled lines) for ± 2 SD, ± 3 SD and ± 4 SD derived from the proposed modified bivariate model have been calculated as described in the Appendix. Essentially, for each person the FT3 and TSH levels are standardized and subtracted to yield a new parameter ZD, which is representative of the distance moved along the average pituitary-thyroid axis. The normal range for ZD is between ± 2 SD, while the other lines (± 3 SD, ± 4 SD) may represent an empirical measure of the probability to suffer from thyroid disease. Contrary to the univariate and classical bivariate approach, this concept allows for interindividual differences in the setpoint of the feedback axis.
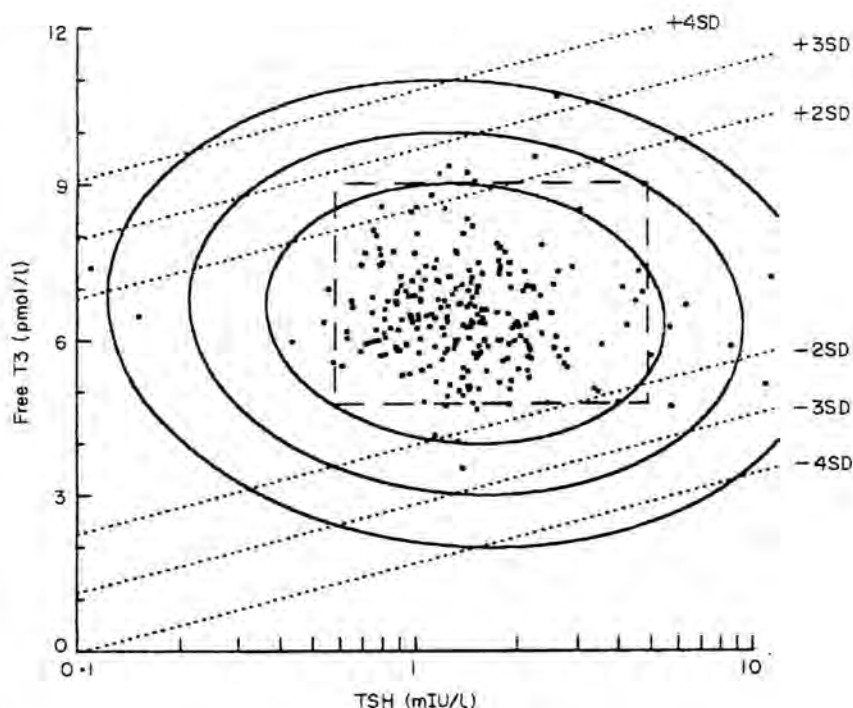
feedback axis and its parallels as depicted in Fig. 3 and described in detail in the Appendix. The average axis is defined by the experimentally found logarithmic shape and the average slope from study B. These zones provide several advantages over the univariate normal range matrix as well as over the bivariate confidence ellipses.

(1) They allow for differences in the setpoint of the pituitary-thyroid axis and are less sensitive to interindividual variations in the slope of the axis than is the conventional approach. It is apparent from the statistical analysis and Fig. 2 that the variability in the setpoint is an important factor for the interindividual differences in the regulation axes. Although an ideal model would take into account the slope of the axis in a given patient, this information is obviously not generally available.

(2) Not only can the binary question, whether a pair of FT3 and TSH levels is within or outside the normal range, be answered but an empirical measure of the probability that a patient with borderline abnormal thyroid function tests suffers from early thyroid dysfunction may be derived in prospective studies. This could prove particularly useful in a more refined classification of subclinical thyroid disease, particularly for research purposes (O'Malley et al., 1989; Ross et al., 1989; Tenerez et al., 1990; Roden et al., 1991; Wartofsky, 1991).

(3) The different stages of thyroid disease (e.g. normal→subclinical hypothyroidism→overt hypothyroidism) are conceptually better represented in adjacent zones rather than by the univariate matrix (Wehmann & Nisula, 1984) or concentric confidence ellipses.

The clinical usefulness of this zonal concept and the assignment of probabilities for thyroid dysfunction to the different zones needs to be established in future studies. Since thyroid function tests are used simultaneously as the tools for defining and diagnosing thyroid disease, only a large prospective study will establish a pattern of borderline abnormal T3 and TSH levels which are associated with an increased risk for thyroid disease. Nonetheless, in addition to the theoretical considerations outlined above, indirect evidence suggests that the proposed concept will prove clinically useful. When the serum T4 levels from a large population of patients with and without thyroid disease are plotted against the logarithm of the TSH concentrations, the data points form a distinct band of constant width along a linear regression line representing the average regulation axis (Spencer et al., 1990). It is evident that in such a situation zones orthogonal to the normalized regression line would represent a more adequate normal range than a univariate box with no direct relationship to the regulation axis. The clinical relevance of the modified bivariate model as depicted

Chopra, I.J. (1991) Nature, sources, and relative biological significance of circulating thyroid hormones. In *Werner and Ingbar's The Thyroid* (eds L. E. Braverman & R. D. Utiger), pp. 126–143. J.B. Lippincott Company, Philadelphia.

Cotton, G.E., Gorman, C.A. & Mayberry, W.E. (1971) Suppression of thyrotropin (h-TSH) in serum of patients with myxedema of varying etiology treated with thyroid hormones. *New England Journal of Medicine*, 285, 529–533.

Helfand, M. & Crapo, L.M. (1990) Screening for thyroid disease. *Annals of Internal Medicine*, 112, 840–849.

Klee, G.G. & Hay, I.D. (1987) Assessment of sensitive thyrotropin assays for an expanded role in thyroid function testing: Proposed criteria for analytic performance and clinical utility. *Journal of Clinical Endocrinology and Metabolism*, 64, 461–463.

Larsen, P.R. (1982) Thyroid-pituitary interaction. *New England Journal of Medicine*, 306, 23–32.

Liewendahl, K. (1990) Assessment of thyroid status by laboratory methods: developments and perspectives. *Scandinavian Journal of Clinical and Laboratory Investigation*, 50, 83–92.

Neter, J., Wasserman, W. & Kutner, M.H. (1990) *Applied Linear Statistical Models* Irwin, Boston.

O'Malley, B.P., Rosenthal, F.D., Exley, A., Falconer-Smith, J.F., Mahabir, J. & Woods, K.L. (1989) Low serum TSH with normal total thyroid hormone levels: an indicator of free T4 excess. *Clinical Endocrinology*, 30, 627–634.

Reichlin, S. & Utiger, R.D. (1967) Regulation of the pituitary-thyroid axis in man: relationship of TSH concentration to concentration of free and total thyroxine in plasma. *Journal of Clinical Endocrinology and Metabolism*, 27, 251–255.

Roden, M., Nowotny, P., Vierhapper, H. & Waldhäusl, W. (1991) Diagnostic relevance of suppressed basal concentrations of TSH compared with the negative TRH test in detection and exclusion of hyperthyroidism. *Acta Endocrinologica (Copenhagen)*, 124, 136–142.

Ross, D.S., Ardisson, L.J. & Meskell, M.J. (1989) Measurement of thyrotropin in clinical and subclinical hyperthyroidism using a new chemiluminescent assay. *Journal of Clinical Endocrinology and Metabolism*, 69, 684–688.

Snedecor, G.W. & Cochran, W.G. (1989) *Statistical Methods*. Iowa State University Press, Ames.

Spencer, C.A., LoPresti, J.S., Patel, A., Guttler, R.B., Eigen, A., Shen, D., Gray, D. & Nicoloff, J.T. (1990) Applications of a new chemiluminometric thyrotropin assay to subnormal measurement. *Journal of Clinical Endocrinology and Metabolism*, 70, 453–460.

Spira, O. & Gordon, A. (1986) Thyroid hormone feedback effects on thyroid-stimulating hormone. In *Thyroid Hormone Metabolism* (ed. G. Hennemann), pp. 535–578. Marcel Dekker, New York.

Staub, J.J., Althaus, B.U., Engler, H., Ryff, A.S., Trabucco, P., Marquardt, K., Burckhardt, D., Girard, J. & Weintraub, B.D. (1992) Spectrum of subclinical and overt hypothyroidism—effect on thyrotropin, prolactin, and thyroid reserve, and metabolic impact on peripheral target tissues. *American Journal of Medicine*, 92, 631–642.

Surks, M.I., Chopra, I.J., Mariash, C.N., Nicoloff, J.T. & Solomon, D.H. (1990) American Thyroid Association guidelines for use of laboratory tests in thyroid disorders. *Journal of the American Medical Association*, 263, 1529–1532.

Tenerez, A., Forberg, R. & Jansson, R. (1990) Is a more active attitude warranted in patients with subclinical thyrotoxicosis? *Journal of Internal Medicine*, 228, 229–233.

Vice, P.A., Clark, F., Schardt, W. & Evered, D. (1976) Studies on the control of thyrotropin secretion in normal man. *Clinical Endocrinology*, 5, 515–529.

Wartofsky, L. (1991) Use of sensitive TSH assay to determine optimal thyroid hormone therapy and avoid osteoporosis. *Annual Reviews of Medicine*, 42, 341–345.

Wehmann, R.E. & Nisula, B.C. (1984) Radioimmunoassay of human thyrotropin: analytical and clinical developments. *Critical Reviews in Clinical Laboratory Sciences*, 20, 243–283.

Technical note

The installation of a commercial resistive NMR imager

By M. A. Smith, M.Sc., Ph.D., J. J. K. Best, M.B., M.Sc., F.R.C.P. (Ed), F.R.C.R., R. H. B. Douglas, D.C.R.(D) and D. M. Kean, M.B., Ch.B., D.M.R.D., F.R.C.R.

NMR Imaging Unit, University of Edinburgh, Royal Infirmary, Edinburgh

A whole body NMR imager has been installed in the Royal Infirmary, Edinburgh for clinical evaluation. This paper gives details of the installation of the first commercial NMR imager to be sited in a hospital environment in the United Kingdom.

NMR IMAGER

The NMR imager is the first production machine manufactured by an Aberdeen-based company.* The design of the imager is based on the "Mark II NMR Imager" developed at Aberdeen Royal Infirmary. Though the physical principles are the same, the computer control circuits and much of the electronics have been redesigned.

The water-cooled, resistive magnet consists of four circular coils, horizontally mounted, producing a field of 0.08T (1 Tesla = 10,000 Gauss) in the vertical direction. The patient enters between the two larger coils, which have a separation of 0.35 m, and lies inside the patient tube which is 0.56 m diameter and 1.2 m long. Wound round the outside of the patient tube are the windings which produce the three orthogonal magnetic field gradients. The RF coil has a slightly larger diameter and is in the form of two linked solenoids in the central region of the patient tube. The overall dimensions of the imager, including the radiofrequency (RF) shield are 2.35 m wide, 2.05 m high and it weighs about 2000 kg. The patient couch extends a further 2.65 m and it weighs 350 kg.

The RF and gradient amplifiers, temperature control, power supply control and NMR lock are contained in one cabinet with the power supply itself in another cabinet. The power supply cabinet is also water-cooled in parallel with the magnet. The imager is controlled by a PDP 11/23+ computer which drives the RF and gradient amplifiers and also analyses the NMR signals. This computer has two RL02 discs for storage and is part of the operator's console, which in addition contains a black and white monitor and a VDU with keyboard. Images in the transverse, sagittal or coronal plane are obtained using two-dimensional Fourier transform, the "spin warp" technique (Edelstein et al, 1980). Saturation recovery and inversion recovery pulse

sequences are used with a suitable time between pulses to give proton density and T_1 images. The computer of the operator's console is linked to a second PDP 11/23, using a serial line, which acts as an independent diagnostic console. The diagnostic console contains a Winchester disc, an 8-inch floppy disc and a magnetic tape unit for patient data storage, plus black and white and colour monitors and a VDU with keyboard.

SITE PREPARATION

The NMR imager is installed in a room which previously had been a laboratory in the University Department of Medicine. The room is part of a single-storey, metal framed building, with girders of the metal frame in the centre of the room. One adjacent room is a store which contains some ferrous material, most of which is rarely moved. In the room where the imager is sited there had been a large treadmill which could be lowered below floor level when not in use. Though this contains a large amount of ferrous material it was not removed but permanently floored over. The specifications from M&D Technology Ltd. required that there should be no ferrous material within 3 m of the centre of the magnet. The material in the storeroom, the vertical support girders and the treadmill are sited at different positions around the magnet site but all are just outside the 3 m limit (Fig. 1). The only ferrous material within the 3 m limit which was removed was a short length of steel trunking sunk into the floor and two central heating radiators along the wall. The laboratory cupboards at the end of the room nearest the magnet are wooden with a metal frame but though they are within the 3 m limit they were not removed.

A separate three-phase supply has been installed for the NMR imager, computers and refrigerator unit. Plastic trunking is used for the electricity cables within the NMR room. Although a water supply was already in the room, a larger 22 mm mains supply has been installed from the adjacent laboratory to increase the flow for the run-to-waste system. A 15 mm mains supply was connected which ran outside the room to the position of the refrigerator unit.

Other modifications made to the room, such as the construction of a partition to create office space, are included in our financial costs for the installation of the NMR imager, though they are not specific for NMR.

Technical note
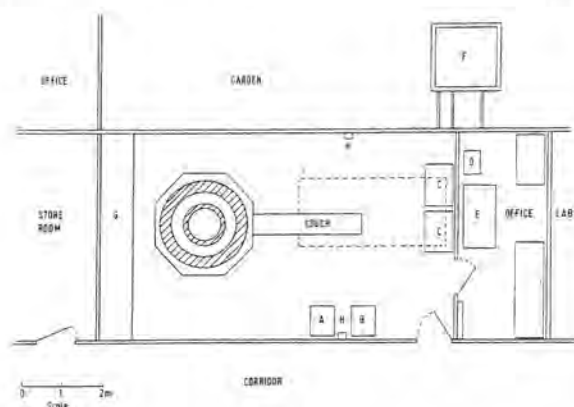
FIG. 1.

Plan view of the NMR Imaging Unit. A—rack containing power control, temperature control, gradient and RF amplifiers. B—power supply. C—operator's console. D—photographic hard-copy device. E—diagnostic console. F—refrigeration unit. G—laboratory bench with storage cupboards. H—vertical metal girders supporting the building. J—position of large metal treadmill stored below floor level. The shaded rings indicate the position of the ring magnets within the imager.

MACHINE INSTALLATION

Before the magnet was delivered, the refrigerator unit was placed in position on a concrete plinth outside the NMR room using a large crane. The suppliers of the unit installed the plumbing necessary for the magnet and power cooling system. A closed-loop water system using 22 mm copper pipe was installed, linking the magnet, power supply and refrigerator with junctions in the flow pipe connected to the 22 mm mains supply, and in the return pipe connected to a pipe which ran to waste. Stopcocks can either isolate the refrigeration unit or the mains and waste pipes, so that it is possible to switch easily from one cooling system to the other.

The magnet was delivered in one piece with the four coils on their supporting frame and the patient tube in position. The magnet was lifted from the lorry, then manhandled along a corridor and into the NMR room. Part of the wall of the room was removed to allow access. The base of the RF shield had already been fixed into position and after the magnet had been pushed into place the castors at the base of each leg of the frame were removed. The magnet stands directly on a concrete floor which forms the foundation of the building.

The magnet operates at 232 A and 100 V when producing a field strength of 0.08 T. To obtain a uniform magnetic field at the centre of the magnet it had to be shimmed. Before this was done, all the cabinets, computers and couch motor assembly, in fact everything which contained ferrous metal, were sited in their permanent positions as shown in Fig. 1. The process of shimming the magnet involved making small adjustments to the relative positions and orientations of

the four magnet coils and two sets of shimming coils. In addition, small amounts of ferrous material were attached to the magnet to make fine adjustments to the uniformity. Unfortunately, at the end of the first shimming procedure, a fault developed on the upper large coil which had to be replaced. The upper coil was lifted from the magnet using a winch and a frame constructed around the magnet, then tipped onto its side so that it could be rolled out of the room. The replacement coil was installed in the same way. When the magnet was shimmed once more, a uniformity of 126 ppm in a 44 cm diameter disc was obtained. After the magnet had been shimmed, the RF shield was fitted and the couch was fixed into position.

OPERATION OF THE IMAGER

The orientation of the coils of the magnet produces a vertical magnetic field, so the fringe field is greatest above and below the magnet, which in our case presents no problem. Magnetic field contours, as low as 0.0005 T, were plotted using a gaussmeter (Fig. 2). It
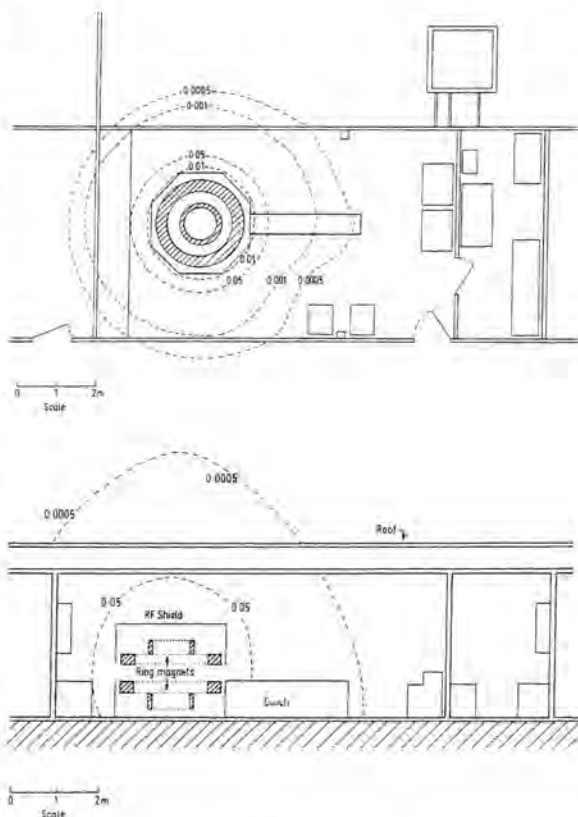
FIG. 2.

Plan and cross-sectional view of the NMR Imaging Unit illustrating the fringe field (in Tesla) of the magnet. The lack of circular symmetry is caused by the ferrous material within the room.

can be seen that there is circular symmetry of the low field contours even though there is ferrous material in the vicinity of the magnet. The 0.0005 T (5 gauss) contour is often quoted to signify the "limit" of the fringe field though this value is far lower than the field strength that might be hazardous to patients with pacemakers or aneurysm clips.

The refrigeration plant successfully maintains the magnet temperature between 23°C and 25°C. The run-to-waste cooling system also works successfully, keeping the magnet at a temperature of about 26°C with a constant water flow of 20 l/min.

The imager is designed with a "standby" mode of operation. This can be used at night to control the current supplied to maintain the magnet at any desired temperature with no water cooling. This is designed to ensure that the core of the magnet is at the correct temperature first thing in the morning for imaging. There is also an NMR feedback device which uses a small NMR probe in the imager to adjust the current and voltage and so maintain a stable field. It is our experience, however, that everything could be switched off at night and that the NMR imager could be used half an hour after switching on in the morning, even with the NMR feedback device disconnected.

Cost of Installation

The cost of the NMR imager with the independent diagnostic console was £399,000, including three years' warranty. Edinburgh received the first imager manufactured by the company and as a consequence, it was expected that there would be "teething troubles" with the imager and that any new developments would be evaluated in Edinburgh. The price paid for the system may not therefore reflect the price of subsequent systems.

The cost of site preparation was £6,500. The largest item of the cost (£5,000) was for the installation of a three phase electricity supply to the NMR Unit and the associated wiring for the electricity supply to the power racks and computers. The cost incurred was less than if an X-ray CT body scanner had been installed rather than an NMR imager, expensive radiation protection measures not being required for the latter.

Summary

It has been demonstrated that a relatively low-cost resistive NMR imager can be installed in a normal hospital environment without many major or expensive modifications. The magnet can be adjusted to give adequate uniformity and there is sufficient RF shielding to give good quality clinical images (Fig. 3). The fringe field of the magnet of this system, which operates at the lowest field strength of any commercial NMR imager, does not present a problem to imaging unit staff (NRPB, 1984).

The long term reliability and detailed specifications with regard to image quality have yet to be determined. These will be determined whilst the imager is being used

A

B

C
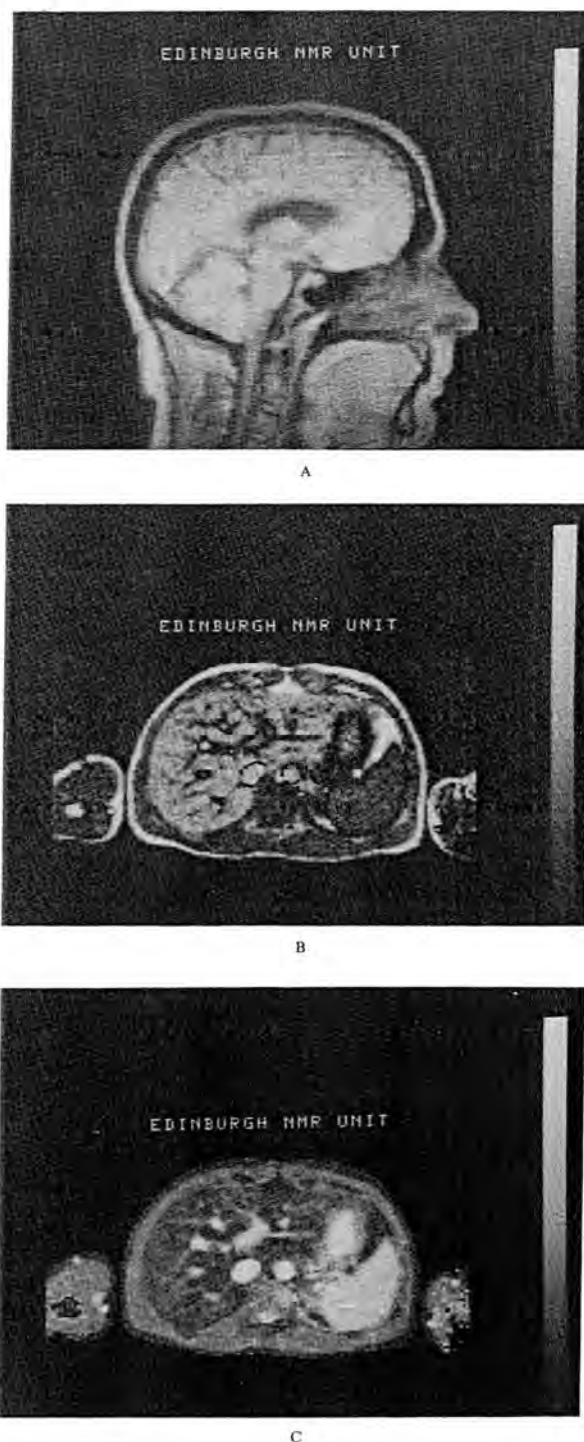
Fig. 3.

Images of the normal head and body using the two types of RF coils: (A) proton density, (B) inversion recovery, (C) calculated T_1.

Technical note

for clinical studies as part of the national clinical evaluation of NMR imaging supported by the Medical Research Council.

REFERENCES

EDELSTEIN, W. A., HUTCHISON, J. M. S., JOHNSON, G. & REDPATH, T., 1980. Spin-warp NMR imaging and applications to human whole body imaging. *Physics in Medicine & Biology, 25,* 751–756.

NATIONAL RADIOLOGICAL PROTECTION BOARD, 1984. *Advice on Acceptable Limits of Exposure to Nuclear Magnetic Resonance Clinical Imaging.* (Her Majesty's Stationery Office, London), ISBN 0-85951-218-5. See also *British Journal of Radiology,* 1983, *56,* 974–977.

Book review

Environmental Radioactivity. NCRP Proceedings No. 5. pp. vi + 284, 1983 (National Council for Radiation Protection and Measurements, Bethesda, Md. 20814 USA), $17.00.
ISSN 0195–7740; No. 5

This publication contains the scientific and briefing sessions of the 19th annual meeting of NCRP and the text of the 7th Lauriston Taylor Lecture given by Merril Eisenbud.

A wide range of topics was covered in the scientific session, including papers on the role of the environment and of natural and man-made sources within it, assessments of radioactivity at the Nevada test-site, in the atolls of the Northern Marshall Islands and at the site of the Three-Mile-Island incident. There were also contributions on environmental modelling, the particular problems associated with long-lived radionuclides, and the ever-present problem of waste disposal. The concluding paper of this section summarised and discussed the current criteria for setting dose-limits for the public.

Merril Eisenbud's lecture, "The human environment—past, present and future" was an interesting and stimulating account of environmental pollution, taken in a fairly broad sense. In contrast to many recent papers on this topic, his treatment was not gloomy, nor were his conclusions pessimistic. It is a pity that his time limit only allowed him to touch on relatively few aspects.

The scientific briefing session contained five papers; mostly reviews of published reports, including that of the NRPB on the Windscale release, the OECD report on the biological behaviour of plutonium and allied transuranic elements, the 1982 UNSCEAR document and two upon USA legislation in the fields of protection and radioactive waste. The proceedings closed with some selected task-group reports.

As usual, the papers are well presented, and continue to maintain the high standard we have come to expect from this Council's publications. There is much in this volume that will be of interest to those engaged in radiation protection and to environmental health physicists.

JOHN R. K. SAVAGE.

I II III

R$_1$CHO or R$_1$COCOOH

IV
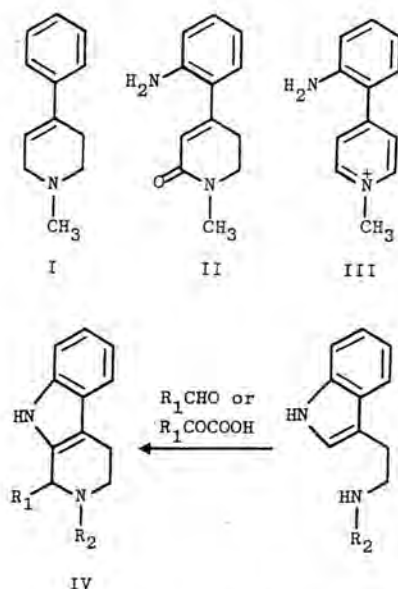
Candidate compounds in the toxicity hypothesis of Parkinson's disease.

(I) MPTP itself.

(II) Ramsden and Williams' proposal.

(III) Fellman and Nutt's alternative.

(IV) 1,2,3,4-tetrahydro-β-carbolines. R$_1$ varies with the aldehyde or ketoacid structure involved. R$_2$ is H or CH$_3$ derived from tryptamine or N-methyltryptamine, respectively. Alternatively, N-methylation may be possible after the cyclisation.

N-methyl derivatives. This hypothesis can be tested by looking for this substance in biological fluids from patients and by pharmacological studies on compounds with neurotoxic activity characteristic of parkinsonism. Although experimental difficulty may arise from the variable C-1 substitutions (R$_1$), this hypothesis should be tested not only for parkinsonism but also for other central-nervous-system diseases.

Division of Clinical Pharmacology,   SATORU OHKUBO
Tokyo College of Pharmacy,   TOSHIHIKO HIRANO
Hachioji, Tokyo 192-03, Japan   KITARO OKA

1. Markey SP, Johannessen JN, Chiueh CC, Burns RS, Herkenham MA. Interneuronal generation of a pyridinium metabolite may cause drug-induced parkinsonism. *Nature* 1984; **311:** 464–67.
2. Heikkila RE, Manzino L, Cabbat FS, Duvoisin RC. Protection against the dopaminergic neurotoxicity of 1-methyl-4-phenyl-1,2,5,6-tetrahydropyridine by monoamine oxidase inhibitors. *Nature* 1984; **311:** 467–69.
3. Langston JW, Irwin I, Langston EB. Pargyline prevents MPTP-induced parkinsonism in primates. *Science* 1984; **225:** 1480–82.
4. Chiba K, Trevor A, Castagnoli N Jr. Metabolism of the neurotoxic tertiary amine, MPTP, by brain monoamine oxidase. *Biochem Biophys Res Comm* 1984; **120:** 574–78.
5. Anon. Brain enzyme is the target of drug toxin: A chemical known as MPTP causes a Parkinson-like state in humans and monkeys: Biochemical and autoradiographical studies are closing in on the mechanism. *Science* 1984; **225:** 1460–62.
6. Rommerspacher H, Honecker H, Barbey M, Meinke B. 6-Hydroxy-tetrahydronorharmane (6-hydroxy-tetrahydro-β-carboline), a new active metabolite of indoalkylamine in man and rat. *Naunyn-Schmiedebergs Arch Pharmacol* 1979; **310:** 35–42.
7. Wyatt RJ, Erdelyi E, DoAmaral JR, Elliott GR, Renson J, Barchas JD. Tryptoline: Formation by a preparation from brain with 5-methyltetrahydrofolic acid and tryptamine. *Science* 1975; **187:** 853–55.
8. Ho BT. Monoamine oxidase inhibitor. *J Pharm Sci* 1972; **61:** 821–37.
9. Neies M, Rommerspacher H. Influence of tetrahydronorharmane (tetrahydro-β-carboline) on the potassium-evoked efflux of (^{3}H)-5-HT and vice versa. *Naunyn-Schmiedebergs Arch Pharmacol* 1980; **311:** 71.
10. Rommerspacher H, Nanz C, Borbe HO, Fehske KH, Müller WE, Wollert V. Benzodiazepine antagonism by harman and other β-carbolines in vitro and in vivo. *Eur J Pharmacol* 1981; **70:** 409–16.
11. Pannier L, Rommerspacher H. Action of tetrahydronorharmane (tetrahydro-β-carboline) on 5-hydroxytryptamine and dopamine-mediated mechanism. *Neuropharmacology* 1981; **20:** 1–8.

BRAIN WATER IN CHRONIC ALCOHOLIC PATIENTS MEASURED BY MAGNETIC RESONANCE IMAGING

SIR,—In magnetic resonance imaging (MRI) the T$_1$ relaxation time is related to the state of water in the tissue.[1] The T$_1$ value, measured in milliseconds, increases as the proportion of free to bound water increases. MRI is therefore a potentially valuable technique in the study of brain water during withdrawal of alcohol in chronic alcoholic patients. It has been used previously in such a study[2] which suggested that there was "decreased free water during intoxication and an increase in brain water during alcohol withdrawal", a somewhat surprising result that the authors admitted was "at variance with current clinical practice which emphasises the role of dehydration in the syndrome and encourages fluid replacement". We have repeated the study in a larger group of patients, since the result could have implications for the treatment of alcoholism.

The subjects were 9 chronic alcoholic patients (7 male, 2 female, aged 29–60 years, mean 46) voluntarily admitted to hospital for detoxification. They had been drinking at least 130 g ethanol per day (mean 180 g per day) before admission and had a 5–15 year history of alcoholism. None was clinically malnourished, or had physical disorders other than raised liver enzymes in serum. Over the first 5 days each patient received a normal diet, intramuscular vitamin B supplement, and decreasing doses of chlordiazepoxide. 9 normal controls, sex and age matched (range 26–62 years, mean 45), were chosen from hospital staff; their alcohol consumption ranged from total abstinence to the equivalent of 80 g ethanol per week.

Measurements were performed using a 0·08T resistive MRI system.[3] All patients were investigated on two occasions, at 24 h and at 7–21 days after cessation of alcohol consumption; controls were investigated once. Measurements of T$_1$ were made from a calculated T$_1$ image of a 12 mm thick transverse section 10 mm above the maximum diameter of the lateral ventricles. To define the T$_1$ in grey and white matter in the frontal, parietal, and occipital regions small regions of interest were defined—for grey matter 20 mm^2 and for white 69 mm^2—and the mean of similar regions in the left and right hemisphere was noted. In addition the T$_1$ value over the whole brain, excluding the cerebrospinal fluid (CSF), was measured. The precision of T$_1$ estimation was estimated from four repeated measurements on 3 normal volunteers over a period of a month. The T$_1$ precision of white matter was 2·8%, grey matter 4·9%, and the whole brain, excluding CSF, 2·6%.

At 24 h T$_1$ over whole brain was higher in alcoholic patients than in controls (see figure). It then falls over the next 7 to 21 days. The change in T$_1$ in the whole brain in alcoholic patients correlated with the time between abstinence and the second measurement (r = −0·81, p<0·01). The mean decrease in T$_1$ in alcoholic patients

T$_1$ values over whole brain of individual patients at 24 h and at 7–21 days after withdrawal of alcohol compared with age-matched normal controls.

Mean±1SE is shown.

in grey matter was $10 \cdot 1$ ms (SE = $6 \cdot 9$ ms) whereas the decrease in white matter was only $0 \cdot 6$ ms (SE = $4 \cdot 0$ ms). The decrease in T_1 in grey matter correlated with the duration of abstinence ($r = -0 \cdot 76$, $p < 0 \cdot 05$). Though the decreases in T_1 over whole brain and in grey matter in alcoholic patients were not significantly different from zero, the reduction is significantly different ($p < 0 \cdot 05$) from the increase previously reported by Besson et al.[2]

The preliminary results of this study suggest that chronic alcoholic patients have a higher T_1 value in the brain than do normal controls. This raised T_1 probably reflects an increase in free water within the brain. During withdrawal from alcohol the T_1 drops, probably because of a decrease in the brain water content. Our findings contradict those of Besson et al[2] but are consistent with the generally accepted hypothesis that the brain becomes excessively hydrated during chronic alcohol consumption and that abstinence results in dehydration of the brain.

We intend to determine in more detail the differences between T_1 in alcoholic patients and normal volunteers, whether the subsequent reduction in T_1 is significant, and if so whether it returns to normal values with prolonged abstinence. A larger number of patients will enable the apparent difference in response between grey and white matter to be explored.

M. A. SMITH
J. CHICK
D. M. KEAN
R. H. B. DOUGLAS
A. SINGER
R. E. KENDELL
J. J. K. BEST

NMR Imaging Unit and
  Department of Psychiatry,
University of Edinburgh,
Edinburgh.

1. Mathur-De Vré R. Biomedical implications of the relaxation behaviour of water related to NMR imaging. Br J Radiol 1984; 57: 955–76.
2. Besson JAO, Glen AIM, Foreman EI, et al. Nuclear magnetic resonance observations in alcoholic cerebral disorder and the role of vasopressin. Lancet 1981; ii: 923–24.
3. Smith MA, Best JJK, Douglas RHB, Kean DM. The installation of a commercial resistive NMR imager. Br J Radiol 1984; 57: 1145–48.

ENDOCRINE ADJUVANT THERAPY FOR BREAST CANCER

SIR,—The six-year follow-up analysis by the Nolvadex Adjuvant Trial Organisation (NATO) of their comparison of tamoxifen with no adjuvant therapy after surgery for early breast cancer (April 13, p 836) focused on oestrogen receptor (ER) content of the primary tumour and on patterns of first relapse. Data from the Ludwig Breast Cancer Trials III and IV,[1] in which one year of daily prednisone $7 \cdot 5$ mg and tamoxifen 20 mg was compared with no adjuvant therapy after surgery for node-positive postmenopausal breast cancer, also cast light on these two issues.

In the Ludwig trials, 32% of patients whose ER status was known had ER values below 10 fmol/mg (taken as the threshold of ER-negativity in previous publications) and 23% had ER values below 5 fmol/mg, compared with 37% in the NATO trial. The higher frequency of ER-negative tumours in the NATO trial might be due to the (few) premenopausal patients included, the limited tumour material available from node-negative patients, or the loss of receptor content during harvesting and transport of the specimens to the laboratory. The NATO investigators suggest that receptor

loss during handling would have yielded a higher percentage of patients whose tumours contained less than 30 fmol/mg than that observed. The higher percentage of patients in the NATO trial with ER measurements below 5 fmol/mg cytosol protein almost certainly included some whose tumours in fact contained higher levels of receptor than that measured and who therefore benefited from adjuvant endocrine treatment.

The investigators provide an analysis of events by first site of recurrence and report that tamoxifen appeared to prevent both local/regional and distant disease. This observation is in contrast to the findings in the Ludwig trials III and IV, which indicated a significant reduction of local and regional recurrences but not of distant metastases.[1,2] The raw recurrence data presented by NATO show that the frequency of distant events was reduced by 17% ($15 \cdot 1\%$ in the tamoxifen-treated group and $18 \cdot 2\%$ in the controls). On the other hand, the incidence of local/regional relapses (also including second primaries which are reported together) was reduced by 46% ($7 \cdot 5\%$ in the tamoxifen group and $13 \cdot 8\%$ in the controls). The table analyses type of recurrence by time in the Ludwig trials. The reduction in mastectomy scar recurrences appeared primarily within the first two years after randomisation, while significant control of regional recurrence and some impact on distant spread was only apparent beyond the first two years. The two-year duration of the tamoxifen treatment in the NATO trial—in contrast to only one year in the Ludwig trial—could therefore account for the early evidence of a survival benefit in the adjuvant-treated group. We do feel, along with our NATO colleagues, that long-term follow-up is needed for a better comprehension of the real effect of adjuvant endocrine treatment in early breast cancer.

A. GOLDHIRSCH
R. D. GELBER
M. N. H. TATTERSALL
C.-M. RUDENSTAM
F. CAVALLI,

Ludwig Institute for Cancer Research,
Bern Branch,
Inselspital,
3010 Bern, Switzerland
        for the Ludwig Breast
        Cancer Study Group

1. Ludwig Breast Cancer Study Group: Randomised trial of chemo-endocrine therapy, endocrine therapy, and mastectomy alone in postmenopausal patients with operable breast cancer and axillary node metastasis. Lancet 1984; i: 1256–60.
2. Goldhirsch A, Gelber RD. Chemo-endocrine versus endocrine therapy in breast cancer. Lancet 1984; ii: 922.

OESTROGEN RECEPTOR STATUS AND CELLULAR COMPOSITION OF BREAST CANCERS

SIR,—In the continuing debate (April 27, p 876) about the predictive value of oestrogen receptor (ER) concentrations in the management of breast cancer[1-3] we risk losing sight of a fundamental flaw in conventional ER assay methods. ER concentrations can now be measured precisely: regrettably the same precision has not always been applied to the assessment of the cellularity of the assayed tumour sample. Indeed, the tissue homogenisation required for conventional assays prohibits any assessment of cellularity or even verification that viable tumour is present in the assayed sample.

Variations in tumour epithelial cellularity (clinically significant ER is assumed to reside in the epithelial compartment of breast

SITES OF FAILURE BY TIME TO FAILURE (AT 48 MO MEDIAN FOLLOW-UP TIME): LUDWIG STUDIES III AND IV

Site of failure	All failures				Failure at <2 yr				Failure at >2 yr			
	P+T		Control		P+T		Control		P+T		Control	
	O	O/E	O	O/E	O	O/E	O	O/E	O	O/E	O	O/E
Mastectomy scar alone	24	0·64	46	1·42	16	0·56	38	1·50	8	0·90	8	1·13
Contralateral breast alone	1	0·21	8	1·93	1	0·38	4	1·71	0	0·00	4	2·22
Regional±local	22	0·61	45	1·45	17	0·75	26	1·28	5	0·38	19	1·77
Distant	84	0·92	86	1·10	60	0·95	59	1·05	24	0·84	27	1·20
2nd primary (not breast)	6	1·00	5	1·00	4	1·08	3	0·91	2	0·88	2	1·16
Death without recurrence	15	1·39	5	0·54	9	1·55	2	0·39	6	1·21	3	0·75
Total failures	152	0·81	195	1·22	107	0·85	132	1·17	45	0·75	63	1·32

P + T = adjuvant endocrine therapy (prednisone + tamoxifen) (n = 320); control = observation only (n = 309). O = observed number of events; O/E = ratio observed/expected number of events.

Nuclear magnetic resonance in hypertrophic cardiomyopathy

M BEEN, D KEAN, M A SMITH, R H B DOUGLAS, J J K BEST, A L MUIR

From the Nuclear Magnetic Resonance Imaging Unit, Royal Infirmary, Edinburgh

SUMMARY The large differences in the spin lattice relaxation times (T_1) of blood and myocardium (measured by nuclear magnetic resonance) allow the heart to be visualised without the use of contrast media. The findings using nuclear magnetic resonance in 11 unselected patients with hypertrophic cardiomyopathy were compared with those in equal numbers of normal subjects and patients with electrocardiographic features of left ventricular hypertrophy. In patients with hypertrophic cardiomyopathy characteristic septal hypertrophy was noted together with variable and sometimes pronounced hypertrophy of the left ventricular free wall, which is consistent with the heterogeneous nature of this disease. The mean (SD) ratio of septal to free wall thickness was 1·5(0·8) for patients with hypertrophic cardiomyopathy, 0·8(0·2) for those with left ventricular hypertrophy, and 0·9(0·2) for normal subjects. Although septal measurements by nuclear magnetic resonance were greater than those obtained by echocardiography there was a significant correlation between the two. Septal and free wall area were significantly smaller in normal subjects. There were no differences in septal or free wall T_1 values between the three groups.

Non-gated nuclear magnetic resonance can detect septal and free wall hypertrophy. With the addition of multiple slice acquisition, rapid estimation of myocardial mass will be possible allowing the potentially important assessment of progression or regression of myocardial hypertrophy.

Hypertrophic cardiomyopathy is characterised by hypertrophy of myocardium, particularly of the interventricular septum, without apparent cause. Distinct histological appearances—such as cardiac muscle cell disorganisation, again mainly of the septum—have been reported.[1] The diagnosis may be confirmed by echocardiography if the typical features (systolic anterior motion of the mitral valve, early aortic valve closure, and disproportionate thickening of the septum relative to the left ventricular free wall) are present. When few of the features are present or if echocardiography is technically difficult than doubt remains. In 1982 Goodwin suggested that angiocardiography was still the most useful investigation.[2]

Nuclear magnetic resonance can be used for both non-invasive visualisation of cardiac structures and tissue characterisation; the second can be achieved by using the spin lattice relaxation time (T_1). The large

differences in the T_1 values of myocardium and blood allow clear separation between cardiac muscle and cavity without the use of contrast medium.[3]

Using nuclear magnetic resonance we therefore examined the appearances of hypertrophic cardiomyopathy by measuring septal and free wall thickness and contrasting T_1 values with those found in concentric left ventricular hypertrophy and normal hearts.

Patients and methods

SUBJECTS

Three groups were examined. The first consisted of 11 unselected patients attending a cardiac review clinic with an established diagnosis of hypertrophic cardiomyopathy based on clinical, echocardiographic, and in two cases angiographic findings (Table 1). The second group consisted of 11 patients with left ventricular hypertrophy based on the electrocardiographic criteria of Romhilt and Estes,[4] of whom nine had World Health Organisation stage III hypertension, one aortic stenosis, and one aortic coarctation. The third group consisted of 11 age matched healthy

Table 1 *Echocardiographic and nuclear magnetic resonance measurements in 11 patients with hypertrophic cardiomyopathy*

Case No	Age (yr)	M Mode echocardiography				Nuclear magnetic resonance			
		Septal thickness (mm)	Posterior LV wall thickness (mm)	SAM	Early closure of aortic valve	Septum		LV free wall	
						Thickness (mm)	Area (cm²)	Thickness (mm)	Area (cm²)
1*	50	14	16	NO	NO	14	4·38	23	4·07
2	55	24	15	NO	YES	23	4·96	7	4·40
3	26	32	20	NO	YES	32	7·35	20	7·17
4	52	30	12	YES	YES	41	7·69	54	8·82
5	45	18	20	NO	NO	26	5·14	23	7·17
6	19	30	16	NO	NO	30	4·62	14	5·57
7*	48	20	18	NO	NO	26	4·93	15	4·53
8	32	32	14	YES	YES	46	9·03	41	8·39
9	68	15	12	YES	YES	29	5·36	27	6·00
10	19	26	12	YES	YES	37	8·21	20	5·67
11	45	14	12	YES	YES	38	6·55	18	5·18

*Sisters.
LV, left ventricular; SAM, systolic anterior motion.

volunteers drawn mainly from hospital staff. In all cases consent was obtained and the study approved by our institute's ethical committee.

NUCLEAR MAGNETIC RESONANCE

Nuclear magnetic resonance was carred out using a commercial (M&D Technology) low field (0·08T) resistive imaging system. Cardiac gating was not used. Three transverse sections with a slice of 16 mm were obtained from each subject with a separation of 20 mm between each section. The pulse sequence used was an interlaced saturation recovery and inversion recovery sequence each with a repetition rate of 1 s and a tau value of 200 ms for the latter. For each section four images were obtained at the end of the 4 min 16 s acquisition: proton density, calculated T_1, inversion recovery, and a "difference" image (proton density-inversion recovery). The inversion recovery and difference images contain both T_1 and proton density information. Of the four images, the calculated T_1 image gave the best contrast between blood and myocardium. The long term precision of T_1 estimation using this particular technique has been found to be 2·7% for a T_1 value of 300 ms.

The section giving best definition between septum and left ventricular cavity was selected for each patient and studied in more detail. Initially, an estimate of the mean and range of T_1 values for myocardium and ventricular blood was obtained in the 33 subjects. The mean (SD) T_1 value for myocardium was 345(28) and for blood 635(124). The window on the T_1 images was set so that all pixels with a T_1 value >450 ms appeared uniformly bright enabling myocardium and blood to be clearly separated. Irregular regions of interest were drawn around the interventricular septum and free wall of the left ventricle using the computer. Computer derived measurements of septal and free wall thickness and area

were made together with total cardiac diameter.

ECHOCARDIOGRAPHY

M mode and real time echocardiography were carried out in the left oblique position within two weeks of the nuclear magnetic study. Septal and free wall diameters were measured from M mode recordings using an Irex-3 phased array system with a 2·5 MHz transducer in the groups with hypertrophic cardiomyopathy and left ventricular hypertrophy. Recordings were made at end diastole at a level just above the mitral valve. Septal and free wall thickness were measured in three consecutive cycles and the mean values noted for each subject. Five of the patients with hypertrophic cardiomyopathy showed systolic anterior motion of the anterior mitral leaflet and seven some degree of early closure of the aortic valve. None of these abnormalities was seen in patients with left ventricular hypertrophy. Two patients did not have echocardiographic features typical of hypertrophic cardiomyopathy, the diagnosis having been established at angiography (cases 1 and 5).

STATISTICAL ANALYSIS

A non-paired Wilcoxon rank test was used for comparison between groups. Student's *t* test was used for comparison of T_1 values between septum and left ventricular free wall with all groups combined.

Results

In eight patients with hypertrophic cardiomyopathy nuclear magnetic resonance showed characteristic appearances with pronounced septal hypertrophy and a variable degree of left ventricular free wall hypertrophy (Figs. 1 and 2). Table 1 shows the results and patient details for the group with hypertrophic car-

Table 2 *Septal and left ventricular free wall spin lattice relaxation times (T_1) in three groups of patients. Values are mean (SD)*

	Septal T_1 (s)	Free wall T_1 (s)
Normal subjects	374 (18)	331 (29)
Patients with ventricular hypertrophy	355 (31)	333 (22)
Patients with hypertrophic cardiomyopathy	352 (27)	342 (24)

diomyopathy. In those patients with secondary left ventricular hypertrophy the free wall and septum appeared of equal thickness, but the muscle mass was greater than in normal subjects. The differences in area and dimension between patients with hypertrophic cardiomyopathy, left ventricular hypertrophy, and normal hearts (Figs. 3 and 4) are summarised below.

SEPTAL AND FREE WALL THICKNESS
There was considerable variation in the thickness of both septum and left ventricular free wall measured by nuclear magnetic resonance in the group with hypertrophic cardiomyopathy (Table 1). Although septal measurements were greater than those obtained with echocardiography there was a significant correlation between the two (r=0·71, p<0·001). The mean ratio of septal to free wall thickness measured by nuclear magnetic resonance and M mode echocardiography was similar at 1·5(0·8) and 1·6(0·6) respectively. The mean ratio of septal to free wall thickness as measured by magnetic resonance imaging was 0·8(0·2) for patients with left ventricular hypertrophy and 0·9(0·3) for normal subjects. In view of the variability of this ratio in patients with hypertrophic cardiomyopathy, there was no statistically significant difference detected between the three groups.
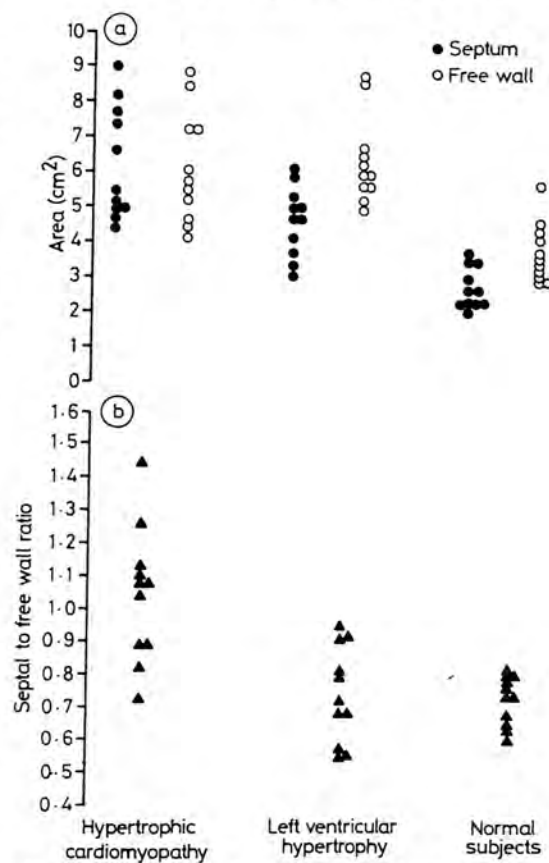
Fig. 2 *(a) Septal and free wall area and (b) ratio of septal to free wall area in individual patients with hypertrophic cardiomyopathy, those with left ventricular hypertrophy, and normal subjects.*
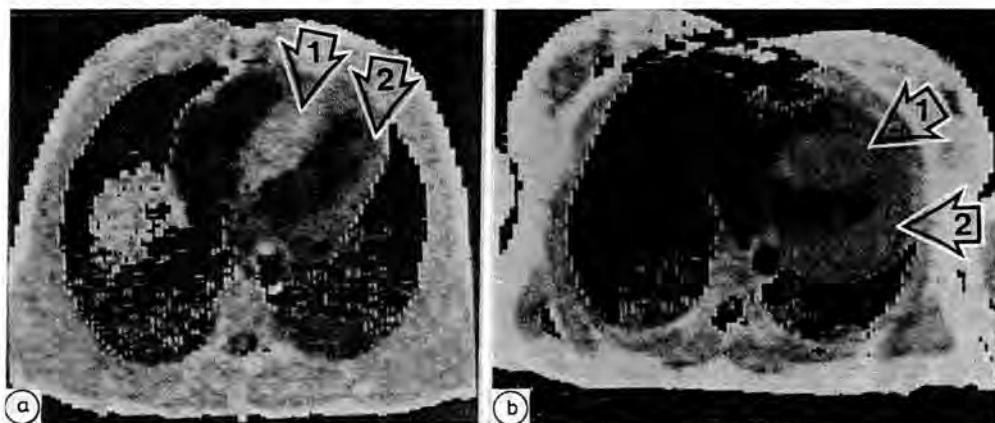
Fig. 1 *Typical appearance of hypertrophic cardiomyopathy by nuclear magnetic resonance showing pronounced septal hypertrophy (arrow 1) (a) with mild left ventricular free wall hypertrophy (arrow 2) (case 10) and (b) with pronounced left ventricular free wall hypertrophy (arrow 2) (case 8).*

SEPTAL AND FREE WALL AREA

There was a significant difference in septal area between normal subjects and both patient groups. Measured area in normal subjects was 2·7 cm^2 compared with 4·6 cm^2 (p<0·05) and 6·1 cm^2 (p<0·05) for patients with left ventricular hypertrophy and hypertrophic cardiomyopathy respectively. Corresponding values for left ventricular free wall area were 3·7 cm^2, 6·3 cm^2 (p<0·05), and 6·1 cm^2 (p<0·05).

TOTAL CARDIAC DIAMETER

The diameter as measured from the right ventricular border to the mid portion of the left ventricular free wall was greater in both patient groups at 138(10) mm and 130(14) mm for patients with hypertrophic cardiomyopathy and left ventricular hypertrophy respectively compared with 120(12) mm for normal subjects. The difference did not reach statistical significance.

SPIN LATTICE RELAXATION TIME (T_1)

Table 2 shows the mean values for T_1. There was no significant difference between patient groups, although septal T_1 was consistently higher than free wall T_1 for all groups (p<0·01).

Discussion

This study shows the ability of nuclear magnetic resonance to outline the interventricular septum and left ventricular free wall and to detect differences in myocardial thickness in patients with increased afterload and hypertrophic cardiomyopathy when contrasted with normal subjects. The pronounced contrast between flowing blood, which gives a high signal intensity, and the chamber walls allows hypertrophy to be demonstrated since there is also contrast between myocardium and surrounding tissues.

Within the group of patients with hypertrophic cardiomyopathy large variations in septal area were found. In those cases in which a diagnosis of hypertrophic cardiomyopathy could confidently be made by nuclear magnetic resonance the findings on echocardiography were more impressive (Table 1). Our unselected population of patients with hypertrophic cardiomyopathy represented the full spectrum of the disease, which is known to be heterogeneous.[5] This variability in septal and free wall size was detected both by echocardiography and by nuclear magnetic resonance.

Steiner, in outlining the applications and potential of nuclear magnetic resonance in cardiac imaging, described the concentric nature of left ventricular hypertrophy in patients with hypertension and aortic stenosis and the non-uniform septal and free wall hypertrophy of hypertrophic cardiomyopathy.[6]

Although these patterns may occur in typical examples, it is important to recognise that both the extent and position of myocardial hypertrophy are variable as illustrated by nuclear magnetic resonance (Figs. 1 and 2).

Stone *et al* recently reported the appearances of hypertrophic cardiomyopathy obtained with non-gated computed tomography using contrast medium in nine patients.[7] Visualisation of the septum was good and showed the variability of the position of maximal septal hypertrophy. Definition of the left ventricular free wall was, however, poor and inadequate for measurements. By using the differences in the relaxation index T_1 between flowing blood and ventricular muscle, nuclear magnetic resonance can allow clear visualisation of both septum and free wall without the use of contrast agents.

It was not the purpose of this study to compare nuclear magnetic resonance with echocardiography as there is a large difference in their cost and stage of development. There is also a wide variation in purchase and installation costs between different nuclear magnetic resonance systems and the variables they measure. The system we used is a low cost low magnetic field system. Echocardiography has contributed to the understanding of hypertrophic cardiomyopathy (for example, in determining the cause and level of obstruction when present[8]) and is of value in making the diagnosis. Echocardiographic features are not, however, specific individually.[5] M mode echocardiography gives diagnostic information in over 85% of patients, but precise measurements of left ventricular dimensions are possible in only 60–65% of patients.[9] Real time echocardiography improves diagnostic ability, and because of its rapidity and widespread availability echocardiography will remain the commonest and most practical technique for confirming hypertrophic cardiomyopathy. Nevertheless, nuclear magnetic resonance is possible in most patients and may be helpful in those in whom echocardiographic quality is poor.

The differences observed between our three groups were from images taken without cardiac gating. The extent by which gating improves resolution in nuclear magnetic resonance is not yet established. Some reports have emphasised the need for cardiac gating to obtain satisfactory anatomical information.[10] Choyke *et al*, however, have shown that images of diagnostic quality were obtained without gating using single spin echo sequences with a very short echo time (10–20 ms).[11] In practice it gives a very similar echo time to that used in our own system. They had noted pronounced degradation of the image with longer echo times and concluded that the previous unfavourable reports using non-gated techniques may have been due to longer echo times used in other centres.

The ability to obtain measurements of myocardial area and thus by multiple slice acquisition to estimate myocardial mass may prove valuable in the follow up of patients with myocardial hypertrophy. Drug treatment in both patients with hypertension and those with hypertrophic cardiomyopathy should ideally result in a reduction in muscle mass. The non-invasive nature of nuclear magnetic resonance makes this an attractive method for long term assessment of such patients.

References

1 Maron BJ. Myocardial disorganisation in hypertrophic cardiomyopathy. Another point of view. *Br Heart J* 1983; **50**: 1–3.
2 Goodwin JF. The frontiers of cardiomyopathy. *Br Heart J* 1982; **48**: 1–18.
3 Crooks LE, Kaufman L. NMR imaging of blood flow. *Br Med Bull* 1984; **40**: 167–9.
4 Romhilt DW, Estes EH Jr. A point-score system for the ECG diagnosis of left ventricular hypertrophy. *Am Heart J* 1968; **75**: 752–8.
5 Chahine RA, Raizner AE, Ishimori T, Montero AC. Echocardiographic, haemodynamic, and angiographic correlations in hypertrophic cardiomyopathy. *Br Heart J* 1977; **39**: 945–53.
6 Steiner RE. Nuclear magnetic resonance imaging of the heart and mediastinum. *Br Med Bull* 1984; **40**: 191–3.
7 Stone DL, Petch MC, Verney GI, Dixon AK. Computed tomography in patients with hypertrophic cardiomyopathy. *Br Heart J* 1984; **52**: 136–9.
8 Nagata S, Nimura Y, Beppu S, Park YD, Sakakibara H. Mechanism of systolic anterior motion of mitral valve and site of intraventricular pressure gradient in hypertrophic obstructive cardiomyopathy. *Br Heart J* 1983; **49**: 234–43.
9 Popp RL. Echocardiographic evaluation of left ventricular function. *N Engl J Med* 1977; **296**: 856–60.
10 Higgins CB, Stark D, McNamara M, Lanzer P, Crooks LE, Kaufman L. Multiplane magnetic resonance imaging of the heart and major vessels: studies in normal volunteers. *AJR* 1984; **142**: 661–7.
11 Choyke PL, Kressel HY, Reichek N, *et al.* Nongated cardiac magnetic resonance imaging: preliminary experience at 0·12 T. *AJR* 1984; **143**: 1143–50.

Two Examples of CNS Lipomas Demonstrated by Computed Tomography and Low Field (0.08 T) MR Imaging

D. M. Kean, M. A. Smith, R. H. B. Douglas, C. N. Martyn, and J. J. K. Best

Abstract: The low field (0.08 T) magnetic resonance (MR) findings in two lipomas of the central nervous system (CNS), one adjacent to the corpus callosum, the other in the cervical cord, are described. The characteristic short T1 of fat and the image acquisition in the sagittal plane permit accurate localisation of these lipomas. Low field MR can provide images of diagnostic quality in a number of CNS lesions. **Index Terms:** Central nervous system, neoplasms—Nuclear magnetic resonance, techniques—Computed tomography.

Whereas the general trend seems to be toward higher field magnetic resonance (MR) imaging, low field imaging is being performed with satisfactory results in a number of centers (1). We report here on the usage of low field (0.08 T) imaging in the cases of fatty tumors of the central nervous system.

MATERIALS AND METHODS

Magnetic resonance investigations were performed using a commercial low field (0.08 T) resistive imaging system, manufactured by M & D Technology Ltd., which has been installed in the Royal Infirmary, Edinburgh (2). A section 12 mm thick was used and the pulse sequence was an interlaced saturation recovery and inversion recovery, each with a repetition time of 1,000 ms and inversion time of 200 ms for the latter. For each section a proton density image, inversion recovery image, and a calculated T1 image were obtained in a total acquisition time of 4 min 16 s.

CASE REPORTS

Case 1

A 32-year-old man was admitted after a seizure that had occurred while he was asleep. He had a previous history of seizures but had never received anticonvulsant therapy. Plain posteroanterior skull radiography showed a faint curvilinear calcification, deep in the left frontal region, parasagittally. Computed tomography (EMI CT 5005) (Fig. 1) showed a large lesion of low attenuation values in the region of the corpus callosum with a rim of calcification anteriorly. With MR the sagittal inversion recovery image (Fig. 2) showed a region of high signal intensity closely related to the corpus callosum. The axial calculated T1 image (Fig. 3) demonstrated the very short T1 of this abnormality. All features seen in both CT and

FIG. 1. *Case 1.* CT scan of lipoma of corpus callosum.

From the NMR Imaging Unit, Department of Medicine, University of Edinburgh, Royal Infirmary, Lauriston Place, Edinburgh EH5 9YW, Scotland. Address correspondence and reprint requests to Dr. D. M. Kean.
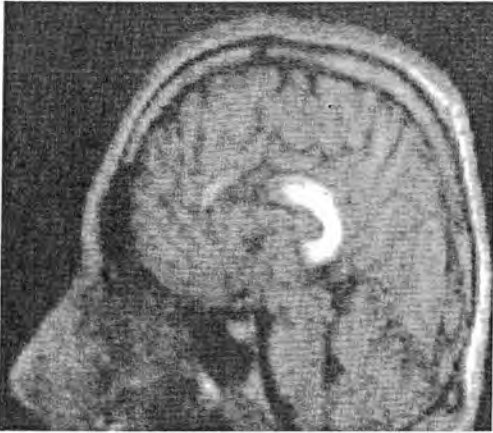
FIG. 2. *Case 1.* Sagittal inversion recovery MR image shows high signal intensity from lipoma.
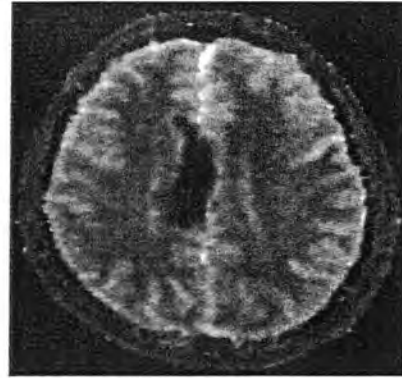
FIG. 3. *Case 1.* Calculated T1 image shows short T1 of lipoma.
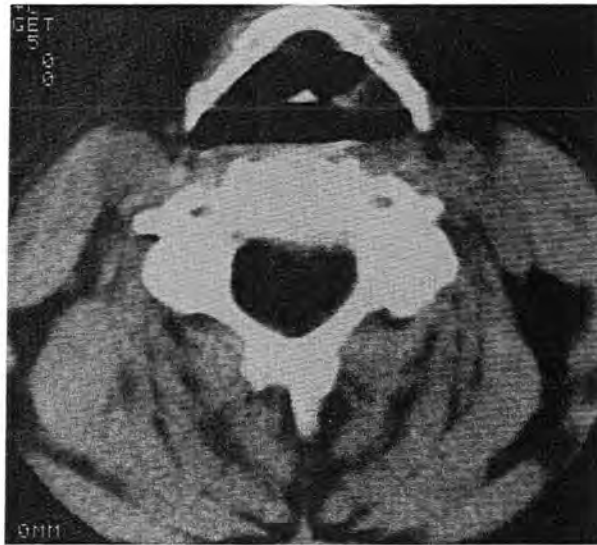
FIG. 4. *Case 2.* CT scan of cervical cord lesion.

FIG. 5. *Case 2.* Sagittal inversion recovery MR image shows high signal intensity from cervical lipoma.

FIG. 6. *Case 2.* Sagittal calculated T1 image shows short T1 of lipoma.

MR are in keeping with the diagnosis of lipoma adjacent to the corpus callosum.

Case 2

A 57-year-old man had a 6 year history of increasing spasticity of the right leg and unsteadiness of gait associated with more recent onset of clumsiness and loss of sensation in both upper limbs. Myelography demonstrated an intradural, extramedullary mass lesion in the cervical region (C2-C7). Figure 4 is a CT scan with intrathecal metrizamide, at the level of the C4 vertebral body. This showed the spinal cord compressed and displaced anteriorly by a large mass with low attenuation values. The sagittal inversion recovery MR image (Fig. 5) showed a large abnormality extending from C2 to C7. The T1 values, as demonstrated by a calculated T1 (Fig. 6), were very short, strongly suggesting that the lesion contained fat tissue. The CT and MR findings were in keeping with the diagnosis of lipoma. At surgery a lipoma that was both adherent to and incorporated within the cord was identified, biopsied, and subsequently shown to be a lipoma.

DISCUSSION

These two cases illustrate that images of good technical quality can be obtained using a low field MR system. Further, the advantages of MR are again demonstrated. In particular we may reemphasize the ability to accurately delineate midline lesions by the use of sagittal plane imaging, and the ability to image spinal cord pathology without the injection of intrathecal contrast material. Finally, we have shown that measurements of magnetic relaxation times, in this case T1, may be useful in characterising lesions such as the two lipomas reported here.

REFERENCES

1. Sepponen RE, Sipponen JT, Sivula A. Low field (0.02 T) nuclear magnetic resonance imaging of the brain. *J Comput Assist Tomogr* 1985;9:237–41.
2. Smith MA, Best JJK, Douglas RHB, Kean DM. The installation of a commercial resistive NMR imager. *Br J Radiol* 1984;57:1145–8.

CHARACTERISATION OF ACUTE MYOCARDIAL INFARCTION BY GATED MAGNETIC RESONANCE IMAGING

M. Been   M. A. Smith
J. P. Ridgeway   J. W. E. Brydon
R. H. B. Douglas   D. M. Kean
J. J. K. Best   A. L. Muir

*Nuclear Magnetic Resonance Imaging Unit, and University
Departments of Medicine, Radiology and Medical Physics, and
Medical Engineering, Royal Infirmary, Edinburgh*

Summary   In studies with gated nuclear magnetic resonance imaging, patients with recent transmural myocardial infarction showed significantly longer spin-lattice relaxation times (T_1) in the infarct area than did healthy volunteers or patients with non-ischaemic or chronic ischaemic heart disease. 10 of the 13 patients had a T_1 longer than that found in any healthy subject or in any patient with other heart disease. Changes in T_1 should prove useful in the assessment of interventions designed to limit infarct size.

Introduction

PROTON magnetic resonance imaging is a non-invasive technique with which body structure can be visualised in multiple planes. It relies on the principle that protons in a static magnetic field will tend to recover to their original position after deflection by a radiofrequency pulse. Anatomical information may be obtained by measuring proton density, which will differentiate between tissues such as muscle and lung.

Measurements of differences in the spin-lattice relaxation time (T_1) and of the spin-spin relaxation time (T_2) allow detailed tissue characterisation. These relaxation parameters are influenced by the ratio of "free" to "bound" water within the tisue.[1] Oedematous tissue would thus have a longer T_1 and T_2 than normal tissue.

In dogs T_1 and T_2 are longer in infarcted than in normal myocardium in vitro.[2,3] Differences in T_1 relaxation times in acute myocardial infarction in man have not been recorded, although an increase in T_2 after acute myocardial infarction has been reported.[4]

The prognosis after myocardial infarction depends on the extent of myocardial damage and residual left ventricular function.[5] Current emphasis on intervention in myocardial infarction designed to limit infarct size highlights the need for techniques that can localise and define ischaemic and infarcted myocardium.[6] Since current methods of assessing myocardial infarct size are imprecise,[7] require repeated blood sampling,[8] or involve the use of radioisotopes,[5] we have explored the use of gated T_1 images to identify the position and size of myocardial infarcts in man.

Patients and Methods

Patients

13 patients with a recent transmural myocardial infarction diagnosed from electrocardiographic (ECG) evidence and the finding of raised levels of heart muscle enzymes were studied 2–12 days after the onset of infarction. 8 patients had ECG evidence of anterior, 3 of inferior, and 1 of predominantly lateral infarction, and in 1 patient the site could not be determined from the electrocardiogram. 6 patients received standard therapy in the coronary-care unit for the first 48 h, and 7 received intravenous thrombolytic therapy. A further 2 patients with subendocardial infarction were also studied. The age range of patients was 37 to 68 years.
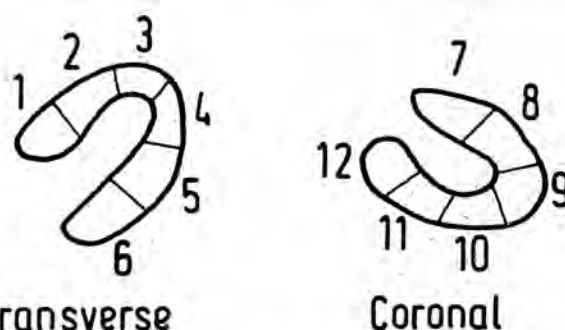
Fig 1—The 12 areas into which the transverse and coronal scans are divided.

The findings of the acute-infarct group were compared with a control population of a further three groups comprising 7 healthy volunteers, 5 patients with chronic ischaemic heart disease and previous infarction, and 5 patients with non-ischaemic heart disease. The age range of these groups was similar to the group with acute infarction.

Magnetic Resonance Imager

The magnetic resonance imager in the Royal Infirmary of Edinburgh is a 0·08T resistive system (manufactured by M&D Technology).[9] It uses an interlaced saturation recovery and inversion recovery sequence from which a T_1 image is obtained. Cardiac gating was achieved by triggering from the R wave of the patient's ECG. Two electrodes were placed on the right side of the trunk and connected to an optical coupling device for relay to the ECG monitor. This prevented electrical interference between the monitor and magnet. Triggering of the image pulse sequence could be varied from every R wave to every second or third R wave to take account of rapid heart rates. The pulse sequence allowed a minimum delay of 230 ms between the upstroke of the R wave and the position within the cardiac cycle to be imaged. Images were obtained close to end systole to avoid the effect of intracavity blood flow.

Imaging Procedure

The study was approved by the local ethical review committee, and written informed consent was obtained from all participants. All patients were in a stable phase at the time of imaging and able to lie flat comfortably. A rapid (16 s) ungated scan was done so that the correct section of the left ventricle to be imaged could be selected. Initially, only one or two full scans with an acquisition time of between 4 and 6 min per section were obtained until we were confident that patients who had recently sustained a myocardial infaretion were able to tolerate the procedure without evidence of stress, such as an increase in heart rate. Imaging time was thereafter increased to allow up to five sections per patient but was still restricted to a maximum imaging time of 30 min per patient. The procedure was well tolerated in all subjects.

Measurement of T_1

The T_1 image was transferred to a diagnostic console and displayed in colour corresponding to the range of T_1 values. The overall visual appearance was noted, and any obvious abnormalities such as wall thinning, pericardial fluid, or obvious area of increased myocardial T_1 were recorded. For all studies the left ventricular wall was divided into six areas for both transverse and coronal scans (fig 1), and the T_1 for each region was measured.

Results

The appearance of normal myocardium was of a uniform T_1 (fig 2), which was seen in both the healthy volunteers and patients with non-ischaemic cardiac disease. The mean T_1
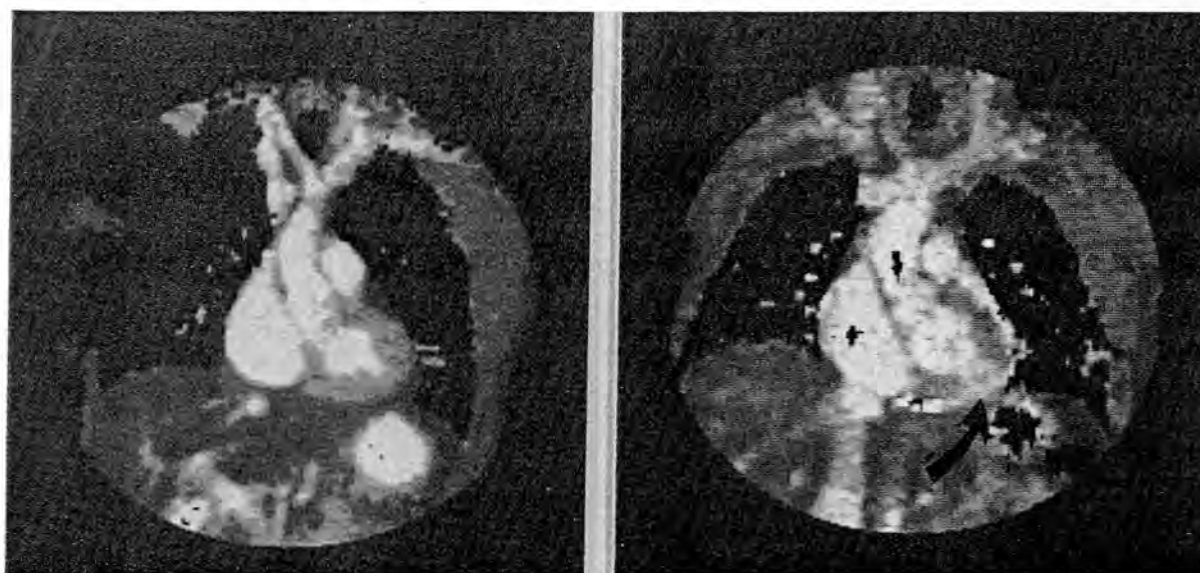
Fig 2—Gated T_1 coronal images of a healthy volunteer (left) and a man 8 days after inferior myocardial infarction (right).

The infarcted heart shows an area of high T_1 in the infero-apical region of the left ventricle above the arrow. There is also a small amount of pericardial fluid seen as a rim of very high T_1.

was 305±25 ms for normal volunteers, which was not significantly different from the T_1 values for the patients with non-ischaemic cardiac disease or old infarction but was lower than for recent infarcts where the mean T_1 was 329±60 ms (p<0·01).

In the group with recent transmural infarction the most dramatic finding was of distinct areas of increased T_1 in the left ventricular wall (table I). The precise area of myocardium involved varied from a localised region of prolonged T_1 (fig 2) to a more diffuse area of patchy increase in T_1. Differences in

TABLE I—MAXIMUM T_1 VALUES IN PATIENTS WITH RECENT MYOCARDIAL INFARCTION

Time since onset of infarction (days)	Site of infarction	Max CK (U/l)	Max T_1 (SD) (ms)	Region of myocardium from which T_1 was obtained (fig 1)
1	Inferior	484	508 (44)	11
2	Anterior	1915	371 (27)	5
3	Anterior	1169	457 (14)	10, 4
3	Anterolateral	2206	324 (58)	1
5	Inferior	946	407 (24)	10
6	Anterior	2640	338 (50)	3
7	Indeterminate	729	429 (19)	11
8	Inferior	*	449 (62)	9
8	Anterior	1660	434 (15)	9, 10
9	Anterior	2215	396 (58)	5
10	Anterior	2050	422 (38)	3
11	Anterior	1982	590 (92)	3
12	Anterior	1585	419 (51)	4

CK = creatine kinase.
*No CK measured; maximum aspartate aminotransferase 146 U/l.

TABLE II—MEAN AND MAXIMUM (±1 SD) T_1

—	Mean T_1 (ms)	Maximum T_1 (ms)
Normal volunteers	305±25	340±17
Non-ischaemic cardiac disease	296±22	316±9
Old infarction	307±27	352±31
Recent infarction	329±60	426±70

maximum T_1 values between the groups were greater than differences in mean T_1 (table II). For patients with recent infarction the maximum T_1 was 426±67 ms. This compares with a maximum T_1 of 352±30 ms for old infarct (more than 2 months) (p<0·05), 316±9 for non-ischaemic cardiac disease (p<0·01), and 339±17 for normal volunteers (p<0·02). 10 of the 13 patients with recent transmural infarction had a region of myocardium with a T_1 longer than 390 ms, whereas none of the other groups contained any areas of myocardium with a T_1 longer than 390 ms. There was no significant difference in the prolongation of T_1 between those treated with and without thrombolytic therapy. Of the 3 patients with recent infarction who did not show areas of increased T_1, all had only one or two sections scanned and it is possible that the region of infarction may not have been included. No regions of high T_1 were seen in the 2 patients with subendocardial infarction. Unsuspected pericardial fluid was noted in 2 patients, pleural effusion in 1, and suspected early aneurysm formation in 1. Patients with previous myocardial infarction had changes such as ventricular dilatation and wall thinning but no areas of increased T_1. A degree of wall thinning was also seen in 3 patients with recent infarction. In patients with inferior myocardial infarction affecting the inferior border of the left ventricle, the area of increased T_1 was often best appreciated on the coronal scan, although it was present on the lowest transverse section as a very broad area of raised T_1.

Discussion

Using a magnetic resonance imager that gives accurate measurements of the relaxation parameter T_1, we have demonstrated that recent myocardial infarction can be visualised in man. We found an average 40% increase in T_1 in areas of suspected infarction in patients imaged between 2 and 12 days after the onset of infarction. A smaller percentage increase in T_1 was reported by Williams et al[2] in biopsy specimens of ischaemic tissue from dogs within 30 min of experimental coronary occlusion. Our findings of increased T_1 with recent but not with old infarction are in keeping with the in-vitro measurements of Brown et al,[10] who showed prolongation of T_1 in canine myocardium 3 h and 4 days after

coronary occlusion, but at 21 days T_1 was more variable, and by 56 days it was shortened.

Higgins et al[3] found a 14% prolongation of T_2 and a good correlation with the percent water content in an experimental model of myocardial infarction and have confirmed these findings in man.[4] In dogs, Wesby et al, having demonstrated a change in spin echo signal intensity in vivo, reported 69% prolongation of T_2 in vitro. It is not yet possible to say whether T_1 or T_2 is superior either in vitro or in vivo. Most magnetic resonance imaging systems are designed so that images of high spatial resolution can be obtained, less emphasis being placed on precise estimation of T_1 or T_2. In such systems the spin echo pulse sequence is generally used for cardiac imaging because it is technically easier to gate and because it produces images of good spatial resolution. Using a system such as this, T_2-weighted images can be obtained and T_1 and T_2 values can be calculated, T_1 with generally poorer accuracy and precision than T_2. However, our method, using inversion recovery, provides a more precise value for T_1. Whether T_1 or T_2 will in the end be the more useful remains to be determined.

The ability to obtain serial sections through the heart suggests that it should be possible to obtain an accurate measure of infarct size with gated images in man. This is of particular importance in assessing interventions designed to limit infarct size. Thrombolytic therapy causes recanalisation and improves blood flow and ventricular function but may cause reperfusion damage or haemorrhagic infarction.[12,13] Our studies have not revealed a significant difference in T_1 values between patients treated conventionally and those with documented coronary reperfusion, but the varying time of imaging from onset of infarction make a more detailed study necessary. With nuclear magnetic spectroscopic analysis Slutsky et al[14] found an increase in T_1 in excised dogs' hearts after 3 h of ischaemia and a slight further prolongation with reperfusion. Brown et al[15] found a differential effect of varying lengths of occlusion and reperfusion on T_1 values in canine hearts. With measurement of T_1 it should be possible to follow the natural history of myocardial infarction and to determine the effect of intervention therapies, including coronary reperfusion.

Correspondence should be addressed to A. L. M., Department of Medicine, Royal Infirmary, Edinburgh EH3 9YW.

REFERENCES

1. Mather-de Vre R. Biomedical implications of the relaxation behaviour of water related to NMR imaging. Br J Radiol 1984; 57: 955–76.
2. Williams ES, Kaplan JL, Thatcher F, Zimmerman G, Knoebel SB. Prolongation of proton spin-lattice relaxation times in regionally ischaemic tissue from dog hearts. J Nucl Med 1980; 21: 449–53.
3. Higgins CB, Herfkens R, Lipton MJ, Sievers R, Sheldon P, Kaufman L, Krooks LE. Nuclear magnetic resonance imaging of acute myocardial infarction in dogs: Alterations in magnetic relaxation times. Am J Cardiol 1983; 52: 184–88.
4. McNamara MT, Higgins CB, Schechtmann N, Botvinick E, Lipton MJ, Chatterjee K, Amparo EG. Detection and characterisation of acute myocardial infarction in man with use of gated magnetic resonance. Circulation 1985; 71: 717–24.
5. Dewhurst NG, Muir AL. Comparative prognostic value of radionuclide ventriculography at rest and during exercise in 100 patients after first myocardial infarction. Br Heart J 1983; 49: 111–21.
6. Kubler W, Doorey A. Reduction of infarct size. An attractive concept: useful—or possible—in humans? Br Heart J 1985; 53: 5–8.
7. Norris RM, Barrat-Boyes C, Heng MK, Sing BN. Failure of ST-segment elevation to predict severity of acute myocardial infarction. Br Heart J 1976; 38: 85–92.
8. Fiolet JWT, TerWelle HF, Van Capelle FJL, Lie KI. Infarct size estimation from serial CK MB determinations: Peak activity and predictability. Br Heart J 1983; 49: 373–80.
9. Smith MA, Best JJK, Douglas RHB, Kean DM. The installation of a commercial resistive NMR imager. Radiology 1984; 57: 1145–48.
10. Brown JJ, Peck WW, Gerber KH, Higgins CB, Strich G, Slutsky RA. Nuclear magnetic resonance analysis of acute and chronic myocardial infarction in dogs: Alterations in spin-lattice relaxation times. Am Heart J 1984; 108: 1292–97.
11. Wesby G, Higgins CB, Lanzer P, Botvinick E, Lipton MJ. Imaging and characterisation of acute myocardial infarction in vivo by gated nuclear magnetic resonance. Circulation 1984; 69: 125–30.

References continued at foot of next column

INDIUM-111 LABELLED MONOCLONAL ANTIBODY TO PLACENTAL ALKALINE PHOSPHATASE IN THE DETECTION OF NEOPLASMS OF TESTIS, OVARY, AND CERVIX

A. A. EPENETOS   D. SNOOK
G. HOOKER   R. BEGENT
H. DURBIN   R. T. D. OLIVER
W. F. BODMER   J. P. LAVENDER

Royal Postgraduate Medical School, Hammersmith Hospital; Charing Cross Hospital; Imperial Cancer Research Fund; and Institute of Urology, London UK

Summary   A monoclonal antibody (H17E2) against placental alkaline phosphatase (PLAP) and testicular placental-like alkaline phosphatase was labelled with indium-111 and used in radioimmunoscintigraphy of 15 patients known or suspected to have germ-cell carcinoma of the testis or carcinoma of the ovary or cervix. Good images of neoplastic lesions were obtained in most patients with active disease. In 1 patient with testicular teratoma and elevated human chorionic gonadotropin who had a normal computed tomography scan, the labelled antibody located microscopic disease in a lymph node, which was then removed. No false positive localisation was seen in patients with PLAP-negative tumours or sites of inflammation. This method may be helpful in the diagnosis, staging, and monitoring of PLAP-positive neoplasms of testicular, ovarian, and cervical origin.

Introduction

RADIOIODINATED polyclonal[1,2] and monoclonal antibodies[3-8] have been shown to localise successfully in a wide range of neoplasms. In-vivo dehalogenation and antibody cross-reactivity with healthy tissues are limitations of this method and may explain the low levels of radioiodine detectable in resected tumours.[9,10]

We selected a new monoclonal antibody (H17E2)[11] against placental alkaline phosphatase (PLAP) and testicular placental-like alkaline phosphatase which shows high reactivity against PLAP-positive tumours and very low, if any, reactivity against healthy tissues.[12] For radiolabelling we used indium-111, which has been shown to produce better tumour-to-healthy-organ (except for liver) ratios than those with radioiodine.[13-16]

Patients and Methods

15 patients, aged 21–70 years (mean 40 years), with testicular (n=8), ovarian (n=6), and cervical (n=1) neoplasms were studied. Written, informed consent was obtained from all patients, and they were skin tested for allergy to mouse antibodies before injection.

Monoclonal Antibody H17E2[11,12]

This mouse IgG1 reacts with placental alkaline phosphatase as well as the leucine inhibitable form of alkaline phosphatase found at low levels in the healthy testis and which cross-reacts with the

M. BEEN AND OTHERS: REFERENCES—continued

12. Jolly SR. Canine myocardial reperfusion injury. Its reduction by the combined administration of superoxide dismutase and catalase. Circulation Res 1984; 54: 277–85.
13. Bresnahan GF, Roberts R, Shell WE, Ross J, Sobel BE. Deleterious effects due to haemorrhage after myocardial reperfusion. Am J Cardiol 1974; 33: 82–86.
14. Slutsky RA, Brown JJ, Peck WW, Stritch G, Andre MP. Effects of transient coronary ischaemia and reperfusion on myocardial edema formation and in vitro magnetic relaxation times. J Am Coll Cardiol 1984; 3: 1454–60.
15. Brown JJ, Strich G, Higgins CB, Gerber KH, Slutsky RA. Nuclear magnetic resonance analysis of acute myocardial infarction in dogs: The effects of transient coronary ischaemia of varying duration and reperfusion on spin lattice relaxation times. Am Heart J 1985; 109: 486–90.

BRAIN WATER MEASURED IN VOLUNTEERS AFTER ALCOHOL AND VASOPRESSIN

Sir,—We have reported[1] that brain water levels in chronic alcoholics are raised during the acute phase of withdrawal and then decrease over 7–21 days of abstinence. We used magnetic resonance imaging (MRI), the T_1 relaxation time being related to the amount of free water in tissues.[2] These findings are consistent with the hypothesis that the brain, in the initial stage of withdrawal, is overhydrated. Vasopressin may have a role in mediating these changes.[3] We have attempted to reproduce these changes in healthy volunteers.

Four male and one female volunteers, mean age 32 (range 26–40), with an average weekly consumption of 16 units of alcohol (range 5–42) had an NMR scan before and 45 min after the consumption of half a bottle of spirits (14 units). The alcohol was consumed over 1½ hours. This produced blood alcohol levels of 143–197 mg/dl at the time of the second scan and caused a mean increase in plasma osmolarity of 12 mmol/kg (after correction for alcohol). We used a 0·08T resistive MRI system.[1]

Measurements of T_1 were made from a calculated T_1 image of a 12 mm thick transverse section 10 mm above the maximum diameter of the lateral ventricles. Measurements were made for the left and right hemispheres of the whole section, excluding CSF, and for individual small areas of grey and white matter in the frontal and occipital regions. Statistical significance of results was calculated using Wilcoxon's paired rank test.

There was a significant decrease in T_1 of the whole section (mean 3·7 ms, p<0·05) (table). In white matter there was a significant decrease when frontal and occipital measurements were analysed together (t = −3·9 ms, p<0·05) and there was a similar trend in grey matter (t = −6·4 ms, NS). The precision of T_1 in grey matter is poorer than that of white matter or of the whole brain.[1] The change in T_1 is consistent with the observation that alcohol inhibits vasopressin and this promotes diuresis and dehydration in the short term.

Three further volunteers (all male, aged 30, 31, and 32 yr) were then scanned daily at 0900 h for 4 days. Day 1 acted as a baseline and the volunteers took vasopressin 20 µl twice daily for the next 3 days. This produced a fall in mean sodium from 140 to 135 mmol/l and in mean plasma osmolarity from 292 to 281 mmol/kg. The T_1 of frontal and occipital white matter increased by a mean of 4·1 ms (consistent with an increase in free water). This increase just failed to reach significance at the 5% level. No general trend was noted in the grey matter or whole slice measurements.

Thus we have demonstrated that we can alter T_1 acutely and in the direction we would expect if the change is due to alterations in the amount of free water in the brain tissue, although the magnitude of the change is about half of that seen in chronic alcoholics.[1] This supports the view that changes in T_1 during withdrawal are due to dynamic changes in water balance.

Isosmotic overhydration has been noted[4] in alcoholics and so have decreased levels of vasopressin in plasma and CSF.[5,6] Eisenhofer and Johnson[7] found that in normal volunteers early suppression of vasopressin is followed by raised levels as the increasing plasma osmolarity overcomes the direct suppression. Perhaps the mechanism of vasopressin release becomes reset in chronic alcoholism. These and other studies[8,9] suggest that water retention, mediated by raised vasopressin levels, may be responsible for some of the clinical features of alcohol withdrawal.

NMR is a safe, non-invasive tool for monitoring changes in tissue hydration, and we plan to look next at changes in total body water, vasopressin, aldosterone, and renin levels over a one week withdrawal period, beginning while the patient is still intoxicated. This research has important clinical implications—both for the treatment of withdrawal symptoms and because of the possibility that vasopressin is involved in the development of dependence on and tolerance to alcohol,[10] and because of case-reports of improved memory in patients with Korsakoff's psychosis given a course of vasopressin.[11]

Department of Psychiatry
and NMR Imaging Unit,
University of Edinburgh,
Royal Edinburgh Hospital,
Edinburgh EH10 5HF

A. J. MANDER
M. A. SMITH
D. M. KEAN
J. CHICK
R. H. B. DOUGLAS
A. U. REHMAN
G. J. WEPPNER
J. J. K. BEST

1. Smith MA, Chick J, Kean DM, et al. Brain water in chronic alcoholic patients measured by magnetic resonance imaging. Lancet 1985; i: 1273–74.
2. MacDonald HL, Bell BA, Smith MA, et al. In vivo correlation of NMR T_1 and brain water. Br J Radiol 1985; 58: 817.
3. Besson JAO, Glen AIM, Foreman EL, et al. Nuclear magnetic resonance observations in alcoholic cerebral disorder and the role of vasopressin. Lancet 1981; ii: 923–24.
4. Beard JD, Knott DM. Fluid and electrolyte balance during acute withdrawal in chronic alcoholic patients. JAMA 1968; 204: 135–39.
5. Noto T, Inoue K, Kitabayashi M, et al. Effect of alcohol intake on the serum AVP levels. Bull Jap Neurochem 1980; 19: 242–45 (in Japanese).
6. Noto T, Kato N, Inoue K, et al. The levels of vasopressin in cerebrospinal fluid of patients with alcoholism. Endocrinol Japan 1982; 29: 121–24.
7. Eisenhofer G, Johnson RH. Effect of ethanol ingestion on plasma vasopressin and water balance in humans. Am J Physiol 1982; 242: R522–27.
8. Sereny G, Rapoport A, Husdan H. The effect of alcohol withdrawal on electrolyte and acid base balance. Metabolism 1966; 15: 896–904.
9. Eisenhofer G, Lambie DG, Whiteside EA. Vasopressin concentration during alcohol withdrawal. Br J Addiction 1985; 80: 195–99.
10. Hoffman PL, Ritzmann RF, Tabakoff B. The influence of arginine vasopressin and oxytocin in ethanol dependence and tolerance. In: Gallant E, ed. Currents in alcoholism: Vol V. New York: Grune and Stratton, 1979.
11. Weingartner H, Gold P, Ballenger JC, et al. Effect of vasopressin on human memory functions. Science 1981; 211: 601–03.

CYSTIC LEUCOMALACIA IN PRETERM INFANT: SITE OF LESION IN RELATION TO PROGNOSIS

Sir,—In your July issue (p 137) we reported the very poor outcome in infants with periventricular leucomalacia (PVL) compared with those who had large intraventricular haemorrhages. We did not distinguish between ischaemic lesions confined to the periventricular areas and those extending further into the white-matter. We have since studied another 7 cases and have become aware of the prognostic importance of the distribution of these lesions (figure). We suggest that the term "periventricular" should be restricted to lesions adjacent to the ventricles in the area of the centrum semiovale, trigone, and optic radiation. Lesions further from the ventricles, at the depth of the sulci in the subcortical region, should be classed as "subcortical leucomalacia" (SCL), on the basis of the post-mortem angiographic studies of Takashima et al.[1] Lesions are prominent in both the subcortical and periventricular regions would be classed as "mixed".

Of the 17 infants studied so far (including the 10 previously reported) 9 had extensive lesions in the periventricular area, 4 in the subcortical region, and 4 were mixed. Although serial ultrasound studies showed the same basic pattern for all lesions, in SCL the areas of increased echogenicity tended to occur earlier after the insult and were especially marked around the interhemispheric fissure, and cysts occurred sooner and persisted far beyond 40 weeks' postmenstrual age.

PVL was seen in preterm infants below 32 weeks' gestation while SCL tended to occur in older preterm infants. Takashima et al[1] suggested that the distribution of the cystic lesions is related to the maturity of the vascular supply. Another suggestion is that the different energy metabolism in the various parts of the brain at

T_1 VALUES (ms) OF LEFT AND RIGHT HEMISPHERES BEFORE AND AFTER CONSUMPTION OF 14 UNITS OF ALCOHOL

Volunteer	Before			After			
	L	R	MEAN	L	R	MEAN	ΔT_1
1	345	347	346	340	349	344·5	−1·5
2	331	331	331	328	333	330·5	−0·5
3	343	353	348	341	344	342·5	−5·5
4	334	336	335	328	328	328	−7·0
5	337	344	340·5	338	335	336·5	−4·0

Technical note

ECG-gated T_1 images of the heart

M A Smith†‡§, J P Ridgway‡, J W E Brydon‡, M Been‖, R H B Douglas†, D M Kean†§, A L Muir‖ and J J K Best†§

† NMR Imaging Unit, ‡ Department of Medical Physics and Medical Engineering, § Department of Medical Radiology and ‖ Department of Medicine, University of Edinburgh, Royal Infirmary, Edinburgh, Scotland

1. Introduction

Magnetic resonance imaging (MRI) has been used to investigate heart disease, either studying abnormal anatomy or attempting to identify pathological alterations of myocardial tissue. The anatomical studies have used cardiac-gated saturation recovery or spin–echo pulse sequences with short time to echo (TE), which produce reasonably high spatial resolution images containing mainly proton density information (Longmore *et al* 1985) or real-time echo planar imaging (Rzedzian *et al* 1983). For information concerning tissue, particularly important for the investigation of myocardial infarction (MI), it may be possible to identify abnormal pathology within the cardiac tissue using the relaxation times T_1 or T_2.

In vitro measurements of excised dog hearts have shown that both T_1 and T_2 increase following recent myocardial infarction (Williams *et al* 1980, Higgins *et al* 1983). The changes in T_1 correlate with changes in the water content of the tissue (Higgins *et al* 1983, Brown *et al* 1984, 1985) demonstrating that the initial increase in T_1 and T_2 is due to tissue oedema. The increase in T_1 is then reversed as the region of the heart wall is replaced by fibrous tissue (Brown *et al* 1984). Increases in T_2 *in vivo* following MI have been demonstrated in dogs (Wesbey *et al* 1984, Pflugfelder *et al* 1985) and in man (Higgins *et al* 1984, McNamara *et al* 1985). In one of these studies T_1 weighted images were also investigated but no increases in signal were detected (Pflugfelder *et al* 1985).

There is a wide variation in the results of the magnitude of the changes in T_1 and T_2 following infarction and also some disagreement concerning the relative merits of T_1 or T_2 in the assessment of MI. We feel that the suggested superiority of T_2 over T_1 is likely to be influenced by the fact that the MRI systems used were not designed to give accurate or precise T_1 values (Pflugfelder *et al* 1985) or that the pulse sequence combination used was more appropriate for T_2 measurements than for T_1 (Higgins *et al* 1983). In order to assess the true value of *in vivo* T_1 measurements of MI in man a pulse sequence specifically designed for T_1 measurement with high precision has been gated with the cardiac cycle to produce gated T_1 images.

2. Methods

A commercial 0.08 T resistive system, installed in a hospital environment for clinical studies (Smith *et al* 1984), has been modified to produce cardiac gated T_1 images. The

imager generally uses a fixed pulse sequence which produces a saturation recovery image, an inversion recovery image and a calculated T_1 image for each section in a 4 min 16 s acquisition time. The imager uses an interlaced saturation recovery and inversion recovery pulse sequence with TR = 1000 ms for both and TI = 200 ms for the latter. One novel feature of the system, which makes it particularly suited to gated cardiac imaging, is the use of an adiabatic fast passage (AFP) pulse to invert the nuclei in the inversion recovery sequence (Hutchinson and Smith 1983). This pulse is very efficient at inverting the nuclei throughout the section imaged and it also has the advantage that it is not slice-selective in the inversion part of the sequence. This latter feature of the inverting AFP pulse is important because of the necessarily long delay between it and the subsequent 90° pulse, which is slice-selective, and which therefore must be synchronised with the cardiac cycle.

The timing of the pulse sequence is controlled by two timing integrated circuits, each with ten channels. In the normal mode of operation one of the timing channels controls the TR interval, which can be fixed at a preset value. This counter works in a free running mode and is automatically re-armed. For the gating sequence, this channel is changed to one shot mode. A single pulse sequence can then be started under direct software control by re-arming the appropriate channels. The computer used in the MRI system is a Digital PDP 11/23 +. The software was programmed to respond to a pulse occurring on one of the status lines and a socket was fitted so that the system could be triggered externally from either a cardiac or respiratory gating pulse.

To obtain an ECG pulse from a subject inside the NMR imager, care was taken to reduce interference on the ECG signal from the RF pulses and also to minimise the noise introduced into the system from any patient connections. It was decided to monitor the ECG and use the R wave to determine the position of systole and diastole in the cardiac cycle rather than the less precise method of using a peripheral pulse from a region such as the finger. It was found that two electrodes placed one on either wrist produced severe interference on the ECG signal from the RF pulse. ECG detection in a perpendicular direction, with one electrode placed on the right shoulder and the other electrode just above the right hip produced no measureable interference from the RF pulses on the ECG signal. Conventional ECG electrodes were used in this position as illustrated in figure 1, the leads being taped to the patient with Micropore to ensure that there were no loops to pick up RF interference. The cables from the two electrodes were twisted together and connected to a rechargeable battery-powered unit 1.2 m from the centre of the magnet which converted the ECG to optical pulses so that it could be transmitted along a 12 m optical fibre. The distance of the battery-powered optical fibre unit from the central region of the magnet was found to be important. If the unit were nearer the centre of the magnet the ferromagnetic material within the unit would degrade the image; if the unit were further away then the electrode leads would act as an aerial for the external RF interference. The optical fibre is connected to a unit to convert the ECG signal into a form that can be fed into a conventional ECG monitor (Kontron Micromon 7141), both of which are sited 4 m from the magnet. The monitor has been modified to produce a pulse immediately after the detection of the QRS complex.

The trigger pulse from the modified ECG monitor is fed into a microcomputer (BBC model B) which in turn produces a pulse which is fed into the MRI system computer to trigger a single NMR signal acquisition. The microcomputer controls the delay between the patient's R wave and the part of the cardiac cycle to be imaged. A window setting can be used such that only R–R intervals within a certain range produce a
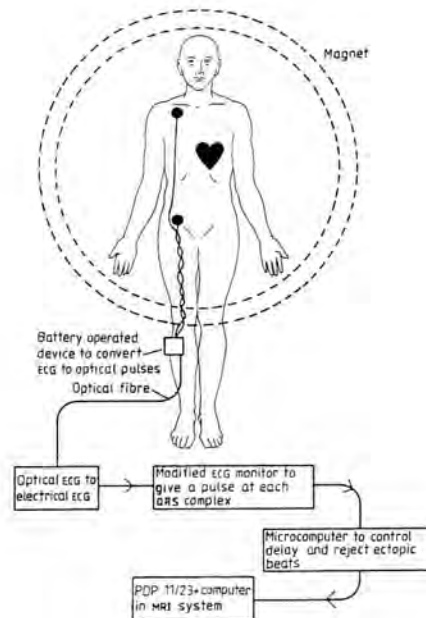
Figure 1. Schematic plan view of subject in MRI system. The positions of the ECG electrodes and leads and the battery powered box, converting the ECG to optical pulses, are shown in relation to the subject and the largest ring magnet.

signal for the MR system: thus ectopic beats are excluded. This is particularly important for end diastolic images as the section is not imaged immediately after the R wave, as is usually the case, but immediately before the succeeding R wave.

The timing of the T_1 gating sequence is illustrated in figure 2. There is a delay of 20 ms between the patient's R wave and the trigger from the ECG monitor due to the QRS complex detection. The delay from this pulse to the start of the AFP inverting
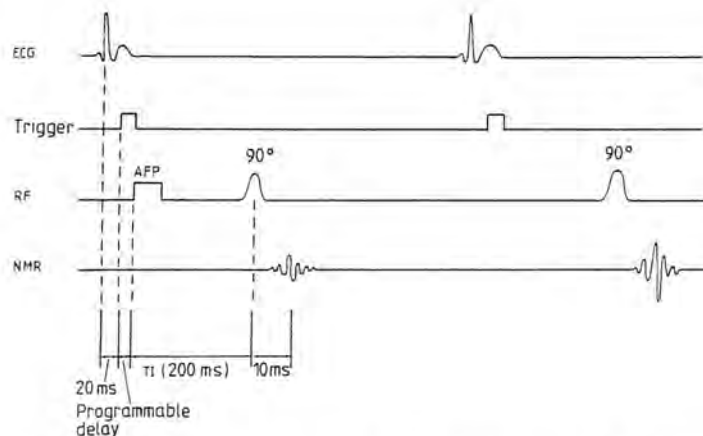
Figure 2. Timing diagram for a gated T_1 image showing inversion recovery and saturation recovery pulses during the interleaved sequence. The trigger from the ECG monitor occurs 20 ms after the upstroke of the R wave. The delay between the trigger pulse and the AFP is controlled by the microprocessor and will be different for each subject. A time from inversion (TI) of 200 ms is shown. The NMR signal is a field echo occurring 10 ms after the 90° pulse.

pulse is controlled by the microcomputer. The time from inversion (TI) can be altered in the main MR acquisition program but is generally set at 200 ms. The time from the trigger pulse and the 90° pulse is identical in both the saturation recovery and inversion recovery parts of the pulse sequence. Thus in both types of pulse sequence resonance occurs in the section at the same part of the cardiac cycle. The field echo occurs approximately 10 ms after the 90° pulse. The shortest delay available between the patient's R wave and the part of the cardiac cycle to be imaged is 230 ms, falling within systole even in patients with heart beat rates as fast as 120 min^{-1}. Signal acquisition can be triggered from every heart beat, though for accurate T_1 estimation every other heart beat is used in subjects with a heart beat rate faster than 70 min^{-1}.

A Perspex phantom was used to check the gated T_1 images. It contained three layers of $CuSO_4$ solution, the central layer having a T_1 of 330 ms and the outer layers a T_1 of 528 ms, and moved up and down with a maximum distance of travel of 5 cm. It was driven by a stepping motor controlled by a microprocessor which enabled either regular motion or motion which simulated an irregular R-R interval to be used. The microprocessor also produced a trigger pulse at the start of each cycle. The frequency of movement studied was $38-70 \text{ min}^{-1}$, equivalent to the frequency of trigger pulses obtained from human subjects, remembering that for heart beat rates greater than 70 min^{-1} a trigger pulse is produced on every second beat.

3. Results

Results obtained from the moving phantom are given in table 1. It can be seen that the precision of the calculated T_1, as demonstrated by the standard deviation of pixel values within the region of interest used, is not degraded by movement. There is a slight variation in T_1 value with TR, as would be expected. However the variation is within the long-term reproducibility (coefficient of variation) of T_1 measurement which is 2.9 and 6.5% for T_1 values 330 and 528 ms respectively.

An example of a cardiac-gated T_1 image of a normal subject at end systole is illustrated in figure 3 with an ungated image of the identical section for comparison. The time to end-systole from the R wave was determined using echocardiography. The

Table 1. Results obtained from phantom when moving at a fixed frequency, at an irregular frequency and when stationary. The $T_1 \pm 2$ SD refers to the mean T_1 within a region of interest ± 2 standard deviations of the T_1 values of the pixels within that region.

Frequency (cycles/min)	TR (ms)	$T_1 + 2$SD (ms)	
		Solution 1	Solution 2
38	1580	337 ± 32	566 ± 90
47	1280	333 ± 34	552 ± 66
56	1070	325 ± 26	524 ± 92
65	920	321 ± 28	497 ± 84
70	860	315 ± 24	493 ± 84
55–67	900–1100	329 ± 24	530 ± 64
50–75	800–1200	326 ± 32	532 ± 94
Static Phantom	1000	330 ± 30	528 ± 90

(a)

(b)
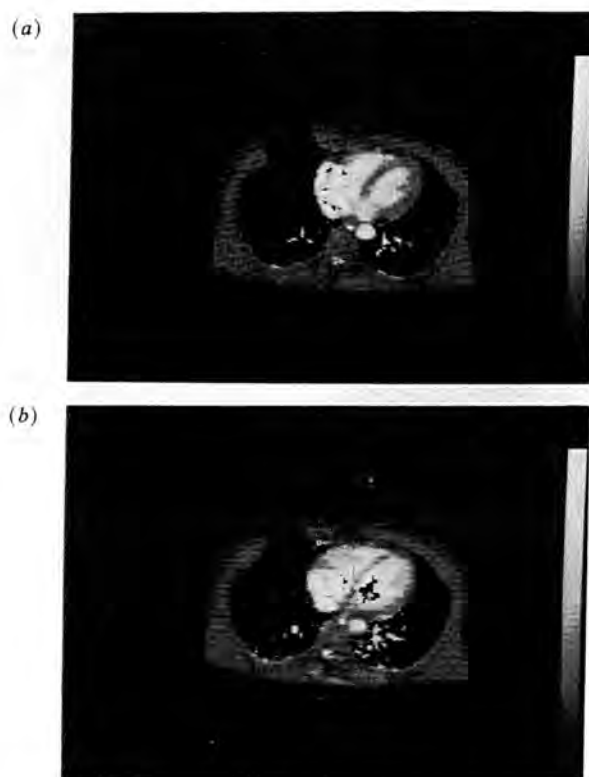
Figure 3. (a) Gated and (b) ungated transverse T_1 images of a normal human subject. The linear grey scale covers the range 50 to 650 ms.

section thickness used was 16 mm and the acquisition time for the gated image just under 4 min. The absence of signal from the anterior chest wall on the right-hand side is caused by the ferromagnetic material in the screening of the cable of the ECG connection. In the gated T_1 image the region of the left ventricular wall can be seen quite clearly with a uniform T_1 value. In the ungated image there is no such region of uniform T_1 corresponding to the ventricular wall; the T_1 value steadily increases from the outer edge of the heart to the centre. Eight small regions of interest were drawn encompassing the whole of the left ventricular free wall and the coefficient of variation of the T_1 values was found to be 3% in the gated image and 10% in the ungated image.

At end-systole the T_1 of the blood is fairly uniform. This is not the case in images later in the cardiac cycle, particularly during early diastole, where the T_1 of blood varies considerably. The cause of this is illustrated in figure 4 which shows the saturation recovery image at different stages during the heart cycle. It can be seen that the image acquired at the beginning of diastole contains a region of very low signal, caused presumably by the turbulence of the blood flowing into the ventricles. As the signal level from this image is the denominator in the equation to calculate T_1, this results in indeterminate values of T_1.

To date the technique has been used on 12 normal volunteers, many of these on more than one occasion, 13 patients with hypertrophic cardiomyopathy and 32 patients with MI, 7 within 4 days and the rest within 12 days of infarction. Occasionally the
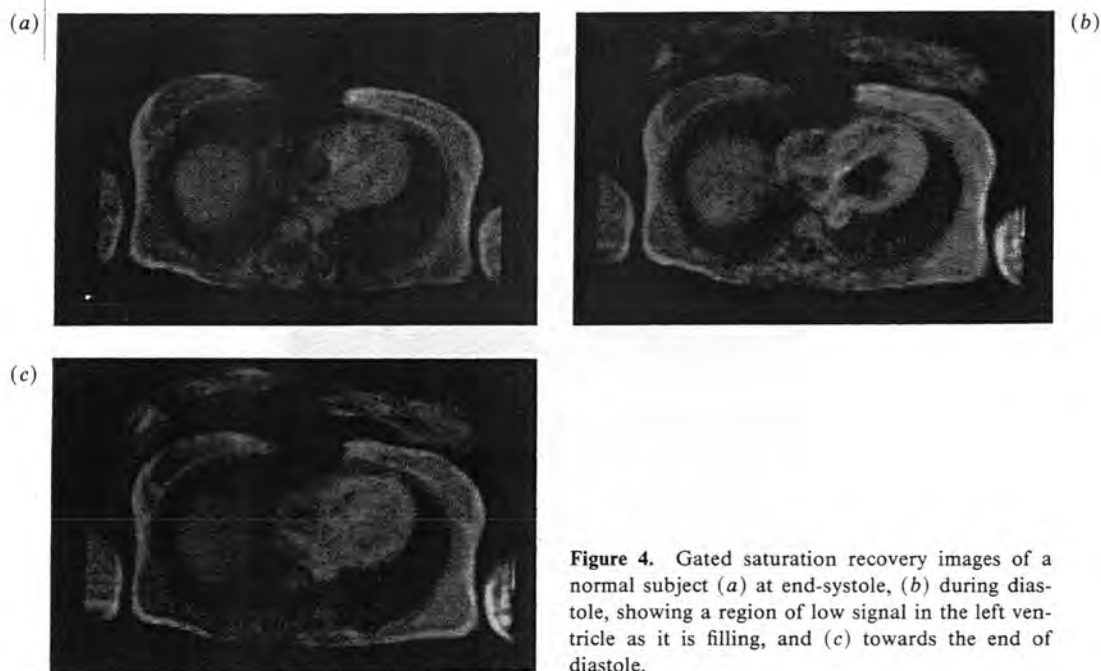
Figure 4. Gated saturation recovery images of a normal subject (a) at end-systole, (b) during diastole, showing a region of low signal in the left ventricle as it is filling, and (c) towards the end of diastole.

position of the two electrodes makes it impossible to produce a trigger pulse from the cardiac monitor. On such occasions the electrode on the right hip is moved to the left side of the patient and the cable to the electrode on the right shoulder is supported away from the chest wall by foam pads so that no signal loss occurs in the region of the heart. The use of this arrangement has improved the ECG signal sufficiently to allow a trigger pulse to be produced in all but one patient. However, the position of the electrode on the left-hand side of the patient causes interference on the ECG from the RF or gradient pulses, depending on the size of the patient and consequent proximity to the gradient windings or RF coil, which can cause unwanted trigger pulses. This can be overcome by gating the signal acquisition on every second, third or fourth pulse, depending on the type of interference. In some instances this can result in a lengthening of the time for an acquisition of a single section.
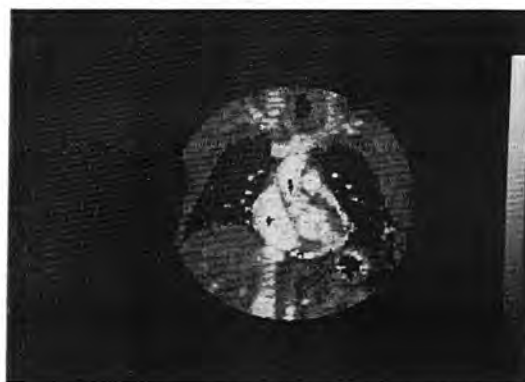
Figure 5. Gated coronal T_1 image of a patient with recent MI. The region of increased T_1, corresponding to infarcted tissue, is indicated.

Patients with recent infarction find the procedure acceptable, a complete investigation of four transverse and one coronal section taking between 20 and 30 min. Regions of increased T_1 have been found in the ventricular wall in patients with a recent infarct (Been et al 1985) and an example is shown in figure 5.

4. Discussion

The ability to obtain ECG-gated T_1 images of sufficient quality and in a sufficiently short time for clinical use has been demonstrated. The commercial system which has been modified has been shown to be particularly suitable for obtaining such images. This technique will be of value in assessing the use of in vivo T_1 measurement to identify abnormal pathology within the ventricular wall, particularly in patients with recent infarction. Most other MRI methods of investigating cardiac disease rely on the identification of wall thinning or abnormal motion using gated spin–echo images, often presented in cine mode. Such techniques can take a long time, particularly if the complete left ventricle is to be studied, which may prove unacceptable for patients with recent infarction. Moreover, echocardiography is already a well established and readily available technique producing similar information.

Many patients with cardiac disease will have an irregular heart beat; even if ectopic beats are not present then the R-R interval will vary during an investigation. Such a variation can produce a significant error in the T_1 estimation when a gated spin–echo sequence with short TR is used. In contrast, our use of a gated inversion recovery sequence with an inverting pulse that is not slice-selective ensures that the typical R-R variations obtained from patients have little effect on the T_1 values obtained.

It would be possible to obtain better linear spatial resolution by increasing the section width, thereby increasing the signal size, or by signal averaging, which would result in a considerably longer acquisition time. However, thicker sections have not been used as these would increase the partial volume effect, which increases with section thickness, as the heart is imaged in the transverse plane which itself is not perpendicular to the ventricular wall. To minimise the time that the patient is inside the MRI system signal averaging is not performed.

Future improvements to the system will be the availability of oblique sections so that the left ventricle can be imaged in a more appropriate plane, either perpendicular to the ventricular wall or along the length of the ventricle through the apex.

References

Been M, Smith M A, Ridgway J P, Brydon J W E, Douglas R H B, Kean D M, Best J J K and Muir A L 1985 Lancet ii 348–50
Brown J J, Strich G, Higgins C B, Gerber K H and Slotsky R A 1985 Am. Heart J. 109 486–90

Brown J J, Wallace W P, Gerber K H, Higgins C B, Strich G and Slotsky R A 1984 *Am. Heart J.* **108** 1292-7

Higgins C B, Herfkens R, Lipton M J, Sievers R, Sheldon P, Kaufman L and Crooks L E 1983 *Am. J. Cardiol.* **52** 184-8

Higgins C B, Lanzer P, Stark D, Botvinick E, Schiller N B, Crooks L, Kaufman L and Lipton M 1984 *Circulation* **69** 523-31

Hutchinson J M S and Smith F W 1983 *Nuclear Magnetic Resonance (NMR) Imaging* ed C L Partain, A E James, F D Rollo and R R Price (Philadelphia: Saunders) pp 231-49

Longmore D B, Klipstein R H, Underwood S R, Firmin D N, Hounsfield G N, Watanabe M, Bland C, Fox K, Poole-Wilson P A, Rees R S O, Denison D, McNeilly A M and Burman E D 1985 *Lancet* i 1360-2

McNamara MT, Higgins C B, Schechtmann N, Botvinick E, Lipton M J, Chatterjee K and Amparo E G 1985 *Circulation* **71** 717-24

Pflugfelder P W, Wisenberg G, Prato F S, Carroll S E and Turner K L 1985 *Circulation* **71** 587-94

Rzedzian R, Chapman B, Mansfield P, Coupland R E, Doyle M, Chrispin A, Guifoyle D and Small P 1983 *Lancet* ii 1281-2

Smith M A, Best J J K, Douglas R H B and Kean D M 1984 *Br. J. Radiol.* **57** 1145-8

Wesbey G, Higgins C B, Lanzer P, Botvinick E and Lipton M 1984 *Circulation* **69** 125-30

Williams E S, Kaplan J I, Thatcher F, Zimmerman G and Knoebel S B 1980 *J. Nucl. Med.* **21** 449-53

Correspondence

In view of the absence of conclusive evidence to support the existence of non-thermal effects we retain our hypothesis that the applied heat dose, which is dependent upon both the temperature obtained and the exposure time, is the critical parameter. In this case extensive thermometry is required to ensure that the patient receives an effective adjunct treatment to radiotherapy.

Yours, etc.,
J. VAN DER ZEE
G. C. VAN RHOON
J. L. WIKE-HOOLEY
**H. S. REINHOLD

Department of Hyperthermia,
Rotterdam Radiotherapy Institute,
Rotterdam, The Netherlands

**Erasmus University,
Rotterdam, The Netherlands
(*Received September 1985*)

REFERENCES

FIELD, S. B. & MORRIS, C. C., 1983. The relationship between heating time and temperature: its relevance to clinical hyperthermia. *Radiotherapy and Oncology, 1,* 179–186.

GIBBS, JR, F. A., PECK, J. W. & DETHLEFSEN, L. A., 1981. The importance of intratumor temperature uniformity in the study of radiosensitizing effects of hyperthermia in vivo. *Radiation Research, 87,* 187–197.

HAHN, G. M., 1982a. Does the mode of heat induction modify drug antitumour effects? *British Journal of Cancer, 45,* 238–242.

——1982b. *Hyperthermia and cancer.* (Plenum Press, New York, London.)

HOLT, J. A. G., 1980. Alternative therapy for recurrent Hodgkin's disease. Radiotherapy combined with hyperthermia by electromagnetic radiation to create complete remission in 11 patients without morbidity. *British Journal of Radiology, 53,* 1061–1067.

MARMOR, J. B., HAHN, N., & HAHN, G. M., 1977. Tumor cure and cell survival after localized radiofrequency heating. *Cancer Research, 37,* 879–883.

OVERGAARD, J., 1985. Rationale and problems in the design of clinical studies. In *Hyperthermic Oncology 1984.* Ed. by J. Overgaard. Vol. II, Review lectures, symposium summaries and workshop summaries (Taylor and Francis, London, Philadelphia), pp. 325–338.

ROBINSON, J. E., HARRISON, G. H., McCULLOCH, D., & McCREADY, W. A., 1981. The effects of microwaves on cell survival at elevated temperatures. *Radiation Research, 88,* 542–551.

SAPARETO, S. A., LI, G. C., WHITE, K. A., HAHN, G. M., VAGUINE, V. A., GIEBELER JR., R. H. & TANABE, E., 1982. Microwave cytotoxicity: lack of in vitro evidence for nonthermal effects at high power levels. *Radiation Research, 89,* 124–133.

The absence of tissue specificity in MRI using *in vivo* T_1 or T_2 determination: true biological variation or technical artefact?

THE EDITOR—SIR,

The discovery by Damadian (1971) that malignant tissue measured *in vitro* has a higher T_1 than normal tissue acted as the stimulus for the development of NMR imaging techniques. In the beginning it was hoped that *in vivo* measurements of relaxation parameters may uniquely identify different tissues or the same tissue in different pathological states, perhaps enabling the differentiation between normal, benign or malignant tissue. However, by the time commercial magnetic resonance imaging (MRI) systems became available in about 1982, the emphasis in MRI system design was generally not on precise or accurate *in vivo* T_1 or T_2 determination but rather higher resolution image production, the images being T_1 or T_2 weighted. It is generally accepted now that neither T_1 nor T_2 are disease-specific, there being too great an overlap for diagnostic purposes.

We feel that this conclusion may be erroneous. The spread of T_1 or T_2 values from a particular tissue may not be due solely to the biological variation but instead may be significantly expanded due to technical errors in their calculation. There are a number of possible sources of error in the *in vivo* relaxation parameter determination.

(a) The calculation of *in vivo* T_1 from a saturation recovery and an inversion recovery pulse sequence will have an error if there is not efficient inversion in the latter sequence. This will occur in all imaging systems when a spatially selective 180° pulse is used or when there is significant radiofrequency inhomogeneity across the image plane. An exception is the system which uses an adiabatic fast passage RF pulse (Edelstein et al, 1980), which efficiently inverts all the nuclei.

(b) Some two-point methods of relaxation parameter calculation are known to be imprecise; for example, two saturation–recovery or two spin–echo sequences with different TR or two inversion-recovery sequences with different TI to calculate T_1 and two spin–echo sequences with different TE to calculate T_2. More precise estimations using such sequences require a larger number of points each with a different TI or TE value to be used.

(c) The spin–spin and spin–lattice relaxation processes may not be characterised by a single exponential.

(d) The width of the tomographic sections used in MRI, particularly when values of T_1 or T_2 are being calculated, can be as thick as 20 mm. As a consequence there can be a significant partial volume effect. The partial volume effect can produce a considerably reduced estimate of the T_1 or T_2 in a pathological lesion which has a higher value than surrounding normal tissues unless the lesion was extremely large. Much thinner section widths must, therefore, be used for accurate *in vivo* T_1 or T_2 determination; the thickness of the section should be about half the diameter of any tissue under investigation and care must be taken to position the section through the centre of the tissue.

(e) It is recognised that cardiac and respiratory movement degrade the resolution of images; this can be avoided by the use of gating techniques. However, not only does it degrade image resolution, it will also produce an error in the calculation of T_1 or T_2 if the tissue is moving.

(f) There can be an error introduced due to subjective operator variation in the choice of region for T_1 or T_2 calculation.

Experience has shown that, as the techniques of *in vivo* T_1 and T_2 determination are improved, so the spread in their values from a particular type of tissue is reduced. Only when the technical errors of T_1 and T_2 measurement are eliminated can we hope to draw any firm conclusions concerning their specificity and consequent clinical use.

Correspondence

We would recognise that in many MRI systems it is not possible to eliminate all the sources of technical error, particularly as there is often limited time available for patient investigation. In the centres which adopt a pragmatic approach to T_1 and T_2 calculation and are investigating its use in the clinical environment, knowing that, for technical reasons, the values obtained may not be entirely accurate, we would suggest that such quantitative values should be defined as T_1^{**} and T_2^{**}. The term T_1 and T_2 would be reserved for what is believed to be true biological relaxation times.

Yours, etc.,
M. A. SMITH,
*D. G. TAYLOR

NMR Imaging Unit,
University of Edinburgh,
Royal Infirmary, Edinburgh
*Department of Physics,
University of Surrey,
Guildford, Surrey
(*Received August 1985*)

REFERENCES

DAMADIAN, R., 1971. Tumour detection by nuclear magnetic resonance. *Science, 171,* 1151–1153.

EDELSTEIN, W. A., HUTCHISON, J. M. S., JOHNSON, G. & REDPATH, T., 1980. Spin-warp NMR imaging and applications to human whole body imaging. *Physics in Medicine and Biology, 25,* 751–756.

Radioprotection by ascorbate *in vitro*: temperature-dependent uptake

THE EDITOR—SIR,

The role of glutathione in radioprotection has been much investigated, but relatively little attention has been paid to ascorbate, which is present at high concentrations in human tumours (Kakar & Wilson, 1974; Moriarty et al, 1977). Both glutathione and ascorbate can act as H-atom donors, although ascorbate is more efficient in electron transfer reactions, and both these reactions may be important in DNA repair processes (Redpath & Willson, 1973; O'Neill, 1983; Willson, 1983). There have been some reports in the literature of radioprotection by ascorbate *in vitro* (Redpath & Willson 1973; O'Connor et al, 1977; Baverstock, 1979) but other workers have found no effect of ascorbate on radiosensitisation by misonidazole (Koch et al, 1979).

As a part of an investigation into the radioprotective role of ascorbate *in vitro*, we have measured the uptake of ascorbate by V79 379A Chinese hamster cells incubated in Eagles' minimum essential medium +10% fetal calf serum at various temperatures. Figure 1 shows the concentration of ascorbate in cells plotted against time of incubation under N_2 at 4°C, 21.5°C and 36°C. The point we would wish to emphasise is the marked temperature-dependence and slow time course of the uptake, with essentially no uptake at 4°C, and intracellular concentrations increasing for several hours at the higher temperatures. In some radiobiological experiments the pre-irradiation incubations are carried out at 4°C in order to reduce toxicity. If the agent of interest is actively transported, or is taken up slowly, both of which appear to apply to ascorbate, a lack of effect could arise from poor intracellular uptake rather than inactivity *per se*. Thus, Koch et al (1979)
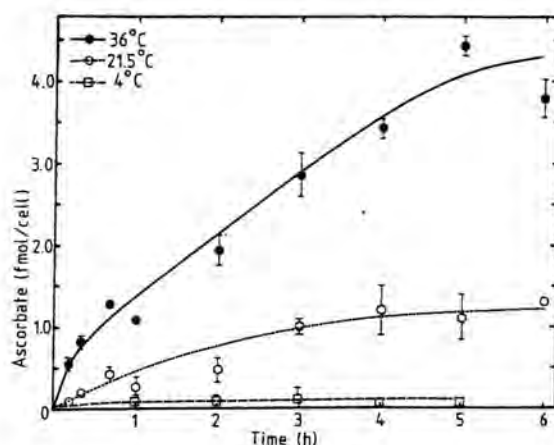
FIG. 1.

Temperature-dependence of the uptake of ascorbate by cells incubated with 0.5 mM ascorbate under N_2. Error bars indicate $\pm$ SD.
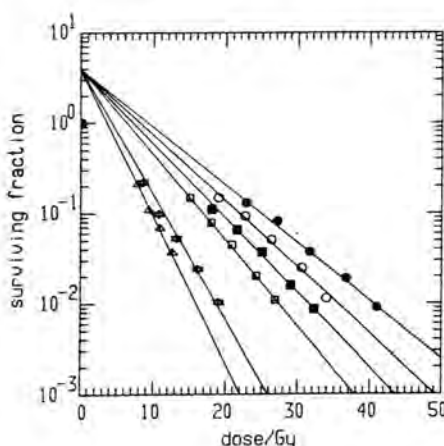
FIG. 2.

Survival curves for cells irradiated under N_2, in the absence or presence of ascorbate. (A) (○) Hypoxic control, (●) 1 mM ascorbate; protection factor (PF) = 1.14. (B) Cells incubated with the inhibitor of glutathione (GSH) biosynthesis buthionine sulphoximine (BSO) (0.1 mM) for 18 h: (□) hypoxic control, (■) 0.2 mM ascorbate; PF = 1.15. (C) GSH depleted cells + misonidazole (0.1 mM): (△) hypoxic control, (✱) 0.2 mM ascorbate; PF = 1.17. In each case, the PF is quoted relative to the paired survival curve in the absence of ascorbate.

showed that ascorbate at 5 mM had no effect on radiosensitivity when the pre-gassing was carried out at 4°C. We have recently shown that if pre-incubation is at room temperature, then ascorbate can afford significant protection in both control and GSH-depleted cells (Fig. 2). Full details will be published elsewhere. We would, therefore, like to take this opportunity to emphasise the importance of measuring the uptake of any

A Description of a Low Field Resistive Magnetic Resonance Imaging System and its Application in Imaging Midline Central Nervous System Pathology

D. M. KEAN, M. A. SMITH, R. H. B. DOUGLAS and J. J. K. BEST

NMR Imaging Unit, University of Edinburgh, Royal Infirmary, Edinburgh

A commercial low field magnetic resonance imaging (MRI) system installed in the Royal Infirmary, Edinburgh at the end of 1983 has since been used for the clinical investigation of over 1000 patients. This system uses an interlaced saturation recovery and inversion recovery pulse sequence which yields four types of clinical image. A T_1 weighted image has been found to be the most sensitive for the detection of pathology. Several examples of pathology with negative X-ray computed tomography examinations including three examples of a syrinx and two cases of tonsillar herniation have been demonstrated using this system. It is suggested that the system could provide a routine clinical service for imaging the central nervous system.

The past four years have seen considerable progress in magnetic resonance imaging (MRI). In the majority of this work imaging systems with field strengths of 0.15 T and above have been used, though some clinical work has been performed at 0.08 T (Hawkes *et al.*, 1980; Bydder and Steiner 1982; Bydder *et al.*, 1982; Brant-Zawadski *et al.*, 1983; Bydder *et al.*, 1983; Gamsu *et al.*, 1983; Herfkens *et al.*, 1983; Hricak *et al.*, 1983a; Hricak *et al.*, 1983b; Smith 1983; Worthington *et al.*, 1983; Kean *et al.*, 1985). Since the major application of MRI appears to be in the investigation of the central nervous system it is necessary to produce satisfactory images of this system with sufficient resolution and pathological contrast within an acceptable patient investigation time.

THE MAGNETIC RESONANCE UNIT

The magnetic resonance machine is a low field 0.08 T system manufactured by M&D Technology Ltd, installed in the Royal Infirmary, Edinburgh (Smith *et al.*, 1984). It employs a resistive magnet whose magnetic field is directed along the vertical axis. The design of the system is closely based on the Aberdeen magnetic resonance imager (Hutchison and Smith, 1983) and uses an interlaced saturation-recovery and inversion-recovery pulse sequence (Fig. 1). The repetition rate (*TR*) and time to inversion (*TI*) are normally 1000 ms and 200 ms respectively resulting in a total data acquisition time of 4 min 16 s for each section.

Four types of clinical image are processed for each section (Fig. 2). The so called 'P' or 'proton density' image (Fig. 3) is obtained from the saturation-recovery pulse sequence which utilises a field echo with an echo-delay time (TE) of 10 ms. This image has the best signal

to noise ratio and consequently the best spatial resolution of the four images, but since there is very little difference between proton density in different normal tissue types and between different pathological tissues little pathological information is contained in this image. The image is not a true proton density image as substances with a very long T_1 relaxation time like cerebrospinal fluid will give very little signal due to the incomplete relaxation of magnetisation between successive pulses with a *TR* of 1 s.

The inversion-recovery pulse sequence employs an adiabatic fast passage (AFP) radiofrequency (RF) pulse to ensure complete 180° inversion of magnetisation throughout the section of data collection. This differs from more conventional 180° RF pulses where it may be
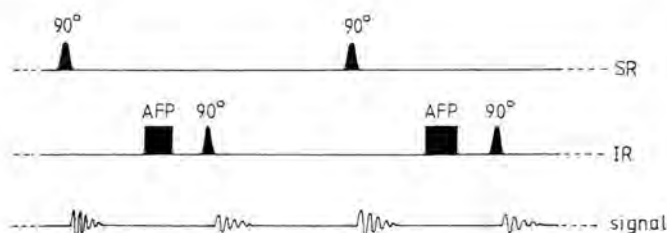
Fig. 1 – The NMR pulse sequence used in the M&D 800 imager.
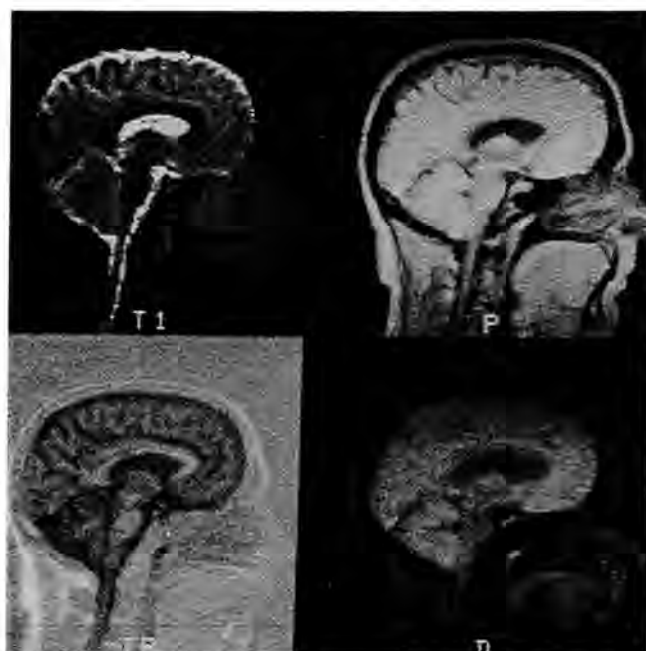
Fig. 2 – The four different types of image produced by the imager.

Fig. 3 – A proton density image.

T_1 weighting will result in regions of prolonged T_1 giving a higher signal intensity.

A calculated T_1 image is obtained from the following equation:

$$T_1 = 200/\ln\{(2 \times \text{'P'})/\text{'D'}\}$$

where 'P' and 'D' represent the pixel values in the proton density and difference images respectively. This image is often useful in confirming the presence of pathology which is suspected on the 'difference' or inversion-recovery image. The T_1 calculation is precise due to the complete inversion achieved by the AFP pulse. The long-term *in vitro* precision over six months varies from 2.3% (coefficient of variation) to 4.1% for T_1 values of between 163 ms and 416 ms respectively. The *in vivo* precision is 4.9% for grey matter and 2.8% for white matter (Smith *et al.*, 1985). An example of a T_1

uncertain whether complete inversion through 180° has been achieved. The inversion-recovery image can be displayed by either a non-modulus or a modulus form of display (Fig. 4). The inversion recovery image is T_1 weighted, allowing for discrimination between tissues of different T_1 values such as grey and white matter. The contrast, that is the difference in signal between two different tissues, will vary with the time allowed for longitudinal relaxation before a 90° pulse is applied (*TI*).

The 'D' or 'difference' image is obtained by subtracting the numerical data of the inversion-recovery pulse sequence from the saturation recovery pulse sequence. This image (Fig. 5) contains much of the spatial resolution of the saturation-recovery image but its T_1 weighting provides much more pathological information. This

Fig. 5 – The 'difference' image.
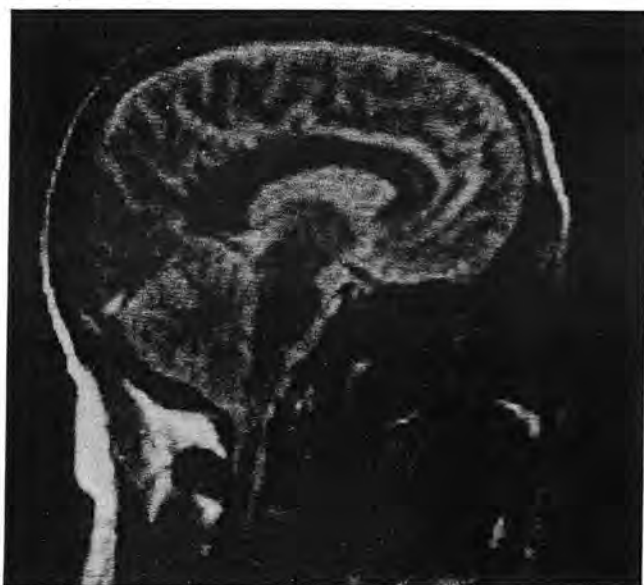
(a)

(b)

Fig. 4 – (a) Modulus form and (b) non-modulus form of the inversion-recovery image.

Fig. 6 – The calculated T_1 image.

image is shown in Fig. 6. The T_1 values can be displayed using a linear grey scale or colour-coded display. The pixel values on the grey scale and the colours on the colour-coded display are directly related to the T_1 value in milliseconds.

THE MACHINE IN CLINICAL PRACTICE

The patient is positioned by means of a light source and is transported into the magnet system on a motor-driven couch. A smaller head coil is fitted into the larger body coil for cranial examination. A 16 s 'fast' scan is used to check the anatomical level before the 4 min 16 s full data collection is begun. There is some T_1 information in the 'fast' scan and this can show pathology such as the subdural collection shown in Fig. 7. This is useful if the patient is unable to cooperate or elderly when chance of movement during the longer scan increases. Fast scans, due to the short TR are also more flow dependent and may be used to confirm the presence of flowing blood within a lesion like an intracranial aneurysm (Fig. 8). Subsequent transverse images above
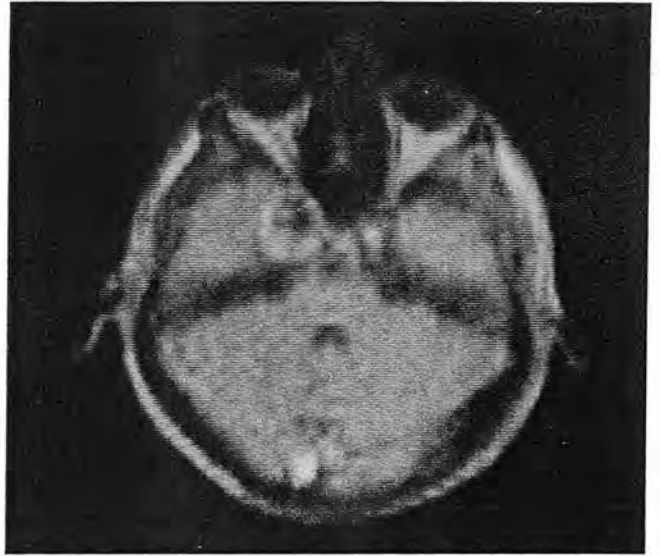
Fig. 8 – 'Fast' image showing high signal from flowing blood in the sagittal sinus and around the thrombus in a cavernous aneurysm.
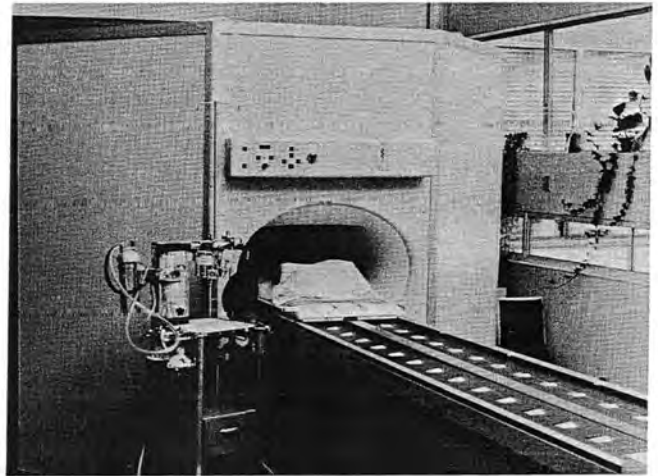
Fig. 9 – An anaesthetic trolley positioned close to the imager.

Fig. 7 – 'Fast' image showing high signal from a subdural collection.
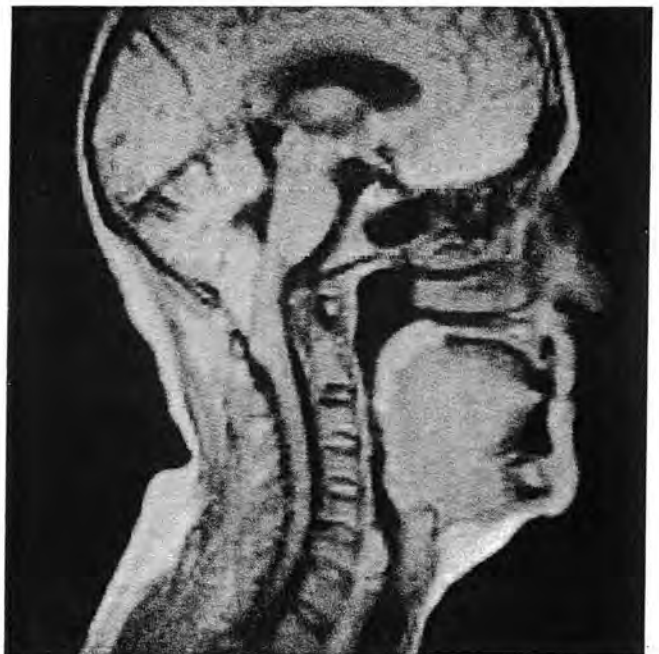
Fig. 10 – Midline sagittal proton density image showing tonsillar herniation to the posterior arch of C2.

or below the first image are then obtained by controlled couch movement. Sagittal and coronal images can also be obtained but at present these are only available through the mid-sagittal and mid-coronal planes of the imaging volume. Slight adjustment to the position of this plane in the midline of the imaging volume may be made by alterations to the static magnetic field. These alterations however are limited and only permit about 1 cm latitude. It is also possible, by moving the patient slightly, to alter the position of the region of interest being imaged.

As with other MRI systems claustrophobia may be a problem, particularly with cranial examinations where the head is more enclosed within the smaller head coil. Gentle persuasion overcomes this problem in all but the most severely claustrophobic. The overall total rejection rate due to claustrophobia is 2%.

To date 49 children have been examined, eight of these under general anaesthesia. Several problems are posed in the administration of general anaesthesia in a magnetic environment but these have been successfully overcome. The problems are minimised by the low mag-
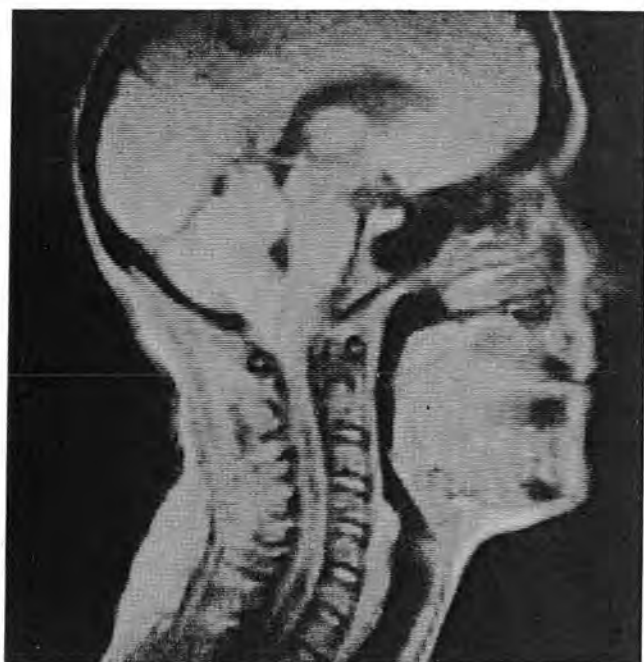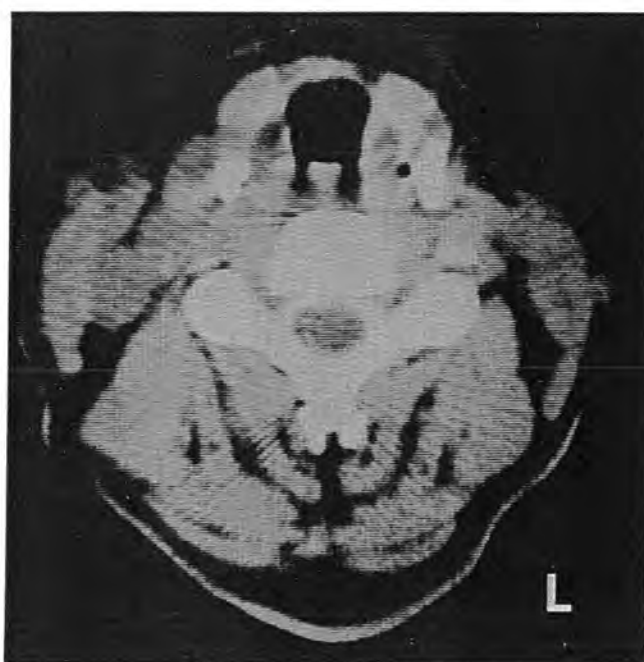
(a)   (b)

Fig. 11 – (a) A midline sagittal proton density image showing central low signal in the cervical cord due to a syrinx cavity. (b) 'Normal' CT scan of the same patient (L+100, W250).

(a)   (b)

Fig. 12 – (a) A midline sagittal inversion-recovery image showing high signal from a large lipoma in the cervical spinal cord. (b) Midline sagittal calculated T_1 image showing the very short T_1 of this lipoma compatible with fat. The displacement of the spinal cord is also shown. (From Kean et al., 1985.)

netic field. It is important that no metal is used in the anaesthetic tubing, particularly at the mouthpiece. Metal stethoscopes cannot be used but an oesophageal stethoscope has proved ideal. A standard anaesthetic trolley causes distortion of the main magnetic field when it is in close proximity to the magnet and adjacent to the RF shield next to the patient couch. Once an anaesthetic trolley is in position however this distortion can be compensated for by adjusting the static magnetic field; and provided it is not moved, the quality of the image is unaffected (Fig. 9). A pulse monitor with a light-emitting diode detector around a digit may be used to monitor the pulse. It is important that all anaesthetic staff are warned of the possibility of danger from projectile metal objects in the proximity of the static field. This hazard however is not so great a problem with a lower field system than with higher field systems. In common with all other MR systems, patients with pacemakers are not allowed within the imaging suite and at present patients with aneurysm clips are not imaged.

CLINICAL RESULTS

Craniovertebral Junction

To date 44 patients with suspected pathology in this region have been examined. The assessment of suspected pathology in this location is made particularly easy by the use of the sagittal imaging plane. This allows the position of the cerebellar tonsils to be accurately defined and any downward displacement of these structures to be easily assessed. Since cortical bone is not visualised by MR the anterior and posterior margins of the foramen magnum are not directly visualised but can be inferred. The clivus, which contains fat, points to the anterior margin of the foramen magnum and the fat in the occipital diploe points to the posterior margin. When the cerebellar tonsils are displaced inferiorly (Fig. 10) they are seen to herniate through the foramen magnum and in this example are seen to approach the posterior arch of the second cervical vertebra.

The presence of a *syrinx* can be rapidly demonstrated by low-field MRI. Figure 11(a) demonstrates a low signal from a syrinx cavity within the cervical cord. This cavity contains CSF which on a proton density image gives a low signal due to its very long relaxation time when examined with a *TR* of 1 s. A moderate degree of tonsillar herniation is also seen. The computed tomography (CT) examination, with intrathecal iopamidol (Fig. 11b), shows a normal sized cord and no evidence of a syrinx.

A *lipoma* in the cervical cord is dramatically shown on inversion recovery and calculated T_1 images (Fig. 12). The short T_1 of this lesion allows a diagnosis of lipoma to be made. The anterior displacement of the cervical spinal cord is also well seen.

Brain Stem

To date 50 patients with suspected pathology in this region have been examined. Lesions in the brain stem cause a non-specific rise in relaxation times. Figure 13a

(a)

(b)

Fig. 13 – (a) Midline sagittal 'D' image showing high signal from a pontine glioma causing effacement of the 4th ventricle. (b) Coronal inversion-recovery image showing very low signal i.e. long T_1 from the same pontine glioma.
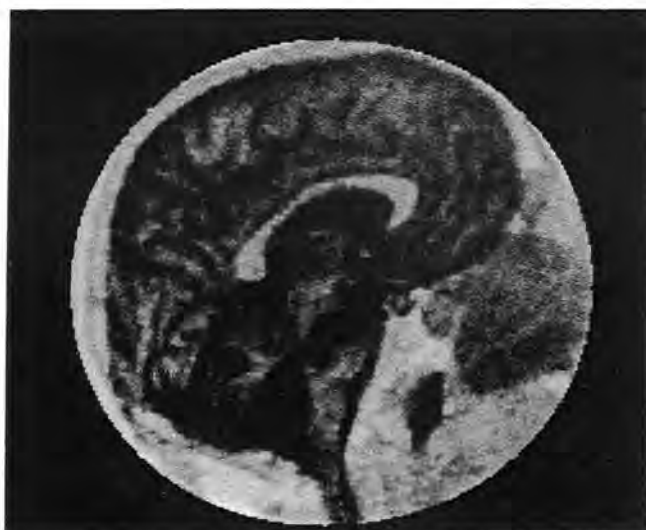
Fig. 14 – Midline sagittal inversion-recovery image showing low signal from a large brain stem infarct.

demonstrates an expanding lesion in the pons, which is effacing the 4th ventricle. The coronal image (Fig. 13b) confirms the intra-axial location of this pathology. Vascular lesions such as brain-stem infarcts are easily demonstrated. Figure 14 demonstrates a region of low signal on an inversion-recovery image corresponding to prolonged T_1 in a large brain-stem infarct. Figure 19 demonstrates a region of prolonged T_1 in the pons in a patient with clinical signs of brain-stem demyelination. It must be pointed out that this T_1 abnormality is not specific and may also be seen in a small area of ischaemia.

Corpus Callosum

This is another structure which is easily assessed by MRI. Figure 16a demonstrates agenesis of the corpus callosum with an associated lipoma. The transverse section (Fig. 16b) shows the separation of the lateral ventri-

cles and the presence of a rounded short T_1 lesion anteriorly.

Pituitary Gland

To date 60 patients with suspected pathology in this region have been examined. MRI does not demonstrate the destruction of cortical bone by pituitary pathology but the presence of most pituitary pathology is easily demonstrated. A very large pituitary macroadenoma is demonstrated in Fig. 17a; although demonstrated well by X-ray CT (Fig. 17b), it should be pointed out that this examination required over 45 1.5 mm sections together with intravenous contrast medium to provide such an image. The spatial resolution of the MRI machine is at present insufficient to demonstrate small pituitary lesions like microadenomas.

DISCUSSION

The advantages of MRI in the investigation of the CNS are now well known and many of these can be obtained from a low-field system. There have now been numerous publications demonstrating the use of MRI in the central nervous system. All of these have shown that MRI is the modality of choice in this region due to the following features:

1. The variability of the pulse sequences give MRI flexibility and allows the examination to be tailored to suit the particular clinical problem since these sequences may be altered to provide more contrast between normal and abnormal tissues which makes MRI a more sensitive technique.
2. The lack of artefact, particularly streaking in the posterior fossa, permits the demonstration of this area along with the craniovertebral junction much better than X-ray CT.
3. The direct acquisition of sagittal and coronal images permits the rapid and accurate localisation of pathology particularly at the cranio-vertebral junction and in the brain stem.
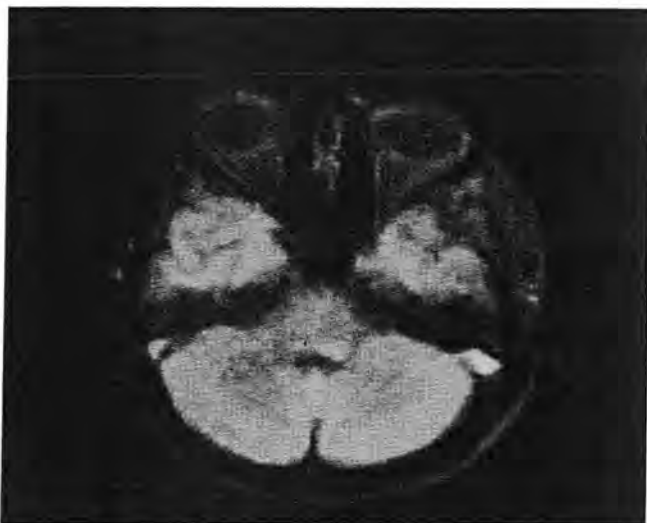
Fig. 15 – Transverse 'D' image showing high signal in the posterior aspect of the pons due to an area of demyelination.
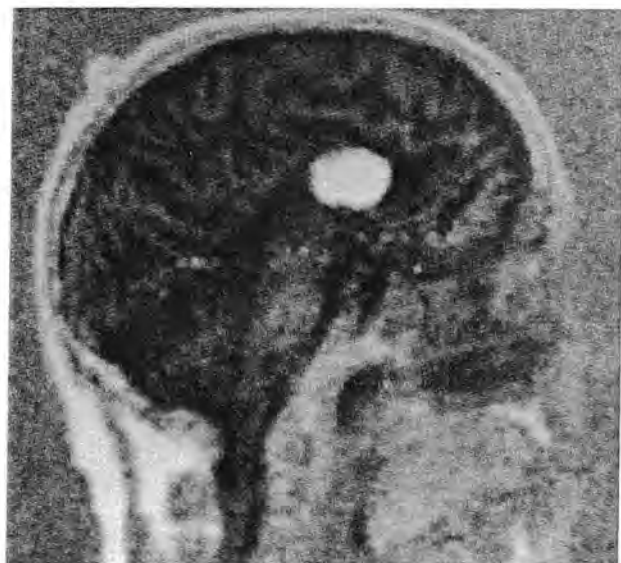
(a)
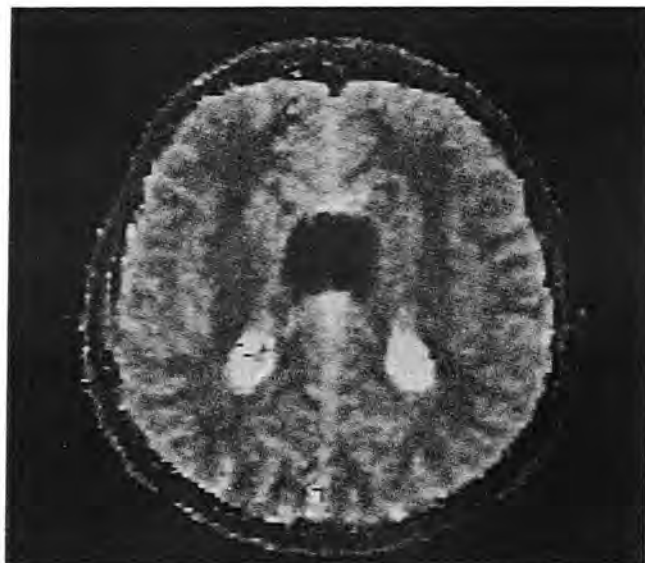
(b)

Fig. 16 – (a) Midline sagittal inversion-recovery image showing high signal from a lipoma of the corpus callosum. (b) Transverse calculated T_1 image showing low signal from the same lipoma. The separation of the lateral ventricles is also seen.
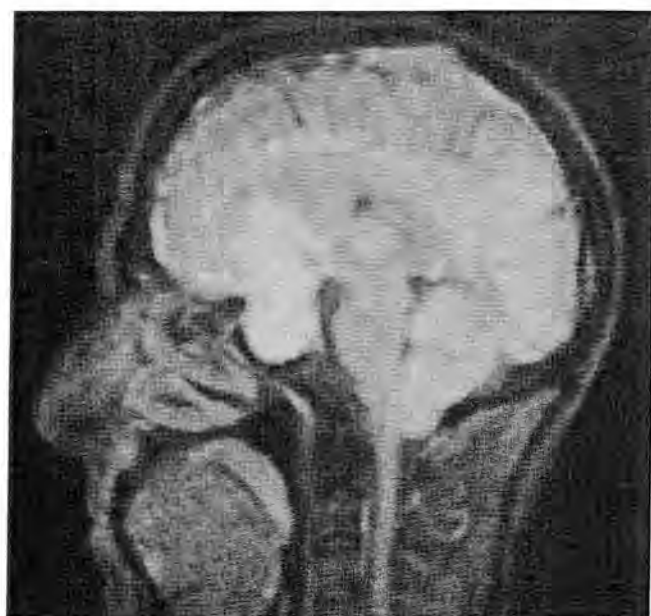
(a)
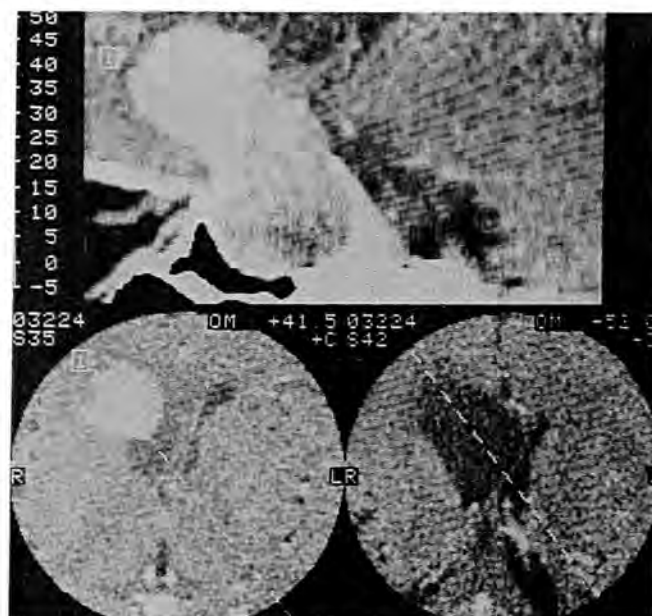
(b)

Fig. 17 – (a) Midline sagittal 'D' image showing a large pituitary macroadenoma extending down into the sella. There is also considerable suprasellar extension. (b) CT scan of the same pituitary macroadenoma (L+40, W150).

These advantages have been demonstrated on systems with a higher field strength than the one described. We believe that the low-field system described is capable of producing excellent clinical results. The most obvious disadvantage is the inferior spatial resolution compared with high-field systems. This drawback may only be a problem in examining regions such as the pituitary and the internal auditory meatus. Signal averaging may overcome this but this would mean a slightly increased imaging time. Another drawback to the system at present is the lack of offset slices in the sagittal and coronal planes. It is planned to upgrade the system with this facility together with the addition of a facility for multiple simultaneous slice acquisition.

In conclusion, we feel that this imaging system, at least when applied to the central nervous system, can provide almost all the advantages inherent to MRI but without many of the problems associated with higher field, higher cost systems; and with the additions of offset slices and multiple simultaneous slice acquisition this system will be capable of providing a routine clinical service in imaging the CNS.

REFERENCES

Brant-Zawadski, M., Davis, P. L., Crooks, L. E., Mills, C. M., Norman, D., Newton, T. H., et al. (1983). NMR demonstration of cerebral abnormalities: comparison with CT. American Journal of Roentgenology, 140, 847–854.

Bydder, G. M. & Steiner, R. E. (1982). NMR imaging of the brain. Neuroradiology, 23, 147–157.

Bydder, G. M., Steiner, R. E., Thomas, D. J., Marshall, J., Gliderdale, D. J. & Young, I. R. (1983). NMR imaging of the posterior fossa in 50 cases. Clinical Radiology, 34, 173–188.

Bydder, G. M., Steiner, R. E., Young, I. R., Hall, A. S., Thomas, D. J., Marshall, J., et al. (1982). Clinical NMR imaging of the brain: 140 cases. American Journal of Roentgenology, 139, 215–236.

Gamsu, G., Webb, W. R., Sheldon, P., Kaufman, L., Crooks, L. E., Birchberg, F. A., et al. (1983). Nuclear magnetic resonance imaging of the thorax. Radiology, 147, 473–480.

Hawkes, R. C., Holland, G. N., Moore, W. S. & Worthington, B. S. (1980). Nuclear magnetic resonance (NMR) tomography of the brain: a preliminary clinical assessment with demonstration of pathology. Journal of Computer Assisted Tomography, 4, 577–586.

Herfkens, R. J., Higgins, C. B., Hricak, H., Lipton, M. J., Crooks, L. E., Sheldon, P. E. et al. (1983). Nuclear magnetic resonance imaging of the cardiovascular system: normal and pathological findings. Radiology, 147, 749–759.

Hricak, H., Crooks, L., Sheldon, P. & Kaufman, L. (1983a). Nuclear magnetic resonance imaging of the kidney. Radiology, 146, 425–432.

Hricak, H., Williams, R. D., Spring, D. B., Moon Jr, K. L., Hedgcock, M. W., Watson, R. A. et al. (1983b). Anatomy and pathology of the male pelvis by magnetic resonance imaging. American Journal of Roentgenology, 141, 1101–1110.

Hutchison, J. M. S. & Smith, F. W. (1983). NMR clinical results: Aberdeen. In Nuclear Magnetic Resonance (NMR) Imaging, eds Partain, C. L., Jones, A. V., Rollo. F. D. & Price, R. R. pp. 231–249, W. B. Saunders Company, Philadelphia.

Kean, D. M., Smith, M. A., Douglas, R. H. B., Martyn, C. N. & Best, J. J. K. (1985). Two examples of CNS lipomas demonstrated by computed tomography and low field (0.08T) MR imaging. Journal of Computer Assisted Tomography, 9, 494–496.

Smith, F. W. (1983). Review: Nuclear magnetic resonance in the investigation of cerebral disorder. Journal of Cerebral Blood Flow Metabolism, 3, 263–269.

Smith, M. A., Best, J. J. K., Douglas, R. H. B. & Kean, D. M. (1984). The installation of a commercial resistive NMR imager. British Journal of Radiology, 57, 1145–8.

Smith, M. A., Chick, J., Kean, D. M., Douglas, R. H. B., Singer, A., Kendell, R. E. et al. (1985). Brain water in chronic alcoholic patients measured by magnetic resonance imaging. Lancet, i, 1273–1274.

Worthington, B. S., Kean, D. M., Hawkes, R. C., Holland, G. N., Moore, W. S. & Corstan, R. (1983). Nuclear magnetic resonance imaging in the recognition of giant intracranial aneurysms. American Journal of Neuroradiology, 4, 835–836.

Technical note

A technique for velocity imaging using magnetic resonance imaging

By J. P. Ridgway, B.Sc., M.Sc. and M. A. Smith, B.Sc., M.Sc., Ph.D.

NMR Imaging Unit and Department of Medical Physics & Medical Engineering, University of Edinburgh, Royal Infirmary, Edinburgh

Magnetic resonance imaging (MRI) is becoming well established as a technique which both shows anatomy and allows tissue characterisation. A further development of the technique allows the imaging of regular movement such as blood flow and cardiac wall motion. In particular, much effort has been put into developing techniques for imaging flowing blood and deducing such parameters as velocity and acceleration.

Early work by Singer (1959) described a technique of blood flow velocity measurement using a "time-of-flight" method. Velocity images have been obtained by this method using a modified version of a spin-echo pulse sequence (Feinberg et al, 1984). Normally, a slice is excited using a selective 90° radio-frequency (RF) pulse and an echo is produced at a later time by applying a selective 180° pulse to the same slice. If moving hydrogen nuclei have, in the meantime, moved out of the slice, no signal will be returned from them, resulting in a reduction in signal intensity from blood vessels in the image. This is the spin washout effect. If, however, the 180° RF pulse is applied to a slice downstream, an echo signal will be returned from excited nuclei having a velocity such that they coincide with the second slice selection. In this way, a series of images can be obtained, each corresponding to a certain range of velocities.

The standard spin-echo technique can also be exploited to produce flow-dependent signals in vessels (Axel, 1984; Bradley et al, 1984; Waluch & Bradley, 1984). The effect, known as paradoxical enhancement, results in vessels appearing to have a much higher intensity than the surrounding tissue. This effect becomes particularly noticeable for shorter repetition times since freshly saturated nuclei moving into the slice will give a stronger signal relative to the surrounding stationary tissue, which is only partially saturated.

In a multi-echo sequence a phenomenon known as even-echo rephasing is also present (Waluch & Bradley, 1984). The magnetic field gradient (subsequently referred to as the gradient) used for slice selection and the gradient used for readout are applied twice in a spin-echo sequence. The first time they are applied, nuclei dephase along the direction of the gradient; the second time, they are applied with opposite polarity and nuclei move back into phase along that direction. If the nuclei are stationary then they will move back exactly

into phase with one another; however, if nuclei are moving along a gradient direction they will have a phase shift at the first echo, having only partially rephased. This phase shift will be linearly dependent on their velocity. All nuclei having the same velocity will have the same phase shift on odd echoes but will have zero phase shift on even echoes, the effect of the gradients having been reversed provided the velocity is constant. Thus, flow can be identified by comparing first and second echo images. On the first echo, flowing blood will appear to have a reduced signal while, on the second echo, the signal will be of higher intensity. We are, of course, neglecting dephasing effects caused by spin-spin relaxation.

Since the non-zero phase shift on the first echo is linearly dependent on velocity, it can be used to measure velocity directly (Bryant et al, 1984; Moran & Moran, 1984; Redpath et al, 1984; Van Dijk, 1984; Moran et al, 1985; Wedeen et al, 1985). In most MRI systems the signal is collected from two channels in quadrature, yielding a real and an imaginary data set. These are usually combined to calculate a modulus image used for diagnosis. These two data sets can, however, be used separately to produce a real or an imaginary image, or can be combined to calculate a phase image. All three of these contain phase information which is normally discarded in the calculation of the modulus image and it is this information which provides a way of imaging velocity.

Although real and imaginary images have been used to demonstrate imaging of velocity, they also contain spin-density information (Moran et al, 1985). The phase image is easiest to interpret and quantify since it contains only motion information and represents a direct linear map of a single velocity component. In order to quantify the velocity measurements accurately, standard spin-echo and field-echo sequences have been modified by adding extra gradient pulses in the direction of required velocity measurement.

To date, this has been done in two ways (Moran et al, 1985); either two identical gradient pulses separated by a 180° RF pulse are inserted, or a bipolar pulse consisting of two successive gradient pulses equal in magnitude and duration but of opposite sign is inserted into the pulse sequence between the 90° RF pulse and the readout gradient. The first of these

Technical note

gradient pulses dephases the nuclei in the applied direction and the second pulse rephases them. Stationary nuclei are all brought back into phase, whereas for nuclei moving along the gradient the rephasing is not complete, leaving them with a phase shift proportional to velocity.

The accuracy of the technique is dependent on the two gradient pulses having exactly the same duration and magnitude over the imaging volume and on the uniformity of the RF, gradient and static fields. A non-uniform field will introduce a spatially dependent phase shift over the image (McVeigh et al, 1985; Norris, 1985b). A technique has been developed (Redpath et al, 1984) to overcome these difficulties by varying the size of the flow-encoding pulses for a number of data acquisitions and applying a 3D Fourier transform technique to the whole set of data. The resultant set of images will be coded in intensity, each corresponding to a certain velocity range, and may be used to reconstruct a simple velocity-coded image. A further limitation of the techniques is that velocities corresponding to a phase shift of greater than $+180°$ or less than $-180°$ will lead to an ambiguity of velocity measurement. This can be avoided by adjusting the magnitude of the gradient so that the resultant phase shifts lie within the range of $\pm 180°$. This paper presents a technique which uses the calculated phase image as a direct measurement of velocity. The problem of field non-uniformity is avoided by using two separate pulse sequences and subtracting the resultant phase images.

METHOD

The technique has been integrated into the standard spin-warp imaging sequence (Edelstein et al, 1980) used on an M&D 0.08 T resistive MRI system (Smith et al, 1984). The slice selection gradients, which are effectively of bipolar form, were initially used to provide the phase

encoding for velocity components perpendicular to the imaging slice (Fig. 1). In order to avoid the appearance of phase shifts due to the spatial non-uniformities of the fields, two pulse sequences were used to produce two phase images which were subtracted to produce the final velocity image. The two pulse sequences were identical except that the timing of the rephasing gradient was later in one than in the other. Phase errors due to the time-independent inhomogeneities in the main field and the RF field would be the same in each case and would, thus, cancel in the final subtracted image. The only remaining phase differences are due to motion, such that for a given velocity component, v, in the direction of the applied slice selection gradient, G, the phase difference is:

$$\phi_{\text{diff}} = -\gamma G v t_w t_{\text{diff}}$$

where t_w is the duration of the rephasing pulse, t_{diff} is the difference in pulse separation for the two pulse sequences, and γ is the gyromagnetic ratio for protons (Fig. 1).

All the computer processing is performed within the acquisition program so that the subtracted phase images are displayed 8 s after acquisition. An ungated velocity image can be obtained in 64 s using a repetition time (TR) of 250 ms. For *in-vivo* imaging, however, the pulse sequences are gated (Been et al, 1985) in order to look at an instantaneous velocity, and consequently the imaging time is dependent on the heart rate. Typically, one section will take about 4 min. The two pulse sequences are interlaced so as to reduce the effects of gross patient movement between scans. The magnitude of the flow pulse gradient, G, is 1.25 mT m^{-1}. For the studies described here, the flow pulse timing was such that $t_{\text{diff}} = 2$ ms and $t_w = 2.4$ ms. The velocity sensitivity can be increased simply by increasing t_{diff}.
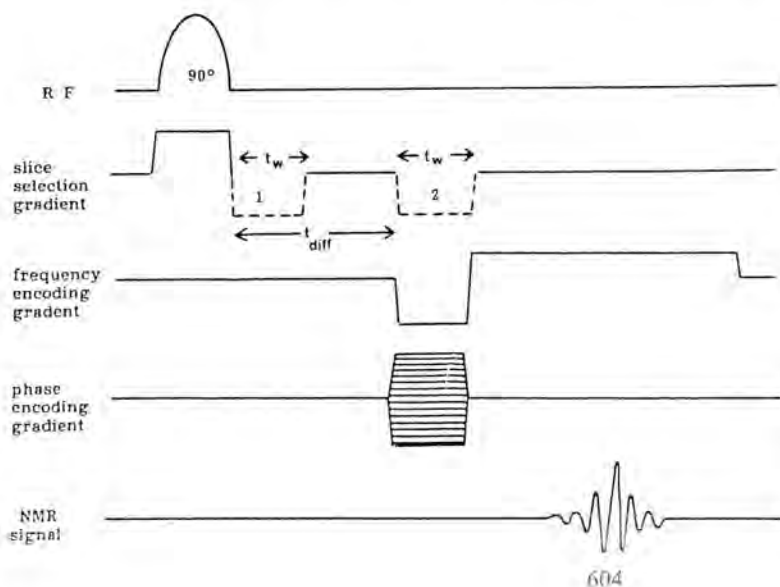

FIG. 1.

A simple adaption of the Aberdeen spin-warp pulse sequence for imaging of velocity through the slice by varying the position of the rephasing gradient (broken line) between positions 1 and 2. Two corresponding phase images are produced and then subtracted to produce the velocity-coded image.
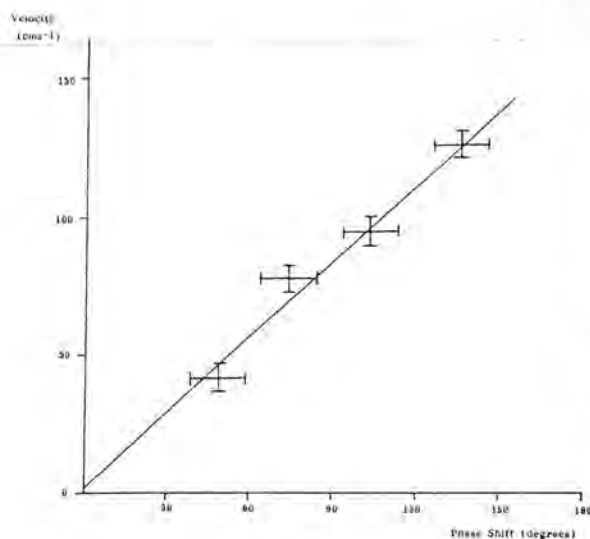
FIG. 2.

Velocity calibration of the flow measurement technique using the pulse sequence in Fig. 1.

Velocity measurements have been calibrated using a simple flow phantom consisting of a 1 cm-inside diameter polythene tube surrounded by a bath of 2.5 mM solution of copper sulphate. The same solution of copper sulphate was pumped through the tube at various known constant rates. The mean flow velocity for the tube was calculated and calibrated against the mean phase shift found within the tube. A number of normal volunteers have been imaged in the neck, thorax and abdomen using the interlaced gated sequence. An initial comparison with continuous wave Doppler ultrasound at 2.5 MHz has been carried out in the abdominal aorta using a Hewlett Packard 77020 Doppler imaging system. Using MRI, a number of delays were used from the electrocardiogram R-wave in order to plot the velocity in the abdominal aorta over the systolic period of the heart cycle. The sample volume for this measurement was taken at the centre of the aortic diameter.

RESULTS

The calibration of the velocity measurement shows a good linear relationship between velocity and phase shift (Fig. 2). Three examples of the volunteer studies are shown in Fig. 3. These images display zero phase shift as mid-grey, positive phase shift of 180° as white and negative phase shift of 180° as black. Where the values in the modulus image are below a certain threshold the phase values are not calculated.

Figure 4 shows the velocity measurements taken in the abdominal aorta compared with those taken from continuous-wave Doppler ultrasound measurements. There is a good agreement in profile shape and timing,
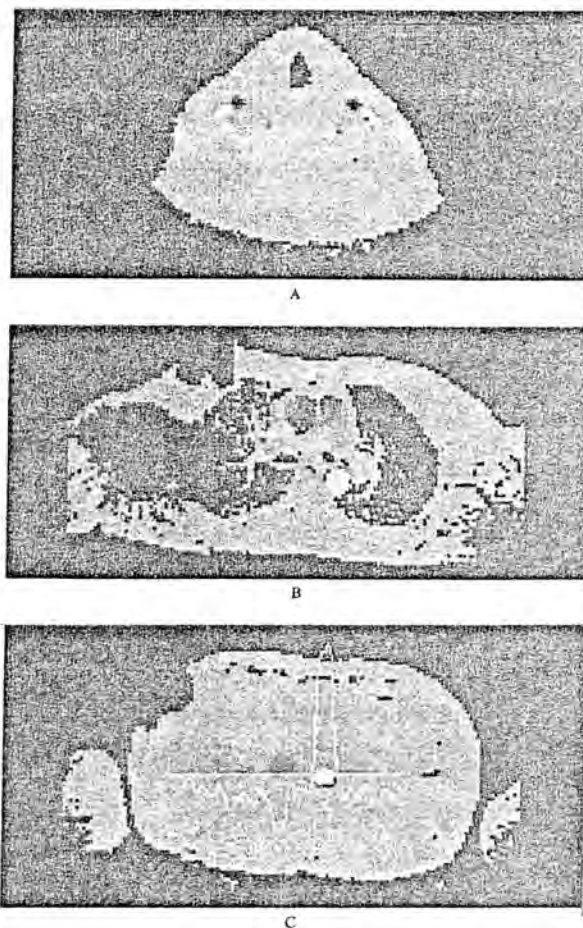
FIG. 3.

(A) A flow image of the neck using the pulse sequence of Fig. 1. This image demonstrates the common carotids and the vertebral arteries as the darker vessels, corresponding to a negative phase shift, and the jugular veins as the lighter vessels, corresponding to a positive phase shift. The surrounding stationary tissue is displayed as mid-grey. (B) A flow image of the thorax showing the ascending and descending aorta. (C) A flow image of the abdomen showing aorta and inferior vena cava. A line profile through both vessels clearly shows the differences in velocities.

although the velocities appear to be lower in the case of the Doppler measurements.

DISCUSSION

It has been shown that velocity measurements are possible on the low field imaging system at Edinburgh with changes only to the pulse sequence and software and without any improvements required on the field homogeneity.

This technique, using phase as a direct measurement of velocity, has advantages over the other techniques
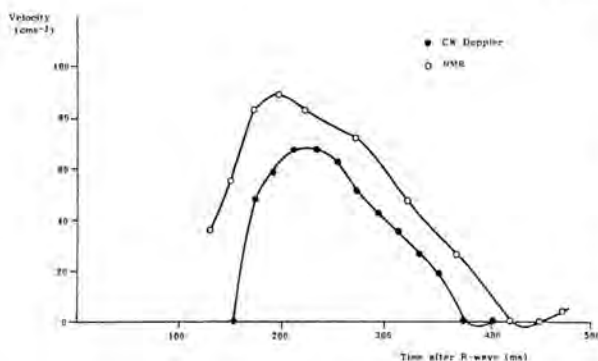
Technical note

Fig. 4.

A velocity flow profile of the systolic period of the heart cycle for the abdominal aorta comparing the results from 11 flow images as shown in Fig. 3C, with results from Doppler ultrasound measurements.

mentioned in the introduction due to its relative simplicity in interpretation, processing and display. The time-of-flight method is restricted to imaging of one particular velocity range per image. Paradoxical enhancement and even echo rephasing are not quantitative measures of flow and can only be used to identify whether flow is present. The 3D Fourier transform method requires many flow encoding stages, whereas the technique described here requires only two sections to produce the final velocity image.

Initially, high flow velocities are being examined since they occur in the larger, better defined vessels. Lower velocities of the order of 1 cm s^{-1} have been imaged by the technique simply by extending the time t_{diff}. However, if this becomes too large then inhomogeneities in the field lead to loss of signal from the imaging slice, so it would be necessary instead to increase the magnitude of the flow gradient.

While peak velocity in the abdominal aorta can easily be imaged, the peak velocity in the ascending aorta is rather more difficult to image due to loss of signal around high velocity gradients over the vessel cross-section (Moran & Moran, 1984; Moran et al, 1985; Wedeen et al, 1985). These large velocity gradients result in a large range of velocities and, hence, a large range of phase shifts being present in the same pixel volume. This phase dispersion causes the signal from the nuclei in the same pixel volume to cancel, resulting in loss of signal, and is often seen as a dark line along the inner surface of the vessel. This effect can be seen even in standard pulse sequences, as the slice selection and signal readout gradients induce accidental phase shifts for nuclei moving in their direction. Of particular importance is the case of mitral-valve stenosis where high-velocity jets are present.

Methods have been suggested to overcome the phase dispersion which causes this loss of signal (Le Roux & Floch, 1985; Pattany & Naylor, 1985). It is proposed to use an adaption of the compensating bipolar pulse technique suggested by Le Roux and Floch, modifying it for use with the basic spin-warp pulse sequence. The compensating bipolar pulse is of opposite polarity to that already in the sequence, so that the dephasing effect is reversed. Figure 5 shows the suggested pulse sequence for use in further work, incorporating compensating bipolar pulses into the technique in all three directions. At present, this is not possible to do due to hardware limitations, although it is hoped to implement it in the near future.

It has already been shown (Norris, 1985a) that double bipolar pulses can be used to image acceleration. The greater the separation between the bipolar pulses, the greater the phase shift for a given acceleration. Thus, phase shifts due to acceleration can be minimised by merging the two middle pulses of the double bipolar flow pulse into one. The velocity measurement is achieved by varying the position in time
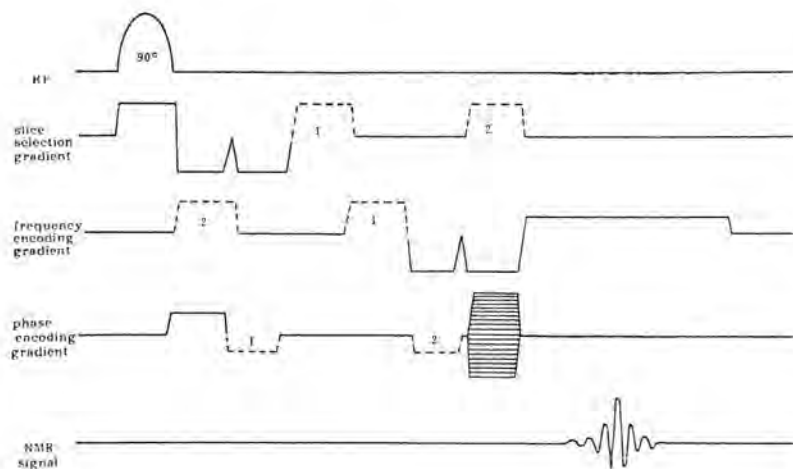

Fig. 5.

A further adaption of the flow pulse sequence of Fig. 1 for measurement of blood flow velocity in all three orthogonal directions. The gradient pulse sequences in the slice selection and frequency encoding directions have two bipolar pulses to compensate for the phase dispersion found in the normal imaging sequence.

of the broken line pulses in Fig. 5 between positions 1 and 2. Using the previous notation, the expression for phase shift is given by:

$$\phi_{\text{diff}} = \gamma G v t_w t_{\text{diff}} + \gamma G a t_w (7 t_w t_{\text{diff}} + t_{\text{diff}}^2)$$

where a is the constant acceleration.

Thus, for conditions where maximum acceleration occurs *in vivo* (200 cm s^{-2}) this would produce at most a 10% error in velocity measurement, given that typical velocities at this point are around 50 cm s^{-1}.

It is proposed to extend the technique to the measurement of flow in all directions in all phases and to pursue further volunteer studies and initial clinical trials. The technique will be compared directly with results from Doppler ultrasound measurements where possible.

REFERENCES

AXEL, L., 1984. Blood flow effects in magnetic resonance imaging. *American Journal of Roentgenology, 143,* 1157–1166.

BEEN, M., SMITH, M. A., RIDGWAY, J. P., BRYDON, J. W. E., DOUGLAS, R. H. B., KEAN, D. M., BEST, J. J. K. & MUIR, A. L., 1985. Characterisation of acute myocardial infarction by gated magnetic resonance imaging. *Lancet, ii,* 348–350.

BRADLEY, W. G., WALUCH, V., LAI, K. S., FERNANDEZ, E. J. & SPALTER, C., 1984. The appearance of rapidly flowing blood in magnetic resonance images. *American Journal of Roentgenology, 143,* 1167–1174.

BRYANT, D. J., PAYNE, J. A., FIRMIN, D. N. & LONGMORE, D. B., 1984. Measurement of flow with NMR imaging using a gradient pulse and phase difference technique. *Journal of Computer Assisted Tomography, 8,* 588–593.

EDELSTEIN, W. A., HUTCHISON, J. M. S., JOHNSON, G. & REDPATH, T. H., 1980. Spin warp imaging and applications to whole body imaging. *Physics in Medicine and Biology, 25,* 751–756.

FEINBERG, D. A., CROOKS, L., HOENNINGER, J., ARAKAWA, M. & WATTS, J., 1984. Pulsatile blood velocity in human arteries displayed by magnetic resonance imaging. *Radiology, 153,* 177–180.

LE ROUX, P. & FLOCH, J., 1985. Cancellation of the shear rate influence on flow velocity imaging. In *Proceedings of the Fourth Annual Meeting of the Society of Magnetic Resonance in Medicine, London, August 19–23, 1985,* pp. 585–586.

MCVEIGH, E. R., HENKELMAN, R. M. & BRONSKILL, M. J., 1985. Spatial dependence of phase in MR images. In *Proceedings of the Fourth Annual Meeting of the Society of Magnetic Resonance in Medicine, London, August 19–23, 1985,* pp. 1248–1249.

MORAN, P. R. & MORAN, R. A., 1984. Imaging true motion velocity and higher order motion quantities by phase gradient modulation techniques in NMR scanners. In *Technology of Nuclear Magnetic Resonance.* Ed. by P. D. Esser & R. E. Johnston (Society for Nuclear Medicine Inc., New York), pp. 149–166.

MORAN, P. R., MORAN, R. A. & KARSTAEDT, N., 1985. Verification and evaluation of internal flow and motion. *Radiology, 154,* 433–441.

NORRIS, D. G., 1985a. Acceleration by NMR. In *Proceedings of the Fourth Annual Meeting of the Society of Magnetic Resonance in Medicine, London, August 19–23, 1985,* pp. 593–594.

NORRIS, D. G., 1985b. Phase errors in NMR images. In *Proceedings of the Fourth Annual Meeting of the Society of Magnetic Resonance in Medicine, London, August 19–23, 1985,* pp. 1037–1038.

PATTANY, P. M. & NAYLOR, G. L., 1985. High velocity flow imaging by even echo rephasing. In *Proceedings of the Fourth Annual Meeting of the Society of Magnetic Resonance in Medicine, London, August 19–23, 1985,* pp. 599–600.

REDPATH, T. W., NORRIS, D. G., JONES, R. A. & HUTCHISON, J. M. S., 1984. A new method of NMR flow imaging. *Physics in Medicine and Biology, 29,* 891–898.

SINGER, J. R., 1959. Blood flow rates by nuclear magnetic resonance measurements. *Science, 130,* 1652–1653.

SMITH, M. A., BEST, J. J. K., DOUGLAS, R. H. B. & KEAN, D. M., 1984. The installation of a commercial resistive NMR imager. *British Journal of Radiology, 57,* 1145–1148.

VAN DIJK, P., 1984. Direct cardiac NMR imaging of heart wall and blood flow velocity. *Journal of Computer Assisted Tomography, 8,* 588–593.

WEDEEN, V. J., ROSEN, B. R., CHESLER, D. & BRADY, T. J., 1985. MR velocity imaging by phase display. *Journal of Computer Assisted Tomography, 9,* 530–536.

WALUCH, V. & BRADLEY, W. G., 1984. NMR even echo rephasing in slow laminar flow. *Journal of Computer Assisted Tomography, 8,* 594–598.

Correlation of human NMR T_1 values measured *in vivo* and brain water content

By H. L. MacDonald, B. A. Bell, M. A. Smith, D. M. Kean, J. L. Tocher, R. H. B. Douglas, J. D. Miller and J. J. K. Best

NMR Imaging Unit, University of Edinburgh, Royal Infirmary, Lauriston Place, Edinburgh and Department of Surgical Neurology, University of Edinburgh, Western General Hospital, Crewe Road, Edinburgh

ABSTRACT

A relationship has been demonstrated between nuclear magnetic resonance (NMR) longitudinal relaxation times (T_1 values) obtained *in vivo* in both normal and oedematous (peritumoral) brain tissue, and measurements of brain water obtained by gravimetric analysis of operative samples. Significant correlations were found in seven patients in both cortex ($r = 0.97$, $P < 0.001$) and white matter ($r = 0.92$, $P < 0.001$). These findings suggest that NMR may prove a useful technique for monitoring brain oedema.

Nuclear magnetic resonance (NMR) T_1 values in body tissue are considered to be related to total water content and to the ratio between "free" and "bound" water (Go & Edzes, 1975; Mathur-De Vré, 1984). Longitudinal relaxation time (T_1) lengthens in oedematous tissue and in a variety of pathological conditions including malignancy. Previous authors (Go & Edzes, 1975; Naruse et al, 1982) have shown a linear correlation between T_1 of experimentally induced cerebral oedema, measured by *in vitro* NMR spectrometry, and brain water, calculated from the weight of wet and dry tissues. The present study was performed in order to examine the relationship between T_1 values, obtained from clinical NMR images of patients about to undergo surgery for cerebral tumour, and brain water measurements obtained by gravimetric analysis of the excised specimens, and also to establish whether T_1 images can be used to predict the degree of cerebral oedema.

METHOD

Patients

All seven patients examined had histologically verified solitary tumours within the brain. Six were gliomas and the seventh a metastasis from an adenocarcinoma of lung. All patients were receiving 4 mg dexamethasone four times a day at the time of imaging and surgery. Four of the patients received 200–500 ml 20% mannitol at the time of dural opening, within 30 min of tissue excision. Six patients underwent lobectomy and one patient had multiple needle biopsies of tumour and peritumoral tissue. The excised specimens were rapidly enclosed in "cling film" and transported to the adjacent laboratory for measurement of brain water content.

Imaging

All patients were scanned the day before surgery with the M&D 800 NMR Imager at the Royal Infirmary, Edinburgh (Smith et al, 1984). For each section an interlaced saturation-recovery and inversion-recovery pulse sequence was used with a repetition time of 1 s for both, and in the latter a T_1 (time to inversion) of 200 ms was used. The slice thickness was 12 mm and the acquisition time 4 min 16 s. A calculated T_1 image was obtained from the saturation-recovery and inversion-recovery images using a two point method. This was felt to be adequate given that most tissues exhibit a single exponential decay curve (Ling et al, 1980). The use of an adiabatic fast passage inversion pulse ensures efficient inversion throughout the section. The mathematical algorithm used produces sufficiently accurate T_1 values (Redpath, 1982) and the long term precision of T_1 values, measured over a 6 month period, varies from 2.3% for $T_1 = 160$ ms to 4.1% for $T_1 = 500$ ms. Between four and eight sections were collected from each patient.

Brain water measurements

Brain water content was measured by microgravimetry using small tissue samples from the lobectomy specimens. The specific gravity (s.g.) of each sample was determined by placing it in a layered gradient column of a mixture of kerosene and bromobenzene oil, that had a high specific gravity at the bottom and a low specific gravity at the top (Marmarou et al, 1978). Two minutes after insertion of the sample into the column, its depth in the oil was measured, and the column was subsequently calibrated by measuring the depth of potassium-sulphate droplets of known specific gravity. The water content of each sample was then calculated from its specific gravity using the formula:

$$\text{g water/g tissue} = 1 - \frac{\text{sample s.g.} - 1}{(1 - 1/\text{solids s.g.}) \times \text{sample s.g.}}$$

derived by Nelson et al (1971). The s.g. of the normal human cortex and white matter solids was determined by wet-weighing 500 mg samples from five patients with normal brain in their operative specimens, and then

H. L. MacDonald et al.

reweighing the same samples after drying to constant weight at 80°C (Nelson et al, 1971).

The lobectomy specimens were sectioned in the transverse plane. Three samples of peritumoral white matter, each weighing about 10 mg, were taken from each site. Each sample was measured in the layered kerosene/bromobenzene density column (Marmarou et al, 1978), and samples of normal cortex and white matter, when present in the specimen, were similarly measured. In two patients, macroscopically oedematous cortex was also sampled. All gravimetric measurements were completed within 15 min of excision of the specimen, to minimise water loss from the tissues. The lobectomy specimen was then fixed for subsequent histological examination.

Analysis

The NMR images were reviewed by the same radiologist and surgeon without reference to the gravimetric data. The sites of tissue sampling had been noted by the surgeon with reference to known landmarks. T_1 values for abnormal tissue were obtained from those sites using the region of interest facility on the diagnostic console. Values for normal tissue were taken by the same method, wherever possible, within the lobe which had been resected.

FIG. 1.

Graph of water content and NMR T_1 values for cortex and white matter. – – – – Linear regression line for normal and abnormal cortex (no mannitol □, with mannitol ■). —— Linear regression line for normal and abnormal white matter (no mannitol ○, with mannitol ●).

RESULTS

A graph of T_1 values plotted against brain water readings for normal and oedematous tissue is shown in Fig. 1. A significant correlation exists between the two measurements for white matter ($r = 0.92$, $P < 0.001$), and cortex ($r = 0.97$, $P < 0.001$). Statistical analysis of the data (Smith et al, 1981) demonstrates that the errors of the techniques account for the spread of the bivariate data about the regression line ($\chi^2 = 36.9$, $P < 0.001$).

DISCUSSION

Brain tumours are often surrounded by a zone of oedema. This form of oedema is regarded by Klatzo (1972) as vasogenic, where oedema fluid emerges through a defective blood-brain barrier and spreads in the extracellular space of the white matter. This preliminary *in-vivo* study confirms in patients with brain tumours the linear correlation between brain water content and NMR T_1 values, previously reported in experimental animal models. Our results, however, highlight differences between white matter, where T_1 increases rapidly as water content rises, and cortex, where the increase is slower. In normal tissue the water content of cortex is greater than that of white matter, our finding of 10% agreeing closely with the 10–15% reported by other authors (Mathur-De Vré, 1984). The T_1 of normal cortex is correspondingly longer than that of normal white matter. Oedema fluid accumulating in cortical tissue is taken up by the cells and is, therefore, influenced by the intracellular macromolecules. The water protons are "bound" in the hydration layer around the macromolecules and this alteration in their
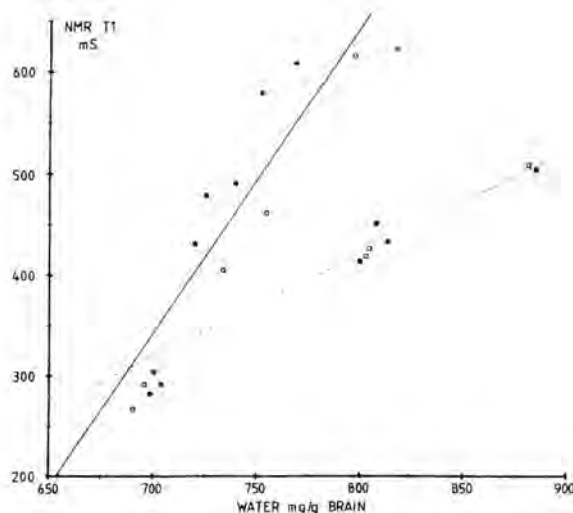
dynamic state shortens their relaxation time (Mathur-De Vré, 1984). In oedematous white matter more water remains in the extracellular compartment. A lower rate of collisions between molecules in this "free" state results in a longer relaxation time. Previous authors, working with rat brain *in vitro*, have attributed the linear increase in T_1 with water content to increase in the "free" water (Go & Edzes, 1975). Although results from our small sample must be interpreted with caution, we have shown a less marked rise in cortex, in keeping with the smaller rise in "free" as opposed to "bound" water. It appears that NMR T_1 values can be used to predict the degree of cerebral oedema in white matter, and possibly in cortex.

Four of our patients received intra-operative mannitol. Measured water content in their peritumoral white matter is lower than might be expected from pre-operative T_1 readings. Magnetic resonance imaging may prove a useful tool in assessing the effect of mannitol and other agents on cerebral oedema.

REFERENCES

Go, K. G. & Edzes, H. T., 1975. Water in brain oedema. Observations by the pulsed nuclear magnetic resonance technique. *Archives of Neurology, 32,* 462–465.

KLATZO, I., 1972. Pathophysiological aspects of brain edema. In *Steroids and Brain Edema.* Ed. by H. J. Reulen and K. Schurmann (Springer-Verlag, Berlin), pp. 1–8.

LING, C. R., FOSTER, M. A. & HUTCHISON, J. M. S., 1980. Comparison of NMR water proton T$_1$ relaxation times of rabbit tissues at 24 MHz and 2.5 MHz. *Physics in Medicine and Biology, 25,* 748–751.

MARMAROU, A., POLL, W., SHULMAN, K. & BHAGAVAN, H., 1978. A simple gravimetric technique for measurement of cerebral oedema. *Journal of Neurosurgery, 49,* 530–537.

MATHUR-DE VRÉ, R., 1984. Biomedical implications of the relaxation behaviour of water related to NMR Imaging. *British Journal of Radiology, 57,* 955–976.

NARUSE, S., HORIKAWA, Y., TANAKA, C., HIRAKAWA, K., NISHIKAWA, H. & YOSHIZAKI, K., 1982. Proton nuclear magnetic resonance studies in brain oedema. *Journal of Neurosurgery, 56,* 747–752.

NELSON, S. R., MANTZ, M. L. & MAXWELL, J. A., 1971. Use of specific gravity in the measurement of cerebral oedema. *Journal of Applied Physiology, 30,* 268–271.

REDPATH, T., 1982. Calibration of the Aberdeen NMR imager for proton spin lattice relaxation time measurements *in vivo. Physics in Medicine and Biology, 27,* 1057–1065.

SMITH, M. A., BEST, J. J. K., DOUGLAS, R. H. B. & KEAN, D. M., 1984. The installation of a commercial resistive NMR imager. *British Journal of Radiology, 57,* 1145–1148.

SMITH, M. A., ELTON, R. A. & TOTHILL, P., 1981. The comparison of neutron activation analysis and photon absorptiometry at the same part-body site. *Clinical Physics and Physiological Measurement, 2,* 1–7.

● *Original Contribution*

A SURFACE COIL DESIGN FOR A VERTICAL FIELD MRI SYSTEM AND ITS APPLICATION IN IMAGING THE BREAST

M. A. Smith*† and D. W. Pye†

*NMR Imaging Unit and †Department of Medical Physics and Medical Engineering,
University of Edinburgh, Edinburgh, United Kingdom

The general design of a flat surface coil for use with a vertical field MRI system is discussed. A development of the design for imaging the breast is used as a specific illustration. The phenomenon of "sympathetic resonance" is described in which transmission and reception is performed on the standard body coil with the surface coil disconnected, its presence amplifying the signal to the body coil from the region of interest. Results show that better quality images can be obtained with the surface coil than with the standard body coil and that the sympathetic resonance mode overcomes to a large extent the limited field of view problem normally associated with a surface coil. A threefold improvement in signal to noise ratio was obtained using the surface coil.

Keywords: Magnetic resonance imaging; Surface coils; Vertical main field; Sympathetic resonance; Breast T_1 imaging.

INTRODUCTION

Tomographic images through human subjects are obtained by magnetic resonance imaging (MRI) using a combination of magnetism and radio-frequency (RF) radiation. The RF coil or coils are either in the form of a combined transmitter and receiver coil, sometimes known as a transceiver, or separate transmitter and receiver coils. It is possible to obtain a significant improvement in the signal to noise ratio (S/N) of the NMR signal by placing a smaller RF coil, generally referred to as a surface coil, close to the patient at the region of interest. Such a coil is generally only a receiver coil, a much larger coil being used as a transmitter. The improvement in S/N produces images of a higher quality but over a restricted region of the patient.

The simplest type of surface coil is a circular loop of conducting material. As the RF field (B_1) must be perpendicular to the main magnetic field (B_0), there is a restriction in the orientation of these surface coils. Most MRI systems have a horizontal magnetic field B_0, which means that a circular surface coil can be used in planes parallel to the patient couch. This is very convenient for imaging regions such as the orbit or breast.[1]

When the main magnetic field B_0 is in the vertical direction, circular surface coils cannot be used in the plane parallel to the patient couch. To image a specific region of the body, different coil configurations must be developed which produce the RF field B_1 in a horizontal plane.

An additional criterion to be considered in the design of a surface coil when a vertical field MRI system is used is that the access for the patient in the vertical direction is generally more restricted than in horizontal field systems. The form of coil for imaging the breast or spine, for instance, must take up the minimum amount of space in the vertical direction. In particular, a flat spine coil would allow imaging with the patient lying supine over it. A further criterion which applies to all breast coils, irrespective of the main field orientation, is that the axillary tail must be imaged as well as the breast.

Although the general design discussed here is applicable to imaging various parts of the body using a vertical field system, and has been tested by us for

imaging both breast and spine, there is particular clinical interest in Edinburgh in the former, and so the technique is specifically illustrated here with the design of a breast coil.

METHODS

A breast coil was developed for the M&D 0.08-T vertical field resistive MRI system sited in the Royal Infirmary, Edinburgh. The patient enters between the faces of the two larger horizontal ring magnets; the distance between the patient couch and the lower face of the upper magnet is 33 cm. One advantage of the vertical field orientation for the main magnetic field is that solenoidal RF coils can be used, resulting in a higher S/N than would be obtained from a similar size saddle coil.[2] The RF coil used for conventional body imaging is a split solenoid, which is situated on the outside of the patient tube containing the gradient windings. The coil is electronically switched between transmit and receive mode. Prior to the development of surface coils, body images were obtained using a 16-mm section width. Calculated T_1 maps were obtained using an interleaved saturation recovery and inversion recovery pulse sequenced with TR = 1000 ms for both and TI = 200 ms for the latter.

Coil design

At the operating frequency of 3.4 MHz the skin depth in copper is less than 0.1 mm. As a consequence it is possible to construct RF coils using copper tube or ribbon. To reduce the resistance of the coil as much as possible, surface coils were constructed using copper pipe with an outside diameter of 8 mm and a wall thickness of 0.6 mm. To construct a surface coil, the appropriate length of copper pipe was straightened and then filled with fine dry sand. The pipe could then be shaped by hand, the sand enabling fairly sharp bends to be obtained without distorting the pipe. Having shaped the coil, the sand was removed. To tune the coil, fixed polystyrene capacitors and nonmagnetic variable capacitors were used. Polystyrene or polyethylene capacitors suffer less RF loss than other types of capacitors. 300-Ω twin feed cable connected the breast coil to the standard M&D preamplifier. When rigid support was required, polycarbonate was used rather than perspex because there is less RF loss with the former.

The surface coils developed for our MRI system used the principle illustrated in Fig. 1. The parallel sections of conductor in the central region of the coil carry current in the same direction resulting in a magnetic field with a significant component perpendicular to the parallel conductors. The return paths of the coil are positioned far enough away from the central region so that the RF field from them does not interfere with the central region. This type of coil can be flat, and such surface coils have been constructed for the spine and mediastinum.

The breast coil design was an extension of this principle and is illustrated in Fig. 2. The breast coil was connected as two loops in parallel and mounted on an expanded polystyrene block in which a trough
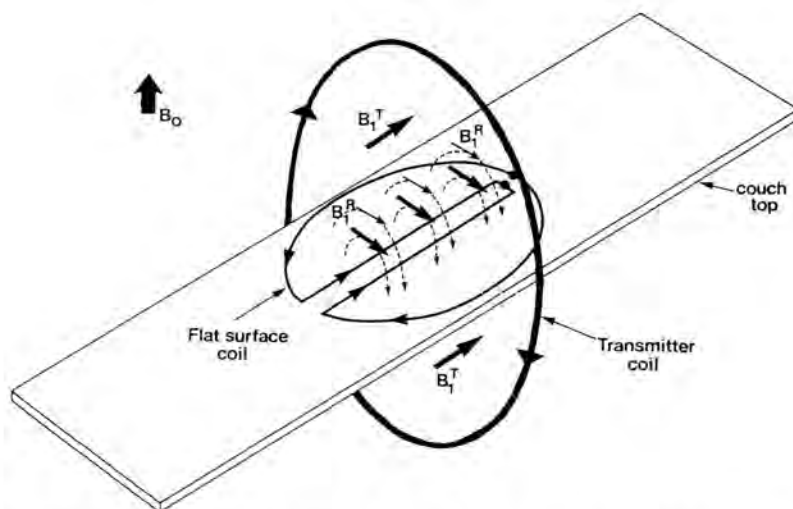

Fig. 1. The transmitter coil produces an RF field B_1^T parallel to and along the long axis of the patient couch. The central conductors of the flat surface coil produce an RF field B_1^R which is perpendicular to both B_0 and B_1^T. The field B_1^R is produced in the region of the central conductors of the flat surface coil; the rest of the flat surface coil is oval in shape, the conductor being sufficiently far from the central region not to interfere with the RF field.

Fig. 2. Prototype breast coil showing the surface coil shaped to fit round the breast when the patient lies prone on the coil support. The curvature of the coil is sufficient for a wide range of breast sizes to be imaged.

was cut. A piece of high-density foam, 1 cm thick, was then placed on top of the coil and the polystyrene block to reduce capacitive coupling between the breast coil and the patient. The subject lies prone with the centre of the breast of interest positioned in the middle of the parallel conductors.

The surface coil was not used to transmit RF radiation; the conventional solenoidal body RF coil was used as a transmitter resulting in uniform spin excitation throughout the tomographic section. The orthogonal orientation of the RF fields associated with the transmitter coil and breast coil, which acted as the receiver, reduced the degree of cross-coupling. The presence of the breast coil did not significantly change the resonant frequency of the body coil, nor was there any interference on the breast coil from transmitted RF radiation. The breast coil was tuned inside the imager at the central position and connected to the preamplifier which had a capacitive loading effect of 60 pF. The pixel size was reduced from 3.5 mm square used for body imaging to 2 mm square and slice thicknesses of 8–12 mm were used.

Coil performance assessment

To assess the performance of the breast coil, the Q factor and the S/N were measured. Two methods were used to determine the Q of the breast coil. The first method to measure Q was performed during the tuning of the breast coil. Two 15-cm-diameter circular copper search coils were placed 20 cm apart, one

either side of the breast coil. One coil was connected to a signal generator and frequency counter, the former being set to the exact reference frequency of the MRI system. The second coil was connected to an oscilloscope and the capacitors of the surface coil adjusted until maximum signal was obtained from the oscilloscope. The Q of the coil was obtained from the equation

$$Q = \sqrt{3} f_{max}/(f_1 - f_2) \ ,$$

where f_{max} equals frequency of maximum signal, f_1 equals frequency above f_{max} at which the signal amplitude is reduced by a half and f_2 equals frequency below f_{max} at which signal is reduced by half. The second method of measuring Q employed a vector impedance meter connected across the surface coil terminals to trace its impedance variation with frequency about 3.4 MHz. This technique was useful for making measurements of Q for both unloaded and patient loaded conditions, search coils being difficult to apply in the latter. All Q values were measured with the breast coil in the imaging position inside the magnet.

A major aspect of our research in Edinburgh into the use of MRI in the breast is the use of T_1 in the investigation of breast disease. As a consequence the image S/N was obtained from the calculated T_1 map for specific section widths and at various distances from the breast coil. The definition of S/N used for evaluation and comparison of surface coils was

$$S/N = \text{mean } T_1/\text{SD} ,$$

where the mean T_1 was obtained from a region of interest containing at least 80 pixels, and SD equals the standard deviation of individual pixel T_1 values within that region.

Coil performance was assessed from images on normal volunteers and also from images of a 7.5-cm-diameter bottle containing $CuSO_4$ with a T_1 of about 200 ms. The bottle was placed in the trough of the breast coil and imaged in the same way as a human subject.

Sympathetic resonance

The phenomenon which we have called "sympathetic resonance" was identified while testing the breast coil. In the conventional surface coil mode the breast coil was tuned to the imager resonant frequency (3.4 MHz) and acted as the RF receiver. However, similar improvements to those obtained using the conventional surface coil mode could be obtained if the large body coil used for transmission was also used for RF detection, with the breast coil still tuned to the resonant frequency but not connected to the preamplifier nor directly coupled to the imager electronics in any way. Images were obtained using the breast coil in this sympathetic resonance mode and also, for comparison, with its connectors shorted so that the coil did not resonate near 3.4 MHz. The principle of a sympathetic resonance coil is illustrated in Fig. 3.

RESULTS

The Q of the patient breast coil for different situations is listed in Table 1. As expected, there is a reduction in Q when the coil is inside the imager and a further reduction when the coil is loaded with a human subject. There is an increase in Q when operating in the sympathetic resonance mode, because the coil is no longer damped by connection to the preamplifier input.

As expected, there is a variation in sensitivity with distance from the breast coil; this variation, however, is less in the sympathetic resonance mode. The calculated T_1 map is obtained from a saturation recovery and inversion recovery image in the usual way, both images having the same signal depth variation. As a consequence, when they are combined, the T_1 map is uniform with depth. However, the decreasing signal in the original images results in a gradual decrease in T_1 S/N with distance from the breast coil. The variation in S/N with depth is shown in Fig. 4 with the S/N for the conventional body coil and head coil[3] shown for comparison. The section width used with the breast coil is narrower than the 16 mm used for routine patient body imaging. The S/N values at different

Table 1. Q values of the breast coil and normal body coil unloaded and loaded with a patient in position

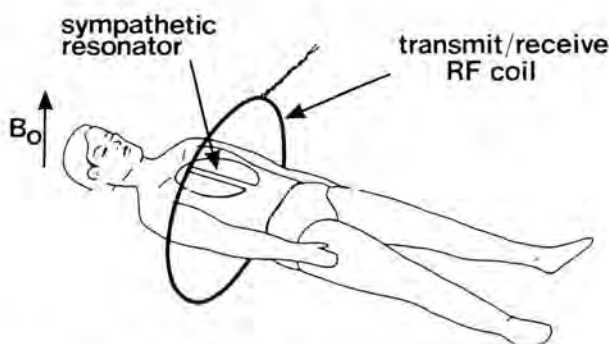|	Q
Breast coil:	
Unloaded	153
With patient	109
Sympathetic resonance:	
With patient	295
Body coil:	
Unloaded	475
With patient	316

Fig. 3. Schematic diagram demonstrating the coil used as a sympathetic resonator. The larger RF coil is used for both transmit and receive. The surface coil is tuned to the resonant frequency but is not directly coupled to the imager electronics in any way.
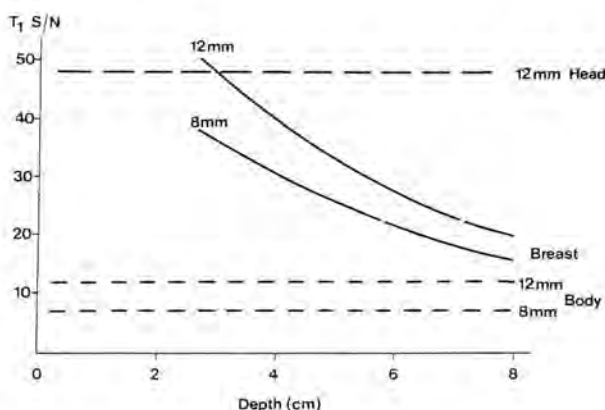

Fig. 4. Variation in S/N in the T_1 image with distance from the surface coil at different section thicknesses. For comparison the signal to noise using the head coil and the large body coil at different section thicknesses is shown.
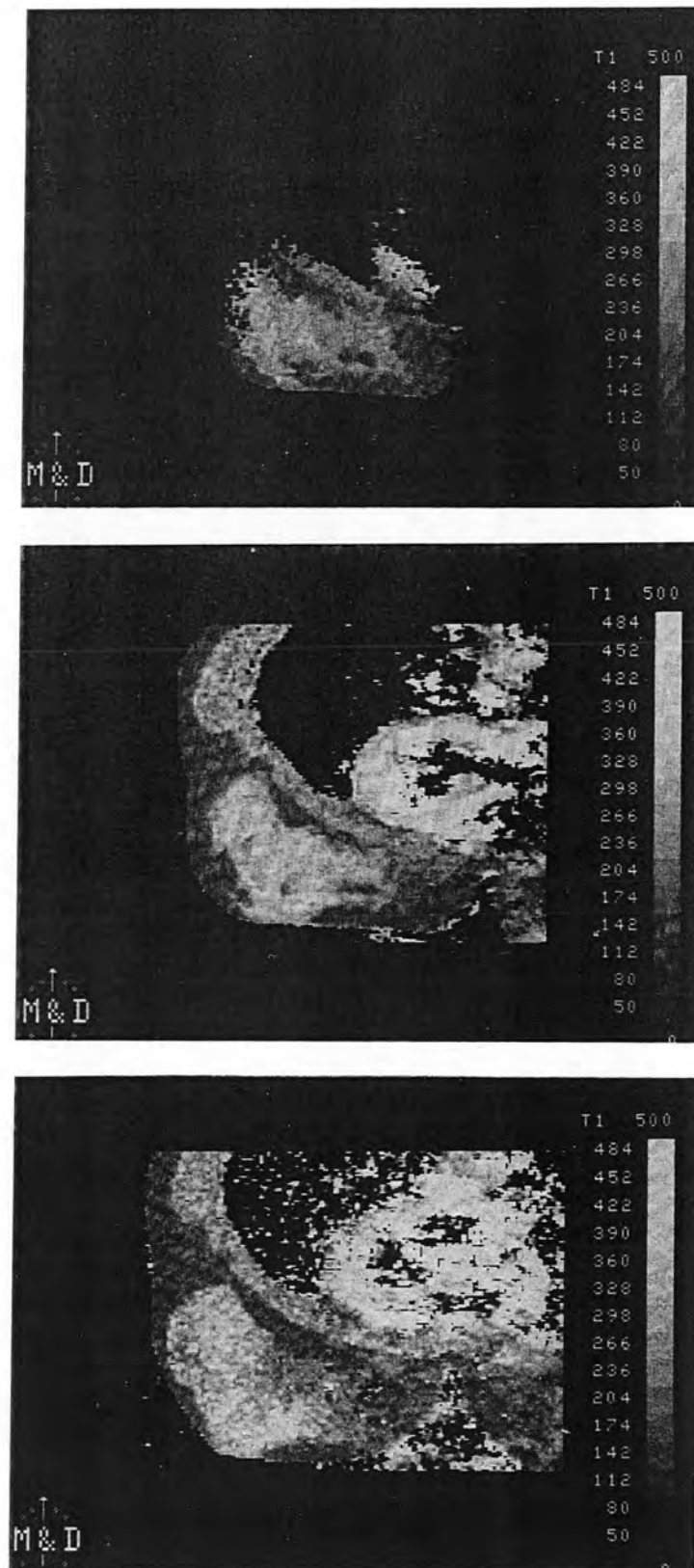
Fig. 5. T_1 images of the same normal breast using a slice thickness of 12 mm with (a) breast coil connected in the conventional manner, (b) breast coil connected in the sympathetic resonance mode and (c) conventional body coil.

Table 2. S/N of a T_1 image with section thickness 10 mm at two different distances from the surface coil. It can be seen that the S/N is better when the breast coil is connected in the conventional manner near the coil but the sympathetic resonance mode is superior at greater distances

	S/N	
	5 cm from coil	9 cm from coil
Receive on breast coil	25.8	14.6
Receive on body coil (sympathetic resonance)	21.9	17.2
Receive on body coil, breast coil shorted (no sympathetic resonance)	9.6	8.6

depths for the breast coil connected in the conventional surface coil mode and also in the sympathetic resonance mode are given in Table 2.

An indication of the improvement obtained using the breast coil on a normal volunteer is illustrated in Fig. 5. For comparison an image is shown using the standard body coil but with the magnet gradients and section width that were used for breast coil imaging. The smaller pixel size and section width used with the conventional body coil produce an apparently noisier image, due to a 75% reduction in signal per pixel, than would be obtained if it were used in its conventional mode. The improvement in image quality compared with the conventional body coil can be seen clearly. This improvement is present when the surface coil is connected in the two different modes though in the sympathetic resonance mode the field of view is larger. This is because the variation in sensitivity with distance from the coil is less in the sympathetic reso-

nance mode and so the image S/N does not deteriorate so quickly.

DISCUSSION

It has been demonstrated that a surface breast coil can be used with a vertical field MRI system to obtain significant improvements in breast image quality. It has also been shown that the depth response of a breast coil can be improved when connected in the sympathetic resonance mode. This is particularly important when investigating regions of abnormal tissue near the chest wall or in the axilla.

It is hoped that the use of this breast coil will enable T_1 maps to be obtained in patients suffering from breast disease with a much thinner section width than could be obtained using the conventional body coil. This will result in a much smaller partial volume error in the T_1 values obtained which may in the past have been partly responsible for the degree of overlap that was found in T_1 values between normal and abnormal tissue.[4]

REFERENCES

1. Stelling, C.B.; Wang, P.C.; Lieber, A.; Mattingly, S.S.; Griffen, W.O.; Powell, D.E. Prototype coil for magnetic resonance imaging of the female breast. *Radiology* 154:457–462; 1985.
2. Hoult, D.I.; Richards, R.E. The signal to noise ratio of the nuclear magnetic resonance experiment. *J. Magn. Reson.* 24:71–85; 1976.
3. Redpath, T.W.; Hutchison, J.M.S. Design of a radiofrequency coil suitable for NMR imaging of heads. *Phys. Med. Biol.* 27:443–447; 1982.
4. Smith, M.A.; Taylor, D.G. The absence of tissue specificity in MRI using in vivo T_1 or T_2 determination: True biological variation or technical artefact? *Br. J. Radiol.* 59: 82–83; 1986.

Cardiac gating in nuclear magnetic resonance imaging

M. A. Smith

NMR Imaging Unit, Royal Infirmary, Edinburgh, UK

In order to obtain NMR images of the heart, and to measure blood flow by NMR, the signal acquisition must be synchronized with the patient's cardiac cycle. Some of the problems of detecting the cardiac cycle within a strong uniform magnetic field without introducing RF interference into the imaging system are discussed. Some general applications of cardiac gated NMR imaging are presented.

KEYWORDS: NUCLEAR MAGNETIC RESONANCE IMAGING, CARDIAC GATING, HEART, FLOW.

Introduction

The basic principles of nuclear magnetic resonance (NMR) have been explained in detail both in this *Journal* [1] and elsewhere [2 and 3]. Essentially the technique involves placing a sample, in our case a human subject, in a strong constant magnetic field. Radiofrequency (RF) radiation is applied at a specific frequency which causes the proton nuclei within the body to resonate; the source of radiofrequency radiation is then switched off and the nuclei continue to resonate emitting RF radiation which can be detected. The size of the NMR signal will be influenced by the amount of protons present, i.e. the proton density. There are two time constants which relate to the exponential decay of two components of the resonance and these are referred to as the relaxation parameters T_1 and T_2. During the transmission and subsequent detection of the RF radiation additional magnetic fields are briefly applied to encode spatial information within the NMR signal. These additional magnetic fields are known as 'magnetic gradients'.

NMR images are produced using a series of RF pulses and the timing and type of pulses used will result in the amplitude of the detection NMR signal containing information not only of the proton density of the sample but also the T_1 and T_2. Thus different pulse sequences can be used in magnetic resonance imaging (MRI) which produce images of the body which contain either mainly proton density information, T_1 information, T_2 information or a combination of two or even three of these parameters. The term 'weighted image' is often used to indicate that the signal intensity of the image is mainly influenced by one particular variable. For example in a T_2 weighted image there will be a lot of information concerning the proton density but the image intensity will also be influenced by the T_2 of the tissue. A T_1 image on the other hand contains purely information related to the T_1 of the tissue. Such an image is sometimes referred to as a 'T_1 map'.

The amount of T_1 or T_2 weighting in an image using a particular pulse sequence will be influenced by the separation between the pulses in the sequence. As the RF pulses in these sequences are often slice selective, difficulties can arise when attempts are made to synchronize the pulses with the cardiac cycle. Not only can the amount of T_1 or T_2 weighting vary during a single scan, thus distorting the final image, but the pulses may not all occur at exactly the same part of the cardiac cycle and so the motion of the heart may not be completely 'frozen'. In addition, the motion of the heart may cause dephasing of the NMR signal resulting in a loss of signal amplitude and low intensity regions in the image.

Cardiac gating is important in MRI, not only to eliminate cardiac motion and phase smearing (figure 1) when imaging the heart, but also to image velocity and flow within the body. It is possible to store velocity information in the phase of the NMR signal [4 and 5] resulting in the production of a phase image the intensity of which is related to velocity. Measurements of pulsatile flow in vessels within the body can only be achieved using cardiac gating.
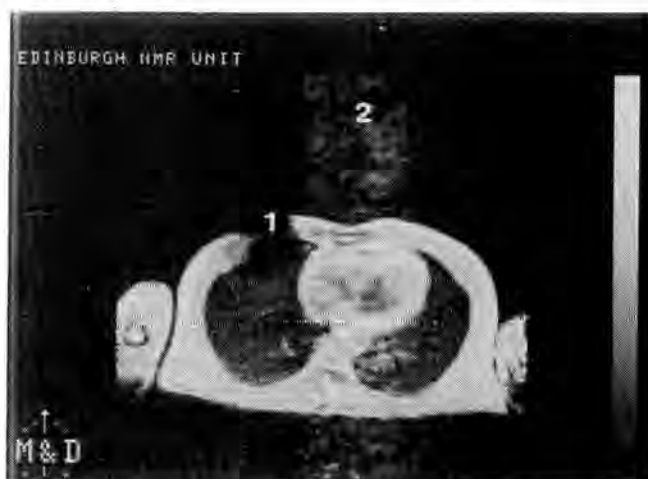

Figure 1. An ungated saturation recovery image, with the ECG leads used for gating connected, showing (1) the loss of signal due to the ECG lead; (2) the 'phase smearing' in the vertical direction caused by the motion of the heart. The absence of signal within the left ventricle is caused by turbulence of the blood and is therefore not a true representation of the ventricular cavity.

The term cardiac 'gating' is something of a misnomer in MRI. In nuclear cardiology signals are emitted from the patient all the time and the patients' ECG is used to define a 'widow' or 'gate' in time during which signals are recorded. Hence the image obtained is cardiac gated. In MRI the image is built up from a number of different NMR signals, usually 128 or 256. These signals are
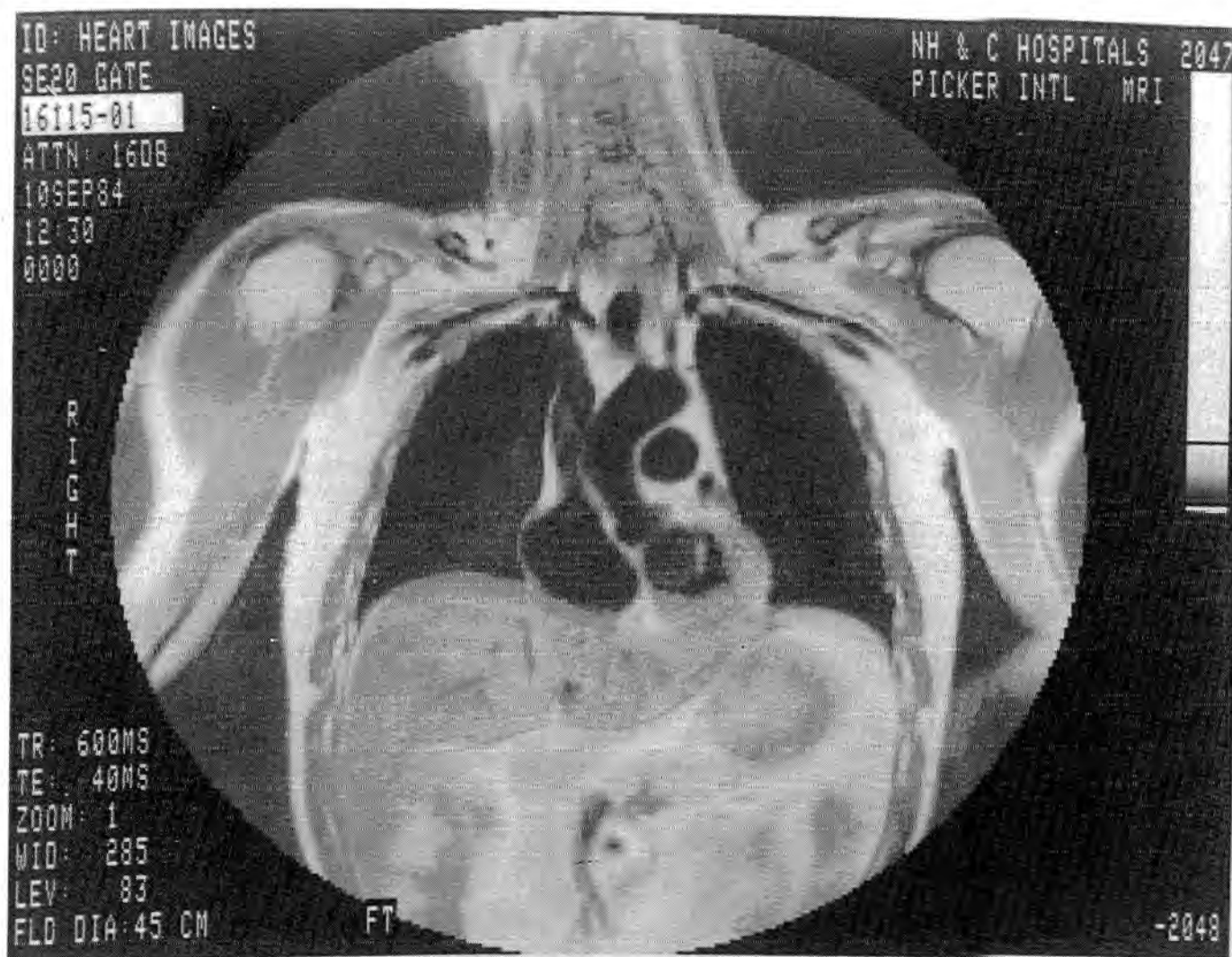
Figure 2. An ECG gated coronal spin echo image at end systole. This sequence produces an image containing mainly proton density information but with high contrast between cardiac tissue and blood. (Courtesy of the National Heart and Chest Hospital.)

produced after a short burst of RF and magnetic gradient pulses which are 'triggered' by the patient's ECG so the NMR signal is obtained in the same part of the cardiac cycle. It is sometimes argued therefore that the term cardiac triggered image is more appropriate.

Detecting the position of the cardiac cycle

There are a number of problems which must be overcome to synchronize the NMR image with the cardiac cycle:

(1) Care must be taken not to introduce an excessive amount of ferromagnetic material into the MRI system. The presence of ferromagnetic material will disturb the magnetic field uniformity and hence can degrade the image.

(2) Both the RF and magnetic gradient pulses can produce interference on any system used to detect the cardiac cycle which is situated inside the MRI system.

(3) The MRI is very sensitive to RF noise and any leads attached to the patient can act as aerials and introduce unwanted noise into the system.

(4) Any system which is developed must not just work for normal volunteers but must be able to tolerate a wide range of abnormal ECGs, compensate for variations in the patient's R-R interval and detect and reject ectopic beats.

A peripheral pulse can be used to identify the cardiac cycle. This has two advantages: the first is that there need be no electrical contact with the patient, and, secondly, any device attached to the patient need be no nearer than 0.5m to the section imaged. The main disadvantage of this technique is that unlike an ECG it does not provide such an accurate determination of the cardiac cycle [6]. Often in cardiac imaging it is required to trigger each signal at end diastole but the delay which exists between end diastole and a peripheral pulse can prevent such images being obtained.

A patient's cardiac cycle is most accurately specified using their ECG. It is possible to detect a patient's ECG using two electrodes, one on either wrist. The advantage of such an arrangement is that the electrodes and cables are away from the region being imaged. The main

disadvantage is that the ECG signal is low but also interference can be detected from RF transmitter and the gradient coils. In our vertical field MRI system it is possible to detect a patient's ECG using two electrodes, one placed on the right shoulder and one placed on the right hip, which produces a larger signal and less interference [7].

It is possible to use some conventional electrodes, which do not contain sufficient ferromagnetic material to distort the image, at low field strengths but in high field systems the amount of ferromagnetic material may produce significant distortion and carbon electrodes may be necessary. Signal loss can occur around the electrode leads (see figure 1) but as the lead is positioned away from the heart, this is quite acceptable. The small local loss of signal is probably due to eddy currents in the screening of the cable; removal of the screening eliminates this signal loss but increases the RF noise introduced into the system.

Transfer of the ECG signal

It is sometimes possible to use a simple filter on the ECG leads to prevent interference being introduced into the MRI system. More common is the use of an optical fibre to transmit the ECG signal. The two ECG leads from the patient are connected to a device which converts the ECG to optical pulses. In Edinburgh a battery-powered module is used with rechargeable nickel-cadmium batteries. This rests at the side of the patient approximately 1.2m from the imaging section and level with the entrance to the imager.

The optical fibre is then connected to a device, this time several meters from the main part of the NMR imaging system, which reconverts the optical pulses to an ECG signal. The signal can then be connected to a modified ECG monitor which produces a trigger pulse at the R wave. A visual display of the ECG has been found to be important to obtain the best position of the electrodes on the patient and also to confirm that the R wave is being detected. In addition the ability to monitor many cardiac patients during the investigation is essential. It must be remembered however that the ECG cannot be considered as diagnostic because of the possible presence of RF and gradient pulses.

Triggering the image acquisition

A NMR image is produced from a number of NMR signals, each obtained with a different phase encoded gradient. In non-gated images the time between each of these signals will be constant for a particular acquisition. However, the time will vary for different types of acquisition typically from about 50ms to 4000ms.

In cardiac gated MRI the trigger pulse initiates a sequence of RF and gradient pulses which produces an NMR signal. The next trigger pulse initiates the production of the next signal and so on until an image is produced. The time from the R wave to the start of each NMR signal production can be altered so that the heart is imaged at any point within the cardiac cycle. RF and gradient interference can produce sharp spikes on the ECG which can be detected as R waves in the ECG monitor producing a trigger pulse. This can be overcome in the software of the MRI system as any such pulses will occur at exact times after the trigger pulse which initiated the signal production. As a consequence pulses detected at such times are ignored.

As in other cardiac gated imaging techniques trigger pulses produced by ectopic beats or from R waves following R-R intervals outwith a predefined range must be ignored. This can be done using a microcomputer or within the main MRI computer itself.

Applications of cardiac gated NMR imaging

In other cardiac imaging techniques there is usually only one parameter which influences the image intensity. In nuclear cardiology it is the isotope concentration, with ultrasound it is tissue reflectivity, and in computerized tomography it is X-ray absorption. In MRI the situation is quite different as we have three separate parameters which can influence the image produced. It is generally true to say that images that are essentially images of proton density can be used to demonstrate anatomy. Pathology, on the other hand, can be imaged using the T_1 or T_2 relaxation parameters.

A cardiac gated image of the heart containing mainly proton density information is shown in figure 2. A spin echo sequence has been used which produces good contrast between blood and cardiac tissue due to the motion of the blood. Such an image would be used to identify abnormal anatomy within the heart or to calculate ventricular volumes and parameters such as ejection fraction and stroke volume [8]. The trigger pulse after the R wave can initiate a number of NMR signals occurring at different parts of the cardiac cycle. The sequence of images so produced, usually 8 or 16, can be displayed in a cine loop mode at the end of acquisition.

Figure 3. A cardiac gated T_1 map showing mainly the left ventricle at end systole. The scale on the right-hand side of the image is calibrated in milliseconds. Generally such images are viewed in colour to highlight increases in the T_1 parameter following myocardial infarction.

327

Figure 4. An ECG gated phase image just above the heart demonstrating flow in the great vessels. Velocity perpendicular to the transverse section is displayed in the image. Sections of the image where there is no motion are displayed as mid grey. Velocity in one direction is displayed lighter, whereas velocity in the opposite direction is displayed darker. The intensity is linearly related to the velocity.

This can be used to demonstrate abnormalities in ventricular wall motion.

Cardiac pathology can be visualised using gated T_1 maps as illustrated in figure 3. Two sequences are used to calculate the T_1 maps, both of which are gated. An important example is the identification of myocardial infarction which results in a local increase in tissue water due to oedema. The anatomy of the heart may appear quite normal even though the pathology is abnormal. The relaxation parameters T_1 and T_2 are both prolonged in regions of oedema and consequently will identify regions of recent infarction that would not be shown on a proton density image [9 and 10]. This time the blood has a high signal corresponding to a high T_1.

The application of cardiac gating in flow measurements is illustrated in figure 4. Moving tissue will influence the phase of the NMR signal; phase maps can therefore be produced in which the image intensity is directly related to velocity and direction. Fairly accurate estimates of flow can be obtained from these velocity measurements and the technique may rival Doppler ultrasound for some applications in the future. To measure pulsatile flow, whether in blood or the CSF, the sequence must be synchronized with the cardiac cycle.

References

1. LERSKI, R. A. (1985) Principles of nuclear magnetic resonance (NMR)—current state of the art. *Journal of Medical Engineering & Technology*, **9,** 112–116.
2. SMITH, M. A. (1985) The technology of magnetic resonance imaging. *Clinical Radiology*, **36,** 553–559.
3. KEAN, D. M. and SMITH, M. A. (1986) *Magnetic Resonance Imaging: Principles and Applications* (William Heinneman Medical Books, London).
4. VAN DIJK, P. (1984) Direct cardiac NMR imaging of heart wall and blood flow velocity. *Journal of Computer Assisted Tomography*, **8,** 429–436.
5. RIDGWAY, J. P. and SMITH, M. A. (1986) A technique for velocity imaging using magnetic resonance imaging. *British Journal of Radiology*, **59,** 603–607.
6. MCNAMARA, M. T. and HIGGINS, C. B. (1984) Cardiovascular applications of MRI. *Magnetic Resonance Imaging*, **2,** 167–184.
7. SMITH, M. A., RIDGWAY, J. P., BRYDON, J. W. E., BEEN, M., DOUGLAS, R. H. B., KEAN, D. M., MUIR, A. L. and BEST, J. J. K. (1986) ECG-gated T_1 images of the heart. *Physics in Medicine and Biology*, **3,** 771–778.
8. LONGMORE, D. B., KLIPSTEIN, R. H., UNDERWOOD, S. R., FIRMIN, D. N. HOUNSFIELD, G. W., WATANALSE, M., BLAND, C., FOX, K., POOLE-WILSON, P. A., REES, R. S. D., DENISON, D., MCNEILLY, A. M. and BURMAN, E. O. (1985) Dimensional accuracy of magnetic resonance in studies of the heart. *Lancet*, **i,** 1360–1362.
9. BEEN, M., SMITH, M. A., RIDGWAY, J. P., BRYDON, J. W. E., DOUGLAS, R. H. B., KEAN, D. M., BEST, J. J. K. and MUIR, A. L. (1985) Characterisation of acute myocardial infarction by gated magnetic resonance imaging. *Lancet*, **ii,** 348–350.
10. MCNAMARA, M. T., HIGGINS, C. B., SCHECHTMAN, N. BOTVINICH, E., LIPTON, M. J., CHATTERJEE, K. and AMPARO, E. G. (1985) Detection and characterisation of acute myocardial infarction in man with the use of gated magnetic resonance. *Circulation*, **71,** 717.

BRAIN WATER MEASURED BY MAGNETIC RESONANCE IMAGING
Correlation with Direct Estimation and Changes After Mannitol and Dexamethasone

B. A. BELL   M. A. SMITH

D. M. KEAN   C. N. J. McGHEE

H. L. MACDONALD   J. D. MILLER

G. H. BARNETT   J. L. TOCHER

R. H. B. DOUGLAS   J. J. K. BEST

Department of Surgical Neurology and NMR Imaging Unit, University of Edinburgh, Royal Infirmary, Edinburgh EH3 9YW

Summary   Brain water content was measured in tissue samples taken at operation from 19 patients with intrinsic cerebral tumours imaged preoperatively by magnetic resonance. A high correlation ($r = 0.94$, $p < 0.0001$) between white matter water content and the longitudinal relaxation time (T_1) enabled water content to be estimated from T_1 to within 4%. 11 patients received dexamethasone and improved clinically but their T_1, and thus brain water content, was unchanged an average of 6 days later. Intravenous infusion of 20% mannitol in 11 patients significantly reduced T_1 in oedematous white matter and tumour within 15 min of administration, and by 30 min the T_1 of oedematous white matter had fallen to a mean of 32.4 (SEM 7.1) ms, corresponding to a reduction in water content of 1.4 (0.3)%.

Introduction

IN 1919 Weed and McKibben[1] showed that the brain bulk of cats could be increased by intravenous infusion of distilled water and decreased by hypertonic (30%) saline or saturated sodium bicarbonate solution. They reported that the cortical capillaries were distended and the intercellular spaces were diminished, but did not examine changes in water content. What are the physical effects of osmotic agents on the brain? Some workers argue that mannitol does not decrease brain water content, but rather changes intracranial vascular calibre[2] and reduces ventricular cerebrospinal fluid (CSF) volume.[3] Others report measurements suggesting that mannitol can reduce brain water content.[4]

In cerebral neoplasms there is relief of symptoms after administration of dexamethasone, and clinical improvement is seen within 24 h. Initially it was thought that steroids produced immediate clinical improvement by reducing the oedema around the tumour, but papilloedema was noted to be slow to resolve.[5] The water content of oedematous brain biopsy samples from untreated tumour patients is higher than in those treated with steroids for 4 days,[6] but a rapid fall in water content in an individual patient coincident with clinical improvement has not been shown. Dexamethasone and other glucocorticoids can reduce high intracranial pressure in tumour patients, but the reduction lags behind steroid administration and clinical improvement by days,[7] although there is evidence that the viscoelastic properties of brain tissue are changed within 24 h of the start of steroid therapy.[8,9] In acute head injury, no such changes are seen.[10]

Computed X-ray transmission tomography (CT) has been used to assess brain water content changes after dexamethasone, and although some investigators have seen changes of about 3 Hounsfield units in oedematous white matter 48 h after starting dexamethasone,[11] changes in density of this order are close to the resolution limits of CT and are influenced by other factors besides water content. Magnetic resonance imaging (MRI) is a better technique than CT for the investigation of brain water. The longitudinal relaxation time (T_1) is mainly determined by the ratio of "free" to "bound" water within tissue.[12] The expected T_1 changes have been shown after alcohol and vasopressin intake,[13] and T_1 correlates with brain water content in vivo.[14]

This study was undertaken to confirm the correlation between T_1 and brain oedema in patients with intrinsic tumours,[14] to investigate water changes in the brain following mannitol administration, and to examine with MRI the effects of dexamethasone.

Patients and Methods

Brain Water Estimations

Brain water was measured in 16 men and 3 women aged 39–73 years (mean 58) having neurosurgery for intrinsic supratentorial tumours of glial (18 patients) or metastatic (1 patient) origin. The site of the tumour allowed a frontal (7 patients), temporal (5 patients), or occipital (6 patients) lobectomy to be done, and biopsies of peritumoural tissue were taken in 1 patient. The lobectomy specimens were sealed immediately in copolymer sheet (Ethicon Ltd, Edinburgh) to prevent evaporative water loss, were taken to a laboratory adjacent to the operating theatre, and were cut transversely as close as possible to the plane of a preoperative MRI of the brain. Peritumoural white matter and, where possible, peritumoural cortex, normal white matter, and normal cortex were sampled from the lobe, and the positions of the samples were marked.

K. J. S. ANAND AND OTHERS: REFERENCES—*continued*

11. Albano JDM, Ekins RP, Maritz G, Turner RC. A sensitive precise radioimmunoassay of serum insulin relying on charcoal separation of bound and free hormone moieties. *Acta Endocr (Kbh)* 1972; **70**: 487–509.

12. Ghatei MA, Uttenthal LO, Bryant MG, Christofides ND, Moody AJ, Bloom SR. Molecular-forms of glucagon-like immunoreactivity in porcine intestine and pancreas. *Endocrinology* 1983; **112**: 917–23.

13. Brown MJ, Jenner DA. Novel double-isotope technique for enzymatic assay of catecholamines, permitting high precision, sensitivity and plasma sample capacity. *Clin Sci* 1981; **61**: 591–98.

14. Sippell WG, Bidlingmaier F, Becker H, et al. Simultaneous radioimmunoassay of aldosterone, corticosterone, 11-deoxycorticosterone, progesterone 17-hydroxyprogesterone, 11-deoxycortisol, cortisol and cortisone. *J Ster Biochem* 1978; **9**: 63–74.

15. Murray AJ, Ballard FJ, Tomas FM. A rapid method for the analysis of N-methylhistidine in human urine. *Analyt Biochem* 1981; **116**: 537–44.

16. Altman DG. How large a sample? In: Gore SM, Altman DG, (eds). *Statistics in practice*. London: British Medical Association, 1982: 6–8.

17. Esler M, Jennings G, Korner P, Blombery P, Sacharias N, Leonard P. Measurement of total and organ-specific norepinephrine kinetics in humans. *Am J Physiol* 1984; **247**: E21–E28.

18. Pathak KS, Anton AH, Sutheimer CA. Effects of low-dose morphine and fentanyl infusions on urinary and plasma catecholamine concentrations during scoliosis surgery. *Anesth Analg* 1985; **64**: 509–14.

19. Solomon S, Bird CE, Ling W, Iwamiya M, Young PCM. Formation and metabolism of steroids in the fetus and placenta. *Recent Progr Horm Res* 1967; **23**: 297–347.

20. Dubois M, Pickar D, Cohen M, Gadde P, MacNamara TE, Bunney WE. Effects of fentanyl on the response of plasma B-endorphin immunoreactivity to surgery. *Anesthesiology* 1982; **57**: 468–72.

21. Stjernstrom H, Jorfeldt L, Wiklund L. The influence of abdominal surgical trauma upon the turnover of some blood borne metabolites in the human leg. *JPEN* 1981; **5**: 207–14.

22. Way WL, Costley EC, Way EL. Respiratory sensitivity of the newborn infant to meperidine and morphine. *Clin Pharmacol Ther* 1965; **6**: 454–61.

23. Panerai AE, Martini A, De Gulio AM, et al. Plasma B-endorphin, B-lipotropin and met-enkephalin concentrations during pregnancy in normal and drug addicted women and their newborn. *J Clin Endocrinol Metab* 1983; **57**: 537–43.

24. Seashore JH, Huszar GB, Davis EM. Urinary 3-methylhistidine excretion and nitrogen balance in healthy and stressed preterm infants. *J Pediatr Surg* 1980; **15**: 400–04.

25. Ballard FJ, Tomas FM, Pope LM, Hendry PG, James BE, MacMohan RA. Muscle protein degradation in premature human infants. *Clin Sci* 1979; **57**: 535–44.

26. Finberg L. Dangers to infants caused by changes in osmolal concentration. *Pediatrics* 1967; **40**: 1031–34.

27. Shaw EA. Neonatal anaesthesia. *Hosp Update* 1982; **8**: 423–34.

28. Lipman N, Nelson RJ, Emmanoulides GC, et al. Ligation of patent ductus arteriosus in premature infants. *Br J Anaesth* 1976; **48**: 365–69.

29. Chugani HT, Phelps ME. Maturational changes in cerebral function in infants determined by 18-FDG positron emission tomography. *Science* 1986; **231**: 840–43.

The samples were then placed in a calibrated layered oil density column for specific gravity measurement and the calculation of water content.[15-17] In 16 patients half of each sample was placed in its fresh state on a small piece of dry aluminium foil that had an accurately predetermined weight. The sample was then dried in an oven at 80°C and reweighed at 24 h intervals until it reached a constant weight, which was then recorded. The wet tissue weight (W) was obtained by subtraction of the foil weight from the fresh weight and the dry tissue weight (D) by subtraction of the foil weight from the dried weight. Wet tissue weight ranged from 8·9 to 484·1 mg, mean 102·8. Water content was expressed as a percentage by weight of the fresh tissue with the formula: % water = (W − D)/ W × 100. Wet and dry weighing of normal samples of brain allowed the derivation of the specific gravity of the solids of human grey and white matter. The specific gravity of the tissue solids is used to calculate water content from the wet tissue specific gravity measurements, and wet and dry weighing also allowed correction of the error introduced by protein in the oedema fluid.[18] The interval between operative lobectomy and completion of the specific gravity measurements was kept to less than 20 min in all cases, so as to limit evaporative water loss from the tissue specimens.

Correlation of T_1 with Brain Water

The patients had MRI the day before surgery by a 0·08 T vertical field resistive MRI system (M & D Technology, Aberdeen). Calculated T_1 maps were obtained by means of an interleaved saturation recovery and inversion recovery pulse sequence with a sequence repetition time of 1000 ms and a time from inversion of 200 ms. Transverse sections through the tumour were obtained, each with a section thickness of 12 mm and an acquisition time of 256 s. Interrogation of the digitally stored T_1 map enabled T_1 values to be measured in any region of a tomographic section. Experiments on normal volunteers showed that the precision of T_1 measurements in the cortex and white matter was 5% and 3%, respectively.[19]

All patients had their operations within 24 h of MRI, and in 6 patients mannitol was given peroperatively to control intracranial pressure. 13 patients did not receive mannitol during surgery. After operation, measurements of T_1 were made from the stored preoperative MRI at sites corresponding as closely as possible to those of brain tissue sampling. The correlation between the measured T_1 and the water content of the samples was assessed by least squares regression analysis, and confidence limits were calculated for the regression line for white matter.

Changes in T_1 with Dexamethasone and Mannitol

11 patients with glial tumours were imaged before steroid administration and were started on dexamethasone 4 mg 6-hourly by mouth immediately after MRI. They had a second MRI 2–11 days later (mean interval 6), and T_1 values for normal cortex, normal white matter, peritumoural white matter, and tumour were measured from the same positions on equivalent sections of the pretreatment and post-treatment scans. All the dexamethasone group had improved clinically by the time the second MRI was done.

17 patients with glial tumours were imaged while having an intravenous infusion of 0·9% saline, after which the infusion fluid was changed to 20% mannitol in 11 patients. Over the next 15 min, 200 ml of infusion fluid was administered to each patient; further MRIs were taken 15 min and 30 min after the control image. On equivalent sections of the control, 15 min, and 30 min images, T_1 values for normal cortex, normal white matter, peritumoural white matter, and tumour were measured at fixed sites by two observers who did not know whether the patient had received 20% mannitol or placebo (0·9% saline), or the timing of the scan.

Changes in T_1 after dexamethasone or mannitol were assessed by non-parametric statistics. Changes from zero were assessed by the Wilcoxon signed rank test and, in the case of mannitol, from patients receiving a placebo infusion by the Mann Whitney test. Results were regarded as significant if p < 0·05.

Results

Comparison of Brain Water Estimations

In the 16 patients for whom there were wet and dry weight brain samples in addition to specific gravity estimations of brain water, gravimetry underestimated tissue water content of oedematous white matter by a mean of 2·4% and of oedematous cortex by a mean of 1·2%.[18]

Correlation of T_1 with Brain Water

In 19 patients there were nine samples of white matter from normal areas of brain and twenty-one from oedematous peritumoural areas. The nine samples of normal white matter had a mean T_1 of 298·0 (SD 15·1) ms and water content of 69·7 (0·7)%, and these are the lowest 9 points on the graph in fig 1A. There was a high correlation (r = 0·94, p < 0·0001) between T_1 and water content with narrow 95% confidence limits. From the image of a single patient the T_1 of white matter allows estimation of water content to within 4%.

In 17 patients there were twelve samples of cortex from normal areas of brain and eight from oedematous peritumoural areas. The twelve samples of normal cortex had a mean T_1 of 464·8 (SD 35·8) ms, and water content of 80·5 (0·8)%, and these are the lowest 12 points on the graph in fig 1B. Oedematous cortex was hard to identify in the lobectomy specimens, since the distribution of peritumoural oedema is largely within white matter, as evident on CT as
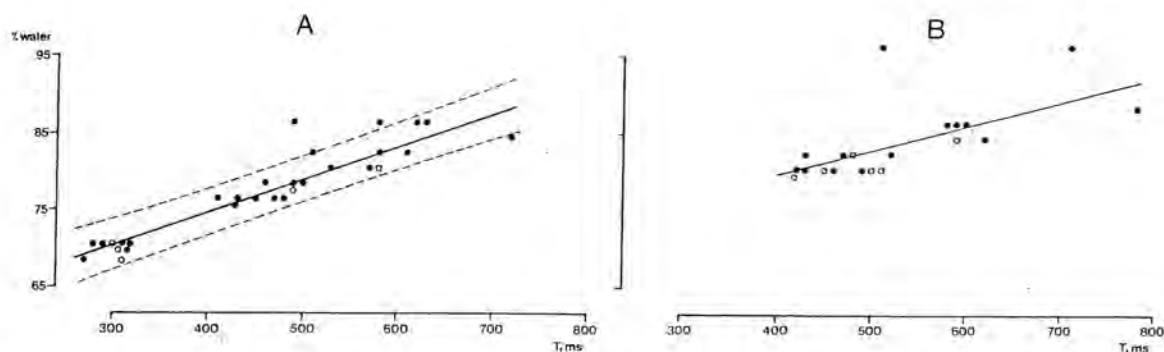

Fig 1—Correlation of white matter (A) and cortex (B) water content with T_1 values.

Open circles, patients who had peroperative mannitol; regression line ——; 95% confidence limits − − −. (A) linear regression line slope = 0·043, constant term = 57·13. (B) linear regression line slope = 0·031, constant term = 66·98.
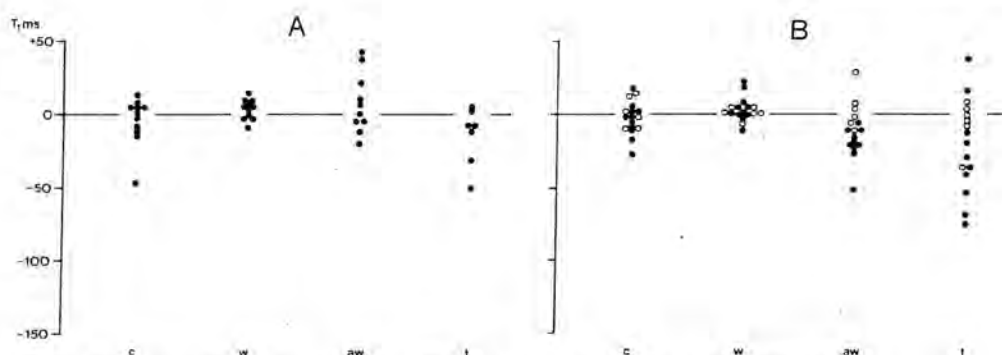
Fig 2—Changes in T_1 measurements after dexamethasone (A) and 15 min after mannitol administration (B).

c, normal cortex; w, normal white matter; aw, abnormal oedematous peritumoural white matter; t, tumour; open circles, patients given placebo.

well as NMR images. In addition the T_1 of cortex was less easy to determine than that of white matter because of the proximity of the CSF in the subarachnoid space, with a consequent partial volume effect, and the smaller area of tissue for measurement on the NMR images. Nonetheless, there was a correlation ($r = 0.65$, $p < 0.002$) between T_1 and water content of cortex; but confidence limits were not calculated because there were insufficient data from abnormal tissue.

Changes in T_1 with Dexamethasone

Dexamethasone had no significant effect on the T_1 of normal cortex and white matter, oedematous peritumoural white matter, or the tumour tissue (fig 2A). We therefore concluded that the water content of these tissues was unchanged by dexamethasone and could not explain the clinical improvement (seen in all patients) by any effect of dexamethasone on the extent of brain oedema.

Changes in T_1 with Mannitol

Mannitol did have an effect in reducing the T_1 of oedematous peritumoural white matter and the T_1 of the tumour tissue, but did not have a significant effect on normal white matter or cortex. After 15 min (fig 2B) the change in the T_1 of the peritumoural white matter and tumour tissue was significantly less than zero (-19.6, SEM 4.0 ms, $p < 0.01$; and -26.9, SEM 11.3 ms, $p < 0.05$, respectively) and for peritumoural white matter it was significantly less than the values obtained during the placebo infusion ($p < 0.01$). 30 min after the intravenous infusion of 20% mannitol was started (fig 3) the mean reduction in T_1 of the peritumoural white matter was 32.4, SEM 7.1 ms ($p < 0.01$) and for tumour was 57.0, SEM 15.6 ms ($p < 0.01$). In both peritumoural white matter and tumour the reduction in T_1
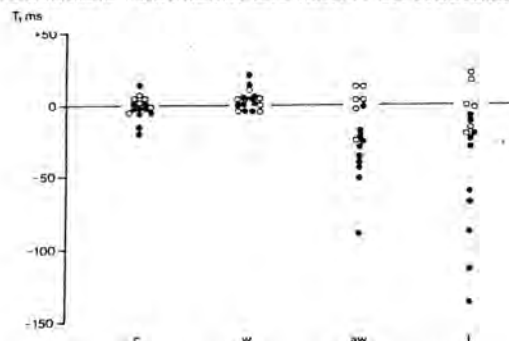
was significantly greater ($p < 0.005$) in patients given mannitol than in those given placebo. The fall of 32.4 ms corresponds to a reduction in water content of 1.4% within the oedematous white matter.

Discussion

This study partly confirms the simple linear correlation between brain water and T_1 reported in animal models of cytotoxic and cryogenic oedema.[20] Within a given tissue (cortex or subcortical white matter) brain water is linearly related to T_1, but the relaxation behaviour of the water molecules in white matter seems to be different from the behaviour of the water in cortex. The water within normal cortical tissue is largely intracellular, the extracellular fluid space being small. When white matter becomes oedematous, water accumulates outside the myelin sheaths, and although it can permeate between the myelin lamellae, it remains largely extracellular.[21] This extracellular oedema fluid in white matter probably has a high free to bound ratio, because of a low concentration of macromolecules in the extracellular space of white matter.

Dexamethasone does not seem to change T_1 in intrinsic tumours and the surrounding oedematous brain, or in the normal brain remote from the tumour, within an average of 6 days of administration. The initial effect of dexamethasone must therefore be mediated by some mechanism other than a change in the water content of the brain. Although resting intracranial pressure is not reduced by steroid therapy for 48 to 72 h, patients are clinically better within 24 h and plateau waves become less frequent. The lumped intracranial elastance, as measured by pressure volume tests, shows a return towards normal over 72 h, but the biggest change is within the first 24 h.[8,9] In patients with posterior fossa tumours, the same clinical response follows steroid therapy over the same time scale, with the disappearance of plateau waves, and yet in these patients the cause of the raised intracranial pressure is predominantly obstructive hydrocephalus rather than brain oedema.[22] This suggests that the first change is an alteration in the viscoelastic properties of brain tissue. The present study shows that brain water is not reduced at this early stage, and to explain the elastance changes some other mechanism, such as a change in cerebral blood volume or alteration in the structural properties of cell membranes, must be invoked.

The intravenous infusion of mannitol reduces T_1, but only in abnormal tissues (tumour and oedematous peritumoural white matter). After rapid intravenous infusion in normal cats, mannitol has been shown to produce considerable pial arteriolar vasoconstriction within 5

Fig 3—Changes in T_1 measurements 30 min after mannitol administration.

minutes of injection, with subsequent vasodilatation at 1 hour.[2] The time course of this vasoconstriction closely matches the reduction in intracranial pressure and blood viscosity that mannitol is known to produce. Some workers argue that the blood viscosity reduction is the primary change and an autoregulatory mechanism is responsible for the vasoconstriction.[2] When autoregulation is impaired, mannitol does not reduce intracranial pressure.[23]

Mannitol lowers haematocrit by drawing water osmotically from tissues other than normal brain, because of the high hydraulic resistance of the normal cerebral capillary wall to water movement (thirty times higher than muscle capillaries and three thousand times higher than mesenteric capillaries).[2,24] This would explain our finding of no change in water content in the normal brain regions of our patients, while in tumour and oedematous peritumoural white matter the water content was reduced. In these abnormal regions, the blood-brain barrier is known to be disrupted from the appearance on contrast enhanced CT and pertechnetate radionuclide scans. The hydraulic resistance of the capillaries in these areas will be low, and mannitol would seem from our findings to withdraw water osmotically from these abnormal tissues.

Our results show that it is possible to estimate tissue water from the T_1 value of white matter with sufficient accuracy to enable small changes in water content to be detected in vivo. They suggest that the early effects of dexamethasone in patients with brain tumours are not mediated by reduction of cerebral oedema, and that mannitol does reduce water content of oedematous brain, but not of normal brain.

REFERENCES

1. Weed LH, McKibben PS. Experimental alteration of brain bulk. *Am J Physiol* 1919; 48: 531–58.
2. Muizelaar JP, Wei EP, Kontos HA, Becker DP. Mannitol causes compensatory cerebral vasoconstriction and vasodilation in response to blood viscosity changes. *J Neurosurg* 1983; 59: 822–28.
3. Takagi H, Saitoh T, Kitahara T, et al. The mechanism of ICP reducing effect of mannitol. In: Ishii S, Nagai H, Brock M, eds. Intracranial pressure V. Berlin: Springer-Verlag, 1983: 729–33.
4. Nath F, Galbraith S. The effect of mannitol on the water content of white matter after head injury in man. *J Neurosurg* 1986; 65: 41–43.
5. Maxwell RE, Long DM, French LA. The clinical effects of a synthetic gluco-corticoid used for brain edema in the practice of neurosurgery. In: Reulen HJ, Schurmann K, eds. Steroids and brain edema. Berlin, Heidelberg: Springer-Verlag, 1972: 219–32.
6. Reulen HJ, Hadjidimos A, Schurmann K. The effect of dexamethasone on water and electrolyte content and on rCBF in perifocal brain edema in man. In: Reulen HJ, Schurmann K, eds. Steroids and brain edema. Berlin, Heidelberg: Springer-Verlag, 1972: 239–52.
7. Kulberg G. Clinical studies on the effect of corticosteroids on the ventricular fluid pressure. In: Reulen HJ, Schurmann K, eds. Steroids and brain edema. Berlin, Heidelberg: Springer-Verlag, 1972: 253–58.
8. Miller JD, Leech PJ. Effects of mannitol and steroid therapy on intracranial volume-pressure relationships in patients. *J Neurosurg* 1975; 42: 274–81.
9. Miller JD, Sakalas R, Ward JD, Adams WE, Vries JK, Becker DP. Methylprednisolone treatment in patients with brain tumours. *Neurosurgery* 1977; 1: 114–17.
10. Gudeman SK, Miller JD, Becker DP. Failure of high dose steroid therapy to influence intracranial pressure in patients with severe closed head injuries. *J Neurosurg* 1979; 51: 301–06.
11. Penn RD. Cerebral edema and neurological function: CT, evoked responses, and clinical examination. *Adv Neurol* 1980; 28: 383–94.
12. Mathur-de Vre R. Biomedical implications of the relaxation behaviour of water related to NMR imaging. *Br J Radiol* 1984; 57: 955–76.
13. Mander AJ, Smith MA, Kean DM, et al. Brain water measured in volunteers after alcohol and vasopressin. *Lancet* 1985; ii: 1075.
14. MacDonald HL, Bell BA, Smith MA, et al. Correlation of human NMR T_1 values measured in vivo and brain water content. *Br J Radiol* 1986; 59: 355–57.
15. Nelson SR, Mantz M-L, Maxwell JA. Use of specific gravity in the measurement of cerebral edema. *J Appl Physiol* 1971; 30: 268–71.
16. Marmarou A, Poll W, Shulman K, Bhagavan H. A simple gravimetric technique for measurement of cerebral edema. *J Neurosurg* 1978; 49: 530–37.

MECHANISM OF EXACERBATION OF RHEUMATOID SYNOVITIS BY TOTAL-DOSE IRON-DEXTRAN INFUSION: IN-VIVO DEMONSTRATION OF IRON-PROMOTED OXIDANT STRESS

P. G. WINYARD   D. R. BLAKE
S. CHIRICO   J. M. C. GUTTERIDGE
J. LUNEC

Department of Rheumatology, Selly Oak Hospital and The Medical School, University of Birmingham; and National Institute for Biological Standards and Control, Hampstead, London NW3

Summary   The mechanism by which a synovial flare occurred in a patient with rheumatoid arthritis after intravenous infusion of iron-dextran was investigated. After the infusion, serum and synovial-fluid iron-binding capacity became saturated, giving rise to low-molecular-mass iron chelates with the capacity to cause oxidative damage ("bleomycin-iron"). At the same time lipid peroxidation and the concentration of oxidised ascorbic acid (dehydroascorbate) increased in both serum and synovial fluid, and red-cell glutathione fell. These changes corresponded closely to an exacerbation of rheumatoid synovitis. Hepatic function was transiently disturbed 7 days after the infusion, reflecting hepatic oxidant stress within the iron-loaded liver. Such changes provide clear evidence that iron-catalysed oxidative reactions influence the inflammatory process in human beings.

Introduction

THE observation that the rheumatoid synovial membrane contains greater than normal deposits of iron[1] led to speculation[2,3] that iron-catalysed generation of toxic free radicals may promote rheumatoid synovitis. The superoxide anion radical and hydrogen peroxide, derived from polymorphonuclear leucocytes (PMN) within the synovial cavity or activated macrophages within the synovial membrane, react together in the presence of transition-metal catalysts (eg, iron) to form the highly reactive hydroxyl radical.[4] This radical is thought to oxidise lipids,[5] proteins,[6-8] ascorbic acid,[9] and other biomolecules within the joint and thus perpetuate inflammation. The oxidation reaction depends on the presence of iron in a suitable form, such as a low-molecular-mass complex (eg, ADP-Fe).[4] As long as iron in synovial fluid or serum is bound to transferrin (serum transferrin is normally about 30% saturated) catalysis of hydroxyl radical formation will not take place.[4] Iron with the capacity to cause oxidative damage can be detected by the bleomycin assay.[10]

B. A. BELL AND OTHERS: REFERENCES—*continued*

17. Marmarou A, Tanaka K, Shulman K. An improved gravimetric measure of cerebral edema. *J Neurosurg* 1982; 56: 246–53.
18. Bell BA, Tocher JL, Smith MA, Miller JD. The accuracy of gravimetric measurement of cerebral oedema in man. *J Neurol Neurosurg Psychiat* (in press).
19. Smith MA, Chick J, Kean DM, et al. Brain water in chronic alcoholic patients measured by magnetic resonance imaging. *Lancet* 1985; i: 1273–74.
20. Naruse S, Horikawa Y, Tanaka C, Hirakawa K, Nishikawa H, Yoshizaki K. Proton nuclear magnetic resonance studies on brain edema. *J Neurosurg* 1982; 56: 747–52.
21. Miller JD. The management of cerebral oedema. *Br J Hosp Med* 1979; 21: 152–65.
22. Brock M, Zillig C, Wiegard H, Zywietz C, Mock P. The influence of dexamethasone therapy on ICP in patients with tumours of the posterior fossa. In: Beks JWF, Bosch DA, Brock M, eds. Intracranial pressure III. Berlin, Heidelberg, New York: Springer-Verlag, 1976: 236–39.
23. Bruce DA, Langfitt TW, Miller JD, et al. Regional cerebral blood flow, intracranial pressure, and brain metabolism in comatose patients. *J Neurosurg* 1973; 38: 131–44.
24. Fenstermacher JD. Volume regulation of the central nervous system. In: Staub ND, Aubrey ET, eds. Edema. New York: Raven Press, 1984.

The British Journal of Radiology

Demonstration of pulsatile cerebrospinal-fluid flow using magnetic resonance phase imaging

By J. P. Ridgway, B.Sc., M.Sc., L. W. Turnbull, B.Sc., M.B.Ch.B., F.R.C.R. and M. A. Smith, B.Sc., M.Sc., Ph.D.

NMR Imaging Unit, Department of Medical Radiology and Department of Medical Physics & Medical Engineering, University of Edinburgh, Royal Infirmary, Edinburgh

ABSTRACT

The study of pulsatile cerebrospinal-fluid (CSF) flow may be useful in diagnosis of certain forms of intracranial disease. Previous techniques used to study CSF flow either are invasive or do not allow accurate measurement. Magnetic resonance imaging (MRI) offers a non-invasive method of studying the CSF pathways. Our technique uses MR phase images and allows quantitative measurement of flow velocities and volume-flow rates. Four volunteers were studied at the level of the second cervical vertebra (C2). The MRI pulse sequence was gated from the R-wave of the subject's electrocardiogram and 12 scans were taken corresponding to different times in the cardiac cycle. The variation in flow velocity throughout the cycle was plotted, and maximum caudad and cephalad flow velocities and flow rates were calculated. Good agreement was found between three of the four volunteers. The mean maximum caudad velocity was 2.91 cm s^{-1} occurring at a mean time of 190 ms after the R-wave. This corresponds to a mean maximum flow rate of 4.13 ml s^{-1}. The total imaging time for each study was about 1 h. Technical developments, allowing simultaneous acquisition of several images throughout the cardiac cycle, will reduce this time significantly.

The cerebrospinal-fluid (CSF) pathways are particularly difficult to study, and to obtain reliable information the haemodynamic conditions must not be altered, for example, by surgical intervention. Radiologists have, for a long time, been aware of the pulsatile nature of CSF flow at fluoroscopy during Pantopaque myelography and in cineradiology of myelography and encephalography (du Boulay, 1966; du Boulay et al, 1972). Estimations of CSF flow using these techniques, which were derived from observation of a television monitor, were inevitably imprecise.

The appearance of flowing fluid using magnetic resonance imaging (MRI) has been the subject of much research, and various techniques have been developed to demonstrate the velocity of blood flow. The effects of blood flow on magnetic resonance (MR) images are dependent on the pulse sequence used, and on the velocity profile of the flow. They can be interpreted as either an increase or decrease in signal compared with stationary material (Axel, 1984; George et al, 1984). The precise variation in signal intensity as a function of velocity is dependent on many factors and is thus difficult to predict.

The nuclear magnetic resonance signal has two components which are referred to as the real and imaginary parts of the signal. These two components can be used to calculate both the modulus and the phase of the signal for each pixel. It is the modulus value that is normally used to obtain the standard clinical MR images. It has been shown, however, that phase images can also be used to quantify flow velocities (Moran et al, 1985). Whereas the modulus MR image contains information on proton density, relaxation time parameters (T_1 or T_2) and flow effects, the phase image contains information on the velocity and direction of flow, as well as phase shifts due to magnetic-field inhomogeneity, chemical shifts, and changes in magnetic susceptibility. The velocity information is usually encoded by adding extra gradient pulses into the pulse sequence (Bryant et al, 1984; Van Dijk, 1984). Alternatively, the bipolar form of gradient pulses which are part of the standard imaging sequence, such as those used for slice selection, can be exploited to provide velocity encoding (Ridgway & Smith, 1986). The range of velocities to be measured can be altered by changing the temporal separation of the two components of the bipolar pulse. Thus, peak velocities in the ascending aorta, and slower venous flow, can both be imaged using the same technique.

Pulsatile CSF flow has been demonstrated in the cerebral aqueduct and pontine cistern using MRI by showing a variation in signal intensity over the cardiac cycle (Bergstrand et al, 1985). An inversion–recovery pulse sequence was used in this study and though a cyclical variation in intensity was shown, no direct quantification of velocity or direction of flow was possible. Phase imaging has not previously been used to image pulsatile CSF flow.

The study describes the extension of a phase imaging technique which was originally developed to measure arterial flow in the body. The technique was modified to measure slow flow in the head and neck.

METHOD

This study was performed using a 0.08 T resistive MRI system manufactured by M&D Technology Ltd.

The imaging technique acquires two phase images, each having different velocity encoding, achieved by varying the temporal separation of the dephase and rephase components of the slice selection gradient (Ridgway & Smith, 1986). The final velocity image is obtained by subtracting these two images, thus eliminating any phase shifts due to field inhomogeneity, chemical shifts or changes in magnetic susceptibility. The technique was modified to image at lower velocity ranges by extending the separation of the bipolar slice selection gradients in one of the velocity-encoding pulse sequences. The difference in separation for the two pulse sequences was thus extended from 2 ms to 12 ms. The maximum measurable velocity, corresponding to a phase shift range of $\pm 180°$, was thus decreased from 120 cm s^{-1} to 20 cm s^{-1} making finer velocity resolution possible. Further modifications involved the inclusion of stronger gradients and the use of a smaller-diameter RF coil, used routinely for head imaging.

The flow measurement was calibrated for mean flow velocities in the range 1–11 cm s^{-1}. A simple continuous-flow phantom was used, incorporating a tube of inside diameter 10 mm, containing copper sulphate solution with $T_1 = 250$ ms. The phantom was fed from a constant head tank and mean flow rates were calculated by finding the time taken for a known volume to pass through the phantom. The MRI pulse sequence was triggered from an external source at a repetition rate corresponding to a heart rate of 75 beats min^{-1}. Each scan was repeated three times and the flow rate recorded before and after each scan.

Four volunteers were imaged, gating the pulse sequence with the subject's electrocardiogram (ECG) (Smith et al, 1986). Heart rates were monitored and images were obtained with delays of 110, 140, 165, 190, 215, 240, 290, 390, 490, 590, 690 and 790 ms after the subject's R-wave. More images were obtained during the systolic period where the velocity variation appeared to be more rapid. The total imaging time for each subject was about one hour.

Prior to this study, one volunteer was imaged at 12 levels in the head and neck at the time during the cardiac cycle when the peak velocity was attained. The resultant images suggested that the peak velocity was higher in the neck than in the head. Imaging too low in the neck resulted in increasing loss of sensitivity with distance from the head coil. As a compromise the level chosen for the four volunteers was at the level of the second cervical vertebra (C2).

The mean phase shift within the ring-shaped subarachnoid space was calculated using two regions of interest; the outer represented the boundaries of the spinal canal and the inner, the spinal cord. From these two regions the mean phase shift within the sub-arachnoid space and its area were determined. The calibration curve was used to determine the velocity from the phase shift, and the area of the subarachnoid space was used to calculate flow.

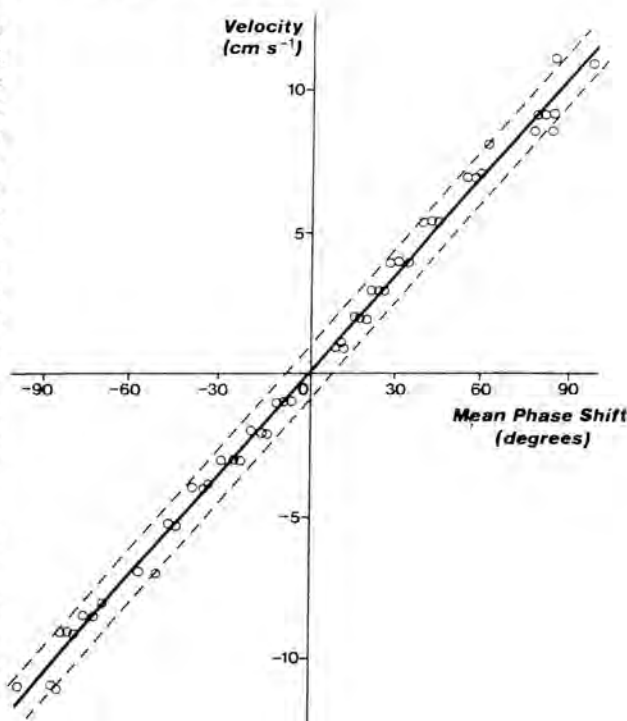In order to assess the reproducibility of the

FIG. 1.

Calibration curve showing calculated mean velocity versus the mean phase shift. The 95% confidence limits with which velocity can be predicted from phase shift are also shown.

technique, expressed as a coefficient of variation, one volunteer was scanned six times at the same level at the time of peak velocity.

RESULTS

The results of the velocity calibration are plotted in Fig. 1, showing 95% confidence limits at ± 0.92 cm s^{-1}. There was a significant correlation ($r = 0.998$, $p < 0.001$) between the phase shift (degrees) and the flow velocity (cm s^{-1}).

A representative transverse section from one of the normal volunteers is illustrated in Fig. 2, showing both the modulus and the phase images. The CSF flow in the subarachnoid space can be seen on the phase image as a ring-shaped area. The displayed intensity of the phase image is related to velocity. Velocity in the caudad direction is represented by lighter shades of grey which correspond to a positive phase shift (Fig. 3A). Similarly, velocity in the cephalad direction is represented by darker shades of grey which correspond to a negative phase shift (Fig. 3B). Mid-grey represents zero velocity, corresponding to zero phase shift.

All volunteers demonstrated pulsatile flow within the subarachnoid space during the cardiac cycle and a representative flow-velocity curve is shown in Fig. 4.
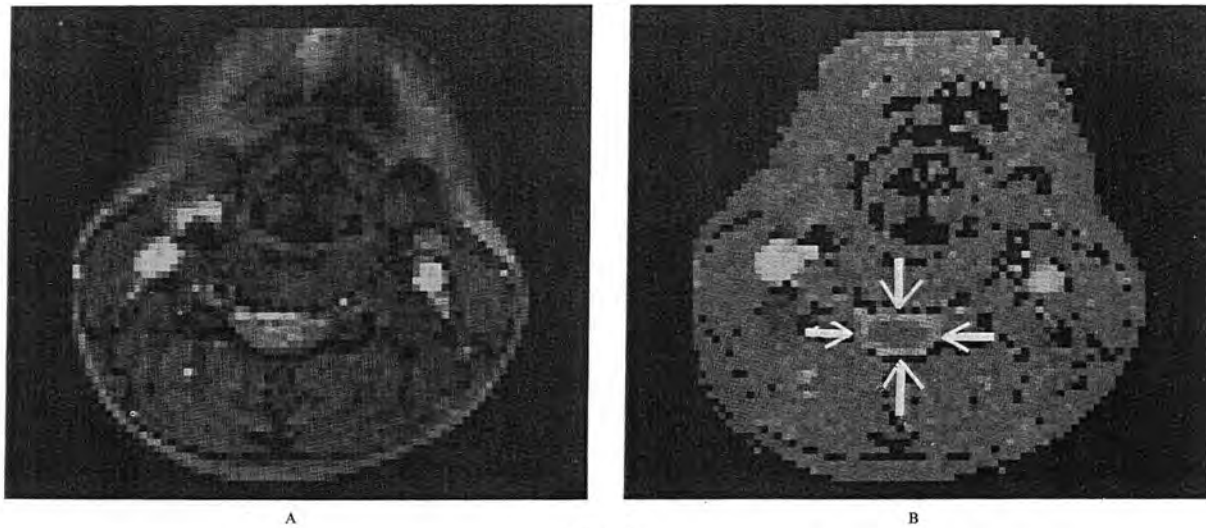
FIG. 2.

Representative section of those used in the volunteer study showing (A) the modulus image and (B) the phase image. The CSF flow is seen on the phase image as a ring of increased intensity (arrows). Also seen are left and right internal jugular veins.

Maximum flow rates, maximum flow velocities and time to peak flow for all subjects are listed in Table I. At intervening times during the cardiac cycle, flow velocities were relatively small and their corresponding phase shifts were not significantly different from phase shifts measured in adjacent soft tissue. The maximum variation in heart rate in any one volunteer was from 65 to 83 beats min^{-1}.

The reproducibility of the repeated scan, analysed once, was 14.4%. However, this figure includes the error associated with the estimation of phase information from a single image which was found to be 8.7%. The reproducibility of the technique itself is therefore 11.5%.

DISCUSSION

This study not only confirms the ability of MRI to demonstrate pulsatile CSF flow, but also demonstrates
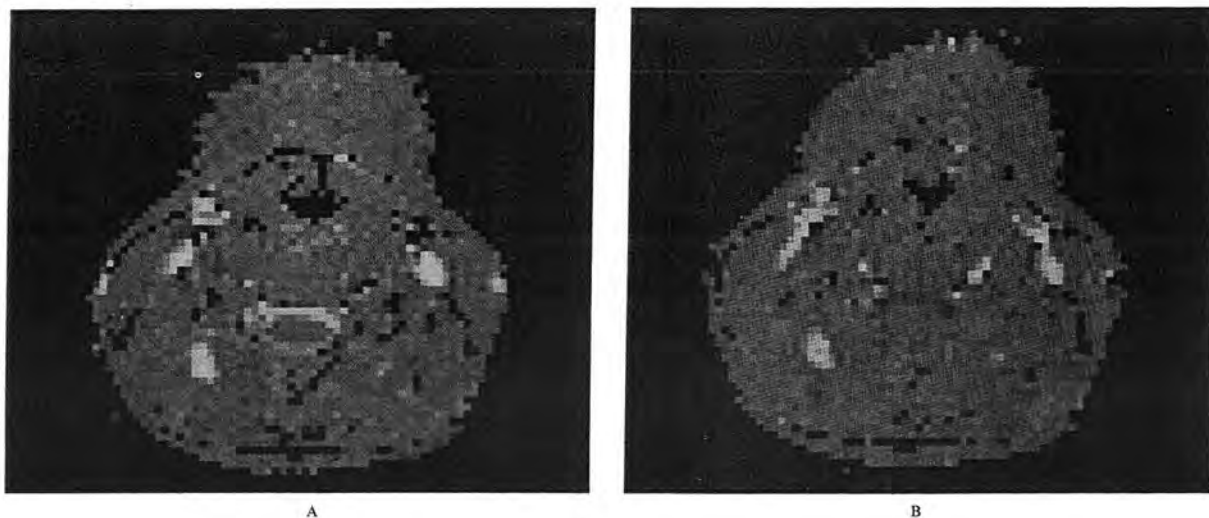

FIG. 3.

Two representative phase images demonstrating the pulsatile nature of the CSF flow: (A) shows caudad flow (positive phase shift); (B) shows cephalad flow (negative phase shift).
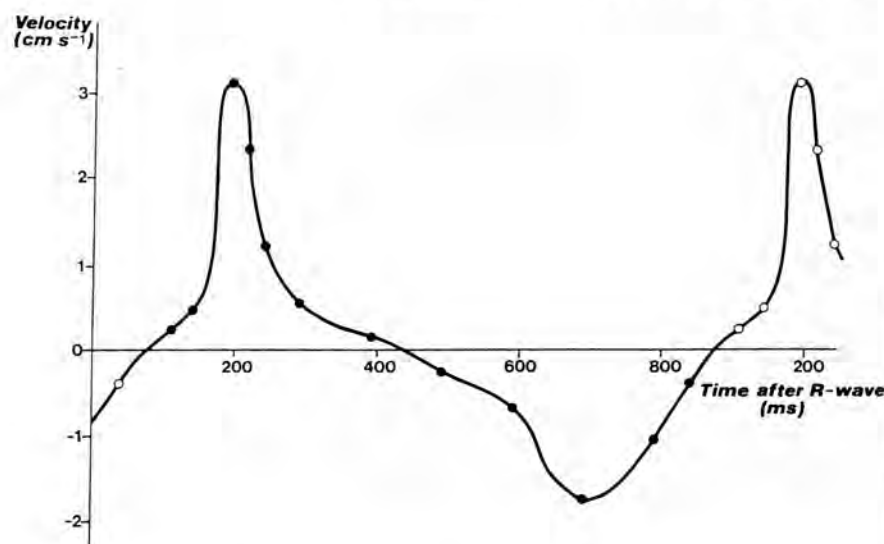
J. P. Ridgway, L. W. Turnbull and M. A. Smith

FIG. 4.

Variation of CSF flow velocity (cm s^{-1}) plotted against time after the R-wave (ms). The set of measured points are shown as filled circles. The same set of points was plotted (open circles) in adjacent ECG cycles to show the continuity of the curve. In this case the average R–R interval was 800 ms (corresponding to a heart rate of 75 beats min^{-1}).

that phase imaging enables quantitative measurement of flow velocity to be obtained with reasonable accuracy. In addition, the direction of flow can be assessed. The technique therefore has advantages over methods which rely on signal intensity (Bergstrand et al, 1985). However, unlike Bergstrand, we have been unable to demonstrate flow within the cerebral aqueduct, though this may be due, in part, to the lower signal-to-noise ratio that is obtained with the lower-field system used in this study.

There is good agreement between the flow rates and velocities obtained in three out of our four normal subjects. Shorter sampling intervals would enable these values to be established more accurately; currently the "peak" caudad and cephalad velocities could be underestimated. The variation in the time to peak CSF flow velocity may be due to many factors including the sampling time, *i.e.* time after R-wave, respiratory rate or variation in heart rate.

At present, the total imaging time for each subject is probably too long for routine clinical use. Simultaneous

multislice acquisition would substantially reduce total imaging time but the spatial location of each section would be different. Alternatively, the acquisition of multiple images of a single section throughout the cardiac cycle, as has been done in cardiac imaging (Waterton et al, 1985) would also reduce imaging time.

This technique offers potential for the investigation of disorders involving the CSF circulation. In the case of complete obstruction, for example, pulsation distal to the obstructing lesion will stop, but it will persist on the cranial side. In addition, du Boulay (1966), using myelographic techniques, observed that when the subarachnoid space was narrowed but not obliterated the amplitude of movement could be considerably exaggerated. Magnetic resonance imaging offers a non-invasive method of studying the direction and velocity of CSF flow in such patients.

TABLE I

MAXIMUM CSF FLOW VELOCITIES AND FLOW RATES

Subject	Max. caudad flow velocity (cm s^{-1})	Max. caudad flow rate (ml s^{-1})	Time of max. caudad flow after R-wave (ms)	Max. cephalad flow velocity (cm s^{-1})	Max. cephalad flow rate (ml s^{-1})	Time of max. cephalad flow after R-wave (ms)	Approximate mean R–R interval (ms)
1	3.17	4.41	190	1.33	1.89	690	750
2	1.78	2.44	215	1.10	1.78	110	750
3	3.57	4.71	165	1.70	2.28	690	800
4	3.12	4.96	190	1.74	2.99	690	800
Mean	2.91	4.13	190	1.47	2.24	—	775
SD	0.78	1.15	20	0.31	0.55	—	29

thank Mrs C. N. Rowan for secretarial services and Mr I. Lennox of the Department of Medical Illustration. We would also like to thank Professor J. J. K. Best and Dr D. M. Kean for their helpful comments and support.

REFERENCES

AXEL, L., 1984. Blood flow effects in magnetic resonance imaging. *American Journal of Roentgenology, 143,* 1157–1166.

BERGSTRAND, G., BERGSTROM, M., NORDELL, B., STAHLBERG, F., ERICSSON, A., HEMMINGSON, A., SPERBER, G., THOMAS, K. & JUNG, B., 1985. Cardiac gated MR imaging of cerebrospinal fluid flow. *Journal of Computer Assisted Tomography, 9,* 1003–1006.

BRYANT, D. J., PAYNE, J. A., FIRMIN, D. N. & LONGMORE, D. B., 1984. Measurement of flow with NMR using a gradient pulse and phase difference technique. *Journal of Computer Assisted Tomography, 8,* 588–593.

DU BOULAY, G. H., 1966. Pulsatile movements in the CSF pathways. *British Journal of Radiology, 39,* 255–262.

DU BOULAY, G., O'CONNELL, J., CURRIE, J., BOSTICK, T. & VERITY, P., 1972. Further investigations on pulsatile movements in the cerebrospinal fluid pathways. *Acta Radiologica Diagnostica, 13,* 496–523.

GEORGE, C. R., JACOBS, G., MACINTYRE, W. J., LORIG, R. J., RAYMUNDO, T. G., YUKIHIKO, N. & MEANEY, T. F., 1984. Magnetic resonance signal intensity patterns obtained from continuous and pulsatile flow models. *Radiology, 151,* 421–428.

MORAN, P. R., MORAN, R. A. & KARSTAEDT, N., 1985. Verification and evaluation of internal flow and motion. *Radiology, 154,* 433–441.

RIDGWAY, J. P. & SMITH, M. A., 1986. A technique for velocity imaging using MRI. *British Journal of Radiology, 59,* 603–607.

SMITH, M. A., RIDGWAY, J. P., BRYDON, J. W. E., BEEN, M., DOUGLAS, R. H. B., KEAN, D. M., MUIR, A. L. & BEST, J. J. K., 1986. ECG-gated T_1 images of the heart. *Physics in Medicine and Biology, 31,* 771–778.

VAN DIJK, P., 1984. Direct cardiac NMR imaging of heart wall and blood flow velocity. *Journal of Computer Assisted Tomography, 8,* 429–436.

WATERTON, J. C., JENKINS, J. P. R., ZHU, X. P., LOVE, H. G., ISHERWOOD, I. & ROWLANDS, D. J., 1985. Magnetic resonance (MR) cine imaging of the human heart. *British Journal of Radiology, 58,* 711–716.

Correspondence

(The Editors do not hold themselves responsible for opinions expressed by correspondents)

Magnetic resonance flow imaging: a possible method for distinguishing communicating syringomyelia from cystic intraspinal lesions

THE EDITOR—SIR,

The important radiological differential diagnosis of syringomyelia is an intramedullary tumour. Magnetic resonance (MR) is now the modality of choice to image the spinal cord and canal (Han et al, 1983; Yeates et al, 1983; Norman et al, 1983). However, differentiation between the cerebrospinal fluid (CSF) contained within a syrinx and a cystic tumour is a potential problem, as there may be little difference in the relaxation parameters (T_1 and T_2) or in the morphology. One possible means of differentiating these conditions is to study CSF flow using a MR phase imaging technique (Ridgway & Smith, 1986; Ridgway et al, 1987), which has recently been developed to allow quantitative measurement of flow velocities, including low values found in CSF flow.

We recently studied a 38-year-old lady who presented with a history of mild spinal-cord disturbance, suggestive of a demyelinating disease. The MR scan showed a probable syrinx extending from the level of the first cervical vertebra to at least the second thoracic vertebra, with some associated tonsillar herniation (Fig. 1). Although in this case the demonstration of a coexisting Chiari malformation established the diagnosis, phase images were obtained in order to detect CSF flow within the syrinx. These were obtained in the transverse plane at the level of the second cervical vertebra; the pulse sequence was gated from the R-wave of the subject's electrocardiogram and images obtained at 50, 225, 300 and 325 ms following the R-wave. Both the time intervals and choice of level corresponded to those used in a previous study carried out on normal volunteers (Ridgway et al, 1987). The cross-sectional area of the syrinx was measured from the images and maximum caudad and cephalad flow rates and velocities were calculated.

Pulsatile CSF flow was demonstrated within the syrinx during the cardiac cycle (Fig. 2). A maximum caudad flow rate of 1.27 ml s^{-1} was achieved at 300 ms following the R-wave. This corresponds to a maximum velocity of 1.63 cm s^{-1}, which was calculated from the area of the syrinx (0.87 cm^2). Cephalad flow was maximum at 50 ms with a flow rate of 0.64 ml s^{-1} and a velocity of 0.86 cm s^{-1}. Due to cord expansion, the subarachnoid space at the level imaged was too small for accurate measurement of CSF flow outside the syrinx to be obtained.

Magnetic resonance phase imaging offers a means of studying the velocity and direction of flow in both normal and pathological CSF circulation. It may prove to be useful non-invasive technique to distinguish communicating and non-communicating forms of syringomyelia, including those associated with spinal-cord tumours, posterior-fossa tumours or cysts, and spinal-cord trauma.

We would like to thank Dr G. Venables for valuable clinical assistance.

Yours, etc.

L. W. TURNBULL
J. P. RIDGWAY
M. A. SMITH
J. J. K. BEST

Department of Medical Radiology,
NMR Imaging Unit,
Department of Medical Physics & Medical Engineering,
University of Edinburgh,
Royal Infirmary of Edinburgh,
Edinburgh EH3 9YW

FIG. 1.

Sagittal proton density image showing fusiform enlargement of the spinal cord. The syrinx cavity is identified as a low-intensity area, vertically orientated, running throughout the length of the cord.
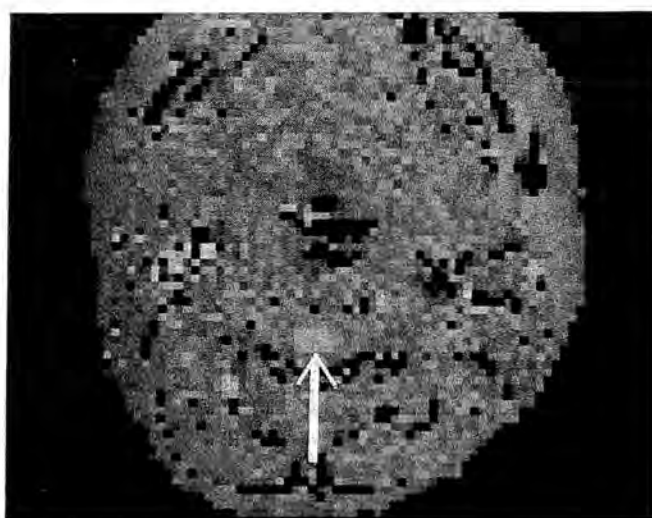

FIG. 2.

Transverse phase image at the level of the second cervical vertebra. The flow within the syrinx is seen as an oval area of increased intensity (arrow). Blood flow within the right deep cervical vein is noted.

Correspondence

REFERENCES

HAN, J. S., KAUFMAN, B., EL YOUSEF, S. J., BENSON, J. E., BONSTELLE, C. T., ALFIDI, R. J., HAAGA, J. R., YEUNG, H. & HUSS, R. G., 1983. NMR imaging of the spine. *American Journal of Roentgenology, 141,* 1137–1145.

NORMAN, D., MILLS, C. M., BRANT-ZAWADZKI, M.; YEATES, A., CROOKS, L. E. & KAUFMAN, L., 1983. Magnetic resonance imaging of the spinal cord and canal: potentials and limitations. *American Journal of Roentgenology, 141,* 1147–1152.

RIDGWAY, J. P. & SMITH, M. A., 1986. A technique for velocity imaging using magnetic resonance imaging. *British Journal of Radiology, 59,* 603–607.

RIDGWAY, J. P., TURNBULL, L. W. & SMITH, M. A., 1987. Demonstration of pulsatile cerebrospinal-fluid flow using magnetic resonance phase imaging. *British Journal of Radiology, 60,* 423–427.

YEATES, A., BRANT-ZAWADZKI, M., NORMAN, D., KAUFMAN, L., CROOKS, L. E. & NEWTON, T. H., 1983. Nuclear magnetic resonance imaging of syringomyelia. *American Journal of Neuroradiology, 4,* 234–237.

Avoidance of ring artefacts in lumbar spine computed tomography in obese patients

THE EDITOR—SIR,

Central ring artefacts (Kowalski & Wagner, 1977) are sometimes unavoidable on computed tomography (CT) in very obese patients, even when meticulous care has been taken with calibration (Seeram, 1982). This is because of low photon transmission and consequent low signal-to-noise ratio (Haaga et al, 1981). The spinal canal is often at the precise centre of the axis of tomographic rotation and, thus, especially liable to be obscured by such artefacts (Fig. 1). This can be avoided by purposely positioning the patient slightly off centre within the gantry aperture so that the spinal canal is removed from the axis of rotation (Fig. 2).

Quantum mottle on the initial lateral scanogram is indicative of low photon transmission and provides a clue that deliberate off-centring may be beneficial.

Yours, etc.,
R. A. R. COULDEN
A. K. DIXON

Departments of Radiology,
Addenbrooke's Hospital, and
University of Cambridge,
Addenbrooke's Hospital,
Cambridge CB2 2QQ
(*Received November 1986*)

REFERENCES

HAAGA, J. R., MIRALDI, F., MACINTYRE, W., LIPUMA, J. P., BRYAN, P. J. & WEISEN, E., 1981. The effect of mAs variation upon CT image quality as evaluated by *in vivo* and *in vitro* studies. *Radiology, 138,* 449–454.

KOWALSKI, G. & WAGNER, W., 1977. Artefacts in CT pictures. *Medicamundi, 22,* 13–17.

SEERAM, E., 1982. Computed tomography technology. *image quality* (W.B. Saunders, Philadelphia), p. 134.
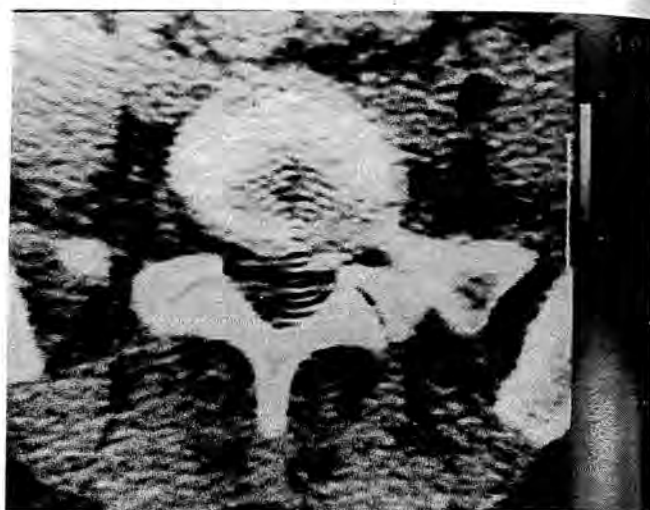
FIG. 1.

Computed tomogram of the L5/S1 disc of an extremely obese patient (W = 1024, L = +45). A central field of reconstruction has been used with a magnification factor of 4.2. The central ring artefacts obscure detail of the disc.
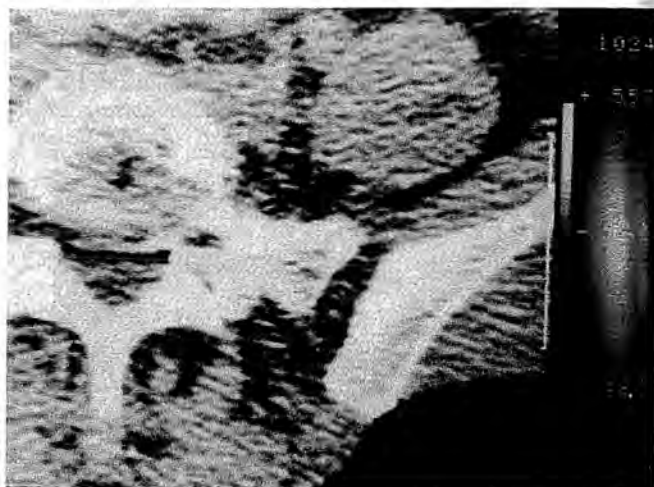

FIG. 2.

The patient has been moved 3.5 cm to the right. The ring artefact is now over the left sacral alum. The degenerate L5/S1 disc is seen more clearly.

Cerebral and Brain Stem Changes After ECT Revealed by Nuclear Magnetic Resonance Imaging

A. J. MANDER, A. WHITFIELD, D. M. KEAN, M. A. SMITH, R. H. B. DOUGLAS and R. E. KENDELL

Nuclear magnetic resonance images of the brain were obtained in fourteen patients with major depression during a course of ECT. The T_1 relaxation time rose immediately after the fit, reaching a maximum 4–6 h later. The T_1 values then returned to their original level; no long-term increase occurred over the course of treatment. These results are consistent with an extensive but temporary breakdown of the blood-brain barrier during ECT.

Nuclear magnetic resonance (NMR) is a long established technique in physics and chemistry, but relatively new in medicine. Nuclei in a constant magnetic field can be made to resonate by the application of an oscillating magnetic field in the radiofrequency range. As the resonance decays to zero the radiofrequency radiation emitted by the nuclei can be detected; this is the basis of the NMR signal. The time taken for the nuclei to return to their original equilibrium position is the spin lattice relaxation time, T_1.

In medical NMR imaging, the signal is usually obtained from hydrogen nuclei (protons) within the body. Since most biological systems consist of 70–90% water, it is these water protons that cause the major component of the NMR signal. Solid tissues have short T_1 values, while relatively fluid tissues have longer ones. The T_1 of grey matter is significantly longer than that of white matter because of their different fat:water ratios. T_1 times can be altered by changes in the ratio of 'free' to 'bound' water in a tissue (Mathur De Vre, 1984) or in its total water content (MacDonald *et al*, 1985). NMR is therefore a useful tool for investigating possible changes in the brain during a course of ECT, particularly as there is no ethical objection to scanning patients repeatedly. Information obtained in this way about changes in the brain induced by ECT may also shed light on the intracerebral changes occurring after spontaneous epileptic fits.

Method

Eleven patients (4 male, 7 female, mean age 49.6 years) had an NMR scan before and after the administration of the first treatment (scans 1 and 2) and again before and after a later treatment (scans 3 and 4) of a course of ECT. A further three patients (all female, mean age 40.3 years) had a scan before and after their last treatment and then six further

scans during the 6 h following the treatment. One of these had a final scan after 25 h. Of the total group of fourteen patients, eleven had bilateral and three had unilateral electrode placings; all of them satisfied Research Diagnostic Criteria for a major depressive episode (Spitzer *et al*, 1978). Patients were excluded if there was a history of serious head injury, brain damage, alcohol abuse or previous radiological abnormality. None had received ECT in the previous 6 months. A standard anaesthetic procedure was used: methohexitone (60–100 mg) and suxamethonium (30–80 mg). Four patients also received diazepam (2.5–10 mg i.v.) before scan 2. The treatment was delivered using an Ectron CC–100 machine, except in one case where a Mecta machine was used. The post-ECT scan was performed as soon as possible after the patient had recovered from the effects of the anaesthetic.

An M&D Technology Ltd 0.08 T resistive magnetic resonance imaging system was used. For each scan, calculated T_1 images were obtained in three planes: a transverse section 10 mm above the maximum diameter of the lateral ventricles, a midline sagittal section of the brain stem, and a coronal section through the parietal and temporal lobes. All sections were 12 mm thick, and the pixel size was 2 mm². Measurement of mean T_1 of the entire area of the transverse section (the grey and white matter together but excluding the cerebrospinal fluid (CSF)) was made. The area of each hemisphere to be sampled was delineated separately using an irregular region of interest; a cursor was used to draw the boundary of the area to be measured directly onto the image of the section as it was displayed on the monitor. The mean T_1 within the region of interest was calculated and displayed. CSF has a high T_1, and is white on the coloured display. It is therefore possible to exclude sulcal CSF by ensuring that it is not included within the boundary of the area to be sampled. In addition, the computer was programmed to present the mean T_1 of the tissues in this area that were within the range 60–600 ms. This range includes grey and white matter, but not CSF, which has a much higher value. This latter method also ensures that in the small regions of interest sulcal CSF is not included in the samples of grey matter that were analysed. Individual small areas of T_1 in the pons, mid-brain (at the level of the

TABLE I
Change in T_1 of the transverse section

| | T_1: ms | | | | | | | |
| | Scan 1 | | Scan 2 | | Scan 3 | | Scan 4 | |
	Mean	s.d.	Mean	s.d.	Mean	s.d.	Mean	s.d.
Unilateral ($n=3$)	350	7	354	7	347	11	348	10
Bilateral ($n=8$)	341	18	348	15	340	10	346	9
Total ($n=11$)	344*	16	350*	13	342**	10	346**	9

*$P<0.01$; **$P<0.05$; all other comparisons NS (Wilcoxon's paired rank test)

optic chiasma) and posterior corpus callosum (sagittal section); frontal and occipital lobes (transverse section) and parietal and temporal lobes (coronal section) were also measured. T_1 was measured at the mid-point of each area. In each case the sample measured had a volume of 1.41 cm³, except the mid-brain and posterior corpus callosum (0.42 cm³).

To control for the effects of the general anaesthetic, five volunteers (three male, two female, mean age 32.6 years) had a transverse section scan before and 30 minutes after an identical anaesthetic procedure.

Results

Patients had a mean of 5.4 treatments given at a mean frequency of 2.4 per week prior to scan 3. As those having unilateral ECT did not show any lateralisation of change in T_1, unilateral and bilateral treatments have been analysed together. There was no significant change in T_1 in any of the areas examined between the beginning and the end of the course of ECT, i.e. when scan 1 was compared with scan 3 and scan 2 with scan 4.

In the transverse section there were significant differences in the mean T_1 of the whole section before and after the individual treatments, i.e. between scans 1 and 2 and between scans 3 and 4 (Table I). The mean change between scans 1 and 2 was 6 ms ($P<0.01$). The rise after bilateral ECT was larger (7.3 ms) than after unilateral ECT (4.0 ms), although this was not significant, probably because of the small numbers in the study. There was a smaller mean increase in T_1 of 4 ms between scans 3 and 4 ($P<0.05$); bilateral ECT produced a larger increase (6.7 ms) than unilateral ECT (1.3 ms), although again this difference was not significant. Patients were scanned sooner after the last ECT (15.8 ± 4 min, range 13–28 mins) than after the first (30.9 ± 16 min, range 15–62 mins), probably because by then they were less depressed and also familiar with the technique ($t=2.69$, d.f.$=19$, $P<0.02$); this suggested that the maximum rise in T_1 may not have occurred within 15 min of treatment. This was shown to be so in the three patients scanned six times during the six hours following ECT (Fig. 1). In the patient scanned after 25 h the T_1 time had returned to below its starting value.

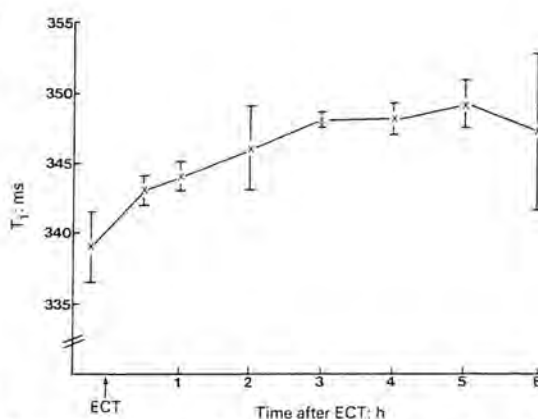The same anaesthetic sequence in the five controls was

FIG. 1 Change in mean T_1 for the three patients scanned over the six hours following ECT.

associated with a non-significant decrease in mean T_1 from 340 ms (s.d. 9 ms) to 336 ms (s.d. 8 ms).

Of the nineteen individual small regions in the grey and white matter, T_1 was found to increase in ten between scans 1 and 2; there was a decrease in seven, and no change in the other two. This increase was statistically significant in the frontal and occipital white matter ($P<0.05$) and in the left temporal grey matter ($P<0.01$). For the 8 patients having bilateral ECT only, there was a significantly decreased T_1 in the right occipital grey matter ($P<0.01$). Between scans 3 and 4 the T_1 in eleven regions increased; there was a decrease in six and no change in the other two.

Discussion

The mean T_1 of the transverse section showed a significant increase after treatment, both at the start and end of a course of ECT, reaching a maximum 4–6 h after the fit. This was shortlived, and no cumulative effects of ECT were noted. The increases reported in this study are likely to be underestimates

of the changes produced by ECT itself, since anaesthesia alone was associated with a fall in T_1.

Measurement of the 19 small regions described above added little further information. Most of the T_1 values in the transverse and coronal sections (20 of 32) increased following treatment. Because there were 64 comparisons involved, it is likely that some of the significant differences arose by chance.

The brain stem showed a non-significant fall in T_1 in five of the six measurements. This may be due to the anaesthetic having a greater effect in this area, and is especially interesting since the brain stem reticular formation is involved in arousal.

Interpretation of changes in T_1 is difficult. There is no good evidence that ECT causes brain damage (Meldrum et al, 1974; Galloway et al, 1981), and recently necroscopy could reveal no pathology attributable to ECT in a patient who had received over 1250 treatments (Lippmann et al, 1985). Similarly, it is unlikely that these T_1 changes represent inflammation or brain damage, since they are reversed so quickly. It is more likely that they are the result of an increase in the total water content of the brain. It is known that ECT produces a temporary breakdown of the blood-brain barrier (BBB) and that this is probably due to the concomitant increase in blood pressure (Bolwig et al, 1977a) and cerebral blood flow (Bolwig et al, 1977b). It is also known that repeated convulsions at short intervals produce cerebral oedema (Laursen et al, 1985). It has been shown that macromolecules leak into cerebral tissue during the temporary breakdown of the BBB induced by ECT (Bolwig et al, 1977a). This would cause an increase in the relative osmotic pressure of the brain. After restoration of the BBB, movement of water from blood vessels into the tissues would therefore occur, and this would provide an explanation for the rise in T_1 over time. It is likely that similar changes occur after spontaneous epileptic fits, although the possibility that the observed changes in T_1 are induced by the electrical stimulus rather then by the subsequent convulsive activity in the brain cannot be excluded.

More work is needed to determine the duration and magnitude of the change in T_1 and to find out if it is related to clinical improvement or the side-effects of treatment.

Acknowledgements

References

BOLWIG, T. G. & WESTERGAARD, E. (1977a) Acute hypertension causing blood-brain barrier breakdown during epileptic seizures. *Acta Neurologica Scandinavica*, **56**, 335–342.

——, HERTZ, M. M., PAULSON, O. B., SPOTOFT, H. & RAFAELSEN, O. J. (1977b) The permeability of the blood-brain barrier during electrically induced seizures in man. *European Journal of Clinical Investigations*, **7**, 87–93.

GALLOWAY, S. P., DOLAN. R. J., JACOBY, R. J. & LEVY, R. (1981) ECT and cerebral atrophy. A computed tomography study. *Acta Psychiatrica Scandinavica*, **64**, 442–445.

LAURSEN, H., GJERRIS, A., BARRY, D. & BOLWIG, T. G. (1985) Cerebral water content and vascular permeability to serum proteins in electrically induced seizures. *Acta Neurologica Scandinavica*, **82**, 123.

LIPPMAN, S., MANSHADI, M. & WEHRY, M. (1985) 1250 electroconvulsive treatments without evidence of brain injury. *British Journal of Psychiatry*, **147**, 203–204.

MACDONALD. H. L., BELL, B. A., SMITH, M. A., TOCHER, J. L., KEAN, D. M., BEST, J. J. K. & MILLER, J. D. (1985) In vivo correlation of NMR T_1 and brain water. *British Journal of Radiology*, **58**, 817.

MATHUR DE VRE, R. (1984) Biomedical implications of the relaxation behaviour of water related to NMR imaging. *British Journal of Radiology*, **57**, 955–976.

MELDRUM. B. S., HORTON, R. W. & BRIERLEY, J. B. (1974) Epileptic brain damage on adolescent baboons following seizures induced by allyglycine. *Brain*, **97**, 407–418.

SPITZER, R. L., ENDICOTT, J. & ROBINS, E. (1978) Research diagnostic criteria: rationale and reliability. *Archives of General Psychiatry*, **35**, 773–782.

*A. J. Mander, MB, BCh, *Registrar, Royal Edinburgh Hospital*, A. Whitfield, MB, BS, FFARCS, *Consultant Anaesthetist, Royal Infirmary, Edinburgh*, D. M. Kean, MB, ChB, DMRD, FRCR, *Senior Research Fellow, NMR Imaging Unit, Royal Infirmary, Edinburgh*, M. A. Smith, BSc, MSc, PhD, *Principal Physicist, NMR Imaging Unit, Royal Infirmary, Edinburgh*, R. H. B. Douglas, DCR, *Senior Radiographer, NMR Imaging Unit, Royal Infirmary, Edinburgh*, and R. E. Kendell, MD. FRCPsych, *Professor of Psychiatry, University of Edinburgh*

*Correspondence: *Professorial Unit, Royal Edinburgh Hospital, Morningside, Edinburgh EH10 5HF*

Serial changes in the T_1 magnetic relaxation parameter after myocardial infarction in man

M BEEN,* M A SMITH,†‡ J P RIDGWAY,‡ R H B DOUGLAS,†
D P DE BONO,* J J K BEST,† A L MUIR*

From the Nuclear Magnetic Resonance Imaging Unit (Departments of *Medicine; †Medical Radiology, and ‡Medical Physics and Medical Engineering, University of Edinburgh), Royal Infirmary, Edinburgh

SUMMARY   A low field resistive nuclear magnetic resonance imaging system (0·08 Tesla) was used to study the in vivo changes in the relaxation parameter T_1 of the left ventricular myocardium from the first day to six months after acute myocardial infarction in 41 consecutive patients admitted to a coronary care unit. T_1 maps were constructed from transverse and coronal images at various times after infarction. Thrombolytic treatment had been successful in 28 patients. Thirty three of the 34 patients studied within two weeks of infarction had a significantly increased T_1 value but this developed only after the third day in four. At day 1–3 the mean (1 SD) maximum T_1 was 413 (29) ms (n = 23) compared with 430 (41) ms (n = 22) at day 4–7, 433 (35) ms (n = 24) at day 8–14, 420 (34) at one month (n = 22), 388 (39) (n = 20) at three months, and 361 (24) (n = 14) at six months. The number of regions of interest with an increased T_1 followed a similar time course. Although the increase in T_1 measured at three months correlated with the initial maximum creatine kinase and with the left ventricular ejection fraction measured at one month, the number of regions with abnormal T_1 from day 4 through to one month correlated best with left ventricular ejection fraction. There was no significant difference in T_1 between patients with or without reperfusion. The rise in T_1 over the first few days together with the prolonged time course of T_1 increase suggests that the increase in T_1 may reflect cellular infiltration as much or more than tissue oedema.

It has been suggested that the magnetic relaxation parameters T_1 and T_2 which are associated with an increase in free water content may be used to demonstrate tissue abnormalities.[1] After experimental canine myocardial infarction in vitro T_1 and T_2 were prolonged, and these changes correlated well with increases in tissue water content.[2 3] In vivo prolongation of both T_1 and T_2 after myocardial infarction has been confirmed in dogs[4 5] and recently in human beings.[6 7] In dogs the changes begin within 30 minutes of coronary occlusion[2] and become more pronounced with occlusions of one, two, and three hours.[2 5] Recently, Pflugfelder et al described the serial changes in the intensity of the in vivo signal in canine myocardial infarction[8] but sim-

ilar studies in human beings have not been reported.

The purpose of the present study was primarily to define the time course of changes in T_1 after acute myocardial infarction in human beings.

Patients and methods

We studied 41 patients with transmural myocardial infarction that was confirmed by both electrocardiographic and creatine kinase changes. Whenever possible, imaging was carried out on day 1–3, day 4–7, day 8–14 and one month, three months, and six months after infarction. Serial imaging was performed on 2–6 occasions (mean 3·4 per patient); however, in two patients adequate images were obtained on one occasion only. Consecutive patients were selected provided that the imager was available, the patient consented, and none of the following exclusion criteria was present: current symptomatic pulmonary oedema, continuing chest pain, major

arrhythmia within 12 hours, previous infarction in the same electrocardiographic territory, or any myocardial infarct in the preceding year.

The study was approved by the local ethics review committee and all patients gave written informed consent.

Ten patients did not have thrombolytic treatment and in a further three thrombolysis was found to be unsuccessful at subsequent coronary angiography (group 1). The remaining 28 patients (group 2) had successful coronary thrombolysis with intravenous anisoylated plasminogen streptokinase complex[9] (n = 23) or recombinant tissue type plasminogen activator (n = 5) (table 1).

The study population was heterogeneous in terms of the site of infarct, rise in creatine kinase, and the use and success of thrombolytic treatment (table 1). Patients on thrombolytic treatment underwent early coronary angiography to determine whether the infarct related vessel was patent, and left ventricular function was assessed by gated blood pool scan.[10] In all patients creatine kinase activity was measured twice a day during their stay in the coronary care unit.

The number of patients in group 1 (n = 13) was smaller than that in group 2 (n = 28) because the use of thrombolytic treatment increased during the study and because non-reperfused patients tended to be less well and were therefore more likely to be excluded from this study.

MAGNETIC RESONANCE IMAGING TECHNIQUE
Patients were imaged with a 0·08 T vertical field resistive magnetic resonance imaging system, manufactured by M & D technology, installed in the Edinburgh Royal Infirmary,[11] and situated between the coronary care unit and the angiography laboratory. Calculated T_1 maps were obtained by an interleaved saturation-recovery and inversion-recovery pulse sequence with a time from inversion (TI) of 200 ms. Inversion was obtained with an

adiabatic fast passage inverting pulse rather than the usual 180° pulse; this is particularly suitable for precise T_1 calculation because it efficiently inverts all the nuclei within the section. In addition, it is not slice selective which means that it inverts all the nuclei within the heart and therefore does not have to be synchronised with the cardiac cycle.

The patient's electrocardiogram was used to trigger the imager such that the 90° pulse in both the saturation-recovery and inversion-recovery sequences occurred in the same part of the cardiac cycle.[12] A field gradient echo of 20 ms was used. The minimum time from the R wave trigger at which imaging can be performed is 230 ms, principally because of the time from inversion (TI) values used. Partly as a consequence of this, but also to obtain tomographic sections of maximum myocardial thickness, images were obtained towards end systole. The pixel size was 3·5 mm × 3·5 mm.

In an attempt to obtain comparable sections on serial studies for individual patients we used the following routine. After attachment of the electrocardiographic leads we used an alignment marker to position the patient on the couch. The lower edge of the xiphisternum was used as the reference level. The distance of subsequent couch movements was recorded from the digital readout provided by the system. Initial images were obtained with a 16 s ungated saturation-recovery sequence as an anatomical guide for the sections to be scanned. Having optimised the image position and recorded its distance from the xiphisternum we performed a gated scan with a slice thickness of 16 mm. To encompass the whole left ventricle, further scans were performed at two or three 15 mm levels cranial or caudal to this or both, and the position was noted to allow equivalent sections to be obtained at subsequent imaging.

A single coronal section through the left ventricle was obtained. The most suitable imaging slice was again selected from rapid ungated images, but in this case the position was adjusted by slightly altering the strength of the magnetic field. Despite the measures described above, it is likely that changing left ventricular geometry over the six month period prevented serial imaging of exactly the same portion of myocardium. For this reason we used the area of highest T_1 found in any region of interest in the infarct territory for analysis.

The imager was triggered by each R wave for heart rates < 75/min and by alternate R waves for faster heart rates. Patients who were scanned during the first 48 hours while in the coronary care unit were moved on a trolley equipped with a defibrillator, and electrocardiographic monitoring was continued throughout.

Table 1 *Data (mean (1 SD)) on the study population*

	Group 1	Group 2
	Coronary occlusion (proven or assumed)	*Coronary reperfusion (proven vessel patency)*
No of patients	13*	28
Anterior infarction	5	19
Inferior infarction	8	9
Age (years)	57 (10)	53 (10)
Peak creatine kinase (U/l)	1889 (800)	1947 (1334)

*Confirmed at angiography[3] or assumed because thrombolysis was not used.

DATA ANALYSIS

For analysis of T_1 values, the myocardium was divided into six sections for each image containing the left ventricular myocardium and cavity. Figure 1 shows the areas into which the myocardium was divided. T_1 values for each of the six sections of every image were obtained by using the computer to draw circular regions of interest within the myocardium. The largest circle that could be placed clearly within the myocardium was used. The area of interest selected was either 0·26 or 0·51 cm², but where wall thinning was considerable the smallest available region of interest (0·08 cm²) was used. This gives a T_1 value of the full thickness of the ventricular wall but with a greater contribution from the central portion of the myocardium. In nine patients there was considerable thinning of the myocardium in the infarct region (eight anterior, one inferior). To avoid the possibility that measurements of myocardial T_1 from this region might be rendered inaccurate by inclusion of intracavitary signal (from blood or thrombus) or extramyocardial signal (from pericardial fat or connective tissue) the region of interest was modified where necessary to encompass the closest lateral position which lay clearly within the myocardium. Attempts at obtaining a T_1 value from the narrowed segment illustrated the necessity for this modification since minor inward or outward adjustment of position resulted in major alterations in T_1.

The maximum T_1 value for each patient investigation was noted as was the number of areas with a T_1 value >390 ms, the value previously identified as the cut off between normal and infarcted tissue.[7] Values for non-affected myocardium were then obtained as follows. On the first image showing an increased T_1 value (>390 ms) we selected the T_1 value from an area anatomically remote from the site of infarction to control for and give information about the variability of T_1 measurements with our system. T_1 values for this selected non-affected region were noted for subsequent examinations.

The data were analysed in both a cross sectional and longitudinal manner. In the cross sectional analysis the maximum T_1 for all patients at each time period after infarction is presented as a mean and 1 SD. The variation in T_1 with time since infarction was studied by fitting a gamma variate curve to the mean maximum T_1 values at each time period and calculating the regression coefficient. The maximum T_1 at day 1–3 was compared with the value obtained from the non-affected region on the same scan by means of a paired Student's t test. Linear regression analysis was used to correlate the maximum T_1 values and the number of areas of increased T_1 with left ventricular ejection fraction and peak creatine kinase
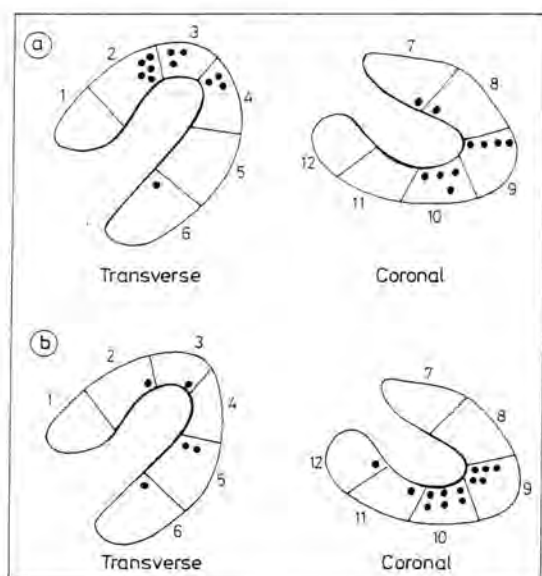

Fig 1 *(a) Regions of myocardium with greatest T_1 value in patients with anterior infarction. Each dot represents the region with the maximum value for a single patient. (b) Regions of myocardium with greatest T_1 value in patients with inferior infarction.*

activity.

Longitudinal analysis of the data was performed by noting the change in T_1 at each study interval.

Results

T_1 VALUES IN THE NON-AFFECTED AREA

For the group as a whole the mean T_1 of the non-affected myocardium at day 1–3 was 320 (19) ms. There was no significant difference in the measured T_1 at any time in the non-affected region, the highest mean value being 326 (18) ms at one month. The range of T_1 values in the 41 patients over all time periods was 274–382 ms, confirming our previous observation that a cut off of 390 ms differentiates between normal and infarcted myocardium.[7]

T_1 VALUES IN THE AFFECTED AREA

Maximum T_1 values

Table 2 shows the results for each patient at the six times after infarction. Maximum T_1 values always occurred in an anatomical position consistent with the electrocardiographic changes (fig 1a and b). But the highest T_1 was not always seen in the same region on serial imaging.

Cross sectional analysis of the data (fig 2) showed that at day 1–3 T_1 was significantly higher in the infarct region than in the non-affected area

Table 2   *Patient details, maximum creatine kinase (CK) and T1 values at intervals shown*

Patient No	Age	Site of infarct	Successful thrombolysis	Max CK	T$_1$ maximum					
					Day 1–3	Day 4–7	Day 8–14	1 mnth	3 mnth	6 mnth
1	39	Lateral	Yes	717	480	—	476	462	397	399
2	45	Inferior	Yes	1261	—	435	443	374	—	—
3	64	Inferior	No	1395	—	—	—	476	427	—
4	58	Inferior	No	1230	415	404	447	454	410	378
5	70	Anterior	Yes	1169	371	—	539	—	—	348
6	55	Anterior	Yes	2624	—	475	—	452	400	389
7	37	Anterior	Yes	3117	366	—	409	399	377	—
8	49	Inferior	No	1529	—	389	468	439	322	356
9	56	Inferior	Yes	2076	—	—	—	—	430	353
10	54	Anterior	Yes	4578	428	507	455	451	408	366
11	60	Anterior	Yes	789	414	472	483	402	—	364
12	46	Inferior	Yes	2361	—	400	379	—	—	344
13	60	Inferior	Yes	1030	435	—	—	—	—	356
14	67	Inferior	Yes	799	378	386	—	—	357	—
15	57	Anterior	Yes	513	—	452	—	—	—	—
16	48	Anterior	Yes	2743	—	—	—	391	—	361
17	53	Anterior	Yes	4565	414	402	420	453	478	372
18	61	Anterior	Yes	3602	—	—	474	—	—	—
19	57	Inferior	No	1301	392	—	397	470	363	344
20	56	Inferior	No	3156	410	—	—	—	—	—
21	73	Anterior	No	699	431	469	468	—	346	385
22	49	Anterior	No	2215	—	—	400	358	358	—
23	42	Lateral	Yes	3719	441	439	438	425	392	—
24	33	Anterior	Yes	1736	442	502	—	405	—	412
25	57	Anterior	Yes	247	429	387	—	—	—	—
26	62	Anterior	Yes	881	—	397	—	—	371	359
27	40	Inferior	No	—	—	460	390	—	360	350
28	42	Anterior	Yes	1652	—	—	396	—	423	338
29	56	Anterior	No	3025	—	—	—	—	—	412
30	63	Inferior	Yes	814	—	—	—	—	364	343
31	52	Inferior	Yes	1286	—	—	—	—	393	347
32	58	Anterior	No	2869	426	—	—	—	—	—
33	61	Anterior	Yes	1701	—	—	408	—	—	—
34	58	Anterior	Yes	4372	435	396	—	424	438	376
35	58	Anterior	Yes	—	—	—	—	—	—	374
36	58	Anterior	Yes	203	402	428	372	429	—	—
37	61	Inferior	Yes	1303	390	365	393	390	346	—
38	44	Anterior	No	2138	404	465	456	427	472	—
39	58	Inferior	No	1216	374	394	469	387	383	—
40	73	Inferior	No	1890	443	—	442	410	355	—
41	62	Anterior	Yes	2723	371	441	443	384	392	—

($p < 0.0001$). T$_1$ continued to rise, reaching a peak at day 8–14 before falling gradually towards normal. Fig 3a–d shows images from one patient at increasing intervals after infarction. The gamma variate curve fitted to the change in peak T$_1$ gave a significant correlation coefficient ($r = 0.95$, $p < 0.001$).

The results of longitudinal analysis, which combined the changes in individual patients, supported the trend shown in fig 2.

Area of raised T$_1$ (fig 4)
In this study 38 of the 41 patients had a maximum T$_1$ of >390 ms. Of the 23 patients who had their first scan between the first and third day after the onset of infarction, five had no regions of interest with a T$_1$ above 389 ms. In four of these, however, the T$_1$ subsequently rose to more than 390 ms by the time of the second scan on day 4–7. Only one patient did not demonstrate a T$_1$ value above 390 ms on at least one scan; the maximum T$_1$ value in this patient was 386 ms.

The number of areas with significantly increased T$_1$ varied greatly both between patients and at different times. The same general pattern to that of the peak T$_1$ values was found. By six months only two patients had any areas of T$_1$ >390 ms.

COMPARISON OF REPERFUSED AND NON-REPERFUSED GROUPS
The maximum T$_1$ and number of areas of increased T$_1$ (above 390 ms) were not significantly different between the two groups at any time period. Neither was there any significant difference in T$_1$ values between those patients in the reperfused group who were treated early (within two hours) and those who were treated later, although there was a trend towards a more rapid fall in the number of areas of raised T$_1$ in the group treated early.

IDENTIFICATION OF INFARCT SITE
For inferior infarcts the maximum T$_1$ was most commonly seen on the coronal image (fig 1a) but
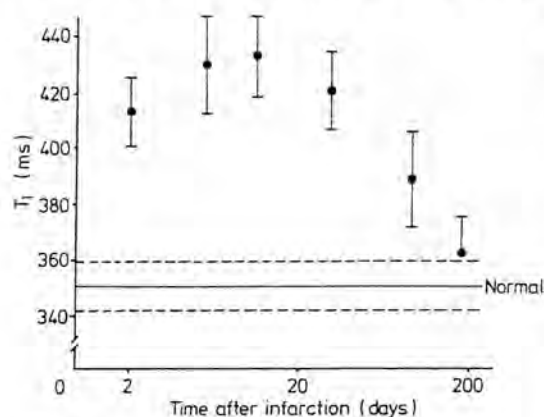
Fig 2 *Mean maximum T_1 values (2 SE) after myocardial infarction. Values were greater than the normal mean maximum T_1 (SE) at first imaging (day 1–3) and tended to increase until the third imaging sequence (day 8–14); values only returned to the mean maximum T_1 values seen in normal subjects six months after infarction.*

maximum T_1 values were more commonly seen on the transverse views when there was an anterior infarct (fig 1b).

CORRELATION OF T_1 WITH OTHER MEASURED VARIABLES

Creatine kinase
Because inferior infarcts tended to have a smaller peak activity of creatine kinase (1471 (581) vs 2162 (428) U/l) and left ventricular function was better preserved (52 (7)% vs 32 (11)%), they were first considered separately from anterior infarcts. There was no significant difference in maximum T_1 values between anterior and inferior infarction, however. There was a correlation (r = 0·59, p < 0·01) between the peak activity of creatine kinase and the maximum T_1 found at three months in the combined groups.

Left ventricular ejection fraction
There was a correlation between ejection fraction and peak T_1 values at one month (r = −0·57, p < 0·05). The number of areas of increased T_1 (> 390 ms) correlated with ejection fraction at 4–7 days (r = −0·63, p < 0·01), 8–14 days (r = −0·53, p < 0·05), and at one month (r = −0·6, p < 0·02).

Discussion

After myocardial infarction T_1 rises in the area of infarction in almost all patients. There is no significant change in T_1 in the unaffected myocardium. This confirms reports of in vitro[2 3] and in

vivo[5 6] experimental studies and those in human infarction.[7 8] The changes may not appear or be appreciable before four days after the onset of infarction, and they reach a peak by the end of the first week. While it is likely that there was some increase in T_1 during the early stages of infarction in all our patients, the magnitude of this increase was not sufficient to permit reliable identification of abnormal myocardium in every case. The values in the five patients who did not have a T_1 > 390 ms on their initial scan ranged from 366 to 378 ms compared with a mean 320 (9) ms in the normal myocardium and they were within our previously reported range for normal myocardium.

Our finding that maximum T_1 values occurred at about two weeks was unexpected. The reported close correlation between T_1 and water content[2] suggests that a more uniform and rapid increase in T_1 would be expected, because myocardial interstitial oedema and mitochondrial swelling occur early after the onset of infarction.[13] The dissociation between the timing of the peak T_1 and the expected peak of myocardial oedema formation may partly be explained by the fact that T_1 depends not simply on the total myocardial water content but also on the binding or interaction of water with biological macromolecules.[1]

The difference between our findings and previous in vitro studies of early changes in T_1 is likely to reflect the major differences between ischaemic human myocardium and excised heart muscle. Not only will the quantity of blood in the intramyocardial vessels differ, as does the coronary anatomy, but in addition there are differences in the state of binding of water within cells. In living systems metabolic processes continuously produce water and its biological state is regulated by cellular processes. That such differences affect T_1 has been demonstrated by comparative in vivo and in vitro T_1 measurements in rabbits.[14]

Our results accord with the in vivo experimental work of Pflugfelder et al who studied the serial changes in relaxation parameters and signal intensity in eight dogs after myocardial infarction.[8] In one animal the increase in signal intensity was only seen 4–6 days after infarction. The timing of peak signal intensity was dependent on the pulse sequence used but occurred between the fourth and thirteenth day. Furthermore, these workers frequently found an area of increased signal intensity on day 20 (the final image) and they commented that the affected area seemed to get smaller. Similarly in our study T_1 values remained raised at one month and even in some patients at three and occasionally six months, but the number of areas of increased T_1 fell more rapidly.
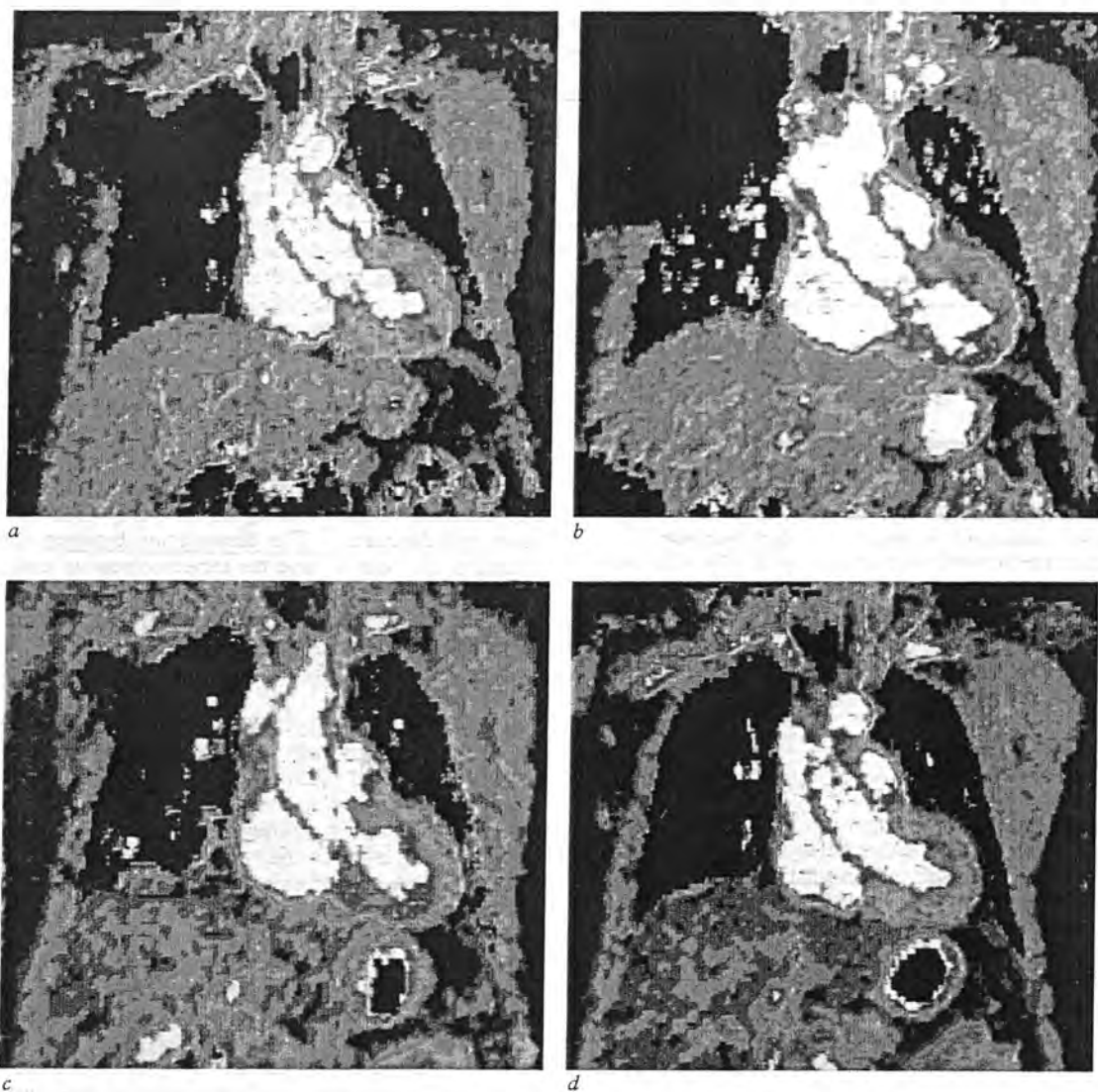
Fig 3 *Sequential coronal images in a patient with inferior infarction: (a) 3 days, (b) 14 days, (c) 1 month, and (d) 3 months after infarction.*

The presence of T_1 prolongation for up to three months confirms that factors other than myocardial oedema are responsible. The classic histological findings[15 16] after myocardial infarction indicate that neutrophils appear after about six hours and increase rapidly after 24 hours, reaching a peak between the third and fifth day.[15 17] Thereafter the number of large mononuclear macrophages increases, reaching a maximum at six weeks and subsequently declining. Other cellular infiltrates also occur, as does prolif-

eration of capillaries which reaches a peak between 3–6 weeks. The histological changes may vary in the same patient at various times.[17] These cellular changes may influence magnetic resonance variables but, as yet, precise histological correlations are not possible. The possibility that T_1 and T_2 changes may provide a method of obtaining in vivo information about pathogenesis is exciting and has received some support from the recent finding that T_2 correlates with the histological severity of rejection in
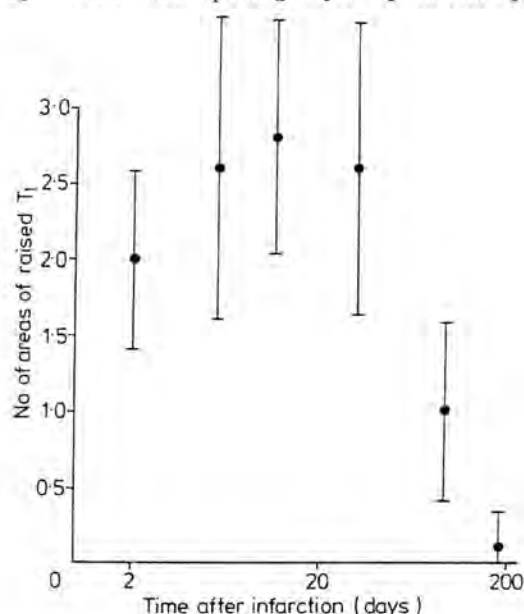
Fig 4 *Number of areas (mean (1 SE)) of myocardium with raised T_1 (> 390 ms) after myocardial infarction. The changes with time follow the same pattern as the changes in maximum T_1.*

heterotopic cardiac transplantation in dogs.[18]

Some studies have suggested that T_2 is better than T_1 for the identification of infarcted tissue, but this may reflect different imaging sequences where the pulse sequence combination used was more appropriate for T_2 measurements than for T_1. Spin echo sequences with a short time to recovery do not contain as much T_1 weighting as an inversion-recovery sequence. In addition, variation in a patient's RR interval can influence time to recovery in the spin echo sequence causing a variable T_1 weighting and, as a consequence, error in the T_1 value. The constant time for inversion used in our technique, coupled with a non-slice selective efficient inverting pulse, minimises the error in T_1 caused by variation in the RR interval.[12]

Ratner *et al* measured endocardial and epicardial T_1 and T_2 and correlates these variables with perfusion measured after 30 and 60 minutes of coronary occlusion.[19] They suggested that the magnitude of change in T_1 and T_2 correlates with the extent of the ischaemic insult. The magnitude of the ischaemic insult is dependent not only on the duration of vessel occlusion but also on vessel size, collateral flow, and the rate of oxygen consumption which all modify the response and determine the infarct size. In this clin-

ical study our means of assessing infarct size were limited. We used the peak creatine kinase activity as a crude assessment of infarct size. There was a correlation with maximum T_1, but only at one month. Thus the maximum level of T_1 seems to correlate poorly with infarct size in clinical practice. Because the kinetics of creatine kinase release are altered by reperfusion we also measured left ventricular ejection fraction at 8–10 days. All patients included in this analysis presented with a first infarct and so the reduction in left ventricular function provides some information about infarct size. The number of areas of increased T_1 did correlate with the ejection fraction at 4–7 days, 8–14 days, and at one month. No correlation was expected at day 1–3 or at three and six months because some patients did not develop changes until after the third day and by three months the area of increased T_1 was considerably reduced. This correlation presumably reflects the amount of myocardium affected by the ischaemic event. Thus the extent of the area with abnormal T_1 values seems a better guide to infarct size than the magnitude of changes in T_1. When this study was undertaken we were unable to perform multiple slice acquisitions but with this capability a precise determination of the volume of infarcted tissue should be possible.

Studies of changes in T_1 in dogs after coronary occlusion and reperfusion have suggested that T_1 is further prolonged by reperfusion,[20] and an increase in cellular swelling after reperfusion has been reported.[13] None the less, we found no significant difference in maximum T_1 between our reperfused and non-reperfused patients. This may reflect a balance between beneficial and harmful[21] effects of reperfusion; however, further analysis of our data in which those given early and late thrombolytic treatment were compared gives no evidence of this. Because time to reperfusion is critically important[22] to the effect of reperfusion, it might be expected that the T_1 values would be different in these groups. There was no significant difference in maximum T_1 or the number of areas showing raised T_1 between those treated within two hours and those treated more than two hours after the onset of symptoms. We noted a trend towards a more rapid fall in the number of areas with a raised T_1 in those treated early. The small numbers in these subgroups and the heterogeneity of the patients (in terms of the vessel affected, the position of the lesion, rate of reperfusion, extent of residual stenosis, collateral flow, disease of other vessels and therefore of infarct size and degree of continuing ischaemia) may be masking real differences.

The factors which produce these alterations in T_1 are complex and as yet we do not know whether changes in T_1 values reflect specific histological

findings. If the demonstrated changes reflect healing then alterations in T_1 may provide an important method for studying a neglected area in our understanding of myocardial infarction.

References

1 Mather-De Vre R. Biomedical implications of the relaxation behaviour of water related to NMR imaging. *Br J Radiol* 1984;57:955–76.

2 Williams ES, Kaplan JL, Thatcher F, Zimmerman G, Knoebel SB. Prolongation of proton spin-lattice relaxation times in regionally ischaemic tissue from dog hearts. *J Nucl Med* 1980;21:449–53.

3 Higgins CB, Herfkens R, Lipton MJ, *et al.* Nuclear magnetic resonance imaging of acute myocardial infarction in dogs: alterations in magnetic relaxation times. *Am J Cardiol* 1983;52:184–8.

4 Wesby G, Higgins CB, Lanzer P, Botvinick E, Lipton MJ. Imaging and characterisation of acute myocardial infarction in vivo by gated magnetic resonance. *Circulation* 1984;69:125–30.

5 Pflugfelder PW, Wisenberg G, Prato FS, Carroll SE, Turner KL. Early detection of canine myocardial infarction by magnetic resonance imaging in vivo. *Circulation* 1985;71:587–94.

6 McNamara MT, Higgins CB, Schechtman N, *et al.* Detection and characterisation of acute myocardial infarction in man with use of gated magnetic resonance. *Circulation* 1985;71:717–24.

7 Been M, Smith MA, Ridgeway JP, *et al.* Characterisation of acute myocardial infarction by gated magnetic resonance imaging. *Lancet* 1985;ii:348–50.

8 Pflugfelder PW, Wisenberg G, Prato FS, Turner KL, Carroll SE. Serial imaging of canine myocardial infarction by in vivo nuclear magnetic resonance. *J Am Coll Cardiol* 1986;7:843–9.

9 Been M, de Bono DP, Muir AL, Boulton FE, Hillis WS, Hornung R. Coronary thrombolysis with intravenous anisoylated plasminogen-streptokinase complex BRL 26921. *Br Heart J* 1985;53:253–9.

10 Muir AL, Hannan WJ, Sapru RP, Boardman AK, Wraith PK, Brash HM. The effects of isoprenaline,

atropine and dobutamine on ventricular volume curves obtained by radionuclide ventriculography. *Clin Sci* 1980;58:357–64.

11 Smith MA, Best JJK, Douglas RHB, Kean DM. The installation of a commercial resistive NMR imager. *Radiology* 1984;57:1145–58.

12 Smith MA, Ridgway JP, Brydon JWE, *et al.* ECG gated T_1 images of the heart. *Phys Med Biol* 1986;31:771–8.

13 Kloner RA, Rude RE, Carlson N, Maroko P, DeBoer LWV, Braunwald E. Ultrastructural evidence of microvascular damage and myocardial cell injury after coronary artery occlusion: which comes first? *Circulation* 1980;62:945–52.

14 Gore JC, Doyle FH, Pennock JM. Relaxation rate enhancement observed in vivo by NMR imaging. In: Partain CL, James AE, Rollo FD, Price RR, eds. *Nuclear magnetic resonance imaging.* London: WB Saunders, 1983:94–106.

15 Lodge-Patch I. The ageing of cardiac infarcts, and its influence on cardiac rupture. *Br Heart J* 1951; 13:37–42.

16 Mallory CK, White PD, Salcedo-Salgar J. The speed of healing of myocardial infarction: a study of the pathologic anatomy in 72 cases. *Am Heart J* 1939;18:647–71.

17 Fishbein ML, Maclean D, Maroko PR. The histopathological evolution of myocardial infarction. *Chest* 1978;73:843–9.

18 Aherne T, Tscholakoff D, Finkbeiner W, *et al.* Magnetic resonance imaging of cardiac transplants: the evaluation of rejection of cardiac allografts with and without immuno-suppression. *Circulation* 1986; 74:145–56.

19 Ratner AV, Okada RD, Newell JB, Pohost GM. The relationship between proton nuclear magnetic resonance relaxation parameters and myocardial perfusion with acute coronary arterial occlusion and reperfusion. *Circulation* 1985;71:823–8.

20 Johnston DL, Brady TJ, Ratner AV, *et al.* Assessment of myocardial ischaemia with proton magnetic resonance: effects of a three hour coronary occlusion with and without reperfusion. *Circulation* 1985;71: 595–601.

21 Braunwald E, Kloner RA. Myocardial reperfusion: a double-edged sword? *J Clin Invest* 1985;76:1713–9.

22 Reimer KA, Lowe JE, Rasmussen MM, Jennings RB. The wavefront phenomenon of ischaemic cell death. I. Myocardial infarct size vs duration of coronary occlusion in dogs. *Circulation* 1977;56:786–94.

Myocardial involvement in systemic lupus erythematosus detected by magnetic resonance imaging

M. Been*, B. J. Thomson*, M. A. Smith†, J. P. Ridgway†, R. H. B. Douglas‡, M. Been*, J. J. K. Best‡ and A. L. Muir*.

*Departments of *Medicine, †Medical Physics and ‡Medical Radiology, Royal Infirmary, Lauriston Place, Edinburgh EH3 9YW, U.K.*

KEY WORDS: Relaxation parameter T1, Lupus activity criteria count.

Myocardial involvement in systemic lupus erythematosus is commonly found at autopsy but seldom recognized clinically or by routine cardiological investigations. As the magnetic resonance relaxation parameter, T1, is altered by changes in tissue cellularity, we carried out magnetic resonance imaging in 10 patients with systemic lupus erythematosus. Five had active systemic lupus erythematosus when assessed using the lupus activity criteria count.

The mean (±SD) T1 was 319±12 in normal volunteers and 321±10 in a second control group with hypertrophic cardiomyopathy. In the group with systemic lupus erythematosus, there was a higher mean value of 336 ms with a wider scatter of individual results (SD±22 ms). In the subgroup of patients with active disease, T1 was significantly higher (349±24) than in either of the two control groups.

In addition, there was an inverse correlation between serum complement and myocardial T1 in patients with systemic lupus erythematosus. Myocardial abnormalities in systemic lupus erythematosus were demonstrated by magnetic resonance imaging even where other non-invasive cardiac investigations were negative. We conclude that T1 calculated from magnetic resonance imaging is often abnormal in systemic lupus erythematosus and probably indicates myocardial involvement.

Introduction

Myocardial abnormalities are frequently found in post-mortem studies of patients with systemic lupus erythematosus[1–3] and discovery of inflammatory infiltration of the myocardial interstitium led to the first description of systemic lupus erythematosus as a 'connective tissue disease'[4]. The diagnosis of myocarditis *in vivo*, however, has remained difficult to establish. The electrocardiogram and chest X-ray are often abnormal in systemic lupus erythematosus but do not clearly differentiate myocardial and pericardial disease[5,6]. Echocardiography may be helpful particularly in the assessment of myocardial function[7,8], but cannot differentiate ischaemic from non-ischaemic dysfunction and is of limited use in determining tissue changes. Thallium imaging reveals perfusion defects in patients with both active and inactive disease[9], but little is known about the underlying

mechanism. The lack of an adequate method for non-invasive assessment of myocardial abnormalities has limited the understanding and recognition of the myocardial component of cardiac involvement in systemic lupus erythematosus.

Magnetic resonance imaging may allow myocardial tissue characterisation. Although we reported that the T1 was not altered in hypertrophic cardiomyopathy[10], these observations were made before we had developed a satisfactory gating technique for magnetic resonance imaging. Increases in the magnetic resonance relaxation parameters, T1 and T2, have been noted after experimental myocardial infarction and relate to myocardial tissue water content[11,12]. We demonstrated an increase in T1 in end-systolic images after myocardial infarction in man[13] but the time of maximum change was at about 14 days after infarction, suggesting that alterations in T1 may reflect cellular repair[14] rather than myocardial oedema alone. This concept is further supported by recent studies of the time course of magnetic-resonance parameter changes after coronary occlusion in both dogs[15] and rabbits[16].

The purpose of the present study was to determine whether the tissue characterisation provided by magnetic resonance imaging could indicate the presence of myocardial involvement in patients with systemic lupus erythematosus and, thereby, provide an index of myocarditis.

Methods

SUBJECTS

Ten female patients with established systemic lupus erythematosus fulfilling the revised American Rheumatism Association criteria[17] were studied. Clinical details of the patients are illustrated in Table 4. Nine patients were free of cardiac symptoms at the time of study, although one of these had a bioprosthetic mitral valve. The tenth patient was in congestive cardiac failure and suffered from recurrent supraventricular dysrhythmias.

Two control groups were also studied. The first was an age- and gender-matched group of eight normal volunteers drawn mainly from hospital staff. The second group consisted of 10 age-matched patients with hypertrophic cardiomyopathy, seven of whom were female.

All patients and volunteers gave written, informed consent prior to magnetic resonance imaging.

INVESTIGATIONS

A clinical history was taken from all patients with systemic lupus erythematosus and a physical examination was performed by one physician (BJT). Blood was taken for estimation of the full blood count, immuno-reactive complement proteins C3 and C4, antibody to double stranded DNA and circulating immune complexes. Disease activity was then assessed using the lupus activity criteria count, a validated index of disease activity which comprises seven primarily clinical variables[18,19]. The presence of two or more positive variables at the time of study indicates active disease. Each subject had a 12-lead electrocardiogram, M-mode and cross-sectional echocardiography on the same day as magnetic resonance imaging. The results of the cardiac imaging were assessed by a second clinician (MB) who was unaware of the clinical assessment.

MAGNETIC RESONANCE IMAGING

Subjects were imaged in a low field (0·08 Tesla) resistive imaging system (M&D Technology). An interleaved saturation recovery and inversion recovery pulse sequence was used to allow accurate measurement of the magnetic relaxation parameter T1. Electrocardiographically triggered cardiac gating was used as described previously[20]. Images were obtained at end-systole with aquisition of each image taking about 5 min. Four contiguous transverse slices, each of 16 mm thickness were obtained, encompassing the left ventricle. A single coronal scan was also obtained at a level that bisected the left ventricle.

The T1 maps which make up the images were

Table 1   *Clinical features of patients with systemic lupus erythematosus*

Patient	Age (years)	Duration of SLE (years)	Clinical manifestations	Blood pressure (mmHg)	Treatment (mg day^{-1})	
					Pred.	Aza.
LC	21	4	—	140/86	12·5	—
MJ	37	2	Alopecia	154/80	25	150
EG	48	2	Arthritis	140/88	15	—
JB	38	6	Arthritis	160/96	15	—
JW	57	14	Arthritis	138/80	2·5	—
CMcD	68	20	—	175/102	10	—
GD	33	4	Arthritis	150/80	—	—
JM	51	10	—	160/80	12·5	—
AR	31	7	Cardiac failure pericarditis, mucosal ulceration, haematuria	150/96	60	50
AL	26	4	—	140/90	—	—

Pred., prednisolone: Aza., azathiaprine; SLE, systemic lupus erythematosus

then analysed by dividing each image of the left ventricular myocardium into six regions of interest to test for homogeneity of signal. From the T1 values obtained, a mean T1 of all regions of interest for each subject was obtained and the maximum T1 in any section noted.

ECHOCARDIOGRAPHY

M-mode and cross-sectional echocardiography were performed using a Hewlett-Packard phased array system with a 3·5-MHz transducer. Left ventricular function was assessed from cross-sectional images and measurement of myocardial thickness and cavity size made from M-mode tracings.

STATISTICAL ANALYSIS

In addition to analysis between three clinical groups, the group with systemic lupus erythematosus was further subdivided into those with and without active disease based on the disease activity

Table 2   ECG and echocardiographic findings in patients with systemic lupus erythematosus

Patient	Age (years)	ECG	ECHO			
			SEPTUM	LV FREE WALL	EDD	ESD
LC	21	Normal	11	14	50	36
MJ	37	Normal	13	14	33	20
EG	48	Normal	11	12	56	30
JB	38	LBBB	12	12	64	56
JW	57	Normal	16	16	50	35
CMcD	68	Non-specific T-wave changes	13	20	44	24
GD	33	Normal	12	14	50	36
JM	51	Left axis Deviation	13	16	63	45
AR	38	AF, widespread T inversion	12	11	64	48
AL	26	Normal	11	11	52	33

SLE, systemic lupus erythematosus; LBBB, left bundle branch block; AF, atrial fibrillation.

Table 3   Magnetic resonance T1 values in volunteers, patients with hypertrophic cardiomyopathy and SLE (complement values are shown for patients with SLE)

Mean T1 (ms)			Complement			
Vol.	HCM	SLE	(C3	C4	ádsDNA	LACC)
321	311	313	(1·01	0·13	elevated	1)
—	314	332	(0·83	0·23	normal	0)
318	320	314	(0·55	0·16	elevated	2*)
334	333	366	(0·51	0·07		2*)
322	324	346	(0·53	0·07	elevated	2*)
—	333	339	(0·67	0·15	elevated	1)
297	320	343	(0·69	0·09	elevated	?*)
332	321	320	(1·23	0·34	normal	0)
314	318	377	(0·53	0·18	elevated	5*)
314	305	313	(0·99	0·27	normal	0)

Vol., volunteers; HCM, hypertrophic cardiomypathy; SLE, systemic lupus erythematosus; áds DNA, antibody to double stranded DNA; LACC, lupus activity criteria count.
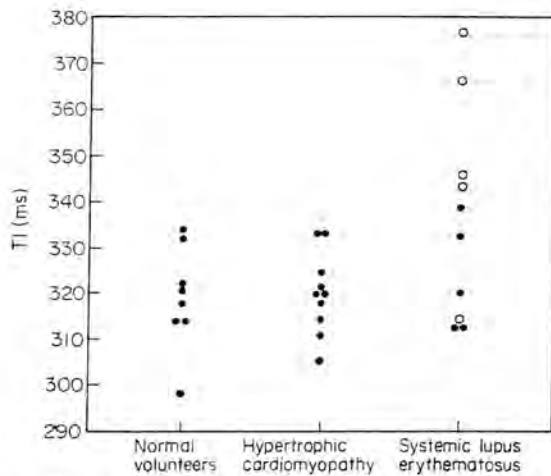*Active disease.

Figure 1 Mean T1 values in normal volunteers, patients with hypertrophic cardiomyopathy and patients with systemic lupus erythematosus. ○, Active disease.

score. Analysis of variance was used to establish whether there was a significant difference between the means of the initial three groups and also between the means of the further subdivision into four groups. Subsequent analysis was performed using a non-paired t-test to decide which group means differed significantly[21].

Correlation between T1 values and complement levels was by linear regression analysis. Significance was accepted at $P < 0.05$.

Results

CLINICAL FINDINGS

The clinical findings in the group with systemic lupus erythematosus are summarised in Table 1.

Active disease, as indicated by a lupus activity criteria count of 2 or more, was present in five of the 10 patients. Eight patients were on prednisolone and two on azathiaprine. Clinical evidence of cardiac disease was only detectable in the one patient with heart failure.

ELECTROCARDIOGRAPHIC AND ECHOCARDIOGRAPHIC
FINDINGS

Four of the group with systemic lupus erythematosus had non-specific electrocardiographic abnormalities (Table 2). The presence of an abnormal electrocardiogram did not relate to disease activity. On echocardiography, mild hypertrophy of the interventricular septum and left ventricular free wall was common (Table 2). Poor left ventricular function was confirmed in the patient with cardiac failure and a dilated left ventricle with moderate contraction was noted in the patient with a mitral-valve replacement.

All patients with hypertrophic cardiomyopathy had evidence of septal hypertrophy, usually with some free-wall hypertrophy.

PERICARDIAL INVOLVEMENT

A small amount of pericardial fluid was noted on the magnetic resonance image in two patients with systemic lupus erythematosus, but was also seen in two normal volunteers and in one patient with hypertrophic cardiomyopathy. The pericardial fluid was not detectable by echocardiography in the normal volunteers or patients with systemic lupus erythematosus but was noted in the patient with hypertrophic cardiomyopathy (in whom the effusion was larger).
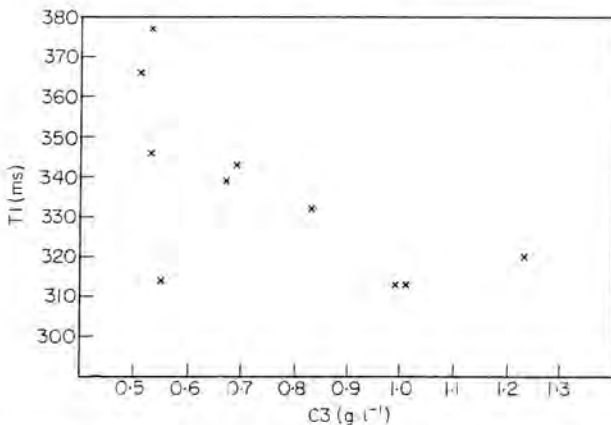

Figure 2 Relationship between MR T1 and the C_3 component of the complement in patients with SLE ($r = -0.67$, $P < 0.05$).
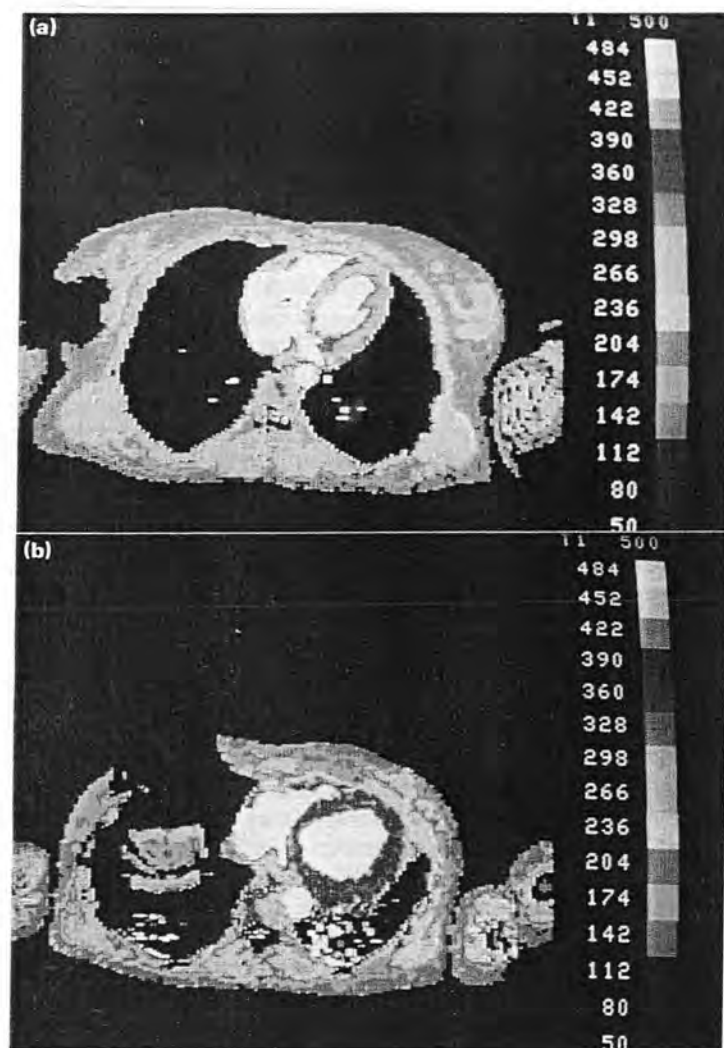
Figure 3 Transverse sections illustrating T1 values in (a) a normal subject and
(b) a patient with active lupus erythematosus. The colour bar shows the T1
values with the normal subject having T1 values of around 300 ms, but the
patient with lupus having a diffuse increase in T1 of around 360 ms.

MAGNETIC RESONANCE IMAGING

The individual mean left ventricular myocardial
T1 for each group is shown in Table 3. The mean T1
(1 standard deviation) for normal volunteers was
319 ± 12 ms), similar to the group with hypertro-
phic cardiomyopathy (321 ± 10 ms). For the group
with systemic lupus erythematosus the mean T1 was
higher at 336 ± 22 ms, this difference being signifi-
cant ($P < 0.05$) when compared to the group with
hypertrophic cardiomyopathy ($N = 10$), but not

when compared to the normal volunteers ($N = 8$).
However, there was marked variability in T1 values
within the systemic lupus erythematosus group
(Fig. 1). Values were particularly elevated in those
with active disease as indicated by the lupus
activity criteria count. For this subgroup the
mean T1 was 349 ± 24 as compared to 324 ± 12 in
the subgroup with inactive disease (Table 3).
Analysis of variance demonstrated a significant
difference between the means at the 0.99 level.

Subsequent analysis demonstrated that the sub-group with active disease was significantly different to both the normal volunteer and hypertrophic cardiomyopathic groups ($P < 0.01$). In addition, T1 showed a negative correlation with serum C3, ($r = 0.67$, $P < 0.05$) in the group with systemic lupus erythematosus (Fig. 2). In the patients with systemic lupus erythematosus and raised T1 values the increase in T1 was diffuse (Fig. 3).

No abnormalities were seen in the electrocardiogram or echocardiographs of the normal volunteers.

Discussion

This study confirms our previous findings that there is little variation in T1 in normal subjects and the T1 is not abnormal in patients with hypertrophic cardiomyopathy[13,10]. Furthermore, it demonstrates that the magnetic relaxation parameter is frequently, but not invariably, raised in patients with active systemic lupus erythematosus. The patients with systemic lupus erythematosus were recruited from those attending an out-patient clinic. They thus tended to have severe disease, reflected by the fact that eight were on steroid therapy (Table 1). However, of the five with active disease at the time of the study, only two had clinical, radiological, electrocardiographic or echocardiographic evidence suggestive of myocardial involvement.

Badui *et al.*[7] found evidence of myocarditis in only 14% of cases using routine non-invasive investigations. Despite the selective nature of the patient group, the fact that four out of the five with active disease had a raised T1 suggests that abnormalities in the myocardium in systemic lupus erythematous are common. It is likely that commonly available cardiac investigations are insensitive to the detection of such myocardial involvement. In two patients with markedly prolonged myocardial T1 values the electrocardiogram was entirely normal.

The possibility that the elevated T1 values might be related to the slight increase in left ventricular wall thickness found in the group with systemic lupus erythematosus is discounted by the normal values in the patients with hypertrophic cardiomyopathy who had marked myocardial hypertrophy.

Increases in myocardial T1 are not specific to systemic lupus erythematosus. We have previously reported increases in T1 following myocardial infarction[13]. However, the pattern of increase is very different in the two conditions. In myocardial infarction there is a localised area of increased T1, with values in the infarcted area rising above 390 ms. There is often associated wall thinning, while the unaffected myocardium has a normal appearance. In contrast, those patients with systemic lupus erythematosus and raised T1 values show a more diffuse pattern of T1 elevation, with values usually not exceeding 400 ms (Fig. 3).

After acute myocardial infarction the time course of the changes is for a localised abnormal area to increase in size up to about 14 days after infarction. There is a gradual return to normal values by six months after the acute event. We have not yet been able to make serial measurements in the patients with lupus erythematosus.

The underlying mechanism for this increase in T1 is not yet clear. Histological findings reported in the myocardium of patients dying of systemic lupus erythematosus include lymphocytic infiltration, sometimes accompanied by myocardial oedema. In addition to the changes following acute myocardial infarction[13] T1 also rises in acute rejection following heterotopic cardiac transplantation[22]. In both these conditions, as in systemic lupus erythematosus, cellular infiltration is a prominent histological feature and may directly or indirectly be responsible for the increase in T1.

Although prolonged myocardial T1 values appear to reflect overall disease activity, one patient with active disease had a normal T1. Although we have no histological proof, increases in T1 may specifically reflect myocardial involvement. It is notable that the one patient with acute cardiac failure had the highest T1.

The likelihood is that increases in T1 documented by this interleaved saturation recovery and inversion recovery pulse sequence reflect altered cellularity of the tissue being examined. The relaxation parameters T1 and T2 depend on the precise pulse sequence using in magnetic resonance imaging. The pulse sequence used in our system given a more precise estimate of T1 than in the more common spin-echo pulse sequence, so some caution has to be taken before applying these results to measurements from other magnetic resonance imaging systems. However, estimates of T1 values from magnetic resonance imaging using inversion recovery sequences may aid in the investigation of other myocardial diseases such as myocarditis, congestive cardiomyopathy, connective tissues diseases other than systemic lupus erythematosus and cardiac rejection after transplantation where myocardial inflammation is suspected.

References

[1] Griffiths GC, Vural IL. Acute and subacute disseminated lupus erythematosus: correlation of clinical and post mortem findings in 18 cases. Circulation 1951; 3: 492–500.

[2] Brigden W, Bywaters EGL, Lessof MA *et al*. The heart in systemic lupus erythematosus. Br Heart J 1960; 22: 1–16.

[3] Bulkley BH, Roberts WC. The heart in systemic lupus erythematosus and the changes induced in it by corticosteroid therapy. Am J Med 1975; 58: 243–64.

[4] Gross G. The cardiac lesions in Libman Sacks disease with a relationship to acute diffuse lupus erythematosus. Am J Pathol 1940; 16: 375–408.

[5] Kong TQ, Kellum RE, Haserik JR. Clinical diagnosis of cardiac involvement in systemic lupus erythematosus. Circulation 1962; 26: 7–11.

[6] Heijtmancik MR, Wright JC, Quint R, Jennings FL. The cardiovascular manifestations of systemic lupus erythematosus. Am Heart J 1964; 68: 119–30.

[7] Badui E, Garcia-Rubi A, Robles E *et al*. Cardiovascular manifestations of systemic lupus erythematosus — prospective study of 100 patients. Angiology 1985; 36: 431–41.

[8] Klinkhoff AV, Thompson CR, Reid JGD, Tomlinson CW. M mode and 2 dimensional echo-cardiographic abnormalities in systemic lupus erythematosus. J Am Med Assoc 1985; 253: 3273–7.

[9] Hosenpud JD, Montanaro A, Hart MV *et al*. Myocardial perfusion abnormalities in asymptomatic patients with systemic lupus erythematosus. Am J Med 1984; 77: 286–92.

[10] Been M, Kean D, Smith MA, Douglas RHB, Best JJK, Muir AL. Nuclear magnetic resonance in hypertrophic cardiomyopathy. Br Heart J 1985; 54: 48–52.

[11] Williams ES, Kaplan JL, Thatcher F, Zimmerman G, Knoebel SB. Prolongation of proton spin-lattice relaxation times in regionally ischaemic tissue from dog hearts. J Nucl Med 1980; 21: 449–53.

[12] Higgins CB, Herfkens R, Lipton MJ *et al*. Nuclear magnetic resonance imaging of acute myocardial infarction in dogs: alterations in magnetic relaxation times. Am J Cardiol, 1983; 52: 184–8.

[13] Been M, Smith MA, Ridgway JP *et al*. Characterisation of acute myocardial infarction by gated magnetic resonance imaging. Lancet 1985; ii: 348–50.

[14] Been M, Smith MA, Ridgway JP, Best JJK, de Bono DP, Muir AL. Serial changes in the T1 magnetic relaxation parameter after myocardial infarction in man. Br Heart J 1988; 59: 1–8.

[15] Pflugfelder PW, Wisenberg G, Prato FS, Turner KL, Carroll SE. Serial imaging of canine myocardial infarction by in vivo nuclear magnetic reasonance. J Am Coll Cardiol 1986; 7: 843–9.

[16] Johnston DL, Homma S, Rokey R *et al*. Serial changes in NMR relaxation times after myocardial infarction; relationship to water content, severity of ischaemia and histopathology over a 3 month period (Abstr). Proc. 5th Annual meeting of the Society of Magnetic Resonance in Medicine, pp. 383–4.

[17] Tan EN, Cohen AS, Fries JF *et al*. The 1982 revised criteria for the classification of systemic lupus erythematosus. Arth Rheumatol 1982; 25: 1271–7.

[18] Urowitz MV, Gladman DD, Goldsmith C, Tozman E. The lupus activity criteria count (Abstr). Arth Rheumatol 1982; 25: 178.

[19] Rubin LA, Urowitz MV, Gladman DD. The mortality in systemic lupus erythematosus: the bimodal pattern revisited. Quart J Med 1985; 55: 87–98.

[20] Smith MA, Ridgway JP, Brydon JWE *et al*. ECG-gated T1 images of the heart. Phys Med Biol 1986; 3: 771–8.

[21] Alder HL, Roessler EB. Introduction to probability and statistics. San Francisco: W H Freeman & Co., 1977: 335–7.

[22] Adherne T, Tscholakoff D, Finkbeiner W *et al*. Magnetic resonance imaging of cardiac transplants: the evaluation of rejection of cardiac allografts with and without immunosupression. Circulation 1986; 74: 145–56.

Brain hydration during alcohol withdrawal in alcoholics measured by magnetic resonance imaging

M.A. Smith, J.D. Chick*, H.M. Engleman, D.M. Kean, A.J. Mander, R.H.B. Douglas and J.J.K. Best

NMR Imaging Unit, University of Edinburgh, Royal Infirmary, Edinburgh and Department of Psychiatry, University of Edinburgh, Royal Edinburgh Hospital, Edinburgh (U.K.)

Twenty-seven patients had a first Magnetic Resonance Imaging (MRI) scan 1 — 3 days after stopping drinking and a second approximately 2 weeks later with no change in whole brain T_1 or T_1 in selected brain areas. Six patients whose first scan was over 36 h after the last drink underwent an increase in whole brain T_1 in the interval to the second scan. The later the first scan was performed the greater was the increase in T_1. These results are compatible with a very early fall in brain water immediately on cessation of drinking (perhaps due to a rebound increase of vasopressin activity) with a return to 'baseline' after two weeks. A third scan after discharge from hospital in 23 individuals who had abstained from alcohol or drank very little did not reveal any further significant change in brain T_1.

Introduction

Water retention within the brain has been postulated as a contributant to some of the clinical features of alcohol withdrawal in chronic alcoholics [1]. In magnetic resonance imaging (MRI), T_1 relaxation time is related to the state of water in the tissue [2]. The T_1 value, measured in milliseconds (ms) increases as the proportion of free to bound water within the tissue increases. In vivo T_1 values have been shown to correlate with the level of brain water [3 — 5] and so may enable a study of brain water during withdrawal of alcohol in chronic alcoholics.

MRI was first used for the investigation of chronic alcoholics by Besson and colleagues [6]. These authors suggested that brain water is diminished during intoxication and increased during alcohol withdrawal. Acute intoxication in occasional drinkers results in a fall in whole brain T_1, compatible with the dehydration which follows acute intake of alcohol [7]. Eisenhoffer and colleagues [1] suggest that such an effect, if chronic, might result on alcohol withdrawal in a rebound increase of vasopressin activity, followed by a return to baseline.

It was therefore hypothesised that whole brain T_1 in alcoholics would be seen to fall from the level at 24 — 48 h following cessation of drinking to a lower level ('baseline') some 2 weeks later. We were unable to perform T_1 measurements in the present study in intoxicated alcoholics immediately prior to admission and thus unable to study the early part of the postulated pattern of changes (that is, the putative rise in brain water and T_1).

Patients and Methods

Chronic alcoholic patients who were about to be voluntarily admitted as inpatients for detoxification to the Alcohol Problems Clinic, Royal Edinburgh Hospital, were fully informed about the study and invited to participate.

*To whom correspondence should be sent.

Twenty-seven patients (18 men, 9 women), were admitted to this study. Their mean age was 44 years (range 26 – 63, S.E.M. 5.2). They were to be scanned within 48 h of admission (day 1) and again approximately on day 15. However, the timing of scans varied according to the availability of the scanner and the requirements of the patients' participation in the ward programme.

In connection with a separate study [8] of cognitive impairment and MRI parameters, results of a scan performed at approximately day 15 were available in a further 42 patients. These patients had not been scanned at or near admission.

Patients had been drinking at least 130 g ethanol/day before admission and had a 5 – 15 year history of alcoholism. No patients were included if they had a history of drug abuse, or were clinically malnourished, or had physical disorders other than raised serum liver enzymes. Over the first 5 days each patient received a normal diet, intramuscular multi-vitamin supplements and decreasing doses of chlordiazepoxide to control withdrawal symptoms.

Our procedures for measuring whole brain T_1 and T_1 in regions of interest in the brain have been described [9]. The inter-operator reliability of our T_1 measurements has been reported [8]. Differences in T_1 values between groups of patients at different times were
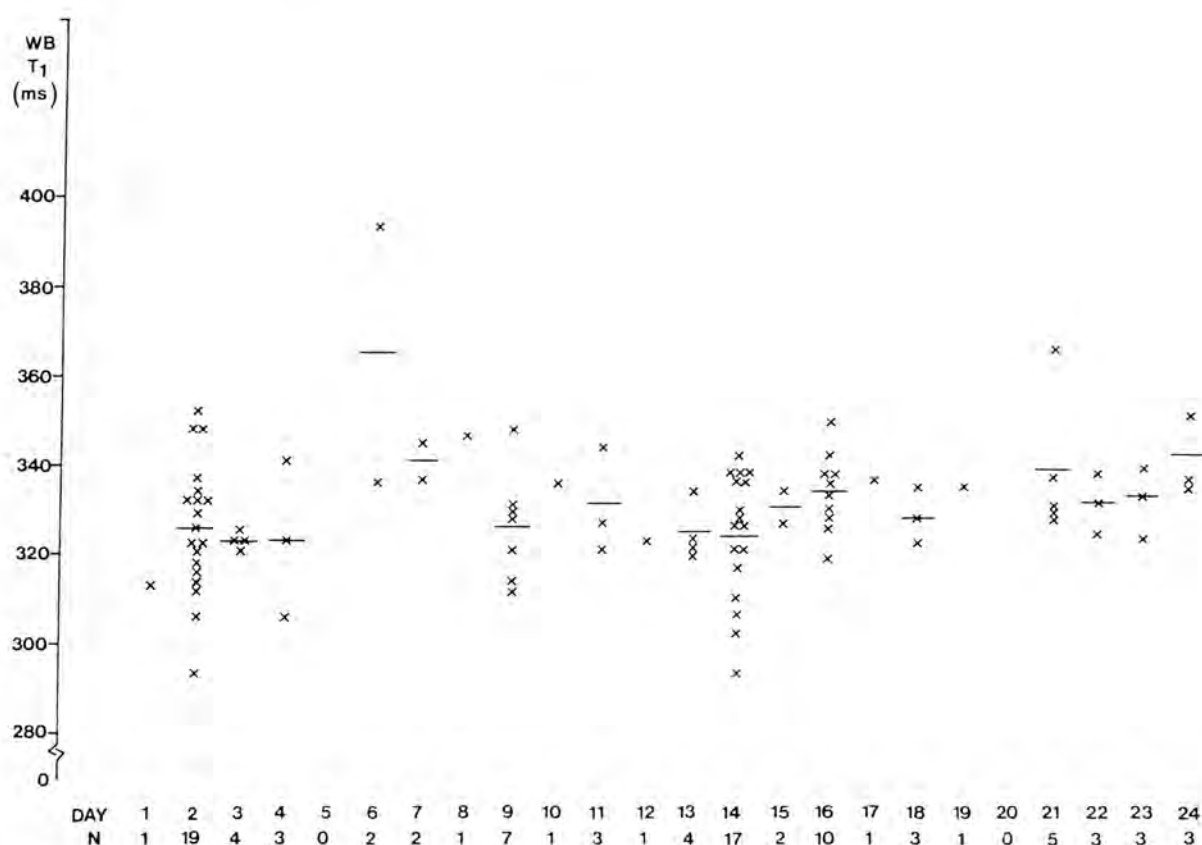

Fig. 1. Whole Brain T_1 measurements with means according to length of time since last drink.

Table I. Mean change in T_1 from Scan 1 to Scan 2 ($\Delta = T_1$ (Scan 2) $- T_1$ (Scan 1)).

		All subjects	Scan 1 within 36 h of last drink	Scan 1 36 – 84 h after last drink
Δ	Frontal White	1.83 ± 9.46	-0.39 ± 2.04	8.50 ± 3.77
Δ	Frontal Grey	0.50 ± 17.51	-1.833 ± 4.26	7.50 ± 6.08
Δ	Parietal White	0.83 ± 9.17	-0.39 ± 2.12	4.50 ± 3.90
Δ	Parietal Grey	-6.75 ± 22.21	-11.17 ± 5.09	6.50 ± 8.17
Δ	Whole brain	0.75 ± 8.89	-1.78 ± 2.01	$8.33^* \pm 2.04$
	n	24	18	6

*Significantly greater ($P = 0.012$) than in those whose first scan was within 36 h of last drink.

compared using Student's t-test. Changes in T_1 in individual patients were assessed using a paired Student's t-test.

Results

Three patients were unavailable for their second scan. The mean whole brain T_1 at the first scan in the 24 patients who had a second scan was 314 ms (range 283 – 338, S.E. 2.71). At the second scan the mean T_1 was also 314 ms (range 283 – 334, S.E. 2.69). T_1 measurements in small areas of interest likewise showed no significant change between scans. Figure 1 illustrates all our available data on whole brain T_1 in the withdrawal period. It includes the subjects on whom only the first scan was done, and subjects from our other study scanned only at day 15 approximately. No trend suggestive of a fall in whole brain T_1 is visible.

Lest the hypothesised fall in T_1 had been early and had been followed by an early 'return to baseline', an analysis of the change in T_1 between the first and second scan was made, comparing those patients who had their first scan within 36 h of the last drink to those whose first scan was later. The 18 patients scanned within 36 h had their second scan at a mean of 13.6 days later (range 9 – 16 days, S.E. 0.43) and the six whose first scan was up to 48 h later had their second scan at a mean interval of 12.3 days since the first (range 9 – 16, S.E. 1.15). This interval was not significantly different ($P = 0.33$).

In those whose first scan had been within 36 h of the last drink, the difference between whole brain T_1 on the first and second scans was insignificant (mean difference -1.78 ms — a fall — range $-15 - +9$, S.E. 2.01). A significant increase occurred, however, in those whose first scan had been up to 48 h later (mean 8.33 ms, range $+2 - +14$, S.E. 2.04; $t = 4.08$, d.f. 5 $P < 0.01$). The difference between the changes in these two groups of patients, (between those scanned within 36 h of admission and those scanned later), is

Table II. Correlation of TIME OF SCAN 1 (post admission) with CHANGE IN T_1 from Scan 1 to Scan 2.

R-values ($* - P < 0.01$) $n = 24$

	Δ WB	Δ FW	Δ PW	Δ FG	Δ PG
TIME OF SCAN 1	0.4048*	0.2434*	0.1080*	0.4076*	0.4242*

significant ($t = 2.73$, d.f. 22, $P = 0.012$) (Table I). The trend was visible but not significant in each of the T_1 measurements made in areas of interest. The later the first scan was performed after the last drink, the greater the change between the first and second scans, as shown by the correlation coefficients given in Table II.

In case our timing of the scans had resulted in our missing any later changes in T_1, another comparison was made. Four patients had the second scan on the 9th or 10th day and 20 patients beyond the 10th day. There was no significant difference when these groups were compared in the mean change between the first and second scans (2.25 ms, S.E. 5.28, range -11 $- +13$ and 0.45 ms, range $-15 - +14$, S.E. 1.97, respectively; $t = 0.36$, d.f. 22, $P = 0.72$).

We had some further data after patients had been discharged from the 2-week ward programme. Seventeen patients from the present study had a further scan 2 months after discharge. There was also a scan at that point in 38 patients in the collateral study already mentioned. The difficulty in using this data is that we were not always certain whether or not an individual had continued to abstain from alcohol during that period. We examined the T_1 values in 23 individuals who had been scanned at about day 15 and had a repeat scan at a mean of 102 days and who as far as we could tell had abstained during that period or drunk very little. No significant change in T_1 in any of the regions of interest or in the whole brain was noted. However, the trend in these apparent abstainers in all our T_1 measures was for a slight increase, but with considerable individual variation (for example, the mean increase in whole brain T_1 was 2.39 ms, range $-11-+19$, S.E. 1.55 ms, $n = 23$).

Discussion and Conclusions

The only possible way in which our data would support the notion that there is a fall in brain water following withdrawal from alcohol is using the sparse data comparing the changes

in those scanned within 36 h of the last drink with those whose first scan was later. Our data would support a fall in T_1 between 36 h and 84 h, with a subsequent return to 'baseline' during the next 10 days approximately. It would have to be postulated, however, that individual differences in 'baseline' T_1 prevented this from emerging in the data on the whole sample as illustrated in Fig. 1.

Our data do not uphold the provisional result which we obtained on our first 9 patients [9]. In that paper, we reported a fall in whole brain T_1 which correlated positively with the length of abstinence prior to the second scan. In our present sample, the correlation between change in whole brain T_1 and interval to the second scan was insignificant (-0.09). Neither were there significant correlations between the change in T_1 in the areas of interest and interval to the second scan.

Further studies should comprise daily measurements beginning on the day prior to admission, when the patient is still drinking, and continuing for 2 weeks.

References

1 G. Eisenhoffer, D.G. Lambie and E.A. Whiteside, Br. J. Addict., 80 (1985) 195.
2 R. Mathur-de Vre, Br. J. Radiol., 57 (1984) 1145.
3 H.L. MacDonald et al., Br. J. Radiol., 59 (1985) 355.
4 D. Barnes et al., J. Neurol. Neurosurg. Psychiatry, 49 (1986) 1341.
5 B.A. Bell et al., Lancet., i (1987) 66.
6 J.A.O. Besson et al., Lancet, ii (1981) 923.
7 A.J. Mander et al., Lancet, ii (1985) 1075.
8 J.D. Chick et al., Alcoholism: Clin. Exp. Res. (1988) in press.
9 M.A. Smith et al., Lancet, i (1985) 1273.

Magnetic resonance spectroscopy *in vivo*

D.A. Porter and M.A. Smith

Division of Radiological Sciences, UMDS, Guy's Hospital, London, SE1 9RT, UK

ABSTRACT

Nuclear magnetic resonance (NMR) has become an important non-invasive investigative technique in medicine and biology. The most recent development has been the ability to perform magnetic resonance spectroscopy (MRS) in selected regions within the human body. Such volumes can be selected by techniques which fall into the following broad categories: surface coil methods, surface coils with depth selection, volume selection and chemical shift mapping. The latter two methods use magnetic field gradients, present on magnetic resonance imaging systems, to select the volume. MRS can be used to measure phosphorus and proton metabolites and hence study tissue biochemistry in-vivo.

Keywords: Medical imaging, magnetic resonance spectroscopy, biochemical analysis.

INTRODUCTION

There has been a great deal of interest in the application of nuclear magnetic resonance (NMR) in the field of medicine and biology over the last 15 years. The initial interest was fueled by the development of techniques of magnetic resonance imaging (MRI) so that now commercial MRI systems are present in many hospitals and research centres. More recently, developments in magnetic resonance spectroscopy (MRS) have provided a non-invasive technique for monitoring biochemical activity from selected regions within the body.

Following the first observations of NMR in 1946 by Bloch[1] and Purcell[2], it has long been possible to obtain *in-vitro* NMR spectra from small samples in liquid or solid form. In 1974 it was demonstrated that NMR can be used to study the major phosphorus containing metabolites in isolated intact tissues[3]. With the development of larger bore high field superconducting magnets came the possibility of acquiring NMR spectra from animal and human tissues *in-vivo*. Nuclei that can be studied by MRS include phosphorus, protons and carbon, all of which play an important role in human biochemistry.

One important requirement for *in-vivo* studies is spatial selection, so that spectra can be collected from a well defined region within the body without contamination by signals originating from tissues not under investigation. After a short account of the basic principles, this article reviews the techniques used to meet the *in-vivo* objectives and presents examples of human *in-vivo* NMR spectra.

PRINCIPLES OF MRS

In order to obtain NMR spectra, the sample to be studied is placed in a strong magnetic field of high homogeneity. The strength of this field is denoted by B_0 and its direction is defined as the z axis. Interaction between the magnetic moment of the nuclei and the static field B_0 results in the preferential alignment of the nuclear spins along the field direction. In this way, a nuclear magnetization is produced along the z axis. An individual nucleus, whose spin is inclined at an angle to B_0, will precess about the field direction at a characteristic frequency:

$$\omega = \gamma B_0$$

where ω is known as the Larmor frequency and γ is the gyromagnetic ratio for the particular nuclear species.

This behaviour is analogous to the precession of the axis of a gyroscope about the Earth's gravitational field. A radio frequency (RF) magnetic field at the same frequency can be employed to tilt the magnetization away from the z axis. This time varying field, denoted by B_1, is applied in a direction perpendicular to B_0. The magnitude and duration of this RF excitation pulse determines the angle of tilt, α, away from the z axis as follows:

$$\alpha = \gamma \int_{0}^{t_p} B_1(t)\ dt \tag{1}$$

where t_p is the pulse duration.

A 180° pulse leaves the nuclear magnetization along the $-z$ axis and a 90° pulse leaves it in the xy plane. The continued precession of the nuclei about B_0 means that any xy component of magnetization present after the RF pulse also precesses about B_0. It is this rotating magnetization that is detected by the induction of an electromotive force (EMF) in a radio frequency receiver coil. The decay of this signal is characterized by two time constants T_1 and T_2. T_1 is known as the longitudinal or spin–lattice relaxation time and describes the relaxation of the system to equilibrium with the nuclear magnetization along the z axis. T_2 is the transverse or spin–spin relaxation time and is a measure of the time during which the individual nuclear magnetic moments that contribute to the rotating xy magnetization remain in phase with each other.

The magnetic field experienced by the nuclei is modified by aspects of its local environment such as the distribution of electrons. As a result, different compounds of the same nucleus will experience marginally different B_0 fields and consequently produce resonances at slightly different frequencies. This change in resonant frequency is known as a chemical shift. Formally, the chemical shift for a compound with resonant frequency, ω, is given by:

$$\text{chemical shift (p.p.m.)} = \frac{\omega - \omega_0}{\omega_0} \times 10^6$$

ω_0 is the resonant frequency of a reference compound which is standard for a given nuclear type. Providing the bandwidth of the RF excitation pulse is sufficient to encompass the entire range of chemical shift for a given nuclear type, the time signal produced by the rotating xy magnetization contains information about the relative signal intensity as a function of chemical shift. This information is retrieved by Fourier transformation of the time signal and allows relative concentrations of different compounds of the same nucleus to be inferred. In order to resolve the different chemical shifts, a high degree of magnetic field homogeneity is required. If this condition is not met the resonant frequency of a nucleus with a given chemical shift will vary significantly across the sample and degrade resolution. Before data can be acquired in an NMR experiment the magnetic field B_0 is adjusted until the required homogeneity is produced. The field homogeneity can be monitored by measuring the line width of a single resonance. The resonance of proton nuclei in water molecules are frequently used for this purpose. This process of B_0 field adjustment is known as shimming. For imaging purposes a uniformity of 1 in 10^5 is sufficient whereas for spectroscopy a uniformity of 1 in 10^7 is required.

SURFACE COIL TECHNIQUES

In 1980 the first *in-vivo* NMR spectra were collected from phosphorus compounds in skeletal muscle and brain of intact rats, using a single turn circular RF coil placed close to the skin[4]. The coil, which is tuned to the appropriate resonant frequency, is positioned so that the coil axis is perpendicular to the static magnetic field B_0. The coil is used both to send the RF excitation pulse and to receive the subsequent RF signal from the irradiated tissues. In conventional *in vitro* NMR spectroscopy a saddle-shaped or solenoidal coil is used to provide a uniform B_1 field over the sample. Under these conditions, different regions within the sample contribute evenly to the detected signal. The inhomogeneous magnetic field associated with a surface coil is used to confine the NMR signal to a region close to the surface of the body. The relative signal strength as a function of spatial coordinates is determined by two factors. Firstly, as a result of the principle of reciprocity[5], the EMF induced in the coil by the rotating magnetization at a given point in the sample is proportional to the magnetic field produced at that same point by unit current flowing through the coil. Secondly, the pulse angle following an RF excitation pulse varies across the sample according to equation (1).

It therefore follows that the relative contribution to the detected signal from a given point in the sample, is proportional to $\alpha \sin \alpha$, where α is the pulse angle at that point. This behaviour can be used to a limited extent to select regions at different distances from the coil. *Figure 1* shows the relative signal received from points in a homogeneous non-conducting sample as a function of distance along the coil axis when a 90° and 180° pulse are generated at the coil centre. Frequency dependent attenuation of the RF signals in conducting biological samples[6] must be considered for a more careful analysis. The behaviour of the surface coil B_1 field away from the coil axis means that regions of high sensitivity selected by adjustment of pulse length have a complex shape. It is not possible to achieve efficient depth selection using simple radio frequency excitation pulses as a result of surface contamination. This arises due to the high B_1 flux near the coil wire, where a large range of pulse angles exist and where the inherent sensitivity is high.

An example of a phosphorus spectrum from a human calf muscle using a 6 cm diameter surface coil is shown in *Figure 2*.

DEPTH SELECTION

A number of techniques have been developed to improve the ability of surface coil methods to select regions of tissue at different distances from the coil.

One approach has been to make the signal received from a given point a stronger function of the pulse angle at that point. In this way the signal is more effectively localized to regions where the pulse angle is close to 90°. This has been achieved by using a series of multiple RF pulses to excite the nuclear magnetization away from its equilibrium direction along the z axis[7]. This contrasts with the simple NMR experiment, outlined above, where a single RF pulse is applied for this purpose.
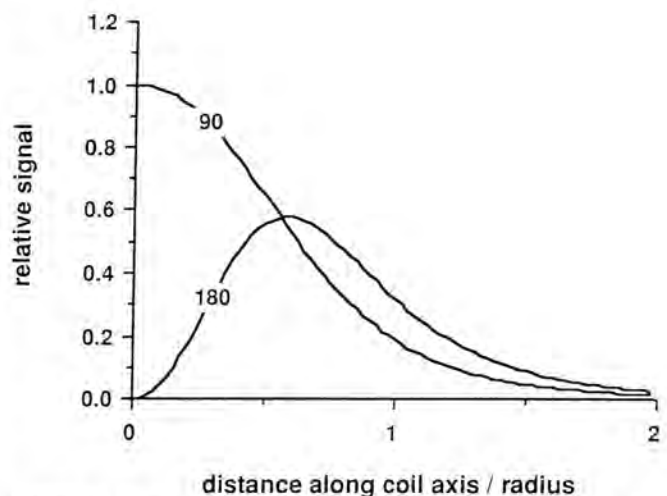

Figure 1 The relative signal strength received by a circular surface coil as a function of the distance along the coil axis. The two curves show how the pulse angle at the coil centre determines the depth from which maximum signal is received
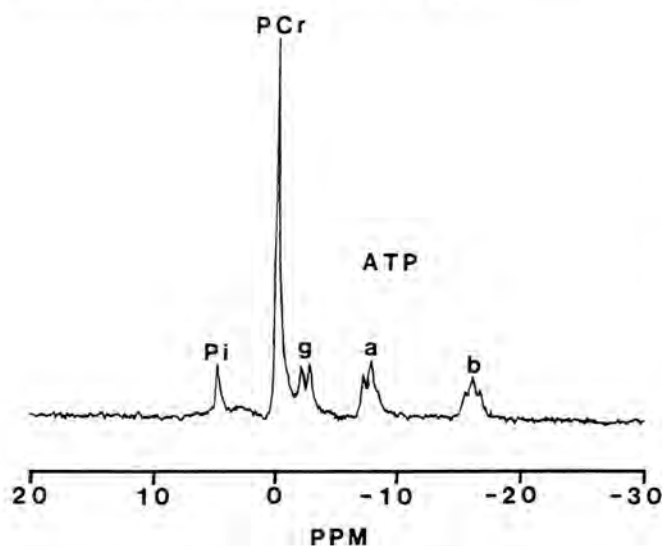
Figure 2 *In-vivo* phosphorus NMR spectrum collected from human calf muscle using a 6 cm surface coil. The frequency decreases from left to right and 0 p.p.m. corresponds to a frequency of about 26 MHz at 1.5 T. The resonances arising from the different phosphorus compounds are labelled as follows: Pi, inorganic phosphate; PCr, phosphocreatine; g, a, b ATP, gamma, alpha and beta adenosine triphosphate

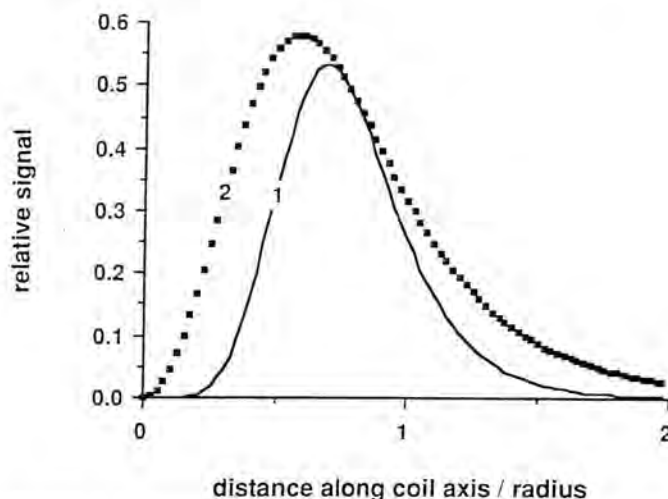distance along coil axis / radius

Figure 3 A comparison of the spatially dependent signal received using the multiple radio frequency (RF) pulse sequence outlined in the text (curve 1) with that produced using a single RF excitation pulse (curve 2). These theoretical curves are plotted for a 180° pulse angle at the coil centre. This pulse angle can be varied to select regions at different distances from the coil

A number of different RF pulse sequences have been used. An example of one of the less complex is a follows: an initial RF pulse of duration l is followed by a second RF pulse of duration $2l$ before signal acquisition. Four separate signal acquisitions are performed in the same way, but the phase difference between the two RF pulses is increased by 90° for each acquisition; 180° phase adjustment of the receiver is also required for alternate acquisitions. Analysis of the motion of the nuclear magnetization during this sequence shows that summation of the four signals produces a signal whose magnitude[7] is proportional to $\alpha \sin^3 \alpha$. *Figure 3* compares this dependence on pulse angle with that obtained from the use of a single RF pulse for excitation.

Other multiple pulse sequences produce signals that are proportional to higher order trigonometrical functions of the pulse length. This greater selectivity to pulse length is accompanied by greater complexity of the sequence and an increase in the number of signal acquisitions required. The problem of avoiding contamination by signals from regions close to the coil has also been addressed by multiple pulse techniques[8].

The introduction of magnetic field gradient techniques provided a more efficient method of selectively receiving a signal from tissue at a given distance below a surface coil. One technique which utilizes a magnetic field gradient in conjunction with a surface coil to produce spatial localization is DRESS (Depth Resolved Surface Coil Spectroscopy)[9]. Superposition of a linear magnetic field gradient upon the B_0 static magnetic field has the effect of making the resonant frequency of the nuclei a linear function of position along the field gradient. Hence, the application of a narrow-bandwidth RF excitation pulse in the presence of the magnetic field gradient only excites spatial

regions of nuclei within the appropriate range of resonant frequency. In DRESS a magnetic field gradient is applied perpendicular to the surface coil plane. The use of a narrow-bandwidth RF excitation pulse, such as an amplitude-modulated sinc function, then has the effect of confining the signal to a plane perpendicular to the field direction and parallel to the surface coil plane. Localization of the signal within the plane is determined by the geometry of the surface coil. The thickness of the selected plane is dependent upon the magnitude of the magnetic field gradient and the bandwidth of the RF pulse.

In this technique the effects of chemical shift must be examined. Consider two compounds of the same nucleus whose resonances are separated by $\Delta\omega$ in the field B_0. The range of frequencies contained within the narrow-bandwidth RF pulse corresponds to slightly
different spatial regions for each of the two compounds. The spatial offset between the two regions is given by:

$$\Delta x = \frac{\Delta\omega}{\gamma G_x} \tag{2}$$

where G_x is the field gradient in the x direction. Clearly, the offset is minimized by using as large a field gradient as possible.

The DRESS technique makes one further modification to the surface coil method of MRS. Separate RF coils are used for excitation and receiving. The coil used for excitation is chosen to have a uniform B_1 field over the sensitive volume of the surface receiver coil. A larger surface coil can be used for the excitation. It is then possible to optimize the signal strength received from the selected plane by applying a 90° pulse to the sample. Pulse length variation, and associated signal reduction, is inevitable if the smaller surface coil is used for the excitation. The Johnson noise received from the sample is determined by the receiver coil dimensions.

Hence, this coil arrangement detects no greater noise than when a single send and receive coil is used.

VOLUME SELECTION

The first technique of volume selection was christened topical magnetic resonance (TMR)[10] and was used to collect the first human *in-vivo* NMR spectrum in 1981 from forearm muscle[11]. Static high order magnetic field gradients are superimposed upon the magnetic field B_0 to produce high field homogeneity in one region only. The signal detected from this region contains highly resolved frequency information, characterized by narrow lines in the spectrum. The detector, which may be a surface coil, also receives signals from the inhomogeneous parts of the body elsewhere. This low resolution information can be filtered out from the signal mathematically to recover the signal originating from the region of high field homogeneity only. The complex nature of the spatial variation of magnetic field means that the volume selected in this manner is irregular and not well defined. The technique is further limited by the requirement that the homogeneous region can only be produced at the centre of the main magnetic field. This makes positioning of the localized volume a difficult task. This method of spatial localization has been superseded by others and is only of historical interest.

More recently, techniques have been developed that achieve localization of the detected signal to a well defined volume, such as a cube, deep within the body. The position and size of the volume is very flexible and changes can be made without repositioning of the subject under investigation. Such methods employ pulsed field gradients that are used in MRI. As in the DRESS technique, described above, the combination of magnetic field gradients and narrow-bandwidth pulses allows the excitation of selected regions of nuclear spins. In DRESS a field gradient is applied in one dimension only, confining the signal to a plane. Field gradients applied in all three dimensions can be used to confine the signal further to a cube. NMR images of the body provide a means of identifying the region from which a spectrum is to be obtained. Then appropriate field gradients and RF pulses are used to acquire localized information from the desired location. The choice of position of the volume is, however, restricted by the sensitive volume of the receiver coil. A number of methods for achieving volume selection have been developed[12-17]. Here we restrict ourselves to the description of two techniques currently implemented on our equipment ISIS[13] and SPARS[14].

ISIS (Image Selected *In-vivo* Spectroscopy) makes use of slice selection in three orthogonal planes. A slice selective 180° pulse applied to a sample leaves the nuclear magnetization with its direction along the $-z$ axis in the selected slice and unperturbed in the $+z$ axis equilibrium direction elsewhere. Application of a non-selective 90° pulse, or detection pulse, rotates the magnetization into the xy plane across the whole sample. The magnetization then rotates in the xy plane as described previously. However, the magnetization in the selected slice

points in the opposite direction to that elsewhere in the sample. As a result there is a 180° phase difference between signals from the two regions so that signal from the selected slice contributes negatively to the total signal. A signal acquired from the same total volume, omitting the 180° slice selective pulse has positive signal contributions from the entire sample. Hence, subtraction of the signal acquired with the slice selection from that acquired without it results in the summation of signal from the selected slice and cancellation elsewhere.

In the ISIS technique this principle is extended to three dimensions to achieve cancellation in all regions except a selected cube. Three orthogonal field gradients are used to produce three selected slices whose intersection is the required cube. The three 180° slice selective pulses are applied successively before the detection pulse. The slice selective pulses can be applied in any combination, ranging from the omission of all three to the use of all three. When no slice selective pulses are applied during the preparation period, before the detection pulse, all regions within the sample contribute positively to the signal. If a single selective pulse is used, a single slice perpendicular to the appropriate field gradient contributes negative signal as above. When two or three slice selections are used, regions experiencing zero or two 180° pulses contribute positively to the signal and regions where one or three 180° pulses have been applied contribute negatively. Signals received using different permutations of the slice selective pulses can be arithmetically combined to cancel signal from everywhere except for the cube formed by the intersection of the three planes, where the signal is summed. Eight separate signal acquisitions are required to achieve this.

As with all techniques that incorporate selective excitation using magnetic field gradients, the spatial localization is a function of chemical shift as described by equation (2). In our case, a maximum magnetic field gradient of 3 mT/m means that Δx is about 1 cm for the range of phosphorus compounds at 1.5 T. Although selective 180° pulses give the optimum signal, the method of cancellation does not depend on the pulse angles used. As a result ISIS can be used in conjunction with RF coils, such as surface coils, with an inhomogeneous B_1 field.

SPARS (SPAtially Resolved Spectroscopy) uses a more complex sequence of magnetic field gradient and RF pulses to produce signals from the selected volume in each signal acquisition. In this case the method does rely on accurate pulse angles and a homogeneous B_1 field is required. Firstly, a non-selective 90° pulse is applied, rotating the magnetization into the xy plane. A combination of pulsed magnetic field gradients and a 180° RF pulse are then used to produce a phase coherence of the nuclear spins in the xy plane. It is then possible to apply a slice selective 90° pulse to rotate the spins within a given slice back along the z axis. The remaining spins in the xy plane become dephased as a result of the position dependent resonant frequency created by the magnetic field applied during the 90° selective pulse. The sequence is repeated and slice selections are performed in the other two dimensions. The

consequence of this is to produce a z magnetization in the selected cube only. A further 90° pulse is applied, rotating this z magnetization into the xy plane and producing a signal from the selected cube.

SPARS requires a longer preparation period prior to data acquisition than ISIS. As a result the application of SPARS is unsuitable for compounds with small T_2 relaxation times, when there is unacceptable loss of signal between excitation and detection. This is true of physiological phosphorus compounds where T_2 values can be as low as 10 ms.

In order to obtain phosphorus brain spectra we have made use of both of the above techniques in our MRI and spectroscopy system shown in *Figure 4*. The human subject is fitted with a phosphorus head coil that is positioned close to the head to optimize sensitivity. The subject is then placed inside the magnet with the head inside the proton imaging coil. *Figure 5* shows the position of the two RF coils during the investigation. Firstly, an image is acquired, from which the position and size of the
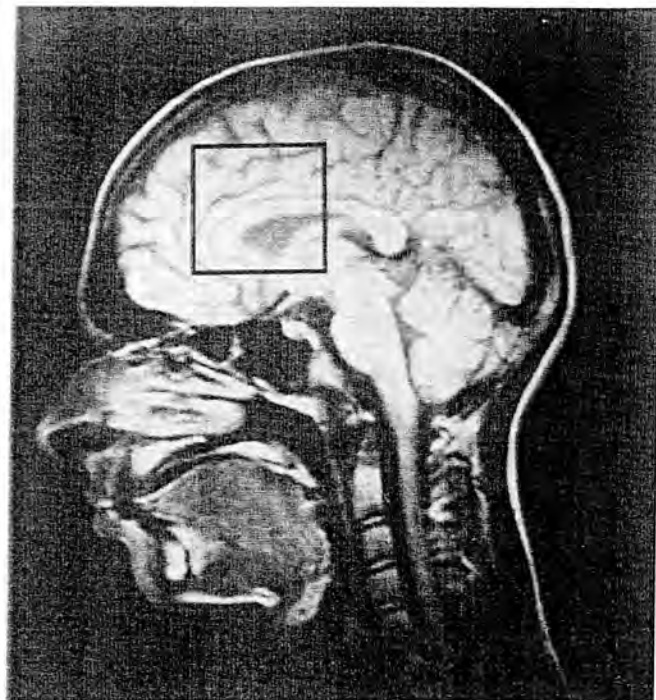
Figure 6 A magnetic resonance image is used to select a volume in the brain from which a phosphorus NMR spectrum is obtained

Figure 4 The 1.5 T Gyroscan Magnetic Resonance Imaging and Spectroscopy system manufactured by Philips Medical Systems. In the foreground the operator can be seen in front of the control console on top of which is the box used to adjust the magnet shim. Through the window can be seen the patient couch and magnet
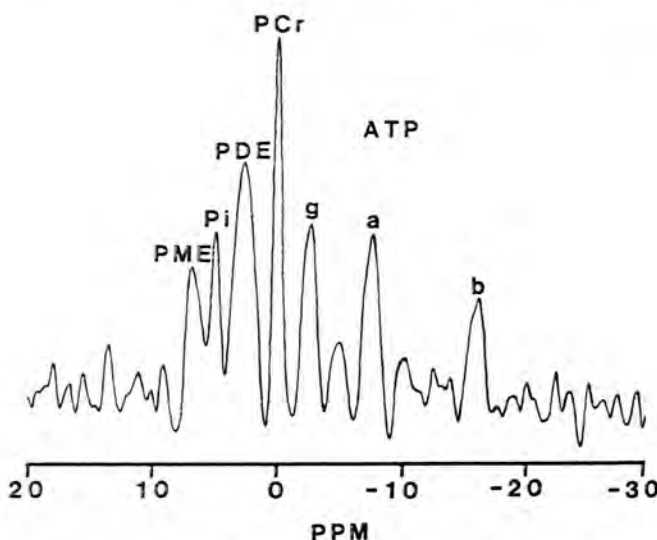

Figure 7 *In-vivo* phosphorus n.m.r. spectrum collected from the brain of a healthy volunteer. The resonances arising from the different phosphorus compounds are labelled as follows: PME, phosphomonoesters; Pi, inorganic phosphate; PDE, phosphodiesters; PCr, phosphocreatine; g, a, b ATP, gamma, alpha and beta adenosine triphosphate

Figure 5 Positioning of the RF coils about the head during acquisition of a phosphorus spectrum from the brain. The proton coil is used both to collect magnetic resonance images to identify the region of interest and to acquire localized proton signals used to shim the static magnetic field B_0

volume to be studied by MRS is determined (see *Figure 6*). The proton coil is then used to collect localized proton signals from the volume of interest using SPARS. The static magnetic field, B_0, is shimmed by varying the current through a series of resistive coils around the magnet bore until the required magnetic field homogeneity of 0.2 to 0.3 p.p.m. is obtained. ISIS is then used to collect a localized phosphorus spectrum; the phosphorus coil is used for both excitation and receiving. A phosphorus spectrum obtained from a $5 \times 5 \times 5$ cm cube in the brain of a normal volunteer is shown in *Figure 7*.

CHEMICAL SHIFT MAPPING

In chemical shift mapping, instead of collecting a single NMR spectrum from a selected region, a map is produced of the spatial distribution of each of the compounds of the nucleus under investigation. One, two and three dimensional versions have been implemented. In a one dimensional method a series of spectra are obtained from a set of parallel planes. In two dimensions an individual NMR spectrum is associated with each pixel and, in three dimensions, with each voxel.

Rotating frame zeugmatography was initially proposed as a proton imaging technique[18]. In this form the spatial distribution of water molecules is mapped, but no chemical shift information is obtained. The method has been modified to enable one-dimensional chemical shift images to be obtained from the human body[19]. A one dimensional B_1 field gradient, of duration t_1, is followed by a period, t_2, of free precession in the homogeneous static field B_0. A series of acquisitions are performed, varying t_1 each time. During the period t_1, the nuclear spins rotate in a plane containing the z axis. The total angle of the rotation during t_1 is given by equation (1). The larger the value of B_1 the higher the frequency of this rotation. Hence, for the linear B_1 field gradient, Fourier transformation with respect to t_1 yields a frequency variable f_1 which linearly describes position in the sample in a direction along the B_1 field gradient. Fourier transformation with respect to t_2 provides the chemical shift information for each of the spatial regions defined by f_1.

A second method for obtaining chemical shift images uses pulsed magnetic field gradients. After the nuclear spins have been excited into the xy plane, an applied linear magnetic field gradient makes the frequency of precession of the nuclei a linear function of position. When the field gradient is removed the frequencies of precession are equal, although a small variation exists dependent on the homogeneity of the static field B_0. However, a phase variation exists in the direction of the applied field gradient, so that the spins are phase encoded with respect to their positions. The signal is acquired, during a period of free precession t_2, after removal of the field gradient. Subsequent signals are collected using different field gradient strengths, so that the resulting phase variation has a different spatial frequency each time. If N signal acquisitions are performed, incrementing the field gradient by the same amount each time, a two dimensional data set is produced comprising the N sets of acquisition times t_2. Two dimensional Fourier transformation of this data produces both chemical shift and positional information. N spectra are produced associated with N slices perpendicular to the applied field gradient. One dimensional chemical shift imaging using phase encoding techniques was first applied to *in-vivo* animal studies in 1983[20] and *in-vivo* human phosphorus chemical shift images were obtained in 1987[21].

By using three orthogonal field gradients for phase encoding, three dimensional chemical shift images of the human body have been produced[22]. All three gradients are applied simultaneously to produce phase encoding in all three directions. The number of acquisitions performed is given by $N_x \times N_y \times N_z$, where N_i is the number of voxels in dimension i. As above the field gradients are removed before signal acquisition. Four dimensional Fourier transformation produces information in three spatial directions along with the chemical shift information. The technique has been used in conjunction with a surface coil to produce chemical shift images of phosphorus in human liver[22] with a voxel size of $2 \times 2 \times 2$ cm.

SUMMARY

MRI has many applications in medicine and would be the investigation technique of choice in a number of clinical conditions. However, the role of MRS in routine clinical practice is much less clear. Many of the above spectroscopic techniques are currently undergoing evaluation of their potential clinical applications. Of particular interest is the non-invasive monitoring of pathological conditions and their response to different therapeutic regimes rather than the use of MRS as a diagnostic tool.

ACKNOWLEDGEMENTS

REFERENCES

1. Bloch F, Hanson WW, Packard M. Nuclear induction. *Phys Rev* 1946; **69**: 127.
2. Purcell EM, Torrey HC, Pound RV. Resonance absorption by nuclear magnetic moments in a solid. *Phys Rev* 1946; **69**: 37-8.
3. Hoult DI, Busby SJW, Gadian DG, Radda GK, Richards RE, Seeley PJ. Observation of tissue metabolites using ^{31}P nuclear magnetic resonance. *Nature* 1974; **252**: 285-7.
4. Ackermann JJH, Grove TH, Wong GH, Gadian DG, Radda GK. Mapping of metabolites in whole animals by ^{31}P n.m.r. using surface coils. *Nature* 1980; **283**: 167-70.
5. Hoult DI, Richards RE. The signal-to-noise ratio of the nuclear magnetic resonance experiment. *J Mag Reson* 1976; **24**: 71-85.
6. Bottomley PA, Andrew ER. RF magnetic field penetration, phase shift and power dissipation in biological tissue: implications for n.m.r. imaging. *Phys Med Biol* 1978; **23**: 630-43.
7. Bendall MR, Gordon RE. Depth and refocusing pulses designed for multipulse n.m.r. with surface coils. *J Mag Reson* 1983; **53**: 365-85.
8. Bendall MR. Elimination of high-flux signals near surface coils and field gradient sample localization using depth pulses. *J Mag Reson* 1984; **59**: 406-29.
9. Bottomley PA, Foster TB, Darrow RD. Depth-resolved surface-coil spectroscopy (DRESS) for *in-vivo* ^{1}H, ^{31}P and ^{13}C n.m.r. *J Mag Reson* 1984; **59**: 338-42.
10. Gordon E, Hanley PE, Shaw D, Gadian DG, Radda K, Styles P, Bore PJ, Chan L. Localization of metabolites in animals using ^{31}P topical magnetic resonance. *Nature* 1980; **287**: 736-8.
11. Cresshull ID, Gordon RE, Hanley PE, *et al*. Localization of metabolites in animal and human tissue using ^{31}P topical magnetic resonance. *Bull Magnet Reson* 1980; **2**: 426.

12. Aue WP, Muller S, Cross TA, Seelig J. Volume-selective excitation: a novel approach to topical n.m.r. *J Mag Reson* 1984; **56**: 350–4.

13. Ordidge RJ, Connelly A, Lohman JAB. Image-selected *in-vivo* spectroscopy (ISIS). A new technique for spatially selective n.m.r. spectroscopy. *J Mag Reson* 1986; **66**: 283–94.

14. Luyten PR, Marien Ad JH, Sijtsma B, den Hollander JA. Solvent suppressed spatially resolved spectroscopy. An approach to high resolution n.m.r. on a whole body m.r. system. *J Mag Reson* 1986; **67**: 148–55.

15. Doddrell DM, Brooks WM, Bulsing JM, Field J, Irving G, Braddeley H. Chemical-shift-encoded excitation. SPACE, a new technique for volume-selected n.m.r. spectroscopy. *J Mag Reson* 1986; **68**: 367–72.

16. Doddrell DM, Bulsing JM, Galloway GC, Brooks WM, Field J, Irving M, Braddeley H. Discrete isolation from gradient-governed elimination of resonances. DIGGER, a new technique for *in-vivo* volume selected n.m.r. spectroscopy. *J Mag Reson* 1986; **70**: 319–26.

17. Kimmich R, Hoepfel D. Volume-selective multipulse spin-echo spectroscopy. *J Mag Reson* 1987; **72**: 379–84.

18. Hoult DI. Rotating frame zeugmatography. *J Mag Reson* 1979; **33**: 183–97.

19. Styles P, Scott CA, Radda GK. A method for localizing high resolution n.m.r. spectra from human subjects. *Mag Reson Med* 1985; **2**: 402–9.

20. Haselgrove JC, Harihara Subramanian V, Leigh JS, Gyulai L, Chance B. One-dimensional imaging of phosphorus metabolites by phosphorus-31 nuclear magnetic resonance. *Science* 1983; **220**: 1170–73.

21. Bailes DR, Bryant DJ, Bydder GM. *et al.* Localized Phosphorus-31 n.m.r. spectroscopy of normal and pathological human organs *in-vivo* using phase encoding techniques. *J Mag Reson* 1987; **74**: 158–70.

22. Bailes DR, Bryant DJ, Case HA. *et al. In-vivo* implementation of three-dimensional phase-encoded spectroscopy with a correction for field inhomogeneity. *J. Mag. Reson.* 1988; **77**: 460–70.

D.J. WEST[1]), M. TARNAWSKI[1]),
M.J. GRAVES[1]), M.G. TAYLOR[1]),
T.S. PADAYACHEE[1]),
V.T. AYTON[1]) and M.A. SMITH[1])

Blood flow imaging by magnetic resonance

Summary. The effects of motion on magnetic resonance signals have been
utilized by many workers to produce quantitative and qualitative flow
data. The Philips MR flow package is able to provide both quantitative
flow information and angiographic images of blood vessels using the same
basic pulse sequence. The authors describe the use of this package in
studies of both normal volunteers and patients, and demonstrate its
potential as an accurate, non-invasive alternative to X-ray angiography
and as a widely applicable tool for measuring in-vivo blood flow.

Atherosclerosis of major arteries is a
very common disease in the Western
world, and the biggest single killer. It
also accounts for a considerable
morbidity resulting from the ischaemic
effects on a wide variety of organs,
leading to angina, transient ischaemic
attacks, claudication, rest pain etc.
Investigation of this disease has, for
many years, relied upon X-ray
angiography which produces high
quality images of the anatomy of the
arteries under study and enables
interventional therapeutic procedures,
most notably angioplasty, to be
performed.
However, X-ray angiography has
several important drawbacks. First, it
is necessary to inject a contrast
medium into the vascular system and,
even with the new low osmolar agents,
this is uncomfortable and not without
a significant morbidity and mortality.
Secondly, the patient is exposed to
X-radiation and, thirdly, as the
femoral artery is punctured, most
angiograms necessitate an overnight
hospital stay with the associated
financial implications.
X-ray angiography has been greatly
improved by digital subtraction
techniques which allow angiography to
be performed as an out-patient
procedure using small catheters, a
lower contrast medium dose and a
possible reduction in X-radiation dose.
Nevertheless, for all this, it still
remains an unpleasant, expensive and
potentially hazardous investigation.
Duplex ultrasound offers a non-
invasive alternative with many
attractions. It is a truly non-invasive
technique, as no significant harmful
effects are known.
However, it too suffers from many
drawbacks.
Ultrasound is attenuated by gas and
bone, so that certain areas of the body
are less accessible and, although
B-scan ultrasound produces images of

vessels, the resolution is poor
compared to X-ray angiography. In
order to study a long vessel, a picture
has to be built up from several
images. Such scans are highly
operator-dependent and time
consuming, and it is sometimes
difficult to identify which vessel one is
imaging.
The volume of blood flowing per unit
of time through named arteries and to
individual organs is a very basic
physiological parameter. A non-
invasive accurate in-vivo method for
measuring blood flow would be of
great value in both clinical and
research situations. The only non-
invasive in-vivo technique at present
applied to measure blood flow
through individual arteries is Doppler
ultrasound. This has proved itself
accurate in those vessels which are
accessible to ultrasound.
However, an inherent problem in the
Doppler technique is that it does not
measure flow directly. Values for
instantaneous velocity are obtained,
which are then integrated throughout
the cardiac cycle to produce a figure
for time-averaged velocity. It is then
necessary to measure the cross-
sectional area of the vessel under
study in order to calculate flow. Thus,
this method involves several stages at
which errors may occur. The need for
accurate measurement of blood vessel
cross-sectional area is a particular
drawback as many vessels, not just

those within the head, are difficult to
image.
Other techniques have also been used
for in-vivo blood flow measurement.
For example, a limited degree of
success has been achieved using
radioactive isotopes, and quantitative
measurements from digital X-ray
angiography. However, these
techniques are invasive.
There is, therefore, a need for a rapid
non-invasive and accurate technique
for imaging the vascular system and
for performing quantitative blood flow
measurements.

MR flow techniques

Flow effects on magnetic resonance
(MR) signals have been known for
over 30 years, and no sooner had the
first magnetic resonance images of the
human body been produced than
workers in several centres were
studying ways of exploiting these
effects to produce quantitative and
qualitative information on blood flow

MR angiography

One of the attractive features of
conventional X-ray angiography is the
production of a projection image of
the contrast-filled blood vessels within
the beam.
However tortuous the vessel may be,
it will be shown throughout its length
(albeit foreshortened in places).
Attempts to provide images of the
blood vessels using MR have generally

1a

1b
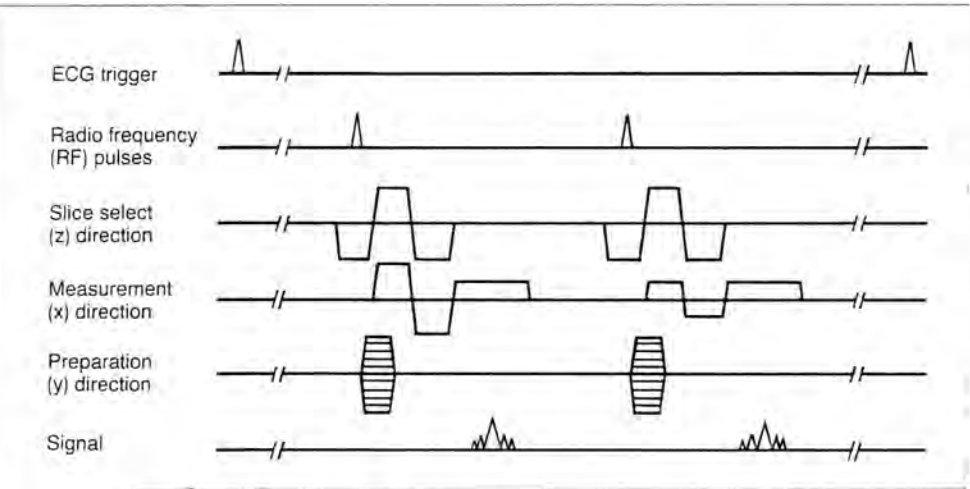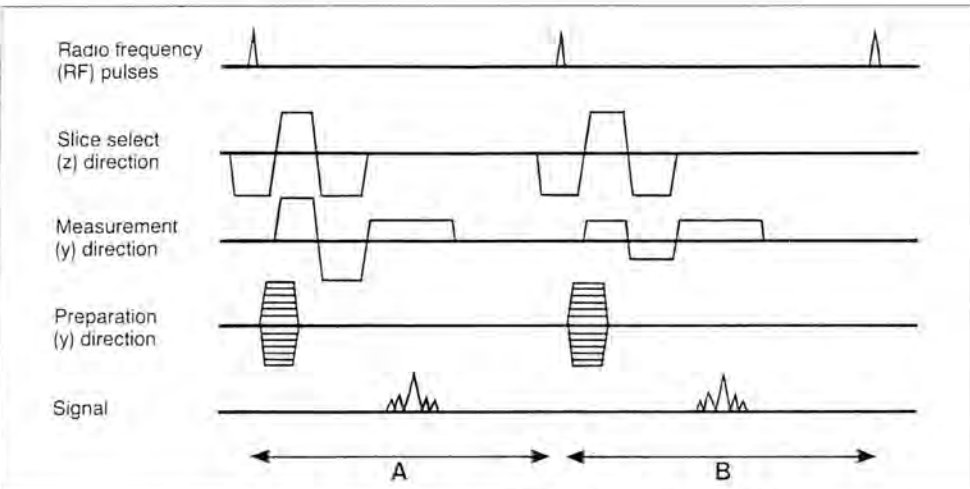
concentrated on simulating such a projection image with a section thick enough to contain all the vessels of interest. These techniques have been collectively termed *MR angiography*. The first technique of MR angiography relied on the different degrees of phase dispersion within voxels in different parts of the cardiac cycle[6,12]. Van Wedeen[13] used a conventional 2D FT spin-echo sequence. Two cardiac-triggered images were acquired: one at systole and the other at diastole. In diastole the blood flow is relatively slow, so

there was no significant phase dispersion, resulting in preservation of the signal from the slow-flowing blood. In the image acquired during systole, however, significant phase dispersion caused a reduction in the signal intensity from the more rapidly flowing blood. The signal from stationary tissue was the same in both images. Subtraction of the systolic from the diastolic image resulted in an MR angiogram.

A disadvantage of this technique is that it will only work where the flow is relatively strongly pulsatile. Vessels

in which there is a constant velocity cannot be imaged. Probably a more important disadvantage is the change in position of some vessels in different parts of the cardiac cycle. Such movement of vessels will produce registration errors when the images are subtracted. A further disadvantage is the variability in the phase dispersion at a fixed point in the cardiac cycle in a patient with vascular disease or with a variable heart rate.

The general technique of MR angiography, which overcomes the problems mentioned above, produces different velocity-dependent phase shifts in two images which can be at the same phase of the cardiac cycle. Stationary tissue will have the same phase shift in each image resulting in zero signal after subtraction. Careful choice of the imaging parameters to produce a phase shift of 180% at the peak velocity likely to be found in the region to be studied will give a maximum signal within the vessel following subtraction.

Van Wedeen et al.[14] use a subtraction of two SE sequences with an unpulsed frequency encoded gradient and different echo times. This variation of TE produces the velocity-dependent phase shift in the subtracted image. Dumoulin et al.[2] inserted an additional bi-polar pulse during the evolution period of a gradient echo sequence. Data for two images were acquired, the polarity of the additional bi-polar pulse being reversed for the second image. This reversal modulates the phase of the moving spins but has no effect on the stationary spins. Groen et al.[4] developed a sequence with the acronym FLAG (Flow Adjusted Gradients); this is the technique we use, and we shall discuss it in detail below.

MR velocity-phase maps
The technique of using MR images to

Fig. 2. MR angiogram of upper legs of normal volunteer. Note good visualization of deep and superficial femoral arteries, but motion artifact obliteration of signal within the pelvis.

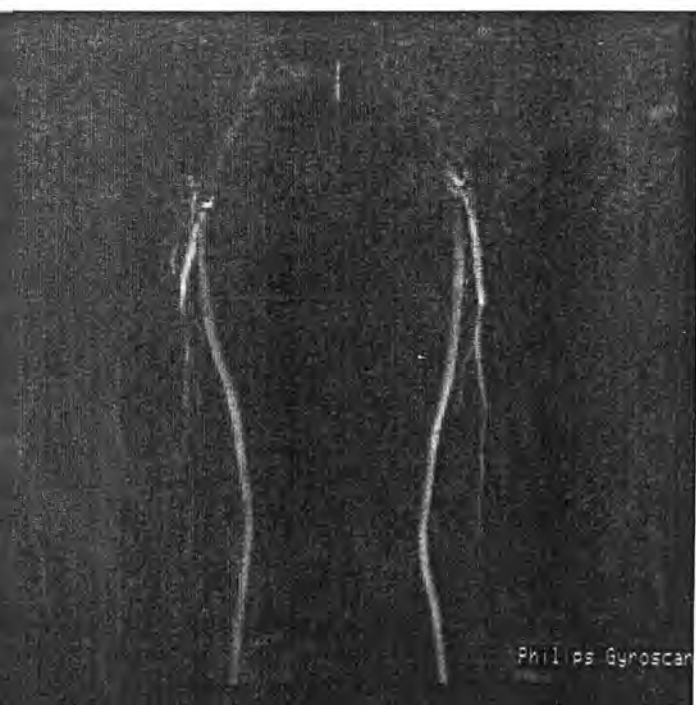Fig. 3. MR angiogram of lower legs of normal volunteer. This is a composite image taken by summing 6 images taken throughout the cycle.

antitate velocity was developed by Bryant et al.[1], Moran and Moran[7] and Van Dijk[11]. These early methods had ere limitations for clinical application, but there have ce been a number of significant advances which make 1ical use practical. Nayler et al.[8] Ridgway and Smith[9] 1 Young et al.[15] utilized a field echo to increase the 1ge of velocities that could be measured. Methods to 2rcome the phase dispersion, which can produce a loss signal, were also developed[8,9]. The technique has also :n extended to measure very slow flow[10].

=e FLAG sequence

the FLAG sequence additional bi-polar gradient pulses added to a field echo sequence to compensate for the ocity-dependent phase shifts. Two images are acquired, : where the bi-polar pulse compensates for velocity, ing zero phase change in flowing blood, and the second h the added bi-polar gradient changed in magnitude ing a velocity-dependent phase shift. For MR iography a thick section is selected and an additional llow gradient is applied in the 'slice select' direction to hase the signal from stationary tissue. Complex traction of the two images gives the required high 1al from flowing blood and zero signal from the kground. For velocity-phase maps, thin sections are

selected and the separate phase images are subtracted. The FLAG sequence is illustrated in Fig 1. In addition to the standard sequence parameters such as slice thickness, matrix size, TE flip angle etc., the following additional operator-adjustable parameters are available: cardiac triggered or continuous acquisition, direction of flow sensitivity, velocity to give the maximum signal or phase difference, and slice dephasing gradient.

Recently there have been a number of developments of the FLAG sequence. The minimum echo time has been reduced to enable thin-section phase maps of the aorta to be acquired with less signal loss; this has also improved the signal-to-noise ratio in MR angiograms.

In a further refinement of the FLAG sequence the flow-sensitive and compensated acquisitions are interleaved within the same cardiac cycle instead of at the same point in adjacent cycles. Consequently the separation is reduced from perhaps 800 ms to 50 ms, reducing the effect of extravascular motion. This technique is referred to as Rapid Sequential Excitation[5].

Our work has been carried out on a Philips Gyroscan MR system operating at 1.5T using the original FLAG sequence, the short echo modification and also the rapid sequential excitation version.

4a

4b

Fig. 4. Comparison of X-ray and MR angiograms of a patient with a block at the origin of the left peroneal artery.
a. X-ray angiogram.
b. MR angiogram demonstrating absence of flow in the left peroneal artery.

Fig. 5. MR angiogram of a patient with patent bilateral femoro-popliteal grafts.

5

MR angiography

Methods

In MR angiography, the acquisition sequence is normally synchronized to the cardiac cycle in order to obtain images at different times within the cycle. This is important in regions such as the lower limb where the flow is very pulsatile, but is not necessary in the carotid arteries where the flow is continuously present throughout the cardiac cycle. Using the standard FLAG sequence to assess flow in the lower limb arteries, we normally collect images at 6 points throughout the cycle, at 75 ms intervals starting 50 ms after the R-wave. We have found a velocity setting of 0.5 m/s to be optimal for the lower leg and cerebral circulation, and 1.0 m/s for the upper leg.

The slice thickness is selected at the minimum which ensures inclusion of all the vessels of interest. A maximum thickness of 10 cm is satisfactory in most circumstances. The direction of flow sensitivity can be set in either of the two co-ordinate axes within the slice. One direction usually suffices, but two directions are sometimes necessary if the vessels are very tortuous. The thick slice under study may be angled if necessary, which is especially useful for examinations of the carotid bifurcation. We generally use

Fig. 6. Comparison of X-ray and MR angiograms in a patient with aortobifemoral trouser graft, and a block of the left superficial femoral artery at its origin with reconstitution via collaterals from the deep femoral artery to the popliteal.
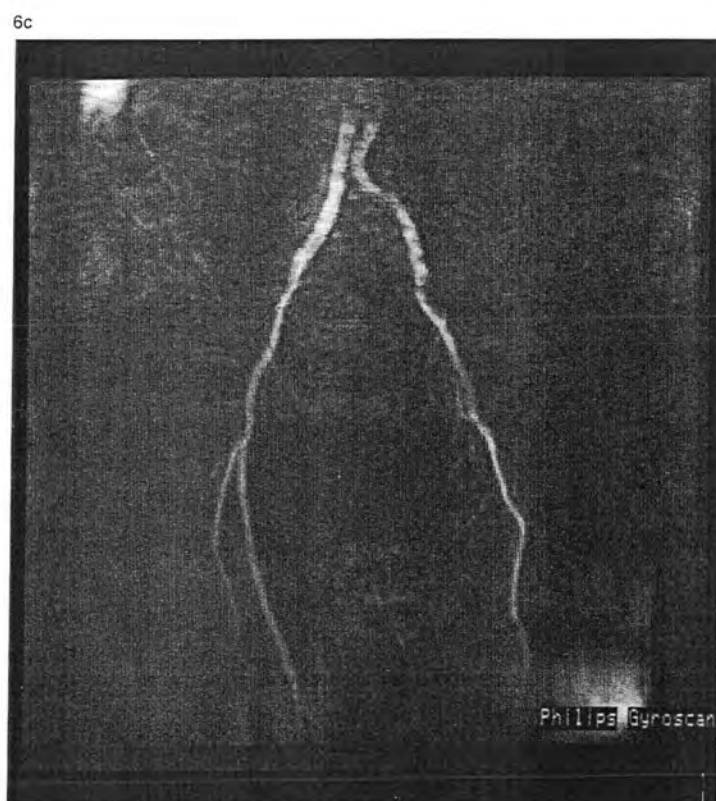a, b. X-ray angiograms.
c, d. MR angiograms.

6a

ILIACS
13-JUL-88   1

6c

Philips Gyroscan

6d

Philips Gyroscan

Fig. 7. Comparison of X-ray and MR angiograms in a patient with a block of the right superficial femoral artery at its origin, and reconstitution of the popliteal. There is also a short block of the left superficial femoral artery at the adductor hiatus.
a. X-ray angiogram.
b. MR angiogram.

Fig. 8. MR angiogram, with sagittal view of the right side of head and neck of a normal volunteer. This demonstrates the common, external and internal carotid arteries, the siphon, the vertebral and basilar arteries and the posterior superior sagittal sinus and transverse sinus.

Fig. 9. MR angiogram of the carotid bifurcation in a normal volunteer. Note the loss of signal in the bulb due to recirculation effect.

7a
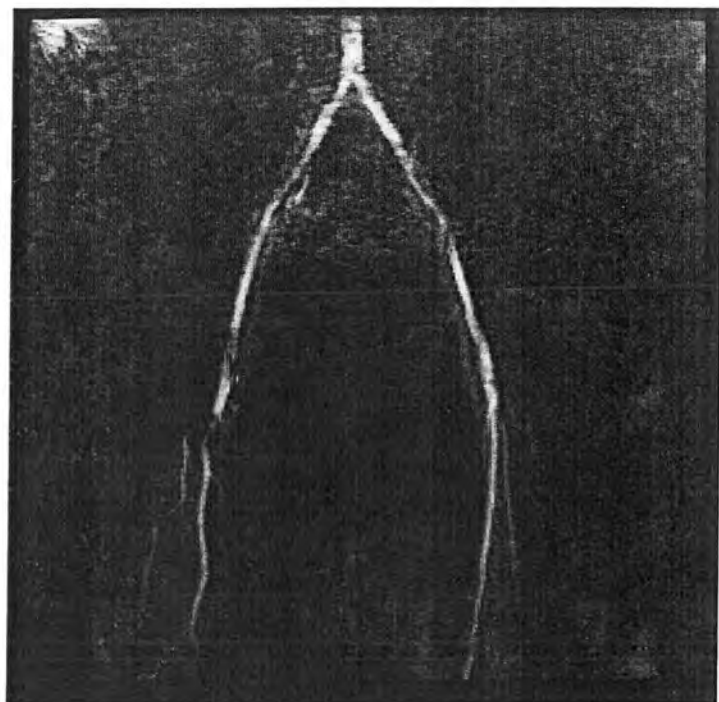
7b
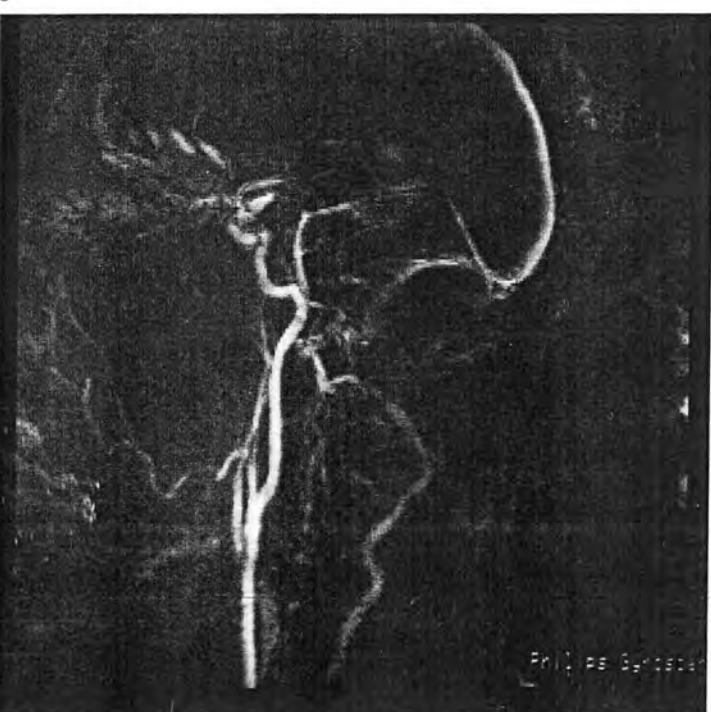
8

9

Fig. 10. Comparison of 3 cm thick midline sagittal MR angiograms in a normal volunteer and a patient with occlusion of the superior sagittal sinus:
a. MR angiogram in a normal volunteer, using velocity encoding of 25 cm per second. Note good visualization of flow in the superior sagittal sinus.
b. Same scan as Fig. 10a in a patient with occlusion of the superior sagittal sinus. Note absence of flow signal from within the sinus.

10b

matrix size of 256 x 256, a TE of 25 ms, a flip angle of ° and four measurements. A slice dephasing gradient is ed to reduce signal from stationary tissue; the magnitude this gradient depends on the thickness of the slice. vestigation of the lower limb arteries from aorta to furcation using the standard FLAG sequence takes 25 nutes for each position, the whole lower limb being vered in two positions making a total imaging time of der one hour. Untriggered angiograms of the head and :k can be obtained in under 10 minutes.

sults in the lower limb
ing the original FLAG sequence, high quality images of femoral, popliteal and lower leg vessels were obtained all normal volunteers (Figs 2, 3). The veins could be dily distinguished from the arteries by their relative ensity at different phases through the cycle and there e very few artifacts. However, as was also found by Laat[3], studies in patients were less satisfactory. The ility of the images was lower in older patients and those h more generalized disease. This is probably due to ient motion.
pite these difficulties we have obtained many

diagnostic studies, such as the example shown in Fig. 4. Particularly high quality images were obtained in a series of 10 patients with femoro-popliteal grafts. All the patent grafts were clearly shown on the MR angiograms, as illustrated in Figure 5.

The quality of the angiograms in the thigh and lower leg was improved with the use of the new sequence with a shorter TE. However, a major problem still remained, in that the abdominal aorta and iliac arteries were impossible to image adequately due to bowel and respiratory motion (Fig. 2). Rapid sequential excitation showed a dramatic improvement in the ability to image the iliac and aortic bifurcation and, for the first time, we were able to routinely visualize the lower aorta and the iliac arteries. We have now used this sequence to study several patients, with excellent results (Figs 6, 7).

Results in the head and neck
Nowadays, most carotid angiography is performed for the detection of atherosclerosis (bifurcation and siphon) or intracranial aneurysm. Non-invasive images with Doppler can compete very strongly with X-ray angiography for carotid bifurcation lesions, but cannot show concomitant

107

Fig. 11. Velocity-phase mapping.
a. *Spin echo transaxial scan through the ascending and descending aorta, used to plan for phase maps.*
b. *MR phase map corresponding to Fig. 11a. This shows a fairly uniform white signal indicating flow into the slice in the ascending aorta, and a black signal indicating flow out of the slice in the descending aorta. The background and the pulmonary artery show a mid-grey signal indicating zero flow vector within the slice.*
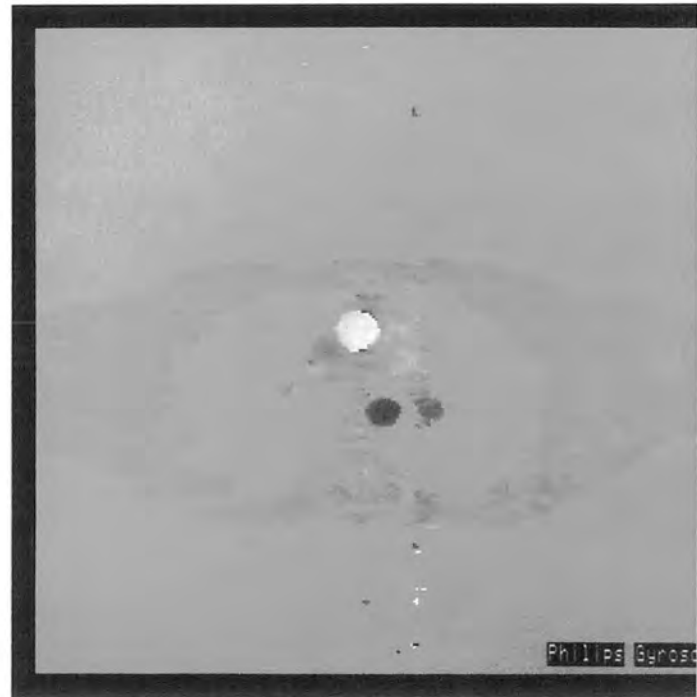**c.** *Sagittal MR phase map of ascending and descending aorta planned from Fig. 11b.*
d. *Colour coded MR phase map as in Fig. 11c, superimposed on the correspondingly orientated spin echo image.*
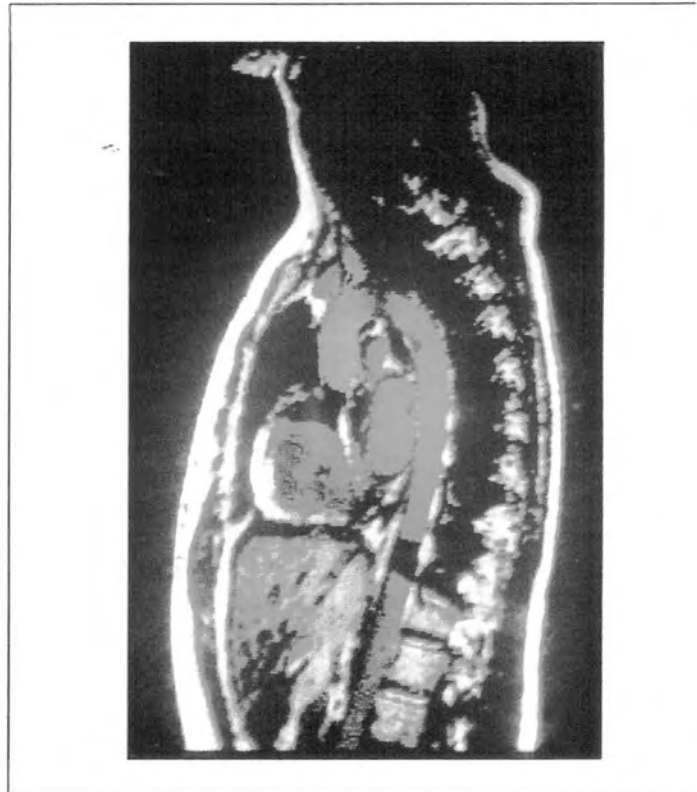
11a
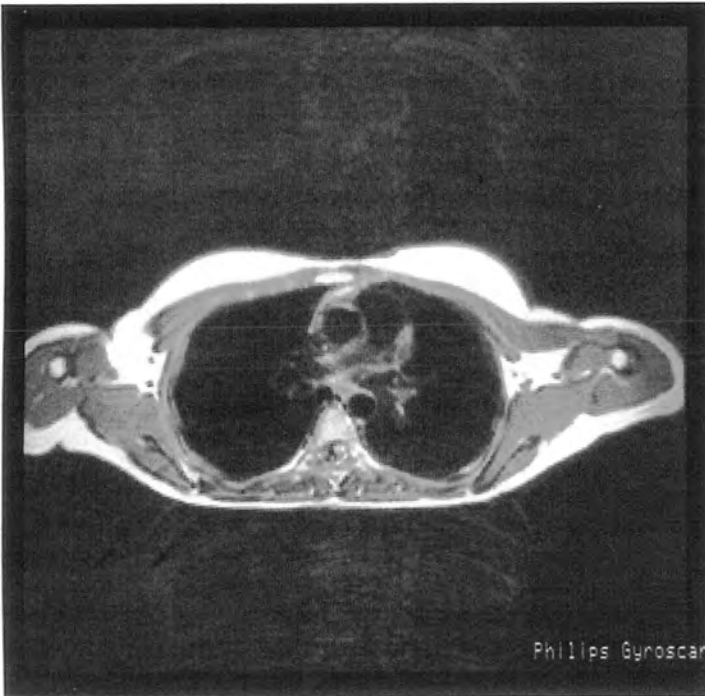
11b

11c

11d

disease of the siphon or intracranial aneurysms.
MR angiography could potentially image both areas
(Fig. 8) and has been applied to imaging the carotid
bifurcation (Fig 9). Studies in this area, however, have
been disappointing for several reasons. First, there is
confusing overlap of the signal from the jugular vein.
Secondly, the spatial resolution is not sufficient to detect
small but nevertheless important lesions and, thirdly, flow
disturbances near the carotid bulb are common, causing
signal loss even in normal volunteers.
The ability of MR to image within the skull and to obtain
flow information in two directions should allow it to be
used to produce angiograms of the intracranial vessels.
Unfortunately, however, the spatial resolution of this
system is not yet sufficient to cope adequately with the
small size of these vessels or to detect small but clinically
significant aneurysms. On the other hand, the cerebral
venous drainage is a large-volume, low-velocity system
which can be usefully imaged with MR angiography. We
have obtained high quality angiograms of the superior
sagittal sinus in normal volunteers (Fig. 10a). In two
patients with proven thrombosis of the superior sagittal
sinus we have demonstrated absence of flow (Fig 10b),
thus confirming the diagnosis which is very difficult to
make clinically, and normally requires high quality
cerebral X-ray angiography.

MR velocity-phase maps
Methods
The same pulse sequences used to produce the MR
angiograms can also be utilized to produce quantitative
phase images whereby the grey scale is proportional to the
velocity of the blood, black representing maximum flow in
one direction, and white representing maximum flow in
the opposite direction. Mid-grey represents stationary
tissue.
It is important to realize that although both the
angiograms and the velocity-phase maps are produced
using the same pulse sequence, the variable parameters and
data processing are very different so that it is not, in
practice, possible to quantitate flow from an angiographic
image.
Velocity-phase maps have potentially more clinical use
than the MR angiographic technique described above.
Unlike Doppler methods, time-averaged flow can be
determined directly by analysing a region of interest
slightly larger than the cross section of the vessel.
It is not necessary to measure the exact area of the vessel,
but only the velocity profile within it. This can then be
used to measure blood flow to individual organs. Time-
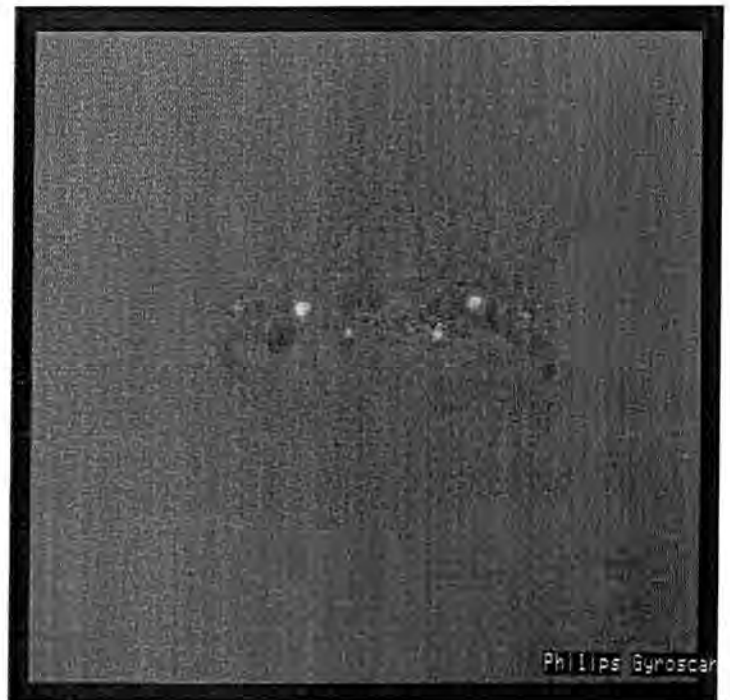
12

averaged or instantaneous velocity can be measured if
desired. Phantom experiments and comparison of our
technique with Doppler ultrasound studies in normal
volunteers have shown it to be accurate for quantifying
both time-averaged velocity and flow. Since clinically, and
in most research situations, the primary interest is in time-
averaged flow or velocity, there is no need to synchronize
the sequence to the cardiac cycle, and continuous
acquisition sequences are used in many vessels. This
significantly reduces the time needed for data acquisition
and processing – a typical study taking about 8 minutes
to acquire.

Results
Typical examples of cardiac-gated phase maps of the
thoracic aorta are shown in Figure 11b and 11c. Phase
maps can be colour coded to give more immediate visual
impact of the direction of flow and, if desired,
superimposed on standard spin echo images (Fig. 11d).
This is likely to have its most important application within
the heart to study flow disturbances arising from
congenital defects.
We have used the technique to measure blood flow in the
common and internal carotid arteries (Fig. 12), middle
cerebral artery (Fig. 13b), renal artery and femoral artery.

Fig. 13. Velocity-phase mapping of the left middle cerebral artery.
a. Sagittal field echo image perpendicular to the left middle cerebral artery before its division. This image is planned from a series of routinely orientated transaxial spin echo head scans which, in almost all cases, adequately demonstrate the course of the middle cerebral artery for planning purposes. Note the high signal in the centre of the vessel at the peak of the parabolic flow profile. Nearer the edges of the vessel there is a large variation of velocities within each voxel which produces dephasing and, therefore, loss of signal.
b. Corresponding phase map from which flow measurements are obtained.

13a
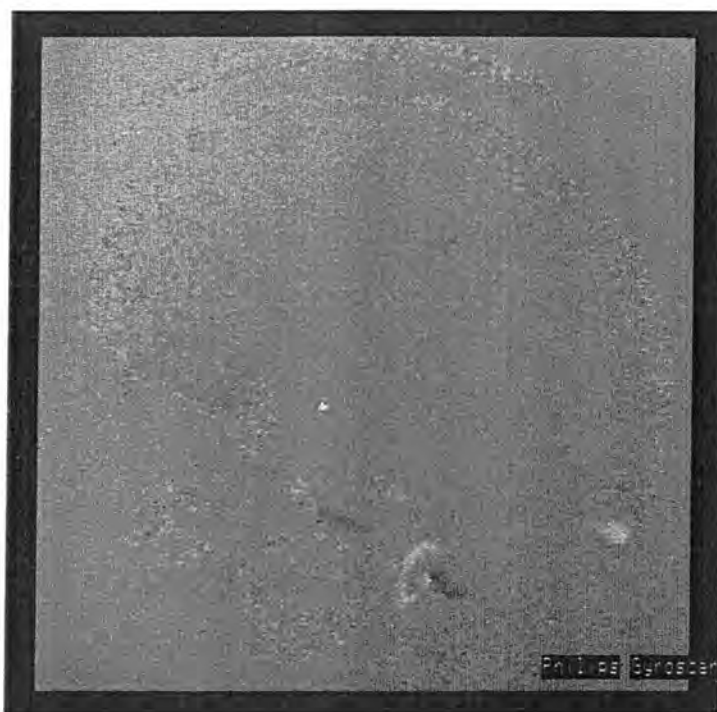
13b

Results from the carotid and femoral arteries were compared with Doppler ultrasound and good agreement was achieved.

The sensitivity of the technique to velocity changes can be of great help as an adjunct to the interpretation of MR angiographic defects. An area of signal loss on an MR angiogram can be due to a stenosis (the high velocity leading to signal loss) or an occlusion. Phase mapping can more clearly define the problem in difficult situations. (Fig. 14).

Conclusions

We now have a technique which, totally non-invasively and with no contrast medium, provides a high quality 'projective' angiogram of all the major vessels of the lower limbs in under one hour. Currently, the technique has clinical applications in the diagnosis of peripheral vascular disease and assessment of femoro-popliteal grafts. X-ray angiography will continue, however, to offer the potential for angioplastic intervention.

MR angiography has immediate application in the investigation of cerebral venous sinus disease and long term potential in the imaging of the intracranial arteries. It is unlikely to ever compete with ultrasound in the

diagnosis of disease of the carotid bifurcation.

MR phase maps can measure flow and velocity accurately and non-invasively through large and medium size vessels. There is a huge potential clinical and research application for the technique.

Fig. 14. Comparison of X-ray angiography and MR velocity-phase mapping in a patient with tight stenosis of the left external iliac artery.

a. X-ray angiogram.

b. MR thin section sagittal phase map along the left external iliac artery demonstrating very high signal at the stenosis where the velocity is very high. Note the dark signal in the iliac vein lying anterior to the artery.

a

14b
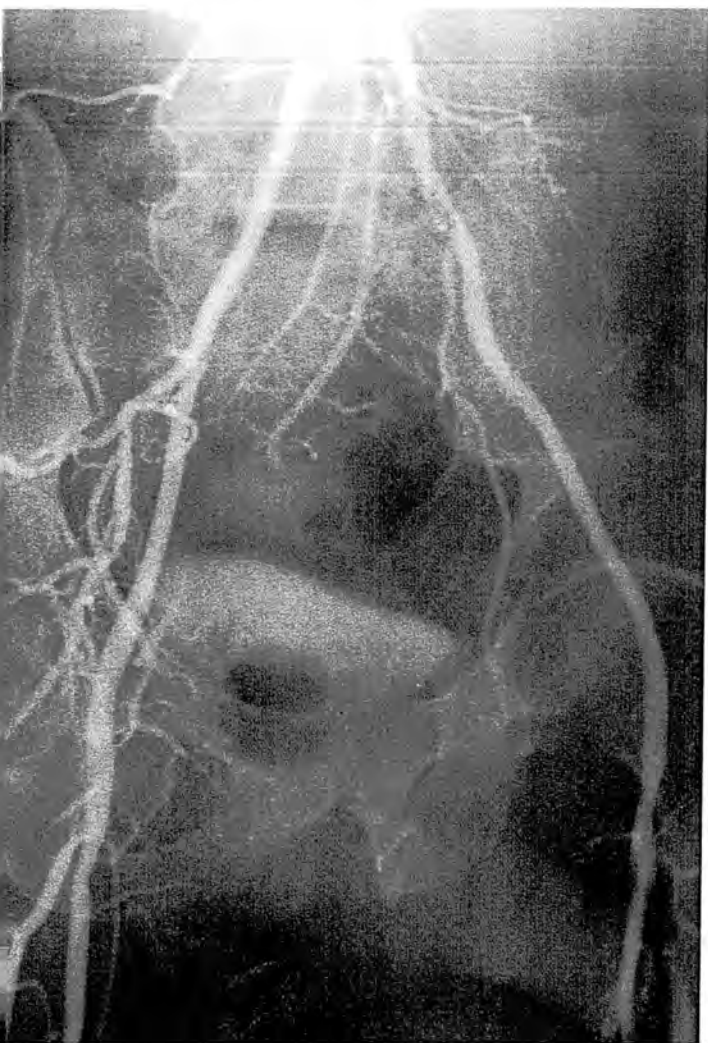
bliography

Bryant, D.J. et al., Measurement of Flow with NMR Imaging using a radient Pulse and Phase Difference Technique, J. Comp. Assist. ɔmog. 8: 588-593 (1984).

Dumoulin, C.L. and Hart, H.R., Magnetic Resonance Angiography, ɪdiology 161: 717-720 (1986).

De Laat, F.L., Vascular Imaging by MR, Digitale Bildgebende ɪrfahren, Eds. G.H. Schneider, E. Vogler, Springer-Verlag: 398 (1987).

Groen, J.P. et al., Design of Flow Adjusted Gradient Waveforms. ɔst. Soc. Mag. Res. Med. 6th Ann. Meet.: 868 (1987).

Groen, J.P. et al., MR Subtraction Angiography by Rapid Sequential citation. Poster Soc. Magn. Reson. Med. 7th Ann. Meet.: 907 (1988).

Macovski, A., A Selective Projection Imaging Application to diology and NMR, I.E.E.E. Trans. Med. Imag. 1: 42-47 (1982).

Moran, P.R. and Moran, R.A., Imaging True Motion Velocity and ᵍher Order Motion Quantities by Phase Gradient Modulation chniques in NMR Scanners, Technology of Nuclear Magnetic sonance, Ed. P.D. Esser and R.E. Johnston, Society for Nuclear ɪdicine Inc, New York, 149-163 (1984).

Nayler, G.L., Firmin, D.N. and Longmore, D.B., Blood Flow aging by Cine Magnetic Resonance, J. Comp. Assist. Tomog 10: ɪ-722 (1986).

Ridgway, J.P. and Smith, M.A., A Technique for Velocity Imaging ng MR Imaging, Brit. J. Radiol. 57: 1145-1148 (1986).

Ridgway, J.P., Turnbull, L. and Smith, M.A., Demonstration of lsatile Cerebro-Spinal Fluid Flow Using Magnetic Resonance Phase aging, Brit. J. Radiol. 60: 423-427 (1987).

Van Dijk, P., Direct Cardiac NMR Imaging of Heart Wall and ᵒd Flow Velocity, J. Comp. Assist. Tomog. 8: 588-593 (1984).

12. Van Wedeen, J. et al., Projective Imaging of Pulsatile Flow with MR, Science 230: 946-948 (1985).

13. Van Wedeen, J. et al., MR Velocity Imaging by Phase Display, J. Comp. Assist. Tomog. 9: 530-536 (1985).

14. Van Wedeen, J. et al., Projective MRI Angiography and Quantitative Flow Volume Densitometry, Mag. Res. in Med. 3: 226-241 (1986).

15. Young, I.R., Bydder, G.M. and Payne, J.A., Flow Measurement by the Development of Phase Differences During Slice Formation in MR Imaging, Mag. Res. in Med. 3: 175-179 (1986).

Technical notes

the softkeys (function keys) and would eliminate the time-consuming transfer from the asymmetrical to the symmetrical mode. If, for example, the $x1$ field wire is to be moved by a distance δx the new value for dx is $dx + \delta x$ and the couch has to be moved a distance $\delta x/2$ such that $x2$ remains constant (Fig. 1). The same would apply for the $x2$, $y1$ and $y2$ field wires.

This software modification would make it possible to alter one edge of a symmetrical field without influencing the remainder and would make a significant impact on the length of time taken to perform the simulation procedure, thereby reducing the likelihood of restlessness and subsequent patient movement.

Magnetic resonance imaging of the infant heart at 1.5 T

By M. A. Smith, BSc, MSc, PhD, *E. J. Baker, MA, MD, MRCP, V. T. Ayton, DCR(R), *J. M. Parsons, MB, BS, MRCP, *E. J. Ladusans, BSc, MRCP and M. N. Maisey, BSc, MD, FRCP, FRCR

Division of Radiological Sciences and *Department of Paediatric Cardiology, United Medical and Dental Schools of Guy's and St Thomas' Hospitals, Guy's Hospital, London Bridge, London SE1 9RT

Magnetic resonance (MR) has been found to be of value in many fields of medicine but has yet to find an established place in the study of diseases of the heart. Published studies of the heart have demonstrated its ability to identify areas of acute myocardial infarction (Been et al, 1985b) and old infarcts (Higgins et al, 1984b), to recognize hypertrophic cardiomyopathies (Been et al, 1985a), pericardial effusions (Stark et al, 1984) and constrictive pericarditis (Soulen et al, 1985). It is, in addition, possible to measure ventricular volumes (Longmore et al, 1985) and images containing blood-flow-related data can be acquired (Ridgway & Smith, 1986; Underwood et al, 1987).

Magnetic resonance imaging (MRI) has been suggested to have a particularly valuable role in the study of the anatomy of the congenitally malformed heart (Higgins et al, 1984a) and imaging studies of a limited number of cases have been published (Jacobstein et al, 1985a,b; Boxer et al, 1986; Didier & Higgins, 1986; Didier et al, 1986; Fletcher & Jacobstein, 1986; von Shulthess et al, 1986). However, in these studies from a small number of research centres there is very little experience in the use of MRI in infants. Since 90% of patients with congenital heart disease present in the first year of life (Hoffman & Christianson, 1978), if MRI is to play a role in the investigation of congenital cardiovascular abnormalities it is essential to be able to image infants within the first year.

Imaging of the heart has generally been performed using low- and medium-field strength magnetic resonance systems with a field strength of 0.6 T or less (Higgins et al, 1985; Didier et al, 1986; Smith et al, 1986; Underwood et al, 1987). Cardiac triggering poses few problems at these field strengths but it has been thought that difficulties may arise with higher-field systems at

1.5 T and above. Despite this, however, the high-field MR systems have a potentially important advantage for the study of congenital heart disease in children; the signal-to-noise ratio from these systems is higher than from low- and mid-field systems resulting in improved spatial resolution or shorter imaging times. Both these advantages are particularly valuable in the study of infants.

An alternative approach for paediatric imaging is to use the echo-planar imaging technique (Rzedzian, 1983). With this method the images can be obtained in 60–120 ms, so that patient and cardiac motion are frozen. A drawback with echo-planar imaging is that, as yet, the image quality is poorer than that obtained using triggered conventional imaging techniques at the same field strength. In addition, the technique is not generally available.

The research described in this paper set out to determine the feasibility of investigating cardiovascular abnormalities in young infants making use of the improved spatial resolution that can be obtained with a high-field MR system.

Imaging technique

The subjects were imaged using a 1.5 T whole-body MR system manufactured by Philips Medical Systems (Gyroscan). To image the heart or the great vessels, the acquisition of the MR image must be synchronized with the patient's heartbeat. To achieve this with a high-field MR system, care must be taken over the positioning of the electrodes. If the three electrodes are placed in the conventional position used for triggering in other imaging modalities, or in MRI at low- and medium-field strengths, unacceptable distortion of the electro-cardiogram (ECG) is produced. The R wave is sharply defined as required but the T-wave amplitude is greatly increased and may be the same size as the R wave, thus

Figure 1. Aortic coarctation in a 6-week-old infant. This section shows clearly the relationship of the left subclavian artery (LSA) to the stricture.

Figure 3. Infant aged 6 months with right lower lobe consolidation. This coronal image demonstrates the hyperinflated right lung with narrowing of the right main bronchus (RB), shown on subsequent images to be caused by the azygos vein and pulmonary artery.

introducing the possibility of incorrect triggering from the T wave. This distortion does not indicate a risk to the patient because it is not caused by the magnetic field disturbing the electrical conduction within the heart but by the motion of conducting material, particularly blood in the great vessels, in the high magnetic field. The distortion is reduced to an insignificant level by placing the three electrodes close together around the left nipple. Pre-gelled disposable silver/silver chloride electrodes (medicotest Q-10-A) were used and the ECG was transmitted using a telemetry system. Specialized electrodes, sometimes proposed for MRI, were not required.

The standard proton radiofrequency (RF) transmit and receive head coil was used. This is circular in cross-section with an internal diameter of 32 cm. The size and

design of the coil enabled the infant to be positioned inside without difficulty and visual contact was possible if necessary throughout the investigation.

The infant was wrapped in a blanket and placed on a thin, firm mattress, which was strapped in a semicircle round the patient to restrict movement. The majority of subjects were imaged supine. The first 12 babies to be imaged were fed immediately prior to the MRI investigation and the investigation was undertaken without sedation. However, although this procedure was successful in most cases, in some, time was needed for them to settle during the investigation and this difficulty increased as infants with more severe abnormalities were studied. Consequently, most subsequent infants were given sedation of 75 mg/kg chloral.

Simultaneous 5 mm sections were acquired using a spin–echo sequence with echo time (TE) of 30 ms and a field of view of 200–250 mm. A matrix size of 256×256 was used but with each image being constructed from 180 signals instead of the usual 256. This resulted in a reduction in scan time with only a slight reduction in

Figure 2. Aortic hypoplasia in a 12-week-old infant. The MR scan clearly demonstrates severe hypoplasia of the whole aortic arch and descending aorta without any localized narrowing. The patient's weakened medical condition and reduced lumen made her a poor candidate for X-ray angiography.

Figure 4. Congenitally corrected transposition in a 10-month-old infant. A smooth-walled anterior left ventricle (LV) and a posterior trabeculated right ventricle (RV) are shown with associated tricuspid (TV) and mitral valves (MV). Other images in the series showed the pulmonary artery arising from the left ventricle and the aorta from the right ventricle.

368

Figure 5. Tetralogy of Fallot in a 19-week-old infant. The ventricular septal defect, valve cusps of the overriding aorta and hypertrophied right ventricle are clearly seen.

spatial resolution in the phase-encoded direction. The MR system was triggered on each heartbeat, even for heart rates as high as 140 beats per minute. Once in position, a series of sections was acquired in the transverse direction from which the angles of obliquity could be obtained. Double-oblique imaging was then used to obtain the appropriate angulation, for example, through the arch and descending section of the aorta. Two signal averages were performed resulting in a typical scan time for a set of seven sections of about 6 min. The total investigation time per patient varies with the complexity of the congenital abnormality; typically, it is currently between 60 and 90 min.

Measurements were performed on a high-contrast resolution phantom and a line pair separation of 1.5 mm and 0.95 mm was obtained in the phase-encoded and frequency-encoded directions, respectively. The RF power absorption for children of different age imaged using the procedure are all below the maximum recommended specific absorption rate (SAR) with a typical value for a 6-week infant of 0.08 W/kg.

Results

The technique has been used to image over 40 infants under the age of 12 months. Electrocardiogram triggering was successfully achieved in all cases and respiratory motion artefacts were not found to be a problem. Constant observation of the patient from the end of the magnet and monitoring of the ECG ensured patient safety. In one instance, an ill, oxygen-dependent infant was imaged with the attendant clinician inside the magnet.

The technique has been successful in imaging a range of congenital disorders including coarctation of the aorta ($n = 22$), atrial and/or ventricular septal defect ($n = 14$), transposition ($n = 5$), Fallot's tetralogy ($n = 3$) and multiple cardiac defects. Images were obtained successfully from all patients and examples showing the quality of images obtained are given in Figs 1 to 5.

Discussion

The superior signal-to-noise ratio obtained with a high-field MR system enables good-quality, thin sections

to be obtained in a reasonably short time period, which we feel is particularly suitable for the investigation of cardiac disease in the infant. Imaging soon after feeding can eliminate the need for any sedation, but for reliable, rapid throughput imaging, mild sedation is required. A series of diagnostic quality images can be obtained in a sufficiently short time to enable MRI to be considered as a possible routine technique for cardiac investigation in these children. Although a rigorous comparative study with ultrasound has not yet been undertaken, our experience suggests that the amount of anatomical detail is at least equal to and generally greater than that achieved using echocardiography. In a number of cases MRI eliminated the need for an X-ray angiogram.

A study is currently in progress to determine the clinical value of MRI in congenital heart disease in infants.

References

BEEN, M., KEAN, D., SMITH, D. A., DOUGLAS, R. H. B., BEST, J. J. & MUIR, A. L., 1985a. Nuclear magnetic resonance in hypertrophic cardiomyopathy. *British Heart Journal*, 54, 48–52.

BEEN, M., SMITH, M. A., RIDGEWAY, J. P., BRYDON, J., DOUGLAS, R., KEAN, D. M., BEST, J. J. & MUIR, A. L., 1985b. Characterisation of acute myocardial infarction by gated magnetic resonance imaging. *Lancet*, ii, 348–350.

BOXER, R. A., LaCORTE, M. A., SINGH, S., COOPER, R., FISHMAN, M. C., GOLDMAN, M. & STEIN, H. L., 1986. Nuclear magnetic resonance imaging in evaluation and follow-up of children treated for coarctation of the aorta. *Journal of the American College of Cardiology*, 7, 1095–1098.

DIDIER, D. & HIGGINS, C. B., 1986. Identification and localisation of ventricular septal defects by gated magnetic resonance imaging. *American Journal of Cardiology*, 57, 1363–1368.

DIDIER, D., HIGGINS, C. B., FISCHER, M. R., OSAKI, L., SILVERMAN, N. H. & CHEITLIN, M. D., 1986. Congenital heart disease: gated MR imaging in 72 patients. *Radiology*, 158, 227–235.

FLETCHER, B. D. & JACOBSTEIN, M. D., 1986. MRI of congenital abnormalities of the great arteries. *American Journal of Roentgenology*, 146, 941–948.

HIGGINS, C. B., BYRD, B. F., FARMER, D. W., OSAKI, L., SILVERMAN, N. H. & CHEITLIN, M. D., 1984a. Magnetic resonance imaging in patients with congenital heart disease. *Circulation*, 70, 851–860.

HIGGINS, C. B., LANZER, P., STARK, D., BOTVINCK, E., SCHILLER, N. B., CROOKS, L., KAUFMAN, L. & LIPTON, M., 1984b. Imaging by nuclear magnetic resonance in patients with chronic ischaemic heart disease. *Circulation*, 69, 523–531.

HIGGINS, C. B., STARK, D. & McNAMARA, M. T., 1985. Magnetic resonance imaging of the heart: a review of the experience in 172 subjects. *Radiology*, 155, 671–679.

HOFFMANN, J. I. E. & CHRISTIANSON, R., 1978. Congenital heart disease in a cohort of 19 502 births with long-term follow-up. *American Journal of Cardiology*, 42, 641–647.

JACOBSTEIN, M. D., FLETCHER, B. D., GOLDSTEIN, S. &

RIEMENSCHNEIDER, T. A., 1985a. Magnetic resonance imaging in patients with hypoplastic right heart syndrome. *American Heart Journal, 110,* 154–158.
—— 1985b. Evaluation of atrioventricular septal defect by magnetic resonance imaging. *American Journal of Cardiology, 55,* 1158–1161.
LONGMORE, D. B., KLIPSTEIN, R. H., UNDERWOOD, S. R., FIRMIN, D. N., HOUNSFIELD, G. N., WATANABE, M., BLAND, C., FOX, K., POOLE-WILSON, P. A., REES, R. S. O., DENISON, D., MCNALLY, A. M. & BURMAN, E. D., 1985. Dimensional accuracy of magnetic resonance imaging in studies of the heart. *Lancet, i,* 1360–1362.
RIDGWAY, J. P. & SMITH, M. A., 1986. A technique for velocity imaging using magnetic resonance imaging. *British Journal of Radiology, 59,* 603–607.
RZEDZIAN, R., MANSFIELD, P., DOYLE, M., GUILFOYLE, D. N., CHAPMAN, B., COUPLAND, R. E., CHRISPIN, A. & SMALL, P., 1983. Real time nuclear magnetic resonance clinical imaging in paediatrics. *Lancet, ii,* 1281–1282.

VON SCHULTHESS, G. K., HIGHASHINO, S. M., HIGGINS, S. S., DIDIER, D., FISCHER, M. R. & HIGGINS, C. B., 1986. Coarctation of the aorta: MR imaging. *Radiology, 158,* 289–296.
SMITH, M. A., RIDGWAY, J. P., BRYDON, J. W. E., BEEN, M., DOUGLAS, R. H. B., KEAN, D. M., MUIR, A. L. & BEST, J. J. K., 1986. ECG-gated T_1 images of the heart. *Physics in Medicine and Biology, 31,* 771–778.
SOULEN, R. L., STARK, D. D. & HIGGINS, C. B., 1985. Magnetic resonance imaging of constrictive pericardial disease. *American Journal of Cardiology, 55,* 480–484.
STARK, D. D., HIGGINS, C. B., LANZER, P., LIPTON, M., SCHILLER, N., CROOKS, L. E., BOTVINCK, E. B. & KAUFMAN, L., 1984. Magnetic resonance imaging of the pericardium: normal and pathological findings. *Radiology, 150,* 469–474.
UNDERWOOD, S. R., FIRMIN, D. N., KLIPSTEIN, R. H., REES, R. S. O. & LONGMORE, D. B., 1987. Magnetic resonance velocity mapping: clinical application of a new technique. *British Heart Journal, 57,* 404–412.

Magnetic resonance imaging at a high field strength of ventricular septal defects in infants

E J BAKER, VICTORIA AYTON,* M A SMITH,* J M PARSONS, E J LADUSANS,
R H ANDERSON,† M N MAISEY,* M TYNAN, NUALA L K FAGG,‡
P E DEVERALL§

From the Departments of Paediatric Cardiology, *Radiological Sciences; §Cardiothoracic Surgery; and
‡Histopathology, Guy's Hospital; and †Cardiothoracic Institute, London

SUMMARY Magnetic resonance imaging at a high field strength has potential benefits for the study of the heart in infants, which is when most congenital heart disease presents. Seventeen infants with various anatomical types of ventricular septal defect were studied by this technique. Good quality, high resolution, images were obtained in every case. There were no major practical problems. The morphology of the defects in all 17 hearts was displayed in great detail. In some instances, the interpretation of the images resembled that of equivalent images from cross sectional echocardiography. But this new technique allowed imaging in planes that cannot be obtained by echocardiography. One particularly valuable plane gave a face on view of the inlet and trabecular components of the septum. This allowed very precise localisation of defects in these areas. The relation between the defects and the atrioventricular and arterial valves was exceptionally well shown in various different imaging planes. One patient in the series had multiple trabecular defects that were clearly shown.

Magnetic resonance imaging gives detailed morphological information about ventricular septal defects.

High resolution cross sectional imaging can provide a precise description of the morphology of defects in the ventricular septum,[1] and echocardiography is a useful investigation in patients with such defects. But newer cross sectional imaging methods have not been evaluated in the study of ventricular septal defects. Gated cardiac magnetic resonance imaging, with imaging systems of low field strength, can detect large defects in older patients.[2,3] The structural diagnosis of congenital heart defects, however, is usually made in infants.[4] This is the age group in which new imaging techniques need to be evaluated.

We studied an unselected series of infants with various types of ventricular septal defect by a magnetic resonance imaging system that operates at high field strength.

Patients and methods

PATIENTS
We studied 17 infants with ventricular septal defects

undergoing clinical assessment at Guy's Hospital (table). The selection criteria were the presence of a known ventricular septal defect and the availability of the infant for imaging. They were aged between three weeks and six months. All had a normal atrial arrangement. Nine had normal cardiac connections. In three there was a discordant ventriculoarterial connection, and one of these infants also had a discordant atrioventricular connection. Two cases had double outlet from the morphologically right ventricle, two others had pulmonary atresia, while the final patient had a common arterial trunk. One patient has since died and the heart has been examined (patient 5). Another has undergone surgical closure of the defect (patient 17).

METHODS
The imaging protocol was described in detail elsewhere.[5] In all patients an initial series of sections was acquired in the transverse plane of the body, encompassing the whole heart. Typically, this required seven sections. Subsequent imaging planes were chosen in the light of the suspected cardiac abnormality and the position and orientation of the cardiac structures as shown on these images. Imaging planes

Table   *Details of patients studied by magnetic resonance imaging at high field strength*

Case No	Age	Morphology demonstrated by magnetic resonance
1	3 mnth	Large muscular inlet defect, multiple small muscular trabecular defects
2	4 mnth	Double outlet of the morphologically right ventricle, anterior aorta, posterior pulmonary trunk overriding a perimembranous confluent defect
3	3 wk	Pulmonary atresia, aorta arising anteriorly from the right ventricle, no central pulmonary arteries, muscular outlet defect
4	4 mnth	Perimembranous confluent defect with overriding by the tricuspid valve and malalignment between the atrial septum and the trabecular ventricular septum
5	3 mnth	Double outlet of the right ventricle with the great arteries arising, side by side, the aorta to the right, complete muscular infundibulum beneath both great arteries, defect with entirely muscular margins
6	6 wk	Doubly committed juxta-arterial defect with muscular posteroinferior border, coarctation
7	4 mnth	Pulmonary atresia with central confluent pulmonary arteries; aortic valve overrides a perimembranous outlet defect
8	6 wk	Perimembranous inlet defect with accessory tricuspid valve tissue partially closing it
9	3 mth	Small perimembranous defect with accessory tricuspid valve tissue
10	1 mnth	Muscular outlet defect, complete muscular subaortic infundibulum coarctation
11	5 mnth	Discordant ventriculoarterial connection, muscular outlet defect with posterior deviation of the outlet septum and subpulmonary stenosis
12	1 mnth	Perimembranous confluent defect with overriding tricuspid valve, overriding aortic valve, and infundibular pulmonary stenosis
13	3 wk	Perimembranous defect with overriding common arterial trunk
14	2 mnth	Small perimembranous defect, coarctation
15	5 mnth	Discordant ventriculoarterial connection, muscular outlet defect
16	1 mnth	Discordant atrioventricular and ventriculoarterial connections; perimembranous outlet defect with overriding pulmonary valve
17	6 mnth	Single large muscular inlet defect

oblique in one or two axes to the standard planes of the body were used in every patient. The angles for these planes were measured individually in each patient from the earlier images. Optimum imaging of the cardiac anomaly was achieved typically in total imaging time of about 90 minutes.

Results

Images of adequate quality for morphological study were obtained in every patient. The electrocardiographic gating was also satisfactory in all instances.

Fig 1 *Magnetic resonance image of oblique coronal section in patient 1. The section includes the ventricular septum and shows multiple muscular defects (arrows), the largest being in the inlet septum. There is no defect in the outlet septum; it appears to be defective because it curves backwards out of the plane of the section.*

Fig 2 *Magnetic resonance image of oblique coronal section in patient 17. There is a single large muscular defect (arrow). The membranous septum was shown to be intact in sections orthogonal to this; because it is thin it appears to be defective in this plane.*

Fig 3 *Magnetic resonance image of oblique transverse, four chamber cut, in patient 2 showing that the defect between the ventricular inlets is perimembranous (arrow). The defect is "roofed" by the area of fibrous continuity between the atrioventricular valves, which are not offset.*
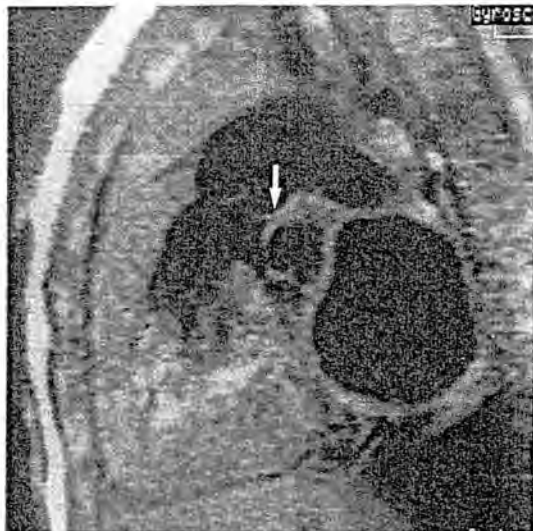
The table lists the descriptions of the morphology that were discernible from the magnetic resonance images. The morphological criteria for the description of ventricular septal defects have been described in detail elsewhere.[1] In the two patients in whom direct observation of the morphology of the defect

Fig 5 *Magnetic resonance image of oblique sagittal cut to show the septum in patient 6 who had a doubly committed juxta-arterial defect. The area of fibrous continuity between the arterial valves is clearly shown (arrow). There is some offsetting between the pulmonary and aortic valves in this section.*

was possible at necropsy or operation the magnetic resonance description of the defects was confirmed.

Although the imaging planes used in each patient were different, some general principles emerged. For

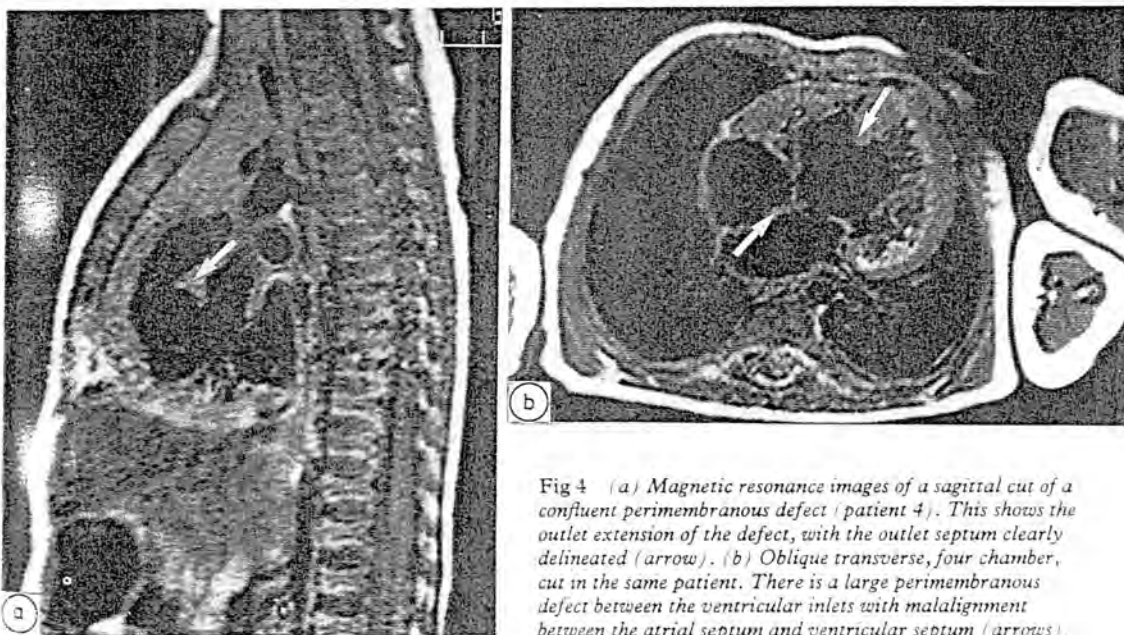Fig 4 *(a) Magnetic resonance images of a sagittal cut of a confluent perimembranous defect (patient 4). This shows the outlet extension of the defect, with the outlet septum clearly delineated (arrow). (b) Oblique transverse, four chamber, cut in the same patient. There is a large perimembranous defect between the ventricular inlets with malalignment between the atrial septum and ventricular septum (arrows).*
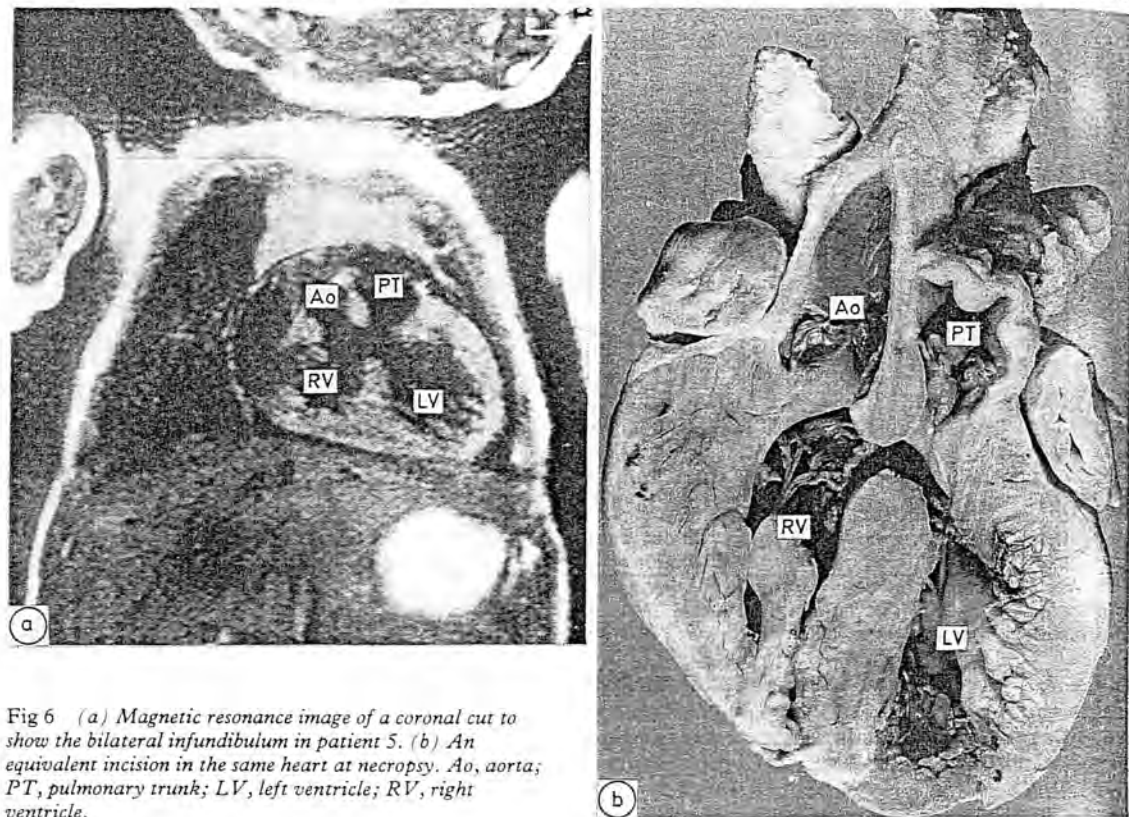
Fig 6   (a) Magnetic resonance image of a coronal cut to
show the bilateral infundibulum in patient 5. (b) An
equivalent incision in the same heart at necropsy. Ao, aorta;
PT, pulmonary trunk; LV, left ventricle; RV, right
ventricle.

instance, the oblique coronal plane was a particularly
valuable imaging plane (rotated around a vertical
axis, and also occasionally a left to right axis, in the
plane of the inlet and trabecular components of the
ventricular septum). This included a large part of the
septum within the 5 mm thick slice. This imaging
plane clearly showed the position of defects in the
inlet and trabecular septum and their relation to the
central fibrous body. This section needed careful
selection of the imaging plane and was not satisfac-
torily achieved in every patient. In patient 1, such a
section clearly showed not only a large muscular inlet
defect, but also several small muscular trabecular
defects (fig 1). In contrast, in patient 17 a similar
image showed a single large defect with entirely
muscular margins in the inlet septum (fig 2). An
oblique sagittal plane rotated around both the ver-
tical and anterioposterior axes was used to show the
ventricles in short axis. A four chamber image,
showing the inlet septum, was obtained from an
oblique transverse plane, rotated around the left to
right and anterioposterior axes (fig 3). Frequently,
even with large defects, the morphology could not be
clearly determined from standard imaging planes.

The use of oblique imaging planes individually
tailored to the morphology seen in each case was
essential (figs 4, 5, and 6). The morphology of the
ventricular septal defects studied in this series was
very varied. There was no standard imaging protocol
that would have provided the best images in every
patient.

Discussion

This series contains examples of a wide variety of
anatomical types of ventricular septal defects. In
every patient, the magnetic resonance study provided
the morphological details to define the anatomy of
the defects present. The high resolution of the images
obtained, even in these small infants, compares
favourably with those from cross sectional echocar-
diography. A unique feature of magnetic resonance
imaging is its capability to image in any plane
through the heart. There should in theory, therefore,
be no feature of the morphology of any ventricular
septal defect that cannot be determined within the
limits of resolution of the images. Further experience
will indicate whether this is indeed true. It is already

clear to us that considerable experience is required in choosing the best imaging plane in individual patients. We believe that the standard series of imaging planes that have been described by others,[6] have no place in the imaging of congenital malformations of the heart. The protocol in each patient has to be matched to the observed anatomy. This is already well established in echocardiography. The same general principles about the interpretation of cross sectional images of the heart apply to magnetic resonance images.

POSITION OF THE DEFECT IN THE VENTRICULAR SEPTUM

Magnetic resonance images in planes that are equivalent to cross sectional echocardiographic imaging planes can be interpreted by the same criteria.[1] Thus the defect can be judged as solely opening between the ventricular inlets, solely between the subarterial outlets, or extending between these areas, when they may be termed "confluent" (fig 5). Although there are no examples in this series, large isolated muscular trabecular defects should be demonstrable in such planes. In addition, we showed a new approach to imaging the ventricular septum that is exclusive to the technique of magnetic resonance imaging. Sections in the plane of, and enclosing, the inlet and trabecular components of the septum produce images comparable to seeing these areas of the septum directly. Defects in these areas can then be precisely localised.

RELATION OF THE DEFECT TO ARTERIAL VALVES

Examples of muscular, perimembranous, and doubly committed juxta-arterial defects all opening between the subarterial outlets are included in this series. The outlet septum cannot be shown face on in the same way as the inlet and trabecular components of the septum. This is because, in hearts with normal connections, the septum curves posteriorly out of the imaging plane. Despite this, extension of defects to open between the subarterial outlets was exceptionally well shown. For example, the fibrous continuity between aortic and pulmonary valve in a patient with a doubly committed defect was very clear (fig 5). A comparison of the necropsy specimen with the magnetic resonance images in a patient with a bilateral infundibulum shows how well this aspect of the anatomy was shown (fig 6). Features such as overriding of arterial valves and deviation of the outlet septum were also well shown.

RELATION OF THE DEFECT TO THE CENTRAL FIBROUS BODY AND ATRIOVENTRICULAR VALVES

The relation of defects to the central fibrous body was shown in various planes. So perimembranous defects were readily distinguished from other defects. Perimembranous defects extending into the inlet septum and roofed by the atrioventricular valves were well shown in a four chamber imaging plane. In two patients in this series such defects were associated with overriding of the tricuspid valve. This was clearly shown (fig 4). In one of these, however, there was echocardiographic evidence of additional straddling of the tension apparatus of the valve that was not evident on the magnetic resonance images.

MULTIPLE DEFECTS

In one patient in this series, the magnetic resonance images clearly showed multiple small trabecular defects in association with a large muscular defect of the inlet septum (fig 1). Only one trabecular defect was shown in this patient on both Doppler colour flow mapping and cineangiography. It is, therefore, possible that magnetic resonance imaging will prove of special value in detecting the presence of multiple defects. Great care is needed to differentiate trabeculations on the right ventricular surface of the septum from true small trabecular defects. By following the defects in contiguous sections from the cavity of the left ventricle to that of the right we were confident that in this patient they were true septal defects. If this is not always done, trabeculations will be falsely identified as septal defects.

THE PLACE OF MAGNETIC RESONANCE IMAGING

There are few practical problems with this imaging technique. The patient must be prevented from moving. We found that light sedation was sufficient for this. The infant does not suffer any discomfort during the imaging procedure and, if well prepared, will generally sleep soundly. The heart rate is constantly monitored and the patient's colour and respiratory motion can be observed from outside the magnet. Cardiac gating was a potential problem because of possible distortion of the electrocardiogram. But we have not found any major difficulty with this. Occasionally the position of the electrodes has to be adjusted to give the best signal, but we have always been able to obtain satisfactorily gating.

Magnetic resonance imaging can, therefore, provide excellent images of ventricular septal defects. Much of the information they contain is comparable with that from cross sectional echocardiography. The images, however, are of high resolution, and new imaging planes that are not possible with echocardiography can be used. This new technique enables a very detailed assessment of the morphology of ventricular septal defects to be made non-invasively. This calls into question the role of

cineangiography in the assessment of infants with ventricular septum defects.

References

1 Baker EJ, Leung MP, Anderson RH, Fischer DR, Zuberbuhler JR. The cross sectional anatomy of ventricular septal defects: a reappraisal. *Br Heart J* 1988;59:339–51.
2 Didier D, Higgins CB, Fischer MR, Osaki L, Silverman NH, Cheitlin MD. Congenital heart disease ited MR imaging in 72 patients. *Radiology* 19 158: 227–35.
3 Underwood SR, Firmin DN, Klipstein RH, Rees RSO, Longmore DB. Magnetic resonance velocity mapping: clinical application of a new technique. *Br Heart J* 1987;57:404–12.
4 Hoffman JIE, Christianson R. Congenital heart disease in a cohort of 19,502 births with long term follow up. *Am J Cardiol* 1978;42:641–7.
5 Baker EJ, Ayton V, Smith MA, *et al.* Magnetic on-ance imaging of coarctation of the aorta in infan use of a high field strength. *Br Heart J* 1989;62:97– 01.
6 Didier D, Higgins CB. Identification and localisation of ventricular septal defects by gated magnetic reson-ance imaging. *Am J Cardiol* 1986;57:1363–8.

Magnetic resonance imaging of coarctation of the aorta in infants: use of a high field strength

E J BAKER, VICTORIA AYTON,* M A SMITH,* J M PARSONS, M N MAISEY,*
E J LADUSANS, R H ANDERSON,† M TYNAN, A K YATES,‡ P B DEVERALL‡

From the Departments of Paediatric Cardiology, *Radiological Sciences, and ‡Cardiothoracic Surgery, Guy's Hospital, and †National Heart and Lung Institute, London

SUMMARY   Nineteen infants with suspected coarctation of the aorta were studied with electrocardiographically gated magnetic resonance imaging on a 1·5 T whole body imaging system. In all cases imaging was successful and produced diagnostic images of high resolution. Coarctation was shown in 12 cases. The position and shape of the coarctation were well displayed by the magnetic resonance images. In addition, they clearly showed the relation of the coarctation to arteries arising from the aortic arch and to the length and diameter of the aortic isthmus and the distal aortic arch. The anatomy was confirmed at operation in all 12 patients, except for two with a small ductus arteriosus (arterial duct), which was not seen in the magnetic resonance images. In the seven remaining patients, coarctation was excluded.

Magnetic resonance imaging produced high quality images that showed the anatomy better than other non-invasive methods. It provided all the anatomical information required for surgical correction.

Magnetic resonance has been promoted as an important advance in the imaging of congenital malformations of the heart and great vessels.[1] As yet, however, there is little evidence that it will either supplant or supplement established imaging techniques. There is no experience in very young children, the age group in which most cases of coarctation now present.[2] We report our experience of imaging the aorta in a group of infants with suspected coarctation with a high field strength magnetic resonance imaging system. The superior spatial resolution of such a system makes it particularly suitable for this age group.

Patients and methods

PATIENTS
Nineteen infants, aged between three days and 10 months, were imaged (table). In every case there was clinical or echocardiographic suspicion of coarctation of the aorta. Infants who were in severe heart failure that required intravenous inotropic support or ven-

tilation were not included; otherwise there were no selection criteria. Four of the patients studied (patients 4, 5, 6, and 10) subsequently had aortograms. Surgical correction was performed in all the cases in which coarctation was confirmed by magnetic resonance imaging.

METHODS
The infants were fed just before the imaging procedure and, if necessary, sedated with 75 mg/kg of chloral hydrate. They were imaged by a 1·5 T whole body imaging system (Gyroscan) manufactured by Philips Medical Systems. Electrocardiogram electrodes were placed closely around the left nipple, an arrangement that minimises the distortion of the electrocardiogram produced by the movement of blood within the high magnetic field. The electrocardiogram was transmitted by a telemetry system. The infants were wrapped in a blanket and their movement was restricted by a firm foam mattress curved in a semicircle around them. They were imaged while supine in a 32 cm diameter proton head coil.

Electrocardiographically gated sections (5 mm thick), separated by 0·5 mm, were simultaneously acquired by a spin echo sequence with an echo time of

Table   *Details of patients studied*

Number	Age	Anatomy shown by magnetic resonance	Surgical findings where different
1	3 wk	Discrete shelf, mild isthmal hypoplasia	Small arterial duct
2	3 wk	Waist lesion, no isthmus, mild distal arch hypoplasia	Agree
3	8 days	Discrete shelf, severe isthmal hypoplasia, patent arterial duct	Agree
4	17 days	Mild isthmal narrowing, no coarctation	—
5	6 days	Discrete shelf, anomalous right subclavian artery proximal to coarctation	Agree
6	2 mnth	Anomalous pulmonary veins to coronary sinus, coarctation excluded	—
7	5 days	No coarctation	—
8	6 wk	Discrete shelf, mild isthmal hypoplasia, ventricular septal defect	Agree
9	10 mnth	Waist lesion, no isthmus	Agree
10	3 mnth	Hypoplasia of abdominal aorta, no coarctation	—
11	3 days	Normal aortic arch	—
12	3 mnth	Discrete shelf, mild isthmal hypoplasia	Agree
13	1 mnth	No isthmus, hypoplasia of distal arch, ventricular septal defect, subaortic infundibulum	Small arterial duct
14	2 mnth	Mild isthmal hypoplasia, discrete shelf, small ventricular septal defect	Agree
15	10 days	Mild isthmal hypoplasia, no coarctation	—
16	2 mnth	Severe isthmal hypoplasia, discrete shelf	Agree
17	12 days	Normal aortic arch	—
18	7 wk	Waist lesion, hypoplasia of distal arch, no isthmus	Agree
19	6 wk	Discrete shelf, distal arch and isthmal hypoplasia	Agree

30 ms. The matrix used was 256 × 256, with a typical pixel size of 0·75 mm. To reduce acquisition time we used 180 phase encoding gradients instead of the usual 256 to produce the image. Two acquisitions of each phase encoding step were averaged. This resulted in a typical scan time for one set of seven sections of about six minutes.

In every case, the initial series of sections was in the transverse plane of the body, encompassing the structures between the arch of the aorta and the diaphragm. This, typically, required seven to nine sections. Subsequent imaging planes, oblique to the standard planes of the body, were chosen to show the area of suspected coarctation. The angles for these planes, chosen individually in each patient, were determined directly from the initial series of transverse images. The most valuable imaging plane for the aortic arch was found to be an oblique sagittal, rotated around a vertical axis, to show the aortic arch (figs 1–5). Occasionally, the imaging plane had to be additionally rotated around an anterioposterior axis to show the aortic arch optimally. A coronal plane, which showed the descending aorta, was also useful in some cases.

In all the patients with coarctation, the area of narrowing was shown in the oblique sagittal plane and at least one other plane, either the transverse or coronal. In most patients it was imaged in all three planes.

Results

Images of diagnostic quality were obtained in every patient. There were no imaging failures. In all patients the electrocardiographic gating was satisfac-
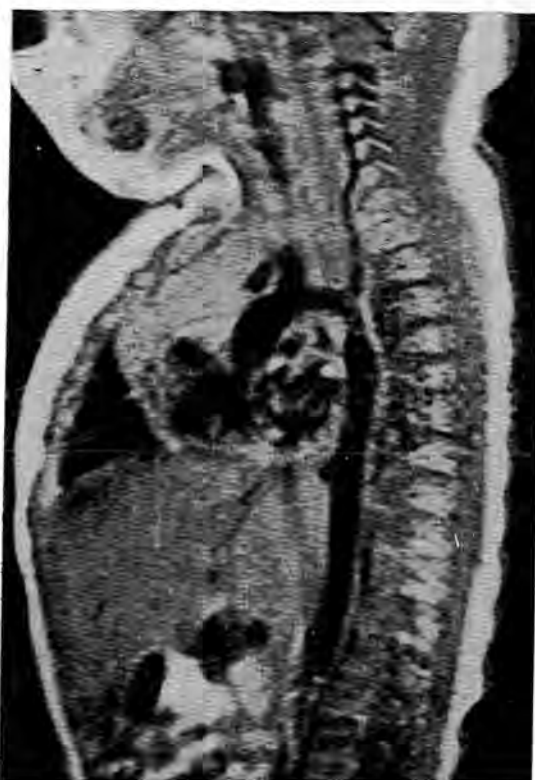

Fig 1   *A normal aortic arch in a three day old infant (patient 11). This image is in an oblique sagittal plane rotated around a vertical axis. There is some mild isthmal narrowing but no coarctation. Cross sectional echocardiography did not rule out the presence of coarctation.*
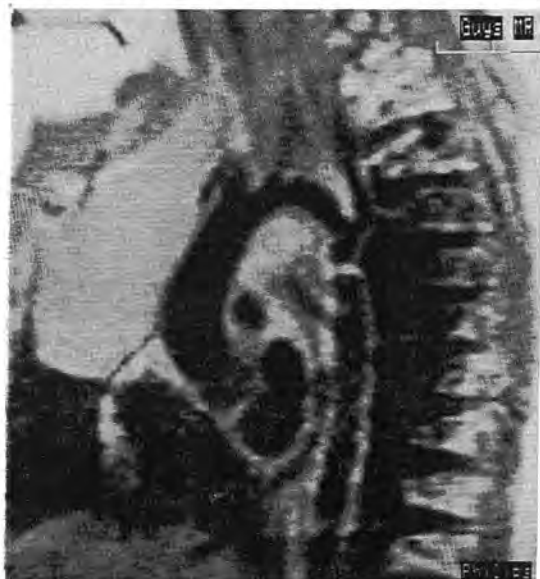
Fig 2 *An oblique sagittal section in a three month old infant with coarctation. There is a discrete shelf across the descending aorta. The length of the aortic isthmus and the relation of the coarctation to the left subclavian artery is clearly seen. There is only very mild isthmal hypoplasia.*
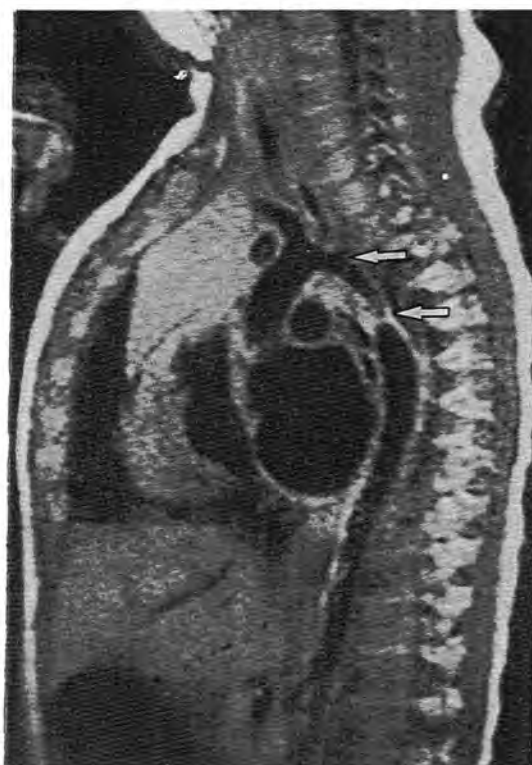

Fig 3 *An oblique sagittal section in another patient aged 10 months with coarctation. In contrast with the anatomy in figure 2, there is a waist like narrowing of the descending aorta. The origin of the left subclavian artery arises at the level of the coarctation and so there is no isthmus.*

Fig 4 *An oblique sagittal section in an infant with a very long, hypoplastic isthmus (between the arrows). The coarctation forms a discrete shelf rather than a waist.*

tory. The diagnosis of coarctation was confirmed in 12 infants. It was excluded in seven. In the first case in which it was excluded (patient 4), we lacked experience in interpreting the magnetic resonance images and so the clinical picture prompted investigation by angiography. The aortogram confirmed normal aortic anatomy. In all the subsequent cases the diagnosis based on magnetic resonance imaging was accepted. Angiography was performed in two other negative cases (patients 6 and 10) to define aspects of the cardiac anatomy other than the aortic arch. In one positive case the arrangement of the branches of the aortic arch was unclear. An aortogram was performed before surgical correction to clarify this. The right subclavian artery arose anomalously just proximal to the coarctation and, in retrospect, this could be seen in the coronal images of the coarctation in this patient. In all the remaining positive cases, surgical correction was performed without further investigation.

Surgical correction confirmed the anatomy in all the patients with coarctation. But in two patients small arterial ducts (ductus arteriosus) were found at
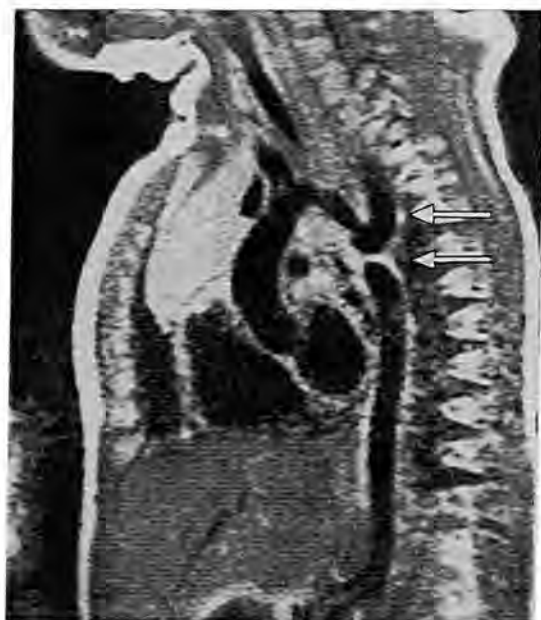
Fig 5 *An oblique sagittal section in an infant with coarctation in the form of a shelf (lower arrow). There is no isthmus and a dilated left subclavian artery (upper arrow) can be seen arising just proximal to the shelf. In this case there is considerable hypoplasia of the distal aortic arch proximal to the origin of the left subclavian artery.*

operation that were not seen in the magnetic resonance images. In practice this was not of clinical importance. In one patient a large arterial duct was shown by magnetic resonance imaging (case 3).

The presence or absence of obstruction in the thoracic aorta could invariably be shown in the initial transverse series of images. Further oblique sagittal images were, however, obtained in all cases to display the anatomy of the aortic arch clearly. From such images the diameter and length of the aortic isthmus were evident. The coarctation shelf, itself, gave a very intense magnetic resonance signal in these T1 weighted images. Images obtained in the coronal plane were valuable in defining the relation of the coarctation to the vessels arising from the aortic arch, particularly the left subclavian artery.

Discussion

To date magnetic resonance imaging of the heart has generally been performed with systems that use low and medium field strengths, $\leqslant 0.6$ T.[3 4] It was thought that it would be difficult to achieve cardiac gating in strong magnetic fields such as 1.5 T. This is because the electrocardiographic signal is distorted by the flow of blood in the high magnetic field. But

the newer, high field strength imaging systems have a potentially important advantage for the study of congenital heart disease. The signal to noise ratio from these systems is considerably better than from those that use low and medium strength fields and so a more favourable compromise between spatial resolution and imaging time can be achieved. These advantages are especially valuable when infants are studied. A major criticism of published reports is that there is almost no experience in the use of gated magnetic resonance cardiac imaging in infants. Indeed, most workers specifically avoided imaging in this age group. Because almost all patients with congenital heart disease present in the first year of life,[2] the anatomical diagnosis of cardiac defects is now generally performed in infancy. An imaging technique, to be of value, must be capable of producing high quality images in this age group.

As we have shown, magnetic resonance images can define the position of the coarctation in the aortic arch, its relation to the arterial duct and the arteries arising from the arch, the length and diameter of the aortic isthmus, and whether the coarctation is a discrete shelf or a waist lesion.[5] Identification of the coarctation is greatly helped by the intensity of the signal from the shelf itself. In infants, this is usually made up of tissue originating from the arterial duct (ductus arteriosus).[6] We always made certain that the shelf could be seen in images in at least two different planes, thus ensuring it was not an artefact produced by the oblique transection of the aorta. In practice, this does not seem to be a problem. In none of our normal patients were the appearances of the aortic arch ambiguous.

We believe that our experience shows that high field strength magnetic resonance imaging can consistently produce high resolution cardiac images in infants. In this series, we have shown that it is possible, with great clarity, to image the aortic arch. The images were of much higher resolution than those obtained with cross sectional echocardiography.[7] In addition, magnetic resonance imaging is non-invasive and safe. It does not use any ionising radiation. It provides all the anatomical information required for surgical repair of the anomaly. It thus has many advantages for studying this age group. Its clinical role requires further evaluation.

References

1 Didier D, Higgins CB, Fischer MR, Osaki L, Silverman

NH, Cheitlin MD. Congenital heart disease: gated MR imaging in 72 patients. *Radiology* 1986;158: 227–35.

2 Hoffman JIE, Christianson R. Congenital heart disease in a cohort of 19,502 births with long term follow up. *Am J Cardiol* 1978;42:641–7.

3 Boxer RA, LaCorte M, Singh S, *et al*. Nuclear magnetic resonance imaging in evaluation and follow-up of children treated for coarctation of the aorta. *J Am Coll Cardiol* 1986;7:1095–8.

4 von Shulthess GK, Higashino SM, Higgins SS, Didier D, Fischer MR, Higgins CB. Coarctation of the aorta:

MR imaging. *Radiology* 1986;158:289–96.

5 Sinha SN, Kardatzke ML, Cole RB, Muster AJ, Wessel HU, Paul MH. Coarctation of the aorta in infancy. *Circulation* 1969;40:385–98.

6 Elzenga NJ, Gittenberger-de Groot AC, Oppenheimer-Dekker A. Coarctation and other obstructive aortic arch anomalies: their relationship to the ductus arteriosus. *Int J Cardiol* 1986;13:289–308.

7 Smallhorn JF, Huhta JC, Adams PA, Anderson RH, Wilkinson JL, Macartney FJ. Cross-sectional echocardiographic assessment of coarctation in the sick neonate and infant. *Br Heart J* 1983;50:349–61.

Magnetic Resonance Imaging of the Brain in Alcoholics: Cerebral Atrophy, Lifetime Alcohol Consumption, and Cognitive Deficits

J. D. Chick, M. A. Smith, H. M. Engleman, D. M. Kean, A. J. Mander, R. H. B. Douglas, and J. J. K. Best

Magnetic resonance imaging of the brain in 69 detoxified alcoholics revealed that relaxation time (T_1) in whole brain and in grey matter and parietal white matter was greater than in age-matched controls. In 48 patients, data on cognitive function and lifetime alcohol consumption were available. With age-controlled, lifetime consumption, and impairment on performance in the cognitive test (a Category Sorting Test) correlated positively with T_1 in whole brain and in selected regions. Impairment in the cognitive test correlated with increased T_1 in whole brain and white matter independently of cerebral atrophy. Alcohol consumption patterns in the following 6 months were unrelated to changes in T_1. The excess water implied by the elevated T_1 values may be intra- or extracellular. It is uncertain whether or not T_1 elevation in alcoholics is a marker of neuronal damage. T_1 elevation appears to be a marker of one type of alcohol-related cognitive impairment.

$\mathbf{E}$ XCESSIVE DRINKING is associated with impaired cognition.[1] There is evidence in some drinkers that a defect in cognition predates the heavy drinking.[2] However, improvements in cognition occur in some alcoholics who become abstinent.[1,3] Also indicators of predrinking intelligence such as early academic attainment and retained verbal skills suggest that the excessive drinking is at least as much a cause of certain types of cognitive impairment as a consequence thereof.[1,2]

Brain shrinkage is also well established,[4,5] and modest correlations between measures of shrinkage (especially central shrinkage) and cognitive impairment have been found.[1,3] The cause of this shrinkage is unknown. However, the cerebellar atrophy of alcoholism is due at least in part to neuronal death.[6] Neuronal death may contribute to the cerebral shrinkage of the alcoholic, a possibility that was raised over 80 years ago.[7] Animal studies have shown that ethanol consumption can cause nerve cell dysfunction and death.[8–11]

A potential marker of nerve cell death in alcoholic patients is, of course, the shrinkage visible in computer tomographic (CT) scans. However, a search for another marker seems justified since the correlations between cognitive impairment indices and CT measurements is, as mentioned, modest at best. An alternative marker might be provided by magnetic resonance imaging (MRI) of the brain. Furthermore, the observation that the histology of neuronal death may show *oedematous* cells[12] suggests a particular importance for MRI.

In magnetic resonance imaging of living tissue the parameter known as T_1 relaxation time is related to the state of water in the tissue.[13] The T_1 value, measured in milliseconds, increases as the proportion of free to bound water within the tissue increases. MRI scanning of brain in the intact patient before neurosurgery has shown that in vivo T_1 measurements predict the degree of brain hydration.[14] Besson et al.[15] were the first to report brain T_1 measurements in a small group of alcoholics but reported only on change in the phase immediately after cessation of alcohol intake.

The present study had four hypotheses: (*a*) that the detoxified alcoholic brain some 2 weeks after the last drink would be overhydrated compared to age and sex matched non-alcoholics; (*b*) that in detoxified alcoholics the degree of overhydration in the brain would be related to the total lifetime consumption of alcohol; (*c*) that this overhydration would predict cognitive impairment; (*d*) that extended abstinence in the posttreatment phase would be associated with reduction of overhydration and improvement in cognitive functioning.

SUBJECTS AND METHODS

Alcoholic patients admitted for detoxification to the Alcohol Problems Clinic at the Royal Edinburgh Hospital were fully informed about the purpose and procedures of the study and invited to participate. Signed consent was obtained. The project was approved by the appropriate Ethics of Research Committee.

Hypothesis 1

Sixty-nine patients (46 males, 23 females) were scanned at the end of detoxification—a mean interval of 14 days after the last alcoholic drink. These 69 patients had a minimum of 5 years of recent heavy drinking. Their mean age was 44 years (range, 22–70; SE, 1.16). None had the clinical features of Wernicke-Korsakoff syndrome, had a history of drug abuse, were clinically malnourished, or had physical disorders other than raised serum liver enzymes. They had all been drinking at least 130 g of ethanol per day during drinking episodes. In Britain, a "standard drink," i.e., a half pint of beer, a glass of wine, or a single measure of spirits, contains 8–9 g ethanol. They spanned the range of socioeconomic

backgrounds, and though half were unemployed none were without a fixed address.

Hypotheses 2, 3, and 4

A subgroup of 48 of the above patients (32 males 16 females) was invited to have cognitive testing and to attend for repeat MRI scans and cognitive testing at 6 months, (though in the event only 26 patients kept the following appointments for both scans and testing). These patients were selected on the basis of their willingness and likely ability to attend for further testing. Their mean age was 44 years (range, 22–70; SE, 1.36). They had mean red cell volumes ranging from 88 to 111 fl (mean, 98.9; SE, 0.98; $n = 42$) and serum γ-glutamyl transpeptidase (GGT) values ranging from 5 to 1000 units (median, 100; mean, 217; SE, 42; $n = 43$). The consumption pattern of this group was studied in more detail. They were asked to give anchor dates throughout their adult lives and commencing with the year in which they first drank alcohol, to reconstruct their typical pattern of drinking month by month during each of the succeeding years. The method is based on that of Skinner and Sheu.[16] Thus an estimate was obtained of cumulative total lifetime alcohol consumption. Inter-rater reliability of this method in 10 patients whose responses were rated by two independent assessors showed an average agreement between assessors of 87%. (Taking the past year's consumption enabled some of the relationships of interest to be analyzed using a recent, rather than a lifetime consumption measure. However, to reduce the total number of tests of significance made, it was decided to concentrate on our cumulative lifetime measure of consumption).

Normal MRI values were available from a group ($n = 26$) recruited from hospital staff and patients' relatives. Their usual alcohol consumption ranged from nil to 80 g ethanol per week. Their ages ranged from 23 to 74 years with a mean of 42 years, and a similar distribution to that of the patients. The ratio of women to men in the normal sample was 14 males to 12 females, that is, a higher proportion of women than in the patients. However a two-tailed t test of the differences in the females and males of the control group found that there were no significant differences in their whole brain T_1 measurements ($p = 0.88$) so the differences in the proportions of the sexes in the control and the alcoholic samples are not considered to be of importance. They may have been of slightly higher mean socioeconomic status than the patients but this was not thought likely to bias the results, though no study of MRI and socioeconomic status has to our knowledge been reported.

Our index of cognitive function was the microcomputer-administered Maudsley Category Sorting Test.[17,18] This provides a measure of abstract reasoning ability and rigidity of thought processes and it is of interest because rigidity of thinking in alcoholics is a major impediment in the psychological treatment of the condition. The subject is required to deduce the categorization system being used by the computer program and to shift his or her set when the program changes. The program offers six different methods and the number of times out of six in which the subject correctly arrives at the solution is counted (CATEGORIES). The number of trials needed to achieve that number of correct solutions is counted (SORTS). The total number of errors made is summed (ERRORS). The number of perseverative errors (errors repeated despite feedback from the program) is totalled (PERSEVERATIONS). We have concentrated on the Category Sorting Test because it has been shown that deficits in this type of function correlate well with CT parameters of atrophy,[19] and are common to both older and younger alcoholics whereas impairments on tests of memory and general intellect tend to be seen only in older patients.[3]

Alcohol consumption in the follow-up period was estimated from the clinic treatment records, and interviews with the patient conducted by a research assistant at 3 months and 6 months. This information was corroborated where possible by an additional interview with a relative and by changes in the serum GGT in those patients who had an elevation of this marker[20] at intake to the study. For some patients only a qualitative report on consumption was available. Patients were categorized as follows for each of the 3-month period: total abstinence; "intermediate" drinking (1–40 g per day); "heavy" drinking (over 40 g per day).

MRI measurements were performed using a 0.08 Tesla-resistive MRI system.[21] Three or four transverse sections were obtained through the brain centered to the maximum diameter of the lateral ventricles. The slice thickness was 12 mm and pixel size was 2 x 2 mm. An interleaved saturation recovery and inversion recovery pulse sequence, with a repetition time of 1000 ms for both and a time from inversion of 200 ms for the latter, was used to obtain a calculated T_1 map of each section. Measurements of the patient's brain T_1 were made from a section approximately 10 mm above the maximum diameter of the lateral ventricles. The T_1 in grey and white matter in the frontal and parietal regions was measured from the T_1 map using small regions of interest generated by the computer. Different size regions of interest were used for grey matter (20 mm^2) and for white matter (69 mm^2) and the mean of similar regions in the left and right hemisphere was noted. Larger irregular regions of interest were also measured to attain mean T_1 values of each cerebral hemisphere. To achieve this an electronic cursor was used to delineate the border of each hemisphere directly on the computer-reconstructed image of the brain as displayed on the monitor. Obvious areas of CSF (which have a very high T_1 and appear white on the coloured image) were avoided. As a further precaution to exclude CSF, the computer was programmed to display the mean T_1 for each hemisphere only for values within the range 60–600 ms. An example of a T_1 map in a patient including the regions of interest used for analysis is shown in Fig. 1.

The precision of the T_1 measurements was estimated from four repeated measurements on three normal volunteers over a period of a month. The T_1 precision of white matter was 2.8%, grey matter was 4.9%, and the whole brain 2.6%.[22] The poorer precision of the measurements of grey matter are due to the fact that it is generally of small volume and adjacent to CSF resulting in partial volume errors. In addition smaller regions of interest are used resulting in a larger error. The interoperator variation of our T_1 measurements was assessed in two independent operators in 20 sections from five different patients. The percentage differences between rates were: whole brain 1.9%; frontal, occipital, and parietal white matter 2.5%; temporal white matter 5.2%; grey matter (all areas) 5.5%. All ratings were blind to the clinical state of the patient, consumption measures, and cognitive test scores. However, control scans were identified as such, and dates of all scans were also known to the raters. T_1 maps were analyzed by three operators; results from the same patient were always analyzed by the same operator.

Atrophy Measurements

Commonly used indices of cerebral atrophy[23] were made by caliper measurement on MRI scans: (a) *Third ventricle*, widest diameter; (b)
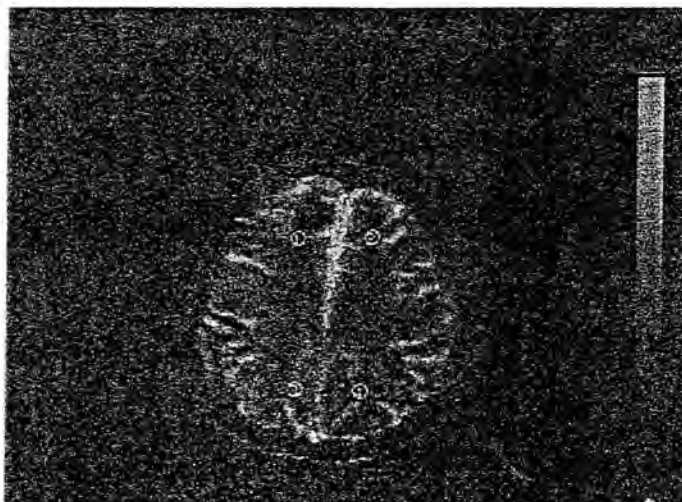

Fig. 1. An example of an MRI scan in a patient indicating region of interest marker.

The Ventricular Index, the distance between the choroid plexuses divided by the maximum width between the frontal horns; (c) *The Huckmann Index*, the sum of the maximum and minimum widths of the frontal horns; and (d) *The mean width of four cortical sulci* was measured on a slice 16 mm above the upper limit of the lateral ventricles, choosing the two widest sulci on each side.

As an attempt at assessing the reliability of these measures in our hands, we checked the correlations between the indices of internal atrophy. The Huckmann index correlated $r = 0.33$ ($p < 0.05$) with the ventricular index and $r = 0.47$ ($p < 0.01$) with "3rd ventricle" ($n = 46$).

Differences in T_1 values within groups of patients at different times were compared using Student's t test. Changes in T_1 were assessed using a paired Student's t test. The relationship between changes in T_1 values, drinking and changes in cognitive function were assessed using linear regression analysis. Partial correlation analysis was used to investigate the relationship between cognitive function and T_1 value and cognitive function and previous drinking history to control for the effect of age and atrophy.

RESULTS

The T_1 values obtained from the patients at 2 weeks and 6 months are given in Table 1 with the results from normal controls for comparison. The most pronounced differences between normals and alcoholic patients are seen in the whole brain and in grey matter T_1 values.

Relationship between T_1, Age, and Alcohol Consumption

In the subgroup studied intensively the mean lifetime drinking total was 775×10^3 g (SE, 104×10^3; range, 71×10^3–3329×10^3). The T_1 values at the time of the first scan correlated positively with the patient's age, significantly so in frontal white matter ($r = 0.49$, $p < 0.01$) and in posterior white matter ($r = 0.41$, $p < 0.05$). Eliminating the effect of age using partial correlation, a significant positive correlation was found between whole brain T_1 in the detoxified patient and the patient's cumulative total life's consumption $r = 0.36$, ($p < 0.01$). (The past year's consumption, which not unexpectedly correlated significantly with lifetime consumption, correlated positively

with parietal white matter T_1 but not significantly w whole brain T_1). ($n = 47$).

Relationship between T_1 and Cognitive Impairment

In the alcoholics given cognitive testing, impairment each of the scores on the Category Sorting Test was relat to an increase in T_1 in all regions of the brain. The findin are shown in Table 2. The effect of age has been controll for. Correlations of each of the test measures with who brain T_1 and with frontal white T_1 were significant either the 99% or 95% levels. The relationships remain significant when the sexes were examined separately. Bo lifetime consumption and past year's consumption cor lated significantly with each of the test measures with a controlled.

Role of Atrophy

Table 3 shows that internal atrophy as measured by t Huckmann index appears to be associated with increase T_1 in white matter, and with impairment in the numb of categories achieved in the sorting test. However, b chance, in the 36 correlations shown in Table 3, tw would be significant at the 5% level.

There is little evidence of a relationship between oth measures of atrophy and either T_1 values or cognitive te impairment. However, the correlation of 0.26 betwee sulcal width and T_1 in frontal grey matter is probabl meaningful in that when patients are divided about th median for sulcal width, the T_1 (frontal grey) is 10 poin higher for those with sulcal width above the median tha for those below the median ($t = 3.3$, $p < 0.01$). Th supports the possibility that CSF in the subarachno space, increased in cortical atrophy, might tend to increas T_1 measurements in grey matter.

Can atrophy account for the relationships shown i Table 2 between T_1 increase and cognitive impairment

Table 1. Mean ± SE (Range) of T_1 in Whole Brain and Regions of Interest and in the Whole Sample of Alcoholics at a Mean of 15.0 Days after Admission

	Whole brain	Frontal white	Parietal white	Frontal grey	Parietal grey	Timing (days after admission)
Control group ($n = 26$)	306 ± 1.69 (290–324)	268 ± 1.58 (252–283)	269 ± 1.97 (248–296)	341 ± 2.09 (326–371)	334 ± 1.50 (310–351)	
Patients—whole sample ($n = 69$)	321 ± 1.67* (283–383)	265 ± 1.49 (230–326)	276 ± 1.45 (230–326)	367 ± 2.28* (314–400)	360 ± 1.76* (321–392)	15.0 ± 0.06 (6–24)
Patients—subgroup with cognitive test ($n = 48$)	325 ± 1.81* (304–383)	266 ± 1.93 (230–326)	277 ± 1.81† (230–326)	373 ± 2.41* (315–400)	361 ± 2.25 (326–392)	15.7 ± 0.8 (6–24)
Patients—subgroup attending for follow-up ($n = 26$)						
First scan	322 ± 1.74* (304–383)	265 ± 1.89 (249–284)	276 ± 1.62 (256–288)	372 ± 2.99* (336–400)	366 ± 2.90* (335–392)	14.0 ± 0.9 (6–23)
Follow-up scan						
< 40 g ethanol per day	324 ± 1.31* (312–333)	266 ± 1.88 (254–285)	280 ± 2.71† (262–301)	373 ± 4.17* (349–406)	365 ± 296* (348–390)	⎰ 192 ± 4.0
> 40 g ethanol per day	330 ± 5.55* (311–378)	270 ± 3.84 (251–298)	277 ± 3.18 (258–293)	374 ± 4.31* (346–393)	363 ± 4.04 (342–392)	⎱ (147–258)

* Patients greater than controls, $p < 0.01$; †$p < 0.05$.

Table 2. Age Controlled Correlation Coefficients of T_1 Values and Estimated Lifetime Consumption with Scores on Components of the Category Sorting Test in Alcoholics at a Mean of 15.7 Days after Admission (*$p<0.01$; †$p<0.05$). (Impairment Results in a Lower Score on Categories, and a Higher Score on Sorts, Errors, and Perseverations).

Category Sorting Test scores [mean ± SE (range)]		Whole brain	Frontal white	Parietal white	Frontal grey	Parietal grey	Lifetime drinking total
Categories	5.42 ± 0.16 (37–136)	−0.44*	−0.50*	−0.42*	−0.24†	−0.17	−0.31†
Sorts	60.90 ± 3.42 (37–136)	0.33†	0.26†	0.19	0.21	0.14	0.37*
Errors	21.00 ± 3.02 (1–90)	0.38†	0.34†	0.30†	0.23	0.20	0.40*
Perseverations	6.33 ± 1.25 (0–35)	0.41*	0.34†	0.29†	0.21	0.25	0.40*
		$n = 48$	$n = 48$	$n = 48$	$n = 48$	$n = 48$	$n = 47$

Table 3. Age-controlled Correlation Coefficients of Atrophy Indices, T_1 Values, and Cognitive Test Scores ($n = 46$)

	Huckmann	Ventricular	Third V	Sulcal width
T_1				
Frontal white	0.33*	0.27	0.14	0.09
Frontal grey	−0.13	0.04	−0.09	0.26
Parietal white	0.39†	−0.10	0.26	0.23
Parietal grey	0.10	−0.15	0.06	0.12
Whole brain	0.03	−0.04	−0.01	0.06
Categories	−0.30*	0.02	−0.21	−0.09
Sorts	0.16	−0.01	0.04	0.03
Error total	0.15	−0.01	0.06	0.07
Perseverations	0.11	−0.01	0.00	0.08

*$p < 0.05$; †$p < 0.01$.

Table 4. Correlation Coefficients of T_1 Values (White Matter and Whole Brain) with Cognitive Test Scores, Controlling for Age and Huckmann Index ($n = 46$)

	Whole brain	Frontal white	Parietal white
Categories	−0.43*	−0.55*	−0.44
Sorts	0.32†	0.40*	0.30†
Errors	0.36†	0.47*	0.40*
Perseverations	0.38*	0.46*	0.40*

*$p < 0.05$; †$p < 0.01$.

Table 5. Correlation Coefficients of T_1 Values in Whole Brain and Grey Matter with Cognitive Test Scores, Controlling for Sulcal Width and Age ($n = 46$)

	Whole brain	Frontal grey	Parietal grey
Categories	−0.43*	−0.21	−0.20
Sorts	0.33†	0.20	0.17
Errors	0.37†	0.21	0.23
Perseverations	0.40*	0.19	0.27

*$p < 0.05$; †$p < 0.01$.

Table 4 shows that internal atrophy did not account for the relationship between raised T_1 in white matter and cognitive impairment. Table 2 showed, as already mentioned, correlations in the expected direction though in general not significant between T_1 in grey matter and cognitive impairment. Table 5 shows little alteration in the size of these correlations when cortical atrophy as measured by sulcal width is controlled for. T_1 in whole brain also remains significantly related to cognitive impairment despite the possible confounding effect of atrophy.

The relative lack of importance of atrophy in this study may partly reflect our measurements. We used indices previously used in CT scans, and by comparison MRI scans lack definition. Our measurements were made by caliper rather than by computer.

Changes in T_1 and Cognitive Function in Relation to Degree of Abstinence

There were 26 patients who reattended for the repeat scan and on whom we had data on consumption of alcohol in the interval (Table 1).

Whether or not patients were deemed to have resumed drinking heavily, the trend was for whole brain T_1 to rise slightly over the 6-month period. Whole brain T_1 measurements at 6 months in those 15 patients who had been abstinent or who had drunk on average less than 40 g of ethanol per day had risen by a mean of 2.33 ms (range, −11 to 29; SE, 2.87) (see also Fig. 2). The mean serum GGT of this group was within the normal range (21 IU/liter, $n = 14$). In those 11 patients who had drunk more than 40 g per day on average during the 6-month period the mean rise in whole brain T_1 was 6.27 ms (range, −15 to 60; SE, 5.94) (see also Fig. 2). This was not a significantly greater mean rise ($p = 0.56$) than in those drinking less than 40 g/day. The mean serum GGT of this group was elevated (178 IU/liter, $n = 10$). The two patients with the highest T_1 values at follow-up were in this group. They were men who had severe long-standing dependence on alcohol for many years and were once again drinking in excess of a bottle of spirits per day (280 g ethanol per day) up to the time of the scan.

There were only nine patients in whom we could be sure that abstinence or near abstinence had been achieved for the whole of the 6-month period. The mean change in whole brain T_1 in these patients was −0.78 ms (range, −11 to 10; SE 2.85). Figure 2 illustrates the pattern of whole brain T_1 changes in individual subjects from the initial scan to the 6-month scan showing abstainers, "intermediate" and "heavy" drinkers separately. Analysis of variance to compare the changes in T_1 values in whole brain and regions of interest over the 6-month period across these three groups defined by increasing posttreatment consumption did not reveal a significant trend for any of the T_1 measurements (frontal white, $F = 1.65$, $p = 0.21$; frontal grey $F = 1.06$, $p = 0.36$; parietal white, $F = 1.92$, $p = 0.17$; parietal grey, $F = 0.26$, $p = 0.77$; whole brain, $F = 0.67$, $p = 0.52$; in each test $df = 2/23$).

There were 25 patients who repeated the Category Sorting Test in a sober state at the time of the 6-month scan. The mean changes in these individuals' scores were: CAT-
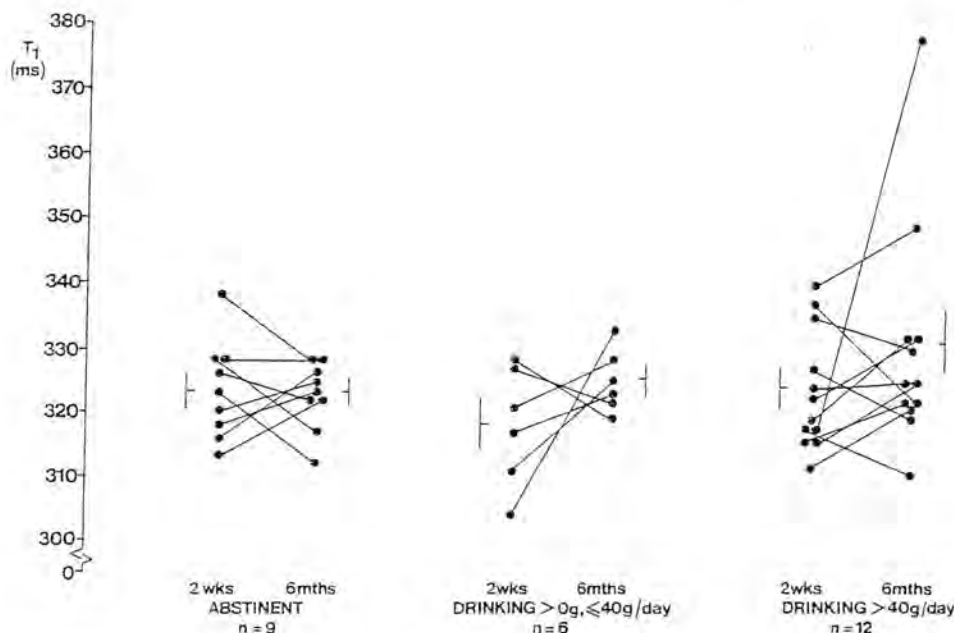
Fig. 2. Whole brain T_1 measurements, separately for those patients who abstained, drank 40 g ethanol per day or less, and who drank over 40 g ethanol per day, to illustrate change between scan at 2 weeks after admission and at approximately 6 months later.

EGORIES, +0.44 (range, −1 to +3; SE, 0.17); SORTS, −5.2 (range, −44 to +18; SE, 3.4); ERRORS, −5.2 (range, −32 to +16; SE, 2.5); PERSEVERATIONS, −0.8 (range, −15 to +7; SE, 1.0). However despite this trend towards amelioration, no significant correlations were found between these changes and changes in T_1.

DISCUSSION

The findings of a raised whole brain T_1 in newly detoxified patients and of a significant relationship between T_1 measurements and both cognitive impairment and the possible cause of that impairment, total lifetime consumption, suggest that T_1 measurements have both potential clinical utility and a neuropathological significance. Cognitive deficits were also linked to increased T_1 in white matter, but not grey matter. The finding that is not corroborative is the lack of difference between controls and patients in frontal white matter T_1, given that cognitive deficits appeared to relate to that measure. Grey matter T_1 measures, while they did distinguish alcoholics from controls did not relate (significantly) to cognitive impairment. This raises the question that our T_1 findings are artefacts due to cerebral atrophy (which would be expected to affect grey rather than white matter T_1 measurements). However, the only T_1 measurement which we made which was significantly related to atrophy was that in frontal grey matter. Thus, while noting that frontal white matter T_1 measurements did not distinguish alcoholics from controls, we feel we have found a relationship between T_1 in whole brain and in white matter that relates to alcohol consumption and to cognitive impairment, and that this is independent of atrophy. We note that Harper et al.[4] have stressed that it is loss of white matter, rather than grey matter, which is most important in alcoholics.

Previous workers have attempted to estimate total life-time consumption[1,16] but its reliability remains in some doubt. Although we have little confidence in the absolute accuracy of the estimates, the rank ordering that the method yields is possibly more reliable. This is supported by our finding a correlation of this estimate with T_1 values, and with cognitive test scores (Table 2). Measures of more recent consumption might be thought to be more reliable. However, while more reliable because the memory is fresher, patients' recent consumption often poorly reflects longer standing patterns of drinking: for example, the patient coming to a clinic has often been trying recently to abstain for periods; or, he has presented for treatment because of one or two especially heavy recent binges. Thus in the general working population, where patterns of drinking are fairly stable over time, a marker such as the serum GGT may correlate well with a measure of recent drinking[20]; while in patients admitted to clinics no apparent relationship is found.[24]

In the "Subjects and Methods" section we explained some of the reasons for our choice of the Category Sorting Test. In addition, its microcomputer-assisted administration makes it an inexpensive and convenient test to perform and reduces tester-induced bias; it tests a psychological function of clinical relevance; previous (unpublished) work in some 150 patients had led us to conclude that among a range of tests it was sensitive to increasing severity of alcoholism. It is not a widely used test in the literature, but it is closely based on the better known Wisconsin Card Sorting Test.[25] Category Sorting Tests are believed to reflect frontal lobe functioning.[17,25] It is notable therefore that the largest correlations between test scores and T_1 in the region of interest measurements were found in frontal tissue. Unfortunately, over a period of 6 months, we believe that a subject who had mastered the test could later recall his method of doing it and so we hesitate to

interpret changes in scores in this test during the follow-up period.

The associations which have been found by other authors between CT changes and cognitive tests suggest that it is central atrophy (i.e., loss of white matter), rather than cortical atrophy (loss of grey matter) which best predicts cognitive impairment, albeit only explaining less than 20% of the variance in cognitive performance overall.[3] Central changes appear to regress less quickly with abstinence than cortical changes.[3] Thus, our failure to find significant correlation between T_1 in grey matter and cognitive impairment is consistent with Bergman[3] and also Ron.[1]

Only slightly over half of the patients invited for a 6-month scan attended, despite repeated arrangements being made in some cases. Only very occasionally did the patient give as a reason that he or she found the enclosed space of the scanner unpleasant. Nonattenders were mostly patients who had resumed drinking and wished to break off contact with the clinic. It is difficult to obtain reliable information on drinking in the follow-up phase without, for example, incorporating at the outset specific monitoring by relatives, or urine, blood, or sweat testing at frequent intervals. It would be premature to conclude that our lack of T_1 reduction in our small number of supposedly abstinent patients indicates that elevated values are permanent in the established alcoholic. However, other follow-up studies of abstinent alcoholics have failed to show improvements in cognitive function[26] and the classic alcohol-related deficit, Korsakoff's syndrome, is marked by persisting permanent alterations in brain cells and persisting cognitive impairment despite abstinence. On the other hand, cortical shrinkage as identified by cerebral tomography sometimes resolves with abstinence.[3] Also, cerebral perfusion, diminished in the newly detoxified alcoholic by comparison to controls, appears to improve with abstinence.[27]

A number of neuropathological processes may occur simultaneously in the alcoholic. An increase in the measured T_1 is a marker of overhydration or oedema of either intra- or extracellular tissue. It remains speculative whether an elevated T_1 is a marker of damaged neurones. Christie et al.[28] have shown that frontal and parietal grey and white matter T_1 values are not elevated in patients with presenile Alzheimer-type dementia when compared to age-matched controls whereas patients with Korsakoff psychosis, abstinent for 1–14 years, (mean, 5 years), have raised cortical T_1 values when compared to age-matched normal controls and to frontal grey and white matter in patients with Alzheimer's disease. (Christie et al. were able to distinguish increased T_1 measurements from atrophy in this study of dementia, supporting our conclusion in the present study that our findings are independent of atrophy). Measurements of T_1, like cortical atrophy, increase with age as also found in a previous study[29] as well of the present study.

In conclusion we believe we have shown that MRI T_1 measurements, especially in white matter, are elevated in alcoholics proportionate to their cumulative alcohol intake and to the degree of impairment on a Category Sorting Test of cognitive function. These findings are analogous to those of ageing. The precise location of the extra water which is presumed to underly this change, and its cause, is unknown. Potentially, MRI T_1 is of clinical value as a marker of alcohol-related brain damage.

ACKNOWLEDGMENTS

REFERENCES

1. Ron MA: The alcoholic brain: CT scan and psychological findings. Psychological Medicine Monograph Supplement 3. Cambridge University Press, 1983

2. Tarter RE, Alterman AI: Neuropsychological deficits in alcoholics: etiological considerations. J Stud Alcohol 45:1–9, 1984

3. Bergman H: Brain dysfunctions related to alcoholism: some results from the Kartad project, in Parsons OH, Butters N, Nathan PL (eds): Neuropsychology of alcoholism: implications for diagnostics and treatment. New York: Guildford, 1987, pp 21–44

4. Harper CG, Kril JJ, Holloway RL: Brain shrinkage in chronic alcoholics: a pathological study. Br Med J 290:501–504, 1985

5. Torvik A, Lindbec CF, Rogde S: Brain lesions in alcoholics; a neuropathological study with clinical correlations. J Neurol Sci 56:233–248, 1982

6. Torvik A, Torp S: The prevalence of alcoholic cerebellar atrophy: a morphometric and histological study of an autopsy material. J Neurol Sci 75:43–51, 1986

7. Horsley V: The effect of alcohol upon the human brain. Br J Inebriety 3:69–91, 1905

8. Durand D, Carlen PL: Decreased neuronal inhibition in vitro after long-term administration of ethanol. Science 224:1356–1361, 1984

9. Walker DW, Barnes DE, Zorneyzer SF, Hunter BE, Kubanis P: Neuronal loss in hippocampus induced by prolonged ethanol consumption in rats. Science 209:711–713, 1980

10. Phillips SC, Cragg BG: Chronic consumption of alcoholics by adult mice: effect on hippocampal cells and synapses. Exp Neurol 80:218–226, 1983

11. Lescaudron L, Beracochea D, Verna A, Jaffard R: Chronic ethanol consumption induces neuronal loss in mamillary bodies of the mouse: a quantitative analysis. Neurosci Lett 50:151–155, 1984

12. Watanabe I, Tomita T, Hung KS, Iwasaki YT: Edematous necrosis in thiamine-deficient encephalopathy of the mouse. J Neuropathol Exp Neurol 40:454–471, 1981

13. Mathur de Vre R: Biomedical implications of the relaxation behaviour of water related to NMR Imaging. Br J Radiol 57:1145–1148, 1984

14. Bell BA, Smith MA, Kean DM, McGhee CNJ, MacDonald HL, Miller JD, Barnett GH, Tocher JL, Douglas RHB, Best JJK: Brain water measured by magnetic resonance imaging: Correlation with direct estimation and changes after mannitol and dexamethasone. Lancet 66–69, 1987

15. Besson JAO, Glen AIM, Foreman EI, et al: Nuclear magnetic resonance observations in alcoholic cerebral disorder and the role of vasopressin. Lancet 2:923–924, 1981

16. Skinner HA, Sheu WJ: Reliability of alcohol use indices: lifetime drinking history and the MAST. J Stud Alcohol 43:1157–1170, 1982

17. Acker C, Acker W, Shaw GK: Assessment of cognitive functions in alcoholics by computer: a control study. Alcohol Alcohol 19:223–233, 1984

18. Acker C: Performance of female alcoholics on neuropyschological testing. Alcohol Alcohol 20:379–386, 1985

19. Meldgaard B, Andersen K, Ahlgren P, Danielsen UT, Sorensen H: Peripheral neuropathy, cerebral atrophy and intellectual impairment in chronic alcoholics. Acta Neurol Scand 70:336–344, 1984

20. Chick J, Kreitman N, Plant M: Mean cell volume and gamma glutamyl transpeptidase as markers of drinking in working men. Lancet 1:1249–1251, 1981

21. Smith MA, Best JJK, Douglas RHB, Kean DM: The installation of a commercial resistive NMR imager. Br J Radiol 57:1145–1148, 1984

22. Smith MA, Chick J, Kean DM, Douglas RHB, Singer A, Kendell RE, Best JJK: Brain water in chronic alcoholic patients measured by magnetic resonance imaging. Lancet 1:1273–1274, 1985

23. Skjodt T, Svensen J, Jacobsen EB, Torfing KF: A comparative study between clinical examinations and computed tomography. Clin Radiol 38:367–370, 1987

24. Latcham R: γ-Glutamyl transpeptidase and mean cell volum Their usefulness in the assessment of in-patient alcoholics. Br J Psychia 149:353–356, 1986

25. Nelson HE: A modified card sorting test sensitive to frontal lot defects. Cortex 12:313–324, 1976

26. Yohman RJ, Parsons OA, Leber WR: Lack of recovery in ma alcoholics' neuropsychological performance one year after treatmen Alcohol Clin Exp Res 9:114–117, 1985

27. Ishikawa Y, Meyer JS, Tonahashi N, et al: Abstinence improve cerebral perfusion and brain volume in alcoholic neurotoxicity withou Wernicke-Korsakoff syndrome. J Cerebral Blood Flow Metabol 6:86 94, 1986

28. Christie J, Blackburn I, Smith MA, Engleman HM, Kean DM Douglas RHB: Magnetic resonance imaging in pre-senile dementia c the Alzheimer-type, multi-infarct dementia and Korsakoff's syndrome Psychol Med 18:319–329, 1988

29. Douglas RHB, Engleman HM, Smith MA: The normal variation in brain T_1: Measurements with age. Proceedings of the Third Europea Society of Magnetic Resonance in Medicine and Biology, 1986, p 60

Phospholipids are visible in ^{31}P n.m.r. spectra of human breast tumours

MARTIN LOWRY,* DAVID A. PORTER,†
CHRISTOPHER J. TWELVES,* PHILIPPA E. HEASLEY,†
PAMELA B. GARLICK,† MICHAEL A. SMITH,†
ROBERT D. RUBENS,* MICHAEL N. MAISEY† and
MICHAEL A. RICHARDS*

*I.C.R.F. Clinical Oncology Unit and †Division of
Radiological Sciences, Guy's Hospital, London SE1 9RT,
U.K.

^{31}P magnetic resonance spectroscopy provides a non-invasive method for studying human tumour biochemistry. *In vivo*, spectral resolution is, however, inferior to that achievable *in vitro*. Furthermore, analysis *in vitro* may assist in determining the chemical composition of the peaks observed *in vivo*. In particular, the peaks commonly known as phosphomonoesters (PME) and phosphodiesters (PDE) may arise from several different compounds. As a preliminary to studies of breast cancer patients, we have characterized the spectra obtained both *in vivo* and *in vitro* from this tumour type.

Tumours (>6 cm) from 15 patients with breast cancer were studied (4 by spectroscopy *in vivo* alone, 8 *in vitro* only and 3 both *in vivo* and *in vitro*). Spectra were obtained *in vivo* with a Philips Gyroscan 1.5 T system using a 5 cm surface coil for volume localization. In 11 patients a biopsy was obtained and rapidly frozen in liquid nitrogen. The specimen was divided and two extracts prepared by homogenization in 6% (v/v) perchloric acid (PCA) and chloroform/methanol (CM), respectively. Spectra from these extracts were obtained with a 9.4 T Bruker AM400 spectrometer.

The spectra collected from PCA extracts of breast tumour specimens consisted of approximately 12 peaks each of

Abbreviations used: PCA, perchloric acid; PME, phosphomonoester; PDE, phosphodiester; CM, chloroform/methanol; GPE, glycerophosphoethanolamine; GPC, glycerophosphocholine.

which was identified and quantified. These results are shown in Table 1. P_i was present in high concentrations while phosphocreatine (PCr) was present in only 6 of the 11 tumours at very low concentrations. Other compounds identified include phosphoethanolamine, phosphocholine, glycerophosphoethanolamine (GPE), glycerophosphocholine (GPC) and nucleotide di- and tri-phosphates. Similar observations have been made on several other tumour types [1, 2, 3].

Comparison of spectra obtained *in vivo* with corresponding spectral regions in the PCA-extract spectra revealed the following major differences. The PCA-extract spectra had greater relative proportions of P_i and PME and smaller PDE than the spectra *in vivo*. In contrast the CM extract showed a large peak in the PDE position (5340 ± 1235 nmol/g wet wt. of tissue), i.e. about 20-fold greater than the combined concentrations of GPE and GPC. The differences in P_i and PME observed between *in vivo* and in the PCA-extract spectra can be explained by saturation effects and n.m.r.-invisible pools. The low PDE in PCA-extract spectra cannot be explained in this way and suggests that some n.m.r.-visible phosphate-containing material has been lost during the extraction procedure. As PCA only extracts the water-soluble metabolites from tissue, one candidate for the missing PDE is phospholipids in cell membranes. The results imply that the PDE peak observed *in vivo* arises primarily from membrane phospholipids. However, phospholipids are generally considered to be n.m.r. invisible owing to their low mobility giving rise to very broad signals. The solution to this apparent paradox lies in the fact that the line-width of the peak is proportional to the magnetic field strength [4]. At the low field strengths used for human spectroscopy *in vivo*, the line-width is small enough for the phospholipid peak to make a significant contribution to the spectrum.

The results of these extract studies have major implications with respect to the interpretation of spectra collected from patients *in vivo*. The finding that the PDE peak is pri-

Table 1. *Concentrations of phosphorus-containing metabolites in human breast tumours*

Individual metabolites were determined by ^{31}P n.m.r. of PCA extracts by calibration of the spectrometer against methylene diphosphonate and correction for saturation effects using separately determined T_1 values. The relative concentrations for spectra *in vivo* were determined from integrals of the appropriate spectral regions. Values shown are the mean $\pm$ s.d. for 11 PCA extracts and 7 spectra obtained *in vivo*.

Peak	Component metabolites	Concentration (nmol/g wet wt.)	Contribution to total area (%)	
			Extracts	*In vivo*
PME			29 ± 9	14 ± 8
	Phosphoethanolamine	1295 ± 491		
	Phosphocholine	554 ± 478		
P_i			36 ± 17	10 ± 3
	Inorganic phosphate	2543 ± 1871		
PDE			5 ± 2	33 ± 8
	Glycerophosphoethanolamine	125 ± 80		
	Glycerophosphocholine	160 ± 65		
PCr			1 ± 1	3 ± 6
	Phosphocreatine	47 ± 57		
γ-ATP			11 ± 4	16 ± 6
	[γ-P]Nucleotide triphosphate	467 ± 230		
	[β-P]Nucleotide diphosphate	223 ± 83		
α-ATP			13 ± 4	18 ± 3
	[α-P]Nucleotide diphosphate	188 ± 72		
	[α-P]Nucleotide triphosphate	430 ± 212		
β-ATP			6 ± 2	11 ± 5
	[β-P]Nucleotide triphosphate	364 ± 179		

marily caused by mobile phospholipids requires that we reconsider the implications of changes in this peak during treatment. Previously it was reasoned that increases in this peak represented the accumulation of GPE and GPC in the tumour as a consequence of cell death [2, 5]. However, if in fact the 'PDE' peak represents phospholipid it could mean exactly the opposite, i.e. an increase in cell proliferation.

1. Evanochko, W. T., Sakai, T. T., Ng, T. C., Krishna, N. R., Kim, H. D., Zeilder, R. B., Ghanta, V. K., Brockman, R. W., Schiffer, L. M., Braunschweiger, P. G. & Glickson, J. D. (1984) *Biochim. Biophys. Acta* **805**, 104–116

2. Desmoulin, F., Galons, J. P., Canioni, P., Marvaldi, J. & Cozzone, P. J. (1986) *Cancer Res.* **46**, 3768–3774
3. Corbett, R. T. J., Nunnally, R. L., Giovanella, B. C. & Antich, P. P. (1987) *Cancer Res.* **47**, 5065–5069
4. Davis, D. G. (1972) *Biochem. Biophys. Res. Commun.* **49**, 1492–1495
5. Daly, P. F., Lyon, R. C., Faustino, P. J. & Cohen, J. S. (1987) *J. Biol. Chem.* **262**, 14875–14878

Molecular graphic displays of antibody–antigen interactions

MALCOLM M. FRASER and
E. JAMES MILNER-WHITE

Department of Biochemistry, University of Glasgow, Glasgow G12 8QQ, U.K.

The three-dimensional structure of the complex between chicken egg white lysozyme and the mouse antibody HyHEL-5 has been determined by X-ray crystallography at 2.5 Å resolution [1]. In this communication, we present photographs of models of the complex displayed on Gemini Challenger graphics workstations. The displays make use of new software based on the CHEMMOD molecular graphics package (U-Microcomputers Ltd, Calver Rd., Warrington, Cheshire WA2 8RF, U.K.) designed for investigating interfaces between macromolecules.

The molecule to be displayed consists of the smoothed α-carbon atoms of the two variable domains of the antibody complexed to lysozyme (Fig. 1). Smoothing was described previously [2] and involves averaging the x, y and z coordinates of five successive α-carbons. Atoms are divided into interacting and non-interacting ones. The non-interacting ones form the bulk of each molecule, being drawn as large grey spheres (diameter 0.4 nm). The less numerous interacting atoms are drawn as pale spheres (diameter 1.5–2.5 nm) to show the contact area.

The variable domains of both light and heavy chains have three hypervariable regions, called L1, L2 and L3 and H1, H2 and H3 [3]. These correspond to the six regions of interacting atoms found, which are labelled as such in Fig. 2. Each is a loop joining strands of β-sheet and L2, L3, H2 and H3
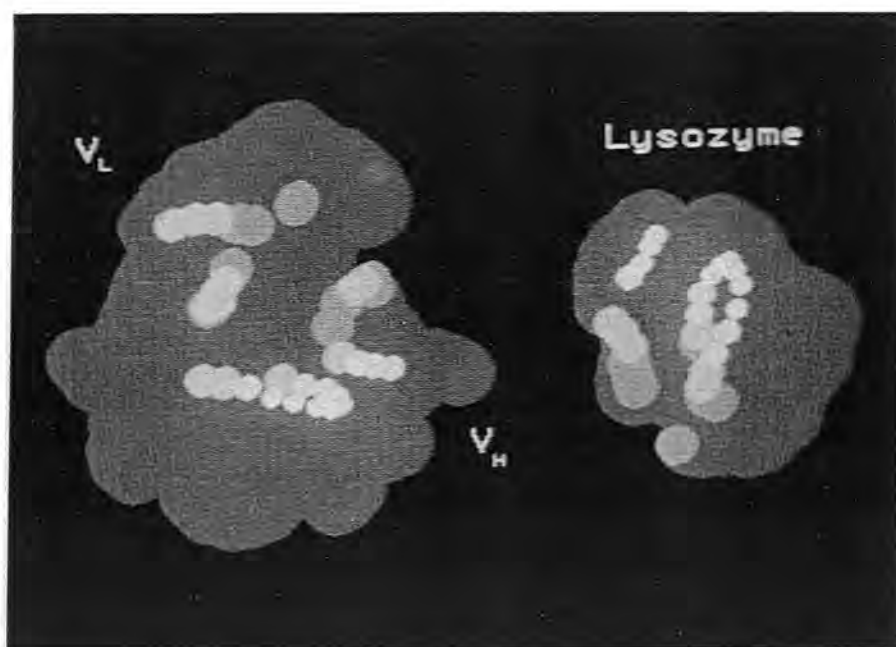

Fig. 1. *The interface between the antibody (two variable domains, VL and VH) and antigen*

Residues that lie within 13 Å of any residue in the other interface are drawn as pale spheres, shaded according to depth. The program originally selects a view along the line joining their centres of gravity. To view the two interacting interfaces simultaneously, the lysozyme molecule is rotated by 180° so that it is placed next to the antibody. Geometricaly this is like opening a book. In the original view the interacting interfaces correspond to middle pages of the book. A simultaneous view of both interfaces is produced by opening the book.